GAMMA-RAY LOGGING WORKSHOP

Grand Junction, Colorado
February 17-19, 1981

Borehole logging methods for exploration and evaluation of uranium deposits

Philip H. Dodd, Robert F. Droullard
and Carl P. Lathan

U.S. Atomic Energy Commission
Grand Junction, Colorado

Borehole logging methods for exploration and evaluation of uranium deposits

Philip H. Dodd, Robert F. Droullard
and Carl P. Lathan

U.S. Atomic Energy Commission
Grand Junction, Colorado

Abstract. Borehole logging is the geophysical method most extensively used in the United States for exploration and evaluation of uranium deposits. Gamma-ray logs, commonly supplemented with a single-point resistance log, currently supply about 80 percent of the basic data for ore reserve calculation and much of the subsurface geologic information.

Truck-mounted rotary drilling equipment is commonly employed; holes usually have a nominal diameter of 4 1/2 inches, range from 25 to 2500 feet in depth, are seldom cased, and may be filled with air or water.

Calibration and quantitative analysis of the gross natural gamma-ray log to obtain equivalent grade and thickness of ore intersections are based on the proportionality between the area under the log curve and the product of the mean equivalent grade and thickness of a radioactive layer.

Rock density and related parameters are calculated from gamma-gamma logs. A different technique permits cancellation of natural radioactivity to obtain density data from ore zones. Calibration and correction factors for nonstandard conditions are determined for each probe in full-scale model holes. GAMLOG and RHOLOG, computer programs written in FORTRAN II for the IBM 7090 computer, are used to quantitatively analyze gamma-ray and gamma-gamma logs to obtain equivalent grade, thickness and bulk density.

Current investigations indicate that natural gamma-ray spectroscopy offers significant additional techniques for exploration and evaluation. Sodium-iodide detectors and single or multichannel pulse height analyzers are used in conjunction with the basic signal conditioning and digital pulse counting system, supplemented with automatic gain or spectrum stabilizers, to make integral or differential measurements of the gamma-ray energies. Certain characteristic photo peaks of thallium-208, bismuth-214, and potassium-40 can be adequately differentiated in spite of extensive scattering in the formation and borehole.

Résumé. La diagraphie des sondages est la méthode géophysique la plus répandue aux États-Unis pour l'exploration et l'évaluation des gisements d'uranium. Les diagrammes de rayons gamma, couramment complété par un diagramme de résistivité à point unique, fournissent généralement environ 80 p. 100 des données de base pour le calcul des réserves de minerai et une bonne parti des renseignements géologiques des couches sous-jacentes.

On utilise en général une foreuse installée sur un camion; les trous ont un diamètre de 4 1/2 po., une profondeur de 25 à 2500 pi., sont rarement tubés et sont soit vide soit remplis d'eau.

La calibration et l'analyse quantitative d'enregistrement brut naturel de rayons gamma effectués pour déterminer la qualité équivalente et l'épaisseur des intersections de minerai sont fondés sur la proportionnalité entre la surface située sous la courbe du diagramme et le produit de l'épaisseur et de la qualité équivalentes moyennes d'une couche radioactive.

La densité des roches et les paramètres connexes sont calculés à partir des enregistrements gamma-gamma. Une technique de différence permet d'annuler la radioactivité naturelle pour obtenir les données densimétriques des zones minéralifères. Les facteurs de calibrage et de correction pour des conditions anormales sont déterminés pour chaque sondage dans les trous d'essai à échelle régulière. Les programmes GAMLOG et RHOLOG écrits en FORTRAN II pour la calulatrice IBM 7090 servent à l'analyse quantitative des diagrammes de rayons gamma et des diagrammes gamma-gamma afin d'obtenir la qualité, l'épaisseur et la densité brute équivalentes.

Les recherches en cours indiquent que la spectroscopie aux rayons gamma naturels offre de nouvelles techniques supplémentaires pour l'exploration et l'évaluation des gisements. Des détecteurs d'iodure de sodium et des appareils d'analyse de tension d'impulsion à canaux simples ou multiples sont utilisés conjointement avec un système de conditionnement des signaux de base et de calcul numérique par impulsion complète par une amplification automatique ou des stabilisateurs de spectre afin de pouvoir effectuer des mesures intégrales ou différentielles des énergies des rayons gamma. Certaines pointes photographiques caractéristiques du thallium-208, du bismuth-214 et du potassium-40 peuvent être bien différenciées en dépit d'une diffusion prononcée dans la formation et dans le sondage.

Natural gamma-ray logging to detect uranium ore was first investigated in 1945. Subsequent improvements in methods and equipment by government and industry have established geophysical logging as a major part of most exploration and evaluation programs. Some 80 percent or more of the basic engineering and geological information used by the uranium mining industry and the Atomic Energy Commission to calculate ore reserves, predict extensions of deposits and for mine planning is derived from logs of non-cored holes. With the resurgence of exploration, particularly as deeper, more widely spaced and costly holes are drilled, the capabilities to extract more information from the hole will significantly assist in the economic search for new districts, new favorable environments, and the reserves and resources required by the growing demands of the nuclear fuel industry.

Borehole measurements, though fraught with problems and pitfalls, offer more than compensating technical and economic advantages. These include reduced coring, sampling and analytical costs; continuous data from which a multitude of sample intervals may be selected and statistically investigated; relatively larger sample volume; certain data may be obtained from previously drilled and cased holes; samples are relatively undisturbed; and analog records, free of subjective observations, are immediately available for qualitative evaluation and correlation.

Contemporary logging programs for uranium evaluation and exploration commonly include analog records of natural gross gamma-ray, single-point resistance, spontaneous potential (SP) and directional measurements. These records are produced by truck-mounted units operated by mining or service companies. Some major companies and individuals elect to log with semi-

portable equipment, without powered winches and often without benefit of chart recorders. It is possible to obtain adequate results for many applications with portable instruments if these are well designed and carefully operated. However, much of the portable instrumentation is poor and operated by untrained personnel which results in less than adequate data for quantitative analysis.

Though not in general use at this time, suitable caliper tools are available and the caliper log is probably the best method for obtaining the hole-size corrections required for quantitative log analysis. Although the feasibility of gamma-gamma logging for radioactive minerals, including ore zones, has been demonstrated by Dodd and Droullard (1965), density-porosity measurements have not been adopted by industry. Resistivity and induced polarization (IP) logs are being tested in the field but are not yet routine or developed to full capability.

Magnetic susceptibility, neutron-neutron, induction and perhaps even neutron activation or photon fluorescence logging appear to warrant research and development for the radioactive mineral industry.

This paper presents a review of a current multipurpose logging system, the principles and methods for calibration, and quantitative analysis of natural gross gamma-ray and gamma-gamma density logs.

Some preliminary observations and comments also are introduced concerning current results from a small project recently initiated by the Grand Junction Office of the U.S. Atomic Energy Commission to investigate techniques and applications of in-hole natural gamma-ray spectroscopy to exploration and evaluation of uranium resources.

General conditions and problems which influence logging

The majority of producing uranium deposits in the United States, and hence the current exploration targets, have relatively small discontinuous substratified configurations and occur in sedimentary rocks which are often poorly indurated. Orebodies are found above, below and astride the water-table. Lithologic units must be defined for correlation and ore zones for economic evaluation, which range from a few inches to tens of feet in thickness.

Rotary seismic-shot-hole type rigs are most commonly employed for drilling. The drilling media may be air, water or natural mud. The holes have nominal diameters of about 4 1/2 inches but may range from 2 to 9 inches. In most cases the holes deviate from the vertical, are rather crooked, and often rough-walled because of caving, washouts, and swelling clay seams. Because of these conditions the probes tend to ride the side and holes have a short life for logging. Not infrequently probes become lodged and must be abandoned. Multiple-purpose probes are desirable to save time in the hole, but excessively complex and costly probes may not be economic.

Although recently exploration drilling has been getting deeper, the holes seldom exceed 2500 feet and usually are 200 to 500 feet deep. Consequently, temperature and pressure conditions are not severe. Massive probes, large cables and powerful winches, such as used for most petroleum logging, are not optimum for uranium logging requirements. This permits the use of smaller and more maneuverable vehicles for logging units which must negotiate steep and narrow hill-side trails and small drill sites. Often a logging unit is expected to service several deep

exploration holes per day or as many as 50 shallow holes in the case of open-pit mining sites. Portable equipment, if properly designed and operated, can meet many of the logging requirements, and indeed may be necessary for certain rugged terrain or for underground long-hole logging.

The holes may be air-filled, water-filled, or partially water-filled; and the interface is seldom encountered at the same depth on successive measurements in the same hole. Heavy muds are seldom used, mud cake is generally thin, invasion by fresh drilling water may be pronounced, and the formational waters are usually fresh to slightly saline. Hence fluid density may be assumed to be 1.0. The intensity of natural gamma radiation ranges from the equivalent of a few ppm uranium from the intrinsic uranium, thorium and potassium in the rocks, through several hundred equivalent ppm in anomalous and mineralized rock, to extreme high-grade zones containing several percent uranium and its gamma-emitting decay products. This great range in natural gamma activity causes severe problems in instrumentation design and logging procedures.

A range in magnitude of gamma activity of 10^5 cannot be adequately spanned by a single detector. To resolve slight variations of lithology or to quantitatively analyze slight anomalies equivalent to a few ppm uranium requires a sensitive detector, yielding at least 50 to 100 counts per second (cps) to achieve adequate statistical precision at reasonable logging speeds. This same detector would generate several hundred thousand cps in a high-grade ore zone of appreciable thickness, which significantly exceeds the capability of current logging instrumentation. Conversely, a detector with adequate sensitivity to measure ore-grade materials without overloading the pulse-transmission and counting instrumentation at perhaps 50,000 or even 100,000 cps would yield too low a count rate from normal lithologic units to achieve an adequate contrast and statistical precision at operational logging speeds.

A similar problem exists in gamma-gamma density logging. If an optimum combination of detector sensitivity, source strength and spacing is selected for adequate statistical accuracy in counting, then if significant additional gamma radiation is encountered in an ore zone, the total count rate may well tax or exceed the linear response capability of the system. The back-scattered radiation from the source in the probe is obscured by the natural gamma radiation from mineralized and ore zones, and special logging techniques are necessary to measure the density of ore zones.

Also, though it may be tempting to use large sensitive crystals for gamma-ray spectral measurements, it is even more imperative not to exceed the gross count rate which the system can achieve without distorting the pulse-height information.

Equipment and instrumentation

Truck-mounted geophysical unit model RD-1A

Logging unit. Figure 1 shows a truck-mounted geophysical unit developed by the Grand Junction Office of the U.S. Atomic Energy Commission for research and development in the field of borehole logging as applied to the search for and evaluation of radioactive mineral deposits. The system is more sophisticated than required for routine logging and is much more complex than units now in routine operation by the mining and service companies. It is used to make natural gamma-ray, neutron,
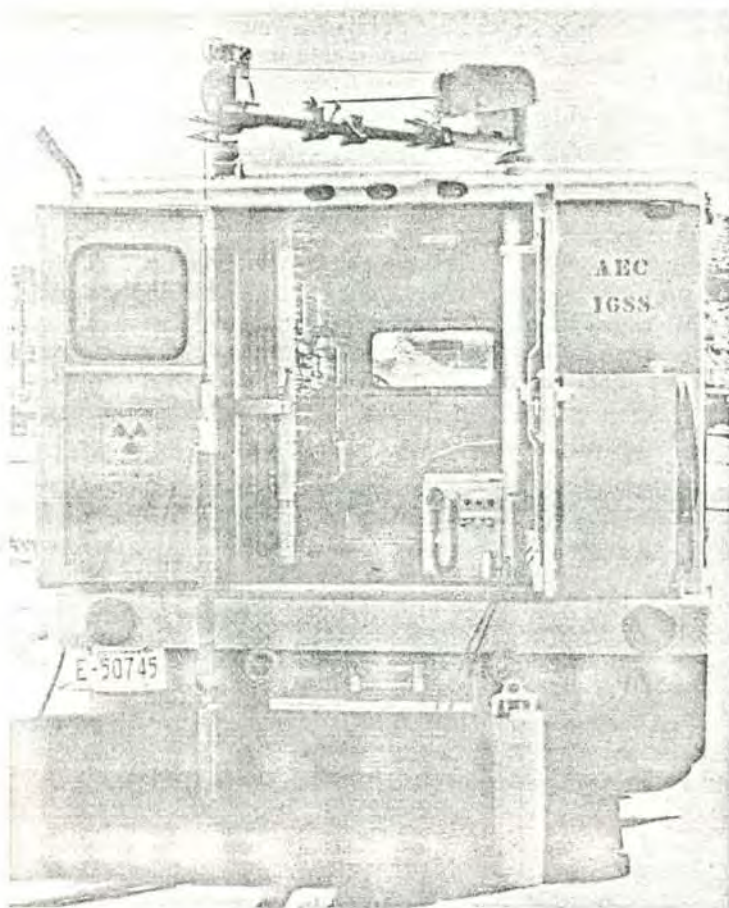
Figure 1. RD-1A multipurpose logging unit developed by U.S. Atomic Energy Commission to support raw materials programs. Down-hole probe is attached to logging cable and large detector for surface spectral measurements is on the ground.

electric, caliper and gamma-gamma density logs. As far as possible, commercially available component instruments and modules were used to assemble this multipurpose system. Primary AC power for this multipurpose system is supplied by a 4 kw generator. Figure 2 is a block diagram of the system.

Nuclear instrumentation

Probes. Activated sodium iodide crystals, ranging in size from $1/2 \times 1/2$ to 5×4 inches, are used for the various applications of measuring gamma rays in boreholes. The crystals are optically coupled to appropriate photo-multiplier tubes, and the output pulses are coupled to the logging cable by means of an amplifier and cable driver.

Logging cable. A double-armored, three-conductor cable of the 3HO type is used for interconnecting the probe and the surface equipment.

Surface equipment (integral and differential counting). The surface end of the 3HO logging cable is connected to an impedance-matching unit which drives a multimode linear amplifier (Ortec model 410). The amplifier provides necessary gain and pulse shaping for the inputs of a single-channel analyzer (Hewlett-Packard model 5583A) and an analog spectrum stabilizer (Hamner model NC-20). The single channel analyzer is used in all three of its operating modes for various applications. Its output pulses are fed to a gating circuit which is controlled by a crystal clock. This unit establishes the dead time of the system and provides selectable dead times, in increments of 1 microsecond, from 2 to 190 microseconds; and its output pulses are used to drive the analog and digital-data readout circuits.

Figure 2. Block diagram, USAEC model RD-1A geophysical logging unit.
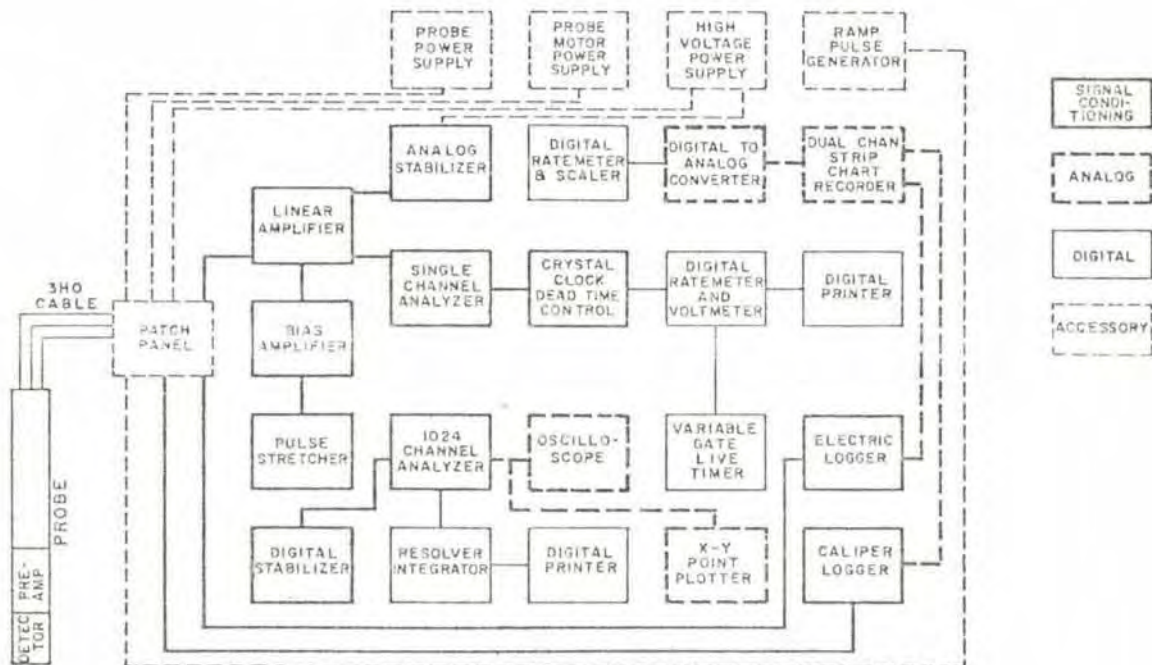
Pulse rate is measured with a scaler-timer (Hewlett-Packard model 5202L) operating as a digital ratemeter. Binary-coded decimal data from this unit are converted to an analog signal by means of a digital-to-analog converter (Hewlett-Packard model 580A), which drives a dual-channel strip-chart recorder (Westronics model SS-11-A/U).

Pulse-rate data for the digital readout are fed to an integrating digital voltmeter (Dymec model 2401B) operating in the frequency mode. An external combination prescaler and time base provides counts-per-second output which can be corrected for dead-time loss by means of a live-timing section controlled by gating signals from the dead-time unit. The BCD output of the digital voltmeter is coupled to a (Hewlett-Packard model 562AR) decimal printer for digital-data output.

Interval control signals for the digital readout are developed in the synchrodriven depth-measuring system through a light-activated pulse generator. Intervals of 0.1, 0.25, 0.50, or 1.00 foot may be selected by a switch.

Surface equipment (gamma-ray spectroscopy). Gamma-ray pulses from the various detectors are routed either directly to a 1024 channel analyzer (TMC model 1001) or are conditioned through the Ortec 410 amplifier followed by a bias amplifier (TMC model 343) and a pulse stretcher (Ortec model 411) prior to height analysis. A digital stabilizer (TMC model 230A) controls both the gain and the baseline of the analyzer.

Analog output from the memory section of the analyzer is viewed on an oscilloscope (Tektronix model RM-647) and readout is by an X-Y point plotter (Houston Omnigraphic model 6550).

A resolver-integrator (TMC model 522RA) is used to process analyzer-memory data, and digital output is recorded on a decimal printer (Franklin model 1200).

Ancillary instrumentation

Surface equipment (electric logging). Potential and current logs are made with an electric logging unit (Mount Sopris model 6-464). Either spontaneous potential or induced polarization logs can be made on the potential channel while the current channel provides either single-point resistance or short-normal resistivity logs. Analog output from this unit is coupled to the Westronics dual-channel strip-chart recorder.

Surface equipment (caliper logging). Signals from the caliper probe are coupled to the digital voltmeter (Dymec model 2401B) operating in the voltage-measuring mode. The borehole diameter is converted to a voltage which is recorded on the digital printer. Analog output is generated by measuring the voltage-to-frequency converter output of the digital voltmeter through the scaler-timer and digital-to-analog converter combination used in nuclear pulse counting.

Test equipment in the Model RD-1A geophysical logging unit includes the aforementioned digital voltmeter and oscilloscope, and a ramp pulse generator (Berkley Nucleonics model GL-3).

Figure 3. Generalized diagram of the natural decay series of uranium, thorium and potassium. Gamma-ray emitters in heavier blocks are of major interest.
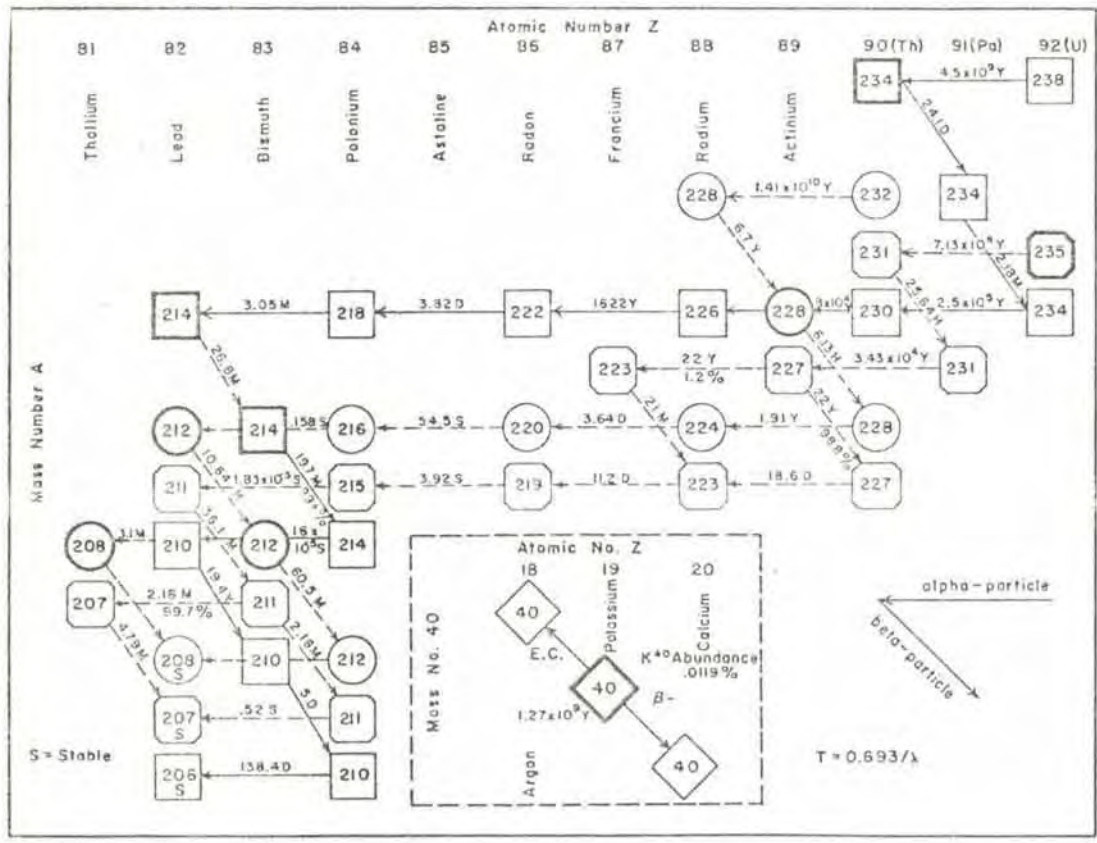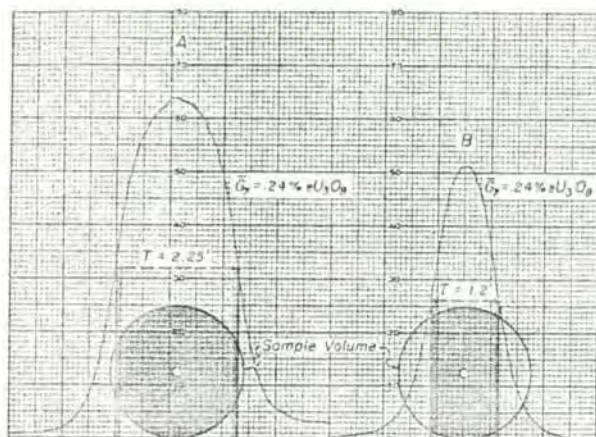
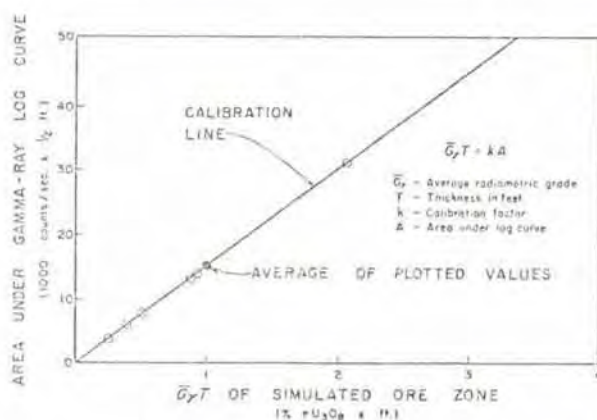Figure 4. Count rate (amplitude of log deflection) depends on both grade and thickness.

Figure 5. The area under the log trace is proportional to the grade-thickness product of the 'ore' zone as demonstrated by six model holes.

The gross natural gamma-ray log

Principle and applications. Gamma rays are emitted by the conversion of potassium-40 to argon-40, by the decay of certain members of both the thorium series, and the uranium series, notably lead-214 and bismuth-214. Figure 3 is a generalized diagram of these decay series in which the gamma-ray emitters of most significance to logging methods have been emphasized by wide-line blocks. These natural gamma rays can be quantitatively detected with logging probes. If uranium is in secular equilibrium with its gamma-emitting daughters, and if there is an insignificant contribution of gamma rays from other sources, then the concentration of uranium in the rocks immediately surrounding a borehole can be determined from a gross-count gamma-ray log with high sensitivity and practical accuracy. Because of the geochemical characteristics of the various radionuclides, these conditions are seldom, if ever, completely fulfilled. Fortunately, for many economically valuable concentrations of uranium, these conditions are sufficiently met, or data may be obtained to supply adequate corrections, to determine the thickness and

mean equivalent grade of the mineralized zone from the gross gamma-ray log and, by calculation, to closely approximate the grade of incremental layers within the zone. Deposits of potassium or thorium may also be evaluated if similar conditions are fulfilled and the response of the logging system has been calibrated in terms of these elements.

In the absence of anomalous radioactivity, a sensitive gamma-ray detector will respond to the differing trace amounts of uranium-, thorium-, and potassium-bearing minerals characteristic of various lithologies; and the gamma log commonly is used to identify formational (rock) units and to correlate thin zones with considerable reliability.

Even with somewhat primitive instrumentation and methods, industry has rather successfully used the gamma log to estimate uranium reserves and to obtain related geological information. Gross-count natural gamma-ray logging is currently the major geophysical method used by the uranium mining industry. It is predicted that at least 6 million feet of borehole will be logged for uranium by this method in the western United States during 1967.

Principles of calibration and analysis

Sample volume concept. The concept of the sample volume is fundamental in devising nuclear logging systems and interpretation methods. For practical purposes, the effective sample volume surrounding a natural gamma-ray detector approximates a spheroid, which by definition contains the material contributing essentially all (some 95 or 98 percent) of the detectable gamma rays; and its radii depend on the energy spectrum of the gamma rays, the scattering and absorption by the medium and the energy threshold of the logging system.

Only when the sample volume is filled with homogeneous material, a condition seldom attained in the geological environment, is the count rate proportional to the grade. Figure 4 illustrates this effect. Logs of two models, which contain the same grade of ore, have different deflections because the 'ore' zones are not of the same thickness and do not occupy an equal sample volume.

Principle of calibration. Scott, *et al.* (1961), empirically and mathematically demonstrated that if the detector is moved up the hole at a constant rate the area under the log curve is proportional to the product of the average radiometric grade and thickness. For practical purposes, this relationship is expressed by the equation

$$\bar{G}_\gamma T = k A \qquad\qquad 1$$

where $\bar{G}_\gamma$ is the average radiometric grade in percent by weight, T is the thickness in feet, k is a constant of proportionality and A is the area under the log curve. The calibration constant k is determined from measurements in full-scale model holes with each probe and for the logging and analytical procedure that will be used. The value obtained for k depends on the sensitivity of the logging system and analytical procedures. In Figure 5 the areas under the log curve of six zones, each differing in thickness or grade, have been plotted against the product of the average grade and thicknesses of the six zones in the model holes. The values for the six ore zones all fall on the line drawn through the average and the origin, demonstrating proportionality.
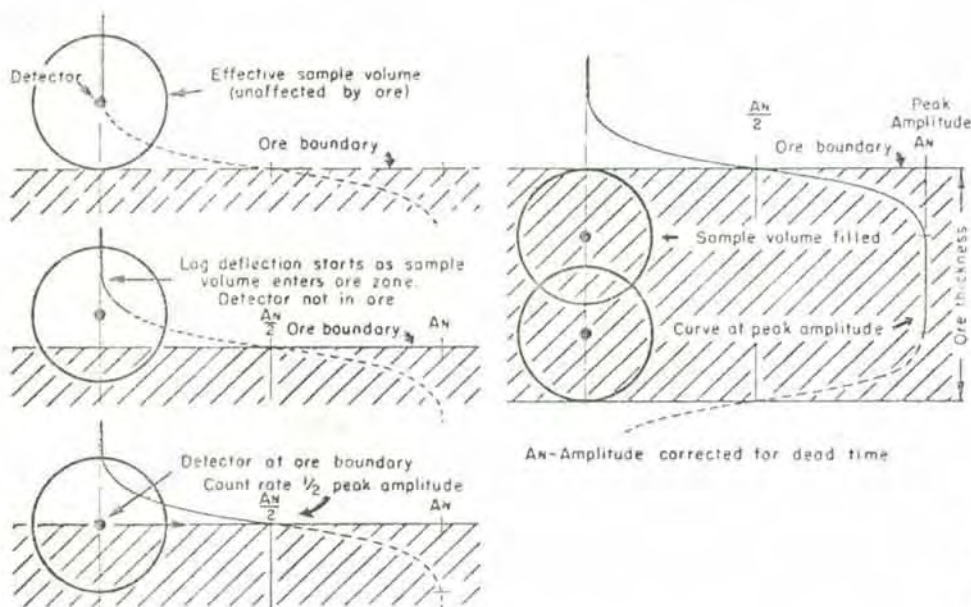
405

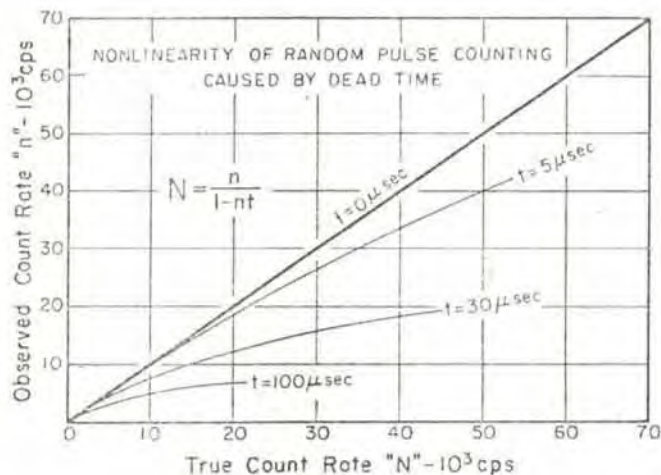Figure 6. The ore boundary is indicated by the half-amplitude point on the anomaly.

Figure 7. Nonlinearity caused by instrument dead time for typical logging systems used by the uranium industry.

of the detector and respective sample volumes, and a representative log trace. When the detector is a distance from the boundary greater than one radius of the sample volume that material in the ore zone will not cause a response. As the detector approaches to within less than one radius, part of the sample volume is occupied and the detector responds even though it may not be in the ore zone. When the detector is at the boundary of a zone which is at least one radius thick, one half of the sample volume is filled and the response will be half that of a full sample volume. For this simple case, the bed boundary is indicated by the half-amplitude point on the log trace. This is also the inflection point on the log curve representing a decrease in the rate of increase in response of the detector to the material in the ore zone.

If the sample volume is not spherical, if the boundary is gradational (or the zone is not homogeneous) and if the zone is less than one radius thick, the method cannot rigorously define the boundary. The thickness is, therefore, an empirically determined estimate which is remarkably good for thicknesses of 2 or more feet; lesser thicknesses tend to be overestimated. Fortunately this does not affect determination of $\bar{G}_\gamma T$, which represents the quantity of radioactive material; it may cause slight 'dilution' and hence underestimation of the average grade of the zone. For practical mining and reserve calculation this error in thickness, which is generally small, can be tolerated or ignored because thicknesses less than 2 feet can seldom be economically extracted without dilution. Perhaps future theoretical work will develop a rigorous technique.

Corrections. Valid quantitative analyses, based on Equation 1 described in the preceding section, depend on the proper application of corrections for nonlinearity in the logging system and for variations of the logging environment from the standard conditions of calibration.

Dead time correction. Assuming that adequate instrumentation is employed, the only significant nonlinearity in the logging system is caused by instrument dead time. If compensation for dead time is not provided in the logging system, such as the crystal clock - dead time module of the RD-1A system, then each numerical

Principle of analysis. From the calibration equation (1), $\bar{G}_\gamma T$ is determined by numerical integration of the response at regular intervals from background to background. The values to be integrated depend on the logging system and may be the deflection of the analog record at regular intervals or, for a digital system, the values recorded at regular intervals while logging. The precision of the integration, and therefore of the analysis, is dependent on the interval and number of the values being integrated. The average radiometric or equivalent grade $\bar{G}_\gamma$ is calculated by dividing the grade-thickness product $\bar{G}_\gamma T$ by the thickness T. The thickness is the distance between the ore or bed boundaries and may be estimated from the log.

A somewhat empirical method has been devised to estimate the thickness T from the log. The method is based on a hypothetical spherical sample volume, which is only a convenient approximation. Figure 6 illustrates the method. It shows a homogeneous ore zone having sharp boundaries, several positions
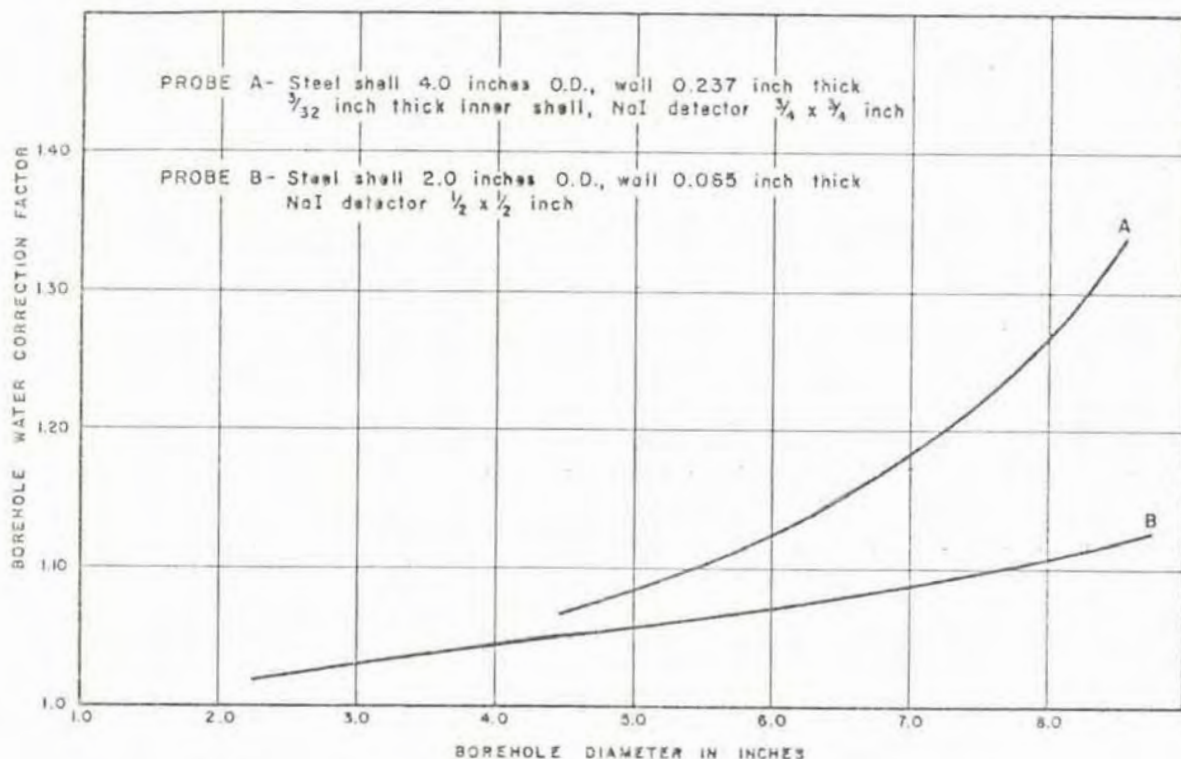
Figure 8. Correction factors for water content and diameter of borehole using typical natural gamma-ray logging probes.

value of the observed count rate n should be corrected statistically using the equation

$$N = \frac{n}{1 - nt} \qquad 2$$

where N is the corrected count rate and t is dead time. Figure 7 shows the nonlinearity caused by dead time of typical logging systems used by the uranium industry. Unless controlled and corrected, dead time will introduce significant errors in the quantitative analysis of any log based on pulse counting. In the case of the natural gamma-ray log, uncorrected dead time results in underestimating grade and overestimating thickness, particularly if very high count rates are generated by sensitive detectors or high concentrations of gamma rays.

Corrections for nonstandard borehole environments. The standard conditions under which the natural gamma-ray logging probes are calibrated have been arbitrarily selected to approximate common field conditions. Any variation in the logging environment from the conditions of calibration may require a correction to standard conditions. Variations in hole size, hole fluid, and drill rods or casing commonly introduce significant nonstandard environments.

At least in the case of gross counting, the correction of the gamma-ray log for variations in size of an air-filled hole up to 8 inches in diameter is insignificant. (For this reason 4 1/2-inch, air-filled, uncased holes have been selected as standard conditions for calibration.) However, if the hole fluid is a significant absorber of gamma rays, such as water or natural mud, then major corrections for hole fluid and size are necessary. Correction
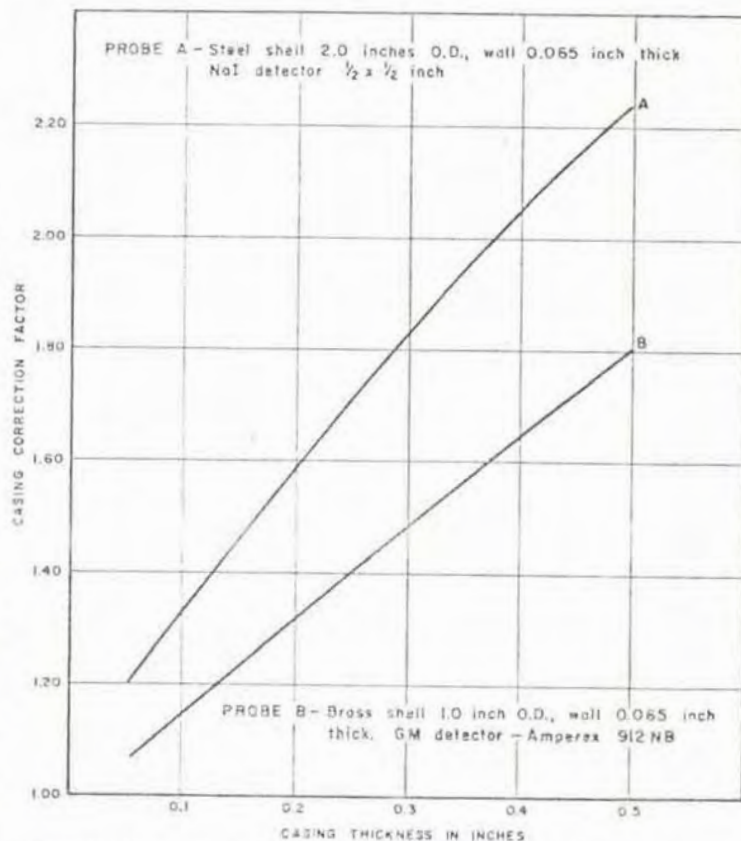

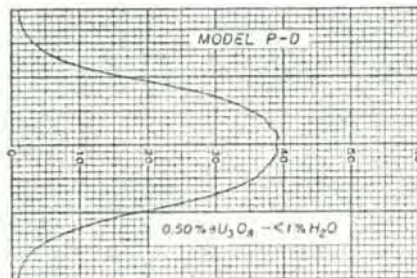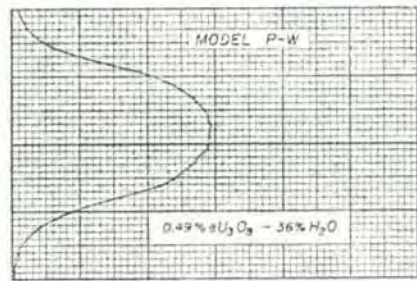Figure 9. Correction factors for wall-thickness of casing using typical natural gamma-ray logging probes.

Figure 10. The attenuation effect of free water in the formation.

curves, Figure 8, are developed for each probe from full-scale models. Factors influencing the correction values are the spectral efficiency of the detector, the probe diameter and the probe shell thickness and material. Heavy barite muds introduce additional problems involving gamma-ray reactions with elements of high atomic number.

Similar curves, Figure 9, are required for each probe to correct for the absorption by casing or drill rods. For practical purposes these corrections are linear for all count rates and may be applied to the area or integrated term of the calibration and analysis equation. Appropriate corrections are indicated by the caliper log and driller's records.

Nonstandard conditions in the formation which modify, scatter and absorb natural gamma rays are less easily determined and the cumulative effects are not well evaluated. These include
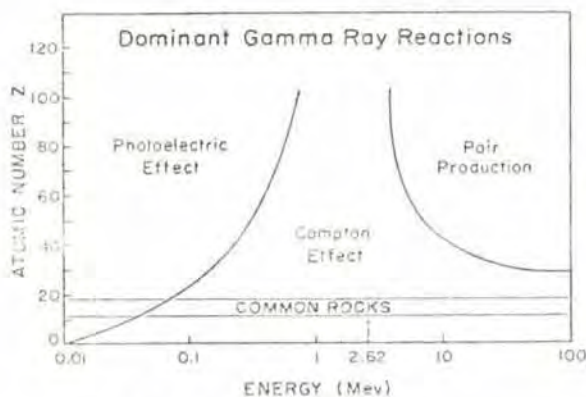

Figure 11. The type of gamma-ray reaction depends on atomic number Z and photon energy. Maximum natural gamma energy and effective atomic number of rocks, and the dominance of compton scatter are indicated by dashed lines.

intergranular fluids and unusual abundance of elements of high atomic number in the rocks.

The effect of free water in the formation is illustrated by the two logs in Figure 10. With the exception of the 36 percent by weight of water in model P-W, these models contain essentially the same materials. However, the log of the water-saturated model has a distinctly lesser amplitude and area under the curve. From empirical investigation and experience, it appears that a factor derived from the relationship

$$\text{Free water correction} = \frac{100 - \% \text{ water in calibration}}{100 - \% \text{ water in formation}} \qquad 3$$

adequately corrects for nonstandard free water content. The percent water in rocks below the water-table may be closely approximated from the gamma-gamma density-porosity log and it is believed that neutron-neutron methods can be developed to obtain this value for unsaturated rocks.

Figure 11 shows the fields of gamma-ray reactions in terms of the gamma-ray energy and the atomic number of the medium. Most of the common rock-forming minerals, especially those of the clastic host rocks for uranium in the western United States, have similar atomic numbers. Consequently the range of the effective atomic number of the rocks is generally narrow, averaging perhaps 15. The maximum energy of natural gamma rays is 2.62 mev. Low-energy photons, either from primary emissions or scatter, are abundant. It is these with energies of 0.14 mev or less which undergo photoelectric absorption, particularly with materials of high atomic number, and are removed from the system. This effect becomes more pronounced with the introduction of more than trace amounts of high atomic number elements, a situation generally difficult if not impossible to evaluate. The effects of nonstandard composition can be minimized by using calibration models which simulate the composition of the common rocks to be logged. Preliminary investigations also suggest that physical or electronic discrimination of low-energy gamma rays, those most influenced by variation in atomic number of the medium, will greatly reduce or largely eliminate compositional effects.

Correction for disequilibrium. In the geochemical environment the major gamma-ray-emitting daughters, such as bismuth-214, often are not in secular equilibrium with the parent uranium-238 (see Figure 3). This is particularly true of many sandstone-type uranium deposits in which the uranium or radium have been selectively transported. In this event, to estimate the true grade of the uranium, a correction must be applied to the equivalent grade indicated by gross gamma-ray measurements. The disequilibrium correction is represented by the ratio of the true grade, determined by chemical analysis, to the equivalent or radiometric grade. This ratio can be estimated by statistical analysis of chemical and 'gamma-only' assays of representative samples from the area, as described by Scott and Dodd (1960). If adequate sample data are available, a regression analysis will relate the disequilibrium ratio and grade; such an analysis indicates the 'best' correction to be applied to each equivalent grade. Lyubavin and Ovchinnikov (1961) suggested that disequilibrium could be detected by spectral logging methods. Preliminary investigations tend to confirm this idea; however, the complexity and extreme

stability of the instrumentation required exceeds or seriously taxes the capability of the instrumentation currently in service.

To calculate ore reserves and make economic evaluations of a uranium deposit may require quantitative analysis of several to several hundred gamma-ray logs. These may have been obtained with more than one logging system, each requiring individual calibration and correction factors. With experience, those logs which indicate a mineralized zone of interest may be selected by inspection.

The equivalent grade and thickness of the anomalies can be determined by 'hand' interpretation methods described in detail by Scott, et al. (1961). Briefly, this involves: (1) selecting the zone boundaries from the half-amplitude points on the sides of the anomaly to determine the thickness T in feet; (2) obtaining the area under the log curve A by summing the count rate values, corrected for dead time, at 1/2-foot intervals between the indicated boundaries, and adding the area of the anomaly which extends outside of the zone boundaries (estimated by applying a 'tail factor' to the sum of the count rates at or adjacent to the boundaries); (3) applying appropriate correction factors to the area; (4) obtaining the grade-thickness product $\bar{G}_\gamma T$ by multiplying the area A by the calibration factor k; and (5) determining the equivalent average grade $\bar{G}_\gamma$ by dividing $\bar{G}_\gamma T$ by T. To some extent portions of anomalies may be selected for analysis to meet mining or economic requirements.

Similar techniques may be applied to determine the equivalent ppm of uranium in formations or selected lithologic units. By this method dispersed amounts of radium and its daughters, which in some cases extend well beyond the limits of the ore, can be detected from relatively wide-spaced exploration holes. However, the gross gamma log of low-intensity anomalies will be significantly influenced by the potassium and thorium content of the rocks.

GAMLOG, a computer program for quantitative analysis of gamma-ray logs was developed by Scott (1962). With subsequent modifications[*] it has become the standard method of analysis to obtain grade and thickness for ore reserve estimation. This program, written in FORTRAN II for the IBM 7090, utilizes 300 or more log deflection values at 1/2-foot intervals and coded control data such as type of logging equipment, k factor, dead time and correction factors to determine and print out the equivalent grade of 1/2-foot layers within the anomaly. The identification and control data are supplied on standard 80-column IBM cards. Log deflection data are digitized from copies or original analog records and punched on cards by a Gerber Digital Data Reader coupled to an IBM 026 key punch. Perforated tape records may be automatically converted to the standard card format, or digital readout on printed tape can be manually transferred to cards by the key-punch operator.

From the calibration equation (1) and the sample volume concept, for an infinitely thick, homogeneous zone, all log deflections, in units of counts per second corrected for dead time, can be shown to be, and any one can be represented by $\bar{N}$. If deflection (count rate) values are taken at 1/2-foot intervals, the number of values will be $2T$. Therefore

$$A = 2\bar{N}T$$
$$\text{and } \bar{G}_\gamma T = k \cdot 2\bar{N}T$$
$$\bar{G}_\gamma = 2k\bar{N} \qquad\qquad 4$$

Therefore, the grade of an anomaly representing a homogeneous, infinitely thick zone, can be determined by multiplying the deflection in corrected counts per second by twice the k factor.

By using Equation 4 the GAMLOG program makes a first approximation of the grades of 1/2-foot layers of an anomaly. Weighting factors for adjacent layers also occupying portions of the sample volume are determined from model studies and hypothetical anomalies are generated for each 1/2-foot layer. These, in turn, are composited into a total anomaly which is compared to the real anomaly. The assigned grades of the individual layers are adjusted by an iterative process until the composited anomaly matches the log anomaly, as shown by Figure 12. The program output shows grade and depth or elevation of the hypothetical layers printed in tabular form.
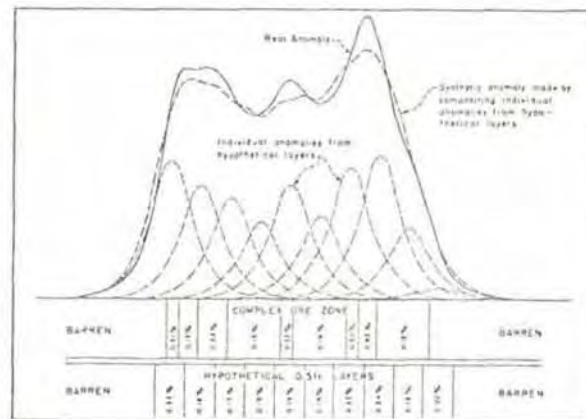

Figure 12. GAMLOG generates synthetic anomalies for hypothetical 1/2-foot layers and adjusts grade of the layers until the composited anomaly matches the log.

Subroutines have been developed to calculate count rates, corrected for dead time, from curvilinear and rectilinear logs which have been digitized in units of inches of deflection and coded range scales. The calculated grade and depth values are used as input data for several computer programs which statistically compute reserves in terms of pounds U_3O_8, tons of ore and average grade and thickness at cut-offs determined by various market prices or production costs per pound (Grundy and Meehan, 1963; Patterson, et al., 1964).

Scattered gamma-ray density log

The scattered gamma-ray density log was introduced in 1951 (Faul and Tittle, 1951) and the principle has been applied to several engineering problems (Homilius, et al., 1958; Roy and Winterkorn, 1957). It is used by the petroleum industry to measure porosity. The physical principles have been well described in the literature (Pickell and Heacock, 1960; Baker, 1957; Homilius and Lorch, 1957; Wahl, et al., 1964; Rodermund, et al., 1961). However, the method cannot be directly applied to determine the density of uranium deposits because the intensity

of natural gamma radiation obscures the scattered gamma rays from the density probe.

To overcome this problem, a method of density logging has been developed which cancels the background of natural gamma radiation and measures the wet bulk density (Dodd and Droullard, 1965). Values for dry density, porosity and water content of the rocks, which are required to evaluate uranium deposits, are derived from the wet density measurement. A digital recording system and a computer program for automatic processing of the data contribute significantly to the practical application of this log.

Principle of scattered gamma-ray density logging

Electron density related to bulk density. The probe used to measure bulk density ρ_b in the borehole contains a collimated source of gamma rays which is separated from the detector. Gamma rays from the source penetrate the rock and are scattered back to the detector. Tittman and Wahl (1965), Czubek and Guitton (1965), and Czubek (1965) have shown that by using a suitable detector and gamma-ray energy the response is proportional to the Compton scattering which is controlled by the electron density ρ_e of the medium. If

$$\rho_e = N_A \ (Z/A) \ \rho_b \qquad 5$$

where N_A = Avogadro's number and Z/A is the ratio of atomic number to atomic weight, then the response is also proportional to the bulk density. Tittman and Wahl (1965), and Danes (1960) have also shown that, with the exception of hydrogen, Z/A of the common rock-forming elements is nearly constant. Therefore, by applying corrections for nonstandard Z/A, the response of the system may be calibrated in terms of ρ_b.

Porosity. Fractional porosity ϕ is calculated from the relationship

$$\phi = \frac{\rho_g - \rho_b}{\rho_g - \rho_f} \qquad 6$$

where ρ_g is the grain density and ρ_f is the fluid density.

Problems and applications in the uranium industry

Special problems. Several of the problems of scattered gamma-ray logging become especially acute when applying the method to the uranium mining industry. Foremost is the wide range and intensity of natural gamma radiation which obscures the back-scattered gamma rays from the source and which places extra demands on the pulse counting system.

The effect of hole size is critical, especially at the smaller diameters. Most holes drilled by the uranium mining industry in the western United States have nominal diameters ranging from 3 to 5 inches and normal variation within this range has a very significant effect on response. Therefore, quantitative density analysis requires accurate measurement of small changes in hole diameter to determine appropriate corrections.

Commonly, the depth to the air-water interface in the hole is unstable, which compounds the problem of correcting for effects of hole fluid.

Information sought from density logging. Dry bulk density, rather than wet density, is used in the volume-to-weight conversion for ore reserve calculations. Many deposits are evaluated by

non-core drilling and logging methods, and the density log can supply the otherwise unavailable bulk-density measurement. Dry bulk density ρ_d may be used in geologic investigations and to evaluate mining problems. For a particular rock type, such as sandstone, the degree of induration or cementation, which is indicated by the density, directly affects its competence under mining stresses and its fragmentation.

Fractional porosity ϕ (Equation 6), is required to calculate ρ_d and the water content of the rock. Porosity data supplement lithologic interpretations from other logs, support geologic studies of ore controls and genesis, and may be used to evaluate water problems encountered in mining. A correction for water content of the host rock is needed to determine ore grade from natural gamma-ray logs.

Saturation S_w, the fraction of the pore space occupied by water, is required to establish the fluid density ρ_f and to calculate the water content. Below the water-table 100 percent saturation may be assumed, at least in the case of rocks having interconnected pore space. Above the water-table saturation may be measured with a neutron log or estimated from experience.

Method for determining density of uranium ore zones. The following method and calculations are used to determine the dry bulk density of uranium-bearing rocks.

Dead time corrections. As in the case of natural gamma-ray or other nuclear pulse counting methods, the response of the density logging system must be corrected for instrument dead time. If not corrected by the logging system it is made by the computer program using Equation 2 and the correction becomes very significant at the high count rates generated by the combined radiation from the source and uranium ore.

Difference method using dual spacing. The intensity of the scattered gamma radiation at the detector is, within certain limits, a function of the source-to-detector spacing. Therefore for a given density, the response of a probe having a short spacing is n_S and
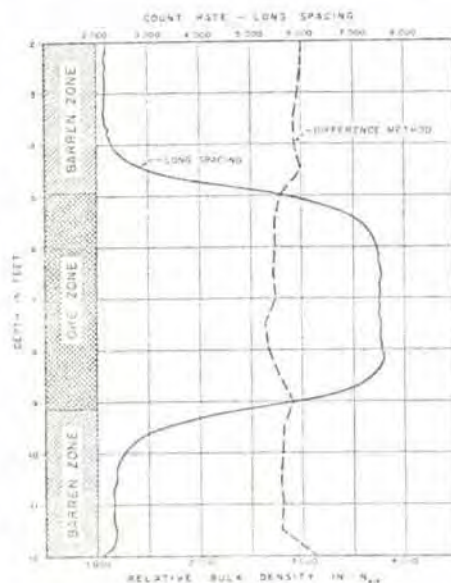

Figure 13. Comparison of density logs of an ore zone, using single spacing and difference methods.

the response for a long spacing is n_L. Corrected for dead time, these become N_S and N_L and both are a function of density. The difference $N_{DIF} = N_S - N_L$ is also a function of density (see calibration curve Figure 15). For a given position in the hole, the intensity of the natural gamma radiation at the detector is a constant which is included in N_S and N_L. This constant is eliminated by subtraction and N_{DIF} remains a function of density unaffected by background radiation (Figure 13).

Therefore, to determine density of naturally radioactive material, two logs are made with a difference in spacing of 4 or more inches. The N_S and N_L values are corrected for borehole effects and the N_{DIF} value is converted to wet bulk density by a polynomial calibration equation (11). To facilitate the difference method, the type 400 density probe has been developed which permits changing the spacing while in the hole (Figure 14).

Calculation of porosity, dry bulk density and water content

Porosity. Having measured the wet bulk density, the fractional porosity may be calculated using Equation 6. A value for grain density ρ_g is determined from the drill cuttings, either by analysis or estimated from inspection of the mineral composition. A value for fluid density ρ_f is determined as follows:

1. Below the water-table ρ_f is assumed to be 1.0 because the pore space is filled with fresh water.

2. Above the water-table ρ_f is equivalent to the water saturation, S_W, because

$$\rho_f = \frac{(\phi_W \cdot \rho_W) + (\phi_a \cdot \rho_a)}{\phi_W + \phi_a} = \frac{\phi_W}{\phi} = S_W \qquad 7$$

where ρ_W is density of water, ρ_a is density of air, ϕ_W is fractional porosity occupied by water, and ϕ_a is the fractional porosity occupied by air. A correction is applied to the ρ_f term to compensate for the A/Z of hydrogen in S_W and the porosity equation (6) is modified to the following form:

$$\phi = \frac{\rho_g - \rho_b}{\rho_g - (S_W \cdot Corr_{A/Z})} \qquad 8$$

Dry bulk density. Dry bulk density ρ_d is calculated by

$$\rho_d = \rho_b - W \qquad 9$$

where W is the weight of water in grams contained in a cubic centimeter of the rock ($W = \phi \cdot S_W$).

Water content. The water content $\%W$, expesssed in percent moisture by weight, is derived from the relationship

$$\%W = \frac{W}{\rho_b} \cdot 100 \qquad 10$$

Calibration for density and borehole effects.

The response of the density logging system to density and borehole effects is calibrated in full-scale model holes. The probe is calibrated for density in standard air-filled holes, 4.5 inches in diameter. The effective bulk densities of the models, which range from 1.62 to 2.85 gm/cm³, are determined by physical measurements, and are corrected to a standard A/Z of 2.0.
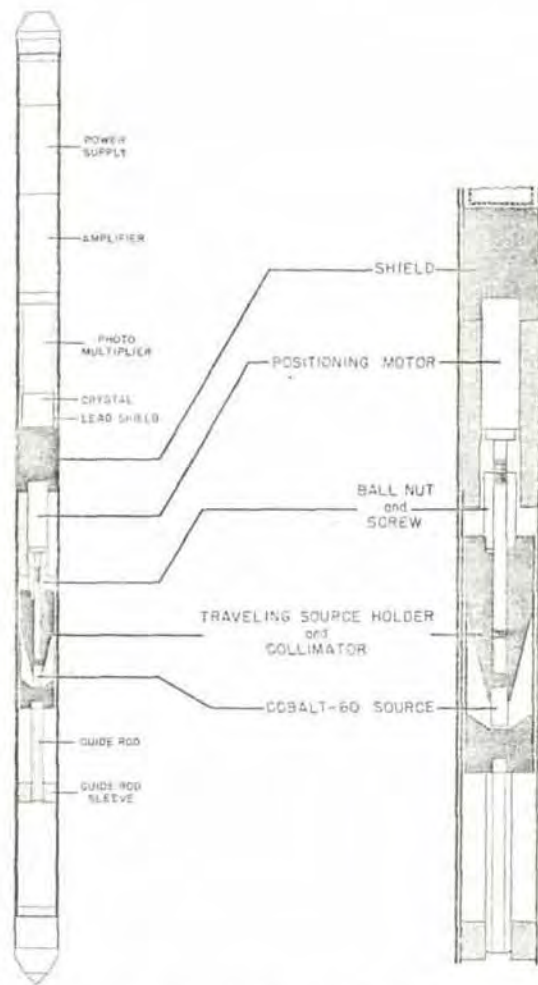

Figure 14. Sectional diagrams of type 400 density probe.

Dual spacing procedure for difference method. The count rates for the short- and long-spacing configurations are measured while the probe is held stationary against the walls of the model holes. These rates are corrected for dead time and the N_{DIF} values computed for each model are plotted versus the bulk density to derive a calibration curve (Figure 15).

WRAP*, a weighted regression analysis program for the IBM 7090 fits a curve to the points and prints out the coefficients and applicable terms of the polynomial calibration equation,

$$\rho_b = a_0 N_{DIF}^n + a_1 N_{DIF}^{n-1} \cdots\cdots + a_{n-1} N_{DIF} + a_n \quad 11$$

Single-spacing calibration. Likewise, the corrected count rates N_S and N_L are plotted and calibration equations similar to Equation 11 are calculated by WRAP for each of the single spacing. These calibrations are used when natural radioactivity of the formation is insignificant and the more sensitive and rapid single-spacing method is satisfactory.
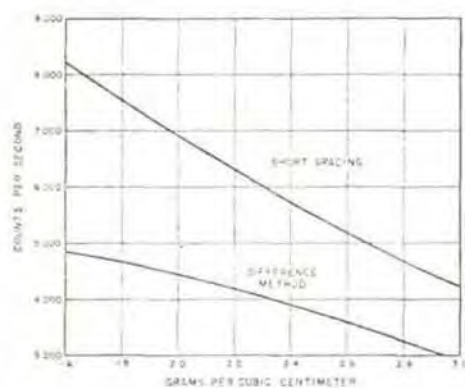
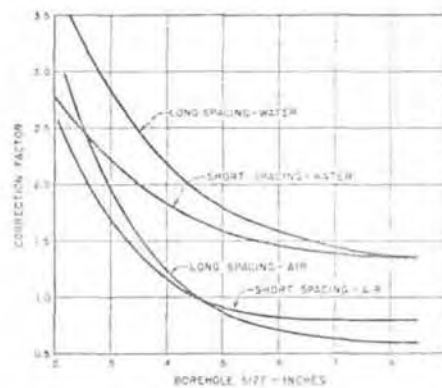Figure 15. Typical calibration curves for type 400 density probe in standard 4.5-inch air-filled hole.

Figure 16. Typical borehole size correction curves for air- and water-filled holes.

Determination of corrections for borehole effects. A model of uniform density which contains 7 holes, ranging in diameter from 2.25 to 8.50 inches, is used to determine correction factors for borehole effects. With the probe held stationary against the wall, the count rates for air-filled and water-filled holes are measured for short and long spacing and the rates corrected for dead time. Corrections are computed to normalize the four sets of data to the standard air-filled hole, 4.5 inches in diameter. Curves showing the correction for diameter in air- and water-filled holes for short and long spacing (Figure 16) are fitted by WRAP which computes the coefficients and applicable terms of four polynomial correction equations similar to Equation 11.

Correction for source decay. The half-life of the Cobalt-60 source is 5.3 years and a correction factor for source decay at the time of logging is applied by the computer to maintain the calibration equation.

Calibration of caliper probe. The caliper system is linear through the operating range and a single-point calibration is made by placing the probe in a metal sleeve of known diameter and adjusting the voltage in the divider circuit to obtain the correct measurement.

Data processing. Automatic data processing contributes significantly to the practical application of the density logging method because many routine manipulations are required to interrelate the data from the several types of logs and to correct the data to standard calibration conditions. Additional manipulations are needed to calculate the dry density, porosity and water content at closely spaced intervals.

RHOLOG*, a computer program written in FORTRAN II for the IBM 7090, has been developed to process the data from the density and caliper logs. The computer calculates and prints out up to 2000 density and associated values in a single hole and determines the average density for zones of special interest. An error code is printed at the appropriate depth if data from associated logs are not available or have been interpolated from adjacent readings, or if they are determined to be invalid for certain portions of the hole. Logs from a given hole may be discontinuous, top and bottom depths of associated logs need not match and, in the absence of specific data, estimates of certain parameters may be used.

*The RHOLOG program was developed by Paul C. deVergie, Grand Junction Office, U.S. Atomic Energy Commission.

The density and caliper logs, including manually entered identification data, are recorded on perforated tape by the logging system. These are converted to punched cards by an IBM 047 tape-to-card converter and additional identification and control data are supplied on manually punched cards. The data cards are listed for editing before being submitted to the computer.

Gamma-ray spectroscopy

Introduction and history. As part of its program to support industry with research and development of new or improved exploration and evaluation tools, the Grand Junction Office of the U.S. Atomic Energy Commission recently initiated a small project to develop applications of gamma-ray spectroscopy to field investigations. The following comments and observations on in-hole spectral measurements are the result of preliminary and exploratory studies.

As early as 1948 and 1949 Hofstadter published on the application of NaI(TI) crystals to detect gamma energies from low-intensity sources. The technique soon became standard laboratory practice. DiGiovanni, et al., (1952), in describing a scintillation logging unit designed for uranium exploration stated, "A further advantage is the fact that the sodium iodide crystal scintillation intensity is directly proportional to the absorbed energy of the incident gamma photon. This makes it possible to obtain gamma energy spectra from the material in the hole (which is extremely useful for determining the nature of the radioactive material therein)."

Laboratory, surface and airborne measurements of gamma spectra are being adapted to the search for radioactive minerals (Adams, 1964; Adams and Fryer, 1964; Pemberton and Seigel, 1966; Foote, 1967).

In spite of numerous references to spectral measurements in the literature, especially since about 1960, the uranium mining industry in the United States has made no concerted effort to adopt this potentially valuable tool for exploration and evaluation. Possibly the lack of interest has stemmed from the temporarily restricted market for uranium, possibly because reliable and stable instrumentation with spectral capability was both expensive and unproven, and possibly because the operational staffs generally considered the whole subject as 'black box' witchcraft. In any event, the advantages of down-hole spectral measurements largely remain to be developed and demonstrated.
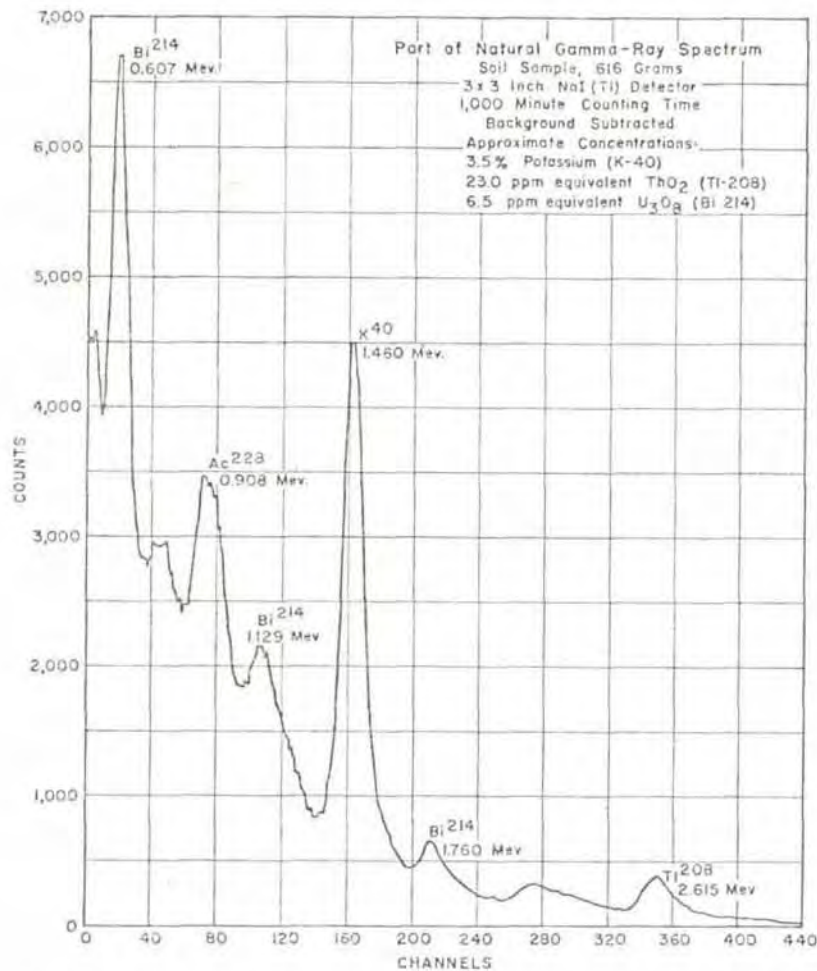
Figure 17. The high-energy portion of the natural gamma-ray spectrum contains prominent photo peaks of thallium-208, bismuth-214, and potassium-40. These can be resolved sufficiently to make spectral identifications and quantitative measurements in the borehole.

Natural gamma-ray spectra. Gamma rays are emitted by at least 24 of the 37 common natural radioisotopes of the thorium and uranium series and potassium. Several natural gamma-emitters, such as bismuth-214, emit gamma photons at many energies. Well over a hundred primary energies have been recognized, and with improved resolution in instrumentation the number is increasing. Compton scatter of the primary photons within the sample produces a more-or-less continuous spectrum of photons with energies below the photopeaks of all primary energies in the source. The gamma-ray emitters of major significance in borehole measurements are shown on the decay series diagram of Figure 3.

Figure 17 shows the high-energy portion of a spectrum for a natural soil sample containing potassium, and uranium and thorium series. The more prominent photopeaks, identified in the figure, are generally believed most useful in down-hole measurements. These include the peak of thallium-208 at 2.62 mev, which is used to indicate natural thorium-232; a bismuth-214 peak at 1.76 mev, used to indicate radium-uranium; and the potassium-40 peak at 1.46 mev, used to measure total potassium.

Problems in down-hole spectroscopy. Good down-hole spectral measurements are more difficult to achieve than those at the surface or in the laboratory. The large sample volume 'seen' by the probe causes the photopeaks of the primary energies, particularly in the low-energy region below .5 mev, to be obscured by fill-in from Compton scatter of all higher energies. As noted by Gregory and Horwood (1961), increasing sample thickness gradually obscures peaks until, for a 1-foot thickness, those peaks representing energies less than one mev are little more than barely discernible shoulders along the spectrum. Therefore, spectroscopy in the borehole based on resolution of photopeaks is restricted to the energy region generally above 1 mev. Even above 1 mev the spectra from large samples measured by the hole probes contain a larger scattered component than 500 to 1000 gm laboratory samples. However, photopeaks can be adequately resolved by a good logging system to be of practical value.

In the low-energy region below 0.5 mev, not only are the photopeaks obscured by scatter, but photoelectric absorption by high Z elements, particularly of photons less than 0.1 mev, distorts the primary spectrum; the low-energy spectrum is sensitive to composition (Kartashov, 1961). In fact, Czubek (1965) and others proposed to measure this absorption of the low-energy photons from a monoenergetic source to calculate effective Z numbers and evaluate composition.

Problems with instrumentation for quantitative spectral measurements down-hole are formidable compared to laboratory and surface work. The proportionality between photon energy and pulse height must be maintained while transmitting the signal through hundreds of feet of logging-type cables to the amplifier and analyzer. Both sensitivity and efficiency for high-energy photons increase with crystal volume. Statistically reliable counting of the selected energy bands is achieved in less time with large crystals. However, the supporting electronics system must be

capable of linear response at the resulting high gross count rate. No single detector is optimum for a wide range of intensity.

Environmental factors are often rigorous. Temperature, in particular, may change rather severely and rapidly. Scintillation-type detectors employing photomultiplier tubes are particularly susceptible to changes in gain with temperature. Spectral measurements preclude operating the system on the gain plateau which overcomes the problem when gross counting. The extended time required to obtain a series of stationary or long dynamic measurements in a deep hole, particularly with fluctuating ambient temperatures, appears to require system gain stabilization.

Sample geometry and environment cannot be controlled in the borehole. Small deviations from calibration conditions may not seriously change the ratio of photons at the energies commonly selected for spectral analysis of uranium, thorium and potassium; but such deviations will affect determinations of absolute concentrations.

Applications to exploration and evaluation. The most obvious and simplest application of gamma spectroscopy is to qualitatively identify the source of gamma radiation. A gross gamma-ray anomaly, whether detected from the air, from a vehicle, on the outcrop, or from a borehole log, is unlabeled as to origin and may not indicate the element of interest. In the search for uranium deposits in sandstone it is not uncommon to find anomalies generated by minor concentrations of thorium-bearing heavy minerals or potassium-rich glauconitic zones. Relatively unsophisticated qualitative spectroscopy will usually identify the source(s) of gamma rays.

Radium haloes are, of course, important guides in uranium exploration. Broad but low-intensity radioactive anomalies, equivalent to only 10 or 15 ppm uranium, are potential targets for wide-spaced preliminary exploration drilling. However, many such apparent gross-count haloes represent facies changes involving intrinsic potassium or thorium minerals. Minor variations, either enrichment or depletion, of perhaps 5 ppm in the uranium-radium concentration, which can be readily obscured by changes in gross radioactivity, may be significant guides to favorable areas for detailed exploration. Similarly Moxham, et al., (1965), found spectral measurements of uranium, thorium and potassium: thorium ratios could be applied to alteration studies as possible halo-like guides to certain copper and copper-lead-zinc deposits in Arizona.

Geological-geochemical environments may be 'fingerprinted' by characteristic ratios or changing ratios of uranium: thorium: potassium. Each of these elements reacts somewhat differently to changes in pH, eH, and to common ion concentrations. For example, because of the increased mobility of the uranyl ions, a depletion in uranium relative to thorium or potassium may indicate a current or paleooxidation environment (Adams and Weaver, 1958). For these studies the absolute concentration need not be determined with extreme accuracy, but the relative values require high precision and sensitivity.

If low-grade deposits of uranium, containing perhaps 100 ppm, become economically significant it will become necessary to quantitatively distinguish between the gamma rays emitted by the uranium decay series and those originating in the potassium or thorium minerals of the host rock. This has already become a problem in evaluation of potential resources. The mining industry

should be alert to and capable of evaluating data generated while exploring for more conventional deposits. Certainly when quantitatively evaluating deposits containing 0.05 percent uranium or less by radiometric methods, it becomes advisable to eliminate any bias imposed by gamma rays from other than the uranium series. Kartashov (1961) discusses the necessity for such in-hole analyses and the probable analytical errors when using a 50 gm NaI(Tl) detector and 10-minute counting time on a small anomaly containing about 50 ppm uranium, 13 ppm thorium and 2.6 percent potassium. The estimated analytical errors were 4.8 percent for uranium, 12.7 percent for thorium and 29.2 percent for potassium. For these measurements extreme sensitivity is not required, and may indeed be undesirable at higher concentrations; but excellent precision and accuracy in absolute concentration is desirable.

Under favorable conditions certain types of disequilibrium in uranium ores may be detected. The low-energy photons from thorium-234, protactinium-234 and uranium-235, which may be differentiated in the laboratory sample, are relatively more proportional to the uranium content than the total spectrum if the uranium-radium series are not in equilibrium. However, these diagnostic photons are buried in a continuum of scattered gammas in the low-energy region and cannot be selectively measured in the borehole. Lyubavin and Ovchinnikov (1961) proposed a method based on the relative fraction of gamma radiation of uranium and its decay products prior to radium and the total gamma radiation of the uranium-radium series. Blake (1965) reported encouraging results from similar preliminary field investigations based on simple ratios between the hard and total spectrum, which were measured by enclosing one of two detectors in the probe with a physical energy filter.

Electronic discrimination can sharpen the differentiation between soft and hard portions of the spectrum. These ratios, which at best yield small percentage changes with disequilibrium, are extremely sensitive to the individual measurements; and the two measurements, to be valid, must represent the same sample and, to be reliable, require instrumentation with almost perfect stability. Minor changes in borehole environment drastically affect the low-energy spectrum and, if not adequately corrected, will cause variation in ratios unrelated to disequilibrium. In spite of these problems, in-hole disequilibrium measurements would be immensely valuable and therefore intensive investigations are warranted to develop reliable operational procedures for disequilibrium logging. Closely spaced or continuous records could be integrated to obtain disequilibrium correction factors which, if applied to the gross gamma log of ore zones, would more accurately indicate the uranium concentration. Even if the disequilibrium is only qualitatively indicated, the logs would be valuable in studying the disequilibrium problem; and a series of measurements might well indicate the position of the sampled zone relative to solution roll fronts described by King and Austin (1966).

Summary

The uranium mining industry increasingly relies on analysis of logs to obtain most of the geological and engineering data from exploration and development drilling.

Natural gamma-ray logs can be quantitatively analyzed by the GAMLOG computer program to determine depth, thickness and

equivalent grade of ore zones and of layers within the anomalous zone. These parameters are used in other computer programs to calculate and evaluate ore reserves. This analysis is based on the relationship between the area under the logging curve (corrected for dead time) and the grade-thickness product.

Backscattered gamma-ray logs can be quantitatively analyzed by the RHOLOG computer program to determine in-place dry bulk density, porosity, and free water in saturated rocks. These parameters are used in the volume-to-weight conversion for ore reserves, to evaluate mining problems, and to correct natural gamma-ray logs. A difference method has been developed to obtain these measurements in naturally radioactive zones.

Calibration and appropriate correction factors for non-standard conditions are obtained from full-scale model holes.

Semiautomatic digitizing of analog records and on-site automatic digital recording contribute significantly to the practical application of computer analysis.

Gamma-ray spectroscopy is being investigated; and in spite of scatter by the large sample, difficulties in linear pulse height transmission on logging cable and problems with environmental stability of spectral instrumentation, it appears to offer powerful new techniques for exploration and evaluation. The sources of high-energy gamma radiation can be identified in the borehole, the relative contribution by the several radioactive series may be evaluated, meaningful radioactive haloes may be differentiated from gross anomalies, geological-geochemical processes and environments may be 'finger-printed', and it may be possible to develop disequilibrium logging methods.

References

Adams, J.A.S., 1964. Laboratory γ-ray spectrometer for geochemical studies. *The natural radiation environment.* Chicago, The University of Chicago Press, p. 485 - 497.

Adams, J.A.S., and G.E. Fryer, 1964. Portable γ-ray spectrometer for field determination of thorium, uranium, and potassium. *The natural radiation environment.* Chicago, The University of Chicago Press, p. 577 - 596.

Adams, J.A.S., and C.E. Weaver, 1958. Thorium-to-uranium ratios as indicators of sedimentary processes: example of concept of geochemical facies. *Bull. AAPG.* 42 (2): 387 - 430.

Baker, P.E., 1957. Density logging with gamma rays. *Trans. AIME.* 120: 289 - 294.

Blake, R.W., 1965. Personal communication.

Czubek, J.A., 1965. Physical possibilities of gamma-gamma logging. *Trans. Symposium on radioisotope instruments and geophysics, Warsaw, Poland.* International Atomic Energy Agency, Vienna, SM-68/34.

Czubek, J.A., and J. Guitton, 1965. Les possibilités d'application de la méthode gamma-gamma à la détermination en place de la densité des minerais d'uranium. Commissariat à l'Energie atomique CEA-R 2720.

Danes, Z.F., 1960. A chemical correction factor in gamma-gamma density logging. *J. Geoph. Res.* 65 (7): 2149 - 2153.

DiGiovani, H.J., R.T. Graveson, and A.H. Yoli, 1952. A drill hole scintillation logging unit, type TU-5-A. U.S. Atomic Energy Commission NYO-4503, p. 1 - 34.

Dodd, P.H., and R.F. Droullard, 1965. A logging system and computer program to determine rock density of uranium deposits. *Trans. Symposium on radioisotope instruments and geophysics, Warsaw, Poland.* International Atomic Energy Agency, Vienna, SM-68/33.

Faul, Henry, and C.W. Tittle, 1951. Logging of drill holes by the neutron-gamma method, and gamma-ray scattering. *Geophysics.* 16: 261 - 276.

Foote, R.S., 1967. Personal communication.

Gregory, A.F., and J.L. Horwood, 1961. A laboratory study of gamma-ray spectra at the surface of rocks. Dept. Mines and Tech. Surveys, Ottawa, Canada, *Mines Branch Research Rpt. R-85.*

Grundy, D.D., and R.J. Meehan, 1963. Estimation of uranium ore reserves by statistical methods and a digital computer. *Memoir 15,* State Bureau of Mines and Mineral Resources, New Mexico Institute of Mining and Technology, Socorro, New Mexico, p. 234 - 243.

Hofstadter, R., 1949. Detection of gamma-rays with thallium-activated sodium iodide crystals. *Phys. Rev.* 75: 796 - 810.

Homilius, J., and S. Lorch, 1957. On the theory of gamma-ray scattering in boreholes. *Geophys. Prospecting.* 5: 449 - 468.

Homilius, J., S. Lorch, and K. Seitz, 1958. Radioactive density determination with the gamma-gamma probe. *Geol. Jb.* 75: 183 - 196.

Kartashov, N.P., 1961. Gamma-spectrometric determination of small amounts of uranium, thorium and potassium in rocks. Translated from *Atomnaya Energiya,* 10 (5): 531 - 533.

King, J.W., and S.R. Austin, 1966. Some characteristics of roll-type uranium deposits at Gas Hills, Wyoming. *Mng. Eng.* 18 (5): 73 - 80.

Lyubavin, Yu. P., and A.K. Ovchinnikov, 1961. Gamma radiation of uranium and its daughter products in radioactive orebodies. *Vopr. rudn. geofiz.* (Problems of mining geophysics), Ministry of Geology and Conservation of Natural Resources U.S.S.R., no. 3, p. 87 - 94.

Moxham, R.M., R.S. Foote, and C.M. Bunker, 1965. Gamma-ray spectrometer studies of hydrothermally altered rocks. *Econ. Geol.* 60 (4): 653 - 671.

Patterson, J.A., P.C. deVergie, and R.J. Meehan, 1964. Application of automatic data processing techniques to uranium ore reserve estimation and analysis. *Quart. Colorado School Mines.* 59: 859 - 886.

Pemberton, R.H., and H. Seigel, 1966. Airborne radioactivity tests – Elliot Lake area, Ontario. *Can. Mng. J.* 87 (10): 81 - 87.

Pickell, J.J., and J.G. Heacock, 1960. Density logging. *Geophysics.* 25 (4): 891 - 904.

Rodermund, C.G., R.P. Alger, and J. Tittman, 1961. Logging empty holes. *The Oil and Gas J.* 59: 119 - 124.

Roy, S.E., and H.F. Winterkorn, 1957. Scintillation methods for the determination of density and moisture content of soils and similar granular systems. *Highway Research Board Bull. 159,* National Academy of Science-National Research Council Pub. 498.

Scott, J.H., 1962. Computer analysis of gamma-ray logs. U.S. Atomic Energy Commission RME-143, p. 1 - 43. Also 1963, *Geophysics* 28 (3): 457 - 465.

Scott, J.H., and P.H. Dodd, 1960. Gamma-only assaying for disequilibrium corrections. U.S. Atomic Energy Commission RME-135, p. 1 - 20.

Scott, J.H., P.H. Dodd, R.F. Droullard, and P.J. Mudra, 1961. Quantitative interpretation of gamma-ray logs. *Geophysics.* 26: 182 - 191.

Tittman, J., and J.S. Wahl, 1965. The physical foundations of formation density logging (gamma-gamma). *Geophysics.* 30: 284 - 294.

Wahl, J.S., J. Tittman, C.W. Johnstone, and R.P. Alger, 1964. The dual spacing formation density log. *J. Petrol. Tech.* 16: 1411 - 1416.

**Fundamentals of
Gamma-Ray Logging**

FUNDAMENTALS OF GAMMA-RAY LOGGING

Robert D. Wilson

Bendix Field Engineering Corporation

INTRODUCTION

The technique of passively observing the gamma radiation emitted by the naturally occurring radioisotopes within earth formations has been in use for over thirty years. In recent years, however, there have been important advances in both the technology and methodology of gamma-ray logging techniques. In addition, active techniques are being developed that stimulate gamma-ray emission from otherwise stable elements.

The gamma-ray signatures observed by both the active and passive techniques permit the quantitative borehole assay of a variety of elements within earth formations. This paper reviews the principles of passive, borehole gamma-ray measurements and the methods of analysis that provide quantitative assays for the elements potassium, uranium, and thorium.

NATURAL FORMATION GAMMA-RAY SOURCES

The three elements potassium (K), uranium (U), and thorium (Th) each have at least one naturally occurring radioactive isotope. ^{40}K is the radioactive potassium isotope and it leads directly to the emission of a single 1461 keV gamma ray from de-excitation of its stable daughter product ^{40}Ar. The two uranium isotopes ^{235}U and ^{238}U occur naturally with an abundance ratio of 0.007 and are both radioactive. These isotopes alpha- and beta-decay through a complex series that terminates with stable isotopes of lead. The single thorium isotope ^{232}Th is radioactive and also decays through a complicated decay series to a stable lead isotope. Dozens of different energy gamma rays are emitted during the decay of both uranium and thorium. The most intense of these gamma rays are emitted by daughter products well down the decay chain from the parent uranium or thorium isotopes.

Principal gamma-ray emitters in the uranium series are ^{226}Ra, ^{214}Bi and ^{214}Pb, and in the thorium series ^{228}Ac, ^{212}Pb, and ^{208}Tl. There are weak gamma rays emitted directly by the parent isotope ^{235}U and by ^{234m}Pa, the second daughter of ^{238}U. These are mentioned here because they represent a so-called "direct" uranium signature that is unaffected by the equilibrium condition of the decay series. Borehole uranium assays based on the ^{235}U or ^{234m}Pa gamma rays are called "direct uranium" assays while those based on the ^{226}Ra, ^{214}Bi, or ^{214}Pb gamma rays are called "equivalent uranium" assays. The term "equivalent" signifies that the uranium assay is based on the gamma-ray intensity from one of the daughter products, such as ^{214}Bi, and that the uranium concentration is equivalent to that which exists for secular equilibrium between uranium and all its radioactive daughter products.

The thorium gamma-ray signatures emitted by the daughter products ^{228}Ac, ^{212}Pb, and ^{208}Tl provide an "equivalent thorium" assay. However,

because of the relatively short half-lives for all the daughters, thorium always exists in a condition of secular equilibrium within earth formations. Hence the equivalent thorium assay is a good measure of the actual thorium content.

Figure 1 shows the relative intensities for the gamma-ray energies emitted by the three naturally occurring elements potassium, uranium, and thorium. Each source spectrum is normalized to unit total intensity. Many of the very low-intensity gamma rays are omitted from the uranium and thorium spectra; yet the complexity of these sources as shown in Figure 1 contrasts sharply with the single-source energy from potassium.

BOREHOLE GAMMA-RAY FLUX SPECTRA

When these sources are uniformly distributed throughout an earth formation, and when a borehole probe is introduced as shown in Figure 2, the gamma-ray energy spectra incident on the probe will appear as shown in Figure 3. (These fluxes were calculated by Mike Evans of the Los Alamos Scientific Laboratory using radiation transport theory. The session entitled "Gamma-Ray Transport Calculations" scheduled for Wednesday morning will be largely devoted to the details of such calculations.)

In the process of transporting from each source location in the formation to the probe location within the borehole, the gamma rays undergo both scattering and absorption interactions. The scattering interactions have the effect of introducing a continuum component to the spectrum that becomes increasingly prominent at low energies. This feature is apparent in all three spectra of Figure 3.

The continuum component for each source peaks at an energy of around 90 keV. The position of this peak is a characteristic of the transporting medium which was a zero porosity sandstone for the results in Figure 3. The absorption interactions have the effect of attenuating the lower energy source lines relative to the higher energy lines. This is obvious, for example, in the thorium spectrum of Figure 3 where the 2614 keV line is much more intense relative to the lower energy lines than in the source spectrum of Figure 1.

DETECTOR RESPONSE TO BOREHOLE GAMMA-RAY SPECTRA

The borehole probe shown schematically in Figure 2 contains one or more gamma-ray detectors that respond to the incident gamma-ray flux (Figure 3) by producing electrical pulses whose amplitudes are proportional to the gamma-ray energy deposited in the detector. These pulses can be analyzed and sorted according to amplitude and the resulting pulse height distribution is stored in a computer memory.

The most commonly used detector for gamma-ray logging is the sodium iodide (thallium activated) scintillator [NaI(Tℓ)]. Other scintillators such as cesium iodide (CsI) and bismuth germanate (BGO) are also in use or under evaluation for logging applications. Recently, solid state germanium detectors have been utilized in borehole probes. They provide a far superior spectral response to the incident borehole gamma radiation but at the expense of significantly decreased detection efficiency. They are also more costly and must be operated at or near liquid nitrogen temperatures.

2

FIGURE 1

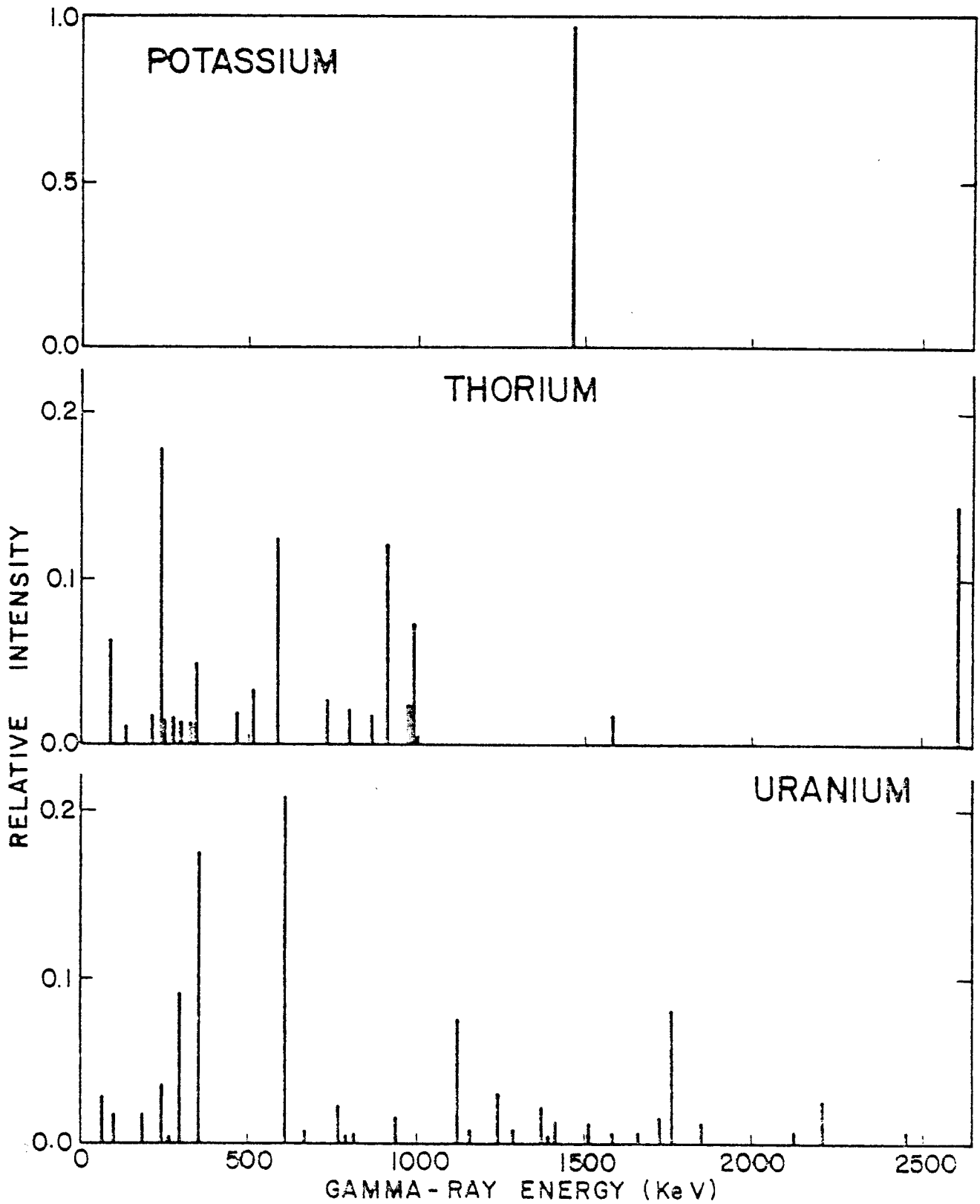## GAMMA-RAY SOURCE ENERGIES AND RELATIVE INTENSITIES FOR NATURALLY RADIOACTIVE ISOTOPES

FIGURE 2

LOGGING TRUCK

INSTRUMENTATION
AND
DRAW WORKS

PROBE
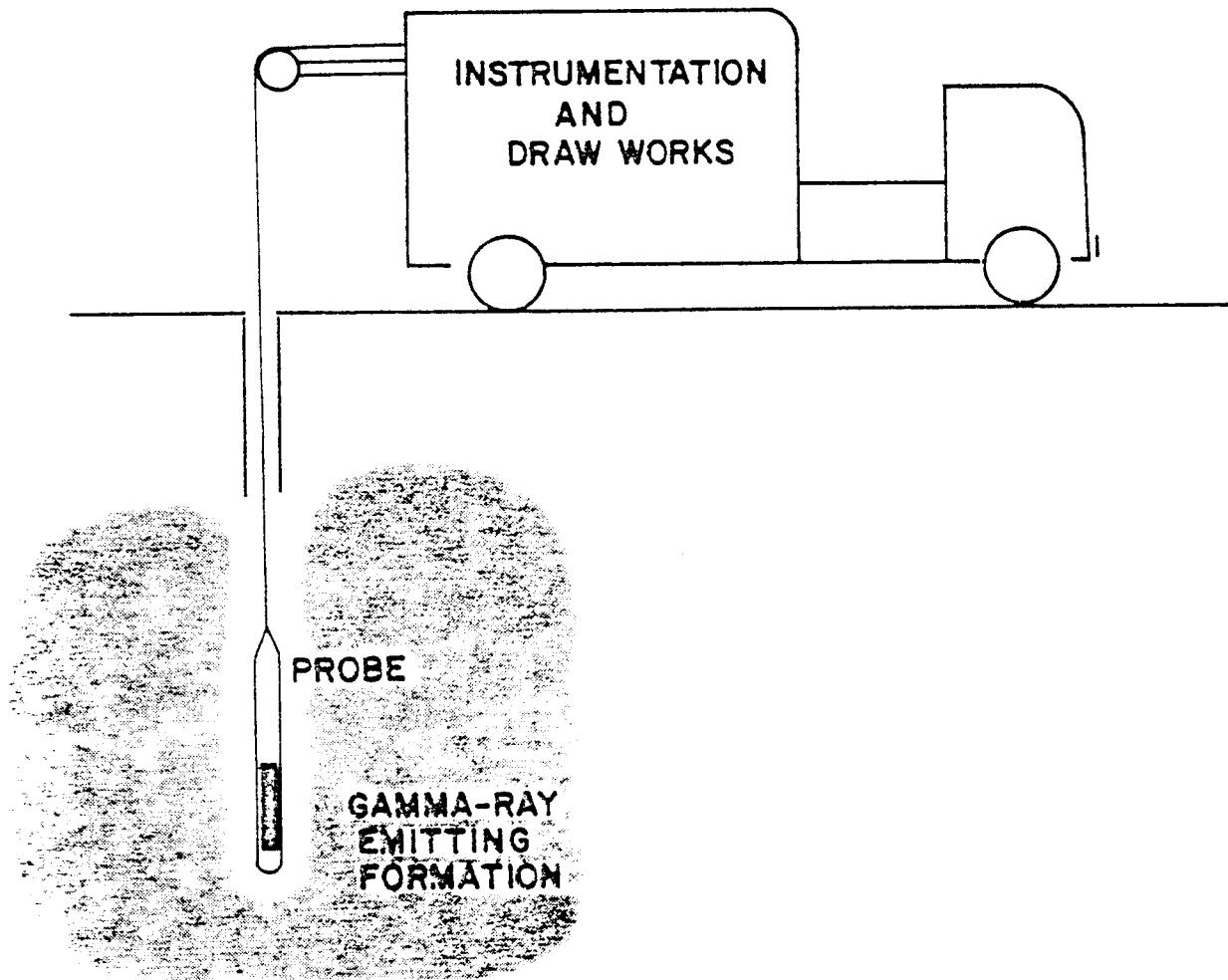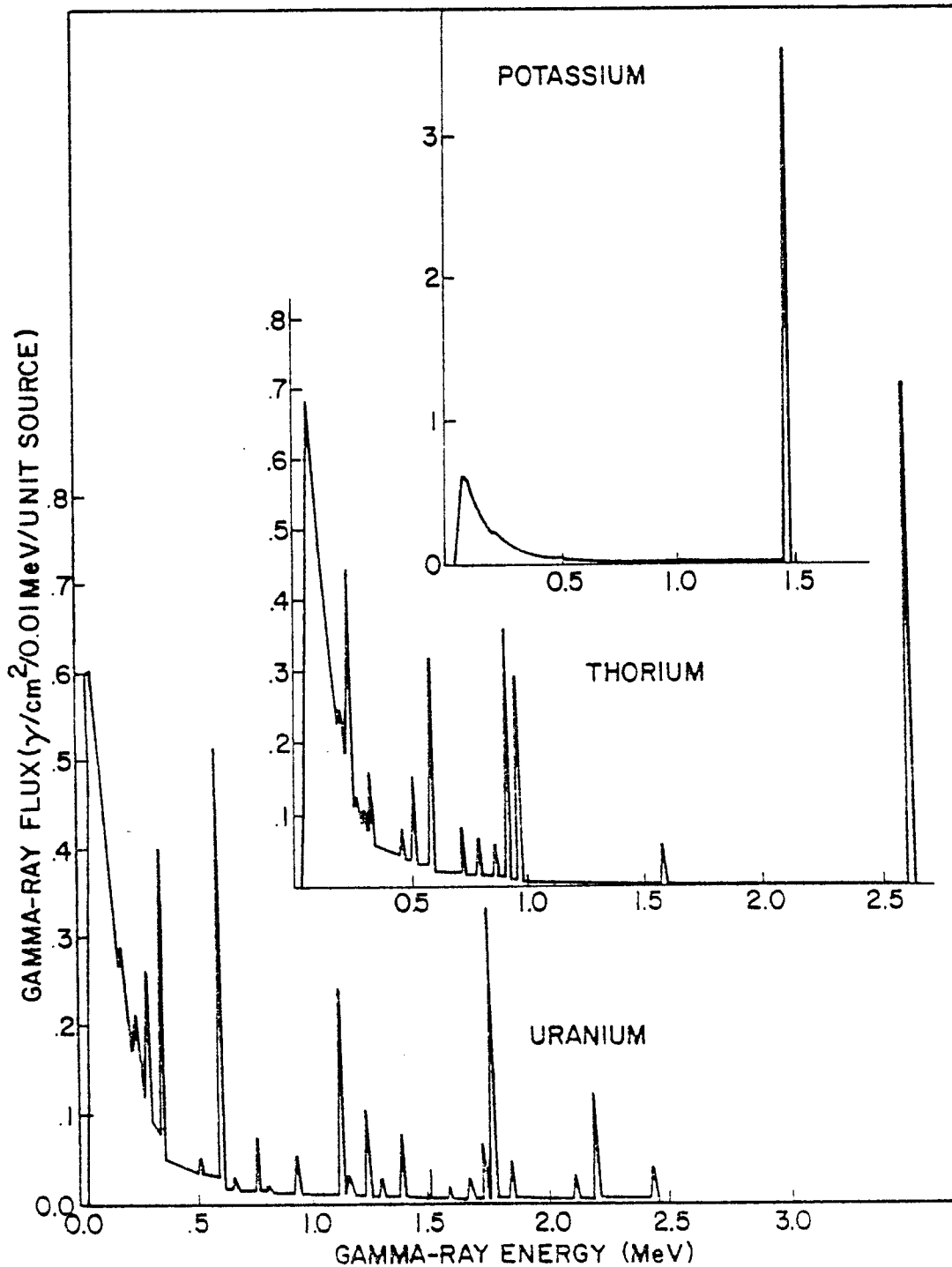
GAMMA-RAY
EMITTING
FORMATION

FIGURE 3

CALCULATED SPECTRA FOR POTASSIUM, EQUILIBRIUM URANIUM, AND THORIUM SOURCES UNIFORMLY DISTRIBUTED IN AN INFINITE SANDSTONE MEDIUM.

Germanium Detector Response

Figure 4 shows the pulse height distributions observed with a germanium probe for the incident borehole fluxes of Figure 3. These spectra were acquired within concrete borehole models enriched in the elements potassium, thorium, and uranium, respectively. The potassium response contains contaminant peaks from the small concentrations of uranium and thorium. The general features of the calculated flux spectra (Figure 3), including continuum shapes and peak locations, agree well with the measured germanium spectra. As the gamma-ray energy increases, the measured peak intensities become progressively smaller relative to calculated intensities because of the decreasing detector efficiency. The continuum shapes observed in the germanium spectra are enhanced both because of the increasing detector efficiency at lower energies and because of Compton scattering of gamma rays within the detector itself. The measured peak in the continuum shape has shifted upward in energy to about 110 keV from the calculated value of 90 keV. This shift is caused by attenuation in the probe shell and cryostat surrounding the germanium detector. (The session entitled "Spectral Logging III: High Resolution Spectroscopy" scheduled for Tuesday evening will be devoted entirely to logging systems that utilize germanium gamma-ray detectors.)

Figure 5 contains the uranium spectrum of Figure 4 but with a semilogarithmic vertical scale and with a greatly expanded horizontal scale. This spectrum is the germanium probe borehole response to a uniformly distributed uranium source that is in secular equilibrium with all its radioactive daughter products. The majority of the peaks appearing in Figure 5 are from the decay of ^{214}Bi. Each one is labeled with its energy in keV. The lowest energy peak observed is at 186 keV and is an unresolved doublet from the decay of ^{235}U and ^{226}Ra. The three peaks above this in energy (242, 295 and 352 keV) are from the decay of ^{214}Pb.

Any one or all of the ^{214}Bi and ^{214}Pb peaks may be used to determine the equivalent uranium concentration. The higher energies are preferable because they represent a larger sample volume and are less perturbed by the effects of borehole and formation matrix variations. The gamma ray at 1001 keV is from the decay of ^{234m}Pa and represents a nearly direct measure of uranium concentration. The peak at 2614 keV and some of the other unlabeled peaks are contaminants from the small thorium concentration in the uranium ore. The 186 keV intensity from ^{235}U could be used as a direct uranium signature. It must be corrected for the ^{226}Ra contribution, however, and it is more susceptible to borehole and matrix variation effects than the higher energy 1001 keV gamma-ray. Because the direct signatures at 186 keV and 1001 keV have very small intensities and are superposed on a relatively large continuum component, performing a passive, direct uranium, gamma-ray log is possible only with the high-resolution germanium detector.

Sodium Iodide Detector Response

Sodium iodide (NaI) is one of several scintillating detector materials that can be used in gamma-ray logging applications. The energy resolution of NaI is far worse than the energy resolution of germanium, but NaI can be fabricated with much larger volumes for superior counting efficiency. Scintillation detectors have the advantage of lower cost and simpler operation
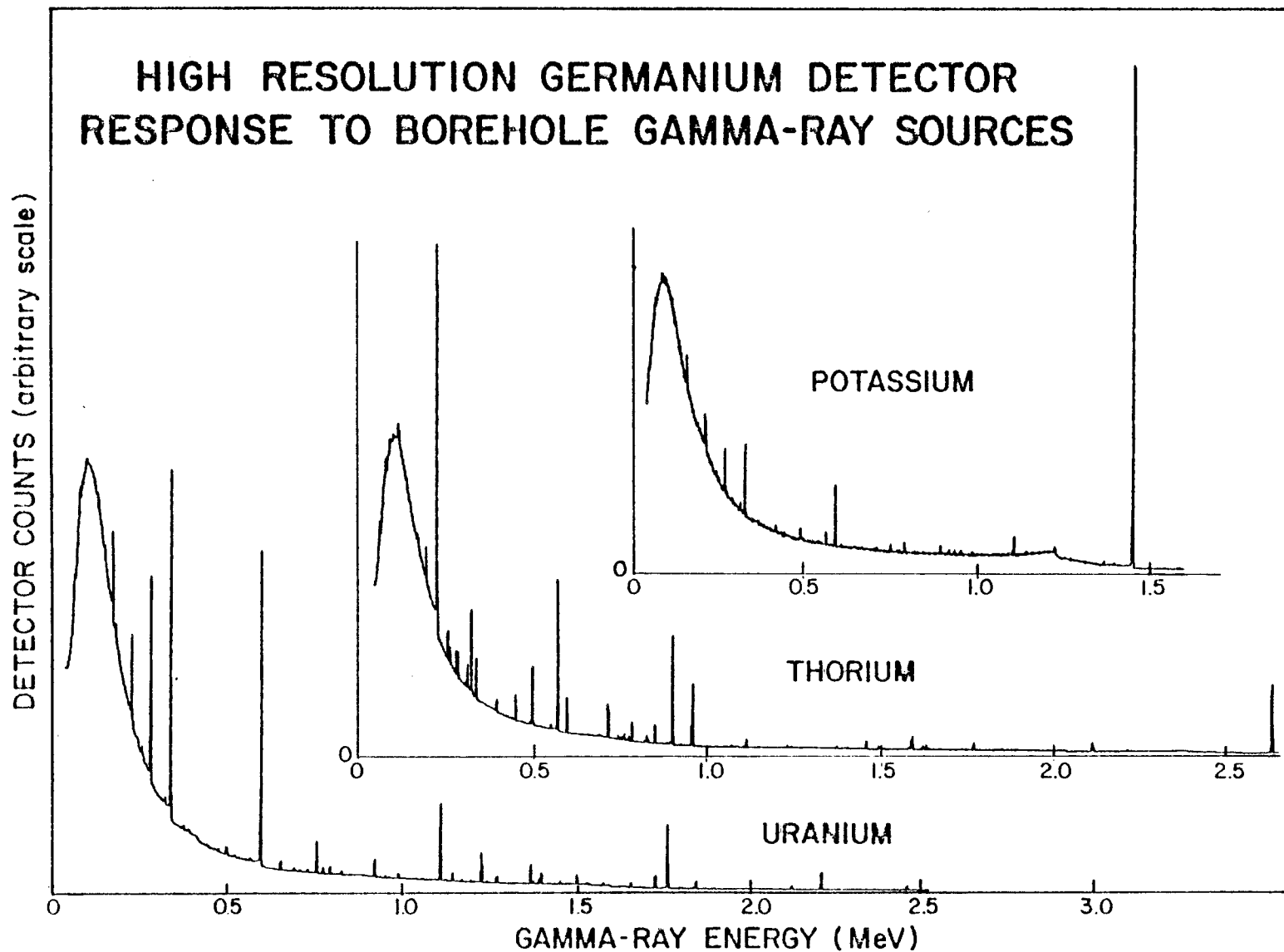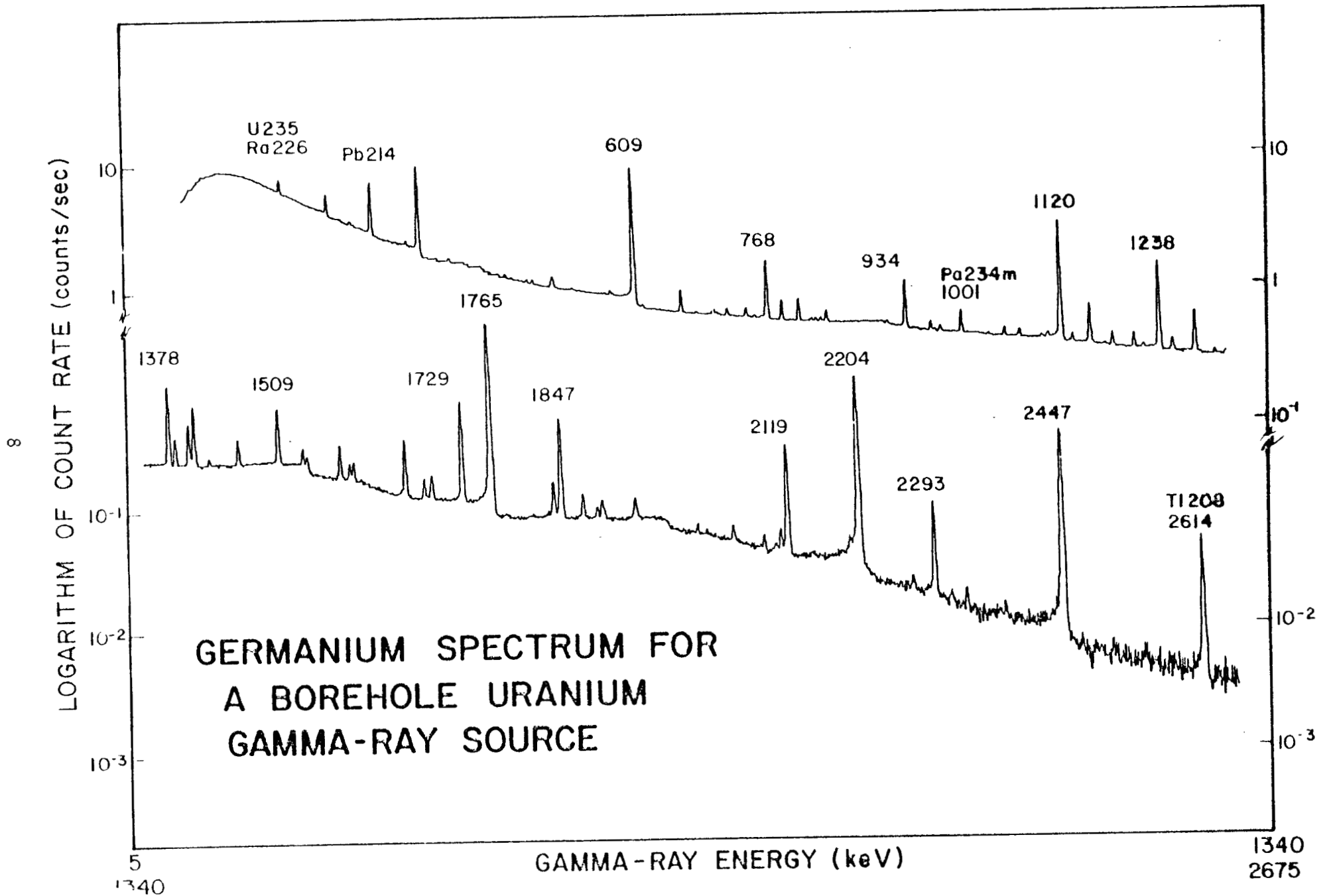
FIGURE 4

HIGH RESOLUTION GERMANIUM DETECTOR
RESPONSE TO BOREHOLE GAMMA-RAY SOURCES

FIGURE 5

GERMANIUM SPECTRUM FOR A BOREHOLE URANIUM GAMMA-RAY SOURCE

than germanium detectors. Of the scintillators, NaI provides the best
gamma-ray energy resolution. Figure 6, for example, shows the response of two
NaI detectors with volumes differing by a factor of about 25. The uranium
source is the same one used to obtain the germanium-detector response shown in
Figure 5. The larger NaI detector is typical of those used in spectral
gamma-ray logging while the smaller detector is typical of those used in
gross-count logging applications.

A comparison of Figure 6 with Figure 5 shows that the NaI energy reso-
lution is worse than germanium by about a factor of 50. The observed count
rates for the large NaI detector in the MeV energy range are greater by about
an order of magnitude while the small NaI detector exhibits count rates about
1/4 that of the germanium detector. The relatively poor NaI energy resolution
results in the identification of only six peaks in the pulse-height distribution.
These peaks are identified by their energies and are all emitted by the decay
of ^{214}Pb and ^{214}Bi as indicated in the abbreviated decay chain schematic at
the bottom of Figure 6.

These spectra clearly show that a direct uranium assay based on the 186
or 1001 keV gamma-ray intensities is not possible with NaI detectors. A
comparison of the large and small NaI detector spectra shows that the
resolution is better for the small detector. This is a typical result and is
due to the manufacturing difficulties encountered in producing long, thin NaI
detectors. This comparison also shows that the relative count rates in the
MeV energy range scale roughly as the detector volume, while at lower energies
(100 to 400 keV) the small detector is relatively more efficient with the
count rates scaling more like the difference in detector surface area. This
effect is most noticeable as an enhancement in the low energy continuum
distribution of the small detector spectrum.

In spectral logging, the 1-3 MeV portion of the spectrum is normally used
while in gross-count logging the entire spectrum is summed to give an integral
response. A portion of the session entitled "Spectral Logging I: Hardware"
scheduled for Tuesday afternoon will be devoted to further discussions of
scintillation detectors and recent detector developments.

For completeness, the large NaI detector responses to the potassium and
thorium borehole sources are shown in Figures 7 and 8. Again, the gamma-ray
producing members of the decay chain are shown at the bottom of each figure.
The peaks are identified with their energies in keV. The thorium spectrum
shows the added minor feature of escape peaks (single and double) from pair
production interactions of the 2614 keV gamma ray in the scintillation
detector. These peaks are too weak to observe in the potassium spectrum
because the 1461 keV gamma ray is not sufficiently far above the pair
production threshold at 1022 keV.

ANALYSIS OF GAMMA-RAY LOGGING DATA

A borehole logging system like the one shown schematically in Figure 2 is
used to acquire gamma-ray spectra as a function of depth. The detector
pulse-height distribution for each depth interval must be energy analyzed
either within the probe or with the surface instrumentation. The resulting
gross-count or spectral data must then be converted to radioelement
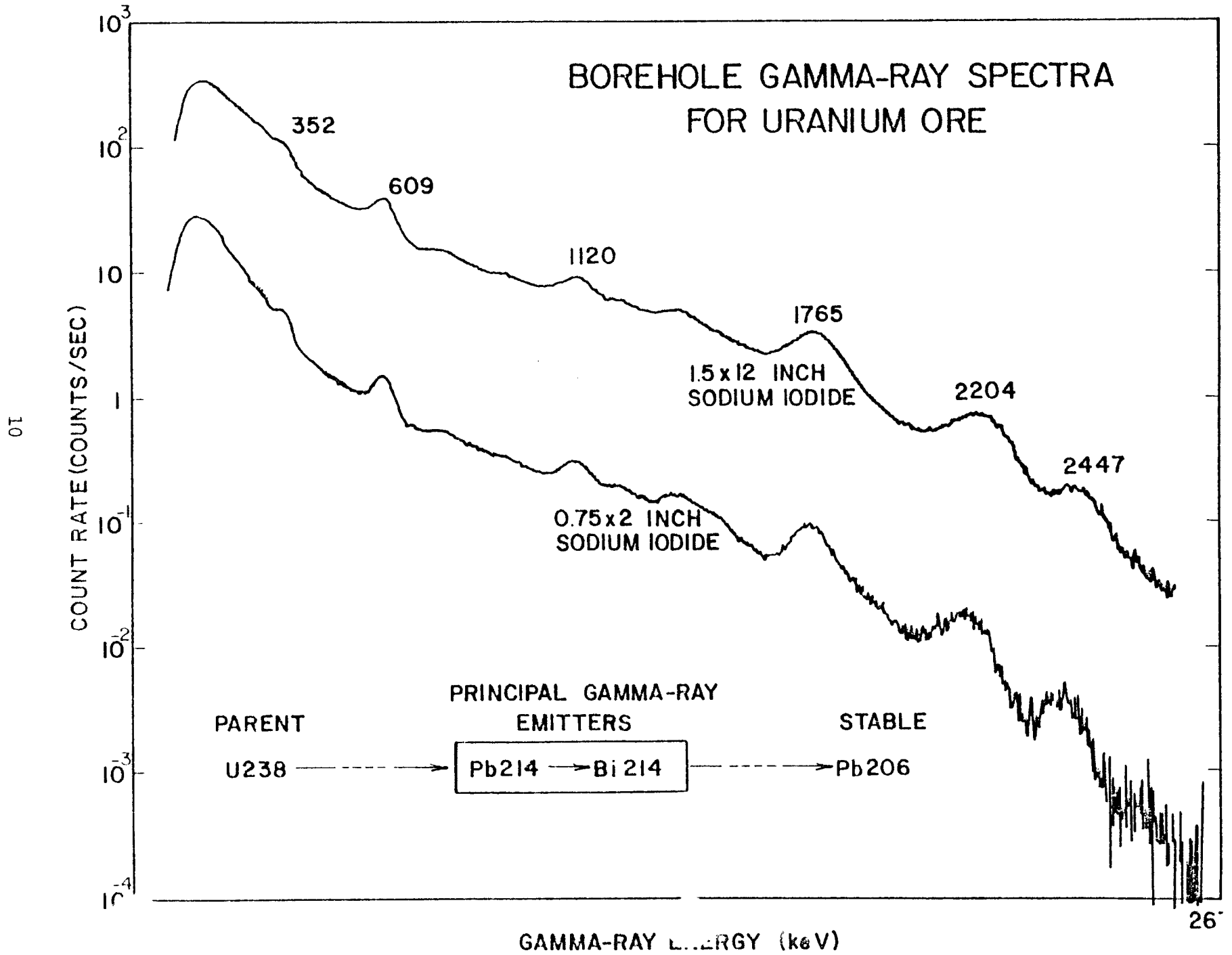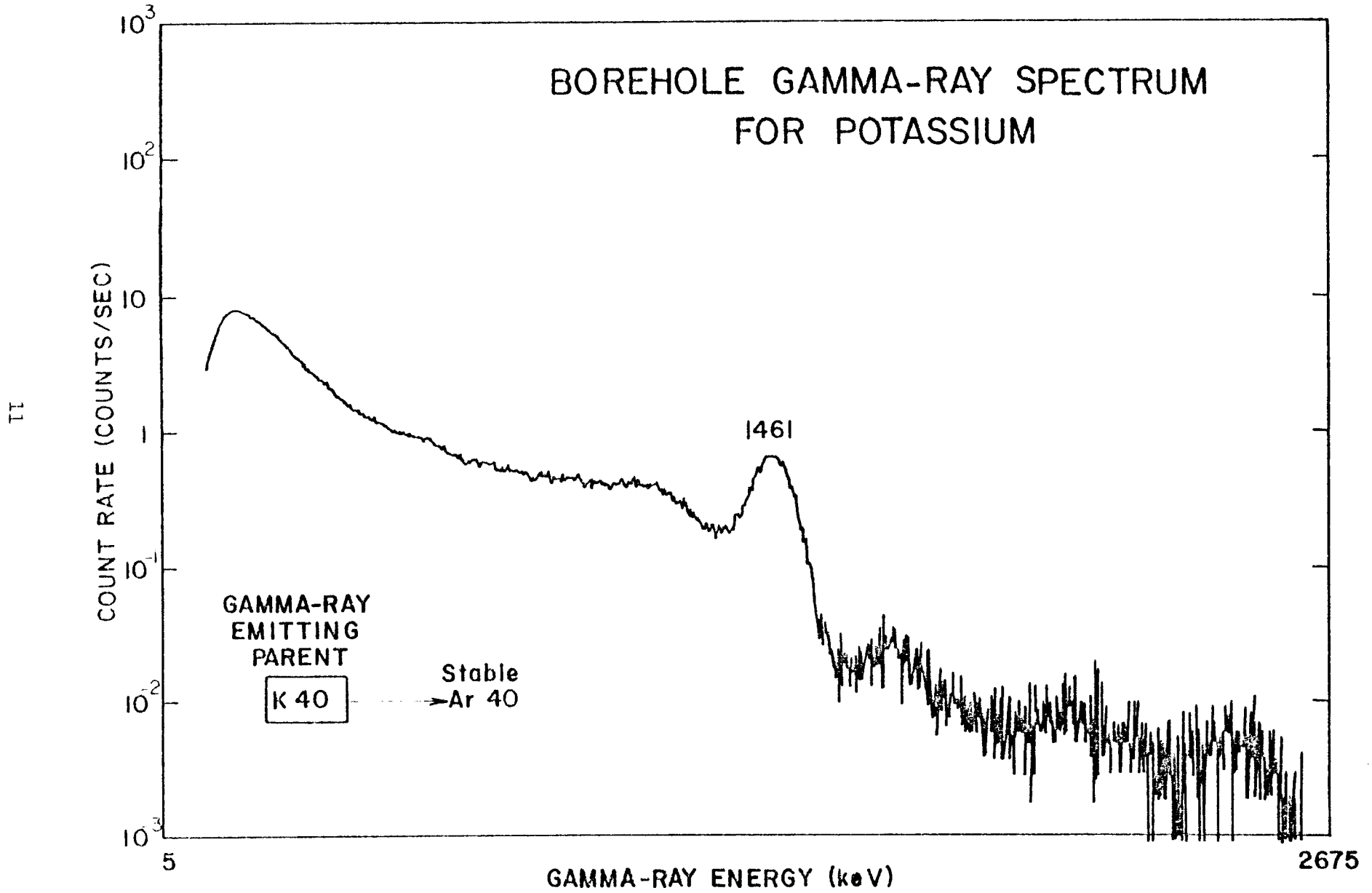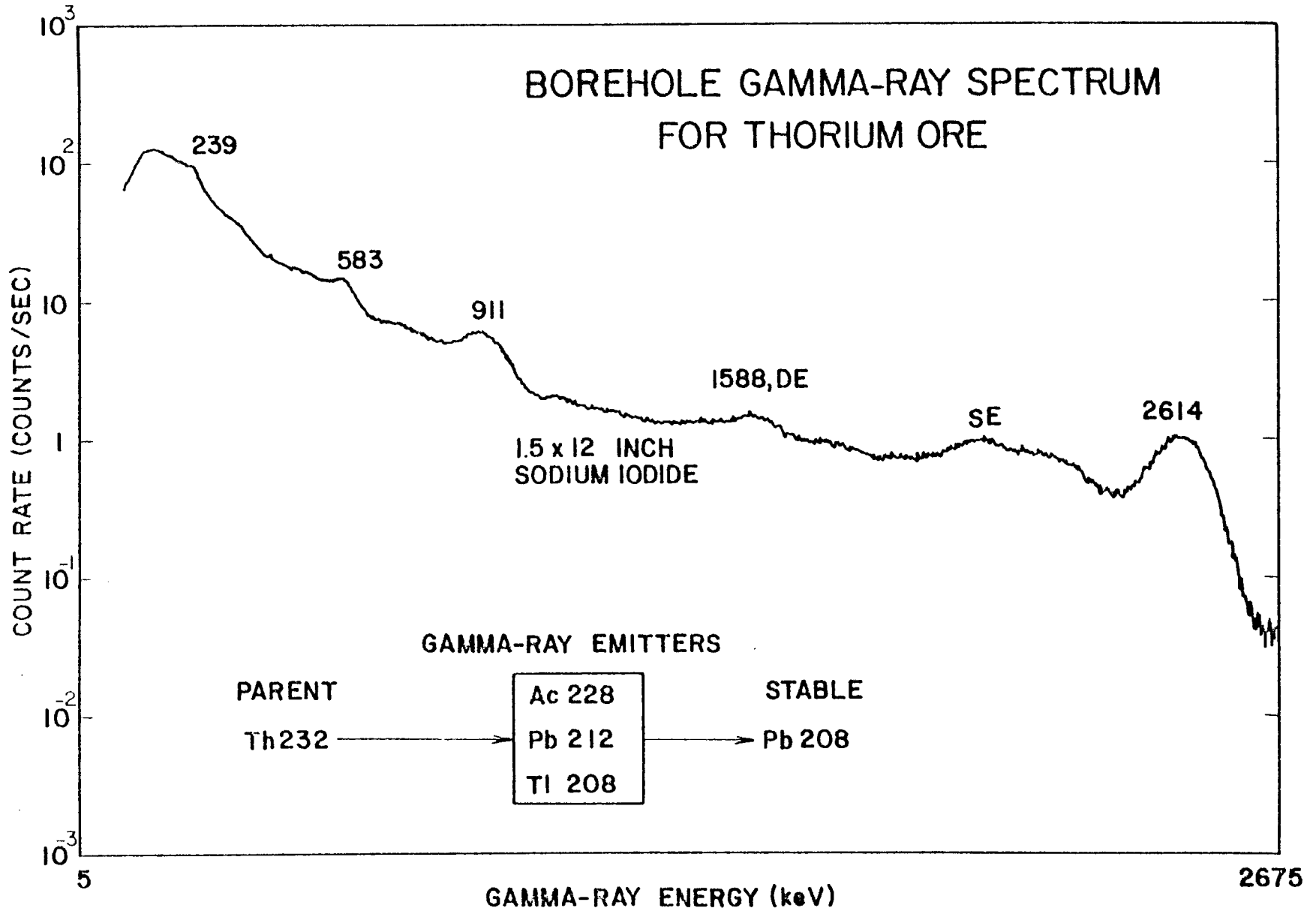concentration using calibration constants that are deduced from a calibration

FIGURE 6

BOREHOLE GAMMA-RAY SPECTRA
FOR URANIUM ORE

FIGURE 7

BOREHOLE GAMMA-RAY SPECTRUM
FOR POTASSIUM

FIGURE 8

BOREHOLE GAMMA-RAY SPECTRUM
FOR THORIUM ORE

239

583

911

1588, DE

SE

2614

1.5 x 12 INCH
SODIUM IODIDE

GAMMA-RAY EMITTERS

PARENT   STABLE

Ac 228
Th 232 ———→ Pb 212 ———→ Pb 208
Tl 208

COUNT RATE (COUNTS/SEC)

GAMMA-RAY ENERGY (keV)

FIGURE 10

URANIUM MODEL
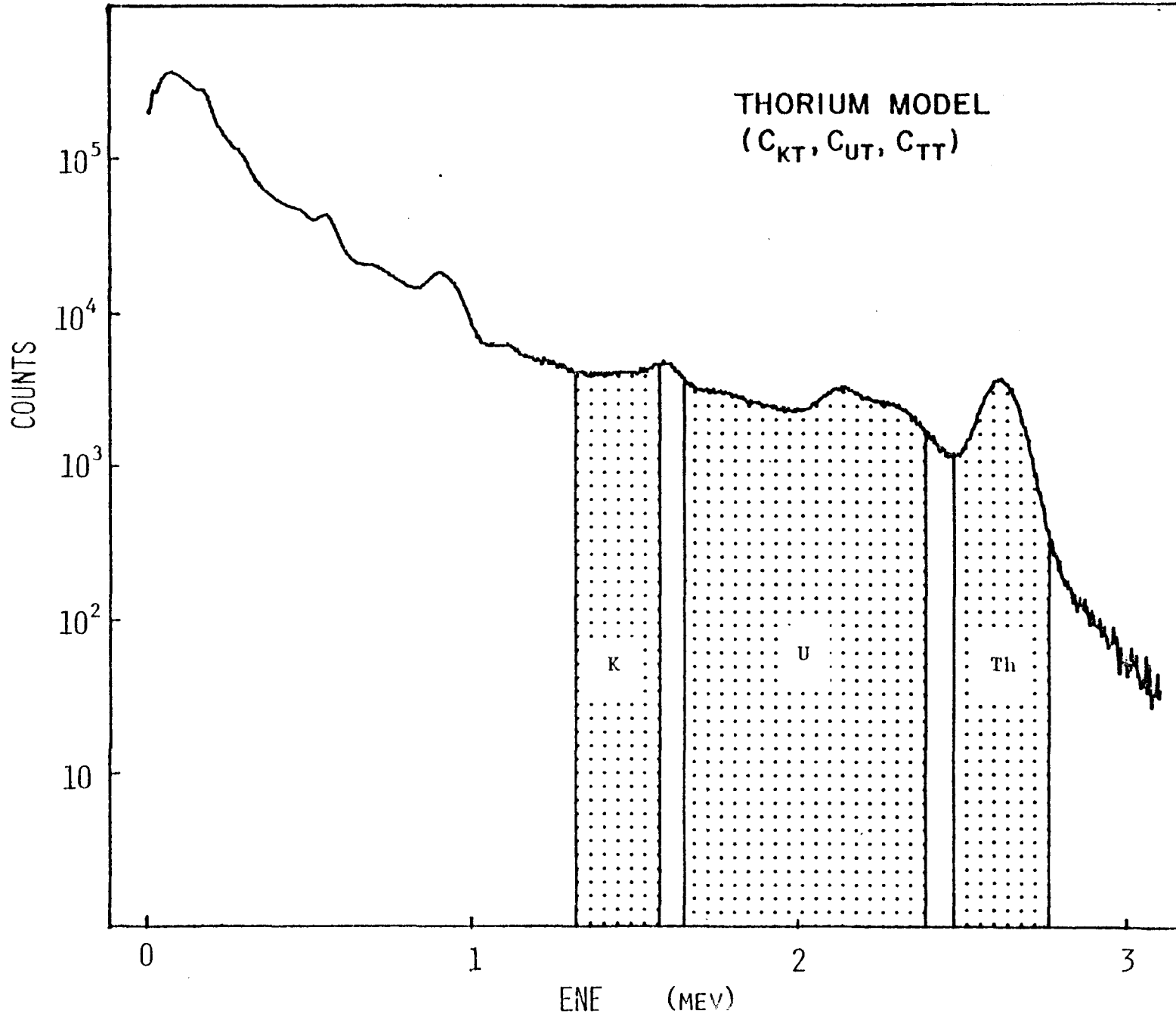(C_{KU}, C_{UU}, C_{TU})

FIGURE 11

THORIUM MODEL
(C_{KT}, C_{UT}, C_{TT})
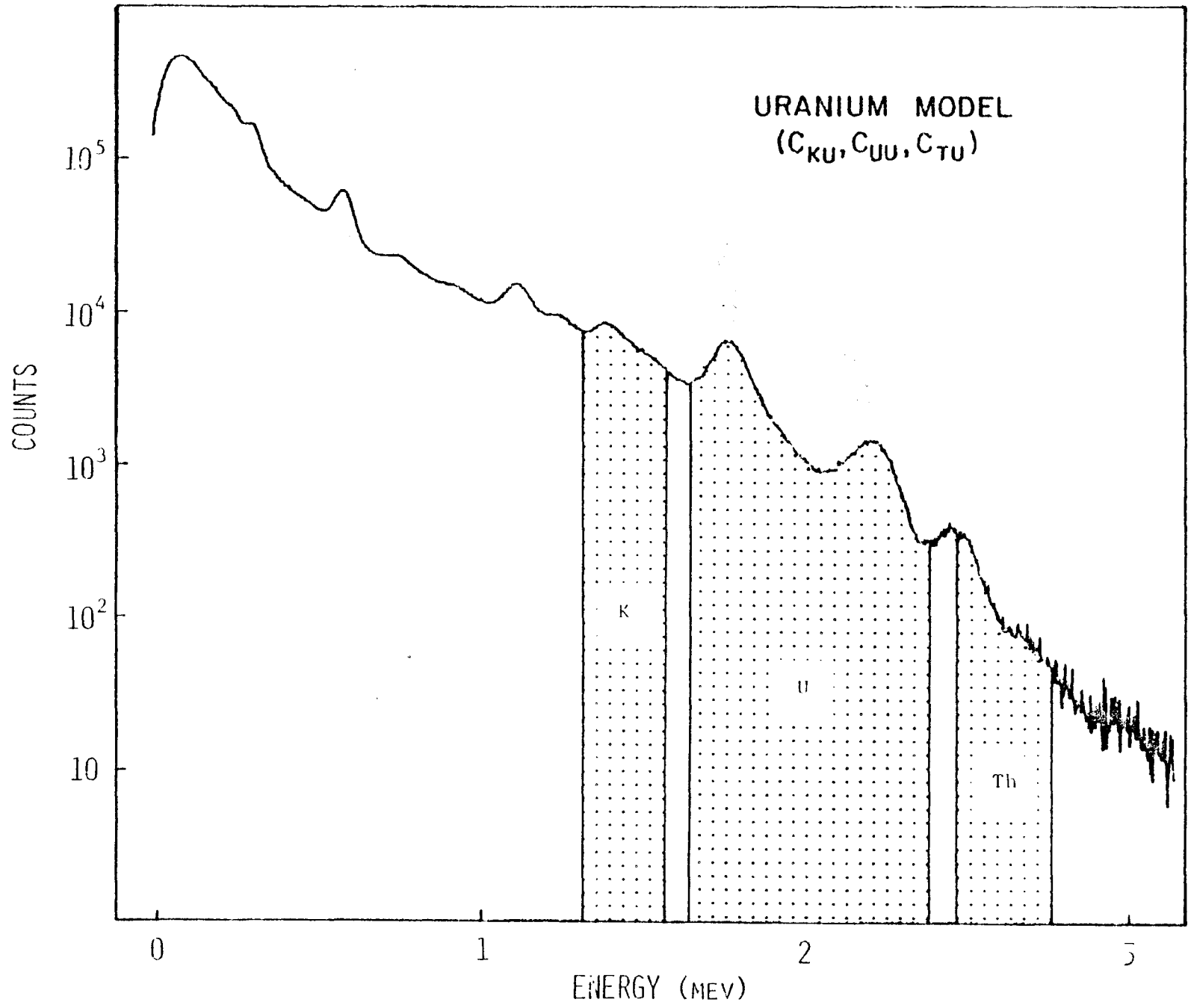
Gross-Count Log Calibration Method

The NaI reponse shown in Figure 6 for the 0.75-inch x 2-inch detector is typical of gross-count logging systems used for uranium exploration. This spectrum is replotted with a linear vertical scale in Figure 12. Three different scales are used to better display the spectral shape at higher energies. Regions of overlap exist to show the effect of scaling changes. Most gross-count logs are performed with systems that integrate or sum the total response shown in Figure 12. The shaded area of this plot shows the detector response to gamma rays with an energy below 400 keV. There are a few probes with filters surrounding the detector that effectively eliminate the response below about 400 keV. The figure shows that for such "filtered" probes about 87 percent of the signal is eliminated. This sacrifice in counting rate may be desirable in order to minimize the non-linear "Z effect" that affects gamma-ray logs performed in high-grade uranium zones.

Gross-count uranium logging systems are calibrated by acquiring integral counting rates as a function of depth through the ore zone of a calibration model. A schematic representation of this calibration method is shown in Figure 13. The equivalent uranium grade G (sometimes called the radiometric uranium grade) and thickness T of this ore zone must be known. When the area A under the log response curve is measured, the calibration constant, or "k" factor, is easily calculated from the equation at the bottom of Figure 13.

RADIOACTIVE DISEQUILIBRIUM AND ITS EFFECT ON GAMMA-RAY LOGS

Earlier in this discussion it was mentioned that equivalent uranium or thorium concentrations based on gamma-ray intensity measurements from daughter products will be equal to the actual parent concentrations only if a condition of secular equilibrium exists. This is always the case for geologic occurrences of thorium. Uranium deposits, however, are sometimes too young for the long-lived daughters preceding the principal gamma-ray emitters to build up to their equilibrium concentrations. For example, a geologic process may have disturbed the equilibrium condition by physically removing members of the decay series. When a disequilibrium condition is known to exist for a uranium deposit, the conventional gross-count or KUT gamma-ray log is not useful unless the disequilibrium factor is known from an independent determination, such as from a core analysis. On the other hand, the high-resolution germanium probe can perform a direct uranium measurement and will provide correct uranium assays independently of the disequilibrium condition.

CONCLUDING REMARKS

The sessions which follow during this three-day workshop will present in-depth discussions of the many gamma-ray logging topics introduced in this fundamentals session. The sessions will be informal so please feel free to contribute your own ideas, research, and comments. The first working session of the workshop is entitled "Calibration Standards" and it will begin immediately after this morning's coffee break.
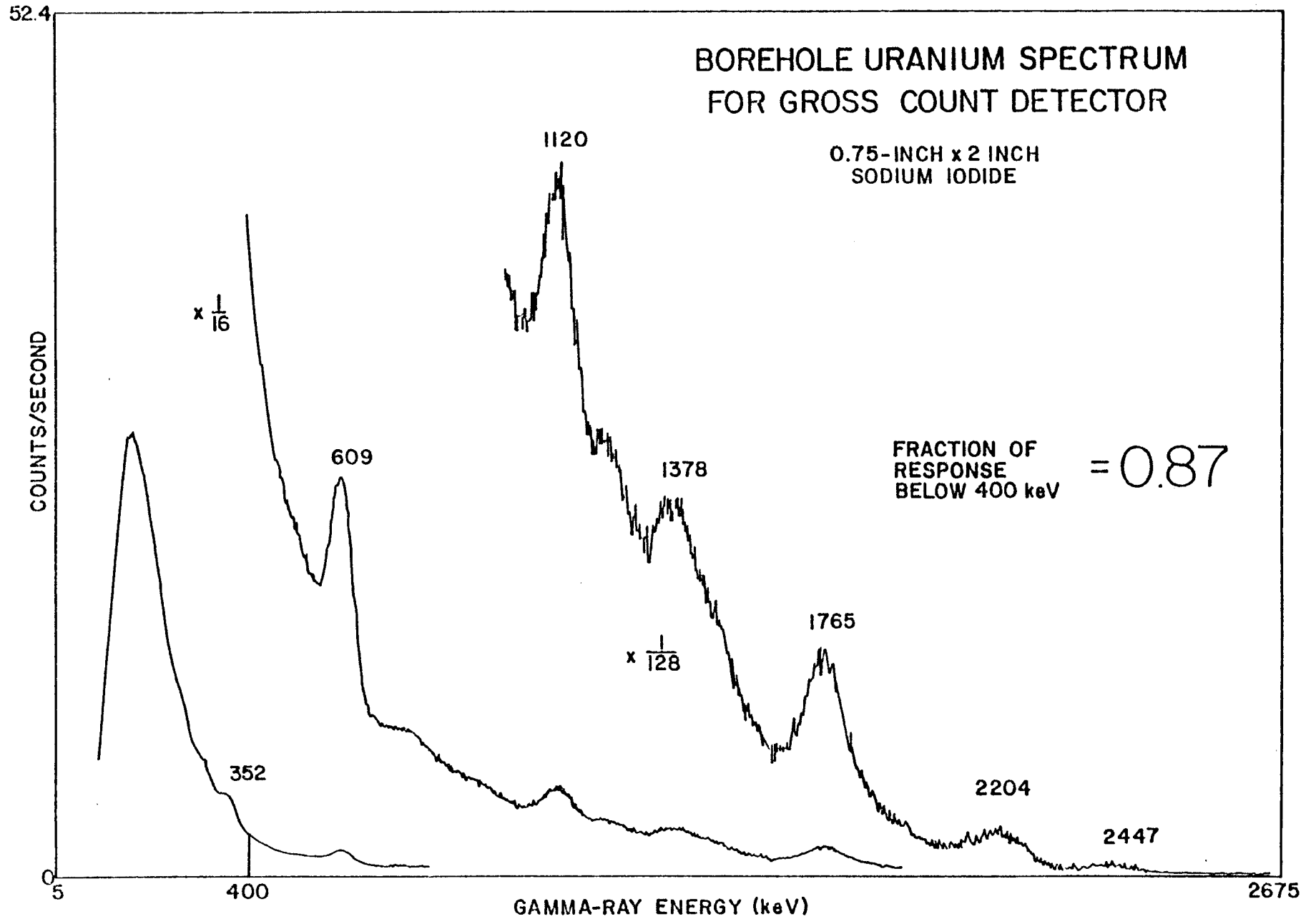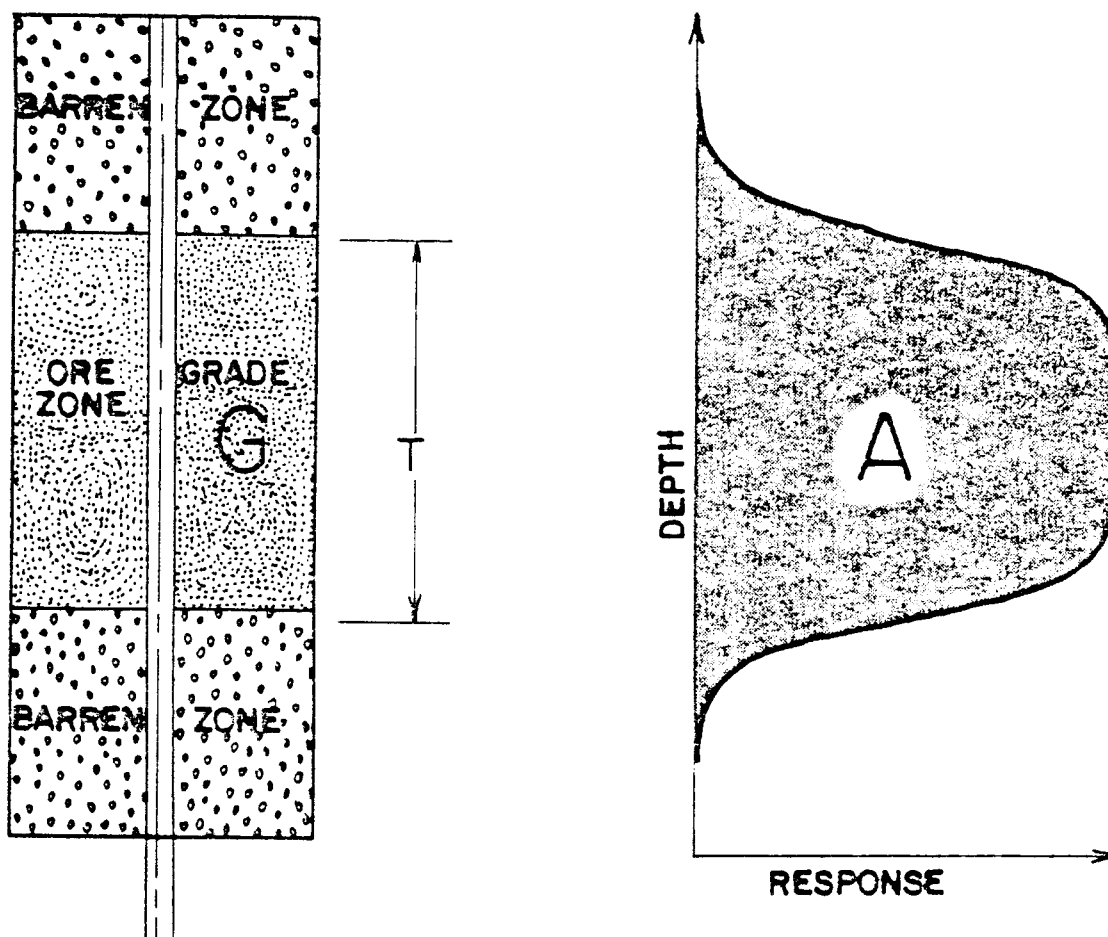
FIGURE 12

BOREHOLE URANIUM SPECTRUM
FOR GROSS COUNT DETECTOR

0.75-INCH x 2 INCH
SODIUM IODIDE

FRACTION OF
RESPONSE $=0.87$
BELOW 400 keV

FIGURE 13

CALIBRATION METHOD FOR
GROSS COUNT GAMMA-RAY LOGS

$$G \cdot T = k \cdot A$$

Spectral Hardware

BENDIX/DOE SPECTRAL PROBES
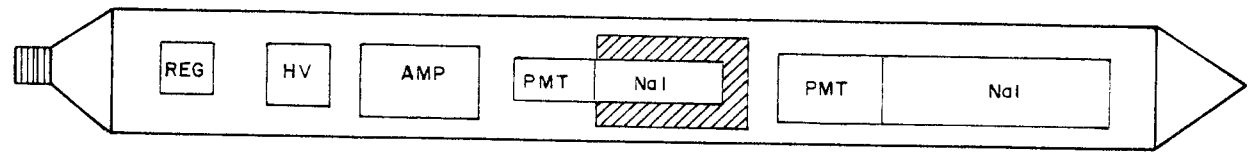
- **PHYSICAL**

  Diameter: 2⅛ to 2⅝ inches
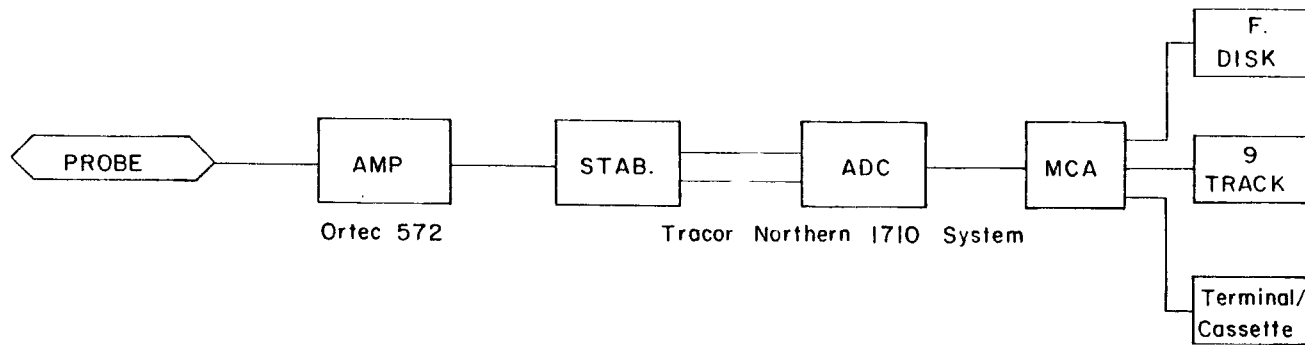 Length: 5 to 9 feet

- **ELECTRONICS**

  Voltage Regulator
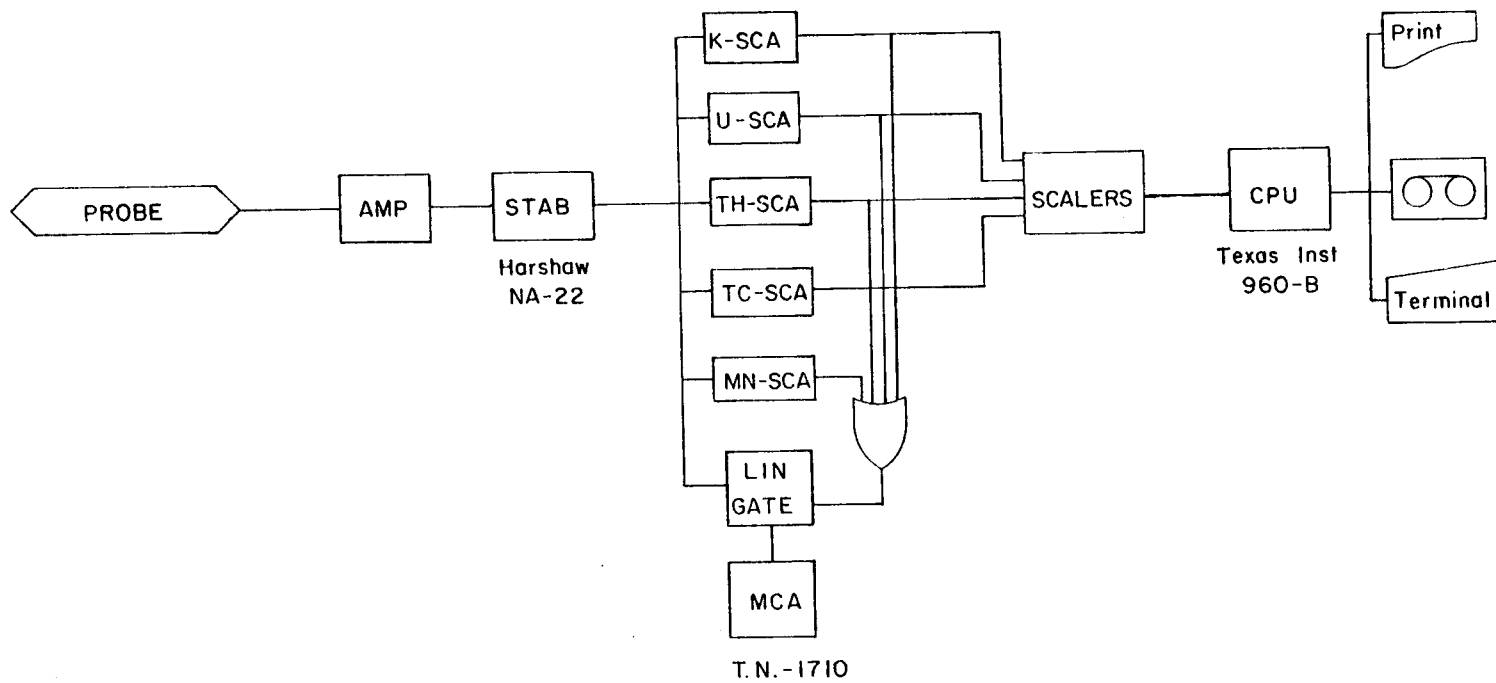 H. V. Supply
  Amplifier/Line Driver

- **DETECTORS**
  NaI(Tl), Ruggedized
  Dual Detectors
  1.5 x 12 inches
  1 x 6 inches (shielded)
  Resolution: 9-11%

PROBE — AMP — STAB. — ADC — MCA — F. DISK / 9 TRACK / Terminal/Cassette

Ortec 572

Tracor Northern 1710 System

SPECTRAL EQUIPMENT - R & D VERSION

PROBE — AMP — STAB — K-SCA / U-SCA / TH-SCA / TC-SCA / MN-SCA / LIN GATE — SCALERS — CPU — Print / Terminal

Harshaw NA-22

MCA

T.N.-1710

Texas Inst 960-B

SPECTRAL EQUIPMENT - FIELD VERSION

**Spectral Calibration and
Correction Methods**

CALIBRATION AND DATA CORRECTION TECHNIQUES

FOR SPECTRAL GAMMA-RAY LOGGING

David C. Stromswold

Robert D. Wilson

Bendix Field Engineering Corporation

Grand Junction, Colorado 81502

INTRODUCTION

As part of its work for the United States Department of Energy (DOE), Bendix Field Engineering Corporation (BFEC) has developed spectral gamma-ray logging hardware and data handling techniques. Calibration of the equipment and correction of the data for borehole and formation effects are two important steps in using logging data to assay for uranium. Procedures for calibrating spectral systems using scintillation detectors are described in the following sections.

Calibration is based on observed count rates in models of known concentration of potassium, uranium, and thorium. The following energy gamma rays are used to identify these elements: 1.46 MeV from ^{40}K, 1.76 and 2.20 MeV from ^{214}Bi (a decay product of uranium), and 2.61 MeV from ^{208}Tℓ (a decay product of thorium). Counts from these gamma rays are recorded for three energy windows which span the intervals shown in Table 1.

Table 1. Spectral Energy Windows.

Identification	Energy Window (keV)
Potassium	1320-1575
Uranium	1650-2390
Thorium	2475-2765

Sodium iodide crystals are used in the probes to detect gamma rays. For logging in low count-rate formations, large (1.5-inch x 12-inch), unfiltered detectors are used, and in regions of higher count rates, data are collected with small (1-inch x 6-inch), filtered detectors. Both detectors are contained in the same probe and selection of the detectors is performed remotely during logging. It is standard BFEC/DOE procedure to start with the large detector and switch to the small detector only after the large detector gives a count rate greater than 1500 counts per second above an energy threshold at 1250 keV. The small detector is thus used on repeated sections of holes when demanded by excessive count rates in the large detector.

Signals from the detectors are shaped and amplified within the probe and sent analog up the logging cable. Uphole the signals are reshaped, amplified, and gain stabilized to provide a constant pulse height for the manganese reference pulses at 835 keV. Spectral discrimination is obtained by either

single-channel analyzers or a multichannel analyzer. Gamma-ray counts in the potassium, uranium, and thorium windows are accumulated for short times (5 to 10 seconds) and then recorded on magnetic tape along with the depth of the probe in the hole.

MODELS

The efficiency of detectors used in logging must be determined in distributed radioactive sources sufficiently large so as to appear to be infinite. In practice this can be accomplished for uranium exploration by having the sources extend approximately 2 feet in every direction from the detector. Such sources are often constructed as cylinders of concrete mixed with radioactive elements. The concrete approximates the density (≈ 2 g/cm^3) of the rock in which logging is to be performed, and the cylinders have holes along their axes for probe insertion. Extended-source models in cylinders having 4-foot diameters are available at Grand Junction and selected field sites.

The primary spectral standards are located at Grand Junction, and they are designated as the potassium (K), uranium (U), and thorium (Th) models. Additional models are available for determining spectral water correction factors; these models are the KUT Water model (KUT WTR) and the D model. (The D model was built for fission-neutron calibration, but it can be used for gamma-ray work.) The grades assigned to these models are given in Table 2.

Table 2. Grades of Models.

Model	%K			ppm U			ppm Th		
Potassium	6.76	±	0.18	2.7	±	0.3	2.4	±	0.6
Uranium	0.84	±	0.24	498.3	±	12.1	5.6	±	1.3
Thorium	1.44	±	0.08	28.3	±	1.0	505.5	±	12.1
KUT WTR	4.90	±	0.29	321	±	19	219.4	±	9.2
D	1.78	±	0.26	576	±	76	7.7	±	1.7

Background measurements are made in a large water tank to reduce the effect of natural radioelements in the calibration area. The concentrations of potassium, uranium, and thorium in the water tank are small and considered to be zero for probe calibration.

Data collected from thin beds of radioactive elements must be processed to remove the averaging effects inherent in logging. Sharp ore/barren transitions can be partially restored if the spatial response of the detector is known. Special thin-bed models are available at Grand Junction for determining the response of detectors to thin uranium beds. These models have 2-inch-thick concrete zones with 0.246 percent eU_3O_8 and are positioned at several angles with respect to a central borehole. The spatial response of a detector can also be determined in calibration models with thick ore zones by logging the interfaces between ore zones and barren zones.

COLLECTION OF CALIBRATION DATA

The gain of the spectral system must be properly adjusted so that the gamma-ray peaks fall in their correct locations for proper identification. This is usually done using a thorium source after the system has warmed up sufficiently (approximately 20 minutes) and the gain stabilizer has been centered on the reference peak from manganese. At a minimum, the 2614 keV peak from the thorium source must occur in a pre-established location in the multichannel analyzer. An improved procedure is to calibrate the multichannel analyzer for gain using the 583 and 2614 keV gamma rays from a thorium source. Once this has been done, the window locations can be checked against their desired positions (Table 1). The use of the 835 keV gamma ray from the manganese stabilization source for energy calibration is not recommended. The apparent energy of this gamma ray changes as the source is moved along the length of the crystal due to nonlinearities in the detector's light output. It is best to use a distributed source for energy calibration.

Before and after calibrating a probe in the models, it is customary to record window count rates from a "field calibrator" source made of thorium ore packed in a tube (approximately 2-inch x 12-inch). The consistency observed in these count rates after local background has been subtracted is used later to test probe operation in the field. Unfortunately some probe malfunctions may not be detected from this test. Observation of the gamma-ray spectra on the multichannel analyzer provides better understanding of the probe's condition.

The counting efficiency of a detector is determined by recording counts in the potassium (K), uranium (U), and thorium (Th) models at a detector depth of 5.5 feet. The K model provides the lowest count rates of all the models, and thus it requires longer counting times than both the U and Th models in order to obtain equivalent counting statistics. Background counts are obtained by placing the probe in a large water tank with the detector at a depth of 5.5 feet. The times needed for collection of adequate data also vary with detector volume and shielding (filters). Counting times used in calibrating a Bendix/DOE spectral probe in the models are given in Table 3.

Table 3. Calibration Counting Times.

Detector Volume V (in3)	Typical Detector Size (inches)	Counting Time (seconds)			
		K Model	U Model	Th Model	Background
15 < V < 25	1.5 x 12	3000	2000	2000	4000
5 ≤ V < 15	1.5 x 3	4500	3000	3000	5000
2 ≤ V < 5	1 x 6 Filtered	6000	4000	4000	5000

ANALYSIS OF CALIBRATION DATA

The calibration data needed for analysis are the counts and counting times (seconds) collected in the three energy windows in the K, U, and Th and background models. These data are used in a computer program (PADCAL) which determines sensitivities and stripping coefficients based on assigned grades

of the models. The program uses linear equations to determine proportionality constants that relate window count rates to model concentrations after background count rates have been subtracted. In a matrix formalism the relationship is

$$R = AC \tag{1}$$

where
  R = 3 x 3 matrix of observed count rates in K, U, and Th models after background has been subtracted
  C = 3 x 3 matrix of concentrations of calibration models
  A = 3 x 3 matrix of proportionality determined from R and C.

The elements of the three matrices are defined as follows:

  R_{ij} = count rate in ith energy window in the jth calibration model after background subtraction;

  $C_{\ell j}$ = concentration of ℓth radioactive element in jth calibration model;

  $A_{i\ell}$ = constant relating count rate in ith energy window with concentration of ℓth radioactive element.

The matrix expression in equation (1) can be written in terms of its individual elements as

$$R_{ij} = \sum_{\ell=1}^{3} (A_{i\ell}C_{\ell j})$$

The convention used in defining the subscripts is:

  1 = Potassium
  2 = Uranium
  3 = Thorium.

Thus, for example, R_{13} is the count rate in the potassium energy window obtained in the thorium calibration model after background subtraction.

The analysis program calculates the proportionality matrix A , its matrix inverse A^{-1}, and the uncertainties in the A and A^{-1} matrix elements. The uncertainties are determined from propagation of the counting statistics in the window counts and the uncertainites in the assigned grades of the calibration models.

Concentrations of K, U, and Th in the field where logging data are collected are calculated using the matrix equation

$$C = A^{-1}R \tag{2}$$

where

  C = 3 x 1 matrix of concentrations to be calculated

  A^{-1} = 3 x 3 matrix of proportionality determined by PADCAL using data from calibration models

  R = 3 x 1 matrix of field count rates (logging data).

4

Equation 2 can be written in terms of its matrix elements as

$$C_i = \sum_{\ell=1}^{3} (A_{i\ell}^{-1} R_\ell)$$

where

C_i = concentration of ith radioactive element

$A_{i\ell}^{-1}$ = $i\ell$ matrix element of A^{-1}

R_ℓ = count rate in ℓth energy window after background subtraction.

The background count rates which are subtracted from field data are taken to be those determined during calibration in the water tank. These values should be acceptable because most of the background is generated by the manganese stabilization source through chance coincidences in which the energies add to reach the spectral windows.

CORRECTIONS TO FIELD DATA

Data collected in the field must be corrected for conditions different from those under which the calibrations were performed. For uranium logging there are two significant borehole conditions for which corrections must be made: (1) the variation of fluid-filled hole diameter, and (2) the presence of steel casing.

Water

Corrections for water in holes of various diameters are determined experimentally using the KUT water factor and D-calibration models. Count rates are collected with the detector in these models for the holes both dry and water-filled. The data are analyzed to determine apparent concentrations of K, U, and Th for the holes wet and dry based on a calibration of the detector in the dry, 4.5-inch holes of the K, U, and Th calibration models.

Water correction factors are determined from the ratio of the calculated concentrations for the wet and dry holes:

$$\text{Water correction factor} = \frac{\text{Calculated concentration, dry}}{\text{Calculated concentration, wet}}$$

Separate correction factors are determined for K, U, and Th and they are used to multiply the (uncorrected) concentrations of these elements calculated from field logging data:

Corrected Field Concentration = (Uncorrected Field Concentration) x (Water Correction Factor).

Separate correction factors must be determined for centralized and side-wall positions of the probe within the hole. Unless there is a mechanical centering device, such as a three-arm caliper, it is customary to assume that the probe rests against a side of the borehole during logging. The sidewall and centralized water correction factors have fundamentally different variations with hole size. The sidewall factors approach a limiting value at large hole diameters, whereas the centralized water factors increase without limit at large diameters.

5

The process of correcting for water in the holes only adjusts the sensitivities of a probe to K, U, and Th. The effect of the water on spectrum shape is not fully incorporated in these corrections because the calibration models presently available are not sufficient to provide data on corrections in addition to the sensitivity factors. The error made by ignoring these additional considerations has been estimated, however, from experimental data for 4.5-inch holes and calculated from theoretical calculations for holes up to 12 inches in diameter. Changes in spectrum shape are reflected by changes in stripping ratios, and for the 4.5-inch hole, the experimental stripping ratios changed by less than 2 percent from wet to dry holes. The calculated variation of stripping ratios with water-filled hole size are shown in Figures 1 and 2 where the stripping ratios have been normalized to their values for 4.5-inch holes. The stripping ratios for a sidewalled probe change by less than 8 percent for holes from 3 to 12 inches in diameter (Figure 1). For a centralized probe, the stripping ratios change by less than 13 percent for the same range of hole diameters (Figure 2). Most uranium logging is performed in the sidewall mode in holes of diameter 7 inches or less. For these situations, the calculated variation in stripping ratios is less than 5 percent, and disregard of such variations should produce acceptably small errors in calculated concentrations from logging data.

The water correction factors for sensitivity to K, U, and Th have been determined experimentally using large, unfiltered detectors, and the resulting correction factors are shown in Figure 3 for the sidewall condition and in Figure 4 for the centralized configuraton. The potassium corrections were measured in the upper barren zone of the D model, the uranium corrections in the ore zone of the D model, and the thorium corrections in the ore zone of the KUT water model. The technique of using different sections of the models for the three correction factors has proven to give better results than using just one location because it minimizes stripping problems.

The correction factors in Figure 3 and 4 are plotted as a function of hole diameter minus probe diameter. The suitability of this parameter for sidewalled probe was tested experimentally for thorium by placing PVC sleeves, with their bottom ends closed around a probe to simulate different probe diameters. The results are shown in Figure 5. Although there is some variation in the correction factors shown, it is clear that using hole diameter minus probe diameter as a water correction parameter is acceptable for sidewall correction factors. Using the same parameter for centralized probes is clearly correct from theoretical considerations.

The correction data in Figure 3 were obtained using a 1.5 x 9-inch NaI(Tℓ) detector in a 2.1-inch diameter probe, and the data have been fitted to a power correction curve:

$$\text{Water Correction (sidewall)} = 1 + ax^b$$

where

   x = hole diameter minus probe diameter (inches)
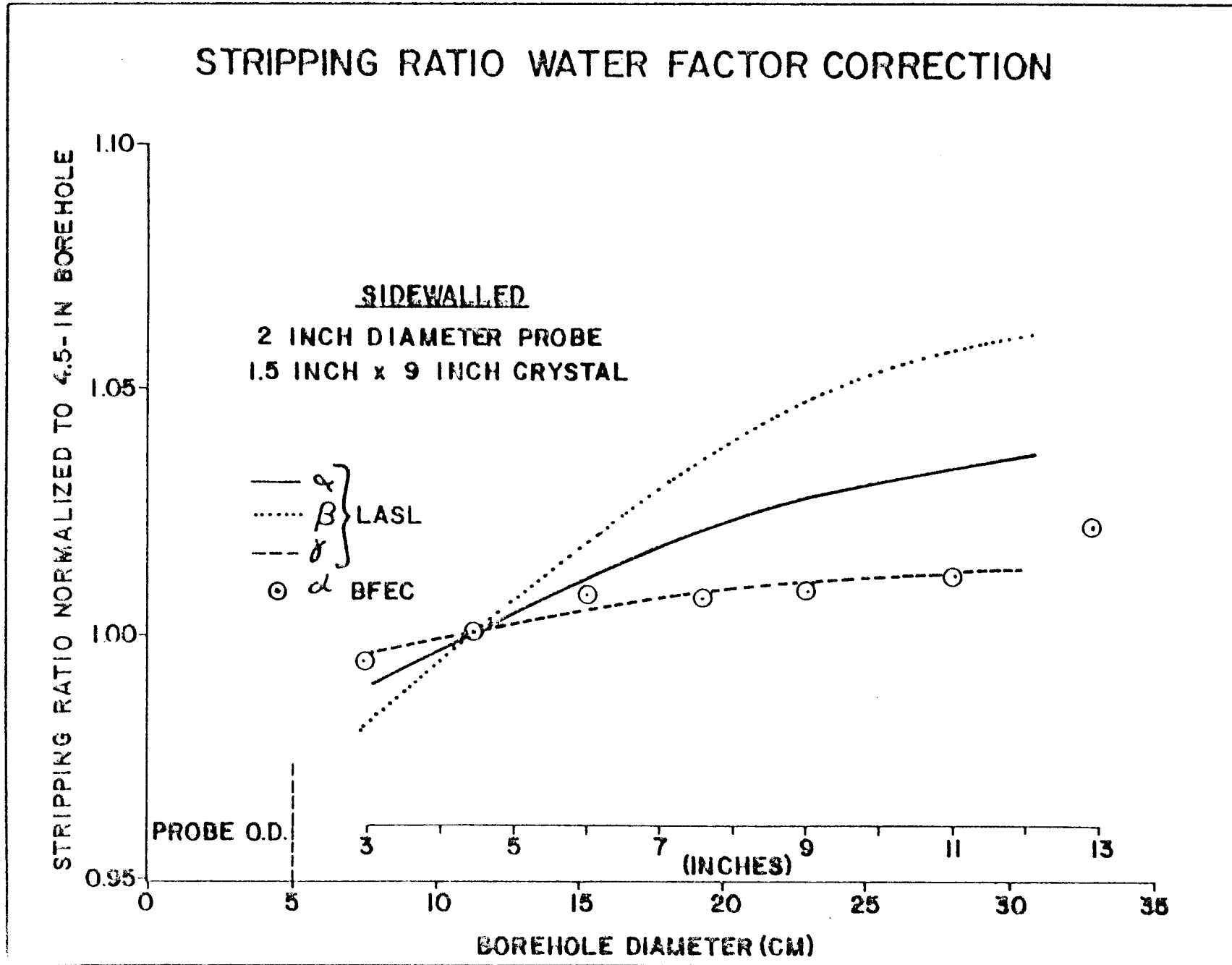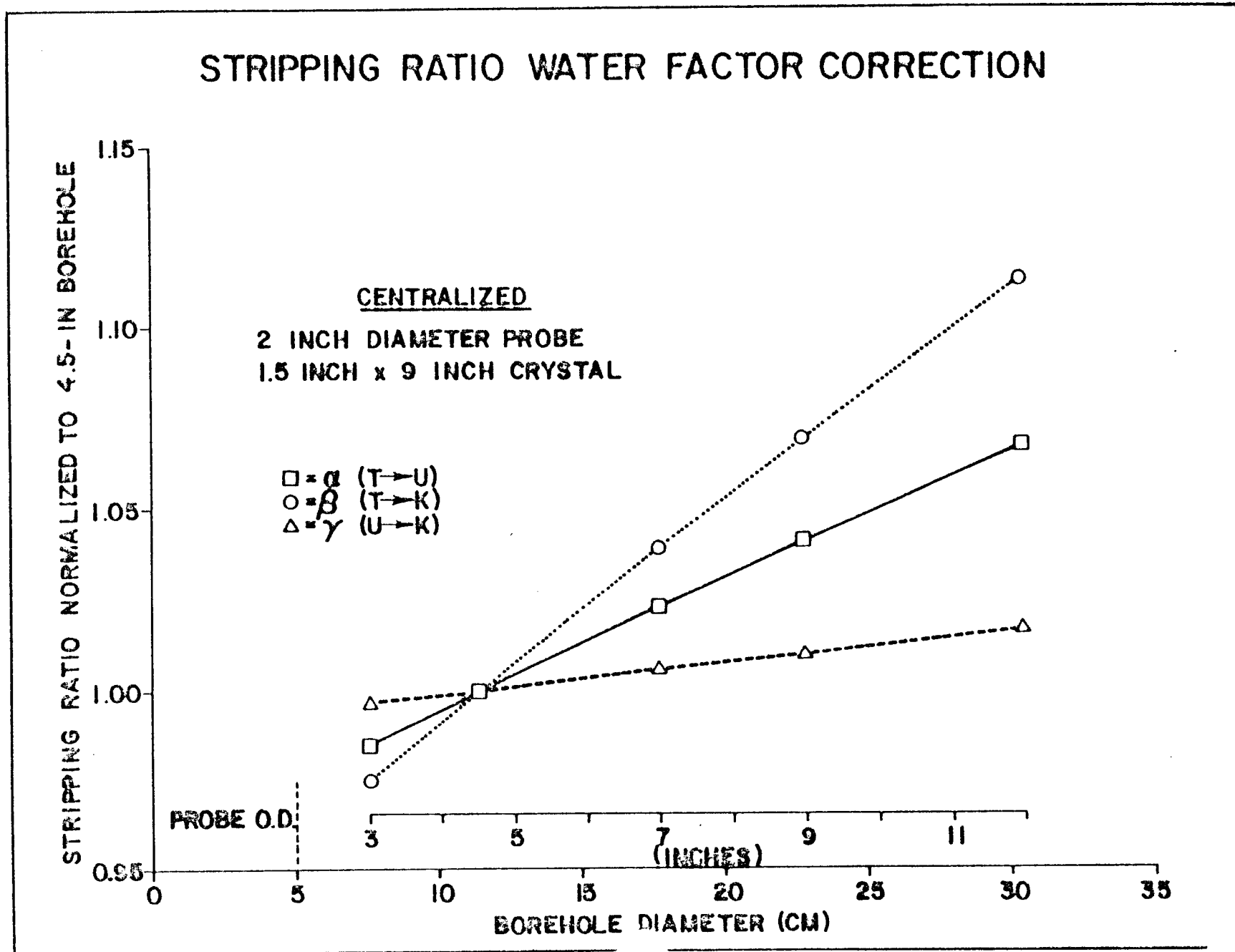 a, b = fitting constants whose values are given in Table 4.

FIGURE 1

STRIPPING RATIO WATER FACTOR CORRECTION

FIGURE 2

STRIPPING RATIO WATER FACTOR CORRECTION

CENTRALIZED

2 INCH DIAMETER PROBE
1.5 INCH x 9 INCH CRYSTAL

$\square = \alpha$ (T→U)
$\bigcirc = \beta$ (T→K)
$\triangle = \gamma$ (U→K)

PROBE O.D.

Y-axis: STRIPPING RATIO NORMALIZED TO 4.5-IN BOREHOLE (1.15, 1.10, 1.05, 1.00, 0.95)

X-axis: BOREHOLE DIAMETER (CM) (0, 5, 10, 15, 20, 25, 30, 35)

(INCHES) (3, 5, 7, 9, 11)

FIGURE 3

WATER CORRECTION FACTORS
FOR KUT SENSITIVITIES
(SIDEWALLED)

POTASSIUM

URANIUM

THORIUM

WATER CORRECTION FACTOR (DRY ÷ WET)

HOLE DIAMETER MINUS PROBE DIAMETER (INCHES)

FIGURE 4

WATER CORRECTION FACTORS
FOR KUT SENSITIVITIES
(CENTRALIZED)

WATER CORRECTION FACTOR (DRY ÷ WET)

POTASSIUM

URANIUM

THORIUM

BOREHOLE DIAMETER MINUS PROBE DIAMETER (INCHES)
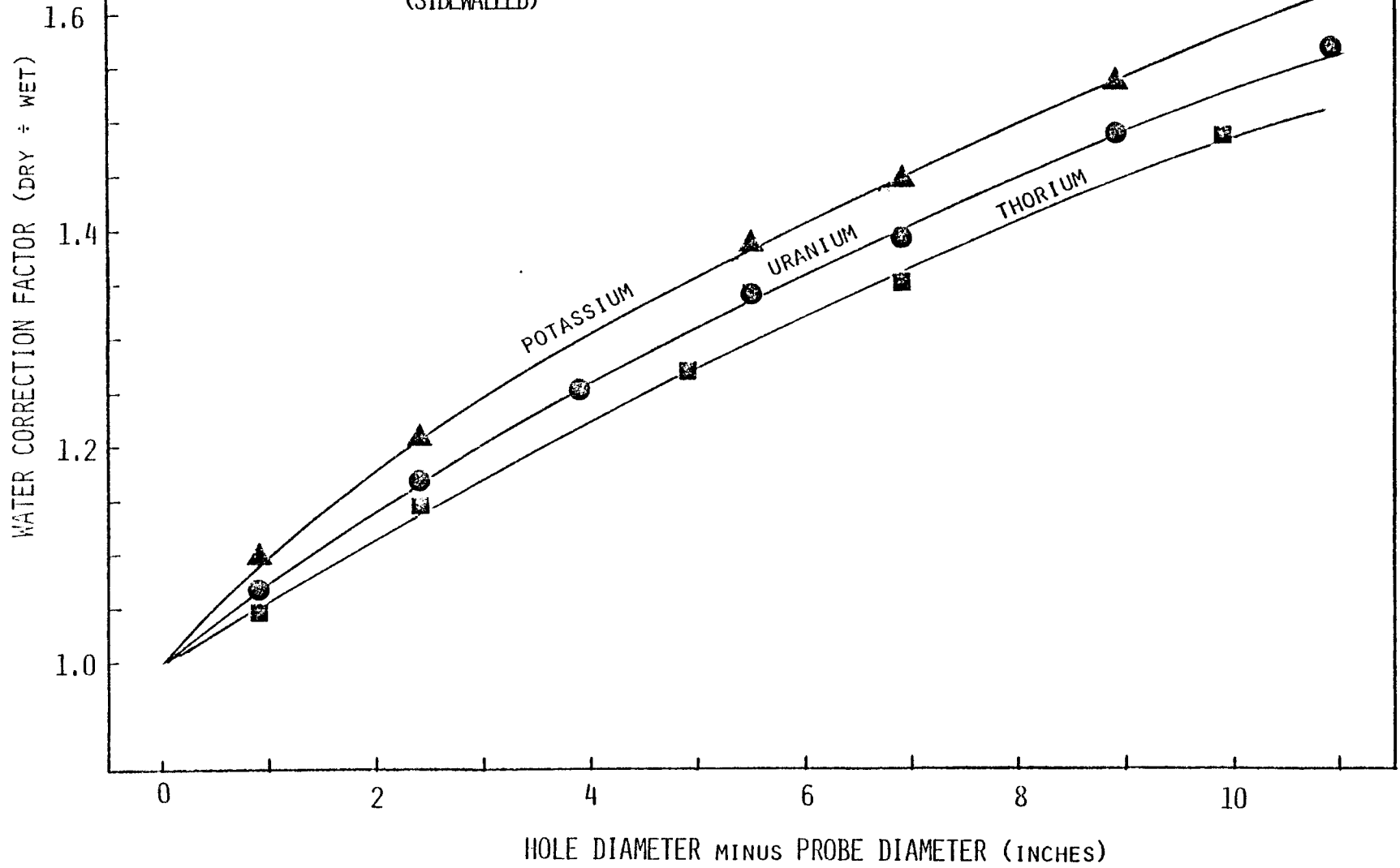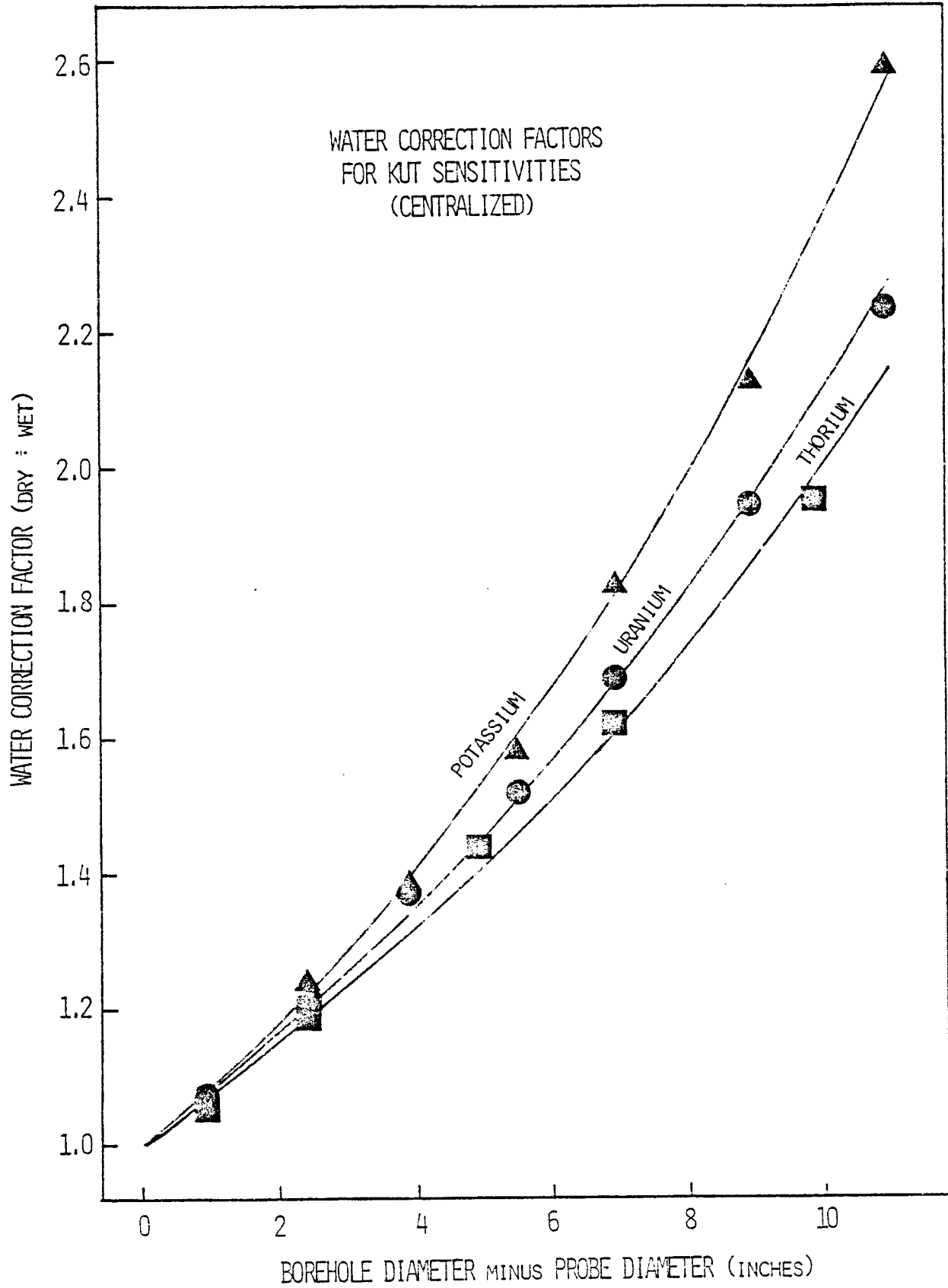
FIGURE 5

THORIUM WATER CORRECTION FACTORS
FOR VARIOUS PROBE DIAMETERS
(SIDEWALLED)
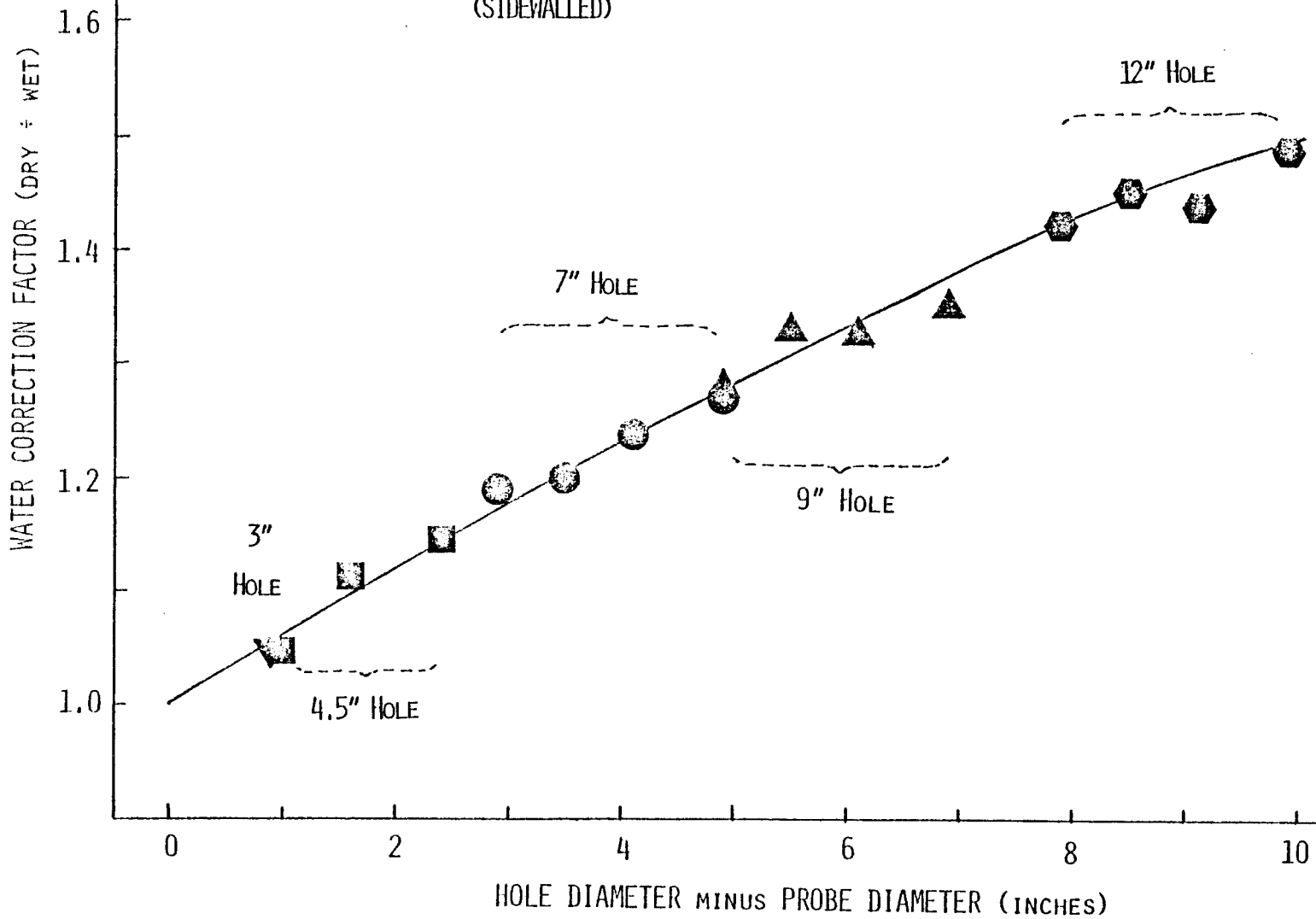
Table 4. Fitting Constants for Sidewall Water Corrections.

Elements	a	b
Potassium	0.1090	0.7375
Uranium	0.0777	0.8484
Thorium	0.0561	0.9662

The water correction data for a 1.5 x 12-inch NaI(Tℓ) detector in a 2.1-inch, centralized probe (Figure 4) have been fitted to the exponential curve

$$\text{Water Correction (centralized)} = c \cdot \exp(dx)$$

where

    x = hole diameter minus probe diameter (inches)
 c, d = fitting constants given in Table 5.

Table 5. Fitting Constants for Centralized Water Corrections.

Elements	c	d
Potassium	0.9912	0.0872
Uranium	1.0116	0.0737
Thorium	1.0031	0.0688

Steel Casing

The presence of steel casing reduces the number of formation gamma rays reaching a detector in a borehole, and corrections must be made to obtain correct concentrations from the logging data obtained in cased holes. Steel casings of thickness 0.06-inch to 0.5-inch are available at Grand Junction for determining casing corrections experimentally. These casings have an inside diameter of 3 inches and they are 4.5 feet long. They are hung individually over a detector and counts are recorded in the K, U, and Th calibration models. In this way, a separate calibration is obtained for each casing thickness, and changes in both sensitivities and stripping ratios can be calculated.

The effect of steel casing is applied to field data by adjusting the calibration matrix, A^{-1}, prior to calculating concentrations from the logs. The steel casing correction factors, F_{ij}, are used to adjust the elements of the A^{-1} calibration matrix as follows:

$$A^{-1}_{ij} \text{ (cased)} = A^{-1}_{ij} \text{ (uncased)} \times F_{ij}$$

The functional form of F_{ij} is taken as

$$F_{ij} = \exp(f_{ij} x)$$

where

    f_{ij} = fitting parameter
    x = number of 0.0625-inch thicknesses of casing
    Values of f_{ij} obtained for a 1.5-inch x 12-inch NaI(Tℓ) detector in a probe having a shell thickness of 0.125-inch are given in Table 6.

Table 6. Steel Casing Parameters for 1.5-inch x 12-inch NaI(Tℓ) Detector.

Parameter	Value
f_{11}	0.072
f_{12}	0.075
f_{13}	0.083
f_{21}	0.000
f_{22}	0.068
f_{23}	0.075
f_{31}	0.000
f_{32}	0.037
f_{33}	0.058

Background Subtraction

There is generally very little background in the K, U, and Th windows which needs to be subtracted from field data. The background counts that do appear come mainly from the manganese stabilization source which emits gamma rays of energy 835 keV. The simultaneous arrival of two manganese gamma rays in the detector can produce a summed pulse which reaches the K or U windows.

The background count rates obtained in the water tank during probe calibration can be used for subtracting background from field data. These count rates, which include the effects of the summed manganese contributions, will decrease with the square of the source count rate as the source decays during its 312-day half life. Backgrounds measured within 2-3 months of field logging should be adequate for most purposes.

No correction is made for pile-up of a manganese gamma ray with a formation gamma ray. Such a correction would be difficult to determine because it varies with formation count rate as well as manganese source strength.

Conclusion

The K, U, and Th models at Grand Junction are the primary standards used in calibrating spectral probes. Data collected in these models are analyzed in a matrix technique to determine counting efficiencies and spectrum stripping parameters for potassium, uranium, and thorium.

Logging data collected in holes that are cased or have diameters different from the standard 4.5 inches of the calibration models must be corrected to give proper assays. The corrections can be determined experimentally using the calibration facilities at Grand Junction.

47.

GAMMA-RAY SPECTROMETRIC CALIBRATION FACILITIES – A PRELIMINARY REPORT

Project 720085

P.G. Killeen
Resource Geophysics and Geochemistry Division

Abstract

Killeen, P.G., Gamma-ray spectrometric calibration facilities – a preliminary report; Current Research, Part A, Geol. Surv. Can., Paper 78-1A, p. 243-247, 1978.

In order to make quantitative measurements of radioelement concentrations with a gamma-ray spectrometer the spectrometer must be calibrated using sources having (1) known radioelement contents, and (2) geometry similar to that in which the measurement will be made. In the case of portable gamma-ray spectrometers the measurement in the field will generally be made on relatively flat outcrop surfaces. This may be simulated using a flat concrete pad approximately flush with the ground surface. In the case of gamma-ray spectral logging, the measurement geometry is, of course, a borehole. In this case model boreholes including appropriate "ore" zones can be constructed in concrete.
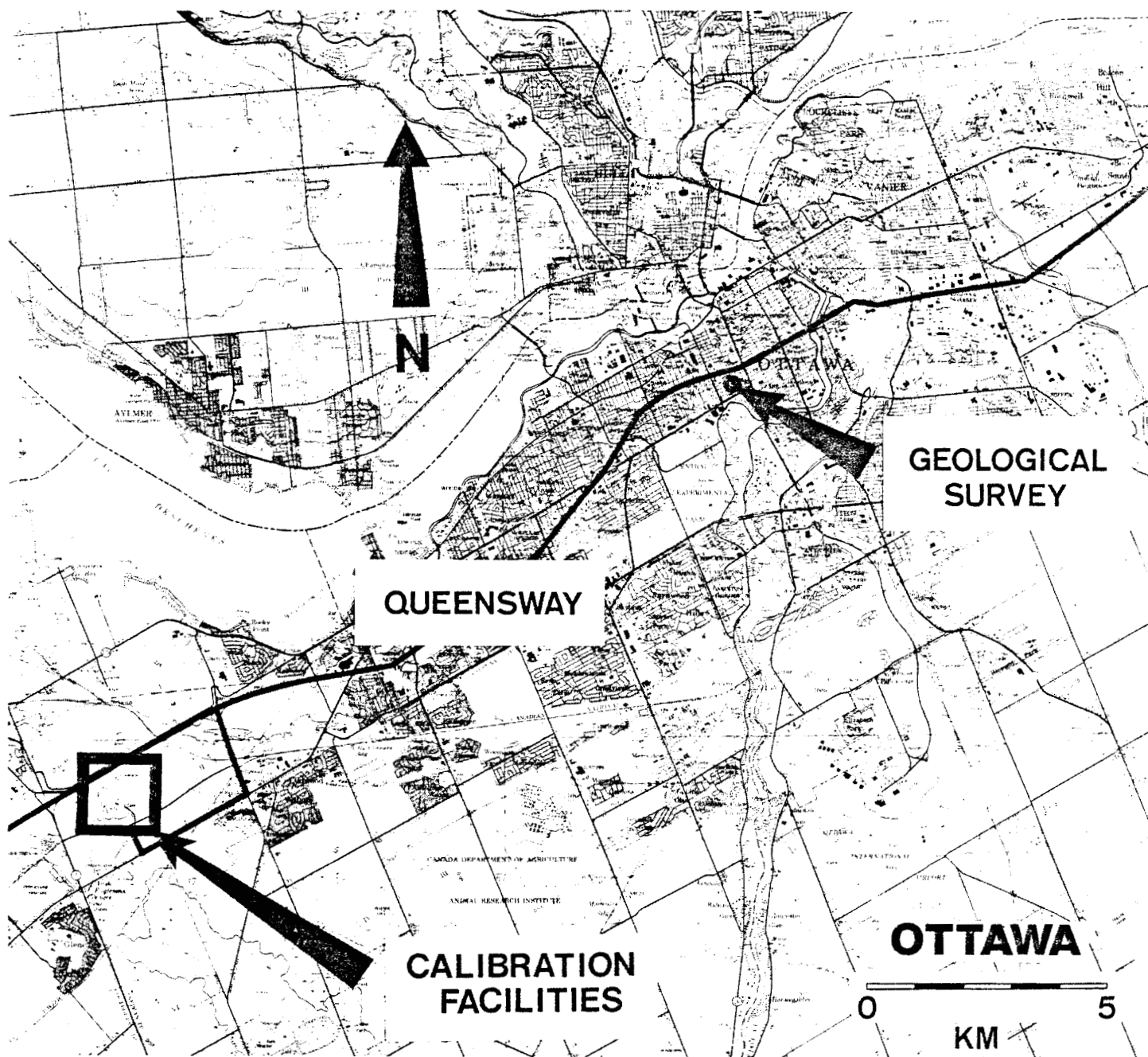
Figure 47.1. Location of the Geological Survey calibration facilities for portable gamma-ray spectrometers and gamma-ray spectral logging equipment.

Introduction

In October 1978, the Geological Survey of Canada completed the construction near Ottawa of extensive calibration facilities for gamma-ray spectrometry equipment as mentioned above. They meet or exceed the recommendations of the IAEA (1976). This paper comprises a preliminary report on the new facilities: their location, description, preliminary analyses of samples taken during construction, and the procedure for obtaining access to the calibration facilities, and preliminary recommended procedures for carrying out the calibration measurements.

Location of the Calibration Facilities

The new calibration facilities are located on the property of the CANMET (E.M.R.) laboratory complex at Bells Corners approximately 10 km west of Ottawa. Figure 47.1 shows the location. The calibration facilities consist of a set of 10 calibration pads for portable spectrometers, located along a gravel road leading to an abandoned quarry in which nine test columns containing the model boreholes are constructed (see Fig. 47.2).

Calibration Pads for Portable Gamma-Ray Spectrometers

The calibration pads are concrete cylinders, 60 cm thick and 3 m in diameter, making effectively infinite sources if the detector of the portable gamma-ray spectrometer is centrally located on and within a few inches of the surface of the pad. Three pads contain different potassium concentrations, three contain different uranium concentrations and three contain different thorium concentrations. The different radioelement concentrations were obtained by adding to the concrete appropriate amounts of uranium ore, thorium oxide, or nepheline syenite for U, Th, and K respectively. A tenth pad, referred to as the blank pad, was constructed with no radioelement additives. The preliminary mean values of the radioelement contents of some of the samples taken during construction are given in Table 47.1. At the time of this writing, not all of the samples have been analyzed. Thus, although subject to revision, these preliminary values indicate the range of concentrations available for calibration purposes. The five pads at Uplands Airport, which had previously been used for calibration of portable instruments, have a very limited range of radioelement concentrations since they were designed for calibrating airborne gamma-ray spectrometers (Grasty and Darnley, 1971) and will continue to be used for that purpose. The new calibration pads should greatly improve the accuracy and repeatability of determinations of calibration factors.

The recommended procedure for carrying out calibration measurements is explained in greater detail on handout sheets provided to users of the calibration facilities. These include a detailed location map, a table of pad numbers with their radioelement concentrations, and information about obtaining clearance for access to the calibration site. This information may be obtained by contacting the Radiation Methods Section, Resource Geophysics and Geochemistry Division of the Geological Survey of Canada.

Basically the calibration procedure for portable gamma-ray spectrometers consists of taking several readings on each pad in order to obtain good counting statistics, with the detector at a slightly different location near the centre of the pad for each reading. Counting times will depend on detector size.
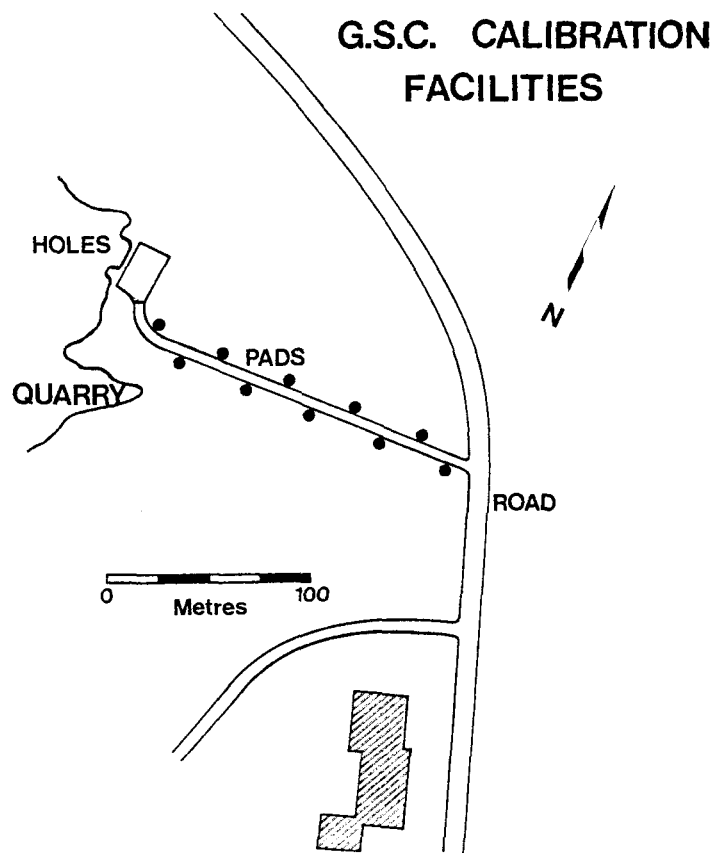

G.S.C. CALIBRATION FACILITIES

Figure 47.2. Detailed locations of the 10 calibration pads and the model holes on the property of the CANMET laboratory complex at Bells Corners.
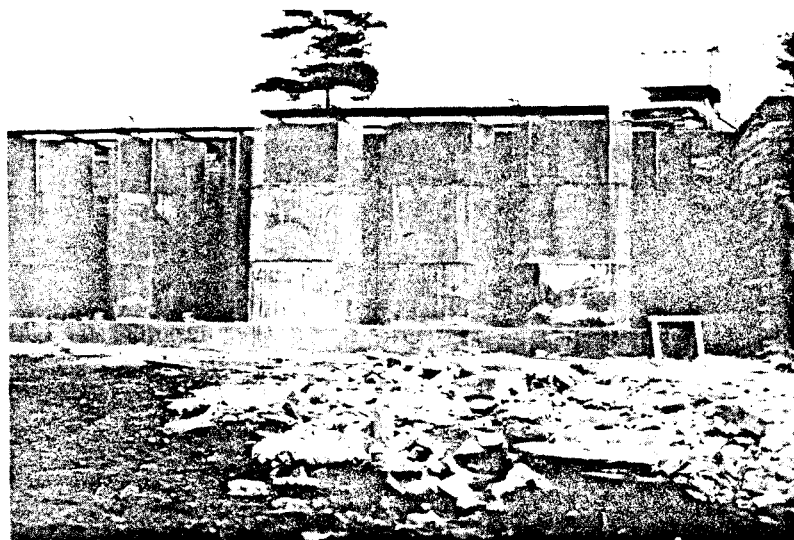

Figure 47.3. The nine concrete test columns viewed from inside the quarry showing the "ore zones" and a logging truck parked above in the working area for calibrating logging systems. (GSC photo 203254-O).

If these data, along with the types and serial numbers of the spectrometers and detectors are given to the Geological Survey, the calibration constants will be computed; there no charge for this service. The use of the calibra constants for computing in situ assays was described Killeen and Cameron (1977).

Table 47.1

Preliminary mean radioelement concentrations
for calibration pads

Pad Number	K%	eU ppm	eTh ppm
PK-1-OT	0.88		
PK-2-OT	1.48		
PK-3-OT	2.87		
PU-4-OT		6.10	
PU-5-OT		42.49	
PU-6-OT		458.15	
PT-7-OT			8.10
PT-8-OT			62.00
PT-9-OT			310.07
PB-10-OT	0.24	0.16	1.39

Model Boreholes for Calibrating Gamma-Ray Logging Systems

For calibration of borehole gamma-ray spectrometers a set of nine models have been constructed along the wall of a rock quarry as shown in Figure 47.3. Each of the models consists of a concrete column 3.9 m in height with an "ore zone" 1.5 m thick sandwiched between an upper and lower barren zone as shown in Figure 47.4. Each test column contains 3 boreholes of diameters A (48 mm), B (60 mm) and N (75 mm) intersecting the ore zones as shown in Figure 47.5. Three of the test columns contain ore zones of different concentrations for potassium, three for thorium, and three for uranium. These ore zones were produced by mixing suitable additives with the concrete as described above for e calibration pads.

The preliminary mean values of the radioelement concentrations in samples taken during construction are given in Table 47.2. Revised radioelement concentration values will be determined and published at a later date when all of the samples have been analyzed. The radioelement concentrations in the barren zones are the same as for the blank pad (PB-10-OT) in Table 47.1.

The calibration procedure for gamma-ray spectral logging equipment consists of three parts: (1) the determination of the stripping factors, (2) the determination of the sensitivity i.e. the relation between count rates and ore grade, and (3) the determination of instrument response characteristics (if the logging data are to be computer processed to improve accuracy and resolution (e.g. Scott et al., 1961; Scott, 1963; Conaway and Killeen, 1978; Killeen et al., 1978).

The stripping factors can be determined relatively quickly by observing the count rates obtained in the uranium and potassium channels of the spectrometer, while the borehole probe is positioned inside a thorium ore zone, and then inside a uranium ore zone. (This would also give the upward stripping factor, i.e. uranium counts in the thorium window.) In practice the count rate should be determined at several positions near the centre of each ore zone in order to obtain an accurate average value. As in the case of the calibration pads, if these data are supplied to the Geological Survey, stripping factors will be computed.

Having determined the stripping factors, these can then be applied to logs recorded in the field. The stripping factors will enable the stripped gamma-ray log to be plotted as shown in the conceptual example of Figure 47.6. From top to bottom in this figure are shown the anomalies in the 4
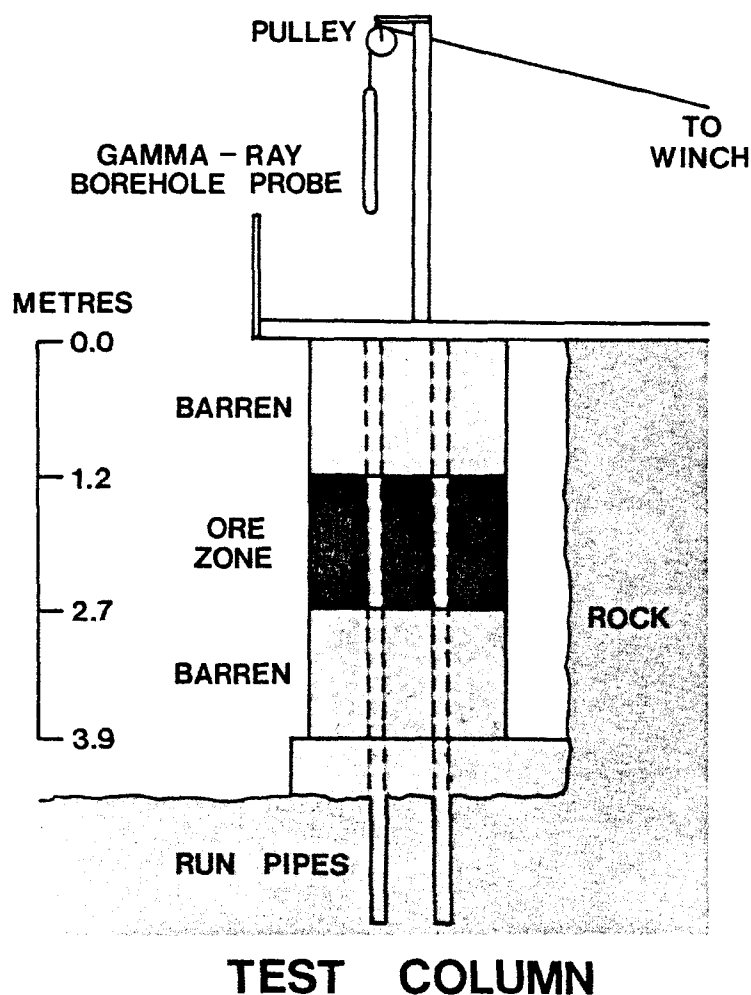

TEST COLUMN

Figure 47.4. Cross-sectional view of a test column, showing two of the three holes in the column, the run pipes which extend 3.0 m below, and the hoist and pulley on top of the column.
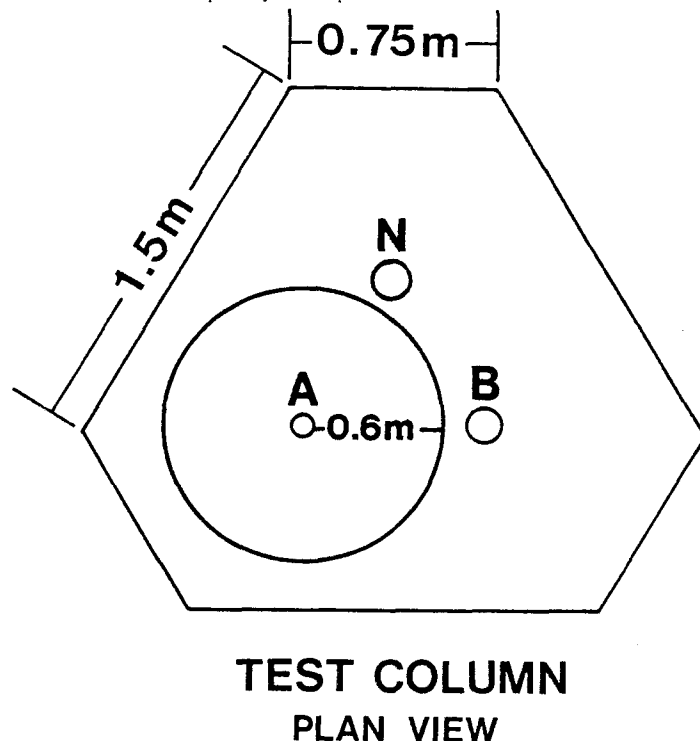

TEST COLUMN
PLAN VIEW

Figure 47.5. Plan view of a test column showing location and spacing of the three sizes of model boreholes.

GAMMA – RAY SPECTRAL LOG

T.C.   K   U   Th

STRIPPED GAMMA–RAY SPECTRAL LOG
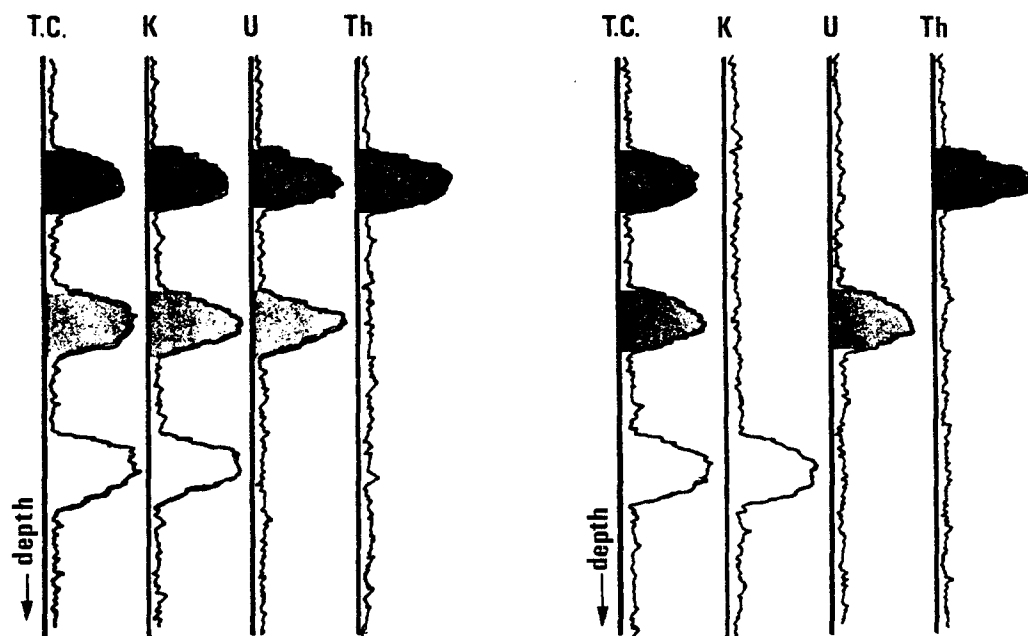
T.C.   K   U   Th

Figure 47.6.

Comparison of unstripped and stripped gamma-ray spectral logs showing anomalies caused by K, U, and Th respectively.

Table 47.2

Preliminary mean radioelement concentrations for test columns

Column Number	K%	eU ppm	eTh ppm
BK-1-OT	0.72		
BK-2-OT	1.14		
BK-3-OT	3.01		
BU-4-OT		14.32	
BU-5-OT		100.67	
BU-6-OT		948.58	
BT-7-OT			8.20
BT-8-OT			34.93
BT-9-OT			347.11

channels of the spectrometer (total count, K, U, and Th) caused by logging through a thorium zone, a uranium zone, and a potassium zone respectively. The left side of Figure 47.6 shows the unstripped log illustrating the ambiguous situation which arises when anomalies appear in the uranium and potassium channels even when no uranium or potassium is present. The right side of Figure 47.6 shows the stripped gamma-ray spectral log, which clearly indicates which of the radioelements caused each of the three anomalies shown in the total count channel.

The ultimate objective of gamma-ray spectral logging is quantitative downhole assaying, particularly of uranium, which is part (2) of the calibration procedure. In this case, the determination of the system calibration constant K is carried out using stripped data obtained as in step (1) above by means of the equation

$$K = \frac{G}{I}$$

Here G is the known radioelement concentration (grade) in parts per million (ppm) and I is the average measured gamma-ray intensity in counts/s near the centre of the ore zone; the

units of K, then, are ppm s/count. The raw field log is then multiplied by K to give the ore grades in cases of uniform ore zones approximately 1 m or more in thickness (i.e. infinitely thick). The grade values obtained for thinner zones will be lower than the actual grade.

In order to enhance the accuracy and resolution of ore grade determinations in thin beds and complex sequences, is necessary to carry out step (3), the determination of t system response characteristics. More information on th can be found in Conaway and Killeen (1978).

The logging equipment calibration facilities are designed to permit calibration of logging systems in both wet and dry holes of sizes A, B, and N, uncased or with various types of casing material.

As in the case of the calibration pads, handout sheets with further information and recommended procedures will be provided to those persons interested in calibrating gamma-ray logging equipment in the model boreholes. The Geological Survey will endeavour to compute the calibration factors for gamma-ray spectral logging systems when the recommended procedures are followed.

It should perhaps also be mentioned here that two model boreholes containing different uranium ore zones have been constructed in Fredericton, in co-operation with the New Brunswick Department of Natural Resources. These two model holes are approximately 125 mm in diameter and may be used in the calibration of total count gamma-ray logging equipment. Future additional calibration facilities are planned for other locations in Canada. These will probably consist of sets of seven calibration pads (2 for each radioelement and one blank), and model boreholes of a simpler design. It is hoped that calibration of gamma-ray spectrometric equipment will become a more common practice in Canada as these calibration facilities become more readily available.

References

Conaway, J.G. and Killeen, P.G.
  1978: Quantitative uranium determinations from gamma-ray logs by application of digital time series analysis; Geophysics, submitted for publication.

Grasty, R.L. and Darnley, A.G.
  1971: The calibration of gamma-ray spectrometers for ground and airborne use; Geol. Surv. Can. Paper 71-17.

IAEA
  1976: Radiometric reporting methods and calibration in uranium exploration; IAEA Technical Report Series No. 174, 57 p.

Killeen, P.G. and Cameron, G.W.
  1977: Computation of in situ potassium, uranium and thorium concentrations from portable gamma-ray spectrometer data; in Geol. Surv. Can., Paper 77-1A, p. 91.

Killeen, P.G., Conaway, J.G., and Bristow, Q.
  1978: A gamma-ray spectral logging system including digital playback, with recommendations for a new generation system; in Current Research, Part A, Geol. Surv. Can., Paper 78-1A, rep. 46.

Scott, J.H.
  1963: Computer analysis of gamma-ray logs; Geophysics, v. 28, p. 457-465.

Scott, J.H., Dodd, P.H., Droullard, R.F., and Mudra, P.J.
  1961: Quantitative interpretation of gamma-ray logs; Geophysics, v. 26, p. 182-191.

**Gamma-Ray Transport
Calculations**

TITLE: A Computer Model for Calculating Gamma-Ray Pulse-Height Spectra for Logging Applications

AUTHOR(S): Michael L. Evans

University of California

LOS ALAMOS SCIENTIFIC LABORATORY
Post Office Box 1663   Los Alamos, New Mexico 87545
An Affirmative Action/Equal Opportunity Employer

A COMPUTER MODEL FOR CALCULATING GAMMA-RAY PULSE-HEIGHT SPECTRA

FOR LOGGING APPLICATIONS

by

Michael L. Evans

ABSTRACT

A generalized computer model has been devised to simulate the emission, transport, and detection of natural gamma radiation from various logging environments. The model yields high-resolution gamma-ray pulse-height spectra that can be used to correct both gross gamma and spectral gamma-ray logs. The technique can help provide corrections to airborne and surface radiometric survey logs for the effects of varying altitude, formation composition, and overburden. Applied to borehole logging, the model can yield estimates of the effects of varying borehole fluid and casing attenuations, as well as varying formation porosity and saturation.

The pulse-height spectrum observed from a detector in a logging environment is computed from the gamma-ray flux incident on the detector surfaces and the response function for the detector. The gamma-ray flux is calculated using a discrete-ordinates transport code, while the detector response function is determined using a Monte Carlo code. This computational procedure is outlined, and examples of the resulting pulse-height spectra are presented. Comparisons between computed and experimental spectra are made for the case of a 1-1/2-in. x 7-in. NaI detector in the borehole logging geometry and for a 3-in. x 3-in. NaI detector in a radiometric survey. These comparisons indicate that the spectrum calculation method is typically accurate to better than 10 per cent.

The response of any instrument is perhaps best understood in terms of a mathematical model that approximates the measurement process. The spectral measurement of radiation fields with scintillation counters involves the transport of radiation from its emission in the source, through various interposed media, to the detector. Interactions of the radiation in the media result in both scattered and unscattered flux components impinging on the detector. The pulse-height spectrum arising from the incident flux spectrum depends on the random nature of the scintillation process and the photomultiplier response.

This measurement process can be modeled by the Monte Carlo method. However, some model geometries result in very weak radiation fluxes incident on the detector. In addition, spectral energy resolution requirements may greatly accentuate the problem of obtaining high-resolution, high-precision pulse-height spectra. Hence, an alternate technique has been chosen to describe the measurement of radiation fields.

The count rate calculation method to be described is straightforward and very flexible in its application. The method can yield photon and/or neutron pulse-height distributions for general geometries and various types of detectors including organic and inorganic scintillators, solid-state detectors, and gas proportional counters. The pulse-height spectrum $c(\vec{r}_d, n)$ observed in a detector in a radiation field given by $\psi(\vec{r}, \vec{\Omega}, E)$ can be computed as:

1

$$c(\vec{r}_d,h) = \iiint R(\vec{r},\vec{\Omega},E,h)\,\vec{\Psi}(\vec{r},\vec{\Omega},E)\cdot d\vec{S}\,d\Omega\,dE \quad , \quad (1)$$

where $c(\vec{r}_d,h)$ is the number of events in pulse-height channel h (cnts/s/MeV) when the detector is located at point $\vec{r}_d$ in the model geometry.

The angular flux $\Psi(\vec{r},\vec{\Omega},E)$ (particles/cm^2/s/sr/MeV) is the number of particles passing through point $\vec{r}$ in the direction $\vec{\Omega}$ having energy E. The angular flux is computed for all points $\vec{r}$ in the model by using a one-, two-, or three-dimensional discrete ordinates code. The number of independent spatial variables modeled depends on the symmetry of the problem geometry. The ONETRAN[1] and TWOTRAN[2] codes are currently being used to compute angular fluxes of interest in the NURE program. Use of these codes results in angular fluxes that are computed only for discrete values of the independent variables $\vec{r}$, $\vec{\Omega}$, and E. That is, values of $\Psi(\vec{r},\vec{\Omega},E)$ are available only at the spatial and angular mesh points specified in the discrete ordinates transport problem. The energy domain is also subdivided into groups of finite width. Thus, Eq. (1) can be written as sums over discrete values;

$$c(\vec{r}_d,h) = \sum_E \sum_{\vec{r}} \sum_{\vec{\Omega}} R(\vec{r},\vec{\Omega},E,h)J(\vec{r},\vec{\Omega},E) \quad , \quad (2)$$

where $J(\vec{r},\vec{\Omega},E) = \vec{\Psi}(\vec{r},\vec{\Omega},E)\cdot d\vec{S}$ is the current at point $\vec{r}$ in the direction $\vec{\Omega}$. The function $R(\vec{r},\vec{\Omega},E,h)$ is the detector response that relates the pulse height h observed for a single incident particle to its point of entry $\vec{r}$ on the surface of the detector, its angle of incidence $\vec{\Omega}$, and its energy E. The discrete nature of the angular flux implies that the response function need be computed only for the discrete values at which Ψ is computed. This greatly reduces the computing effort required to determine (or map) the response function for a given detector. Even so, $R(\vec{r},\vec{\Omega},E,h)$ can still be a very large matrix, depending especially on the resolution required in the energy (E) and pulse-height (h) variables. The angular flux spectra of the airborne and subsurface gamma-ray transport studies utilize an energy structure containing 265 groups and require pulse-height spectra having 10-keV resolution. Thus, a 265-channel by

300-channel matrix is needed to describe the response of the detector to gamma rays incident on the detector at a single point $\vec{r}$ with a single angle of incidence $\vec{\Omega}$. Clearly, then, certain simplifying assumptions must be made if high-resolution, high-precision response function maps are to be generated in reasonable computer execution times.

Radiometric logging is performed in source/detector geometries that frequently result in radiation fields that vary only slowly in magnitude and direction over the detector surface. This is true of airborne and surface surveys for which the source is large compared with the survey height. In borehole logging, the variation in the radiation field is small for both centralized and sidewalled geometries, provided the ore-bearing formation is large compared with the detector length. However, the radiation field can vary significantly in magnitude and direction over the detector surface when logging through thin, ore-bearing zones. In particular, the polar dependence of the field can vary considerably as a function of distance from the ore zone.

A good approximation to the pulse-height distribution observed in the logging geometries described above is given by

$$c(\vec{r}_d,h) = \sum_E \sum_\theta \left[\sum_\phi \sum_{\vec{r}} R(\vec{r},\theta,\phi,E,h) \right]$$
$$\times \left[\sum_\phi \sum_{\vec{r}} J(\vec{r},\theta,\phi,E) \right] \quad , \quad (3)$$

where the first term is the effective detector response $R_e(\theta=\theta_c,E,h)$ for a given polar angle of incidence $\theta=\theta_c$, formed by summing responses resulting from radiation incident on the detector surface at all points $\vec{r}$ and azimuthal angles ϕ. The effective detector response is computed at each angle θ_c for which the discrete ordinates code provides angular flux values. The second term is an equivalent incident current impinging on the detector surface at points $\vec{r}$ from the directions ϕ. If this equivalent current adequately describes the average magnitude and azimuthal direction of the incident current, and if the detector response can be accurately estimated, then Eq. (3) should

2

yield acceptable estimates of the resulting pulse-height distribution. These assumptions are critical to practical evaluation of Eq. (1). If a separate detector response function were required at all possible points of incidence $\vec{r}$, angles of incidence θ and ϕ, and radiation energy E, an intractable computer problem would result. A tractable solution is obtained by assuming that the pulse-height distribution depends strongly on only E and θ, and is weakly dependent on ϕ and $\vec{r}$. Using this scheme, the detector response need be explicitly determined for only E and θ, while an implicit sum over $\vec{r}$ and ϕ is deemed sufficient to describe the detector response for geometries in which the $\vec{r}$ and ϕ dependence of the incident particle current is weak and can be replaced by an equivalent sum as well.

Accurate estimates of the effective detector responses R_e can be computed for cylindrically symmetric detectors by mapping with broad parallel beams incident at the polar angles θ_c. Detectors not having cylindrical symmetry will, in general, exhibit significant variation in response with the azimuthal angle of incidence. Since the detector response code GAMRES[3] used in these studies presently treats only detectors that are right circular cylinders, we will restrict the following discussion to detectors having that shape. Consideration of detectors having other shapes would entail modification of both the response function code as well as the folding Eq. (3) to explicitly include the effects of detector azimuthal response. In practice, the restriction to cylindrical detector geometry is of little concern, since most detectors used for radiometric logging and surveys are right circular cylinders.

The effective detector response $R_e(\theta=\theta_c,E,n)$ has been computed for a 3-in. by 3-in. NaI crystal using a broad parallel beam of gamma rays incident on the end face of the crystal ($\theta_c=0°$). That response function map is shown in Figs. 1 and 2, which are three-dimensional perspective plots of the energy vs pulse-height surface. Both plots use logarithmic (base 10) response scales so that the features of the surface at high energies such as the full-energy peak and the first and second escape peaks can be clearly identified. The perspective of Fig. 2 was obtained by rotating the plot of Fig. 1 clockwise about the response axis.

The folding expression in Eq. (3) will be used to obtain estimates of the pulse-height distributions observed in both the airborne and subsurface geometries. While other folding techniques may yield more accurate estimates for certain geometries and detectors, preliminary results indicate that Eq. (3) will yield adequate pulse-height spectra for the logging geometries of interest. Likewise, the use of a broad parallel beam for response function determination may be inferior to other beam/detector configurations for certain detector sizes and shapes. However, the agreement between computed and measured pulse-height spectra for the airborne and subsurface geometries has been good in the initial comparisons.

The scheme for calculating pulse-height distributions $c(\vec{r}_d,n)$ using Eq. (3) is summarized schematically in Fig. 3. The one-dimensional discrete ordinates transport code ONETRAN is used to compute the angular flux values $\Psi(\vec{r},\vec{\Omega},E)$ for the logging geometry of interest, while the analogue Monte Carlo transport code GAMRES is used to determine the effective detector response $R_e(\theta=\theta_c,E,n)$. Values of $\Psi(\vec{r},\vec{\Omega},E)$ for different geometries and $R_e(\theta=\theta_c,E,n)$ for different detectors are stored in separate files that serve as input to the folding code ENFOLD. This code performs the summations indicated in Eq. (3) to determine the theoretical pulse-height distribution $c(\vec{r}_d,h)$ for a given detector location $\vec{r}_d$. Thus, this generalized procedure permits easy calculation of pulse-height spectra for different detectors (varying in type, shape, and size) and different logging configurations (varying in geometry, composition, and size).

Examples of pulse-height distributions generated in this way are shown below. The flux spectra $\Psi(\vec{r}=0,E,n)$ observed at the center of an 11.43-cm (4.5-in.) diam, air-filled, uncased, infinitely long borehole are shown in Figs. 4-6 for a K, U, and Th source spectrum, respectively. The source was distributed homogeneously in the formation ($\rho = 2.138$ g/cm^3, P = 0.3, S = 1.0) surrounding the borehole and corresponded to a dry-weight concentration of 16.48 per cent K, 4.37-ppm U, and 13.4-ppm Th, respectively. Pulse-height distributions observed in a 1-1/2-in. by 7-in. NaI detector centered coaxially in the borehole are shown in
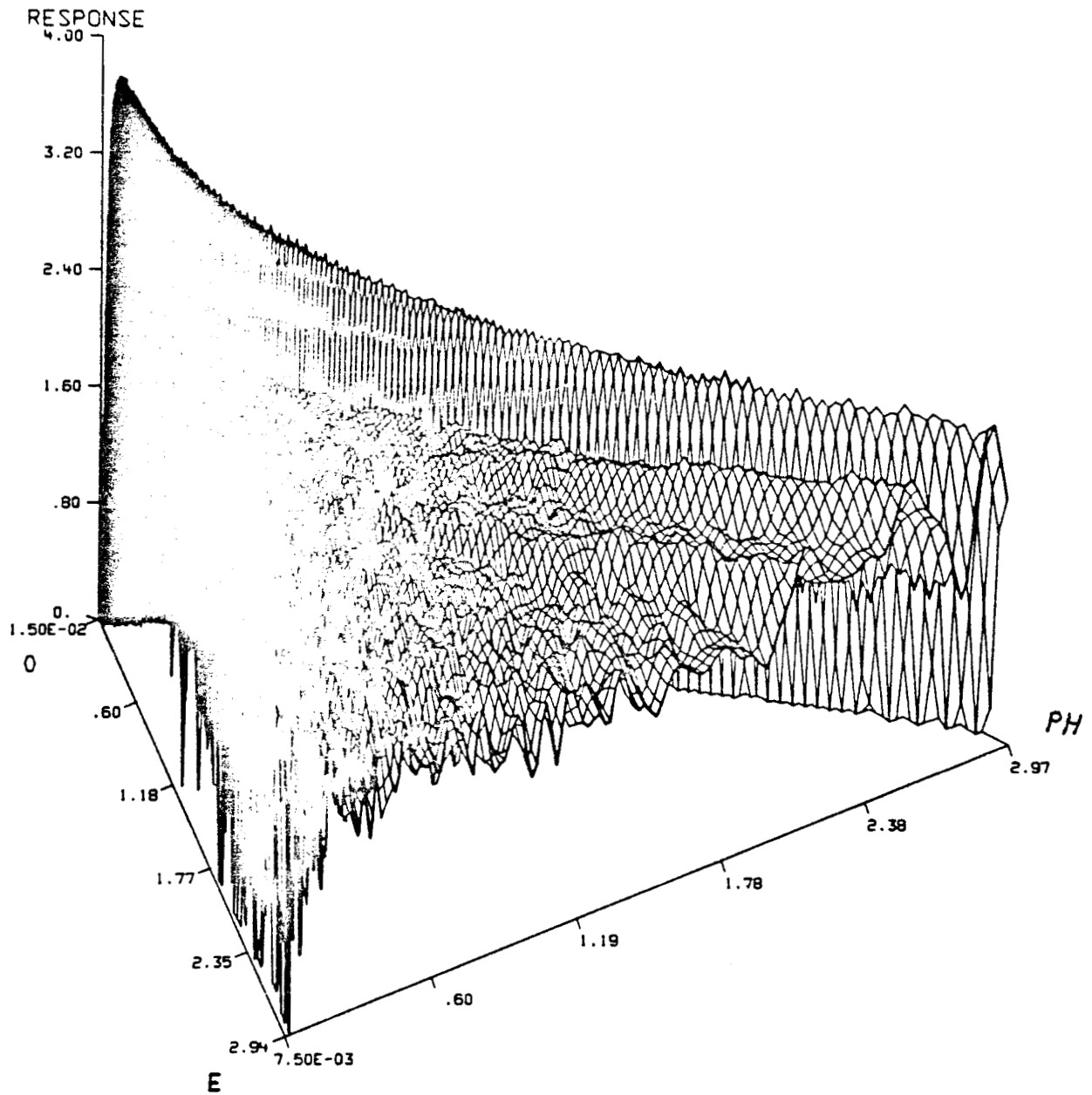
3

Fig. 1 The response function map calculated for a 7.62-cm-diam x 7.62-cm-long (3-in. x 3-in.) cylindrical NaI scintillator for incident photons having energies in the range of 15 keV to 2.94 keV. Both the energy (E) and pulse-height (PH) axes are visible. Note that the response axis is logarithmic (base 10).
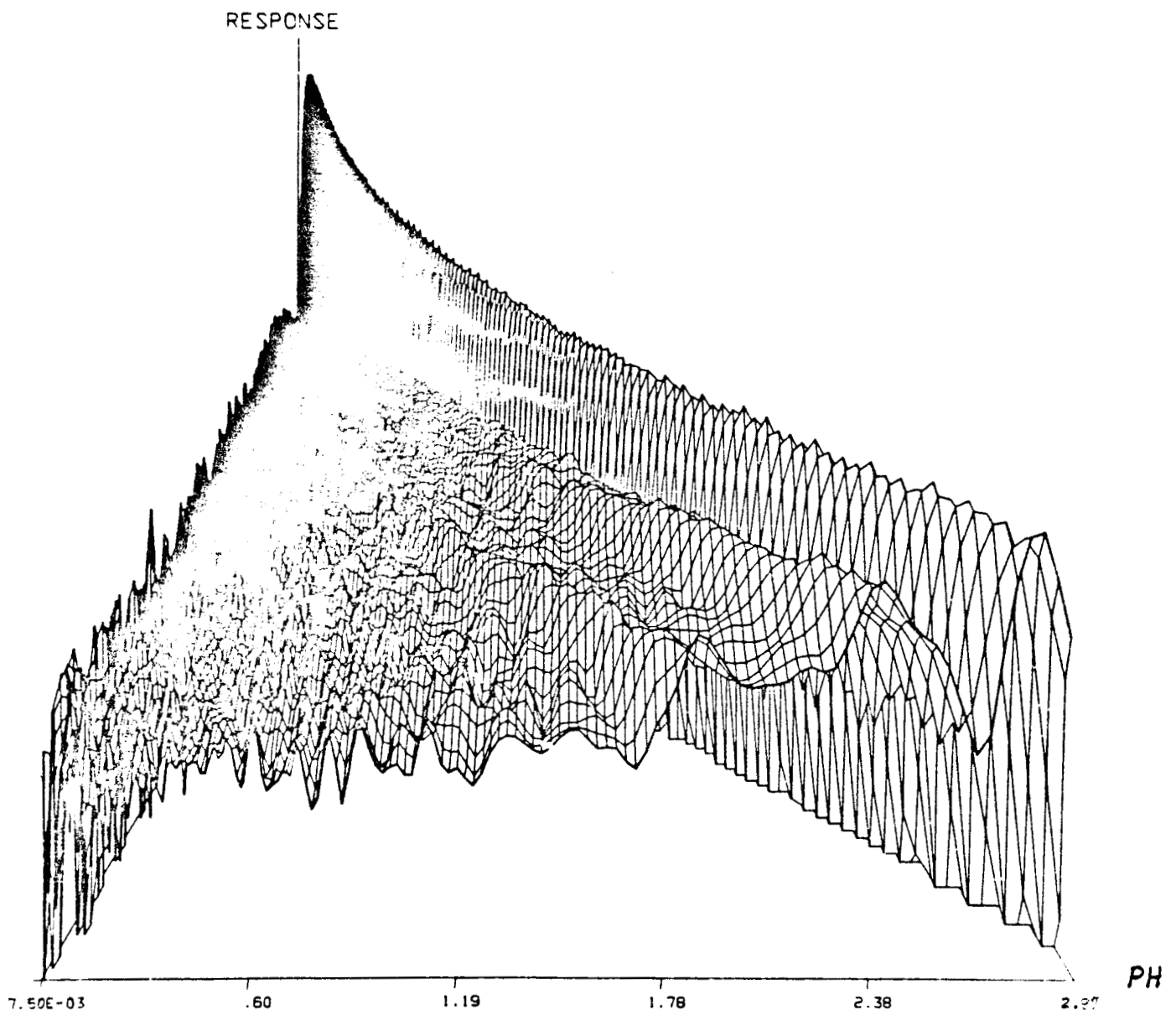
Fig. 2   The response function map of Fig. 1 viewed from a different perspective.   The map has been rotated clockwise about the response axis relative to Fig. 1.
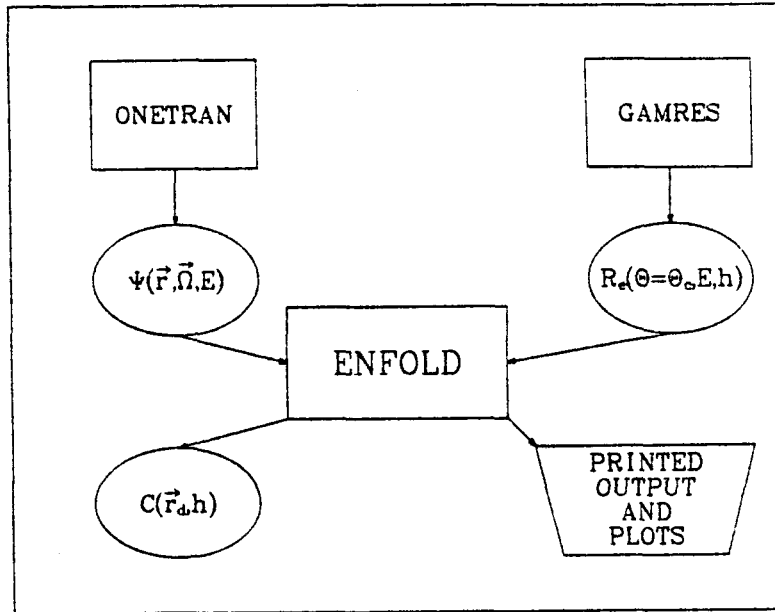
Fig. 3 Flowchart of method for calculating pulse-height distributions.
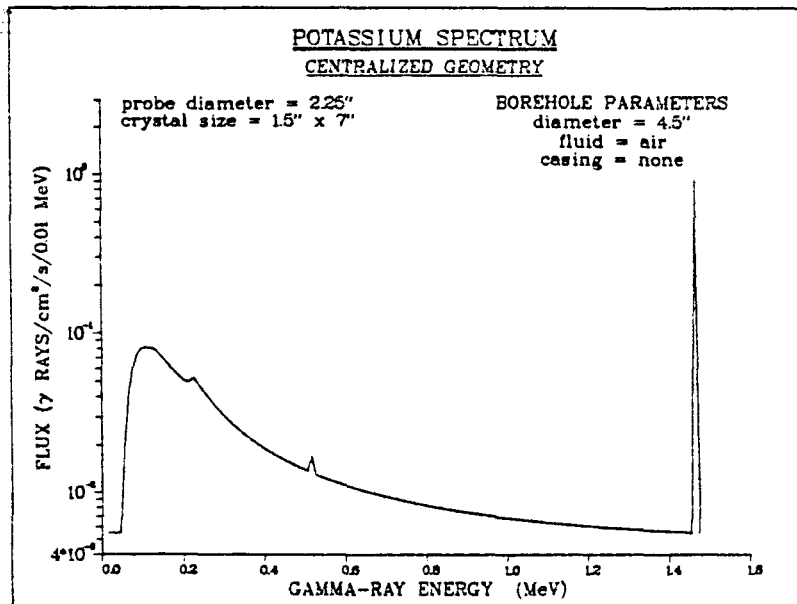
Fig. 4 Calculated flux spectrum at the center of an 11.43-cm (4.5-in.) diam, air-filled, uncased, infinitely long borehole. The borehole is surrounded by sandstone having a density of 2.14 g/cm^3 and a dry-weight potassium concentration of 16.48 per cent.
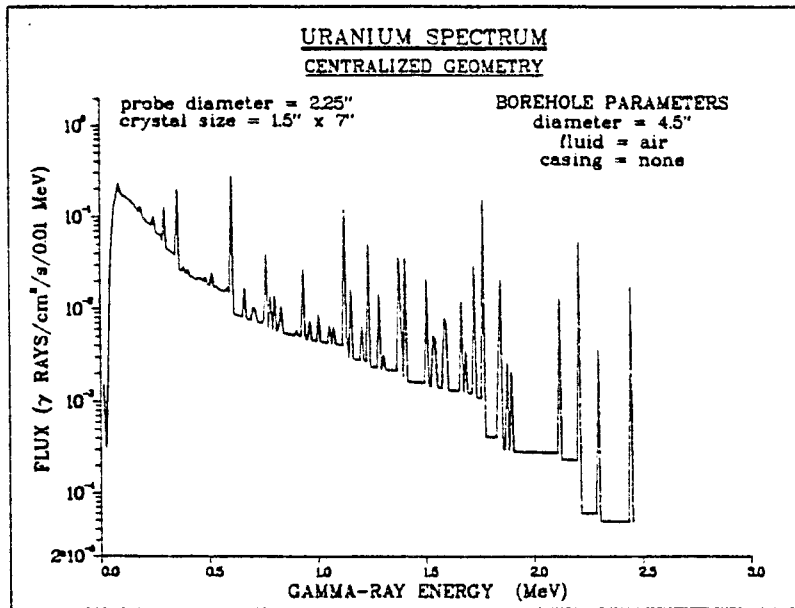
URANIUM SPECTRUM
CENTRALIZED GEOMETRY

probe diameter = 2.25"
crystal size = 1.5" x 7"

BOREHOLE PARAMETERS
diameter = 4.5"
fluid = air
casing = none

FLUX (γ RAYS/cm³/s/0.01 MeV)

GAMMA-RAY ENERGY (MeV)

Fig. 5 Flux spectrum calculated for a uranium source dry-weight concentration of 4.37 ppm. All parameters other than the source were identical to those for Fig. 4.
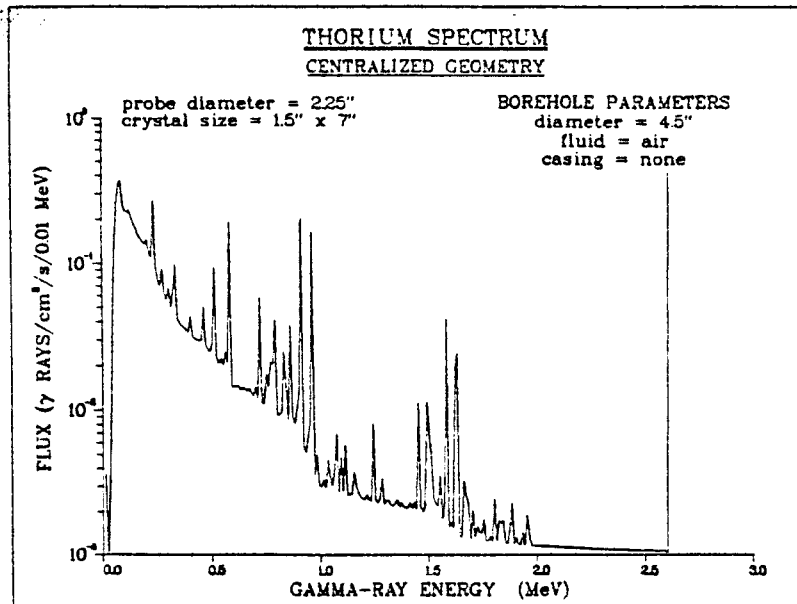

THORIUM SPECTRUM
CENTRALIZED GEOMETRY

probe diameter = 2.25"
crystal size = 1.5" x 7"

BOREHOLE PARAMETERS
diameter = 4.5"
fluid = air
casing = none

FLUX (γ RAYS/cm³/s/0.01 MeV)

GAMMA-RAY ENERGY (MeV)

Fig. 6 Flux spectrum calculated for a thorium source dry-weight concentration of 13.4 ppm. All parameters other than the source were identical to those for Fig. 4.

7

Figs. 7-9. The detector is inside a 2.25-in. o.d. probe shell having a 1/8-in.-thick iron wall. The formation and borehole parameters are identical to those used to compute the flux spectra of Figs. 4-6. These pulse-height spectra are written on a disk file so that further processing of the spectra can be performed to provide information on the change in spectral shape caused by varying borehole and/or detector parameters.

The accuracy of the count rate calculation method is demonstrated in Figs. 10-13. The first three figures compare theoretical pulse-height distributions with those observed in the K, U, and T borehole calibration models of the US Department of Energy (DOE) Grand Junction facility. The KUT models are used as standards for calibration of gamma-ray spectral logging equipment.[4] Each of the theoretical pulse-height distributions were synthesized from the individual K, U, and Th spectra of Figs. 7-9. Radioelement concentrations were assigned to each model from dry-weight chemical assays performed on samples taken from each model. These concentrations were used as weighting factors in synthesizing the composite pulse-height spectra of Figs. 10-12.

The calculation simulated as closely as practicable the calibration models, the logging probe, and the NaI detector contained in the probe. The radioelements were assumed to be homogeneously distributed in the formation surrounding the borehole. The pulse-height distributions were computed and measured with the logging probe sidewalled.

The comparisons between theoretical and experimental pulse-height distributions presented in Figs. 10-12 are absolute. No normalization of the theoretical count rate curves has been made. The agreement between theory and experiment is generally very good. All three comparisons exhibit a discrepancy at low pulse-height values caused by differences in the nonlinearity of the experimental NaI crystal and that assumed in the computer model. Measurement of the actual nonlinearity function for the detector crystal of interest and use of this function in the computer model would eliminate this discrepancy in pulse-height scaling between the theoretical and experimental distributions.

Examination of Fig. 10 reveals that the K, U, and Th grade assignments in the potassium model are perhaps too low, assuming that the synthesized theoretical spectrum is accurate. The energy resolution assumed for the NaI detector in the computer model appears to be slightly greater than that of the actual crystal, accounting for some of the discrepancy between the pulse-height distributions in the 1.46-MeV ^{40}K peak.

The agreement between the theoretical and experiment pulse-height distributions is best for the uranium model. The computed distribution predicts the response to better than 5 per cent for the 1.765-MeV peak of the uranium series. The divergence of the curves for pulse heights greater than about 2.6 MeV is due to the presence of an LED gain stabilization peak in the experimental spectrum, which, of course, is not simulated in the computer model.

The thorium model yielded the greatest discrepancy between theoretical and experimental spectra. The small disagreement for the 2.615-MeV peak of the thorium series is due, once again, to the slightly larger value of detector energy resolution assumed in the computer model. The apparent discrepancies near 1.1, 1.3, and 1.8 MeV correlate strongly with the occurrence of lines in the uranium series. This implies that the uranium concentration assumed in the calculation was too low, given that the computer model accurately predicts the response to the uranium series (as demonstrated in Fig. 11). These results serve to illustrate the usefulness of the count rate calculation method as an aid in assigning radioelement concentrations to calibration models in a self-consistent manner.

The comparisons of theoretical vs experimental pulse-height distributions shown in Figs. 10-12 are probably not the optimal way to evaluate the accuracy of the calculated spectra. Subtle differences in detector energy resolution and nonlinearity between the actual detector and the simulation make precise comparison of the pulse-height spectra difficult at best. These problems can be mitigated by comparing window count rates rather than channel count rates, since the former tend to average out small variations in the pulse-height spectra resulting from differences between the actual and simulated detector resolution and nonlinearity.
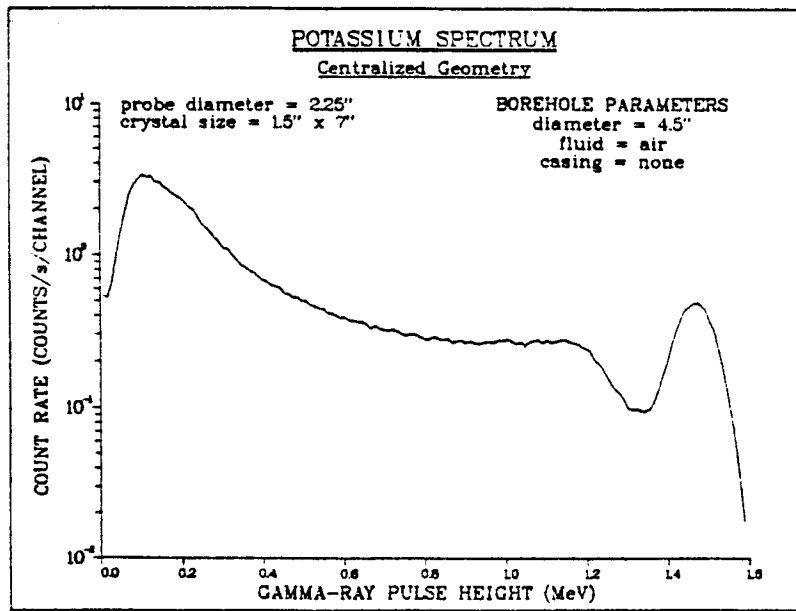
Fig. 7 Theoretical pulse-height spectrum for a 3.81-cm-diam x 17.78-cm-long (1-1/2 in. x 7-in.) NaI detector centered coaxially in a 11.43-cm-diam (4-1/2-in.-diam), air-filled, uncased borehole. The detector was contained within a probe having 0.32-cm (1/8-in.) iron walls and a 5.72 cm O.D. (2-1/4 in. O.D.). The pulse-height spectrum corresponds to the flux spectrum of Fig. 4 for a potassium source.
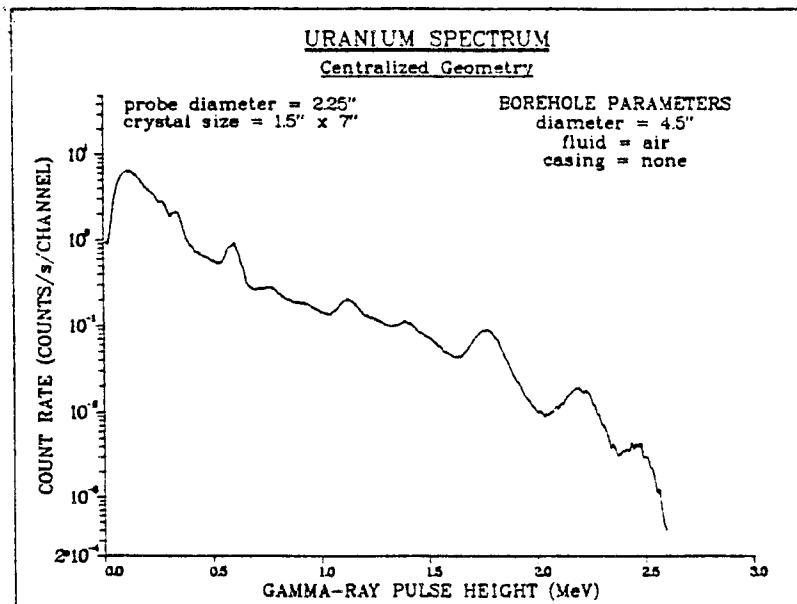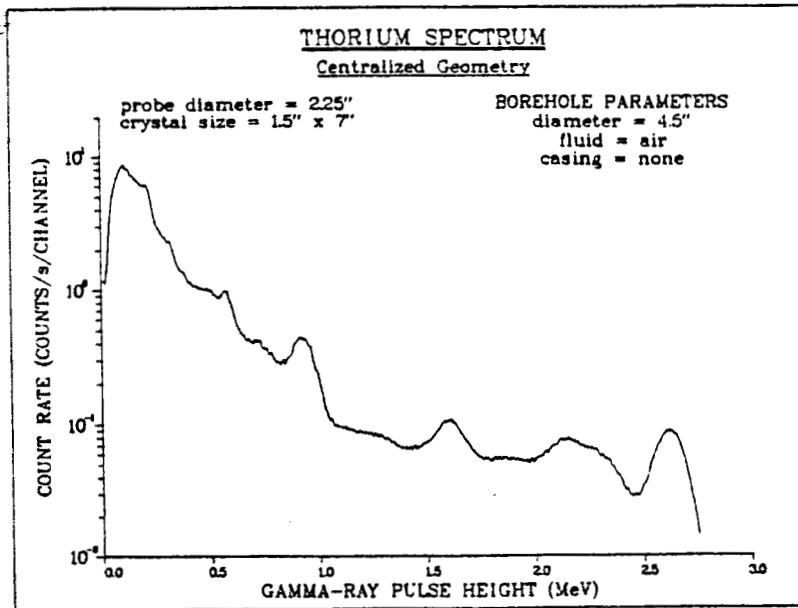

Fig. 8 Pulse-height spectrum computed for a uranium source dry-weight concentration of 4.37 ppm. All parameters, other than the source, were identical to those for Fig. 7.

THORIUM SPECTRUM
Centralized Geometry

probe diameter = 2.25"
crystal size = 1.5" x 7"

BOREHOLE PARAMETERS
diameter = 4.5"
fluid = air
casing = none

Fig. 9 Pulse-height spectrum computed for a thorium source dry-weight concentration of 13.4 ppm. All parameters other than the source were identical to those of Fig. 7.
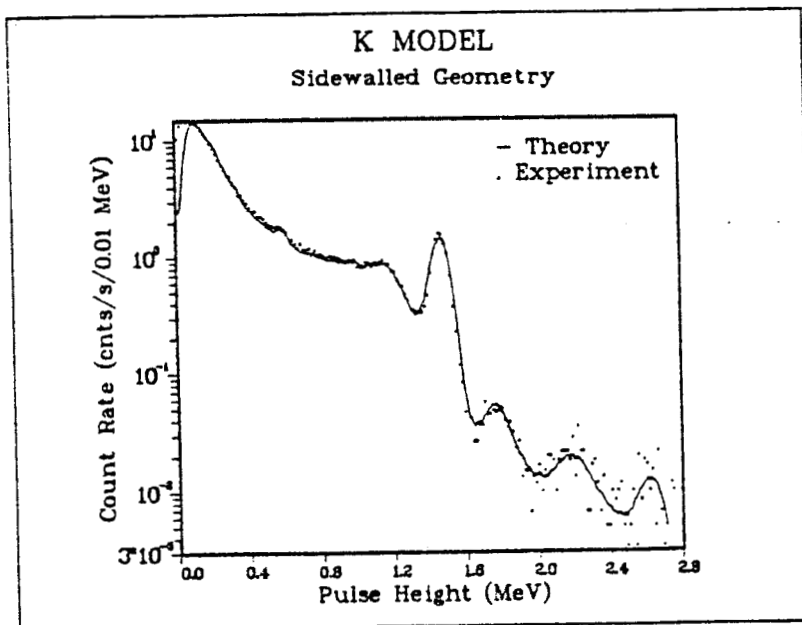

K MODEL
Sidewalled Geometry

– Theory
. Experiment

Fig. 10 Comparison of theoretical and experimental pulse-height spectra observed in the K model at the DOE Grand Junction calibration facility. The computed spectrum was synthesized from K, U, Th spectra similar to those of Figs. 7-9, assuming radioelement concentrations determined from sampling the K model and performing chemical analysis.
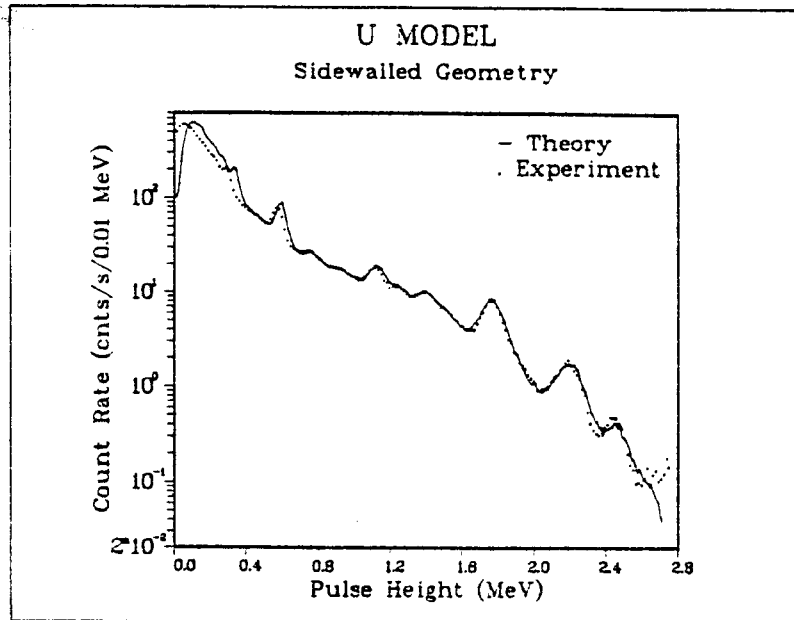
10

Fig. 11 Comparison between theoretical and experimental pulse-height distribu-
tions observed in the DOE Grand Junction U model. As in Fig. 10, the
comparison is between absolute count rates, that is, no normalization
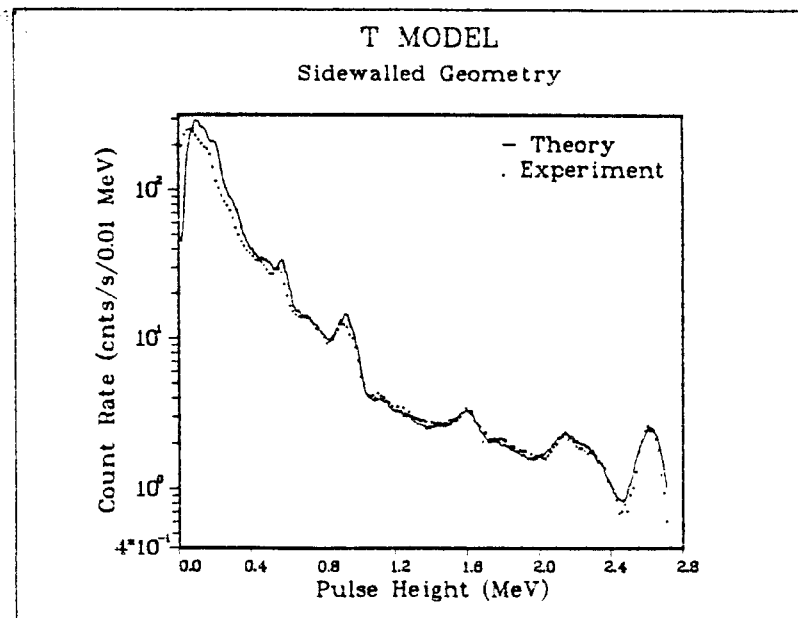has been performed on the count-rate values.

Fig. 12 Theoretical vs experimental pulse-height spectra observed in the DOE
Grand Junction Th model. The spectra of Figs. 10-12 assume the probe
is side-walled in the borehole.

11

A comparison between theoretical and experimental window count rates is shown in Fig. 13 for aerial gamma-ray spectral logging. The experimental window sensitivities were taken by Lovoorg[5] with a 3-in. by 3-in. NaI detector on the concrete calibration pads constructed at Riso National Laboratory in Denmark. The pads contain known K, U, and Th concentrations with the U and Th in secular equilibrium with their daughters. The detector was placed on the surface of the pads for data taking. The computer model simulated the actual physical configuration as closely as possible. In particular, the 3-in. by 3-in. NaI detector was modeled well with regard to energy resolution and pulse-height nonlinearity.

The theoretical KUT window sensitivities agree very well with the experimental values. The poorest agreement occurs for the thorium sensitivity, where the theoretical value is 7.7 per cent smaller than the experimental value. Data taken more recently by Lovoorg (but as yet unpublished) in a worldwide round robin study at many calibration facilities, suggests that a sensitivity of about 3.31 for potassium and 0.125 for thorium are more accurate average values. If this is so, then the agreement between the theoretical and experimental sensitivities improves to about 2.1 per cent for potassium, 1.4 per cent for uranium, and 4.0 per cent for thorium.

REFERENCES

1. T. R. Hill, "ONETRAN: A Discrete Ordinates Finite Element Code for the Solution of the One-Dimensional Multigroup Transport Equation," Los Alamos National Laboratory report LA-5590-MS (June 1975).

2. K. D. Lathrop and F. W. Brinkley, "TWOTRAN II: An Interfaced, Exportable Version of the TWOTRAN Code for Two-Dimensional Transport," Los Alamos National Laboratory report LA-4848-MS (July 1973).

3. M. L. Evans, "NDA Technology for Uranium Resource Evaluation," Los Alamos National Laboratory report LA-6996-PR (October 1977), 24-32.

4. M. A. Mathews, Carl. J. Koizumi, and Hilton B. Evans, "DOE-Grand Junction Logging Model Data Synopsis," DOE report GJBX-76(78).

5. L. Lovoorg, L. Botter-Jensen, P. Kirkegaard, and E. M. Christiansen, Nucl. Instru. and Meth., 167 (1979), 341.

KUT Window Sensitivities

Airborne Geometry

	S_K (cnts/s/%k)	S_U (cnts/s/ppmU)	S_T (cnts/s/ppmTh)
Experiment (Lovborg)	3.17	0.288	0.130
Theory (Evans)	3.38	0.284	0.120

Fig. 13 Comparison of theoretical vs experimental KUT window sensitivities for aerial gamma-ray spectrometric surveys.

Spatial Deconvolution

Spatial Deconvolution for Spectral Gamma-Ray Logging

David C. Stromswold

Robert D. Wilson

Bendix Field Engineering Corporation

Grand Junction, Colorado 81502

The process of logging a formation often provides an inaccurate represen-
tation of the spatial distribution of radioactive materials, especially when
the formation contains thin zones of ore. The log shows a general representa-
tion of the ore's distribution, but sharp zone changes are washed out and
appear on the log as gradual transitions. The data can be deconvolved
spatially to produce a better representation of the formation if the response
of the detector to thin zones is known. This response can be measured
directly in calibration models such as the thin-bed models, or it can be
calculated from logging data collected in thick-zone models which have a sharp
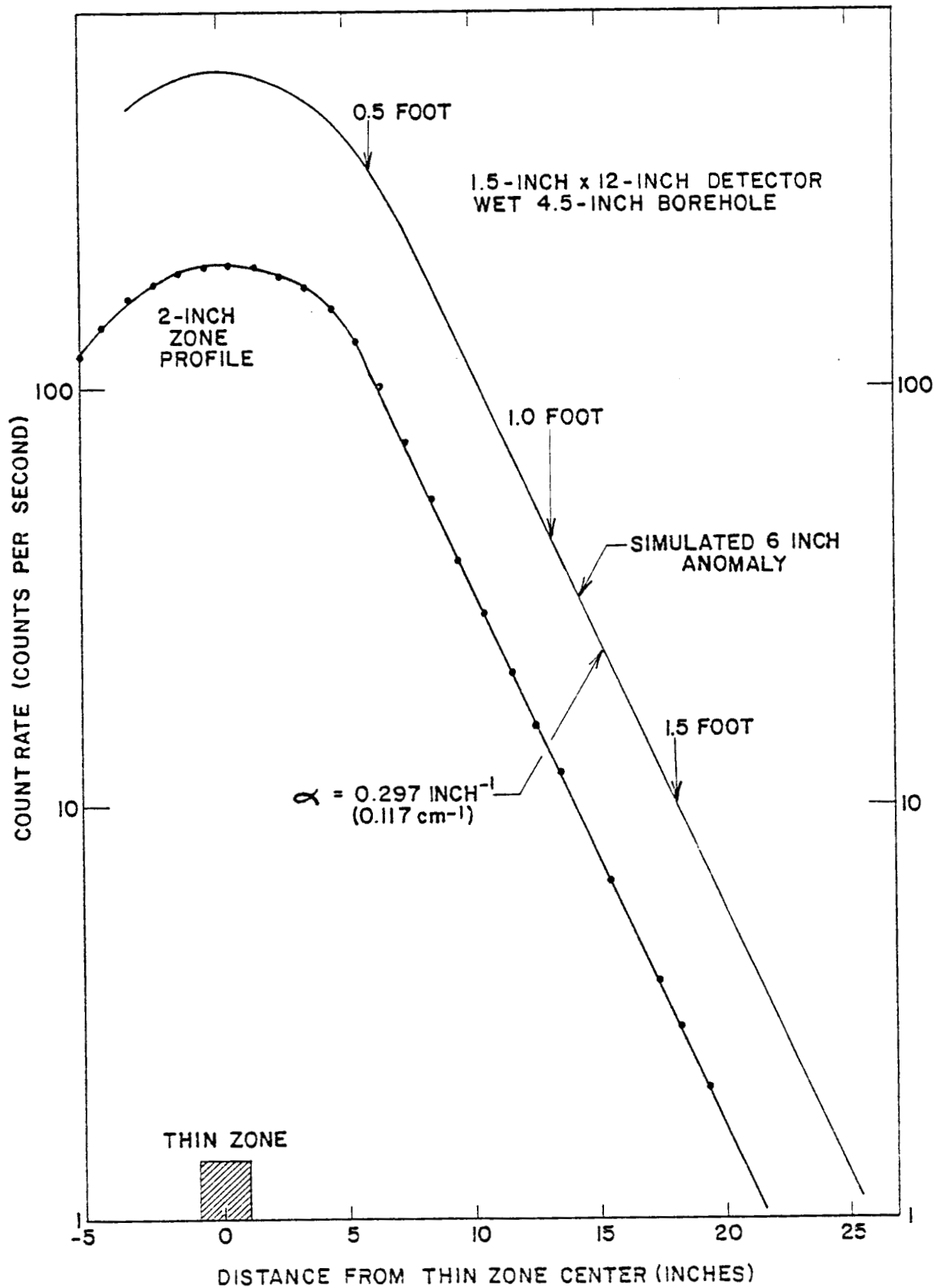transition between an ore zone and a barren zone.

Two techniques for spatially deconvolving gamma-ray logs have been used:
GAMLOG, which deconvolves using a series of half-foot weighting coefficients,
and the inverse digital filter based on an exponential fall-off of the signal
from thin zones. Data were collected in the calibration models to determine
spatial deconvolution parameters for a 1.5-inch x 12-inch NaI detector and a
filtered 1-inch x 6-inch NaI detector in a 2.1-inch diameter probe having a
0.1-inch-thick steel wall.

GAMLOG

In the GAMLOG technique (Scott, 1963), an iterative procedure is used to
calculate a series of 0.5-foot-thick anomalies. Weighting factors for 0.5-foot
intervals comprise a symmetric 5-point filter which is passed over the
logging data to sharpen the log's transitions between zones of differing ore
grades. The weighting factors can be determined experimentally for the
uranium energy window using the 90° bed of the thin-bed calibration model.
The simulated half-foot anomaly needed for GAMLOG can be obtained from the
2-inch-thick zone data from the thin-bed model by summing logging data from
three adjacent 2-inch zones. When this was done for a 1.5-inch x 12-inch
detector, the data in Figure 1 were obtained for a simulated half-foot
anomaly. The data in the figure have already had background subtracted as
determined in the barren portion of the model far from the ore zone. The
curve drawn through the data is a visual fit to the points. GAMLOG weighting
coefficients can be determined from the relative counting rates at 0.5-foot
intervals from the peak at the center of the simulated ore zone. Resulting
coefficients are listed in Table 1 for the case with the borehole dry and
water filled (as in Figure 1). Weighting coefficients are also listed for the
filtered 1-inch x 6-inch detector with the borehole dry. Notice that the
coefficients for the 1-inch x 6-inch detector fall off more rapidly from the
center value than do the ones for the 1.5-inch x 12-inch detector. This is in
agreement with expectations that a long detector will have a more spread out

FIGURE 1

URANIUM WINDOW THIN ZONE RESPONSE

1.5-INCH x 12-INCH DETECTOR
WET 4.5-INCH BOREHOLE

0.5 FOOT

1.0 FOOT

SIMULATED 6 INCH ANOMALY

1.5 FOOT

2-INCH ZONE PROFILE

$\alpha = 0.297 \text{ INCH}^{-1}$
(0.117 cm^{-1})

THIN ZONE

COUNT RATE (COUNTS PER SECOND)

DISTANCE FROM THIN ZONE CENTER (INCHES)

spatial response to a thin zone than will a short detector. The addition of water to the 4.5-inch borehole had little effect on the weighting coefficients for the 1.5-inch x 12-inch detector.

Table 1. GAMLOG Weighting Coefficients for Uranium Window.

Detector	Hole (4.5-inch)	Distance (feet) 0.0	0.5	1.0	1.5
1.5 x 12	Dry	1.000	0.570	0.108	0.020
1.5 x 12	Wet	1.000	0.573	0.105	0.018
1 x 6 filtered	Dry	1.000	0.365	0.060	0.010

The coefficients in Table 1 must be normalized to their sum so that they do not affect the grade-thickness product of the log. For example, the values for the 1.5-inch x 12-inch detector in the dry hole must be divided by $1.000 + 2(0.570) + 2(0.108) + 2(0.020) = 2.396$ to obtain proper normalization. In addition, the coefficients listed are only for the uranium energy window, but in the absence of thin-bed models for determining weighting coefficients for potassium and thorium, the values in Table 1 are assumed to be approximately correct for K and Th also.

Inverse Filter

A second method of spatially deconvolving gamma-ray logs is the inverse digital filter technique (Conaway and Killeen, 1978). This is a noniterative method which assumes that the response of a point-sized detector to an infinitesimally thin zone is the double-sided exponential

$$I(z) = \frac{\alpha}{2} \exp(-\alpha|z|)$$

The constant alpha (α) depends on several factors including borehole diameter and fluid content. The inverse filter used to deconvolve a gamma-ray log consists of three coefficients:

$$\frac{-1}{(\alpha\Delta z)^2} \, , \quad 1 + \frac{2}{(\alpha\Delta z)^2} \, , \quad \frac{-1}{(\alpha\Delta z)^2}$$

where Δz is the digital sampling interval along the borehole.

Values of alpha can be determined from thin-zone models directly or by differentiating the count rates obtained from logging an interface between thick zones of a model having a large grade difference. The differentiation produces a hypothetical count rate profile that would be observed from an infinitesimally thin ore zone located at the interface between the two thick zones. When the profile is plotted on semilogarithmic paper, the slope of the curve gives the value of alpha (Conaway, 1980).

Data from the thin-bed model were used to determine alpha for the 1.5-inch x 12-inch and filtered, 1-inch x 6-inch detectors. After plotting background subtracted count rates on a semilogarithmic graph, the data which fell along straight lines were entered in an exponential curve fitting routine to

determine alpha. In this way, tails of the curves which departed from an exponential relationship were avoided, and possibly better values of alpha were obtained than would have been determined from strictly graphical methods. Resulting values of alpha are given in Table 2 for the uranium energy window. In the absence of suitable thin-bed models for K and Th, these same values are assumed to be correct for K and Th also.
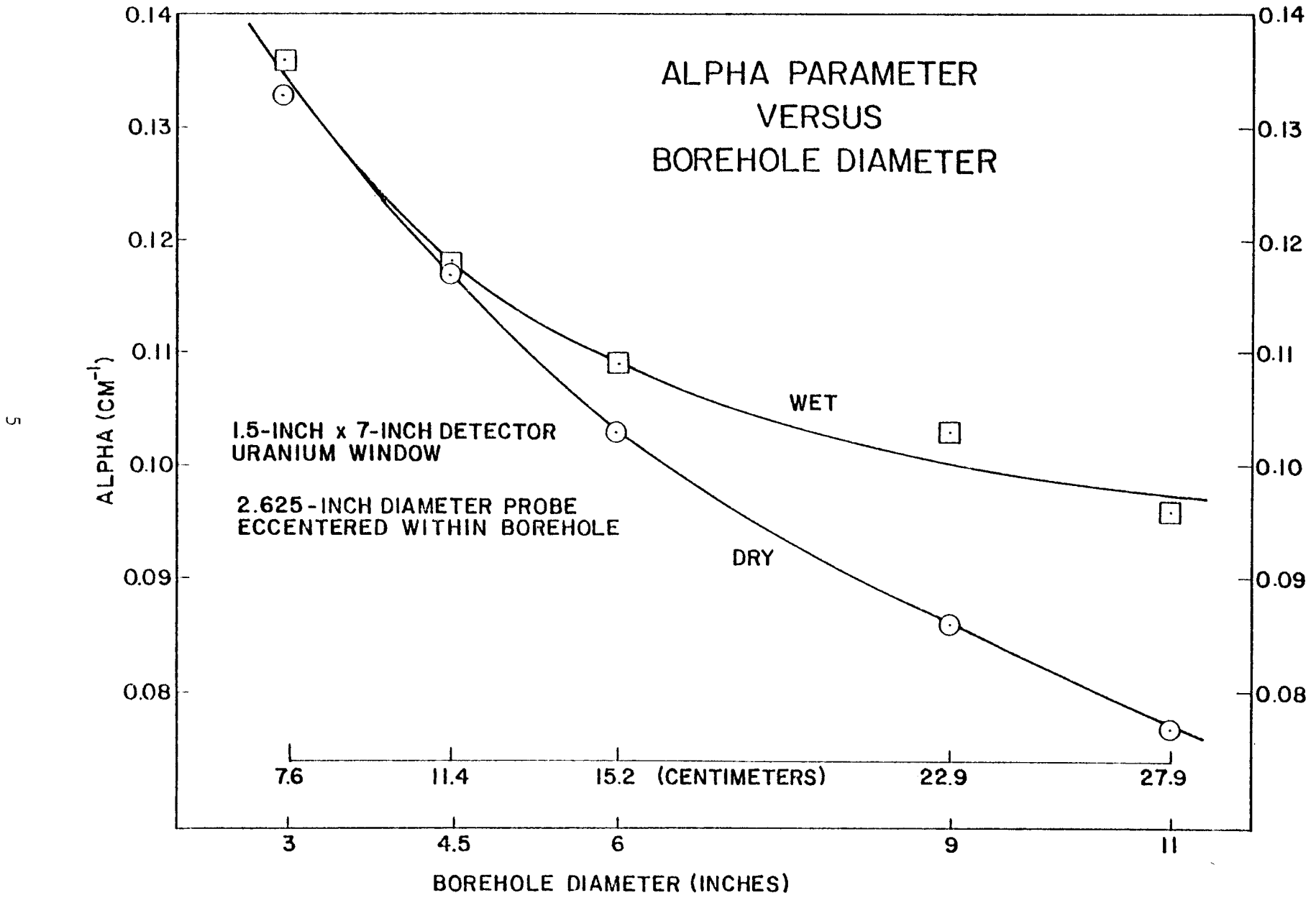
Table 2. Alpha Parameters from Thin-Bed Model

Detector	Hole (4.5-inch)	Alpha in^{-1}	Alpha cm^{-1}
1.5 x 12	Dry	0.286	0.113
1.5 x 12	Wet	0.297	0.117
1 x 6 filtered	Dry	0.299	0.118

The variation of alpha with hole diameter was determined from data collected in the D Model using a 1.5-inch x 7-inch NaI(Tℓ) detector in a 2.6-inch-diameter probe having a 0.1-inch-thick steel shell. Logging data were collected across the ore zone/barren zone interface in holes of diameter 3 to 11 inches for both dry and water-filled conditions. The values of alpha obtained are given in Table 3 and plotted in Figure 2. At small hole diameters (4.5 inches and less), the alphas show little significant difference between the wet and dry holes. However, for the larger holes, alpha is distinctly smaller when the holes are dry. The smaller alphas imply that the signal from a thin zone falls off less rapidly in air than it does in water. The decreased fall off in air is reasonable from attenuation considerations applied to gamma-ray propagation through the air or water of the borehole.

Table 3. Alpha Parameters for 1.5-inch x 7-inch NaI Detector.

Hole Diameter (inches)	Alpha (in^{-1}) dry	wet	Alpha (cm^{-1}) dry	wet
3	0.338	0.346	0.133	0.136
4.5	0.298	0.301	0.117	0.118
6	0.261	0.276	0.103	0.109
9	0.214	0.262	0.084	0.103
11	0.196	0.244	0.077	0.096

FIGURE 2

ALPHA PARAMETER
VERSUS
BOREHOLE DIAMETER

1.5-INCH x 7-INCH DETECTOR
URANIUM WINDOW

2.625-INCH DIAMETER PROBE
ECCENTERED WITHIN BOREHOLE

WET

DRY

ALPHA (CM^{-1})

(CENTIMETERS)

7.6   11.4   15.2   22.9   27.9

BOREHOLE DIAMETER (INCHES)

3   4.5   6   9   11

References

Conaway, J. G., 1980, Direct determination of the gamma-ray logging system response functions in field boreholes: Geoexploration, v. 18, p 187-199.

Conaway, J. G. and P. G. Killeen, 1978, Quantitative uranium determinations from gamma-ray logs by application of digital time series analysis: Geophysics, v. 43, p. 1204-1221.

Scott, J. H., 1963, Computer analysis of gamma-ray logs: Geophysics, v. 28, p. 457-465.

EXPERIMENTAL SPATIAL DECONVOLUTION

PARAMETERS FOR GROSS GAMMA-RAY LOGGING

David C. Stromswold

Bendix Field Engineering Corporation

The process of obtaining a gamma-ray log of a formation often provides an inaccurate representation of the spatial distribution of radioactive materials, especially when the formation contains thin zones of ore. The log shows a general representation of the ore's distribution, but sharp zone changes are washed out and appear on the log as gradual transitions. The logging speed, gamma-ray path length through the formation, and the length of the detector contribute to the creation of the gradual transitions rather than the sharp boundaries which may actually be present. This smearing does not affect the total grade-thickness product, but it is often desirable to know the grades and thicknesses of the ore layers separately.

The logging data can be deconvolved spatially to produce a better representation of the formation if the response of the detector to thin zones is known. This response can be measured directly in calibration models such as the Grand Junction thin-bed models, or it can be calculated from logging data collected in other models where there is a sharp transition between a thick ore zone and a thick barren zone. The calculational approach with thick zones was chosen for this study because a variety of hole diameters was desired and the gross gamma-ray water-factor model provided the necessary hole diameters.

GAMLOG Parameters

Two techniques for spatially deconvolving gamma-ray logs are used in the uranium exploration industry. The first one is the iterative procedure used in the program GAMLOG to resolve a series of half-foot concentration anomalies. In this technique, weighting factors are determined for half-foot intervals from a hypothetical anomaly which is 0.5-foot thick and within which the radioelemental concentration is uniform. These weighting factors comprise a symmetric five-point filter which is passed over the original logging data to sharpen the log's transitions between zones of differing ore grades.

The weighting factors can be determined experimentally by logging through an ore zone/barren zone interface in a calibration model. The response of the probe to a hypothetical half-foot anomaly positioned at the interface between the two thick zones can be calculated from the logging data by subtracting count rates separated by half-foot intervals in the original log (Scott, 1963). When the count rate differences are plotted, a curve is obtained which peaks at the location of the interface and falls off on each side. From the magnitude of the curve at the peak and at successive half-foot intervals on each side of the peak, the weighting factors are obtained. For ease of comparison, the weighting factor for the peak is generally assigned the value 1.00 and the other weighting factors are expressed as fractions of this peak height (e.g., 0.23 for the 0.5-foot points, 0.04 for the 1.0-foot points, and

0.01 for the 1.5-foot points). When the weighting factors are applied to logging data, they are normalized to give a total weight of unity so that the grade-thickness product is not disturbed. Thus each weighting factor is divided by the sum of all the weighting factors [e.g., they are divided by 1.00 + 2(0.28) + 2(0.04) + 2(0.01) = 1.66]. This division will not be included in the results presented here, however, because it complicates comparison of weighting factors determined for different borehole conditions.

Weighting factors have been determined for the filtered Bendix probe using the method described above. [This probe has an outside diameter of 2.4 inches, and it contains a 1.25 x 1.75-inch filtered NaI(Tl) detector.] Logging data were collected with the probe sidewalled in three different diameter holes of the gross-gamma water-factor model. A plot of the count rates obtained in the dry 4.5-inch diameter hole is shown in Figure 1 as an example of the data. The corresponding simulated half-foot anomalies obtained by subtracting count rates at half-foot intervals are shown in Figure 2. In that figure the peak on the left represents a half-foot thick anomaly positioned at the interface between the ore zone and the upper barren zone; the peak on the right represents a half-foot thick anomaly at the interface between the ore zone and the lower barren zone. Note that the curve in the center region between the two peaks is not well defined because of the large scattering of the points. The scattering there is due to the large uncertainty obtained from subtracting high count rates which are almost the same in magnitude through the center region of the model.

Weighting factors calculated from the barren zone portions of the count-rate difference curves are given in Table 1. The weighting factors increase as the hole diameters increase because the gamma rays travel farther through the borehole than they would through the concrete of the model. The increased penetration distance results in a greater percentage of the gamma rays reaching the detector when it is far from the anomaly. For the 4.5-inch hole, the same values for the weighting factors were obtained for both dry and wet holes due to the uncertainty in the experimental results. Ideally, the weighting factors should have been slightly smaller for the wet hole due to the decreased range of the gamma rays through water.

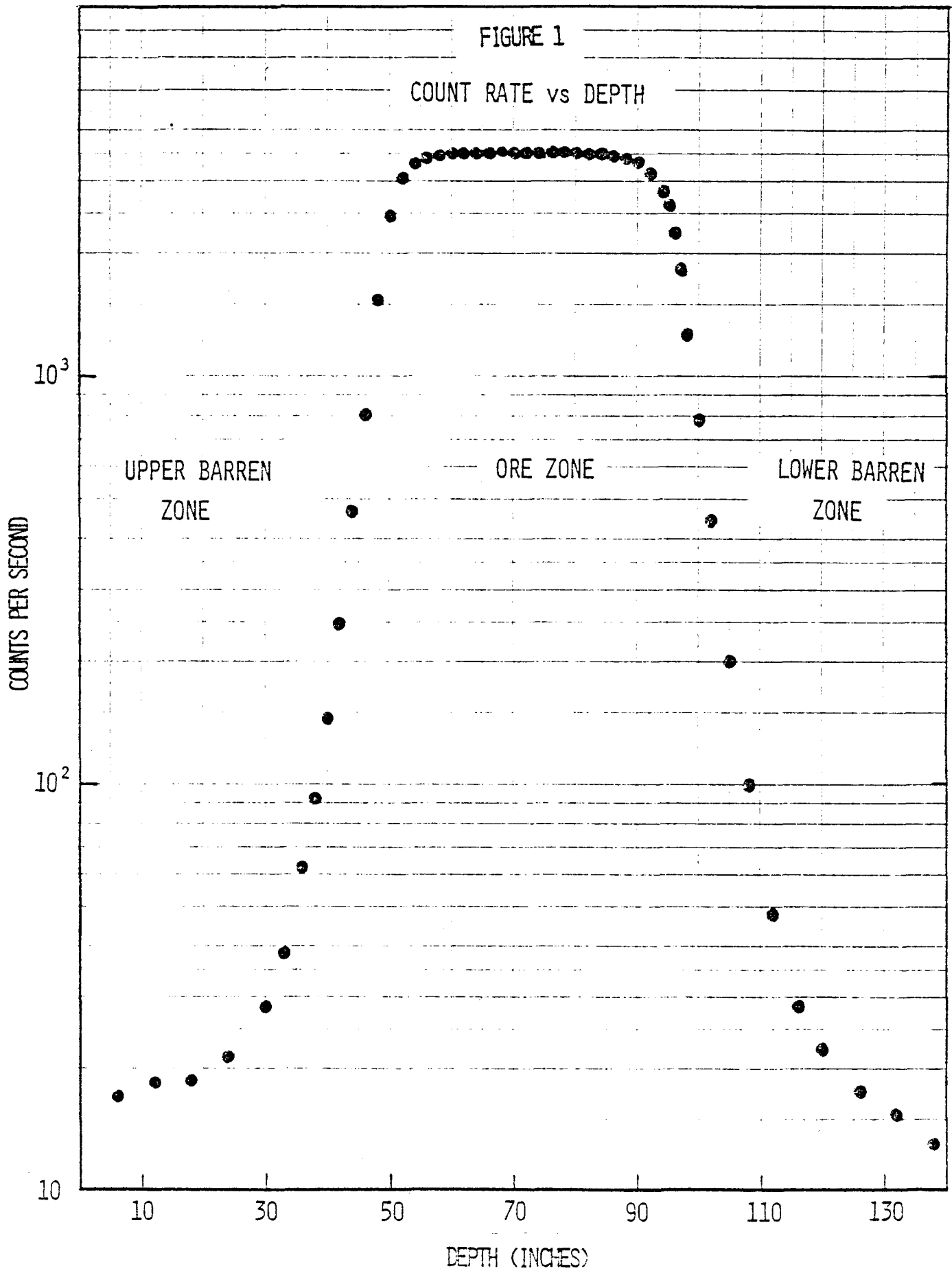Table 1. Weighting Factors for Filtered Bendix Probe

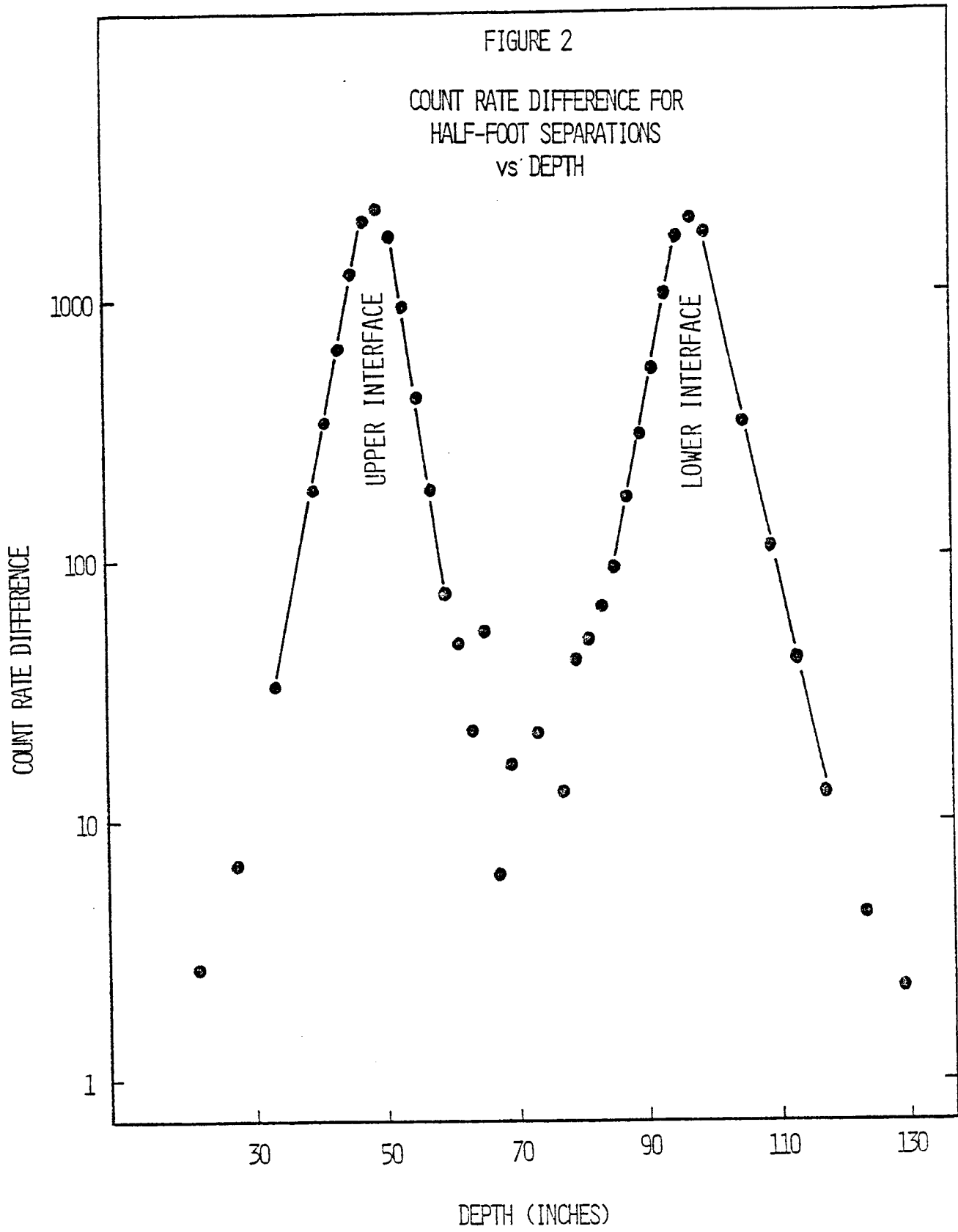| Hole Diameter (inches)	Hole Condition	Weighting Factors*			
		0.0 ft	0.5 ft	1.0 ft	1.5 ft
4.5	Dry	1.00	0.28	0.04	0.01
4.5	Wet	1.00	0.28	0.04	0.01
6.6	Wet	1.00	0.30	0.05	0.01
8.6	Wet	1.00	0.31	0.06	0.01

*Estimated uncertainty in weighting factors is ± 0.01.

Weighting factors were also determined for the Century 9055 probe (1.8-inch outside diameter, unfiltered 0.875 x 4-inch NaI detector). They are presented in Table 2 for the probe sidewalled in holes of diameter 2.4 inches to 8.6 inces in both dry and water-filled conditions. For dry holes the 0.5-foot weighting factors vary from 0.27 for the 2.4-inch hole to 0.41 for the 8.6-inch hole. This is a 47 percent variation when compared to the value

FIGURE 1

COUNT RATE vs DEPTH

UPPER BARREN ZONE — ORE ZONE — LOWER BARREN ZONE

COUNTS PER SECOND

DEPTH (INCHES)

3

FIGURE 2

COUNT RATE DIFFERENCE FOR
HALF-FOOT SEPARATIONS
vs DEPTH

for the 4.5-inch hole. The same weighting factor varies by 38 percent when the holes are filled with water. The greater variation in the air-filled holes is explained by the increased range of the gamma-rays through air.

Table 2. Weighting Factors for Century

Model #9055 Probe

Hole Diameter (inches)	Hole Condition	Weighting Factors*			
		0.0 ft	0.5 ft	1.0 ft	1.5 ft
2.4	Dry	1.00	0.27	0.04	0.00
2.4	Wet	1.00	0.27	0.03	0.01
4.5	Dry	1.00	0.30	0.05	0.01
4.5	Wet	1.00	0.29	0.05	0.01
6.6	Dry	1.00	0.38	0.09	0.02
6.6	Wet	1.00	0.33	0.06	0.01
8.6	Dry	1.00	0.41	0.11	0.03
8.6	Wet	1.00	0.38	0.08	0.02

*Estimated uncertainty in weighting factors is ± 0.01.

Inverse Filter Alpha Parameters

A second method for spatially deconvolving gamma-ray logs is the inverse filter technique espoused by Conaway and Killeen (1978) of the Geophysical Survey of Canada. This is a non-iterative technique that assumes the response of a point-sized detector to an infinitesimally thin zone is the double-sided exponential

$$I(z) = \frac{\alpha}{2} \exp(-\alpha|z|) \tag{1}$$

The constant alpha (α) depends on several factors including borehole diameter and fluid content, and z is the distance of the detector from the thin zone.

Values of alpha can be determined from thin-zone models directly or from differentiating the count rates obtained from logging an interface between two thick zones of a model. The differentiation produces a hypothetical count rate profile that would be observed from an infinitesmally thin ore zone located at the interface between the two thick zones. When the profile is plotted on semilogarithmic paper, the slope of the curve gives the value of alpha (Conaway, 1980).

In the present experiments, the values of alpha were obtained by first plotting the differential count rates on semilogarthmic graphs and then selecting the data which fell along straight lines in the barren zone for entry into an exponential curve fitting routine to determine alpha. In this way, tails of the curves which departed from an exponential relationship were avoided, and better values of alpha were obtained than could be determined from strictly graphical methods. The results for the filtered Bendix probe sidewalled in the gross gamma-ray water model are shown in Table 3 for hole diameters from 4.5 inches to 8.6 inches. For water-filled holes, the value of alpha decreased from 0.31-inch^{-1} to 0.27-inch^{-1} as the hole diameter

5

increased from 4.5 inches to 8.6 inches. This corresponds to a 13 percent change in alpha as a function of water-filled hole size. The smaller values of alpha mean that the gamma-rays are less attenuated in the larger diameter water filled holes. This is reasonable because the gamma-rays will travel farther through water than through the concrete of the calibration model. Only the 4.5-inch hole was logged dry, and a value of 0.29-inch^{-1} was obtained for alpha. The decrease in alpha from 0.31-inch^{-1} for the same hole filled with water is again consistent with attenuation differences for gamma rays in air and in water.

Table 3. Alpha Parameters for Filtered Bendix Probe.

Hole Diameter (inches)	Hole Condition	Alpha (inch^{-1})
4.5	Dry	0.29
4.5	Wet	0.31
6.6	Wet	0.30
8.6	Wet	0.27

Values of alpha were also determined for the Century 9055 probe side-walled in the gross gamma water model, and they are given in Table 4. Both dry and water-filled holes of diameter 2.4 inches to 8.6 inches were used. Over this range of diameters, alpha varied from 0.34-inch^{-1} to 0.23-inch^{-1} in the dry holes and from 0.34-inch^{-1} to 0.27-inch^{-1} in the water-filled holes. These values correspond to 37 percent and 22 percent variations for the dry and water-filled holes, respectively, as compared to the alphas for the standard 4.5-inch hole. Alpha for the Century probe changes more rapidly with hole size than it does for the Bendix probe. This is due to the unfiltered condition of the Century probe. The absence of a filter makes a probe more sensitive to the low energy gamma-rays which are strongly influenced by borehole conditions. The filter in the Bendix probe removes most of the low energy gamma-rays, and changes in that part of the spectrum do not affect the observed count rates strongly.

Table 4. Alpha Parameters for Century Probe.

Hole Diameter (inches)	Hole Condition	Alpha (inch^{-1})
2.4	Dry	0.34
2.4	Wet	0.34
4.5	Dry	0.30
4.5	Wet	0.32
6.6	Dry	0.24
6.6	Wet	0.29
8.6	Dry	0.23
8.6	Wet	0.27

References

Conaway, J. G., 1980, Direct determination of the gamma-ray logging system response functions in field boreholes: Geoexploration, v. 18, p 187-199.

Conaway, J. G. and P. G. Killeen, 1978, Quantitative uranium determinations from gamma-ray logs by application of digital time series analysis: Geophysics, v. 43, p. 1204-1221.

Scott, J. H., 1963, Computer analysis of gamma-ray logs: Geophysics, v. 28, p. 457-465.

SPATIAL DECONVOLUTION APPLIED TO GAMMA RAY LOGGING: A REVIEW

John G. Conaway
McPhar Geophysics

Introduction and Background

Ideally, we would like gamma ray logs to give exact information
regarding the quantity and distribution of radioactive material (say,
uranium ore) with depth along a borehole. In this ideal gamma ray
log, radiation itensity I would be exactly proportional to the radio-
element concentration or grade G at any given depth, or G = KI where K
is the system calibration constant or K=factor. In practice, many
factors interfere with this ideal, and distort the shape of the log.
Data processing techniques of several types can be used to reduce this
distortion, thereby causing the processed gamma ray log to approach the
desired ideal. These techniques as a group can be termed spatial
deconvolution techniques.

Among the factors which limit spatial resolution in gamma ray logs
are the effect of the analog ratemeter time constant (for analog systems),
the effect of detector length, and the effect of borehole parameters
including diameter, casing, and fluid. In general, the most significant
distortion results from the fact that the gamma rays from a radioactive
zone obviously are not constrained to travel in that zone, but, in fact,
propagate in all directions; solid rock is translucent to gamma rays.
Thus, a thin radioactive zone perpendicular to the borehole (Figure 1a)
does not cause a sharp anomaly as shown in Figure 1b, but rather a
smeared anomaly spread over perhaps 1 - 2 m perpendicular to the thin

zone (Figure 1c). This smeared anomaly may be called the geologic

impulse response, a term meant to indicate that the smearing is

unavoidably inherent in the physical situation, and is not a result

of instrument deficiencies or other external effects. The geologic

impulse response is a function of gamma ray energy, and formation

parameters such as density, fluid content, and equivalent atomic

number

The relationship between radioelement distribution and gamma ray

log response has been considered theoretically and experimentally by

a number of authors. Suppe (1957) summarized the Russian effort to

that date. Further work by Suppe and Khaykovich (1960) and Davydov (1970)

laid the foundation for the concept of the geologic impulse response,

which was introduced by Conaway and Killeen (1978a). In addition,

Davydov proposed an inversion (spatial deconvolution) scheme which, with

some modification, has proven quite useful in dealing with the geologic

impulse response. Roesler (1965) applied gamma ray logging for making

quantitative determinations of K_2O in East German potash deposits. His

work is notable especially for his consideration of the relationship

between detector length and spatial resolution; Roesler did not suggest

a solution for this problem. J.A. Czubek has expended considerable

effort over the course of his career on describing theoretically the

shape of gamma ray anomalies (Czubek, 1961; 1962; 1969) and on the

spatial deconvolution problem (Czubek, 1971; 1972). Jonas (1975)

attempted to apply some of Czubek's numerical deconvolution techniques,

however, Czubek and Zorski (1976) report that Jonas applied the

techniques incorrectly. Jonas has certainly not been alone in his problems in applying Czubek's interpretation techniques. The level of knowledge in nuclear theory and mathematics required to follow much of Czubek's important work in nuclear logging is unfortunately beyond the experience of the majority of applied geophysicists.

In North America, parallel effort has lead to other numerical interpretation techniques for gamma ray logs. In particular, Scott et al (1961) demonstrated that, although the expression $G = KI$ is not valid for unprocessed gamma ray logs, under ideal conditions the average grade $\overline{G}$ over a complete gamma log anomaly having area A (from background to background) can be computed from $\overline{G} = KA/T$ where T is the total thickness of the radioactive zone, and K is the same calibration factor described earlier. Scott (1962) and Scott (1963) presented a computer program which was designed to improve the accuracy of gamma ray logs for determining the distribution of radioactive material. This was the well-known GAMLOG program, which represented the earliest application of spatial deconvolution to gamma logs.

GAMLOG, which is still in widespread use today, uses an iterative approach to the problem of improving the accuracy and resolution of gamma ray logs. The response of the logging system to a thin zone of radioactive material is first determined using data from model boreholes. Given that the equation $\overline{G} = KA/T$ is valid, then the anomaly resulting from any complex sequence of radioactive zones is simply the sum of the anomalies resulting from the individual zones. The experimentally determined thin zone response function is applied to the raw field log

and the result fed back in the form of an error signal. This process continues iteratively until the desired degree of improvement occurs, or until the practical limit imposed by noise is reached.

Through the efforts of the MIT Geophysical Analysis Group and others in the 1950's and 1960's, digital time series analysis was established as a powerful group of related techniques for the analysis of data gathered sequentially in time or space. In geophysics these techniques are associated largely with seismology, although they are equally applicable in other areas, including borehole logging. Drawing upon these techniques, and the work by Czubek (1971), Davydov (1970), and Suppe and Khaykovich (1960) mentioned earlier, Conaway and Killeen (1978a) considered separately the effects of the geologic impulse response, detector length, ratemeter time constant (analog systems) and sampling interval (digital systems). That paper also contained a number of computer-simulated gamma ray logs illustrating these effects both in the ideal case and in the presence of statistical noise (unavoidable in nuclear logging), using a combined inverse filter (spatial deconvolution) and smoothing technique.

Conaway and Killeen (1978b) compared the inverse filter technique (Conaway and Killeen, 1978a) with Scott's iterative technique (Scott, 1963). Theoretically the two techniques give identical results in the ideal case. In practice, slight differences between the processed logs result from unavoidable approximations made in applying both techniques. Inverse filtering has the advantage that it requires only on the order of 3% as much computer time as iteration. In addition, whereas iterative

processing requires that an entire log (or at least a complete anomaly) be available to the computer before processing can begin, inverse filtering is a one-pass sequential operation and thus can be applied in real time during the logging operation, given suitable equipment.

The System Response Function

The log which is produced by a given logging system in the vicinity of a thin zone ("spatial impulse") of radioactive material perpendicular to the borehole is called the system impulse response, or the system response function. In an infinitesimally thin borehole using a point detector the system response function $\phi(z)$ would generally resemble Figure 1c, and could be approximated by the equation

$$\phi(z) = \frac{\alpha}{2} e^{-\alpha |z|} \tag{1}$$

as given by Davydov (1970) based on Suppe and Khaykovich (1960). Here z is depth along the borehole and α is a parameter referred to as the shape constant.

Equation (1) describes a double-sided exponential, which has a corresponding simple exact digital inverse filter (Conaway, 1980a). The beauty of this equation for this application is in its simplicity. By determining the behavior of α under various conditions, the exact inverse filter is adapted easily to changing conditions. Moreover, under favorable conditions α may be determined directly from field logs (Conaway, 1980b), thus providing a check on values arrived at by other means (model boreholes and theoretical studies).

Under the conditions considered by Scott et al (1961) in their derivation of the relationship $\overline{G}$ = KA/T, gamma ray logs obey the principle of superposition. This means that various distorting effects may be removed from the data separately, and in any order (at least to the limit that they may be removed at all). Thus, it is not necessary that the system response function correspond precisely with equation (1). In general, the radiation intensity outside of the radioactive zone will die away essentially exponentially with distance. This is a sufficient condition to use the inverse filter based on equation (1). After application of this filter, some residual distortion will exist in the log near the radioactive zone, the extent depending on borehole diameter, detector size, ratemeter time constant, etc. These may also be considered individually.

Variations in the Shape Constant

The shape constant α in equation (1) provides a simplified means of studying the effects of borehole, formation, and instrumental parameters on the shape of the system response function. Such effects have been considered by many authors including Czubek (1961; 1966; 1969; 1971; 1972), Rhodes and Mott (1966), McDonald and Palmatier (1969), Davydov (1970), Conaway and Killeen (1978a), Conaway (1979, 1980a, 1980b, 1981), and Conaway et al (1979, 1980). Other work by BFEC and LASL (e.g. Wilson, 1979; Stromswold, 1979) will be reviewed separately by those groups in these proceedings.

An increase in the value of α indicates a more rapid decrease in radiation intensity with distance from the radioactive zone. This condition may, in general, be brought about by :

(a) An increase in formation density.

(b) An increase in pore fluid density (e.g. from air to water).

(c) A decrease in dip angle between the radioactive zone and the normal to the borehole (until perpendicularity or 0° dip).

(d) An increase in borehole fluid density (e.g. from air to water to heavy mud).

(e) A decrease in borehole diameter (allowing proportionately less radiation to travel in the borehole).

(f) An increase in the equivalent atomic number Zeq of the formation.

(g) Restriction of the detected gamma rays to unscattered photons (e.g. the 1.76 MeV ^{214}Bi window of uranium).

(h) For unscattered gamma rays, a decrease in the energy of the spectral discrimination window.

The reader is referred to the abovementioned works for further information on these factors.

Conclusions

Improving the accuracy of gamma ray logs for quantitative radio-element determinations may be achieved by several spatial deconvolution techniques. These techniques have resulted from research in a number

of countries over a period of more than 20 years. Appropriate choice
of equipment, logging technique, and data processing can produce a
log with markedly better accuracy and spatial resolution than normally
obtained.

GEOLOGY   RADIOELEMENT   GAMMA-RAY INTENSITY
           CONCENTRATION
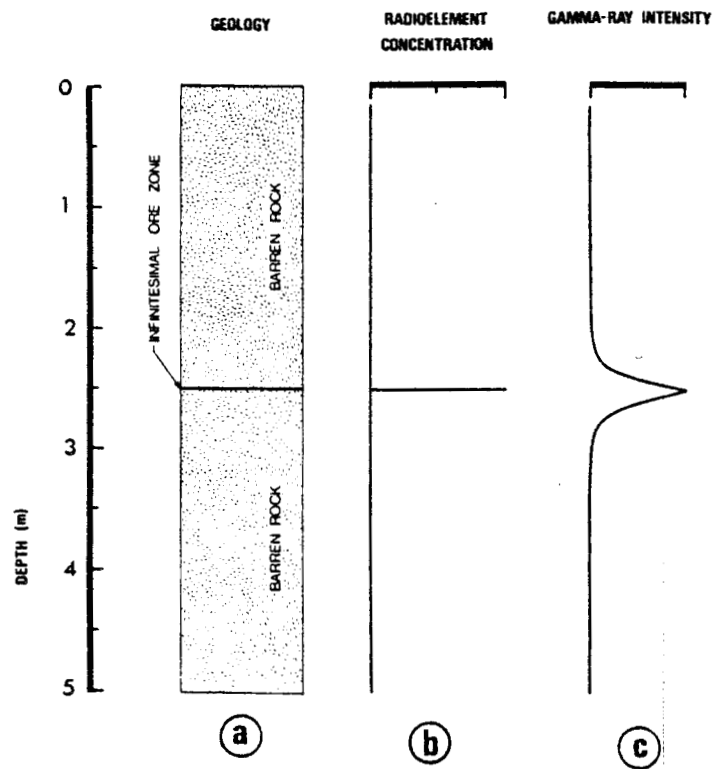
Figure 1

(a) Geologic column showing an infinitesimally thin radioactive ore zone sandwiched between two thick barren zones, a 'geologic impulse' of radioactive ore.

(b) Plot of radioelement concentration with depth corresponding to Figure 1a.

(c) Noise-free response of a point-detector to the thin ore zone, the 'geologic impulse response'.

REFERENCES

Conaway, J.G.
    1979:   Problems in gamma-ray logging: The effect of dipping
            zones on the accuracy of ore grade determinations; in
            Current Research, Part A, Geological Survey of Canada,
            Paper 79-1A, p.41-44.

    1980a: Exact inverse filters for the deconvolution of gamma-
            ray logs; Geoexploration, v.18, p.1-14.

    1980b: Direct determination of the gamma ray logging system
            response function in field boreholes, Geoexploration,
            v.18, p.187-199.

    1981:   Deconvolution of gamma ray logs in the case of dipping
            radioactive zones, Geophysics, v.45.

Conaway, J.G., Allen, K.V., Blanchard, Y.B., Bristow, Q.,
Hyatt, W.G., and Killeen, P.G.
    1979:   The effects of borehole diameter, borehole gluid, and
            casing thickness on gamma ray logs in large diameter
            boreholes: in Current Research, Part C, Geological
            Survey of Canada, Paper 79-1C, p.37-40.

Conaway, J.G., Bristow, Q., and Killeen, P.G.
    1980:   Optimization of gamma-ray logging techniques for uranium;
            Geophysics, v.45, p.292-311.

Conaway, J.G. and Killeen, P.G.
    1978a: Quantitative uranium determinations from gamma-ray logs
            by application of digital time series analysis;
            Geophysics, v.43, p.1204-1221.

    1978b: Computer processing of gamma-ray logs: iteration and
            inverse filtering, in Current research, part B:
            Geogical Survey of Canada, Paper 78-1B, p.83-88.

Czubek, J.A.
    1961:   Some problems of the theory and quantitative inter-
            preation of the gamma-ray logs; Acta Geophysica Polonica,
            v.9, p.121-137.

    1962:   The influence of the drilling fluid on the gamma-ray
            intensity in the borehole; Acta Geophysics Polonica,
            v.10, p.25-30.

    1966:   Physical possibilities of gamma-gamma logging; in
            Radioisotope Instruments in Industry and Geophysics,
            volume 2, International Atomic Energy Agency Proceedings
            Series, IAEA, Vienna.

Czubek, J.A.
    1969:   Influence of borehole construction on the results of
              spectral gamma-logging: in Nuclear Techniques and
              Mineral Resources, International Atomic Energy Agency
              Proceedings Series, IAEA, Vienna.

    1971:   Differential interpretation of gamma-ray logs: I: Case
              of the static gamma-ray curve; Report No. 760/1, Nuclear
              Energy Information Center, Polish Government Commissioner
              for Use of Nuclear Energy, Warsaw, Poland.

    1972:   Differential interpreation of gamma-ray logs: II: Case of
              the dynamic gamma-ray curve: Nuclear Energy Information
              Center, Polish Gov. Comm. for Use of Nuclear Energy,
              Warsaw, rep. no. 793/1.

Czubek, J.A. and Zorski, T.
    1976:   Recent advances in gamma-ray log interpretation;
              International Atomic Energy Agency Advisory Group
              Meeting on Evaluation of Uranium Resources, Rome, Italy.

Davydov, Y.B.
    1970:   Odnomernaya obratnaya zadacha gamma-karotazha   skvazhin
              (One dimensional inversion problem of borehole gamma
              logging); Izvestiya Vysshoya Uchebnoye Zavedeniya
              Geologiya i Razvedka, No.2, p.105-109 (in Russian).

Jonas, J.T.
    1975:   Digital data processing techniques applied to the natural
              gamma-ray log; M.S. thesis T-1778, Colorado School of
              Mines.

McDonald, W.J., and Palmatier, E.D.
    1968:   Predicting nuclear log response; Journal of Petroleum
              Technology, v.21, p.1421-1426.

Rhodes, D.F. and Mott, W.E.
    1966:   Quantitative interpretation of gamma-ray spectral logs;
              Geophysics, v.28, p.410-418.

Roesler, R.
    1965:   Ein neues Auswerteverfahren fur radiometrische
              Bohrlochmessungen uter besonderer Berucksichtigung der
              K_2O-Bestimmung aus Messungen der naturlichen Gammastrahlung
              in Bohrlochern; Freiberger Forschungshefte, C180, Geophysik,
              VEB Duetsch. Verlag Fur Grundstoffindustrie, Leipzig.

Scott, J.H.
  1962:   The GAMLOG computer program: U.S. Atomic Energy Commission
               rep. RME-143, September, Grand Junction, CO.

  1963:   Computer analysis of gamma-ray logs; Geophysics,
               v.28, p.457-465.

Scott, J.H., Dodd, P.H., Droullard, R.F., and Mudra, P.J.
  1961:   Quantitative interpreation of gamma-ray logs; Geophysics,
               v.26, p.182-191.

Stromswold, D.C.
  1979:   Measurement of the deconvolution parameter "α" for
               uranium; Spectral Gamma-Ray Borehole Logging Technical
               Note, Bendix Field Eng. Corp., Grand Junction, Col.

Suppe, S.A.
  1957:   Gamma-ray borehole logging; in Radiometric Methods in
               the Prospecting of Uranium Ores, V.V. Alekseev,
               A.G. Grammakov, A.I. Nikonov, and G.P. Tafeev, ed.,
               Translation available as AEC-tr-3738 (Book 2), U.S.
               Atomic Energy Agency.

Suppe, S.A. and Khaykovich, I.M.
  1960:   Resheniye pryamoi zadachi gamma-karotazha v sluchaya
               slozhnogo raspredeleniya radioaktivnogo elementa v
               aktivykh plastakh (Solution of the linear problem of
               gamma logging in the case of a complex distribution of
               the radioactive element in the active strata); Voprosy
               Rudnoi Geofiziki, Issue I (in Russian).

Wilson, R.D.
  1979:   Log deconvolution with the inverse digital filter;
               Spectral Gamma-Ray Logging Technical Note 9, Bendix
               Field Engineering Corp., Grand Junction, Colorado.

Reduction and Analysis
of Field Logs

HOLE TRUCK DEMO LOG   TRUCK 1980
AREA HOLIDAY INN, GJ COLO   SER # 5
OPER R. PRICE   DATE   02-17-81

K(A) PCT   CALIPER   INCHES
0   5.0   20   4   1.0   7

U(A) PPM
0   25.0   100

T(A) PPM
0   10.0   40
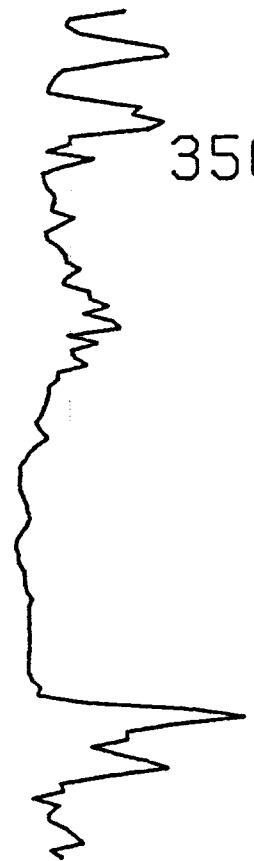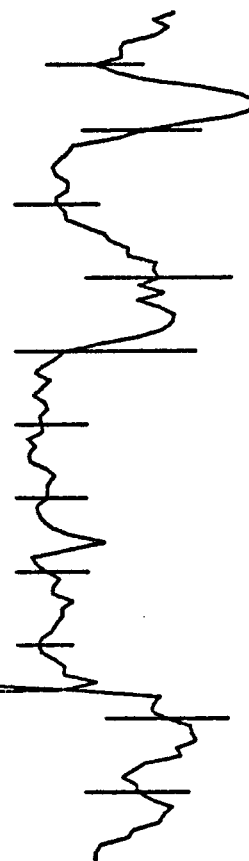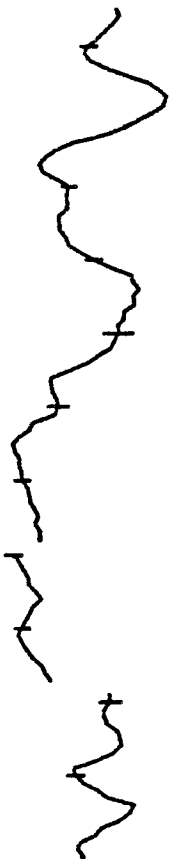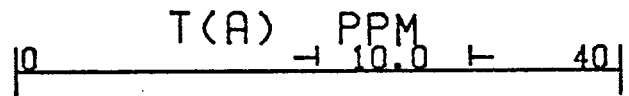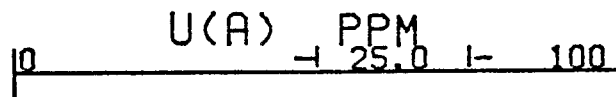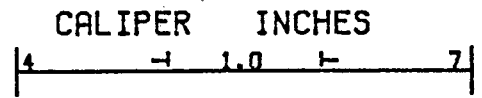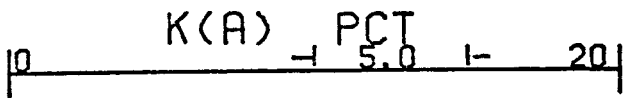
350

400

FIELD PROCESSING FOR LARGE NaI DETECTOR

CASING CORRECT $A_{3\times3}^{-1}$ & $A_{2\times2}^{-1}$

DETERMINE CALCULATION MODE (3x3 OR 2x2)

DETERMINE EXTENDED COUNTING TIME
    COUNT RATE & TIME

REMOVE TOOL BACKGROUND FROM
    COUNT RATE

CALCULATE K,U,T CONCENTRATIONS & UNCERTAINTIES

IF NaI DETECTOR IN BOREHOLE FLUID
    THEN CORRECT KUT CONCENTRATION

DETERMINE CALCULATION MODE
(3x3 or 2x2)

IF SMALL NaI DETECTOR
$\qquad$ THEN GO TO 2x2

$\vdots$

IF $(R_k - B_k)$ R_{KL}
$\qquad$ THEN GO TO 3x3

$\vdots$

PREVIOUS CALC MODE?

WAS 3x3

$$\text{IF} \left| \frac{\sigma C_k}{C_k} \right| > L_2$$

THEN GO TO 2x2

$\vdots$

(3x3) CALCULATE K,U,T
USING $A_{3 \times 3}^{-1}$

WAS 2x2

$$\text{IF} \left| \frac{\sigma C_k}{C_k} \right| < L_3$$

THEN GO TO 3x3

$\vdots$

(2x2) CALCULATE U,T
USING $A_{2 \times 2}^{-1}$

HOLE TRUCK DEMO LOG   TRUCK 1980

AREA HOLIDAY INN, GJ COLO   SER # 5

OPER R. PRICE   DATE   02-17-81

K(RAW) CPS
0   20.0   80

U(RAW) CPS
0   20.0   80

T(RAW) CPS
0   2.5   10
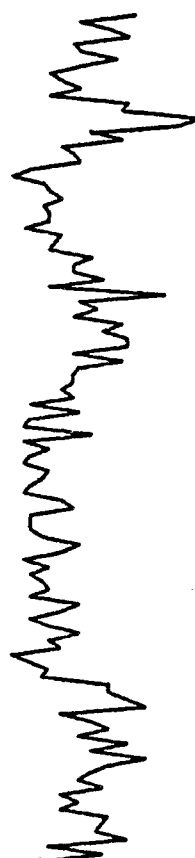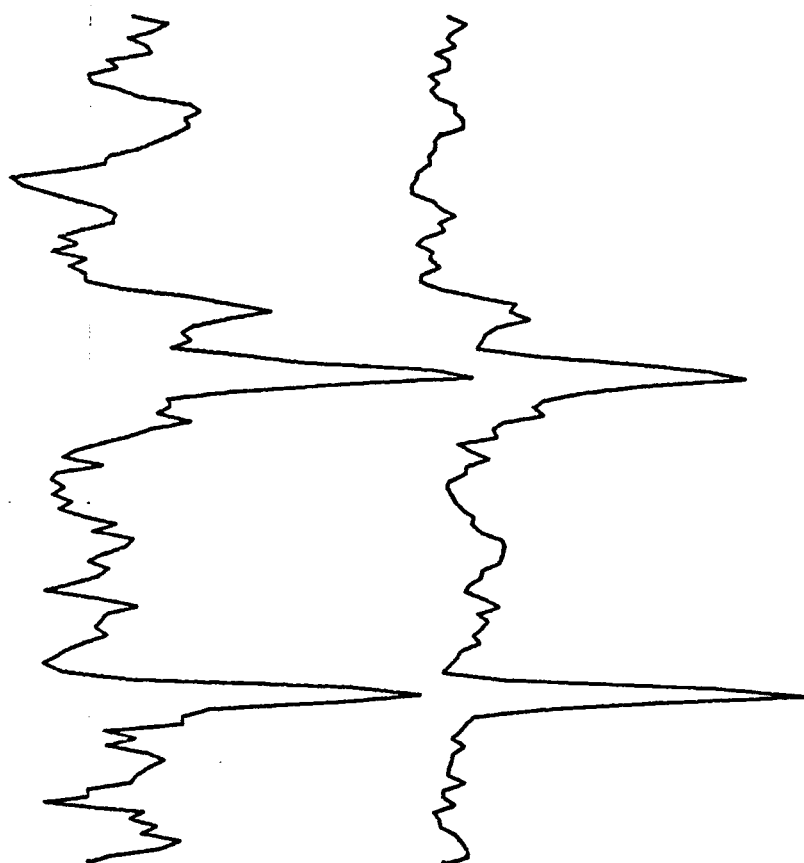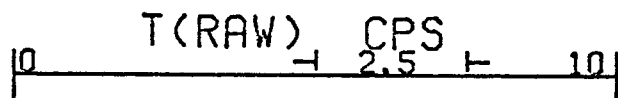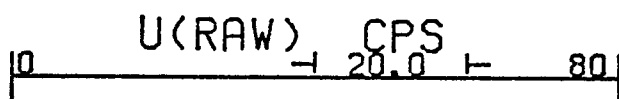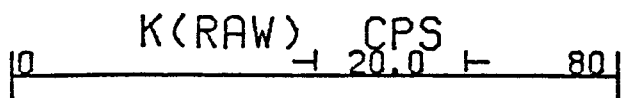
350

400

HOLE   TRUCK DEMO LOG   TRUCK 1980
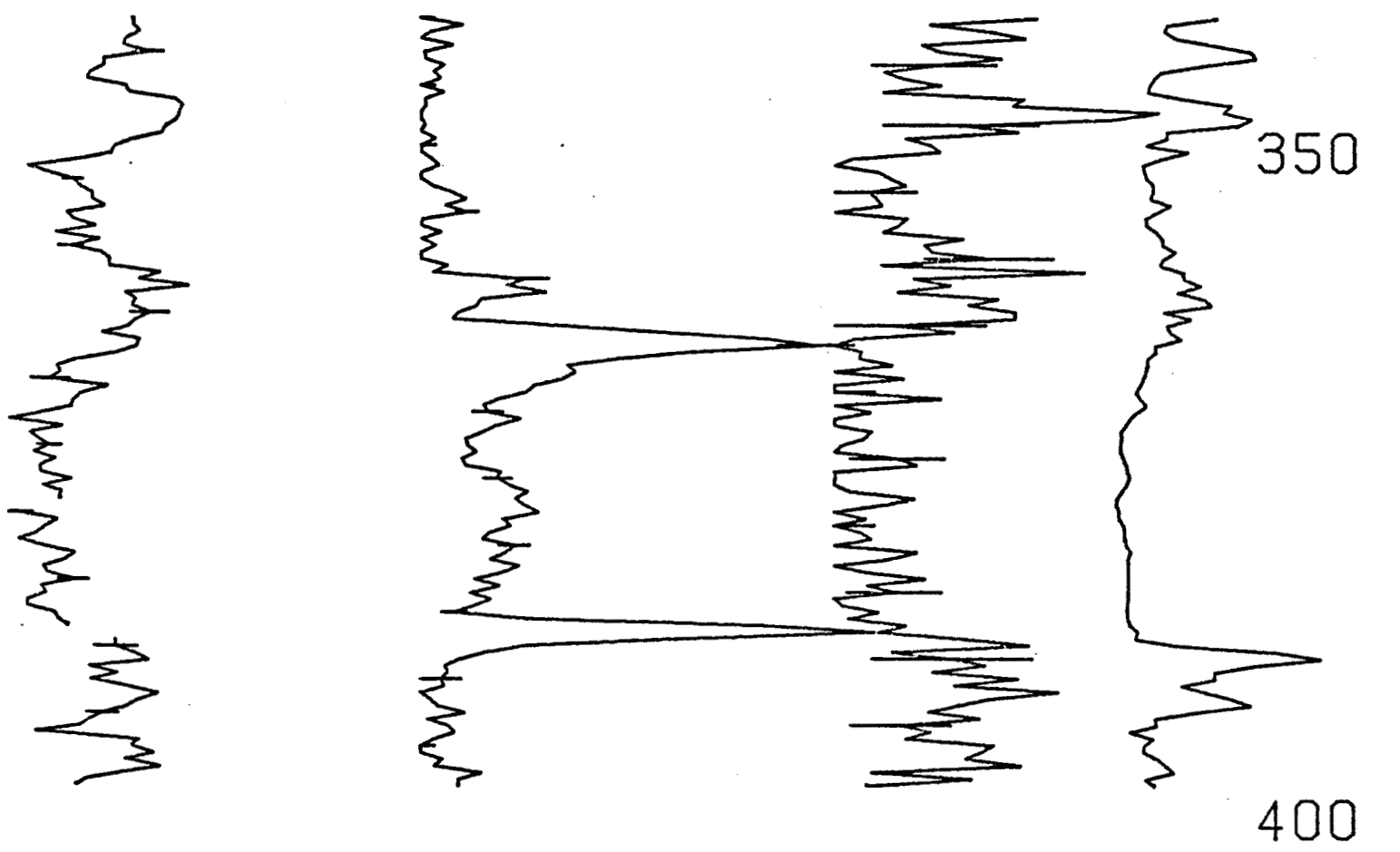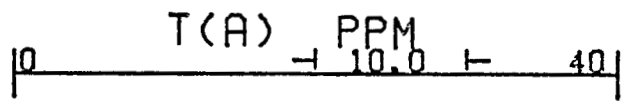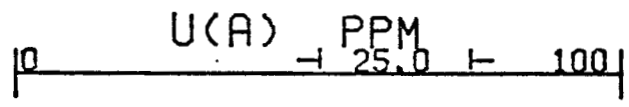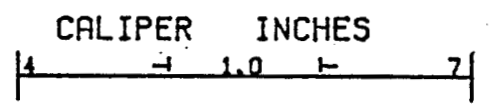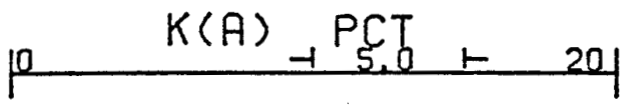
AREA HOLIDAY INN, GJ COLO   SER # 5

OPER R. PRICE   DATE   02-17-81

K(A) PCT   CALIPER   INCHES

|0   5.0   20| |4   1.0   7|

U(A) PPM

|0   25.0   100|

T(A) PPM

|0   10.0   40|

350

400

6.

THE EFFECTS OF BOREHOLE DIAMETER, BOREHOLE FLUID, AND CASING THICKNESS ON GAMMA RAY LOGS IN LARGE DIAMETER BOREHOLES

Project 740085

J.G. Conaway, K.V. Allen, Y.B. Blanchard,
Q. Bristow, W.G. Hyatt, and P.G. Killeen
Resource Geophysics and Geochemistry Division

Abstract

The response of a gamma ray logging system to a thin zone of radioactive material depends on a number of instrumental, borehole, and formation parameters. This paper considers the effects of borehole diameter, borehole fluid, and casing thickness on the shape of the system response function and the area beneath it in total-count gamma ray logging.

Introduction

The noise-free response of a gamma ray logging system to a thin zone of radioactive material perpendicular to the borehole is called the system response function. The shape and amplitudes of the gamma ray log from a borehole are determined by the ore distribution and the system response function; thus, successful quantitative interpretation of the log depends on a knowledge of the form of the system response function. The shape and area of this function depend on many instrumental, formation, and borehole parameters. In this paper we consider the effects of three borehole parameters: borehole diameter (over the range from 9-33 cm), borehole fluid (air or water), and casing thickness (from 1.6-12.7 mm steel casing). The results presented here are based on tests in the borehole calibration models located at the U.S. Department of Energy radiometric calibration facilities at Grand Junction Colorado (Mathews et al., 1978).

Theoretical Background

The theoretical basis for quantitative interpretation of gamma ray logs is given by the equation

$$\bar{G}T = KA \qquad (1)$$

(Scott et al., 1961). Here, A is the area beneath a given anomaly on the gamma ray log, T is the thickness of the radioactive zone causing the anomaly, $\bar{G}$ is the average radioelement concentration or grade over that thickness, and K is the constant of proportionality. Equation (1) assumes that the system is linear (i.e. follows the principle of superposition). The constant K is generally determined in model calibration boreholes under standard conditions of casing thickness, borehole diameter, and borehole fluid. If these conditions are different in the field than in the model, the sensitivity of the system to a given radioelement may change, requiring a compensating change in K (usually applied in the form of separate correction factors, e.g. Dodd and Eschliman, 1972).

The validity of equation (1) is independent of the shape of the system response function. However, if the gamma ray log is to be deconvolved to produce a record of radioelement concentration as a function of depth (e.g. Scott, 1963; Conaway and Killeen, 1978) then the shape of the system response function must be known at least approximately so that an appropriate deconvolution operator can be derived.

A digital inverse filter for deconvolution of gamma ray logs has been given by Conaway and Killeen (1978) based on earlier work by Suppe and Khaikovich (1960), Davydov (1970),

and Czubek (1971) wherein the noise-free response $\phi(z)$ of a point detector to a thin zone of radioactive material at depth $z = 0$ was approximated by

$$\phi(z) = \frac{\alpha}{2}e^{-\alpha|z|} \qquad (2)$$

where α is a constant for a given set of instrument, borehole, and formation parameters. The inverse filter coefficients are given by

$$\left(-\frac{1}{(\alpha \Delta z)^2}, \quad 1 + \frac{2}{(\alpha \Delta z)^2}, \quad -\frac{1}{(\alpha \Delta z)^2} \right) \qquad (3)$$

where Δz is the sampling interval along the borehole.

A simple method for determining α which is valid in either model or field boreholes has been discussed by Conaway (in press). All that is required is a digital log across an interface between a barren zone and an ore zone, where the barren zone is essentially homogeneous over a distance of perhaps 1.5-2 m away from the interface (Fig. 6.1a). It is not necessary that the ore zone be homogeneous or infinitely thick. The constant (except for statistical noise) 'background' radiation intensity in the barren zone is subtracted from each discrete value, and the resulting data are plotted as the natural logarithm of the count rates ('background' corrected) as a function of depth (Fig. 6.1b). The desired value of α is the slope on this plot of the linear anomaly flank outside of the ore zone. This technique is more difficult to apply to data from an analog logging system because of the distortion introduced by the analog ratemeter (Conaway, in press). This semi-log slope technique for determining α is useful for studying the behavior of the system response function as a function of borehole diameter, borehole fluid, and casing thickness, and will be used in subsequent sections of this paper.

Steel Casing

Figure 6.2a shows a plot of gamma ray intensity as a function of depth measured in a model borehole containing a 1.5 m thick 'ore' zone between two barren zones, for no casing and for six thicknesses of steel casing (1.6, 3.2, 4.8, 6.4, 9.5, and 12.7 mm). The borehole is water filled and 11.4 cm in diameter. All of the curves have been normalized so that their areas are equal, for comparison; this has no effect on the computed value of α. The digital sampling interval $\Delta z = 3$ cm, logging velocity $v = 0.3$ m/min, and the detector is 25 x 75 mm NaI(Tl) with the lower energy threshold of the instrument set at 100 keV.
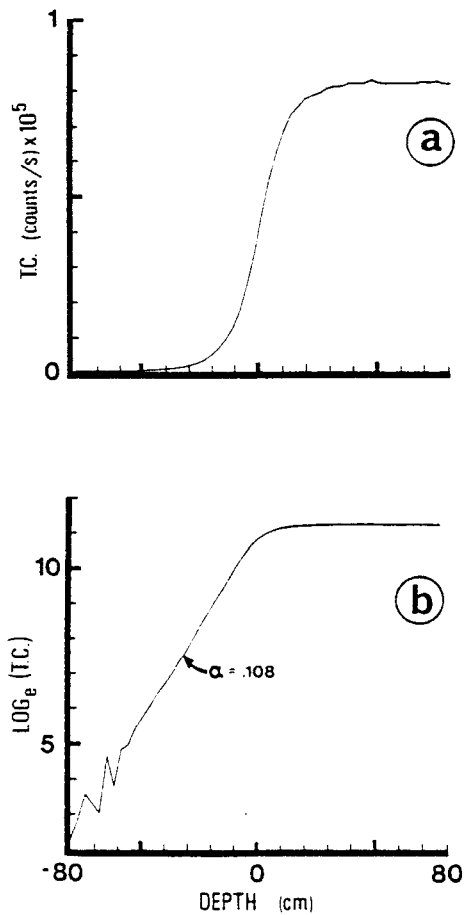
(a) Measured total count (T.C.) gamma ray response across a barren zone/ore zone interface.

(b) Natural logarithm of data in Figure 6.1(a) (background subtracted) plotted against depth. Units of α are cm^{-1}.
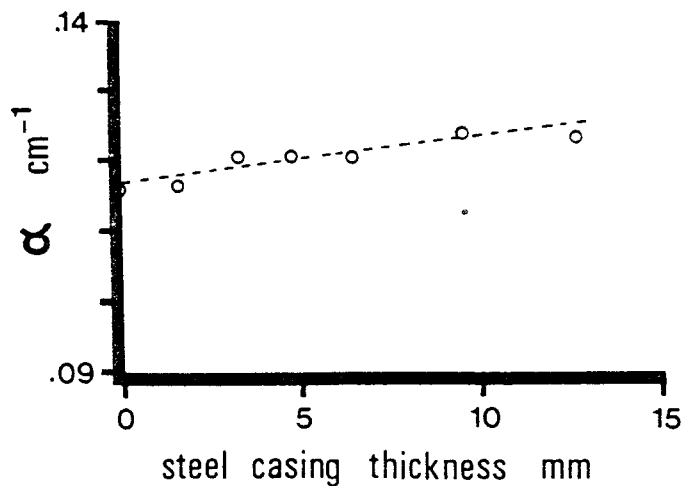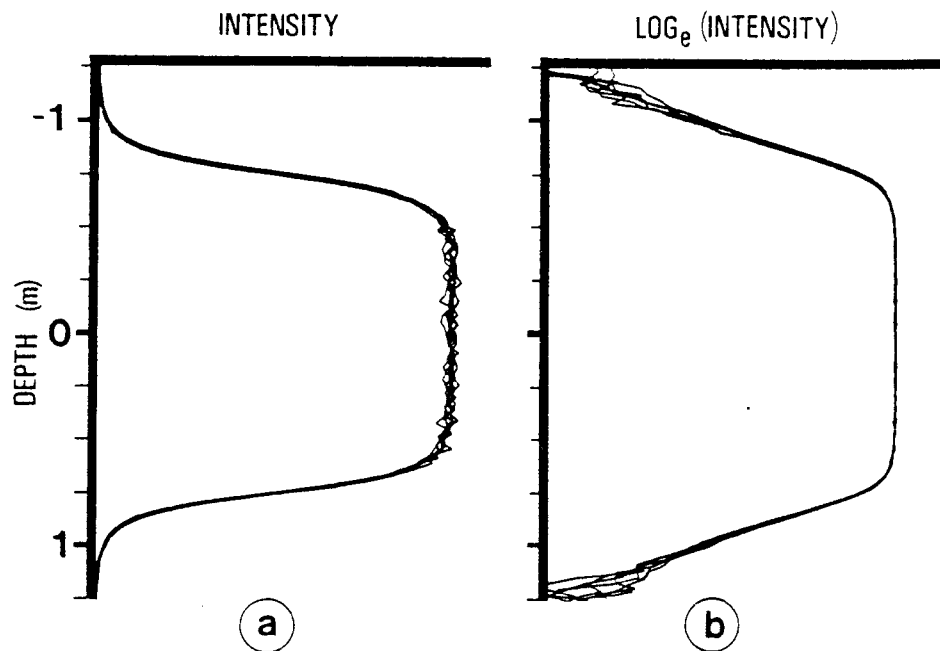
Figure 6.1.

(a) Seven logs through a model ore zone with different thicknesses of steel casing, as described in text. All areas have been normalized to a constant value.

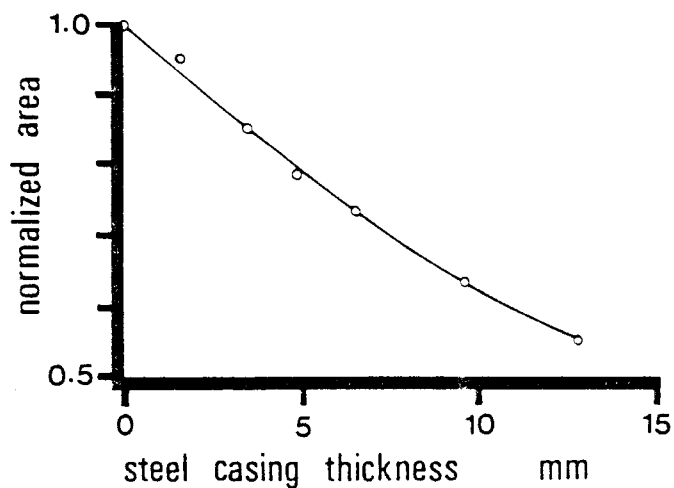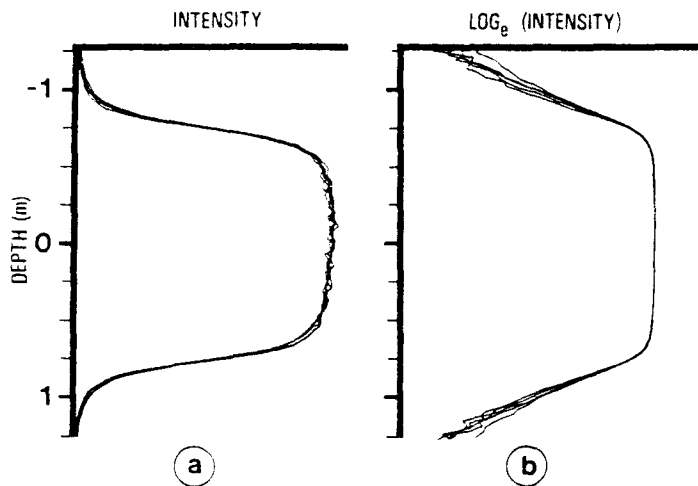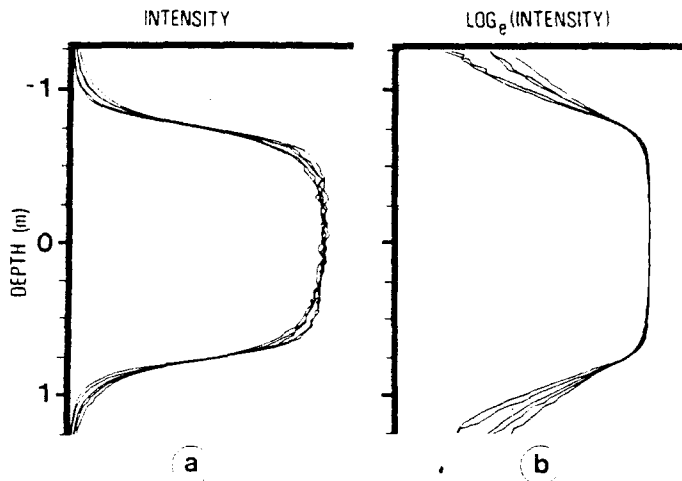(b) Semi-log plot of the data shown in Figure 6.2.a, background subtracted.

Figure 6.2.

Figure 6.3. Plot of α as a function of steel casing thickness based on data shown in Figure 6.2b. The straight line through the experimental points is not meant to imply that the data follow a linear pattern; statistical scatter is too large to determine this reliably.

Figure 6.4. Plot of anomaly area as a function of steel casing thickness, normalized to a value of 1 for no casing.

38

INTENSITY   LOG$_e$ (INTENSITY)

(a) (b)

(a) Five logs through a model ore zone in uncased water-filled boreholes of different diameters, as described in text. All areas have been normalized to a constant value.

(b) Semi-log plot of the data shown in Figure 6.5a, background subtracted.

Figure 6.5.

INTENSITY   LOG$_e$ (INTENSITY)

a . b

(a) Five logs through a model ore zone in uncased air-filled boreholes of different diameters. as described in text. All areas have been normalized to a constant value.

(b) Semi-log plot of the data shown in Figure 6.6a, background subtracted.

Figure 6.6.

It is clear from Figure 6.2a that the casing has little effect on the shape of the log. Subtracting the background and plotting the natural logarithm as described above gives Figure 6.2b. In spite of considerable statistical noise outside of the ore zone in this figure, some divergence of the curves can be seen as distance from the ore zone increases. Figure 6.3 shows a plot of α as a function of casing thickness based on a least-squares fit on the linear portion of the anomaly flanks in Figure 6.2b, over the range from 6-36 cm outside of the ore zone, on both sides.

Figure 6.4 shows the effect of casing on the total area of the anomaly, normalized to 1 for no casing. The inverse of this curve would give multiplicative casing correction factors which can be applied to gamma ray curves with different casing thickness. It should be emphasized that Figures 6.3 and 6.4 are dependent upon instrumental characteristics, and correction factors should be individually determined for each probe and logging system.

Borehole Diameter and Fluid

The effect of borehole diameter on α has been discussed by Suppe and Khaikovich (1960) and Davydov (1970) based on experimental results, and by Czubek (1971) based on an analytical expression for the point detector system response function. The data given in the present paper were obtained in five water-filled model boreholes of different diameters (8.9, 11.4, 17.8, 22.9 and 33 cm) through the same 1.5 m thick ore zone (Figure 6.5a). In all cases the borehole probe was kept in contact with the borehole wall throughout the log. The logs shown in Figure 6.5a have been normalized to give uniform area, as explained previously. These same logs ('background' corrected) are plotted on semi-log co-ordinates in Figure 6.5b. Examination of Figure 6.5b shows that the anomaly flanks are not completely linear. The corresponding normalized logs for the same boreholes air-filled are given in Figures 6.6a and 6.6b. The differences caused by the various borehole diameters are more pronounced in the case of air-filled boreholes. In large diameter boreholes, the ore zone will be detected from a greater distance if the borehole is air-filled rather than water-filled due to increased radiation passing through the borehole fluid in the case of air. This explains why there is a greater difference between the results in air and in water for large diameter boreholes than for small diameters.

The values of α determined using the semi-log slope technique, based on the data shown in Figures 6.5 and 6.6 are plotted in Figure 6.7. Figure 6.8 shows the total area under the anomaly curves for the five borehole diameters, both air and water filled, normalized to the 8.9 cm diameter case. In the case of an air-filled borehole one expects very little change in area, whereas for the water-filled case the curve asymptotically approaches a constant area corresponding to the case of infinite diameter (i.e. logging along a flat wall). If the probe were centred, of course, the curve for the water-filled case would asymptotically approach zero.
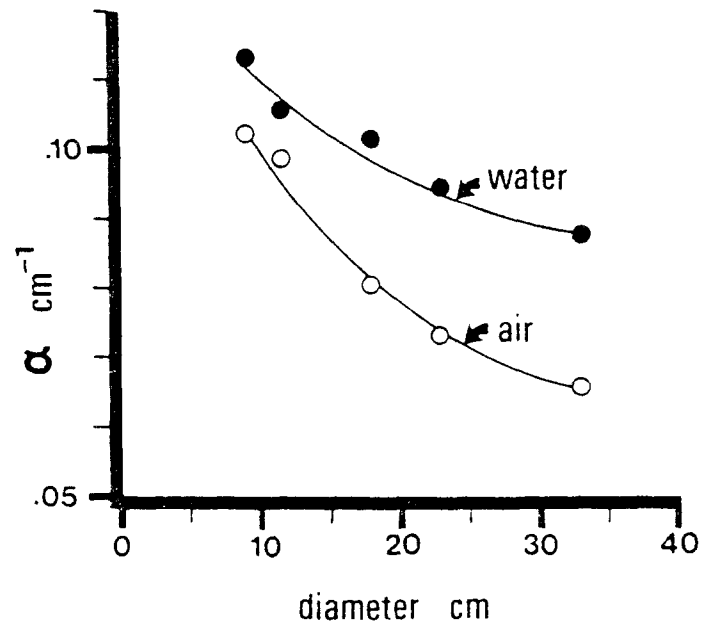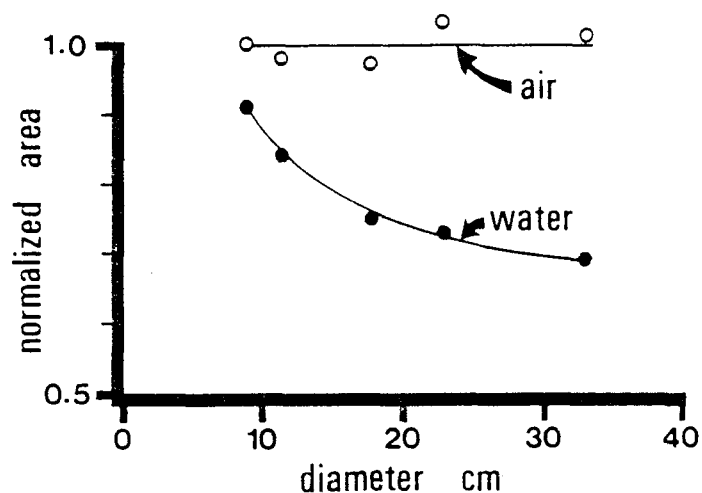

Figure 6.7. Values of α as a function of borehole diameter, as explained in text.

Figure 6.8. Area under the anomaly curves from boreholes of various diameters through a model ore zone, normalized to 100 per cent for air-filled case.

Discussion and Conclusions

In this paper we have illustrated the variations in the shape of the system response function (in particular the variations of the constant α in equation (2)) with changes in borehole diameter, borehole fluid, and steel casing thickness, for total count logging. In addition, variations in the system sensitivity (i.e. area beneath the response function) with these same borehole parameters have been described.

Results such as these, obtained with a particular set of equipment, should not be used to derive correction factors for other equipment. These factors should be determined individually for each logging system. The results presented here, however, serve to illustrate the effects which can be expected under these conditions.

In the case of gamma ray spectral logging equipment, correction factors should be determined individually for each spectral window, for best results. Differences between the behavior of the different windows under various conditions may be small, but this should be verified experimentally rather than assumed.

Acknowledgments

The authors thank J.M. Carson and K.A. Richardson for helpful comments and suggestions, and the U.S. Department of Energy and Bendix Field Engineering Corp. personnel for expediting the logging of the model boreholes at Grand Junction Colorado.

References

Conaway, J.G.
    Direct determination of the gamma ray logging system response function in field boreholes (in press)

Conaway, J.G. and Killeen, P.G.
    1978: Quantitative uranium determinations from gamma ray logs by application of digital time series analysis; Geophysics, v. 43, p. 1204-1221.

Czubek, J.A.
    1971: Differential interpretation of gamma ray logs: I. Case of the static gamma-ray curve; Report No. 760/I, Nuclear Energy Information Centre, Polish Government Commissioner for Use of Nuclear Energy, Warsaw, Poland.

Davydov, Y.B.
    1970: Odnomernaya obratnaya zadacha gamma-karotazha skvazhin (one dimensional inversion problem of borehole gamma logging); Izv. Vyssh. Uchebn. Zaved., Geol. I. Razvedka, No. 2, p. 105-109 (in Russian).

Dodd, P.H. and Eschliman, D.H.
    1972: Borehole logging techniques for uranium exploration and evaluation; in Uranium Prospecting Handbook, S.H.U. Bowie, M. Davis, and D. Ostle. eds., Inst. Min. Metall., London.

Mathews, M.A., Koizumi, C.J., and Evans, H.E.
    1978: DOE - Grand Junction logging model data synopsis; Bendix Field Eng'g Corp. publication GJBX-76(78). Grand Junction, Colorado.

Scott, J.H.
    1963: Computer analysis of gamma-ray logs; Geophysics, v. 28, p. 457-465.

Scott, J.H., Dodd, P.H., Droullard, R.F., and Mudra, P.J.
    1961: Quantitative interpretation of gamma-ray logs, Geophysics, v. 26, p. 182-191.

Suppe, S.A. and Khaikovich, I.M.
    1960: Resheniye pryamoi zadachi gamma-karotazha v sluchaye slozhnogo raspredeleniya radioaktivnogo elementa v aktivykh plastakh (Solution of the linear problem of gamma logging in the case of a complex distribution of the radioactive element in the active strata); Voprosy Rudnoi Geofiziki, Issue I (in Russian).

BIBLIOGRAPHY OF PUBLICATIONS RELATED TO
GEOLOGICAL SURVEY OF CANADA PROJECT 740085:
BOREHOLE GEOPHYSICS (NUCLEAR TECHNIQUES)

1. Killeen, P.G.

    1975:   Nuclear techniques for borehole logging in mineral explora-
            tion; in Borehole Geophysics applied to Metallic Mineral
            Prospecting - a review. Ed. by A.V. Dyck, Geol. Surv.
            Can. Paper 75-31, pp. 39-52.

2. Killeen, P.G.

    1976:   Portable borehole gamma-ray spectrometer tests; Geol. Surv.
            Can. Paper 76-1A, pp. 487-489.

3. Killeen, P.G. and Bristow, Q.

    1976:   Uranium exploration by borehole gamma-ray spectrometry
            using off-the-shelf instrumentation; Exploration for
            Uranium Ore Deposits (Proc. Symp. Vienna, 1976) IAEA
            Vienna, pp. 393-414.

4. Killeen, P.G.

    1976:   Trends in gamma-ray logging of mineral exploration bore-
            holes; CIM Bulletin March 1976 (Abstract).

5. Killeen, P.G. and Bristow, Q.

    1976:   A backpack portable borehole gamma-ray spectral logging
            system with digital recording; in Geophysics - A Key to
            Energy Independence: 46th Annual Meeting of the S.E.G.
            (Abstract), p. 105.

6. Killeen, P.G. and Dyck, A.V.

    1977:   Geophysical logging of MacDougall Core Hole 1A, Prince
            Edward Island; Appendix 3, p. 23 in R.D. Howie, Geologi-
            cal Studies and Evaluation of MacDougall Core Hole 1A,
            Western Prince Edward Island, Geol. Surv. Can. Paper 77-20.

7. Killeen, P.G.

    1977:   Calibration facilities for downhole uranium assay with a
            borehole gamma-ray spectral logger; in Geophysics - Global
            Reflections: 47th Annual Meeting of the S.E.G. (Abstract)
            p. 39.

8. Killeen, P.G.

    1977:   Gamma-ray spectral logging for uranium assay; in Canadian
            Exploration Geophysical Society (KEGS) Monthly Circular,
            November.

9. Bristow, Q.

    1977:   A system for the offline processing of borehole gamma-ray
            spectrometry data on a NOVA minicomputer; Geol. Surv. Can.
            Paper 77-1A.

10. Killeen, P.G., Conaway, J.G. and Bristow, Q.

    1978:   A gamma-ray spectral logging system including digital play-
            back with recommendations for a new generation system; in
            Geol. Surv. Can. Paper 78-1A, pp. 235-241.

11. Conaway, J.G. and Killeen, P.G.

    1978:   Quantitative uranium determinations from gamma-ray logs by
            application of digital time series analysis; Geophysics,
            Vol. 43, No. 6, pp. 1204-1221.

12. Killeen, P.G. and Conaway, J.G.

    1978:   New facilities for calibrating gamma-ray spectrometric log-
            ging and surface exploration equipment; CIM Bull., Vol. 71,
            No. 793, pp. 84-87.

13. Conaway, J.G. and Killeen, P.G.

    1978:   Computer processing of gamma-ray logs: iteration and in-
            verse filtering; in Geol. Surv. Can. Paper 78-1B, pp. 83-88.

14. Conaway, J.G.

    1978:   Problems in gamma-ray logging: thin zone correction factors;
            in Current Research, Part C, Geol. Surv. Can. Paper 78-1C,
            p. 19-21.

15. Bristow, Q. and Killeen, P.G.

    1978:   A new computer-based gamma-ray spectral logging system; in
            Geophysics Golden Gateway to Energy, 49th Annual Meeting of
            the S.E.G. (Abstract), pp. 117-118.

16. Conaway, J.G. and Killeen, P.G.

    1980:   Gamma-ray spectral logging for uranium; CIM Bull., Vol. 73,
            No. 813, pp. 115-123.

17. Conaway, J.G.

    1979:   Problems in gamma-ray logging: the effect of dipping beds
            on the accuracy of ore grade determinations; in Current
            Research, Part A, Geol. Surv. Can. Paper 79-1A, pp. 41-44.

18. Conaway, J.G.

    1979:   Computer processing of gamma-ray logs: a program for the
            determination of radioelement concentrations; in Current
            Research, Part B. Geol. Surv. Can. Paper 79-1B, pp. 27-32.

19. Conaway, J.G.

    1979:   Uranium ore concentrations from gamma-ray logs; Paper
            presented 81st. CIM Annual General Meeting. Abstract
            in CIM Bull., V. 72, pp. 96-98.

20. Killeen, P.G.

    1979:   Gamma-ray logging problems in high grade uranium ore
            zones; CIM Bull. (Abstract) Vol. 72, No. 803, p. 98.

21. Killeen, P.G.

    1979:   Application of gamma-ray spectral logging to uranium
            exploration; in Technical Program, Abstracts and Bio-
            graphies, 49th Annual International Meeting of the S.E.G.
            (Abstract), p. 99.

22. Conaway, J.G., Allen, K.V., Blanchard, Y.B., Bristow, Q., Hyatt, W.G.
    and Killeen, P.G.

    1979:   The effects of borehole diameter, borehole fluid, and
            steel casing thickness on gamma-ray logs in large dia-
            meter boreholes; in Current Research, Part A, Geol. Surv.
            Can. Paper 79-1C, pp. 37-40.

23. Conaway, J.G., Bristow, Q. and Killeen, P.G.

    1980:   Optimization of gamma-ray logging techniques for uranium;
            Geophysics, Vol. 45, No. 2, pp. 292-311.

24. Conaway, J.G.

    1980:   Exact inverse filters for the deconvolution of gamma-ray
            logs; Geoexploration, Vol. 18, p. 1-14.

25. Conaway, J.G.

    1980:   Uranium concentrations and the system response function
            in gamma ray logging; in Current Research, Part A, Geol.
            Surv. Can., Paper 80-A, pp. 77-87.

26. Bristow, Q.

    1979:   Airborne and vehicle mounted geophysical data acquisition
            system controlled by Nova minicomputers; in Proceedings
            of the 6th Annual Data General User's Group Meeting, New
            Orleans, Dec. 4-7, 1979.

27. Conaway, J.G.

    1980:   Problems associated with gamma ray logging for the evalua-
            tion of high grade uranium deposits; Transactions, American
            Geophysical Union (Abstract), Vol. 61, No. 17, April 22, 1980,
            p. 415.

28. Bristow, Q., Conaway, J.G. and Killeen, P.G.

    1980: A microprocessor-based software-controlled portable bore-hole-logging system; Transactions, American Geophysical Union (Abstract), Vol. 61, No. 17, April 22, 1980, p. 415.

29. Killeen, P.G., Conaway, J.G. and Bristow, Q.

    1980: The application of inverse filtering to borehole gamma-ray spectral logging, Transactions, American Geophysical Union (Abstract), Vol. 61, No. 17, April 22, 1980, p. 415.

30. Conaway, J.G., Killeen, P.G. and Hyatt, W.G.

    1980: A comparison of bismuth germanate, cesium iodide, and sodium iodide scintillation detectors for gamma ray spectral logging in small diameter boreholes; in Current Research, Part B, Geological Survey of Canada, Paper 80-1B, p. 173-177.

31. Conaway, J.G.

    1980: Direct determination of the gamma-ray logging system response function in field boreholes; Geoexploration, 18, p. 187-199.

32. Killeen, P.G., Bristow, Q. and Conaway, J.G.

    1980: "Real time" deconvolution of gamma-ray logs with a new generation portable logging system; The Log Analyst, (Abstract), Vol. 21, No. 2, p. 23.

33. Conaway, J.G., Killeen, P.G. and Bristow, Q.

    1980: Variable formation parameters and nonlinear errors in quantitative borehole gamma-ray log interpretation; in Technical Program, Abstracts and Biographies, 50th Annual International Meeting of the S.E.G. (Abstract) p. 121-122.

34. Conaway, J.G.

    1981: Deconvolution of gamma-ray logs in the case of dipping radioactive zones; Geophysics, Vol. 46, No. 2, p. 198-202.

Project 740085

John G. Conaway and P.G. Killeen
Resource Geophysics and Geochemistry Division

Abstract

Conaway, John G., and Killeen, P.G., Computer processing of gamma-ray logs: Iteration and inverse filtering; in Current Research, Part B, Geol. Surv. Can., Paper 78-1B, p. 83-88, 1978.

For nearly two decades an iterative computer technique has been used for processing gamma-ray logs to determine the distribution of uranium along a borehole. Recently an inverse filter technique has been developed for the same application. Analysis of the iterative technique shows that it approaches theoretical equivalence with the inverse filter technique as the number of iterations increases. In tests with gamma-ray borehole logs with a sampling interval of 10 cm there was little difference in the results produced by the two methods. In practice a sampling interval shorter than 10 cm should be used to improve resolution and reduce aliasing errors. In this case a smoothing filter is required with both techniques to reduce the high-frequency noise.

The inverse filter technique generally requires less than 5 per cent as much computing time as iteration, and may be accomplished using an 'open-ended' algorithm, thereby making possible on-line processing of the data using a minicomputer or microprocessor, concurrent with the logging of the borehole.

Introduction

An iterative computer technique for determining radio-element concentrations from gamma-ray borehole logs has been in routine use in the United States since it was first introduced by Scott et al. (1961), and Scott (1962; 1963). Recently an inverse filter technique has been presented by Conaway and Killeen (in press) which is intended for the same purpose – determining radioelement concentrations from gamma-ray logs. A number of questions regarding the two techniques immediately present themselves: Are the results from the two methods equivalent? Which is more efficient? What are the advantages and disadvantages of each? The answers to these questions can be obtained from theoretical considerations, computer studies, and tests with gamma-ray borehole logs.

First a brief review of the theory is necessary. Consider the case of an infinitesimally thin radioactive ore zone embedded in a thick sequence of barren rock (Fig. 13.1a). The function expressing the distribution of radioactive material with depth is an impulse or 'spike' (Fig. 13.1b) having a flat amplitude spectrum (Fig. 13.2, curve a). This is the desired output of a gamma-ray logging system in the presence of a thin ore zone – a spike proportional in height to the ore grade. The actual output which would be obtained under noise-free conditions using a point-detector would resemble Figure 13.1c. This curve, called the geologic impulse response or GIR (Conaway and Killeen, in press), has an amplitude spectrum similar to Figure 13.2, curve b.

The purpose of computer processing of the raw data is to convert the geologic impulse response (Fig. 13.1c) into the spike (Fig. 13.1b) within the limitations imposed by noise. In other words, in the ideal case the data are processed to make the amplitude spectrum of the GIR (Fig. 13.2b) flat, as shown in Figure 13.2a.

Inverse Filtering

Representing the geologic impulse response function (Fig. 13.1c) by the symbol s(z), the relationship between the noise-free gamma-ray log c(z), and the distribution of radioactive material along a borehole, g(z), is given by

$$c(z) = g(z) * s(z) \qquad \dots\dots\dots\dots\dots\dots\dots\dots\dots\dots (1)$$

where the symbol * denotes convolution (see e.g. Kanasewich, 1973, for a discussion of convolution). In the frequency domain this is expressed as

$$C(\omega) = G(\omega) \cdot S(\omega) \qquad \dots\dots\dots\dots\dots\dots\dots\dots\dots (2)$$
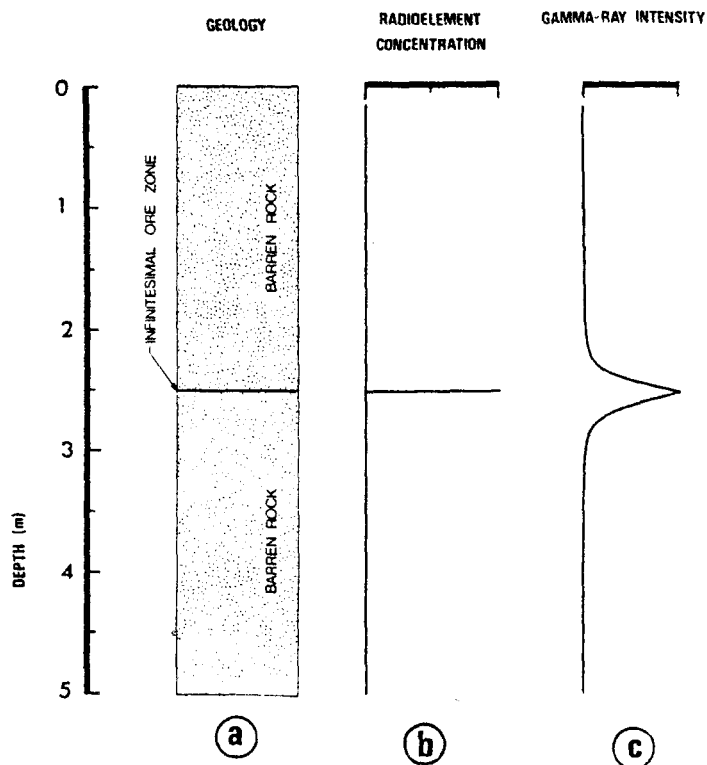

Figure 13.1

(a) Geologic column showing an infinitesimally thin radioactive ore zone sandwiched between two thick barren zones, a 'geologic impulse' of radioactive ore.

(b) Plot of radioelement concentration with depth corresponding to Figure 13.1a.

(c) Noise-free response of a point-detector to the thin ore zone, the 'geologic impulse response'.

where $C(\omega)$, $G(\omega)$ and $S(\omega)$ are the Fourier transforms of $f(z)$, $g(z)$, and $s(z)$, respectively. Thus in the frequency domain the distribution of radioactive material is given by

$$G(\omega) = C(\omega) \cdot \left(\frac{1}{S(\omega)} \right) \quad \dots \dots \dots \dots \dots \dots \dots \dots (3)$$

Letting

$$F(\omega) = \frac{1}{S(\omega)}$$

then in the space domain

$$g(z) = c(z) * f(z) \quad \dots \dots \dots \dots \dots \dots \dots \dots (4)$$

where the inverse filter $f(z)$ is the Fourier transform of $F(\omega)$.

In the special case of the infinitesimally thin ore zone (Fig. 13.1)

$$C(\omega) = S(\omega)$$

Therefore, from equation (3)

$$G(\omega) = S(\omega) \cdot \left(\frac{1}{S(\omega)} \right) = 1$$

In theory, then, the flat spectrum of the impulse has been recovered by inverse filtering, in the absence of noise.

The Iterative Algorithm

The heart of the computer program given by Scott (1962), as well as of the modern counterpart of that program, is an iterative algorithm which, in its simplest form, is shown in the flow chart given in Figure 13.3. The step enclosed in the dashed box, that of setting negative grade values equal to zero will be ignored for the present. Letting the contribution of the ith step in the iteration to the value of $g(z)$ be given by $b_i(z)$, from the flow chart we have:

initial state	$b_0(z) = c(z)$
contribution of first iteration	$b_1(z) = c(z) - c(z)*s(z)$
contribution of second iteration	$b_2(z) = c(z) - 2c(z)*s(z) + c(z)*s(z)*s(z)$
contribution of third iteration	$b_3(z) = c(z) - 3c(z)*s(z)$ $+ 3c(z)*s(z)*s(z) - c(z)*s(z)*s(z)*s(z)$

Expressing this in the frequency domain, where the contribution of the ith step in the iteration is $B_i(\omega)$,

$$B_0(\omega) = C(\omega)$$

$$B_1(\omega) = C(\omega) - C(\omega) \, S(\omega)$$

$$B_2(\omega) = C(\omega) - 2C(\omega) \, S(\omega) + C(\omega) \, S^2(\omega)$$

$$B_3(\omega) = C(\omega) - 3C(\omega) \, S(\omega) + 3C(\omega) \, S^2(\omega) - C(\omega) \, S^3(\omega)$$

In general terms, then

$$B_i(\omega) = C(\omega) \left[1 - S(\omega) \right]^i \quad \text{where } i = 0,1,2,\dots, n$$

Thus, in the frequency domain the processed log after n iterations, $G_n(\omega)$, is given by

$$G_n(\omega) = \sum_{i=0}^{n} B_i(\omega) = \sum_{i=0}^{n} C(\omega) \left[1 - S(\omega) \right]^i$$

or

$$G_n(\omega) = C(\omega) \sum_{i=0}^{n} \left[1 - S(\omega) \right]^i \quad \dots \dots \dots \dots (5)$$

It can be shown that the series

$$\sum_{i=0}^{n} \left[1 - S(\omega) \right]^i$$

converges to $1/S(\omega)$ as n becomes large, for all values of $\_$ such that

$$0 \leqslant \left| 1 - S(\omega) \right| < 1 \quad \dots \dots \dots \dots \dots \dots \dots \dots (6)$$

(see e.g. Sokolnikoff and Sokolnikoff, 1941). As can be seen from Figure 13.2b, the condition given by equation (6) will be valid. Thus, after many iterations the value of $G_n(\omega)$ approaches

$$G_n(\omega) = C(\omega) \cdot \left(\frac{1}{S(\omega)} \right) \quad \dots \dots \dots \dots \dots \dots (7)$$

which is identical to equation (3). Thus it has been shown that the inverse filter technique and the iterative technique for processing gamma-ray logs are theoretically equivalent operations.

Referring once again to the flow chart for the iterative algorithm (Fig. 13.3) consider the step shown in the dashed box, that of setting negative ore grade values equal to zero. As will be shown more fully later, the iteration process amplifies high frequencies while exerting relatively little effect on low frequencies. Thus, the scatter in the iterated ore grade values is greater than the scatter in gamma-ray counts. This means that some of the processed ore grade values may be negative; however, the mean grade over a given zone will be correct. The act of setting negative grade values equal to zero introduces statistical bias, causing the mean calculated grade over the zone to be erroneously high. In general this is a small effect, but since this step in the processing of the log is unnecessary and invalid, it should be eliminated.
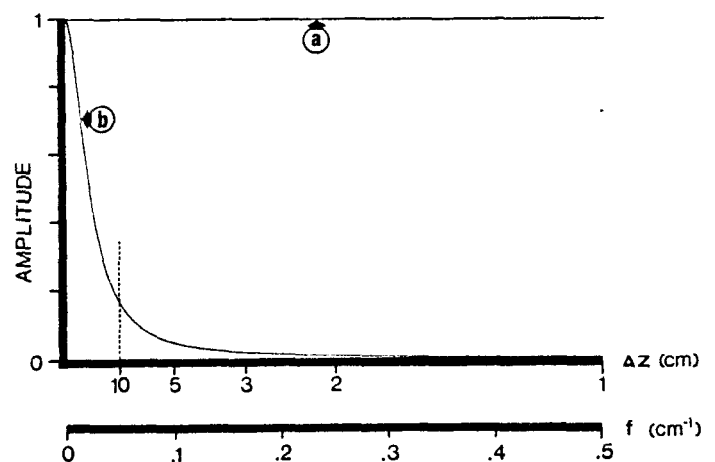
Figure 13.2

(a) Amplitude spectrum of a spike (Fig. 13.1b).

(b) Amplitude spectrum of the noise-free geologic impulse response (Fig. 13.1c). Two horizontal axes are shown for convenience. The lower one, spatial frequency (f), is given by $f = \omega/2\pi$. The upper scale is calibrated in sampling interval (Δz), to make it easy to study the amplitude spectra in relation to the Nyquist frequency f_N for various sampling intervals, where $f_N = 1/2\Delta z$. The amplitude spectrum is a plot of amplitude as a function of spatial frequency (f); the upper horizontal axis, Δz, is provided for reference only. Note especially the signific~ amount of energy at frequencies higher than Nyquist frequency for $\Delta z = 10$ cm (dashed line).
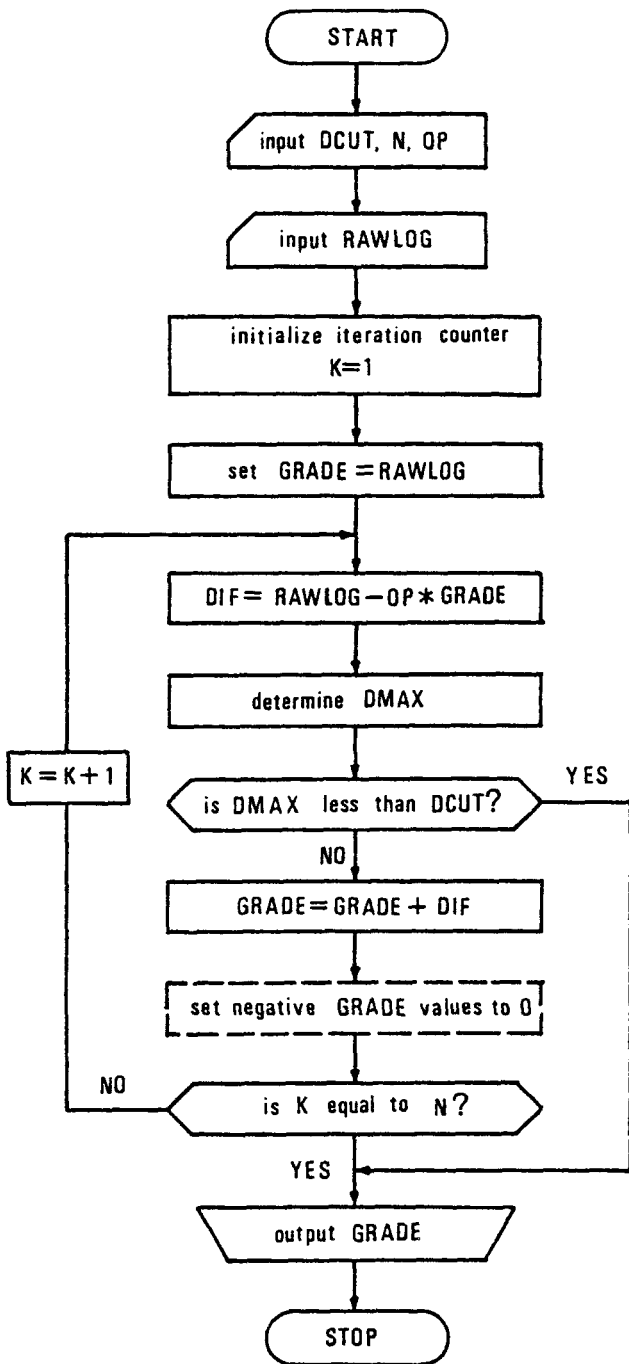
Figure 13.3. Flow chart for the iterative algorithm used for determining ore grade values from a gamma-ray log. The parameters used are:

N — the number of iterations to be performed.

OP — the digitized system impulse response function determined in a model borehole.

RAWLOG — the array containing the raw gamma-ray log.

GRADE — the array containing the approximate grade values being iterated.

DIF — defined in flow chart.

DMAX — maximum value of DIF.

DCUT — assigned cutoff value of DMAX to stop processing before N iterations have been reached.

Figure 13.4. Amplitude spectrum of the theoretical inverse operator (curve a) and of the 3-point approximate inverse operators for sampling intervals of 1 cm (b), 3 cm (c), 5 cm (d), and 10 cm (e).

Figure 13.5. Amplitude spectrum of the noise-free geologic impulse response (shown in Fig. 13.2b) after application of the theoretical inverse operator (a), and approximate inverse operators corresponding to sampling intervals of 1 cm(b), 3 cm (c), 5 cm (d), and 10 cm (e).

Iteration and Inverse Filtering in Practice

The problem of developing an inverse filter operator for processing gamma-ray logs may be approached from many directions. Perhaps the simplest solution has been presented by Conaway and Killeen (in press), based in part on earlier work by Czubek (1971) and Davydov (1970). Here the GIR is approximated by the function

$$s(z) = \frac{\alpha}{2} e^{-\alpha|z|} \qquad \qquad \ldots\ldots\ldots\ldots\ldots\ldots\ldots\ldots\ldots(8)$$

where the constant α is most easily determined in a model borehole. This function has been found to provide a reasonable fit to the experimentally determined response function with Geological Survey of Canada gamma-ray logging equipment. The amplitude spectrum of the theoretical inverse operator is shown as curve a in Figure 13.4. This theoretical inverse operator may be approximated by a simple 3-point operator given by

$$\left(-\frac{1}{(\alpha\Delta z)^2}, \quad 1 + \frac{2}{(\alpha\Delta z)^2}, \quad -\frac{1}{(\alpha\Delta z)^2} \right). \qquad \ldots\ldots\ldots(9)$$
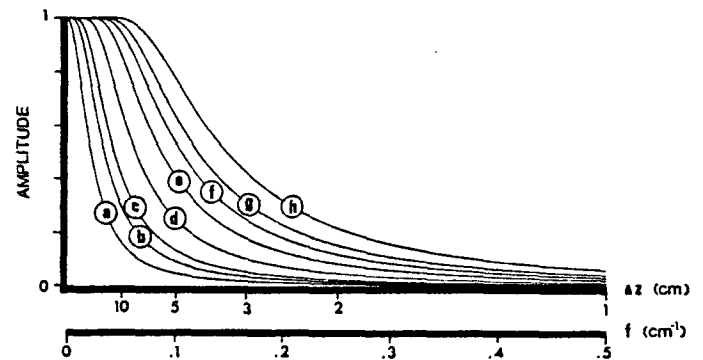
Figure 13.7. (a) Amplitude spectrum of the noise-free geologic impulse response. The other curves show the amplitude spectrum of the GIR after 1 iteration (b), 2 iterations (c), 5 iterations (d), 10 iterations (e), 15 iterations (f), 20 iterations (g), and 30 iterations (h).

Figure 13.6. Amplitude spectrum of geologic impulse response with noise, after application of theoretical inverse operator (a), and approximate inverse operators corresponding to sampling intervals of 1 cm (b), 3 cm (c), 5 cm (d), and 10 cm (e).

The amplitude spectra for this operator for sampling intervals Δz = 1, 3, 5, and 10 cm are also shown in Figure 13.4 as curves b through e, respectively.

If the assumed shape of the GIR represents a good approximation in a given case, then the noise-free amplitude spectrum of the GIR processed with the exact inverse operator would resemble Figure 13.5 curve a. The approximate inverse operator would produce spectra resembling curves b through e, depending on the sampling interval. The effect of noise on the processed amplitude spectrum is shown in Figure 13.6 curves a through e. Two points are immediately apparent: (1) The operator performance improves as Δz decreases (Fig. 13.5) and (2) a low-pass filter will be required if a sampling interval much shorter than 10 cm is used (Fig. 13.6). It can be seen from Figure 13.2, curve b that a significant amount of information may be present at frequencies higher than the Nyquist frequency for Δz = 10 cm (vertical dashed line). Thus, to reduce errors due to aliasing of this high frequency information a sampling interval shorter than 10 cm should be used.

In the case of the iterative processing technique, Figure 13.7 curve a shows the noise-free amplitude spectrum of the GIR; curves b through h show the shape of the spectrum after 1, 2, 5, 10, 15, 20, and 30 iterations, respectively. Similarly, Figure 13.8 shows the iterative results with a noise level identical to that used in producing Figure 13.6. Here it can be seen once again that a smoothing filter is needed for sampling intervals significantly less than Δz = 10 cm. Although it may seem at first that the noise level of the processed log may be controlled sufficiently by stopping after fewer iterations when processing data obtained at smaller sampling intervals, in fact this technique

does not give results as good as those which may be obtained by using more iterations and a smoothing filter. This latter technique gives more accurate information at low frequencies and a better cutoff at higher frequencies.

Two examples are presented to illustrate some of the points discussed above. Figure 13.9a shows a portion of a digitally recorded gamma-ray log run at v = 3 m/min with sampling interval Δt = 2 s (Δz = 10 cm). The log was processed iteratively (10 iterations) and is plotted as Figure 13.9b. The inverse filtered log (approximate operator) is given as Figure 13.9c. Figures 13.9b and 13.9c have been plotted on a scale of gamma-ray intensity rather than ore grade to facilitate comparison of the 3 curves. The agreement between the two processed logs, while not exa is very close. In order to process the raw gamma-ray . (Fig. 13.9a), which has approximately 160 gamma-ray readings, the iterative technique required on the order of 14 500 multiplication operations and 18 000 additions or subtractions. The inverse filter method required only about 500 multiplications and 500 additions. Thus in this case inverse filtering is more efficient by a factor of about 30 in terms of computation time.

As a second example, consider the gamma-ray log shown in Figure 13.10a. This log is from the same section of the borehole as Figure 13.9, but run at a speed of 1 m/min with Δt = 2 s (Δz = 3.3 cm), thus giving similar counting statistics to Figure 13.9. Figure 13.10b shows the iterated log after 10 iterations. This processed log is rather noisy, and a smoothing filter should be used. The program as it stands now does not have a provision for smoothing, since it has traditionally been used with a sampling interval of 10-15 cm. Figure 13.10c shows the deconvolved and smoothed log produced using a 9-point combined smoothing and approximate inverse operator (see Conaway and Killeen, in press). The resolution here is somewhat better than in Figure 13.9, where Δz = 10 cm. To process the log shown in Figure 13.10 the inverse filter technique required about 4500 multiplications and a similar number of additions, while the iterative technique, even without smoothing, required about 135 000 multiplications and 145 000 additions or subtractions. Once again this represents a difference in computational efficiency of about 30:1 in favour of inverse filtering. Figure 13.10b can be smoothed to give results similar to Figure 13.10c, if a suitable smoothing routine is incorporated into the computer program. Selection of a suitable length of smooth operator of a given type is a matter requiring s experience. This decision is perhaps best made on the ba...
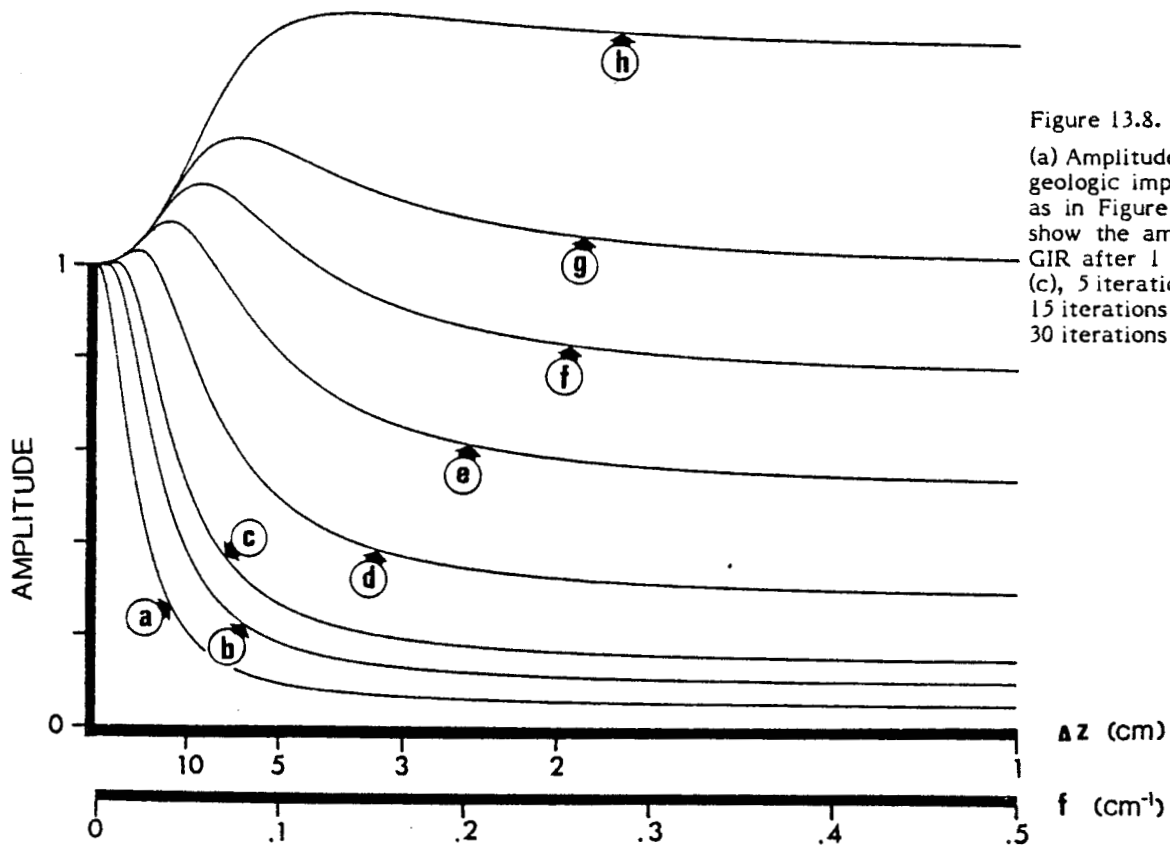
Figure 13.8.

(a) Amplitude spectrum of the geologic impulse response with noise as in Figure 13.6. The other curves show the amplitude spectrum of the GIR after 1 iteration (b), 2 iterations (c), 5 iterations (d), 10 iterations (e), 15 iterations (f), 20 iterations (g), and 30 iterations (h).
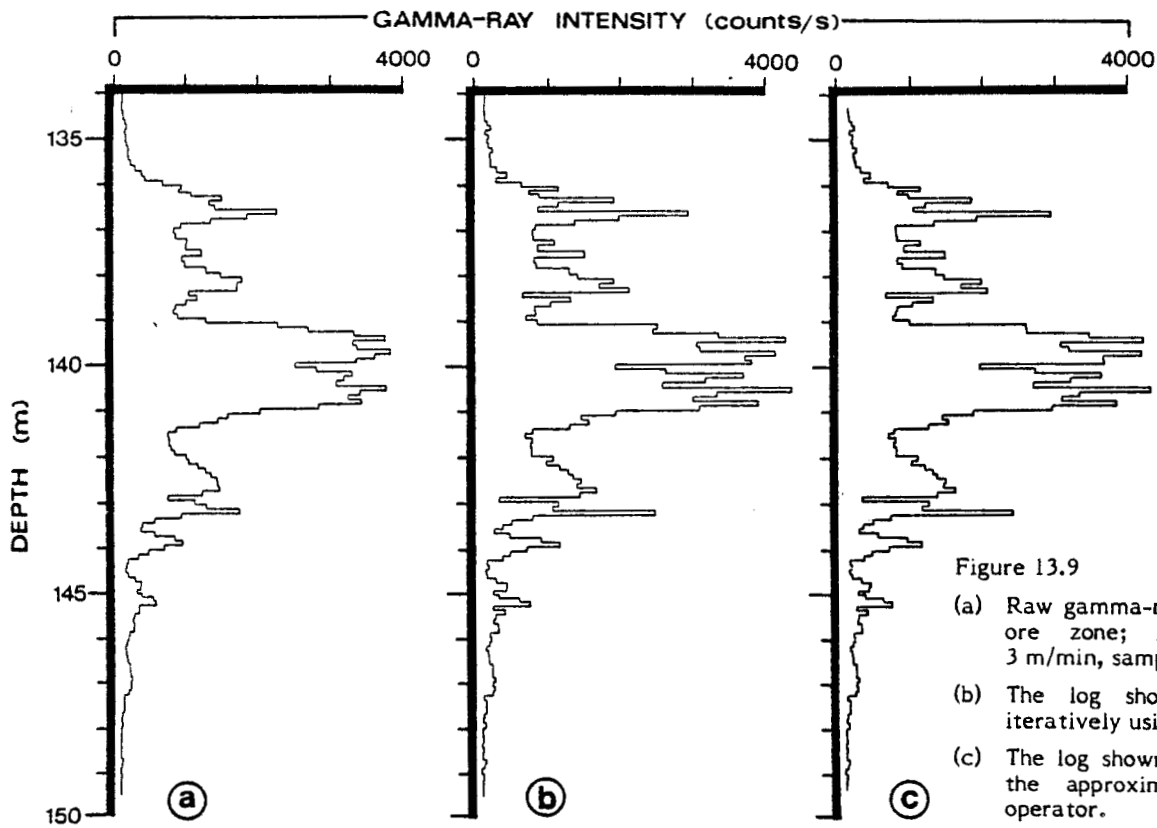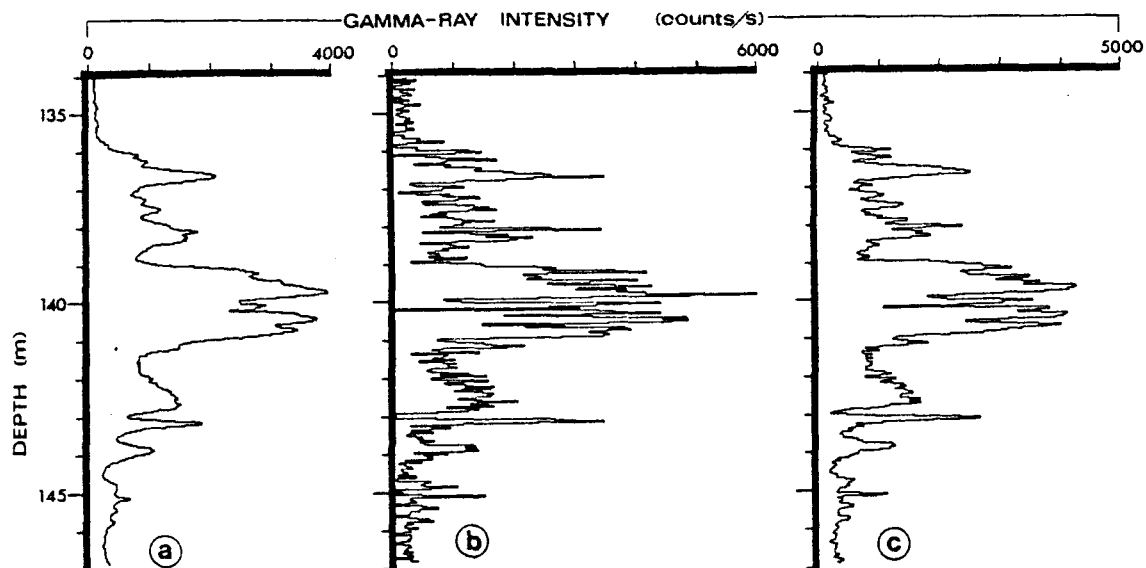

Figure 13.9

(a) Raw gamma-ray log from a uranium ore zone; logging velocity $v = 3$ m/min, sampling interval $\Delta z = 10$ cm.

(b) The log shown in (a) processed iteratively using 10 iterations.

(c) The log shown in (a) processed with the approximate 3-point inverse operator.

GAMMA-RAY INTENSITY (counts/s)

Figure 13.10

(a) Raw gamma-ray log from the same ore zone as in Figure 13.9; logging velocity v = 1 m/min, sampling interval Δz = 3.3 cm.

(b) The log shown in (a) processed iteratively using 10 iterations.

(c) The log shown in (a) processed with the approximate 3-point inverse operator.

of studies of the repeatibility of several processed logs obtained in the same borehole under the same conditions. The best smoothing operator will be the shortest one which still produces results of acceptable repeatibility.

Conclusions

It has been demonstrated that the iterative and inverse filter techniques for processing gamma-ray borehole logs are theoretically equivalent operations. From the example log with a sampling interval Δz = 10 cm (Fig. 13.9) it is clear that, while the approximate inverse filter and the iterative technique with 10 iterations give very similar results, the inverse filter method is many times more efficient computationally. From the amplitude spectra and the example log with Δz = 3.3 cm (Fig. 13.10) it can be seen that a sampling interval less than 10 cm should be used for improved resolution and to reduce aliasing errors; a smoothing filter is required with either method for the shorter sampling intervals.

Because discrete convolution is a sequential operation, the inverse filter technique requires little core memory, and allows the data to be processed on-line concurrently with the logging operations using a minicomputer or microprocessor. It is likely that the next generation of portable digital gamma-ray logging equipment will include such a facility. A proposed system of this type has been described by Killeen et al. (1978).

References

Conaway, J.G. and Killeen, P.G.
    Quantitative uranium determinations from gamma-ray logs by application of digital time series analysis; Geophysics, v. 43 (in press).

Czubek, J.A.
    1971: Differential interpretation of gamma-ray logs: I. Case of the static gamma-ray curve: Report no. 760/1, Nuclear Energy Information Center of the Polish Government Commissioner for Use of Nuclear Energy, Warsaw, Poland.

Davydov, Y.B.
    1970: Odnomernaya obratnaya zadacha gamma-karotazha skvazhin (One dimensional inversion problem of borehole gamma logging): Izv. Vyssh. Uchebn. Zaved., Geol. i. Razvedka, no. 2, p. 105-109 (in Russian).

Kanasewich, E.R.
    1973: Time sequence analysis in Geophysics; Calgary, University of Alberta Press.

Killeen, P.G., Conaway, J.G. and Bristow, Q.
    1978: A gamma-ray spectral logging system including digital playback, with recommendations for a new generation system; in Current Research, Part A, Geol. Surv. Can., Paper 78-1A, p. 235-241.

Scott, J.H.
    1962: The GAMLOG computer program; U.S.A.E.C. Report RME-143, Grand Junction, Colorado.

    1963: Computer analysis of gamma-ray logs; Geophysics, v. 28, p. 457-465.

Scott, J.H., Dodd, P.H., Droullard, R.F., and Mudra, P.J.
    1961: Quantitative interpretation of gamma-ray logs; Geophysics, v. 26, p. 182-191.

Sokolnikoff, I.S. and Sokolnikoff, E.S.
    1941: Higher mathematics for engineers and physicists; McGraw Hill, New York.

John G. Conaway and P.G. Killeen
Resource Geophysics and Geochemistry Division

Abstract

Conaway, John G., and Killeen, P.G., Computer processing of gamma-ray logs: Iteration and inverse filtering; in Current Research, Part B, Geol. Surv. Can., Paper 78-1B, p. 83-88, 1978.

For nearly two decades an iterative computer technique has been used for processing gamma-ray logs to determine the distribution of uranium along a borehole. Recently an inverse filter technique has been developed for the same application. Analysis of the iterative technique shows that it approaches theoretical equivalence with the inverse filter technique as the number of iterations increases. In tests with gamma-ray borehole logs with a sampling interval of 10 cm there was little difference in the results produced by the two methods. In practice a sampling interval shorter than 10 cm should be used to improve resolution and reduce aliasing errors. In this case a smoothing filter is required with both techniques to reduce the high-frequency noise.

The inverse filter technique generally requires less than 5 per cent as much computing time as iteration, and may be accomplished using an 'open-ended' algorithm, thereby making possible on-line processing of the data using a minicomputer or microprocessor, concurrent with the logging of the borehole.

Introduction

An iterative computer technique for determining radioelement concentrations from gamma-ray borehole logs has been in routine use in the United States since it was first introduced by Scott et al. (1961), and Scott (1962; 1963). Recently an inverse filter technique has been presented by Conaway and Killeen (in press) which is intended for the same purpose – determining radioelement concentrations from gamma-ray logs. A number of questions regarding the two techniques immediately present themselves: Are the results from the two methods equivalent? Which is more efficient? What are the advantages and disadvantages of each? The answers to these questions can be obtained from theoretical considerations, computer studies, and tests with gamma-ray borehole logs.

First a brief review of the theory is necessary. Consider the case of an infinitesimally thin radioactive ore zone embedded in a thick sequence of barren rock (Fig. 13.1a). The function expressing the distribution of radioactive material with depth is an impulse or 'spike' (Fig. 13.1b) having a flat amplitude spectrum (Fig. 13.2, curve a). This is the desired output of a gamma-ray logging system in the presence of a thin ore zone – a spike proportional in height to the ore grade. The actual output which would be obtained under noise-free conditions using a point-detector would resemble Figure 13.1c. This curve, called the geologic impulse response or GIR (Conaway and Killeen, in press), has an amplitude spectrum similar to Figure 13.2, curve b.

The purpose of computer processing of the raw data is to convert the geologic impulse response (Fig. 13.1c) into the spike (Fig. 13.1b) within the limitations imposed by noise. In other words, in the ideal case the data are processed to make the amplitude spectrum of the GIR (Fig. 13.2b) flat, as shown in Figure 13.2a.

Inverse Filtering

Representing the geologic impulse response function (Fig. 13.1c) by the symbol s(z), the relationship between the noise-free gamma-ray log c(z), and the distribution of radioactive material along a borehole, g(z), is given by

$$c(z) = g(z) * s(z) \qquad \dots\dots\dots\dots\dots\dots\dots\dots\dots\dots\dots (1)$$

where the symbol * denotes convolution (see e.g. Kanasewich, 1973, for a discussion of convolution). In the frequency domain this is expressed as

$$C(\omega) = G(\omega) \cdot S(\omega) \qquad \dots\dots\dots\dots\dots\dots\dots\dots\dots\dots (2)$$
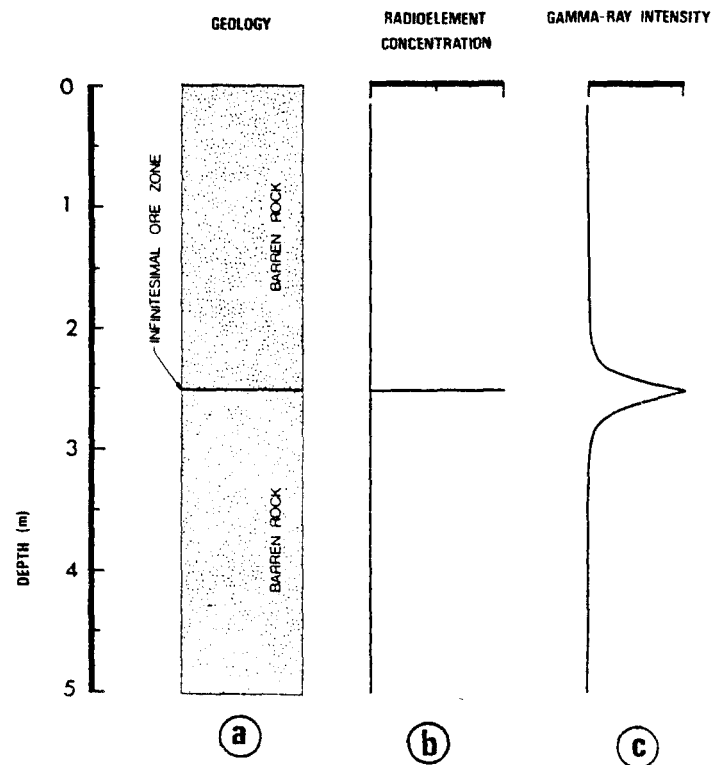

Figure 13.1

(a) Geologic column showing an infinitesimally thin radioactive ore zone sandwiched between two thick barren zones, a 'geologic impulse' of radioactive ore.

(b) Plot of radioelement concentration with depth corresponding to Figure 13.1a.

(c) Noise-free response of a point-detector to the thin ore zone, the 'geologic impulse response'.

where $C(\omega)$, $G(\omega)$ and $S(\omega)$ are the Fourier transforms of $f(z)$, $g(z)$, and $s(z)$, respectively. Thus in the frequency domain the distribution of radioactive material is given by

$$G(\omega) = C(\omega) \cdot \left(\frac{1}{S(\omega)}\right) \quad \dots\dots\dots\dots\dots\dots\dots\dots(3)$$

Letting

$$F(\omega) = \frac{1}{S(\omega)}$$

then in the space domain

$$g(z) = c(z) * f(z) \quad \dots\dots\dots\dots\dots\dots\dots\dots\dots\dots(4)$$

where the inverse filter $f(z)$ is the Fourier transform of $F(\omega)$.

In the special case of the infinitesimally thin ore zone (Fig. 13.1)

$$C(\omega) = S(\omega)$$

Therefore, from equation (3)

$$G(\omega) = S(\omega) \cdot \left(\frac{1}{S(\omega)}\right) = 1$$

In theory, then, the flat spectrum of the impulse has been recovered by inverse filtering, in the absence of noise.

The Iterative Algorithm

The heart of the computer program given by Scott (1962), as well as of the modern counterpart of that program, is an iterative algorithm which, in its simplest form, is shown in the flow chart given in Figure 13.3. The step enclosed in the dashed box, that of setting negative grade values equal to zero will be ignored for the present. Letting the contribution of the ith step in the iteration to the value of $g(z)$ be given by $b_i(z)$, from the flow chart we have:

initial state	$b_0(z) = c(z)$
contribution of first iteration	$b_1(z) = c(z) - c(z)*s(z)$
contribution of second iteration	$b_2(z) = c(z) - 2c(z)*s(z) + c(z)*s(z)*s(z)$
contribution of third iteration	$b_3(z) = c(z) - 3c(z)*s(z)$ $+ 3c(z)*s(z)*s(z) - c(z)*s(z)*s(z)*s(z)$

Expressing this in the frequency domain, where the contribution of the ith step in the iteration is $B_i(\omega)$,

$$B_0(\omega) = C(\omega)$$

$$B_1(\omega) = C(\omega) - C(\omega) S(\omega)$$

$$B_2(\omega) = C(\omega) - 2C(\omega) S(\omega) + C(\omega) S^2(\omega)$$

$$B_3(\omega) = C(\omega) - 3C(\omega) S(\omega) + 3C(\omega) S^2(\omega) - C(\omega) S^3(\omega)$$

In general terms, then

$$B_i(\omega) = C(\omega) \left[1 - S(\omega)\right]^i \quad \text{where } i = 0,1,2,\dots, n$$

Thus, in the frequency domain the processed log after n iterations, $G_n(\omega)$, is given by

$$G_n(\omega) = \sum_{i=0}^{n} B_i(\omega) = \sum_{i=0}^{n} C(\omega) \left[1 - S(\omega)\right]^i$$

or

$$G_n(\omega) = C(\omega) \sum_{i=0}^{n} \left[1 - S(\omega)\right]^i \dots\dots\dots\dots\dots(5)$$

It can be shown that the series

$$\sum_{i=0}^{n} \left[1 - S(\omega)\right]^i$$

converges to $1/S(\omega)$ as n becomes large, for all values of S such that

$$0 \leqslant \left| 1 - S(\omega) \right| < 1 \quad \dots\dots\dots\dots\dots\dots\dots\dots(6)$$

(see e.g. Sokolnikoff and Sokolnikoff, 1941). As can be seen from Figure 13.2b, the condition given by equation (6) will be valid. Thus, after many iterations the value of $G_n(\omega)$ approaches

$$G_n(\omega) = C(\omega) \cdot \left(\frac{1}{S(\omega)}\right) \quad \dots\dots\dots\dots\dots\dots(7)$$

which is identical to equation (3). Thus it has been shown that the inverse filter technique and the iterative technique for processing gamma-ray logs are theoretically equivalent operations.

Referring once again to the flow chart for the iterative algorithm (Fig. 13.3) consider the step shown in the dashed box, that of setting negative ore grade values equal to zero. As will be shown more fully later, the iteration process amplifies high frequencies while exerting relatively little effect on low frequencies. Thus, the scatter in the iterated ore grade values is greater than the scatter in gamma-ray counts. This means that some of the processed ore grade values may be negative; however, the mean grade over a given zone will be correct. The act of setting negative grade values equal to zero introduces statistical bias, causing the mean calculated grade over the zone to be erroneously high. In general this is a small effect, but since this step in the processing of the log is unnecessary and invalid, it should be eliminated.
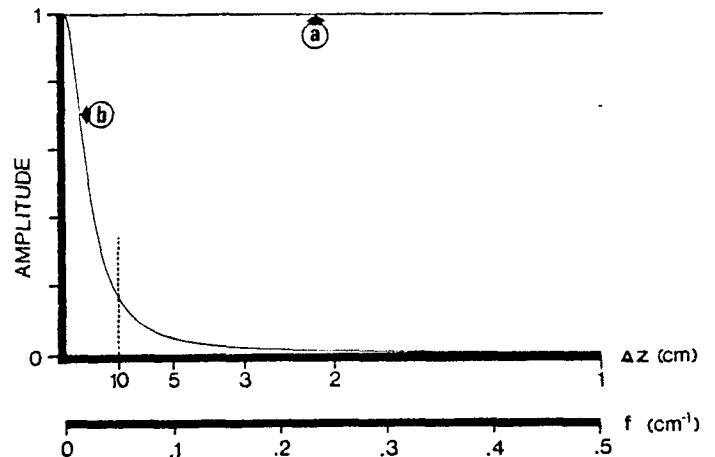

Figure 13.2

(a) Amplitude spectrum of a spike (Fig. 13.1b).

(b) Amplitude spectrum of the noise-free geologic impulse response (Fig. 13.1c). Two horizontal axes are shown for convenience. The lower one, spatial frequency (f), is given by $f = \omega/2\pi$. The upper scale is calibrated in sampling interval (Δz), to make it easy to study the amplitude spectra in relation to the Nyquist frequency f_N for various sampling intervals, where $f_N = 1/2\Delta z$. The amplitude spectrum is a plot of amplitude as a function of spatial frequency (f); the upper horizontal axis, Δz, is provided for reference only. Note especially the significant amount of energy at frequencies higher than Nyquist frequency for $\Delta z = 10$ cm (dashed line).
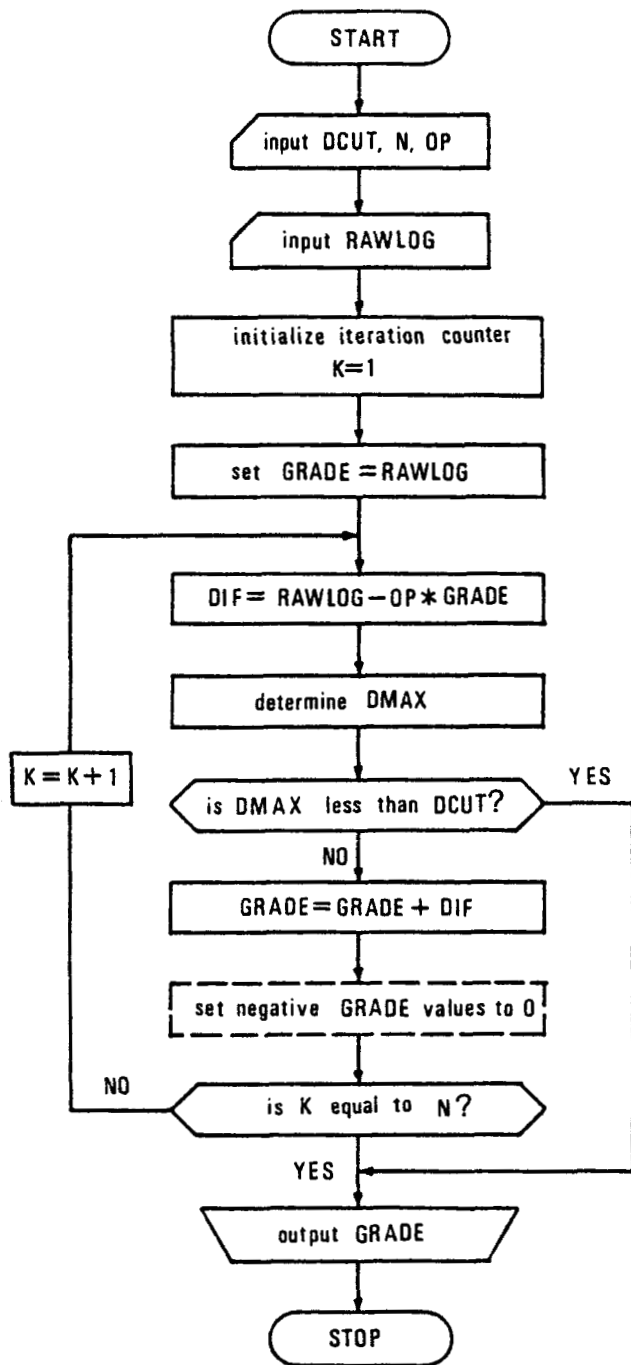
Figure 13.3. Flow chart for the iterative algorithm used for determining ore grade values from a gamma-ray log. The parameters used are:

N — the number of iterations to be performed.

OP — the digitized system impulse response function determined in a model borehole.

RAWLOG — the array containing the raw gamma-ray log.

GRADE — the array containing the approximate grade values being iterated.

DIF — defined in flow chart.

DMAX — maximum value of DIF.

DCUT — assigned cutoff value of DMAX to stop processing before N iterations have been reached.

Figure 13.4. Amplitude spectrum of the theoretical inverse operator (curve a) and of the 3-point approximate inverse operators for sampling intervals of 1 cm (b), 3 cm (c), 5 cm (d), and 10 cm (e).

Figure 13.5. Amplitude spectrum of the noise-free geologic impulse response (shown in Fig. 13.2b) after application of the theoretical inverse operator (a), and approximate inverse operators corresponding to sampling intervals of 1 cm(b), 3 cm (c), 5 cm (d), and 10 cm (e).

Iteration and Inverse Filtering in Practice

The problem of developing an inverse filter operator for processing gamma-ray logs may be approached from many directions. Perhaps the simplest solution has been presented by Conaway and Killeen (in press), based in part on earlier work by Czubek (1971) and Davydov (1970). Here the GIR is approximated by the function

$$s(z) = \frac{\alpha}{2} e^{-\alpha|z|} \quad \dots\dots\dots\dots\dots\dots\dots\dots\dots\dots\dots(8)$$

where the constant α is most easily determined in a model borehole. This function has been found to provide a reasonable fit to the experimentally determined response function with Geological Survey of Canada gamma-ray logging equipment. The amplitude spectrum of the theoretical inverse operator is shown as curve a in Figure 13.4. This theoretical inverse operator may be approximated by a simple 3-point operator given by

$$\left(-\frac{1}{(\alpha \Delta z)^2}, \quad 1 + \frac{2}{(\alpha \Delta z)^2}, \quad -\frac{1}{(\alpha \Delta z)^2} \right). \quad \dots\dots\dots\dots(9)$$
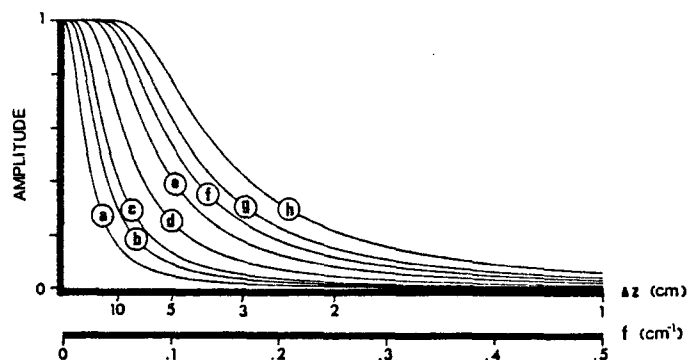
Figure 13.7. (a) Amplitude spectrum of the noise-free geologic impulse response. The other curves show the amplitude spectrum of the GIR after 1 iteration (b), 2 iterations (c), 5 iterations (d), 10 iterations (e), 15 iterations (f), 20 iterations (g), and 30 iterations (h).

Figure 13.6. Amplitude spectrum of geologic impulse response with noise, after application of theoretical inverse operator (a), and approximate inverse operators corresponding to sampling intervals of 1 cm (b), 3 cm (c), 5 cm (d), and 10 cm (e).

The amplitude spectra for this operator for sampling intervals Δz = 1, 3, 5, and 10 cm are also shown in Figure 13.4 as curves b through e, respectively.

If the assumed shape of the GIR represents a good approximation in a given case, then the noise-free amplitude spectrum of the GIR processed with the exact inverse operator would resemble Figure 13.5 curve a. The approximate inverse operator would produce spectra resembling curves b through e, depending on the sampling interval. The effect of noise on the processed amplitude spectrum is shown in Figure 13.6 curves a through e. Two points are immediately apparent: (1) The operator performance improves as Δz decreases (Fig. 13.5) and (2) a low-pass filter will be required if a sampling interval much shorter than 10 cm is used (Fig. 13.6). It can be seen from Figure 13.2, curve b that a significant amount of information may be present at frequencies higher than the Nyquist frequency for Δz = 10 cm (vertical dashed line). Thus, to reduce errors due to aliasing of this high frequency information a sampling interval shorter than 10 cm should be used.

In the case of the iterative processing technique, Figure 13.7 curve a shows the noise-free amplitude spectrum of the GIR; curves b through h show the shape of the spectrum after 1, 2, 5, 10, 15, 20, and 30 iterations, respectively. Similarly, Figure 13.8 shows the iterative results with a noise level identical to that used in producing Figure 13.6. Here it can be seen once again that a smoothing filter is needed for sampling intervals significantly less than Δz = 10 cm. Although it may seem at first that the noise level of the processed log may be controlled sufficiently by stopping after fewer iterations when processing data obtained at smaller sampling intervals, in fact this technique

does not give results as good as those which may be obtained by using more iterations and a smoothing filter. This latter technique gives more accurate information at low frequencies and a better cutoff at higher frequencies.

Two examples are presented to illustrate some of the points discussed above. Figure 13.9a shows a portion of a digitally recorded gamma-ray log run at v = 3 m/min with sampling interval Δt = 2 s (Δz = 10 cm). The log was processed iteratively (10 iterations) and is plotted as Figure 13.9b. The inverse filtered log (approximate operator) is given as Figure 13.9c. Figures 13.9b and 13.9c have been plotted on a scale of gamma-ray intensity rather than ore grade to facilitate comparison of the 3 curves. Th agreement between the two processed logs, while not exe is very close. In order to process the raw gamma-ray . (Fig. 13.9a), which has approximately 160 gamma-ray readings, the iterative technique required on the order of 14 500 multiplication operations and 18 000 additions or subtractions. The inverse filter method required only about 500 multiplications and 500 additions. Thus in this case inverse filtering is more efficient by a factor of about 30 in terms of computation time.

As a second example, consider the gamma-ray log shown in Figure 13.10a. This log is from the same section of the borehole as Figure 13.9, but run at a speed of 1 m/min with Δt = 2 s (Δz = 3.3 cm), thus giving similar counting statistics to Figure 13.9. Figure 13.10b shows the iterated log after 10 iterations. This processed log is rather noisy, and a smoothing filter should be used. The program as it stands now does not have a provision for smoothing, since it has traditionally been used with a sampling interval of 10-15 cm. Figure 13.10c shows the deconvolved and smoothed log produced using a 9-point combined smoothing and approximate inverse operator (see Conaway and Killeen, in press). The resolution here is somewhat better than in Figure 13.9, where Δz = 10 cm. To process the log shown in Figure 13.10 the inverse filter technique required about 4500 multiplications and a similar number of additions, while the iterative technique, even without smoothing, required about 135 000 multiplications and 145 000 additions or subtractions. Once again this represents a difference in computational efficiency of about 30:1 in favour of inverse filtering. Figure 13.10b can be smoothed to give results similar to Figure 13.10c, if a suitable smoothing routine is incorporated into the computer program. Selection of a suitable length of smooth operator of a given type is a matter requiring s experience. This decision is perhaps best made on the ba.
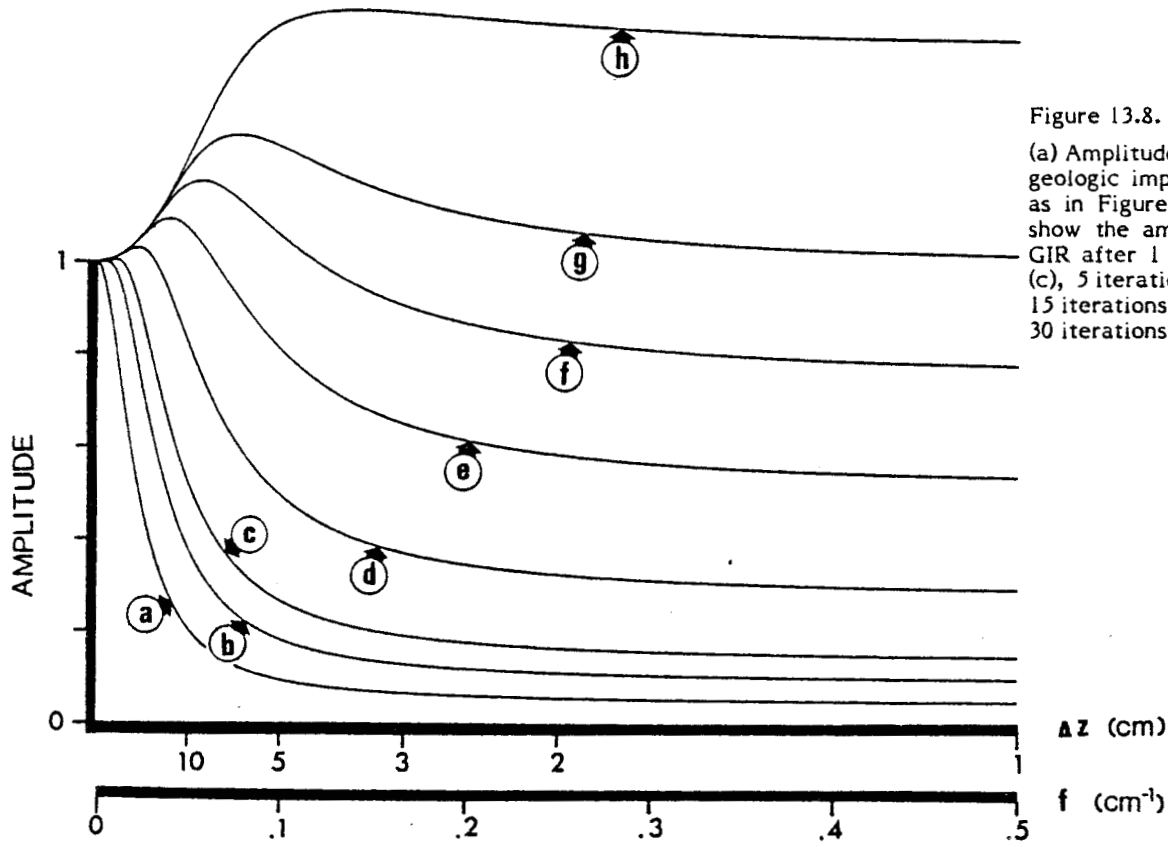
86

Figure 13.8.

(a) Amplitude spectrum of the geologic impulse response with noise as in Figure 13.6. The other curves show the amplitude spectrum of the GIR after 1 iteration (b), 2 iterations (c), 5 iterations (d), 10 iterations (e), 15 iterations (f), 20 iterations (g), and 30 iterations (h).
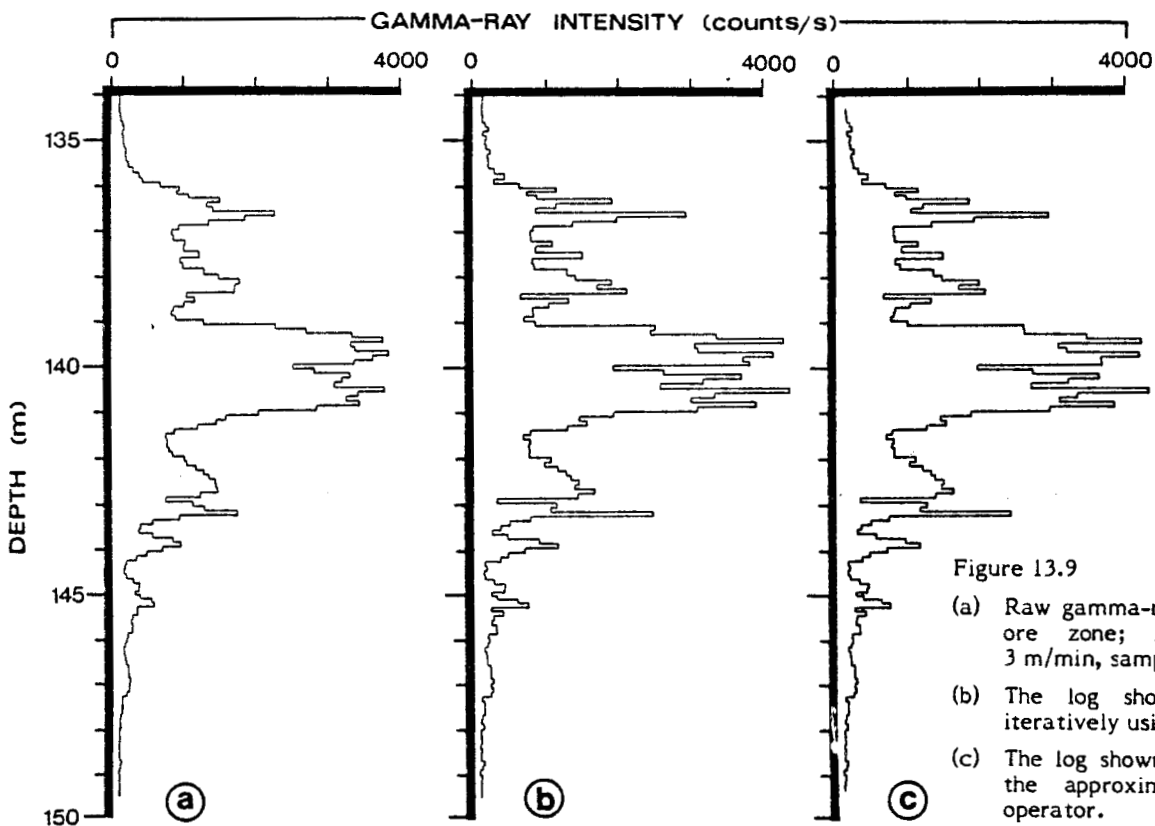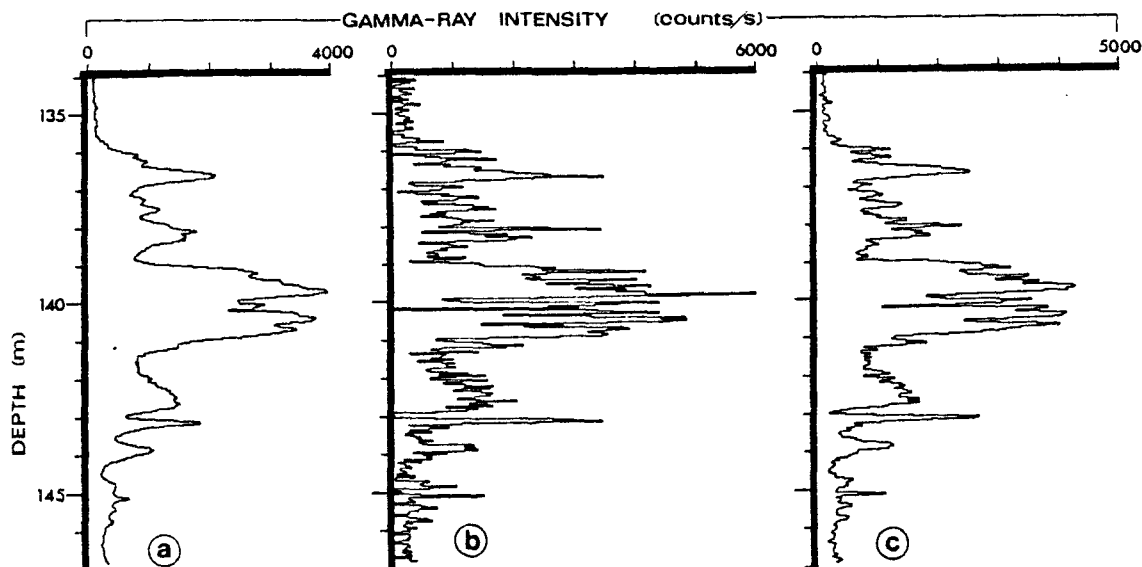

Figure 13.9

(a) Raw gamma-ray log from a uranium ore zone; logging velocity $v = 3$ m/min, sampling interval $\Delta z = 10$ cm.

(b) The log shown in (a) processed iteratively using 10 iterations.

(c) The log shown in (a) processed with the approximate 3-point inverse operator.

GAMMA-RAY INTENSITY (counts/s)

Figure 13.10

(a) Raw gamma-ray log from the same ore zone as in Figure 13.9; logging velocity v = 1 m/min, sampling interval Δz = 3.3 cm.

(b) The log shown in (a) processed iteratively using 10 iterations.

(c) The log shown in (a) processed with the approximate 3-point inverse operator.

of studies of the repeatibility of several processed logs obtained in the same borehole under the same conditions. The best smoothing operator will be the shortest one which still produces results of acceptable repeatibility.

Conclusions

It has been demonstrated that the iterative and inverse filter techniques for processing gamma-ray borehole logs are theoretically equivalent operations. From the example log with a sampling interval Δz = 10 cm (Fig. 13.9) it is clear that, while the approximate inverse filter and the iterative technique with 10 iterations give very similar results, the inverse filter method is many times more efficient computationally. From the amplitude spectra and the example log with Δz = 3.3 cm (Fig. 13.10) it can be seen that a sampling interval less than 10 cm should be used for improved resolution and to reduce aliasing errors; a smoothing filter is required with either method for the shorter sampling intervals.

Because discrete convolution is a sequential operation, the inverse filter technique requires little core memory, and allows the data to be processed on-line concurrently with the logging operations using a minicomputer or microprocessor. It is likely that the next generation of portable digital gamma-ray logging equipment will include such a facility. A proposed system of this type has been described by Killeen et al. (1978).

References

Conaway, J.G. and Killeen, P.G.
Quantitative uranium determinations from gamma-ray logs by application of digital time series analysis; Geophysics, v. 43 (in press).

Czubek, J.A.
1971: Differential interpretation of gamma-ray logs: I. Case of the static gamma-ray curve: Report no. 760/I, Nuclear Energy Information Center of the Polish Government Commissioner for Use of Nuclear Energy, Warsaw, Poland.

Davydov, Y.B.
1970: Odnomernaya obratnaya zadacha gamma-karotazha skvazhin (One dimensional inversion problem of borehole gamma logging): Izv. Vyssh. Uchebn. Zaved., Geol. i. Razvedka, no. 2, p. 105-109 (in Russian).

Kanasewich, E.R.
1973: Time sequence analysis in Geophysics; Calgary, University of Alberta Press.

Killeen, P.G., Conaway, J.G. and Bristow, Q.
1978: A gamma-ray spectral logging system including digital playback, with recommendations for a new generation system; in Current Research, Part A, Geol. Surv. Can., Paper 78-1A, p. 235-241.

Scott, J.H.
1962: The GAMLOG computer program; U.S.A.E.C. Report RME-143, Grand Junction, Colorado.

1963: Computer analysis of gamma-ray logs; Geophysics, v. 28, p. 457-465.

Scott, J.H., Dodd, P.H., Droullard, R.F., and Mudra, P.J.
1961: Quantitative interpretation of gamma-ray logs; Geophysics, v. 26, p. 182-191.

Sokolnikoff, I.S. and Sokolnikoff, E.S.
1941: Higher mathematics for engineers and physicists; McGraw Hill, New York.

A COMPARISON OF BISMUTH GERMANATE, CESIUM IODIDE, AND SODIUM IODIDE SCINTILLATION DETECTORS FOR GAMMA RAY SPECTRAL LOGGING IN SMALL DIAMETER BOREHOLES

Project 740085

J.G. Conaway, P.G. Killeen, and W.G. Hyatt
Resource Geophysics and Geochemistry Division

Abstract

Preliminary studies comparing a 19 x 76 mm bismuth germanate scintillation detector ($Bi_4Ge_3O_{12}$, commonly called BGO) to thallium activated sodium iodide (NaI(Tl)) and sodium activated cesium iodide (CsI(Na)) detectors of the same size have been completed. The potential advantage of BGO in gamma ray spectrometry is due to its high density ($7.13 g/cm^3$), which is almost twice that of the most commonly used detector material, NaI(Tl) ($3.67 g/cm^3$). The increased stopping power for high energy gamma rays of the high density BGO is evident in both the gamma ray logs and gamma ray spectra recorded in the model boreholes at the Geological Survey's calibration facility at Bells Corners, Ontario. The calibration factors (stripping factors and proportionality constants) for the three types of detectors are tabulated and compared both for the standard set of energy windows commonly used in portable spectrometers and for a set of wider energy windows which offer improved accuracy under some circumstances. The relative performance of the three detectors for determining uranium concentrations (using both sets of windows) was computed and tabulated for a range in U/Th concentration ratios from 10:1 to 1:10. A reduction of more than 50% in statistical errors in uranium determinations was found in comparing the BGO detector to NaI(Tl). CsI offers a more modest improvement of about 10%. In hardrock mining applications where the borehole diameter imposes a severe detector size restriction, the BGO detector appears to offer considerable advantages for uranium exploraton and evaluation.

Introduction

A problem that is well known in gamma ray spectrometry for geophysical exploration is the low gamma ray count rate measured in the high energy windows utilized for thorium (2.62 MeV) and uranium (1.76 MeV) determinations, leading to large statistical uncertainties in computed dioelement concentrations. Two approaches to solving this problem are to increase the counting time in any given location, or increase the detector volume. In gamma ray spectral logging the counting time depends on the logging speed, and extremely slow logging speeds are economically unattractive. The detector size, on the other hand, is limited by the diameter of the borehole. In hardrock mining and exploration, boreholes with diameters of 60 mm or less are common; often the logging must be done inside casing or drill rod, which further decreases the available space. Commonly a scintillation detector of diameter on the order of 19 mm must be used for gamma ray spectral logging, and these small detectors are extremely inefficient at high gamma ray energies (see Killeen and Bristow, 1976). Greater efficiency may be obtained with a detector which has higher density and/or atomic number (Z). Tests over the past few years with sodium activated cesium iodide detectors (CsI(Na)) which have a density of $4.51 g/cm^3$ have shown a significant improvement over thallium activated sodium iodide (NaI(Tl)), (density $3.67 g/cm^3$) in counting statistics for the high energy windows. In addition CsI(Na) detectors are more resistant to both thermal and mechanical shock than NaI(Tl). Another scintillating material, bismuth germanate ($Bi_4GE_3O_{12}$, commonly called BGO), has recently become available in sufficiently large sizes to be used for borehole logging. With a density of $7.13 g/cm^3$ it would seem to have considerable promise for borehole applications.

Table 18.1 shows some of the physical properties of the three scintillating materials considered in this study. The gamma-scintillation efficiency is a measure of the light output of the scintillating crystal. CsI(Na) has a light output

nearly 85 per cent of NaI(Tl). However the light output of BGO is only 8 per cent that of NaI(Tl) and hence the energy resolution will be poorer. BGO, like CsI(Na), is a rugged scintillating material; in addition BGO is not hygroscopic, unlike the other two detector materials. The energy resolution measurements (based on a ^{137}Cs source) for the three 19 x 76 mm detectors used in this study are also given in Table 18.1. BGO detectors with better energy resolution than the one used in this study are possible as indicated by the work of Nestor and Huang (1975).

The decay constant, also given in Table 18.1, is comparable for all three detector materials. Note that thallium activated cesium iodide CsI(Tl) (not considered here) has different properties from CsI(Na) including a longer decay constant and lower light output. A long decay constant will impose an upper limit on the count rate to which the detector may respond. When a gamma ray causes a scintillation in the detector before the previous scintillation has decayed, the two events cannot be distinguished.

Experimental Apparatus

A series of experimental measurements were made with each of the three 19 x 76 mm scintillation detectors, NaI(Tl), CsI(Na), and BGO. The NaI(Tl) detector was considered the standard for comparison. The GSC DIGI-PROBE logging system was used for all the measurements. This minicomputer-based, truck-mounted logging system has been developed for such R and D work by the Geological Survey, and is described briefly by Killeen et al. (1978), and in greater detail by Bristow (1980). The logging system is built around a 16-bit minicomputer operated interactively via a keyboard with a CRT display having alphanumeric and graphic capabilities. The system can record 256 or 1024 channels of gamma-ray spectral logging data on 9-track tape as often as every 0.25 s. For the purpose of this investigation, 256 channel (12 keV per channel) gamma ray spectra were recorded.

Table 18.1

Properties of the three detector materials compared
in this paper, as specified by the supplier,
Harshaw Chemical Co.

Material	Decay Constant (μS)	Density (g/cm^3)	Relative γ Scintillation Conversion Efficiency (%)	Side-On Energy Resolution (%)
NaI(Tl)	.23	3.67	100	11.2
CsI(Na)	.63	4.51	85	12.6
Bi$_4$Ge$_3$O$_{12}$	.30	7.13	8	24.5

The energy resolution of the detectors was measured by the authors with a small ^{137}Cs source alongside the detector.

Table 18.2

Window energy limits (keV) used to determine the
calibration factors in this paper

Window	TC	K	U	Th
Standard	400-3000	1360-1560	1660-1860	2410-281
Wide	400-3000	1360-1560	1610-2300	2400-3000

Stripping Factors

α = ratio of Th gamma rays in U window to Th gamma rays in Th window

β = ratio of Th gamma rays in K window to Th gamma rays in Th window

γ = ratio of U gamma rays in K window to U gamma rays in U window

a = ratio of U gamma rays in Th window to U gamma rays in U window

b = ratio of U gamma rays in Th window to U gamma rays in K window

g = ratio of K gamma rays in U window to K gamma rays in K window

Total Count Window Proportionality Constants
(CPS = counts/second)

K_K = % K/CPS in total count window

K_U = ppm U/CPS in total count window

K_{Th} = ppm Th/CPS in total count window

K, U, and Th Window Proportionality Constants

C_K = % K/CPS in K window

C_U = ppm U/CPS in U window

C_{Th} = ppm Th/CPS in Th window

Note that the factor K_U is equivalent to the so-called 'K-factor' commonly used in gross count gamma ray logging where all the gamma rays are assumed to originate from the radioactive decay series of uranium.

These K-factors and C-factors are used as the constant of proportionality K in the equation (Scott et al., 1961):

$$\overline{G}T = KA \qquad (1)$$

depending on which radioelement is causing the anomaly, and which spectral window is being used. In equation (1), $\overline{G}$ is the average grade over a zone of thickness T. A is the area under the corresponding anomaly on the gamma ray log. In the centre of a uniform ore zone of effectively infinite thickness, equation (1) reduces to

$$G = KI \qquad (2)$$

where I is the measured gamma ray intensity.

The CsI(Na) detector used in these studies was implanted with an ^{241}Am stabilization source emitting alpha particles exhibiting gamma equivalent energies on the order of 4 MeV. A small fraction of these alpha particles exhibited gamma-equivalent energies in the 0.4-3 MeV energy range of interest in these studies. This 'background' count rate was quite low compared to the observed intensities in the U and Th model ore zones, and those data were easily corrected. In the case of potassium, however, the background was on the same order as the count rate in the potassium model, and hence values of the calibration factors determined in the borehole are not listed in Table 18.3 for CsI(Na).

All measurements were made by interchanging detectors in the same borehole probe. In this way no parameters except those due to the detector and its integral-mount photomultiplier tube changed during the comparison tests.

Calibration checks were made before and after each measurement to minimize the potential problem of gain shifts. Because of the versatility made possible by full spectral recording it is possible to reproduce gamma ray spectral logs using energy windows of any desired widths or positions in the gamma ray energy spectrum. Comparisons were therefore made with two sets of energy windows as shown in Table 18.2. The 'standard' windows represent those commonly used in portable and airborne gamma ray spectrometers. The 'wide' uranium window has the advantage of including the 2.24 MeV gamma ray peak from the uranium decay series, but the disadvantage of an increased scattered thorium component in the uranium window. This requires a larger stripping factor α (see Conaway and Killeen, 1980; Killeen, 1979) to remove the thorium component from the uranium window. The wide thorium window is useful when working with BGO because of the poorer energy resolution of this material.

Experiments in Model Boreholes

All measurements were made with the above described logging system in the model boreholes at the Geological Survey's calibration facilities at Bells Corners, near Ottawa. These model boreholes consist of a set of nine concrete columns 3.9 m in height, each with a simulated ore zone 1.5 m thick sandwiched between upper and lower barren zones. Each test column contains three boreholes of diameters 48 mm (size A) 60 mm (size B) and 75 mm (size N) intersecting the ore zones. Three of the test columns contain 'ore' zones of different concentrations for potassium, three for thorium and three for uranium. These are described in more detail by Killeen (1978); Killeen and Conaway (1978) and Killeen (1979).

Gamma ray spectral logs were run in the high grade U, Th, and K model holes using each of the three detectors; also a 5 minute gamma ray spectrum was accumulated and recorded with each detector with the logging probe stationary in the centre of the 'ore' zones. All tests were performed in the B-size holes, water filled. From these data, all of the required calibration fractors for a gamma ray spectral logging probe were derived (see Conaway and Killeen, 1980) for the three detectors for each of the two sets of energy windows shown in Table 18.2. The results are given in Table 18.3. The meaning of each of these factors has been discussed by Conaway and Killeen (1980) and is summarized below.

Table 18.3

Calibration factors obtained for 3 different
detector materials, each detector having
dimensions 19 x 76 mm.

Windows →	Standard			Wide		
Detector Material →	NaI	CsI	BGO	NaI	CsI	BGO
↓ Calibration Factor						
α	1.5	1.2	0.65	5.0	3.7	1.9
β	2.1	1.6	0.92	2.0	1.5	0.85
γ	1.8	1.6	1.2	1.0	0.87	0.65
a	0.04	0.05	0.07	0.02	0.03	0.04
b	0.05	*	0.02	0.05	*	0.03
g	0.03	*	0.04	0.12	*	0.13
K_K	0.39	*	0.16	-	-	-
K_U	0.91	0.80	0.33	-	-	-
K_{Th}	1.9	1.6	0.81	-	-	-
C_K	4.7	*	1.2	-	-	-
C_U	39	31	10.5	22	17	5.6
C_{Th}	128	73	25	122	70	23

Asterisks indicate factors which could not be determined for the CsI detector because of background problems, as described in text.

Horizontal dashes indicate instances where the wide windows are identical to the standard windows

From Table 18.3 it is easy to see that the BGO detector has much lower stripping factors (α, β, γ) than NaI(Tl), and that the values for CsI(Na) are intermediate. The reason for the decrease in stripping factors is the higher detection efficiency of CsI(Na) and especially BGO at the high energies. This is evident in the comparison of gamma ray spectra shown in Figure 18.1. These spectra were recorded as 5 minute stationary measurements with each of the three detectors in the centre of the 350 ppm thorium 'ore zone' of the model holes. The spectra shown in Figure 18.1 are linear plots with the same vertical count-rate scale; note that these plots are in CPS/channel. The high energy peak at 2.615 MeV from ^{208}Tl in the thorium decay series is much larger in the spectrum observed with BGO than in the spectrum observed with NaI(Tl), and even the CsI(Na) shows an improvement over NaI(Tl).

Figure 18.2 shows the spectra recorded with the three different detectors positioned in the centre of the 950 ppm uranium ore zone in the high grade uranium test column. The 1.76 MeV peak from ^{214}Bi which is generally used for uranium determinations is obviously greatly enhanced by the BGO detector, and to a lesser extent by the CsI(Na). This improvement in count rate in the uranium window is even more apparent in the three uranium logs shown in Figure 18.3. These three logs through the 950 ppm uranium model ore zone represent the deadtime corrected gamma ray count rate in the uranium channel using 'standard' energy windows (see Table 18.2). The uranium log obtained with the CsI(Na) detector shows about a 25 per cent increase in count rate over NaI(Tl) and the BGO detector shows a count rate increase by a factor of about 4 over NaI(Tl). Since there is no appreciable thorium in this ore zone the relative count rates shown in Figure 18.3 are true indications of the higher efficiency of the BGO detector at high energies.

Table 18.4

Computed performance of the three 19 x 76 mm detectors
for determining uranium concentrations in
a mixed U-Th environment.

Concentration Ratio U/Th	Standard Windows			Wide Windows		
	NaI	CsI	BGO	NaI	CsI	BGO
10	1.00	0.90	0.51	0.81	0.72	0.39
1.0	1.00	0.91	0.47	0.93	0.83	0.39
0.1	1.00	0.93	0.42	1.06	0.94	0.39

Values given are error limits (one standard deviation) in the uranium computations normalized to the NaI standard windows for each radioelement concentration ratio. Clearly, the smaller the relative error, the better the detector's performance.

The comparison can be put in more quantitative terms if the C-factors in Table 18.3 are compared. These figures represent the number of parts per million (or percentage in the case of potassium) required to produce one count per second for each radioelement in the appropriate energy window. Thus, using the standard windows, C_U for NaI, CsI, and BGO detectors are 39, 31 and 10.5 respectively, which indicates that BGO is 3.7 times as sensitive to uranium as NaI(Tl). Even CsI(Na) is 1.26 times as sensitive as NaI(Tl). The thorium window proportionality constant C_{Th} for the three detectors shows improvements over NaI(Tl) by a factor of 1.75 times and 5.1 times for CsI(Na) and BGO respectively. For the wide windows the improvement factors for uranium C_U are 1.3 and 3.9 for CsI(Na) and BGO, and for thorium C_{Th} the improvement factors over NaI(Tl) are 1.74 and 5.3 for CsI(Na) and BGO respectively. Thus a similar improvement is observed for both 'standard' and 'wide' windows.

Statistical Errors in Uranium Determinations

What effects do these improvements in count rate and changes in the stripping factors have on the determination of uranium concentrations in a mixed U-Th environment? Using the calibration factors in Table 18.3 and the statistical analysis described below we can arrive at some conclusions about the degree of improvement over NaI(Tl) which is possible with CsI(Na) and BGO detectors.

Ignoring the contribution of K, which would be negligibly small even in a low grade uranium ore zone, we can extend equation (2) to the case of a mixed U-Th zone by writing the equations
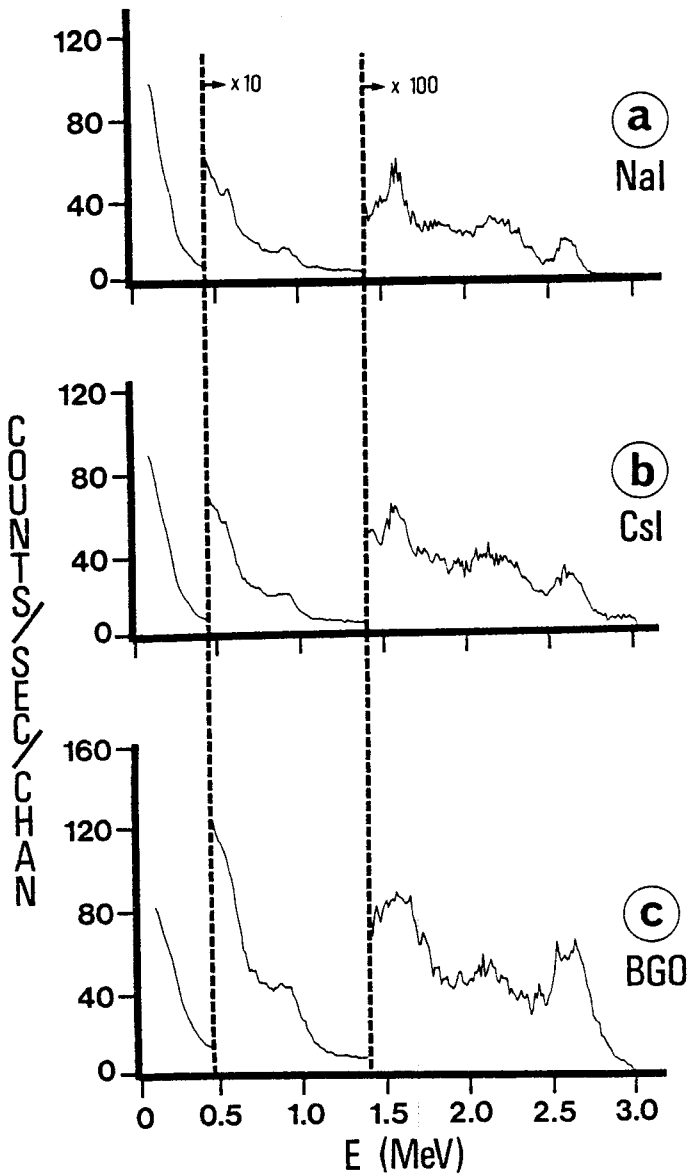
$$G_U = C_U (I_U - \alpha I_{Th}) \tag{3}$$

$$G_{Th} = C_{Th} (I_{Th} - a I_U) \tag{4}$$

where G_U is uranium grade, I_U is the gamma ray intensity in the unstripped uranium window, G_{Th} is thorium grade and I_{Th} is the gamma ray intensity in the unstripped thorium window; a and α are stripping factors described earlier. Solving equations (3) and (4) for I_U and I_{Th} we get

$$I_U = \frac{1}{1-a\alpha} \left[\frac{G_U}{C_U} + \frac{\alpha G_{Th}}{C_{Th}} \right] \tag{5}$$

$$I_{Th} = \frac{1}{1-a\alpha} \left[\frac{G_{Th}}{C_{Th}} + \frac{a G_U}{C_U} \right] \tag{6}$$

350 ppm Th

The standard deviation σ of the statistical noise in the stripped U window is (e.g. Chase and Rabinowitz, 1968):

$$\sigma = (I_U + \alpha I_{Th})^{\frac{1}{2}} \qquad (8)$$

and thus the relative error E in the uranium determination · given by

$$E = \frac{\sigma}{I_{Us}} = \frac{(I_U + \alpha I_{Th})^{\frac{1}{2}}}{(I_U - \alpha I_{Th})} \qquad (9)$$

If desired, E may be multiplied by 100 to give percentage error. The relative errors for the three detectors were computed from equation (9) for three U/Th ratios, 10:1, 1:1, and 1:10. These results are given in Table 18.4, normalized to the error for the NaI(Tl) detector (standard windows) for each U/Th ratio.

950 ppm U

a. 256 channel gamma ray spectrum (12 keV per channel) recorded in 350 ppm thorium model ore zone using a 19 x 76 mm NaI(Tl) detector.

b. Same as (a) but using a 19 x 76 mm CsI(Na) detector. Note that at the high energy end of the spectrum the count rate does not drop to zero as in the NaI(Tl) spectrum (a). This is due to the implanted [241]Am source, as explained in text.

c. Same as (a) but using a 19 x 76 mm BGO detector.

Figure 18.1

Using these equations it is possible to compute the expected count rate in a given spectral window for a specified concentration of uranium and thorium. We are concerned here with the statistical errors in the uranium window count rate, after stripping. The count rate in the stripped uranium window I_{Us} is (ignoring potassium)

$$I_{Us} = I_U - \alpha I_{Th} \qquad (7)$$

Figure 18.2. 256 channel spectrum recorded in 950 ppm uranium model ore zone using

a. NaI(Tl) detector,

b. CsI(Na) detector and

c. BGO detector

COUNTS/SEC
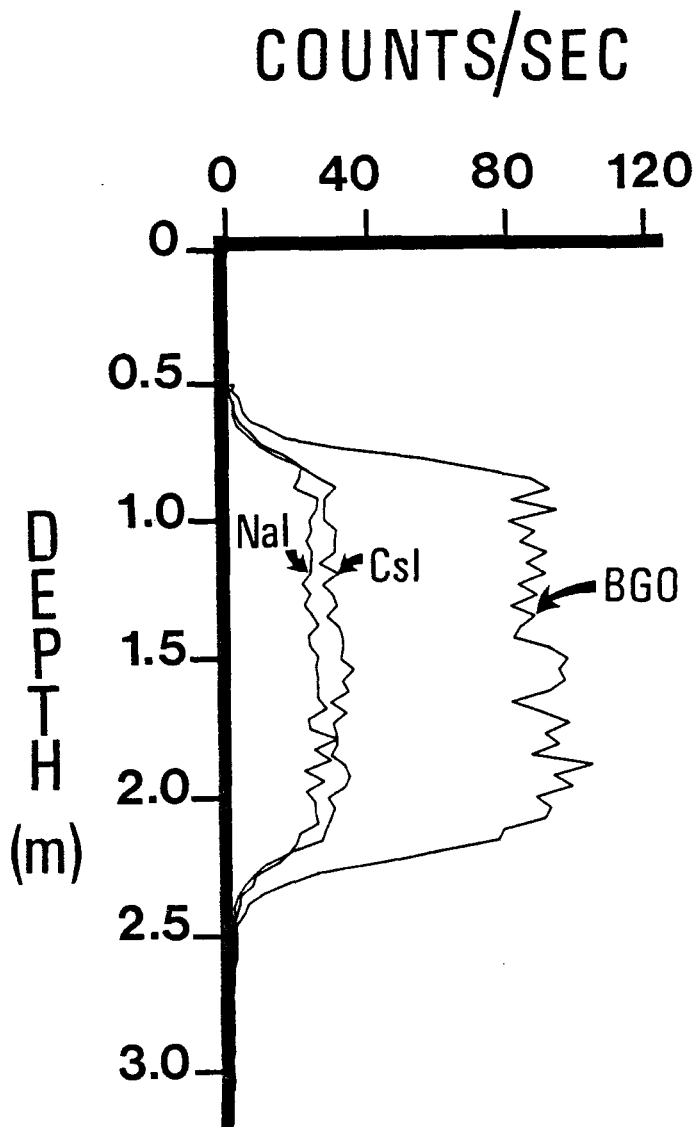
Figure 18.3. Plot of gamma ray intensity as a function of depth using the standard uranium spectral window and three different detector materials, as indicated.

Several conclusions can be drawn from Table 18.4 for the 19 x 76 mm detector size.

1. The wide windows are better than the standard windows for all 3 detector materials for U/Th ratios of 10:1 and 1:1. For BGO the wide windows are also better for the 1:10 U/Th ratios, but this is not true for NaI(Tl) or CsI(Na).

2. CsI(Na) exhibits a relative error improved by about 10% compared to NaI(Tl) with the same window widths.

3. BGO produces an improvement in relative error on the order of 50 per cent or more under all conditions.

Conclusion

It is clear that BGO is the best of the three detector materials tested for slim hole gamma ray spectral logging. BGO's improved ruggedness compared with NaI(Tl) is also an advantage. At present the price of BGO is on the order of double the price of the other detector materials, however, this price differential is still not high enough to rule out the use of BGO in spectral logging, considering its great advantages in slim probes.

Note that the results obtained in these tests are dependent on probe characteristics, detector size, and borehole conditions. It may be expected that the observed advantages of BGO will in general decrease with increasing detector size.

References

Bristow, Q.
1980: NOVA-based airborne and vehicle mounted systems for real-time acquisition, display and recording of geophysical data; in Proceedings of the 6th Annual Data General Users Group Meeting, New Orleans, Dec. 4-7, 1979.

Chase, G.D. and Rabinowitz, J.L.
1968: Principles of radioisotope methodology; Burgess Pub. Co., Minneapolis, 633 p.

Conaway, J.G. and Killeen, P.G.
1980: Gamma-ray spectral logging for uranium; Canadian Institute of Mining and Metallurgy Bulletin, v. 73, no. 813, p. 115-123.

Killeen, P.G.
1978; Gamma-ray spectrometric calibration facilities – a preliminary report; in Current Research, Part A, Geological Survey of Canada, Paper 78-1A, p. 243-247.

1979: Gamma ray spectrometric methods in uranium exploration – application and interpretation; in Geophysics and Geochemistry in the Search for Metallic Ores; Peter J. Hood, Editor; Geological Survey of Canada, Economic Geology Report 31, p. 163-229.

Killeen, P.G. and Bristow, Q.
1976: Uranium exploration by borehole gamma-ray spectrometry using off-the-shelf instrumentation; in Exploration for Uranium Ore Depos Proceedings Series, International Atomic Ene Agency, Vienna, p. 393-414.

Killeen, P.G. and Conaway, J.G.
1978: New facilities for calibrating gamma-ray spectrometric logging and surface exploration equipment; Canadian Institute of Mining and Metallurgy Bulletin, v. 71, no. 793, p. 84-87.

Killeen, P.G., Conaway, J.G., and Bristow, Q.
1978: A gamma-ray spectral logging system including digital playback, with recommendations for a new generation system; in Current Research, Part A, Geological Survey of Canada, Paper 78-1A, p. 235-241.

Nestor, O.H. and Huang, C.Y.
1975: Bismuth germanate: a high-Z gamma-ray and charged particle detector; Institute of Electrical and Electronics Engineers Transactions on Nuclear Science, NS-22, p. 68-71.

Scott, J.H., Dodd, P.H., Droullard, R.F., and Mudra, P.J.
1961: Quantitative interpretation of gamma-ray logs; Geophysics, v. 26, no. 2, p. 182-191.

MULTIPIT, A METHOD FOR
CALIBRATION OF LOGGING SYSTEMS

by
Merle E. Crew

U.S. Department of Energy
Grand Junction, Colorado

TABLE OF CONTENTS

MULTIPIT, A METHOD FOR
CALIBRATION OF LOGGING SYSTEMS

by

Merle E. Crew

Abstract

A method of calibration of gamma-ray logging equipment is presented which uses
data from 2 or more model holes. Input to the program is a series of count
rates at equal intervals, from background to background for each model hole
used. The corresponding grade thickness products (GT) are stored in the
program. Using this data a simultaneous solution is made, finding the value
for dead time that gives a minimum value of the sum of the least squares of
the differences between the calculated and the known grade thickness products.
Having found the dead time that gives the best least squares fit to a linear
equation, the slope of the line is the proportionality constant or K factor.

Introduction

Historically there have been many methods to determine dead time of a logging
system. This must be known to correct the observed counts per second before
any attempt can be made to apply the principle of AK = GT, where A is the area
under the curve, K is the proportionality constant, G is the mean radiometric
grade, and T is the thickness of the anomaly in the model hole, (Reference 1),
to determine the calibration constant for a probe. The most common method
used is a simultaneous solution of data from two model holes which varies the
dead time until the ratio of the areas under the curve of the two models
equals the ratio of the known grade thickness product of the models,
(Reference 2). The TWOPIT method will give some variance to results depending
upon which pair of model holes are used and works best when there is maximum
difference in the grades, and consequently count rates, of the models used in
the calculation.

In this paper a method will be presented which uses data from any 2 or more
model holes and simultaneously solves for the dead time which gives the best
least squares fit to a line, plotting the area under the curve against GT
values for the respective model holes, thus meeting the condition that
AK = GT.

Products of any equipment manufacturer mentioned in this paper are for
descriptive information only and do not constitute an endorsement.

Concept

The method proposed here as a prime method for calibration of gamma-ray
logging equipment, uses data from any 2 or more model holes to simultaneously
solve for the dead time and K factor that will give the best least squares fit
to a line when plotting area under the curve against GT values for the
respective model holes.

Area under the curve has commonly been plotted against GT values to confirm general agreement with the principle that AK = GT but there is no evidence to indicate use of the method to simultaneously solve for dead time and K factor.

The important concept presented here is that there is but one value for dead time, when used to correct the observed counts per second for the data from a series of model holes, that will give the best fit to a straight line when area under the curve for each model is plotted against the GT for the respective model.

The least squares method of fitting a straight line to a set of data points is a standard mathematical procedure and need not be described.

Table 1 is a listing of dead times from minus one to plus 1.5 microseconds by 0.1 microsecond increments and the corresponding sum of the squares of the differences for each value when a least squares fit is made to the points as determined by that particular dead time. Although it is impossible to have negative dead times they are included here to show a continuous function with a discrete minimum attained with one specific value for dead time.

TABLE 1

Dead time in microseconds	$\Sigma(y-y_1)^2$
-1.0	0.012709
-0.9	0.011300
-0.8	0.010001
-0.7	0.008813
-0.6	0.007738
-0.5	0.006777
-0.4	0.005931
-0.3	0.005201
-0.2	0.004590
-0.1	0.004099
0	0.003728
0.1	0.003479
0.2	0.003355
0.3	0.003356
0.4	0.003484
0.5	0.003740
0.6	0.004127
0.7	0.004645
0.8	0.005296
0.9	0.006082
1.0	0.007004
1.1	0.008065
1.2	0.009265
1.3	0.010607
1.4	0.012092
1.5	

The simplest strategy for solution would be to start at a slightly negative value of dead time and test for sum of the squares of differences at 0.01 microsecond increments until a minimum value is attained. The MULTIPIT program is an iterative method of incrementally increasing the dead time used to correct the observed count rates. For each value of dead time used, the observed counts, at equal increments (commonly 0.5 foot) from background value to background value, are dead time corrected and summed to give total area under the curve. When areas have been obtained for all model holes being considered, a least squares fit is made to a line, and the sum of the squares of differences calculated. This value is then compared to the value obtained from the previous iteration. If the new sum is smaller than the previous sum, another increment of dead time is made and another iteration continues. If the value of the sum of the squares of the difference is larger than the previous sum it indicates that a minimum was reached somewhere in the interval of the two previous increments. The program then backs up two increments, reduces the dead time increment by one tenth and proceeds with iterations at the smaller dead time increments.

The MULTIPIT program starts at 0 microseconds and increments first by 1 microsecond, then 0.1 microsecond, then 0.01 microseconds, and terminates when the minimum least squares value has been found using 0.01 microsecond intervals. Since modern equipment has dead times generally less than 1 microsecond, a solution is found without excessive iterations and the 0.01 microsecond lower limit gives more than adequate precision.

When the best fit has been determined, the dead time used and the slope of the line or K factor are printed and are the calibration factors. The sum of the squares of the differences and a plot of the line with points for each model hole are also output as indicators of goodness of fit. The results of the program are shown in Appendix A. Appendix B is a list of the data input for the various model holes and Appendix C is a listing of the program as used on the Tectronix system.

The relationship, AK = GT, demands that the calibration line pass through the origin, therefore the restrictive form of the equation for a straight line, $y = nx$, is used to meet this condition.

Options

The MULTIPIT program on the Tectronix system will accept data at one-tenth foot intervals for up to 19 model holes. Provision is made in the program to use the maximum number of model holes or to omit or select any combination down to a minimum of 2 model holes. This is useful to test if there is a significant difference in the results using model holes in the lower grade ranges versus using model holes in the higher grade range. Due to experimental error possible in collecting the data, and possible minor error in grade assignments of the various model holes, identical results cannot be expected in these two cases.

Data input can be in any units, either English or metric. If the input is at one-half foot intervals, the slope of the line, or K factor, will be for one-half foot intervals or if data input is 0.2 foot then the K factor is appropriate for data collected at this interval. The same applies to data collected in the metric system. If full metric conversion is desired it would also be necessary to change the program stored values for grade thickness product from foot-percent values to meter-percent values.

Options are programmed for various methods of data entry. Digital data may be entered directly as counts per second on the keyboard or analog data may be entered as scale units with the range factor being entered for internal conversion to counts per second. The program will also accept data directly from the Tectronix digitizing table and is programmed to list the data in counts per second and to reproduce the curve as a check on the accuracy of digitizing.

Discussion

The data used to test the MULTIPIT concept was collected by Bendix Field Engineering Corp., (Contractor to the U.S. Department of Energy) using logging unit number 1709 with an unshielded probe number 301. This is a zero dead time compensated probe and the calibration, as determined by currently used methods, was 1.696 microseconds dead time and a K factor of 0.00002495. Data was used from model holes N3, U3, U2, and U1. Physical and analytical data on the model holes is listed in Logging Model Data Synopsis, (Reference 3).

Comparative results of the solution discussed herein and the currently used method are presented in Tables 2 and 3.

TABLE 2

MULTIPIT
dead time = 0.25 microsecond
K factor = 0.00002577
$\Sigma(y-y_1)^2$ = 0.00335

	N3	U3	U2	U1
Area	40806	69182	169009	328332
GT	0.9976	1.7975	4.3691	8.4563
Calc. GT	1.0515	1.7826	4.3548	8.4601
diff.	-0.0539	+0.0149	+0.0143	-0.0038

TABLE 3

Current method
dead time = 1.696 microsecond
K factor = 0.00002495
$\Sigma(y-y_1)^2$ = 0.00720

	N3	U3	U2	U1
Area	41047	69939	173546	345428
GT	0.9976	1.7975	4.3691	8.4563
Calc. GT	1.0241	1.7450	4.3210	8.4941
diff.	-0.0265	+0.0525	+0.0481	-0.0378

From the above tables it is evident that neither method exactly fits the assigned grade of the model holes, however, using the sum of the squares of the differences between the assigned grade thickness and the calculated grade thickness product as an index, the value for the MULTIPIT method is less than half of that for the current method.

Conclusions

The method proposed for calibration of logging equipment is an iterative method of varying the dead time to find the best least squares fit of the data from 2 or more model holes to a straight line, thus meeting the requirements of the generally accepted principle that AK = GT.

It has been shown that the MULTIPIT program gives better fit of the test data to a straight line than the currently used method. It would seem logical that a method which uses a spectrum of data points and simultaneously solves for dead time and K factor would be superior to the present method which estimates the dead time from certain pairs of models, then determines the K factor from a single model on the low end of the GT ranges.

Application of the MULTIPIT method also has promise of refining the grade assignments of the model holes at Grand Junction and field locations. If repeated use of the method with different logging systems shows consistent deviation of certain models from the calibration line, it would be strong evidence that the grade of that model should be adjusted.

The gamma-ray logging calibration facility of the U.S. Department of Energy at Grand Junction, Colorado and its associated field model holes at Casper, Wyoming; Grants, New Mexico; and George West, Texas is the only known facility with a sufficient number of model holes to fully utilize this method. Since this is the prime calibration facility for the entire uranium industry, adoption of the MULTIPIT method would give the industry more uniform calibration effective over the entire range of grades that might be encountered in exploration or development drill holes.

Acknowledgements

REFERENCES

1. Scott, J. H., Dodd, P. H., Droullard, R. F., and Mudra, P. J.,
   Quantitative Interpretation of Gamma-Ray Logs: U.S.A.E.C.,
   RME-136, 1960.

2. Crew, M. E., and Berkoff, E. W., 1979, TWOPIT, A Different Approach
   to Calibration of Gamma-Ray Logging Equipment: The Log Analyst,
   Nov-Dec., 1970, p. 26-32.

3. Mathews, M. A., Koizumi, C. J., and Evans, H. B., DOE-Grand Junction
   Logging Model Data Synopsis, GJBX-76(78), 1978.

Appendix A

Program MULTIPIT Results

*** PROGRAM MULTI-PIT RESULTS ***

DATE

COMPANY	B.F.E.C.	SUM OF SQUARES	0.003340
UNIT #	1709	DEAD TIME	2.500E-007
PROBE #	301	K FACTOR	2.577E-005

CORRECTED AREAS	ASSIGNED GT"S	CALCULATED GT"S	DIFFERENCE
U-1 = 328332	8.4563	8.4601	-0.0038
U-2 = 169009	4.3691	4.3548	+0.0143
U-3 = 69182	1.7975	1.7826	+0.0149
N-3 = 40806	0.9976	1.0515	-0.0539

8

*** MULTI-PIT RESULTS ***

DATE
COMPANY   B.F.E.C.
UNIT #   1709
PROBE #   301
DEAD TIME   2.500E-007
K FACTOR   2.577E-005

GT VALUES

CORRECTED AREAS
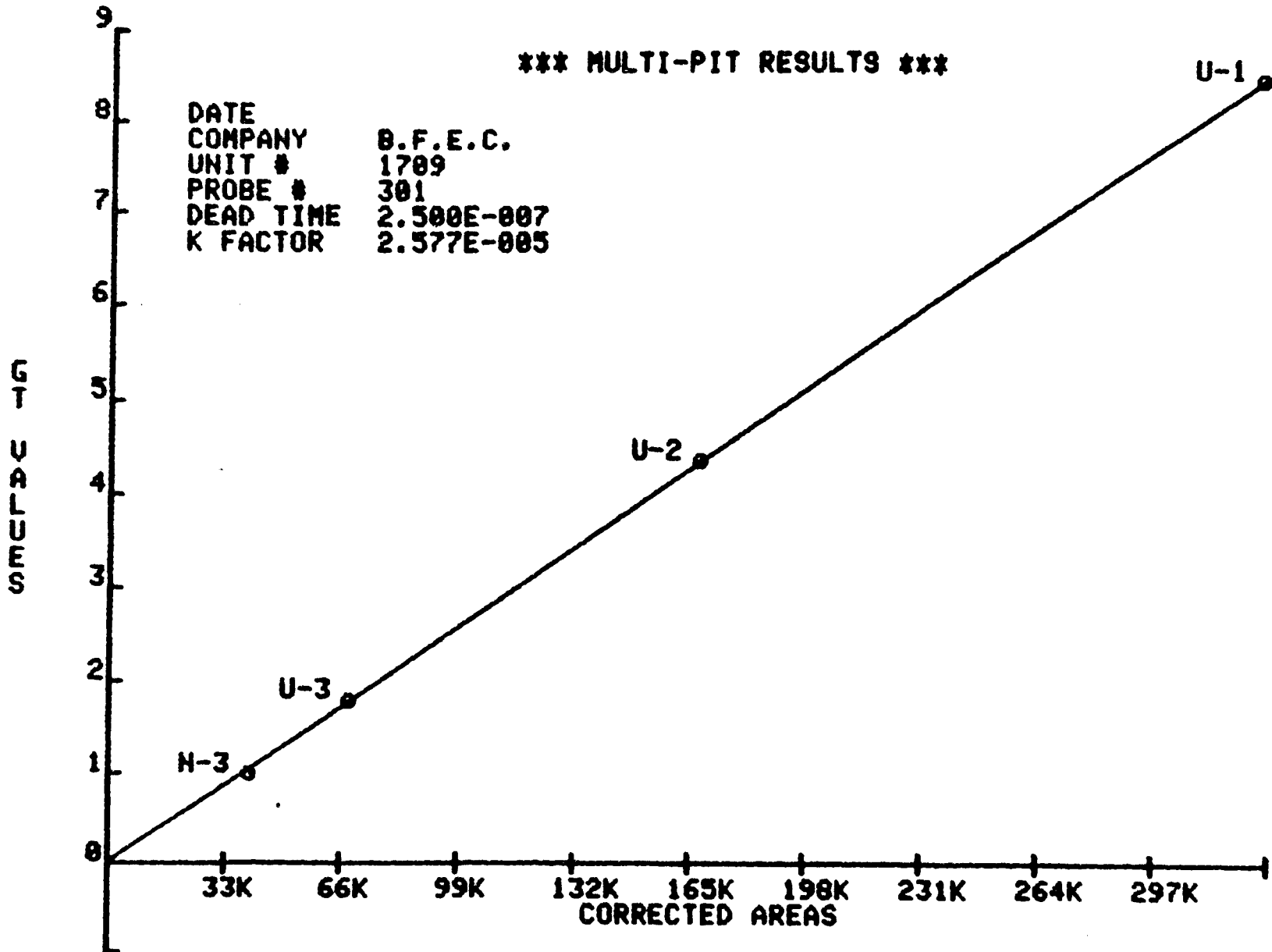
Appendix B

Input Data

*** INPUT DATA FOR PIT U-1 ***

DATA ENTRY CODES ARE AS FOLLOWS

    ENTER 0 FOR LAST ENTRY
    ENTER 2 TO DELETE LAST DATA POINT ENTERED
    ENTER 3 TO RESTART ENTRY FOR THIS PIT

297.6
1267.2
5980.8
22937.6
35616
37776
38076.8
38172.8
37977.6
37763.2
35792
25312
6976
1312
297.6

*** INPUT DATA FOR PIT U-2 ***

DATA ENTRY CODES ARE AS FOLLOWS

    ENTER 0 FOR LAST ENTRY
    ENTER 2 TO DELETE LAST DATA POINT ENTERED
    ENTER 3 TO RESTART ENTRY FOR THIS PIT

137.6
496
2435.2
10624
18441.6
20057.6
20358.4
20438.4
20352
20080
18745.6
12224
3126.4
592
140.8

*** INPUT DATA FOR PIT U-3 ***

DATA ENTRY CODES ARE AS FOLLOWS

    ENTER 0 FOR LAST ENTRY
    ENTER 2 TO DELETE LAST DATA POINT ENTERED
    ENTER 3 TO RESTART ENTRY FOR THIS PIT

67.2
214.4
931.2
4137.6
7593.6
8342.4
8451.2
8518.4
8508.8
8348.8
7708.8
4812.8
1129.6
227.2
60.8

*** INPUT DATA FOR PIT N-3 ***

DATA ENTRY CODES ARE AS FOLLOWS

    ENTER   0   FOR LAST ENTRY
    ENTER   2   TO DELETE LAST DATA POINT ENTERED
    ENTER   3   TO RESTART ENTRY FOR THIS PIT

256
380.8
899.2
2892.8
4300.8
4576
4652.8
4636.8
4624
4684.8
4300.8
3299.2
976
211.2
73.6

UNITED STATES ATOMIC ENERGY COMMISSION

GRAND JUNCTION OFFICE

MINING DIVISION

TWOPIT, A DIFFERENT APPROACH TO CALIBRATION
OF GAMMA-RAY LOGGING EQUIPMENT

by

M. E. Crew and E. W. Berkoff

April 1969
(Grand Junction, Colorado)

CONTENTS

ILLUSTRATIONS

TABLES

APPENDIX

TWOPIT, A DIFFERENT APPROACH TO CALIBRATION OF GAMMA-RAY LOGGING EQUIPMENT

ABSTRACT

The standard method of calibrating gamma-ray logging equipment is to first determine dead time, then log test pit N-3 in the Grand Junction AEC compound and determine the K-factor by the equation $K = \dfrac{GT}{A}$.

This paper suggests a different method, using a computer to solve for apparent dead time and a K-factor. Input to the computer is derived from logs of two test pits with different grades and grade-thickness products, and consists of the value of the GT (grade-thickness product) for each pit and a series of observed counts taken at equal intervals from background to background in each pit. A Fortran computer program for processing this data has been developed for use on IBM 1401 and IBM 1130 computers, but can easily be adapted to any digital computer of similar or greater size.

The method described is not represented to be a calculation of true instrumental dead time, but is a method of arriving at a dead time type correction for several effects combined.

Advantages of the method are (1) determination of dead time type effects based on counting geometry and count rates the same as encountered in field logging, and (2) a calibration based on both a high grade and a low grade pit rather than on a single grade pit.

INTRODUCTION

The construction of the Casper test pits in the summer of 1967 provided the first uniform-high-grade, apparent-infinite-thickness ore zone in a full scale model bore hole. Analysis of both AEC and company logs of these pits, which were obtained using conventional geiger or scintillation probes

resulted in under-interpretation of the high grade pit to varying degrees. Investigations into the reasons for this under estimation led to development of the two-pit concept as a means for correcting for the discrepancy.

To calibrate gamma-ray logging equipment for quantitative evaluation of uranium ore, it is essential to know the dead time of the system. This may be determined electronically or by the two-source method wherein first a background measurement is taken, then a first source is placed close enough to the probe to give a medium counting rate for the system and the count rate in cps taken. Next a second source is placed adjacent to the first and the count rate for both sources combined is determined, then the first source removed the count rate for the second source only is determined.

Dead time can then be calculated by the following equation: [1]/

$$\text{Dead time} = \frac{\dfrac{\sqrt{C^2 + 3DY} - C}{3D}}{2}$$

where
$$C = M_3^2 + M_B^2 - M_1^2 - M_2^2$$
$$D = M_3^3 + M_B^3 - M_1^3 - M_2^3$$
$$Y = M_1 + M_2 - M_3 - M_B$$

and M_1 = count rate in cps, first source

M_2 = " " " " , second source

M_3 = " " " " , both sources

M_B = " " " " , background

After dead time has been determined, the next step is to determine the proportionality constant or K-factor which relates the response of the system, commonly expressed in terms of area under the curve, to grade-thickness product. This is done by logging a test pit of known grade-thickness, applying

appropriate correction for dead time, using the equation $N = \dfrac{n}{1 - nt}$, to each observed count rate, n, to obtain true count rate, N, and using the sum of the true count rates ΣN, as a value for the area, A, under the log curve then substituting in the equation

$$AK = GT \qquad\qquad (2)$$

as developed by Scott, et al, [2/].

Area, as used in equation (2) consists of the observed counts area plus the dead time correction area and is normally obtained by summing the dead time corrected count rates at half foot intervals and is thus in units of half feet times counts per second. The value of K is commonly calculated to relate the area so derived to the GT but can be computed for any interval of integration.

Figure 1, shows the relationship between observed count rate and dead time corrected count rate on a log of the Casper high pit with a grade of 2.242% eU_3O_8 made with a scintallation probe having 3/4 x 1 inch crystal and 5 micro seconds dead time. The area between the observed and corrected log curves represents the loss in area, or gamma-rays detected, because of system dead time.
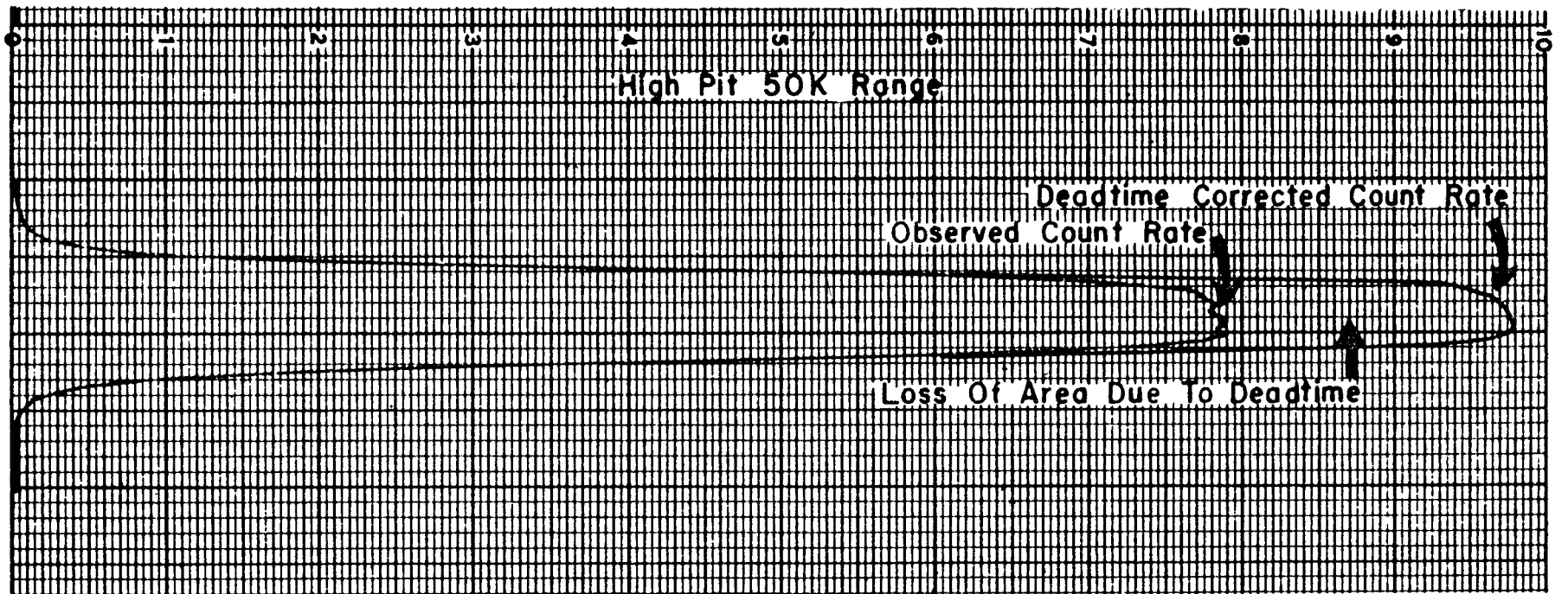
Figure I. Loss of Area Due to Deadtime

TWO PIT CONCEPT

The method described in this report is not represented to be a calculation of true instrumental dead time, but instead a method of arriving at a dead time type correction for the entire logging system which will result in a closer approximation to equivalent radiometric grade throughout the entire range of count rates encountered in gamma-ray logging of drill holes.

The entire concept to be shown here is based on the previously mentioned equation (2).

$$AK = GT$$

where A = sum of dead time corrected counts

K = proportionality constant of system

G = mean radiometric equivalent grade

T = thickness in feet

Now consider the case of two test pits with different grade-thickness products in which

$$A_1 K = (GT)_1$$

represents the low grade pit and

$$A_2 K = (GT)_2$$

represents the high grade pit. Since the above relationships are true, it can also be said that

$$\frac{A_1 K}{A_2 K} = \frac{(GT)_1}{(GT)_2}$$

and since the expression K cancels out that

$$\frac{A_1}{A_2} = \frac{(GT)_1}{(GT)_2} \tag{3}$$

The expression A is defined as the sum of the dead time corrected counts and may be written

$$A = N_1 + N_2 + N_3 \ldots N_z \tag{4}$$

and it is known that

$$N = \frac{n}{1-nt} \tag{5}$$

where N = dead time corrected count rate

n = observed count rate

t = dead time in seconds.

Therefore, by substituting, equation (4) can be written as

$$A = \frac{n_1}{1-n_1 t} + \frac{n_2}{1-n_2 t} + \frac{n_3}{1-n_3 t} \ldots \frac{n_z}{1-n_z t} \tag{6}$$

and by substituting again, equation (3) can be rewritten as

$$\frac{\dfrac{n_1}{1-n_1 t} + \dfrac{n_2}{1-n_2 t} + \dfrac{n_3}{1-n_3 t} \ldots \dfrac{n_z}{1-n_z t}}{\dfrac{m_1}{1-m_1 t} + \dfrac{m_2}{1-m_2 t} + \dfrac{m_3}{1-m_3 t} \ldots \dfrac{m_z}{1-m_z t}} = \frac{(GT)_1}{(GT)_2} \tag{7}$$

using the term m in the denominator to designate observed counts in the high grade pit whereas the n in the numerator represents observed counts in the low grade pit.

In equation (7) GT_1 and GT_2 are known values and the various values for the n and m terms are observed values, thus leaving t as the only unknown in the equation. A direct algebraic solution is difficult if not impossible because of the indefinite length of the series, but a computer solution by trial and error is relatively simple. First the ratio of the two GT values is determined, then by trial and error, the computer solves for the dead time that will make the ratio on the left side of the equation equal to the ratio of the GT products.

A description and lising of the computer program called TWOPIT which solves the equation is attached as Appendix A.

A close approximation to the dead time evaluation by the above computer method can be made manually or with a desk calculator using ratios of peak observed counts in the respective pits rather than area under the curve, provided that the "ore" zones in the models are of uniform grade and the thickness is equal to or greater than the diameter of the effective sample volume influencing the detector, generally 3 feet or slightly less; or provided that thickness T_1 is equal to thickness T_2 and the ore zones are homogeneous with respect to grade.

It has been shown by Scott, 3/, that under certain conditions

$$G = 2KN \qquad (8)$$

Then following the same reasoning as described above with respect to areas under the curve and grade thickness products it can be said that

$$\frac{G_1}{G_2} = \frac{N_1}{N_2}$$

By similar substitutions for N and solution for dead time, t, this is reduced to

$$t = \frac{n - Rm}{nm\,(1-R)} \qquad (9)$$

where t = apparent dead time, in seconds

    n = peak observed count, low pit

    m = peak observed count, high pit

    $R = \dfrac{\%\ eU_3O_8,\ \text{low pit}}{\%\ eU_3O_8,\ \text{high pit}}$

Results obtained by this short-cut method are generally within one microsecond of the value obtained by the TWOPIT program.

APPLICATION

Effect of Dead Time

To understand the importance of accurate dead time determination, it is necessary to consider the effect of dead time on the interpretation of gamma-ray logs.

Figure 2 shows dead time correction curves for 5, 10, 20, 30, and 40 microseconds. The previously mentioned equation (5) $N = \frac{n}{1-nt}$ was used in construction of the graphs. As a guide for interpreting this chart, lines have also been drawn to show a 50% and a 100% correction to observed count rates. Because of uncertainties involved in determining a true dead time value, and the large effect resulting from a small change in dead time at high count rates, it would be advisable to choose equipment with detector size and dead time characteristics such that not greater than a 50% correction to observed counts would be required at the highest count rates encountered in ore hole logging. Using this criteria it can be seen that the maximum observed counts should not exceed 65,000 cps for a system with 5 microseconds dead time, 33,000 cps for 10 microseconds, 17,500 cps for 20 microseconds, etc.

Another way of determining the possible error that is introduced by a small error in dead time determination is illustrated in Figure 3. This figure shows the approximate relationship between peak observed count rate and equivalent % U_3O_8 by equation (8), G=2KN modified to $G=2K \frac{n}{1-nt}$.

A value for K of .00002 was used for construction of the graphs. This value is within the range encountered for 3/4 x 1 inch crystals in scintillation logging probes.

At an observed count rate of 30,000 cps it is evident from the graph that if 5 microseconds are used the interpreted grade would be 1.41% eU_3O_8, whereas if 10 microseconds are used the grade would be 1.71%--a difference of 0.30%,and as dead times were increased the same microseconds difference
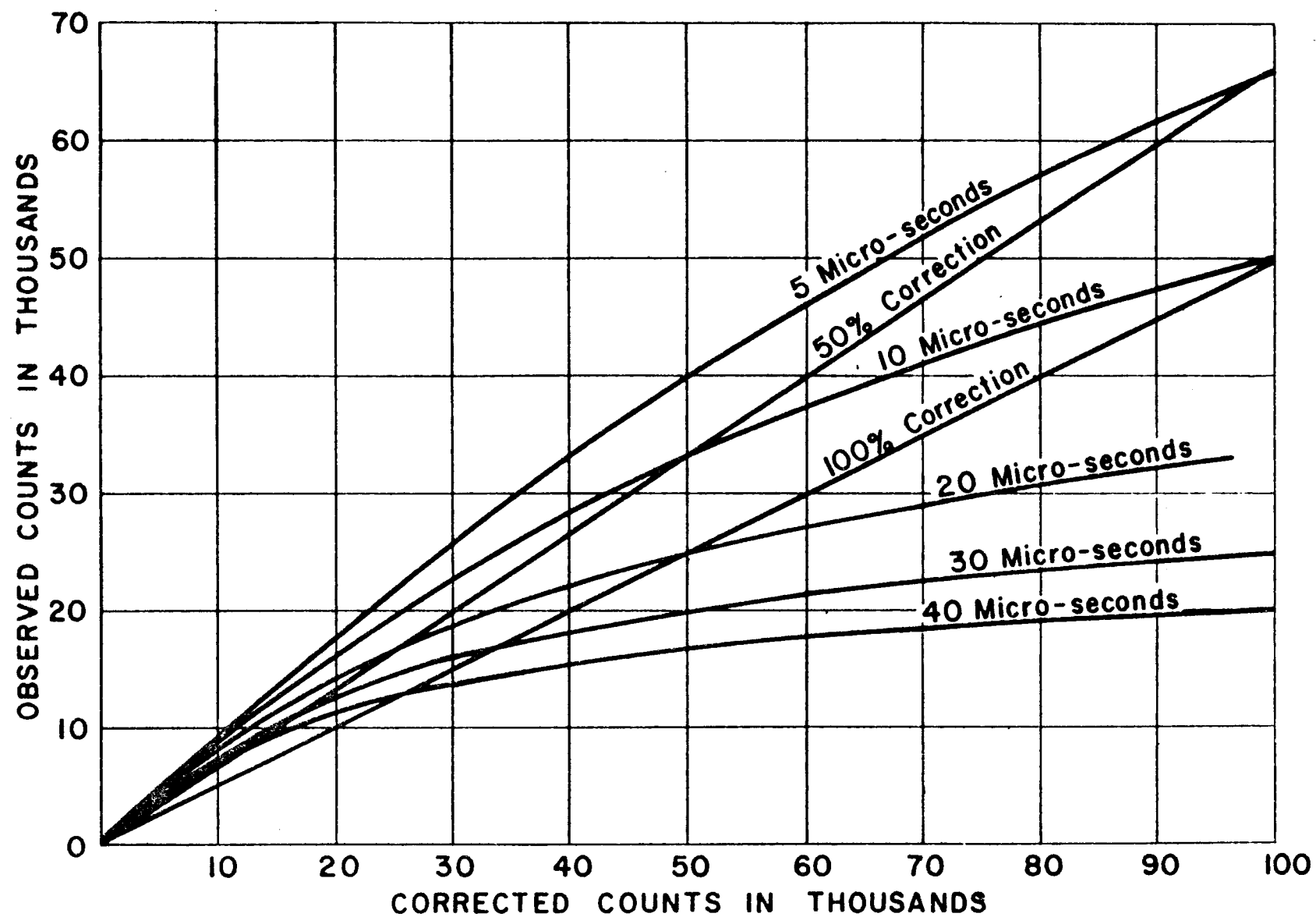
Figure 2. Deadtime Correction Curves

- 6 -
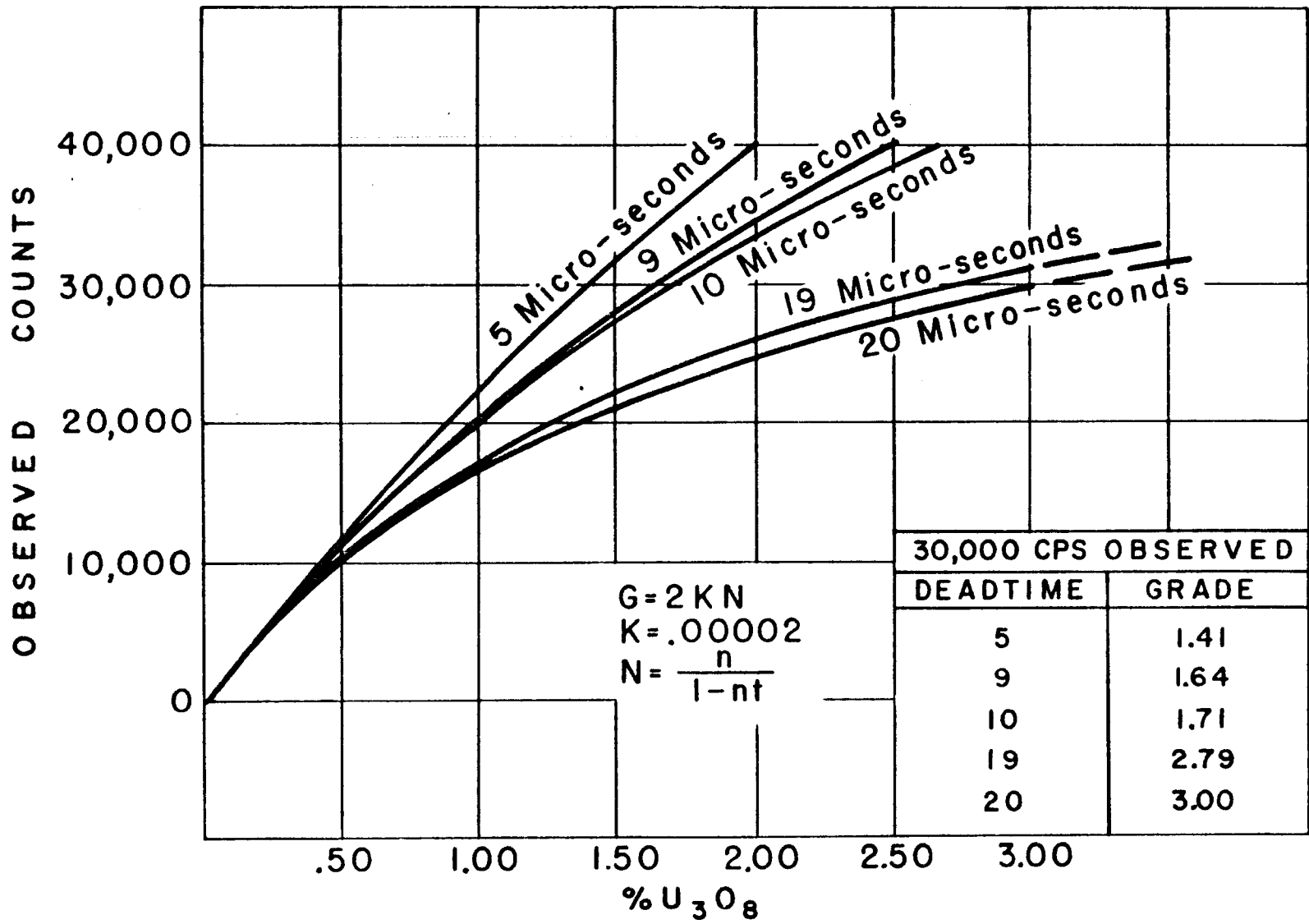
Fig. 3. Effect of Deadtime on Grade

would create a progressively increasing error. To see this effect more clearly, consider a 1 microsecond difference between 9 and 10 microseconds and between 19 and 20 microseconds at a rate count of 30,000 cps. The interpreted grades at 9 and 10 microseconds are 1.64% and 1.71% eU_3O_8 respectively; a difference of .07%, while the interpreted grades at 19 and 20 microseconds are 2.79% and 3.00% eU_3O_8; a difference of 0.21% or 3 times as great an effect as 1 microsecond had between 9 and 10 microseconds.

It is obvious that dead time plays a vital role in interpretations and must be determined in a manner which will reduce possible error to a minimum.

Evaluation

To support the premise presented in this paper, the Casper test pits were logged with Unit LP-1, probe 4. This is an AEC owned logging unit developed, constructed, and operated by Lucius Pitkin, Inc., an AEC service contractor. The following table shows the conventional factors and the factors arrived at by the TWOPIT program:

TABLE 1

Interpretation Factors for Probe 4

	Conventional	TWOPIT
Deadtime (microseconds)	4.9	8.66
K Factor	.00001948	.00001925

Figure 4 is a reproduction of the TWOPIT computer program output which generated the TWOPIT factors shown in Table 1.

The data, taken at half foot intervals from the analog record of the test pit logs, were interpreted using both conventional and TWOPIT factors. The total area under the curve was used rather than the customary "tail factor" method. Results are shown in Table 2.

- 11 -

From the results shown, it is obvious that there is little difference at grades in the range of the low grade test pit, but that the error is reduced considerably by use of TWOPIT factors in the grade range of the high grade pit.

The question now is: At what grade does the difference become significant? There is no definite answer to this but a relative comparison of the two methods through a range of grades can be shown by plotting observed counts against percent eU_3O_8 using the previously mentioned approximate relationship, G=2KN, and converting observed counts to corrected counts before substituting in the equation. Figure 5 is such a comparison of TWOPIT and conventional factors for probe 4.

It must be remembered that the tables and figures are for specific pieces of equipment and that each logging tool is somewhat different from every other in its response, thus each unit and probe combination must be individually evaluated rather than using a general correction for all combinations.

PROGRAM TWOPIT RESULTS

DATE OF COMPUTER RUN   APRIL 9, 1969
NO RANGE CORRECTION USED FOR THIS DATA

PITS	CASPER PITS		DATE LOGGED 01/24/69
COMPANY	LUCIUS PITKIN		LOG READINGS TAKEN AT 0.50 FOOT INTERVALS
UNIT	LP-1		RATIO - GT(LOW)/GT(HI) = 0.1476360
PROBE	4		APPARENT DEADTIME USED = 8.660 MICROSECONDS
XL SIZE = .75X1.00			WHEN RATIO-AREA(LOW/AREA(HI) = 0.1476771

<table>
<tr><td colspan="2" align="center">LOW PIT DATA
GT = 0.99300</td><td colspan="2" align="center">HI PIT DATA
GT = 6.72600</td></tr>
<tr><td align="center">OBSERVED
COUNTS</td><td align="center">CORRECTED
COUNTS</td><td align="center">OBSERVED
COUNTS</td><td align="center">CORRECTED
COUNTS</td></tr>
<tr><td align="center">100.</td><td align="center">100.</td><td align="center">200.</td><td align="center">200.</td></tr>
<tr><td align="center">300.</td><td align="center">301.</td><td align="center">700.</td><td align="center">704.</td></tr>
<tr><td align="center">1150.</td><td align="center">1162.</td><td align="center">2850.</td><td align="center">2922.</td></tr>
<tr><td align="center">4900.</td><td align="center">5117.</td><td align="center">14500.</td><td align="center">16582.</td></tr>
<tr><td align="center">7650.</td><td align="center">8193.</td><td align="center">34100.</td><td align="center">48390.</td></tr>
<tr><td align="center">8150.</td><td align="center">8769.</td><td align="center">39750.</td><td align="center">60616.</td></tr>
<tr><td align="center">8020.</td><td align="center">8619.</td><td align="center">40000.</td><td align="center">61200.</td></tr>
<tr><td align="center">7950.</td><td align="center">8538.</td><td align="center">40250.</td><td align="center">61787.</td></tr>
<tr><td align="center">6700.</td><td align="center">7113.</td><td align="center">38350.</td><td align="center">57420.</td></tr>
<tr><td align="center">2800.</td><td align="center">2870.</td><td align="center">24500.</td><td align="center">31098.</td></tr>
<tr><td align="center">550.</td><td align="center">553.</td><td align="center">6250.</td><td align="center">6608.</td></tr>
<tr><td align="center">170.</td><td align="center">170.</td><td align="center">1400.</td><td align="center">1417.</td></tr>
<tr><td align="center">80.</td><td align="center">80.</td><td align="center">350.</td><td align="center">351.</td></tr>
<tr><td>AREA</td><td align="center">=   51583.</td><td>AREA</td><td align="center">=   349295.</td></tr>
<tr><td>K FACTOR</td><td align="center">=   0.00001925</td><td>K FACTOR</td><td align="center">=   0.00001926</td></tr>
</table>

Figure 4
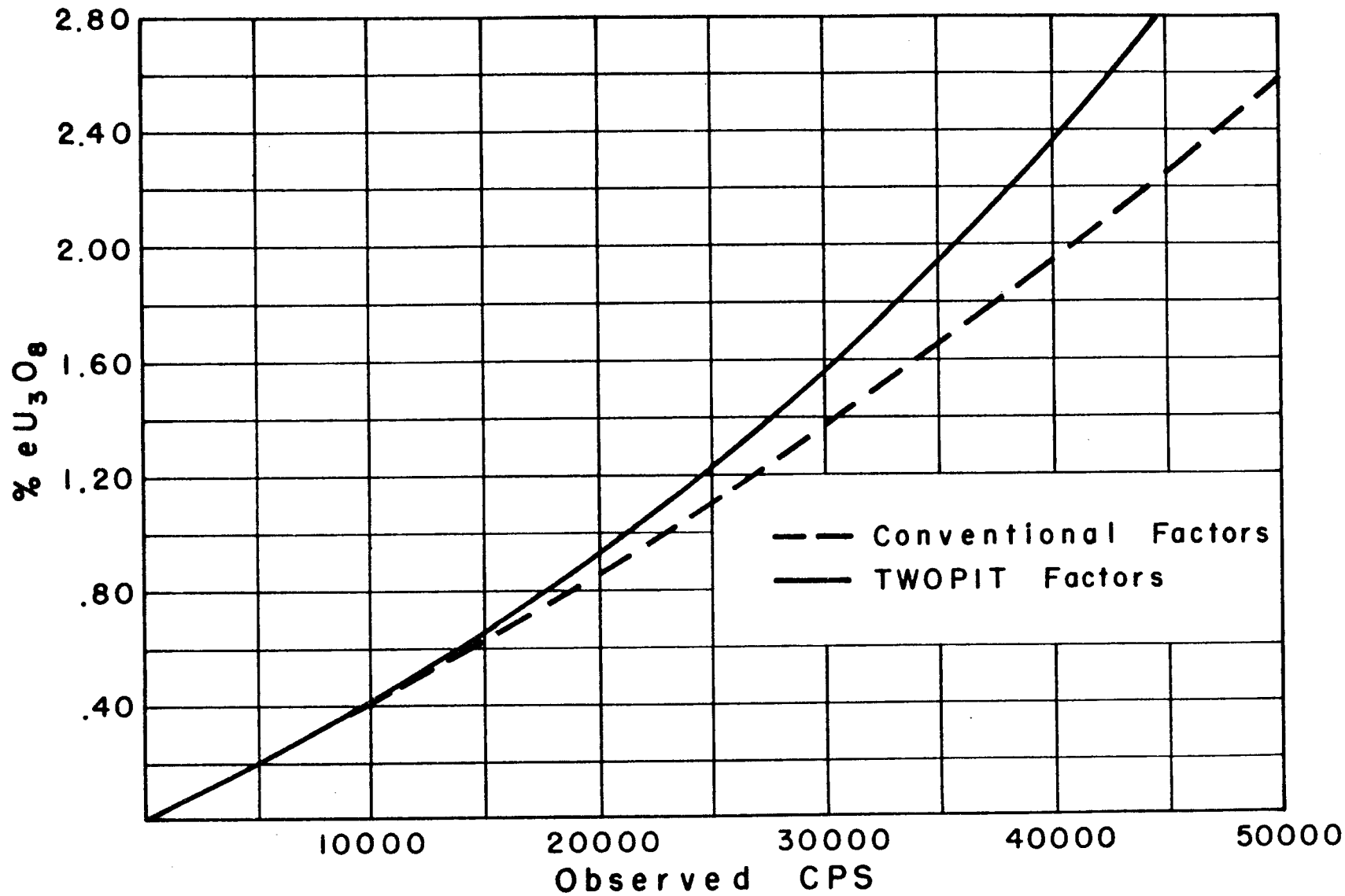
Figure 5. Comparison of TWOPIT and Conventional
Fac rs for Probe 4

TABLE 2
INTERPRETATION OF TEST PIT LOGS, UNIT LP-1, PROBE 4

	LOW PIT				HIGH PIT	
Observed Count	Dead Time Corrected Count			Observed Count	Dead Time Corrected Count	
	Conventional	TWOPIT			Conventional	TWOPIT
100	100	100		200	200	200
300	300	301		700	702	704
1,150	1,157	1,162		2,850	2,890	2,922
4,900	5,021	5,117		14,500	15,609	16,582
7,650	7,948	8,193		34,100	40,941	48,390
8,150	8,489	8,769		39,750	49,365	60,616
8,020	8,348	8,619		40,000	49,751	61,200
7,950	8,272	8,538		40,250	50,138	61,787
6,700	6,927	7,113		38,350	47,224	57,420
2,800	2,839	2,870		24,500	27,842	31,098
550	551	553		6,250	6,447	6,608
170	170	170		1,400	1,410	1,417
80	80	80		350	351	351
Total Area = 50,202	51,583				292,870	349,295
Area x K=GT = .9779	.9930				5.7051	6.7239
Thickness = 3.0	3.0				3.0	3.0
GT/T=% eU$_3$O$_8$= .326	.331				1.902	2.241
Accepted Value .331	.331				2.242	2.242
% error - 1.51	0.00				-15.17	-0.04

SUMMARY

The method described in this report is not represented to be a calculation of true instrumental dead time but instead a method of arriving at a dead time type correction for the entire logging system which will result in a closer approximation to equivalent radiometric grade throughout the entire range of count rates encountered in gamma-ray logging of drill holes.

The dead time effect calculated is a combination correction to compensate for true instrumental dead time, non linearity of ratemeter, recorder errors including improper zero adjust, and a photoelectric absorption effect of low energy gamma-rays by high concentrations of uranium (Dodd, personal communication). It is thus a total system evaluation that can be affected by many things other than true dead time.

Certain cautions must be taken before using the method, but in general these cautions are the same for conventional calibration techniques. The equipment used should:

1. Have linear response between all ranges.

2. Have constant electronic dead time, not rate sensitive.

3. Have linear counting capability above the rate encountered in the high grade pit.

4. Operate on the plateau region for the detector and give repeatable results.

If the above equipment conditions are met, the TWOPIT method will give calibration factors which will result in errors of interpretation no greater than the error in the assigned radiometric grades of the test pits.

REFERENCES

1/ Bellar, L. S., Farrar, H. IV, 1965, Determination of Paired-Pulse
    Resolution of Random Counting Systems, Report NAA-SR-MEMO-11132,
    Atomics International Division, North American Aviation Corp., AEC
    Contract AT (11-1) GEN. 8.

2/ Scott, J. H., Dodd, P. H., Droullard, R. F., and Mudra, P. J., 1961,
    Quantitative Interpretation of Gamma Ray Logs: Geophysics, Vol. XXVI,
    No. 2, p. 182-191.

3/ Scott, J. R., 1962, the GAMLOG Computer Program: RME-143, USAEC.

National Uranium Resource Evaluation

SPECTRAL GAMMA-RAY
LOGGING STUDIES

Bendix **Field Engineering
Corporation**

Grand Junction Operations
Grand Junction, CO 81502

January 1981

SPECTRAL GAMMA-RAY LOGGING STUDIES

Robert D. Wilson
and
David C. Stromswold

Bendix Field Engineering Corporation
Grand Junction Operations
P.O. Box 1569
Grand Junction, Colorado

January 1981

PREFACE

This is a progress report on spectral gamma-ray logging studies conducted
during the period from 1978 to 1980. Its contents first appeared as a
series of unpublished technical notes. The series has now been edited and
compiled.

The results presented are based mainly on experiments performed at the United
States Department of Energy (DOE), Grand Junction calibration facility. The
theoretical calculations of gamma-ray transport were performed at the Los
Alamos Scientific Laboratory (LASL) in work funded by DOE, Grand Junction.

An explanation and diagrams of the equipment used in the Grand Junction
experiments are included in the appendix of this report.

ACKNOWLEDGMENTS

CONTENTS

CONTENTS (Cont'd)

ILLUSTRATIONS

ILLUSTRATIONS (Cont'd)

9

11

CALIBRATION

INTRODUCTION

Calibration of radiation probes for exploration purposes relates the count rate in the probes' detectors to the concentrations of radioelements producing the counts. For spectral gamma-ray probes, calibration relates the number of gamma rays in specific energy windows to concentrations of potassium (K), uranium (U), and thorium (Th). The methods of collecting and analyzing calibration data are discussed in the following sections.

CALIBRATION THEORY

The number of gamma rays observed by a detector is assumed to be a linear function of the surrounding radioelement concentrations. Thus, an observed count rate R due to concentration C of gamma-emitting elements can be written

$$R = AC \tag{1}$$

where A is a proportionality constant.

Ideally, only gamma rays from a single radioactive source contribute to counts in a limited energy range or window; however, it is possible for gamma rays with energy initially outside a window to shift into the window (e.g., by Compton scattering). Because of this energy shift, it is necessary to calculate the contributions in each energy window from gamma rays of all the possible sources. The right side of equation (1) can be expanded as follows to show contributions to the counts, R, from all gamma rays:

$$R = AC + \sum (A'C') \tag{2}$$

where the summation (Σ) is over all gamma emitters that contribute to R by energy shifts into the R window. For potassium, uranium, and thorium (KUT) analysis, there are three terms on the right side of equation (2):

$$R = A_1 C_1 + A_2 C_2 + A_3 C_3 \tag{3}$$

where C_1, C_2, and C_3 represent the concentrations of potassium, uranium, and thorium, respectively.

Because R can represent the count rate in any energy window, it is convenient to adopt the following index notation:

$$R_i = \sum_{\ell=1}^{3} A_{i\ell} C_\ell \tag{4}$$

17

where

R_i = count rate in ith window
C_ℓ = concentration of ℓth radioactive element
$A_{i\ell}$ = constant relating count rate in ith window to the concentration of ℓth element.

For KUT analysis the following index convention is used:

i = 1 <=> potassium (K) window (1.32 MeV to 1.57 MeV)
i = 2 <=> uranium (U) window (1.650 MeV to 2.390 MeV)
i = 3 <=> thorium (Th) window (2.475 MeV to 2.76 MeV)
ℓ = 1 <=> potassium (K)
ℓ = 2 <=> uranium (U)
ℓ = 3 <=> thorium (Th).

For data collected in borehole models, where the concentrations of K, U, and Th are known, an additional index is added to the count rate and concentration variables to identify the calibration model used. Thus, equation (4) becomes:

$$R_{ij} = \sum_{\ell=1}^{3} A_{i\ell} C_{\ell j} \tag{5}$$

where the added index "j" indicates the model. The following convention is used for j:

j = 1 <=> model with large relative K concentration (K model or K pit)

j = 2 <=> model with large relative U concentration (U model or U pit)

j = 3 <=> model with large relative Th concentration (Th model or Th pit).

The double indices are interpreted as follows:

R_{ij} = Count rate in ith window in jth model
$C_{\ell j}$ = Concentration of ℓth radioelement in jth model
$A_{i\ell}$ = Constant relating count rate in ith window to the concentration of the ℓth radioelement.

Equation (5) can be written in the matrix form

$$R = AC \tag{6}$$

where R, A, and C are all 3x3 matrices. Inverting equation (6) gives

$$A = RC^{-1} \tag{7}$$

18

and

$$A^{-1} = CR^{-1} \qquad (8)$$

where C^{-1} is the matrix inverse of C, and A^{-1} is the matrix inverse of A. Equations (7) and (8) determine the calibration matrices A and A^{-1} from counting data, R, collected in the models where the concentrations, C, are known. A computer program (PADCAL) has been written to perform the actual matrix calculations (Stromswold and Kosanke, 1978).

The calibration matrices A and A^{-1} relate the response of the radiation detector in counts per second to the concentration of radioelements producing the counts. These calibration matrices provide a means for analyzing count rate data collected in the field where concentrations are not already known. The equation for converting count rate to concentration is

$$C = A^{-1}R \qquad (9)$$

where A^{-1} is the 3x3 calibration matrix, and C and R are 3x1 matrices. The three elements of the R matrix are the count rates observed in the K, U, and Th windows. The calculated concentration matrix has as its three components the concentrations of K, U, and Th.

Equation (9) can be written in non-matrix notation as follows:

$$C_i = \sum_{\ell=1}^{3} (A_{i\ell}^{-1} R_\ell) \qquad (10)$$

where C_i is the concentration of the ith radioelement, $A_{i\ell}^{-1}$ is the (i,ℓ) element of the A^{-1} matrix, and R_ℓ is the count rate in the ℓth energy window.

CALIBRATION METHODS

The spectral gamma-ray KUT probes are calibrated using the borehole models located at Grand Junction, Colorado. Three models (pits) are used for calibration, and each has an enhanced concentration of potassium, uranium, or thorium. The models are labeled by their prominent radioelement although each model contains traces of all three radioelements. The concentrations of these models are given in Table 1-1.

For KUT borehole probes, background count rates are from the radioactive source contained in the probe and used for energy stabilization. These background rates are determined using a large water tank or reported count rates for the standard BFEC detector and source configurations (Technical Note 2). The background count rates for the KUT energy windows are subtracted from measurements in each of the borehole models.

Table 1-1. Concentrations of Borehole Calibration Models

Model	% K	ppm U	ppm Th
K	6.76 $\pm$ 0.18	2.7 $\pm$ 0.3	2.4 $\pm$ 0.6
U	0.84 $\pm$ 0.24	498.3 $\pm$ 12.1	5.6 $\pm$ 1.3
Th	1.44 $\pm$ 0.08	28.3 $\pm$ 1.0	505.5 $\pm$ 12.1

NOTE: Statistical uncertainties quoted are one standard deviation.

The detectors used in the KUT probes are NaI(Tℓ) crystals of various dimensions. All crystals are larger than those generally used for gross-gamma surveys. Typical gross-gamma detectors have volumes less than 2 cubic inches, whereas most KUT detectors used by Bendix Field Engineering Corporation (BFEC) have volumes larger than 10 cubic inches. These larger volumes make it possible to collect statistically significant data in the K, U, and Th windows at logging speeds up to 5 feet/minute with counting periods of 5 to 10 seconds.

Several KUT probes contain two NaI(Tℓ) crystals. For these probes, the crystal having the smaller volume is used only when mineralized zones are encountered which are radioactive enough to overload the counting capability of the larger crystal. The physical specifications of the KUT probes built and operated by BFEC are given in Table 1-2.

The counting times used for calibrating the KUT probes in the models vary with both the probe and the calibration model used. These counting times are given in Table 1-3 for the three borehole models and the water tank. The counting times scale approximately as the inverse of the detector volume with the result that the precision in the calibration data is essentially independent of detector size. The detector volumes have been divided into three categories as follows:

$$25 \text{ in}^3 \text{ to } 35 \text{ in}^3 \text{ (large volume)}$$

$$15 \text{ in}^3 \text{ to } 25 \text{ in}^3 \text{ (medium volume)}$$

$$5 \text{ in}^3 \text{ to } 15 \text{ in}^3 \text{ (small volume)}.$$

The inclusion of the volume ranges in Table 1-3 provides a means for determining appropriate calibration times for detectors in newly constructed probes.

Until recently, probes have been calibrated in the models by collecting data at five separate points within each model. The process of moving the probe several times during calibration is time consuming for the operator; hence, the need for these separate data collections has been tested by comparing the averages of the five points with the data from the single point at the center of the ore zone. The data used in these tests are the regular calibration data collected over a period of 8 months. The results are shown in Table 1-4.

20

Table 1-2. Specifications of KUT Probes

Probe I.D.	Number of Detectors	Detector Dimensions diameter x length (inches)	Detector Volume (in^3)	Probe Outside Diameter (inches)	Comment
231	1	2 x 5	15.71	2-5/8	
232	1	2 x 5	15.71	3-1/2	Insulated for high temperature boreholes
241	2	1.75 x 3 2 x 10	7.22 31.42	2-5/8	
242	2	1.75 x 3 2 x 10	7.22 31.42	2-5/8	
251	2	1 x 6 Filtered 1.5 x 12	4.71 21.21	2 - 1/8	For narrow boreholes
252	2	1.5 x 3 1.5 x 12	5.30 21.21	2	For narrow boreholes
253	2	1.5 x 3 1.5 x 9	5.30 15.90	2	For narrow boreholes

21

Table 1-3. Calibration Counting Times

Probe I.D.	Detector Volume Range (in^3)	Counting Time (seconds)			
		K Model	U Model	Th Model	Water Tank
241-L 242-L	$25 \leq V < 35$	1500	1000	1000	2000
231 232 252-L 253-L	$15 \leq V < 25$	3000	2000	2000	4000
241-S 242-S 252-S 253-S	$5 \leq V < 15$	4500	3000	3000	5000

Note: The "L" and "S" on the Probe I.D. designate long and short detectors in dual detector probes.

The closeness of the averaged calibrations to the single point calibrations shows that it is necessary only to collect data at the center of the ore zone for acceptable calibrations. The uniformity of the data in Table 1-4 also shows that there is no difficulty in positioning the probe at the center of the ore zone. As a check on equipment operation two separate data collections are now made during calibration without moving the probe. Consistency between two sets of data provides confidence that the equipment did not malfunction (e.g., stop prematurely) during data collection.

SUMMARY

Calibration data for spectral gamma-ray probes are collected in the Grand Junction models. The counting times for collecting these data vary with detector size, and appropriate times have been presented in Table 1-3 for a range of detector volumes.

The collected data are analyzed using matrix mathematics to obtain the conversion factors between count rates and concentrations and to determine the gamma-ray scatter components that produce interferences among the discrete energy windows. In this technique of analysis, calibration consists of determining the matrix A^{-1} using equation 8. A^{-1} can then be used to calculate (equation 9 or 10) unknown concentrations in the field based on observed count rates.

Table 1-4. Comparison of Calibration Data Taken at One Point and at Five Points

Date of Calibration	Probe I.D.	Counting Time (Sec)	K CHANNEL				U CHANNEL				Th CHANNEL			
			Mid-Point Counts	Mid-Point Counts/Second	5-Point Average Counts/Second	Average Counts for 5 Points	Mid-Point Counts	Mid-Point Counts/Second	5-Point Average Counts/Second	Average Counts for 5 Points	Mid-Point Counts	Mid-Point Counts/Second	5-Point Average Counts/Second	Average Counts for 5 Points
K Model														
6/6/78	252-S	600	5240	9.033±.12	8.983	5390.2	718	1.196±.04	1.133	680.2	70	0.116±.01	0.115	69.0
6/5/78	252-L	400	14552	36.380±.30	36.102	14440.8	1779	4.440±.10	4.430	1772.2	215	0.537±.03	0.503	201.2
6/5/78	242-S	600	10361	17.268±.16	17.103	10262.	1749	2.915±.06	2.988	1793.0	57	0.095±.01	0.116	69.8
6/1/78	242-L	400	21568	53.920±.36	53.930	21572.2	2523	6.307±.12	6.451	2580.6	260	0.650±.04	0.648	259.2
5/25/78	242-L	400	20573	51.432±.35	51.295	20518.2	2867	7.167±.13	7.119	2847.8	284	0.710±.04	0.720	288.2
3/29/78	252	400	6062	15.155±.19	15.081	6032.6	6062	2.295±.07	2.330	932.0	107	0.267±.02	0.303	121.4
3/29/78	231	400	10627	26.567±.25	26.835	10734.2	1388	3.470±.09	3.494	1397.8	228	0.570±.03	0.529	211.8
3/29/78	242-S	400	4357	10.892±.16	10.944	4377.6	654	1.635±.06	1.664	665.8	66	0.165±.02	0.158	63.2
3/29/78	242-L	400	22388	55.970±.37	55.730	22292.0	3566	8.915±.14	9.049	3619.6	425	1.062±.05	1.038	415.4
2/21/78	252	400	6059	15.147±.19	15.194	6077.8	711	1.777±.06	1.845	738.0	80	0.200±.02	0.196	78.6
2/14/78	242-S	400	4350	10.875±.16	10.749	4299.6	644	1.610±.06	1.651	660.4	69	0.172±.02	0.139	55.6
2/13/78	242-L	400	22638	56.595·.37	56.334	22533.0	3254	8.135±.14	7.9205	3168.2	277	0.692±.04	0.736	294.4
U Model														
6/6/78	252-S	300	25167	83.890±.52	83.576	25073.0	23266	77.553±.50	77.362	23208.6	411	1.370·.06	1.464	439.2
6/5/78	252-L	200	69983	349.915±1.32	348.128	69625.6	71556	357.780·1.33	357.011	71402.2	1999	9.995±.22	10.012	2002.4
6/5/78	242-S	300	31732	105.773·.59	105.906	31772.2	26720	89.066·.54	89.130	26739.2	494	1.646·.07	1.822	546.8
6/1/78	242-L	200	96290	481.450·1.55	480.534	96106.8	97005	485.025·1.55	488.830	97766.0	2589	12.945·.25	13.033	2606.6
5/25/78	242-L	200	97554	487.770·1.56	486.062	97212.4	102841	514.205·1.60	514.345	102869.0	3373	16.865·.29	16.684	3336.8
3/29/78	252	200	29766	148.830·.86	149.313	29862.6	29686	148.430·.86	148.855	29771.0	923	4.615±.15	4.606	921.2
3/29/78	231	200	49153	245.765·1.10	246.105	49221.0	50071	250.355±1.11	250.088	50017.6	1636	8.180·.20	8.513	1702.6
3/29/78	242-S	200	19533	97.665±.69	96.580	19316.0	17736	88.680·.66	87.634	17526.8	319	1.595±.08	1.481	296.2
3/29/78	242-L	200	98845	494.225·1.57	491.311	98262.2	104254	521.270·1.61	521.287	104257.4	3212	16.060·.28	16.171	3234.2
2/21/78	252	200	29332	146.660·.85	147.034	29406.8	28546	142.730·.84	142.213	28442.6	685	3.425·.13	3.384	676.8
2/14/78	242-S	200	19627	98.135·.70	96.823	19364.6	16956	84.780·.65	84.468	16893.6	292	1.460·.08	1.432	286.4
2/13/78	242-L	200	98688	493.440·1.57	491.567	98313.4	102359	511.795·1.59	511.587	102317.4	3032	15.160·.27	15.521	3104.2
Th Model														
6/6/78	252-S	300	9418	31.393·.32	30.974	9292.2	18435	61.450·.45	60.869	18265.8	4861	16.203·.23	16.116	4834.8
6/5/78	252-L	200	24161	120.805·.77	119.983	23996.6	50247	251.235·1.12	250.090	50018.0	15245	76.225·.61	77.034	15406.8
6/5/78	242-S	300	14217	47.390·.39	47.214	14164.4	22512	75.040·.50	74.710	22412.6	5254	17.513·.24	17.230	5168.4
6/1/78	242-L	200	35197	175.985·.93	175.090	35018.2	65980	329.900·1.28	329.660	65932.2	21331	106.655·.73	106.690	21338.2
5/25/78	242-L	200	34022	170.110·.92	170.570	34114.6	67233	336.165·1.29	336.240	67247.2	20741	103.705·.72	103.700	20740.8
3/29/78	252	200	9963	49.815·.49	49.570	9914.2	21530	107.650·.73	106.390	21278.2	6038	30.190·.38	30.270	6053.2
3/29/78	231	200	16706	83.530·.64	83.310	16661.0	32456	162.280·.90	161.470	32294.0	12033	60.165·.54	59.000	11800.4
3/29/78	242-S	200	8094	40.470·.44	39.510	7901.0	14841	74.205·.60	73.780	14755.0	3376	16.880·.29	16.840	3368.8
3/29/78	242-L	200	35017	175.085·.93	174.480	34896.2	67632	338.160·1.30	336.940	67388.2	21955	109.775·.74	108.870	21773.6
2/21/78	252	200	9982	49.910·.49	50.210	10041.6	20731	103.655·.71	103.570	20713.4	6067	30.335·.38	30.190	6037.6
2/14/78	242-S	200	8201	41.005·.45	40.780	8156	14829	74.145·.60	73.540	14706.8	3127	15.635·.27	15.700	3140
2/13/78	242-L	200	35282	176.410·.93	175.720	35143.4	66861	334.305·1.29	333.760	66751.2	22299	111.495·.74	111.740	22348

Note: Uncertainties are one standard deviation.

Technical Note 2

KUT BACKGROUND CORRECTIONS

ABSTRACT

Measurements have been completed that identify and quantify the sources of
background for Bendix KUT probes. Results of these measurements show that the
only significant source of background is instrumental and is from the pile-up
of 0.835 MeV ^{54}Mn pulses into the K and U energy windows. Pile-up count
rates are presented for the standard Bendix KUT detectors: the 1-inch x 6-inch
filtered and the 1.5-inch x 12-inch unfiltered-sodium iodide (NaI)
scintillators.

The K, U, and Th window count rates contributed by ^{54}Mn pile-up were
determined as a function of source strength. The pile-up contribution to the
Th window count rate is negligible except for source strengths much higher
than those employed with Bendix probes. The K and U window count rates
contributed by ^{54}Mn pile-up are significant, especially for the smaller
1-inch x 6-inch filtered detector, for the range of source strengths employed
with Bendix KUT probes.

Analytic polynomial fits were obtained for the K and U window pile-up count
rates as a function of ^{54}Mn source strength for the two NaI detector sizes.
These analytic expressions may be used in KUT log analysis algorithms to
subtract the instrumental background count rates from KUT calibration data and
from field logs.

For the nominal logging conditions where uranium and thorium concentrations
are in the few ppm range, the effect of ^{54}Mn pulses piling up with formation
gamma-ray pulses is negligible. At higher uranium and thorium grades (greater
than 100 ppm) this effect remains less than 1 percent and may be neglected.

When ^{54}Mn pile-up count rates are not available because of a nonstandard
detector configuration or because of incomplete knowledge of the ^{54}Mn source
strength, direct measurements may be obtained in a low background model now
available at the Grand Junction calibration facility.

INTRODUCTION

In the calibration of spectral gamma-ray probes, test models of known
potassium, uranium, and thorium concentration are used to relate count rates
to concentrations. Background counts which are not related to the test model
concentrations must be subtracted from both the calibration data and from
subsequent field data. This technical note discusses the theory of background
subtraction for KUT logging probes, and presents background measurement
results and a correction procedure.

THEORY OF KUT BACKGROUND SUBTRACTION

The calibration of a KUT probe is discussed in Technical Note 1. Background
count rates are subtracted from the calibration data before they are related
to concentrations. The resulting 3 x 3 calibration matrix is called A^{-1}.
Concentrations are calculated from field KUT logs using the matrix equation

$$C = A^{-1}R \qquad (1)$$

where C is a 3 x 1 matrix whose elements are the desired concentrations of potassium (%), uranium (ppm), and thorium (ppm) and R is a 3 x 1 matrix whose elements are the measured, unstripped count rates for potassium (K), uranium (U), and thorium (Th).

Concentrations are determined by subtracting background count rates before multiplying by the calibration matrix A^{-1}:

$$C_B = A^{-1}(R-B).\qquad\qquad(2)$$

In equation (2), B is a 3 x 1 matrix containing the background count rates for K, U, and Th, and C_B is the background corrected concentration matrix. Comparing equations (1) and (2) it is clear that the calculated concentrations will be too high if background is not subtracted from the observed counting data.

ORIGIN OF BACKGROUND COUNTS

In this discussion, background counts are defined as counts in a detector which are not attributable to the presence of K, U, or Th. In KUT probes containing a radioactive source for energy stabilization, this source can be a major contributor to background. In KUT probes used by Bendix, ^{54}Mn sources of approximate strength 0.7 and 4 microcuries are used to stabilize the large and small detectors, respectively. This source produces a gamma ray of energy 0.835 MeV, which is well below the KUT energy windows. However, the chance arrival of two 0.835 MeV gamma rays at the same time in a detector produces a sum or pile-up spectrum that looks similar to the pulse height spectrum from a single gamma ray having approximately twice the energy of the individual gamma rays. This pile-up spectrum extends in energy to twice 0.835 MeV or 1.67 MeV and gives counts in both the K and U energy windows.

Chance coincidences can also occur with one 0.835 MeV gamma ray from ^{54}Mn and another gamma ray from a different source. When the summed energies fall in the K, U, or Th windows, they produce background counts. In mineralized zones where uranium or thorium is present, there is an abundance of low energy gamma rays due to Compton scattering. These gamma rays can have chance coincidences with ^{54}Mn gamma rays and contribute to the background. This contribution is not constant, rather it is a function of the concentrations of radioactive elements in the formation.

A second source for background counts is cosmic rays and their secondary radiations. Cosmic rays are charged particles that enter the earth's atmosphere. The energy of cosmic rays is generally much higher than that of the K, U, and Th windows, and consequently few cosmic rays contribute directly to the background. The interactions of cosmic rays with material near the detector, however, can produce gamma rays which contribute to background counts. These contributions are negligible when the probe is more than a few feet below the surface of the ground. Only during calibration in shallow holes and at the ground level is there any cosmic-induced background.

Background counts can be produced by the presence of radioactive elements that emit gamma rays having energies within K, U, or Th windows. This origin of background is generally minor compared to other origins of background counts, and it seldom produces serious problems for data analysis.

26

Finally, background counts can come from the photomultiplier tube on the detector. These counts are low in energy, and they do not produce any significant contributions to the K, U, and Th windows in a properly operating probe.

BACKGROUND MEASUREMENTS

The background measurements reported here were performed in two distinct geometries but always employed a 2.125-inch diameter Bendix KUT probe with analog signals driven through 3000 feet of 4HO logging cable. Pulses from the logging cable were reshaped using an Ortec 572 spectroscopy amplifier and then analyzed with a Tracor Northern model 1710 multichannel analyzer.

In the first geometry, the KUT probe was placed inside a lead cylinder approximately 1.4 inches thick having an inside diameter of 4.5 inches and a length of 5 feet. This arrangement was used to measure pile-up count rates in the KUT energy windows as a function of ^{54}Mn source strength.

The second geometry became available at a later time and represents a superior shielding arrangement. The probe is placed within a water filled tank 6.5 feet in diameter and 8 feet long. The tank is constructed to accept liners of various diameters attached along its axis. A 4.5-inch diameter PVC liner was used to simulate the standard borehole condition. This arrangement was used to determine the origin of KUT probe background counts.

Identification of Background Sources

A 1.5-inch x 9-inch NaI detector with the standard probe and signal processing system was placed at a depth of 5.5 feet at the center of the water filled tank. In one measurement, a 0.6 microcurie ^{54}Mn source was taped to the detector wall at its approximate midplane. In another measurement, the detector was placed at the same depth but without the ^{54}Mn source. Both measurements were for 2000 seconds. Figure 2-1 shows the spectra for these two measurements. Both spectra contain 1024 channels. The plots are semilogarithmic with the vertical axis expressed in counts/channel. The KUT energy windows and the ^{54}Mn pilot window are labeled in the figure. The ^{54}Mn spectrum shows clearly the pile-up or sum distribution that occurs between the source energy of 0.835 MeV and twice this energy at 1.670 MeV. The sum peak occurs at the lower edge of the U window. K window pile-up counts are from the continuum portion of the sum spectrum. The spectrum without the ^{54}Mn source shows some structure at energies below the KUT windows. This is most likely caused by high energy cosmic-ray produced interactions in the detector. These interactions yield saturated pulses from the linear amplifier along with associated low amplitude reflection pulses due to the 3000-foot logging cable. The saturated pulses are excluded by the upper level discriminator of the multichannel analyzer but the low amplitude reflections appear as low energy peaks in the spectrum. The count rates from this background source are negligible when compared to those from the nominal ^{54}Mn strength of 0.6 microcuries. The very few counts observed above 1.67 MeV and including the Th window are the same for both spectra, showing that there is no pile-up contribution to the Th window. The measurement without a ^{54}Mn source was repeated but with the probe inside a 4.5-inch diameter PVC liner centered within the water filled tank. Measurements were taken with the probe at the same 5.5-foot depth and with the PVC liner both dry and water
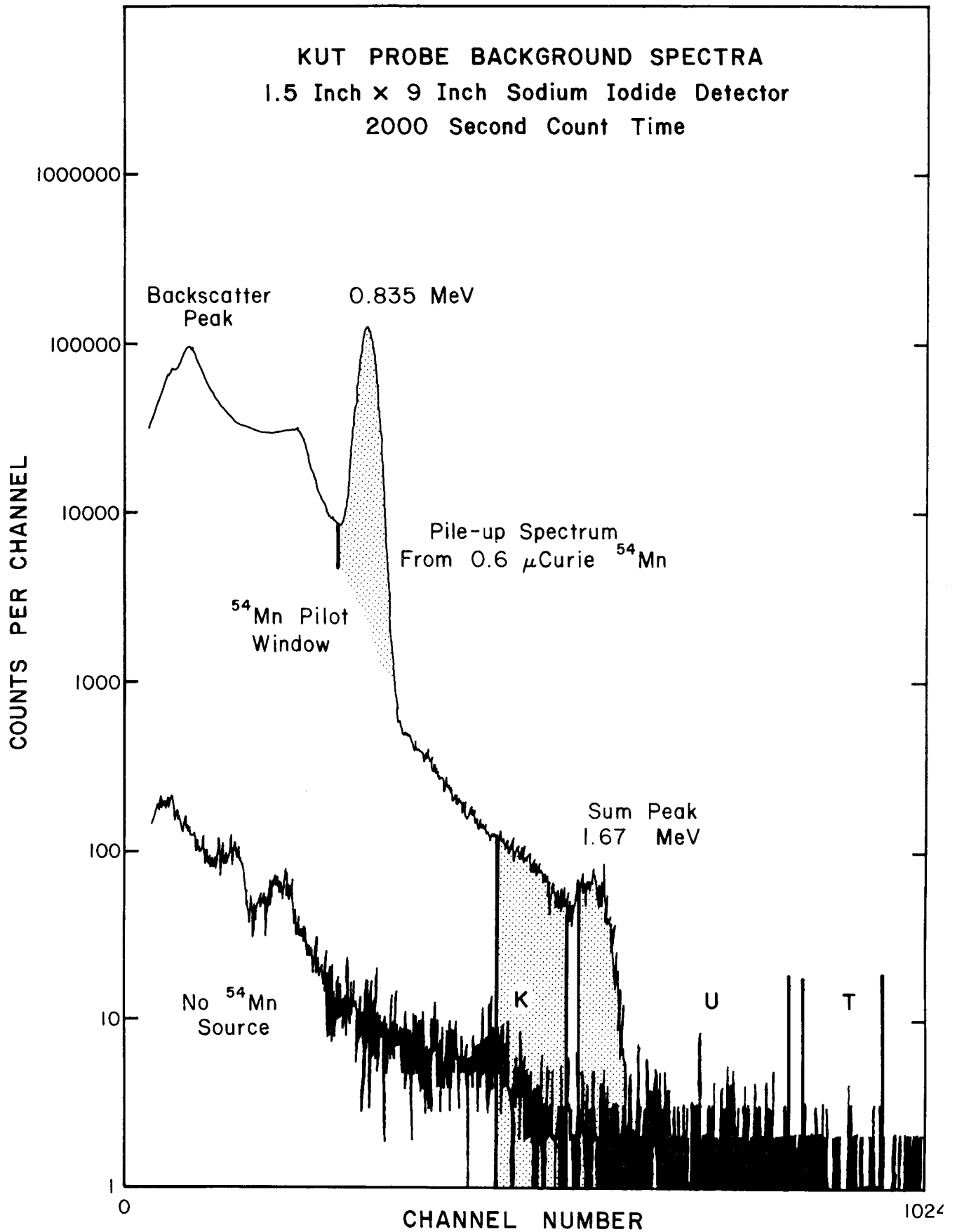
Figure 2-1.   KUT probe background spectra as acquired within the low
background water tank.

28

filled. Results were virtually identical to the previous measurement without the liner. Results of all 4 measurements are summarized in Table 2-1.

Table 2-1. Background Measurements for a 1.5-inch x 9-inch NaI Detector
As Taken in the Water-Filled Tank

Measurement Condition	K Window (cps)	U Window (cps)	Th Window (cps)
0.6 µCi ^{54}Mn	3.83	1.34	0.036
No ^{54}Mn or liner	0.16	0.17	0.024
No ^{54}Mn, dry liner	0.15	0.16	0.036
No ^{54}Mn, Water filled liner	0.15	0.16	0.037

It is clear from these results that when KUT probes are placed in the calibration models at a depth of 5.5 feet to obtain calibration data the pile-up count rates from the ^{54}Mn source are the only significant source of background. The 0.6 µCi strength is typical of the ^{54}Mn sources employed with the large detector in Bendix KUT probes. Count rates observed in the K and U windows without a ^{54}Mn source are negligible in comparison. The observed Th window count rates are negligible in all 4 measurements, having a thorium concentration equivalent of less than 0.3 ppm.

There is another effect that tends to complicate the ^{54}Mn pile-up background correction when measurements are performed in formations or models with high uranium or thorium concentrations. When count rates from the low energy continuum region of the spectrum from uranium or thorium become comparable to the ^{54}Mn count rates then the chance that a ^{54}Mn pulse will sum with a low energy formation gamma-ray pulse becomes significant. Simultaneous with this effect is the random pile-up of low energy uranium or thorium pulses with each other. This effect can both remove from and add to the K, U, and Th window count rates.

These two effects that involve random summing of formation gamma-ray pulses either with ^{54}Mn pulses or with each other are grade dependent. Corrections, therefore, are nearly impossible to make. These effects are second order in nature for the vast majority of logging environments. They are probably not important until uranium or thorium concentrations exceed several hundred ppm, and then only when using the larger of the detectors in Bendix KUT probes.

For the present, KUT background corrections will include only the ^{54}Mn pile-up count rates. These rates will be subtracted from both calibration and field data. Future KUT logging systems should include down-hole linear gating circuitry to reduce count rates on the logging cable and uphole pile-up rejection circuitry to eliminate those events which are randomly summed.

^{54}Mn Pile-up Count Rates

1.5-inch x 12-inch Sodium Iodide Detector. The ^{54}Mn pile-up distribution contributes to both the K and U windows, but only slightly to the Th window count rates (See Figure 2-1). Pile-up spectra were obtained for a range of ^{54}Mn source strengths to determine the K and U window pile-up count rates as

29

a function of source strength. The ^{54}Mn gamma-ray sources were always taped to the detector wall at its approximate midplane. Certain source strengths were obtained by combining two or more of the ^{54}Mn sources. All measurements were performed in the lead cylinder described earlier. Table 2-2 contains the basic instrumental background data for the 1.5-inch x 12-inch NaI detector. The window counts corresponding to zero ^{54}Mn source strength are due to external background transmission through the shield. Table 2-3 contains the data as reduced to count rates and as corrected for the contribution from the external background.

Table 2-2. Instrumental Background for the 1.5-inch x 12-inch NaI Detector as Contributed by Pile-Up Counts from the ^{54}Mn Stabilization Source.

^{54}Mn Source Strength (μC)	K Window Counts	U Window Counts	Th Window Counts	Count Time (Seconds)
0	9610	7405	1599	6000
0.31	13764	8698	1648	6000
0.42	20773	11640	1883	6000
1.16	73276	27322	1763	6000
3.91	833986	309254	9433	6000

Table 2-3. Net Instrumental Background Count Rates for 1.5-inch x 12-inch NaI Detector. The Count Rates for No ^{54}Mn Source Have Been Subtracted From the Rates for Each Source Strength.

^{54}Mn Source Strength (μC)	K Window (cps)	U Window (cps)	Th window (cps)
0.31	0.692	0.216	0.008
0.42	1.86	0.706	0.048
1.16	10.61	3.32	0.027
3.91	137.4	50.31	1.31

Figure 2-2 is a plot of the numerical results presented in Table 2-3. This is a semilogarithmic plot of both the K and U window pile-up count rates from the ^{54}Mn source. The pile-up contribution to the Th window is negligible for all but the highest source strength of 3.91 microcuries. Since this strength is never used with the 1.5-inch x 12-inch detector of the Bendix KUT probes, the pile-up background will be neglected for the thorium window. The horizontal axis is expressed both in microcuries of ^{54}Mn and in terms of the ^{54}Mn pilot window count rate. For the 1.5-inch x 12-inch detector, the pilot window yields the following:

$$2400 \pm 20 \ \frac{\text{counts/sec}}{\mu\text{curie } ^{54}\text{Mn}}$$

The pilot window count rate will be utilized later in the recommended correction procedure for KUT field logs. Analytical expressions fit to these data will always be given as a function of the ^{54}Mn pilot window count rate. The solid curves shown in Figure 2-2 are the result of third order polynomial

30
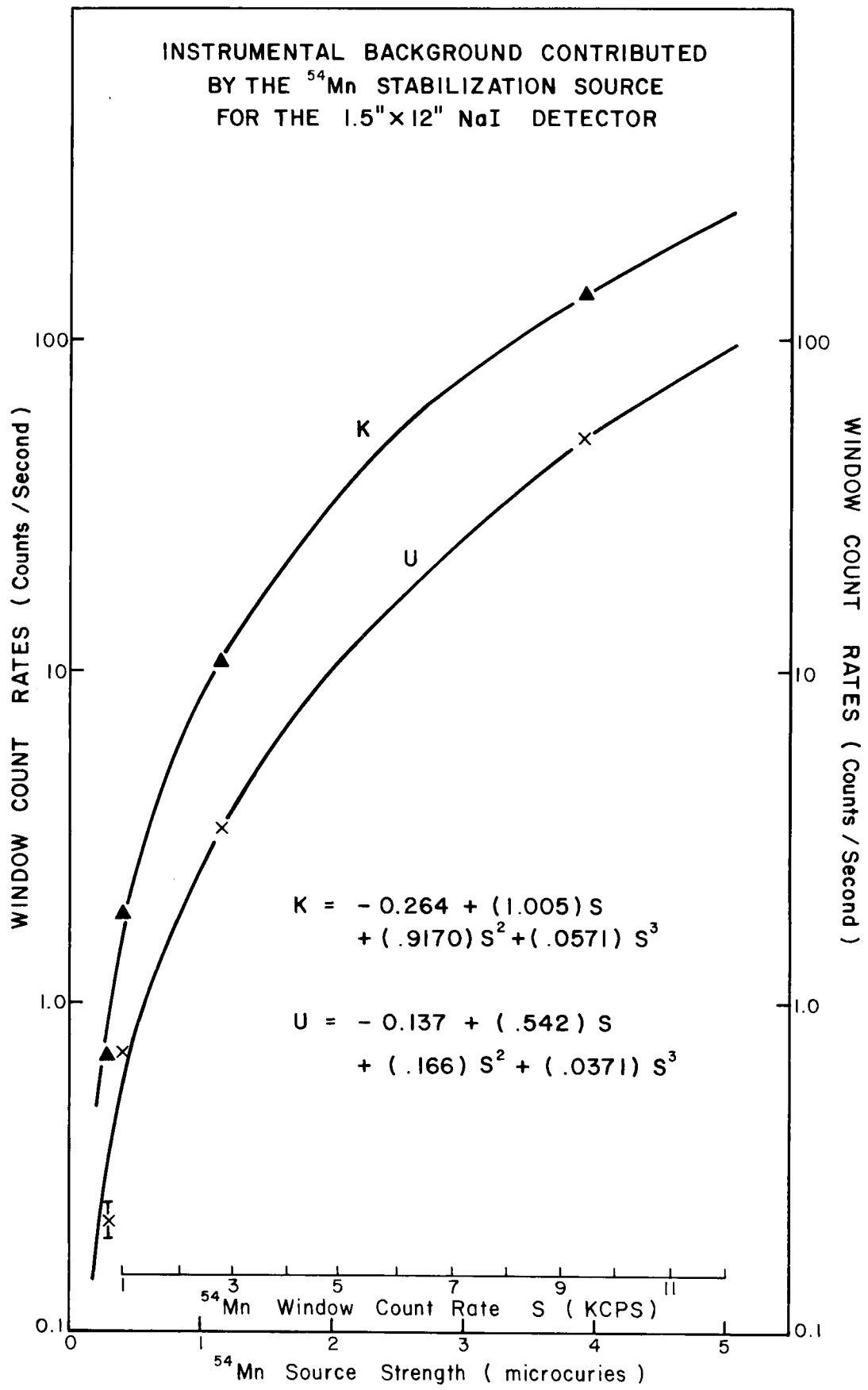
Figure 2-2. ⁵⁴Mn pile-up background count rates for the 1.5-inch x 12-inch NaI detector as acquired within the lead shield.

least squares fits to the measured results. The corresponding analytical expressions are given on the figure, where pilot window count rate S has units of thousands of counts/second (KCPS). These expressions represent excellent fits to the measured data over the range of source strength from 0.3 to 4 microcuries. The uncertainties for the measured data are smaller than the symbols plotted in Figure 2-2 with the exception of the U window count rate for the 0.3 microcurie source strength. For this point the uncertainty is shown as a vertical bar.

1-inch x 6-inch Filtered NaI Detector. The experimental arrangement for these measurements was the same as for the 1.5-inch x 12-inch detector. A larger range of ^{54}Mn source strengths was employed because of the smaller crystal size. K, U, Th, and ^{54}Mn pilot window counts were obtained from the spectrum for each source strength. The results are summarized in Table 2-4. Table 2-5 contains the data reduced to count rates and corrected for the external background contribution. As with the 1.5-inch x 12-inch detector data, the ^{54}Mn pile-up contribution to the thorium window is negligible for all but the highest source strengths of 4.08 and 6.10 microcuries. Figure 2-3 is a semilogarithmic plot of the numerical results contained in Table 2-5. For the 1-inch x 6-inch filtered detector, the pilot window yields

$$418 \pm 6 \ \frac{counts/sec}{\mu curie \ ^{54}Mn} \ .$$

The analytic expessions presented for K and U instrumental background count rates result from third order polynomial least squares fits to the logarithm of the measured data. The fits were made to the logarithm of the measured data because direct polynomial fits were unsatisfactory. The dependent variable S represents the ^{54}Mn pilot window count rate in thousands of counts per second (KCPS). The fits represent the data well for the range of source strengths from 0.5 to 6 microcuries. The dashed curve is a visual fit to the very small pile-up contribution to the Th window at the higher source strengths.

Table 2-4. Instrumental Background for the 1-inch x 6-inch Filtered NaI Detector as Contributed by Pile-Up Counts From the ^{54}Mn Stabilization Source.

^{54}Mn Source Strength (μC)	K Window Count	U Window Count	Th Window Count	Count Time (Seconds)
0.0	6757	6317	1299	25200
0.59	12414	9188	1711	32911
1.04	13655	7212	1024	20898
1.04	8039	4324	633	12100
1.62	15188	6277	792	14000
2.61	43046	14252	1138	20000
4.08	29906	7024	268	3500
6.10	58429	14322	364	3800

Figure 2-3. ^{54}Mn pile-up background count rates for the 1-inch x 6-inch
filtered NaI detector as acquired within the lead shield.

Table 2-5. Net Instrumental Background Count Rates for the 1-inch x 6-inch Filtered NaI Detector. The Count Rates for No ^{54}Mn Source have been Subtracted from the Rates for Each Source Strength.

^{54}Mn Source Strength (μ C)	K Window (cps)	U Window (cps)	Th Window (cps)
0.59	0.109	0.028	0.0004
1.04	0.385	0.094	-0.0026
1.04	0.396	0.107	0.0008
1.62	0.817	0.198	0.005
2.61	1.884	0.462	0.005
4.08	8.28	1.76	0.25
6.10	15.11	3.52	0.44

CORRECTION OF KUT LOGS

The nominal ^{54}Mn source strengths employed in Bendix KUT probes are approximately 0.7 microcuries for the 1.5-inch x 12-inch detector and 4 microcuries for the filtered 1-inch x 6-inch detector. ^{54}Mn has a relatively short half life of 312.5 days. As the source decays during its use, its strength could drop by up to a factor of two. When KUT field logs and calibration data are corrected for the ^{54}Mn instrumental background, the current source strength must first be computed. The source strength can be expressed either in microcuries on in terms of the pilot window count rate. When the ^{54}Mn source is located at the midplane of either detector size, the KUT window pile-up count rates can be estimated from the strength in microcuries. Quite often, however, the source is not located at the detector midplane in Bendix probes. When this is the case, the pile-up corrections must be estimated from the pilot window count rate. Figures 2-2 and 2-3 contain analytic expressions for K and U window pile-up count rates with the pilot window count rate as the independent variable. The current value of the source strength for a given KUT field log or calibration run can be either measured from the pilot window count rate in thousands of counts per second (KCPS) or it can be computed by decay correcting an earlier pilot window count rate measurement using the equation

$$S = S_0 \exp\left[-\lambda(t-t_0)\right] \tag{3}$$

where S_0 is the source strength expressed as a pilot window count rate (KCPS) at some initial time t_0 (in days), λ is the ^{54}Mn decay constant and is equal to 2.218×10^{-3} days^{-1}, and t is the current time (in days). Once the current ^{54}Mn source strength has been determined, the K and U window count rates are computed from the analytic polynomial fits to the measured instrumental background data presented in Figures 2-2 and 2-3 and reproduced below.

1.5-inch x 12-inch NaI Detector

$$K = -0.264 + (1.005)S + (0.9170)S^2 + (0.0571)S^3 \tag{4}$$
$$U = -0.137 + (0.542)S + (0.166)S^2 + (0.0371)S^3 \tag{5}$$

1-inch x 6-inch Filtered NaI Detector

$$\log K = -1.416 + (2.486)S - (0.8853)S^2 + (0.1219)S^3 \qquad (6)$$
$$\log U = -2.022 + (2.572)S - (1.0230)S^2 + (0.1616)S^3 \qquad (7)$$

The instrumental background from ^{54}Mn pile-up counts in the Th window is negligibly small for the range of source strengths employed in Bendix probes and can be neglected in this correction procedure.

Equations (4) and (5) should be used only for the range of source strengths from 0.3 to 5 microcuries (pilot window count rates from 0.72 to 12 KCPS) and equations (6) and (7) for the range from 0.5 to 7 microcuries (pilot window from 0.21 to 3 KCPS). Beyond these ranges, for example at zero source strength, the equations give unphysical results.

If equations (4) through (7) cannot be used to estimate ^{54}Mn pile-up count rates, either because the source strength is not known or because the detector size or type is different, then the pile-up count rates should be measured directly. One of the B model tanks at the Grand Junction calibration facility has been filled with water and can be used as a low background model for such measurements.

Having determined the ^{54}Mn pile-up count rates appropriate for a given probe, the next step in this correction procedure is to subtract K and U window rates from both the calibration model data and from each point of the unstripped digital KUT log. Now one may proceed with the normal log reduction procedure.

SUMMARY

Measurements have shown that the pile-up of ^{54}Mn stabilization pulses is the only significant source of background for KUT logging probes both during calibration and during field logging. The pulse pile-up count rates in the K, U, and Th windows were measured for a range of ^{54}Mn source strengths appropriate to the 1-inch x 6-inch filtered and the 1.5-inch x 12-inch unfiltered detectors used in Bendix KUT probes. The pile-up count rates are significant only for the K and U windows. Analytical expressions were fit to these data that give the K and U window pile-up count rates as a function of source strength.

A procedure is presented that corrects KUT calibration data and field logs for this instrumental background. The background correction does not significantly alter results of the KUT calibration but it is an important correction when performing lithology-type field logs with the 1.5-inch x 12-inch detector where uranium concentrations are in the few ppm range. For example, for a nominal 0.7 microcurie ^{54}Mn source strength, the pile-up count rates are about 4.5 counts/second and 1.3 counts/second in the K and U windows, respectively. This corresponds to 0.8 percent potassium and 1.9 ppm equivalent uranium. For the nominal 4 microcurie source strength used with the filtered 1-inch x 6-inch detector, the pile-up count rates are about 8 counts/second and 1.7 counts/second in the K and U windows, respectively. This corresponds to 12 percent potassium and 24 ppm equivalent uranium. The large grade equivalents for the small crystal point to the limited value of this detector for lithology logging. It is intended for use only when uranium or thorium grades are high and it will not provide good potassium results in any situation.

Technical Note 3

BOREHOLE WATER FACTOR CORRECTIONS

INTRODUCTION

Water factor corrections to gamma-ray logging data are designed to correct probe response for the varying gamma-ray signal attenuation resulting from changes in the water-filled borehole diameter. These corrections are crudely applied to total gamma-ray logging data by introducing a single factor for a given probe and borehole, based on the size of the bit used to drill the hole. Such a correction obviously cannot account for localized borehole diameter variations, viz, washout zones. For spectral gamma-ray (KUT) logging, the borehole water attenuation problem is much more complicated. As of 1978 no correction was made to KUT field logs because the existing water factor data are considered inadequate. Since BFEC KUT probes are calibrated under dry borehole conditions in the Grand Junction models, field logs in water-filled holes will yield results that are systematically low. The corresponding error in the KUT assay for a 2.0-inch diameter probe and a 4.5-inch, water-filled borehole is between 15 and 25 percent and rises to as much as 100 percent for a 9-inch-diameter, water-filled borehole.

There have been attempts to obtain KUT water factor correction curves utilizing the "old" total gamma water factor model. There are difficulties with the procedures employed to generate these curves and with the fact that the model is not entirely suitable for spectral gamma-ray probes.

A new procedure is recommended for obtaining K, U, and Th water factor corrections. Curves are presented, based on results from the "new" KUT water factor model.

PREVIOUS ATTEMPTS TO DETERMINE KUT WATER FACTOR CORRECTIONS

Before construction of the new KUT water factor model, measurements of K, U, and Th window intensities were obtained by Mark Mathews within the ore zone of the "old" total gamma water factor model. The ore zone for this model assays at 0.321 percent U_3O_8, but potassium and thorium values are unavailable. Mathews' results were announced in an internal BFEC memo to H. B. Evans, dated June 14, 1977. He presented curves of unstripped dry/wet window intensities versus borehole diameter. These curves were represented as correction factors and showed the greatest effect for the thorium window. One would expect just the opposite effect; that is, the gamma-ray attenuation coefficient is lowest for thorium and hence should require the smallest water factor correction. However, the curves are based on unstripped results, and since the ore zone contains high grade uranium with most probably nominal concentrations of potassium and thorium, all three energy window count-rates contain large contributions from the uranium gamma-ray signal. Under these conditions, one might expect all three curves to be roughly coincident.

The fundamental difficulty with this attempted approach to KUT water factor corrections is that the K, U, and Th window intensities are unstripped prior to forming the dry/wet correction ratio. Without stripping, the corrections are valid only for the K, U, and Th concentrations contained in the water factor model. These relative concentrations are not available for the old

37

water factor model. The corrections will be incorrect, to varying degrees, for any other combination of relative concentrations. This is especially so for the K window, which receives large contributions from the U and Th signals.

RESULTS FROM KUT WATER FACTOR MODEL

Measurements that Characterize the New Model

The new KUT water factor model was completed by BFEC personnel at about the time our efforts to improve KUT data reduction methods began in July 1978. The only data available on the new model were its design grades and physical dimensions. It was necessary then to obtain data on the actual grades of potassium, uranium, and thorium, to determine the extent of any inhomogeneities in the model, and to obtain probe response profiles with depth.

Borehole KUT Assay Within Each Hole Size

After the calibration of the 1.5-inch x 9-inch NaI(Tℓ) crystal of probe 253L in the K, U, and Th models, the probe was placed at the center of the mixed ore zone for each of the five hole sizes within the water factor model. The mixed zone is 5 feet thick and is sandwiched between 3-foot thick barren zones. The design grades for the mixed zone were 4 percent potassium, 350 ppm equilibrium uranium, and 250 ppm thorium. The measurements were performed for 1000-second counting periods with the borehole dry and the probe side-walled. Assay results are presented in Table 3-1 and plotted in Figure 3-1.

Theoretical arguments predict that probe response in a dry hole will be independent of hole size so long as the mixed ore zone always presents an effectively infinite medium to the probe. Results in Figure 3-1 seem to be independent of hole size for potassium and uranium within the measurement precisions, while there is a systematic decrease in the thorium assay amounting to about 1 percent from the 3-inch to the 12-inch hole size. The decrease is attributed to the fact that for the thorium signal the model no longer has the appearance of an infinite medium in the axial direction (the ore zone thickness to hole diameter ratio has dropped to 60/12 = 5.0). The probe now "sees" the upper and lower barren zones to some degree. The assays reported here are based on equivalent dry grades of the calibration models and hence represent <u>dry</u> bulk grades for the KUT water factor model ore zone. These results are systematically above the design grades, especially for potassium, where the assays are about 25 percent high. Part of the difference with potassium may be due to large absolute uncertainties in stripping ratios caused by the assay errors for the U and Th calibration models.

Depth Profiles

Measurements were performed at 1-foot intervals through the mixed zone and into both barren zones of the new water factor model. The resulting profile shapes were acquired for the 4.5-inch and 12.0-inch boreholes. Profiles which were similar, but only about the mixed zone center, were acquired for the remaining borehole sizes. The intent was to determine homogeneity of the model and to identify effects of the finite model thickness on profiles, especially for the largest hole sizes. Figures 3-2 through 3-4 show the depth
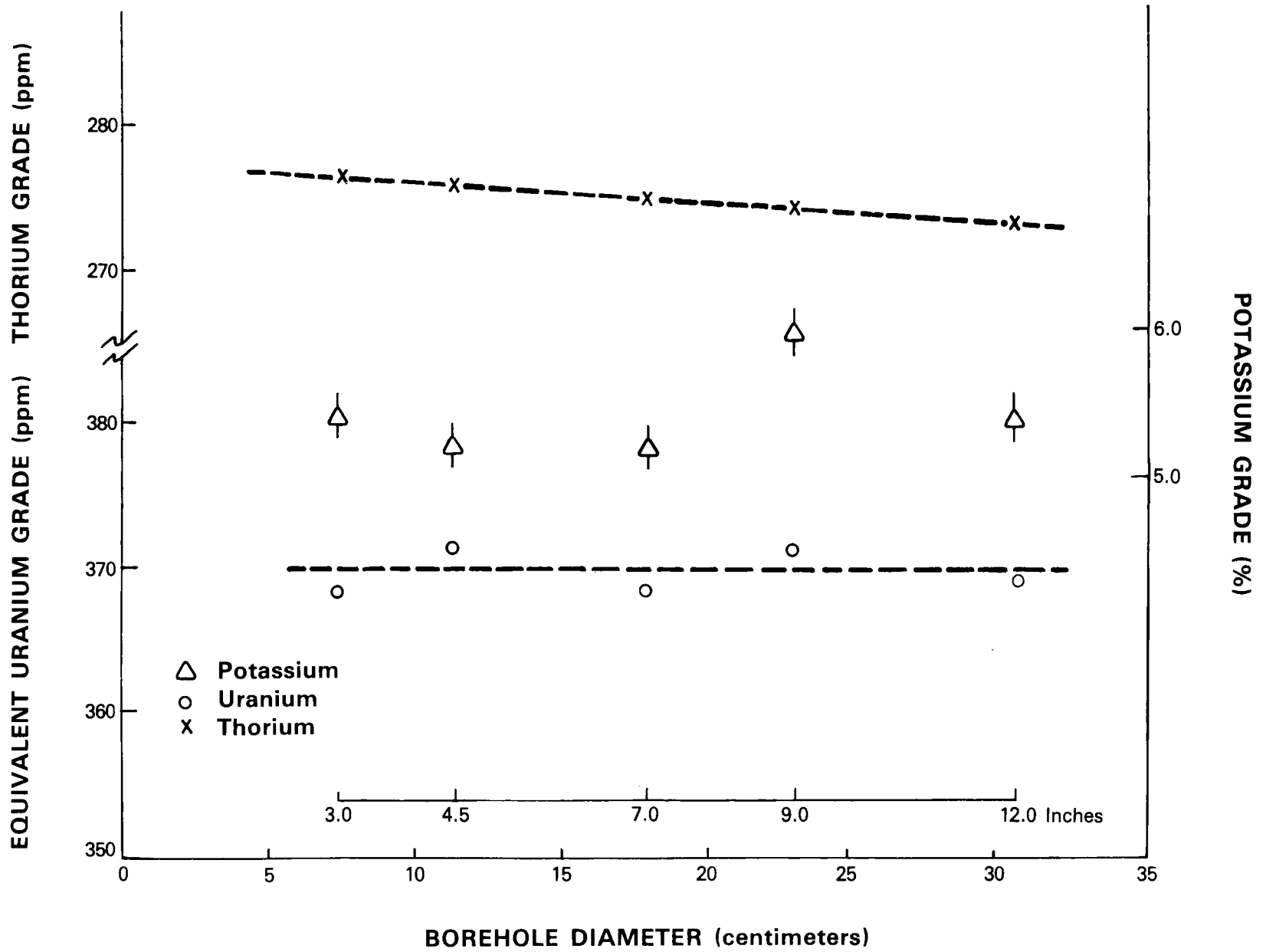
Figure 3-1. KUT concentrations for borehole assay of dry water factor model.
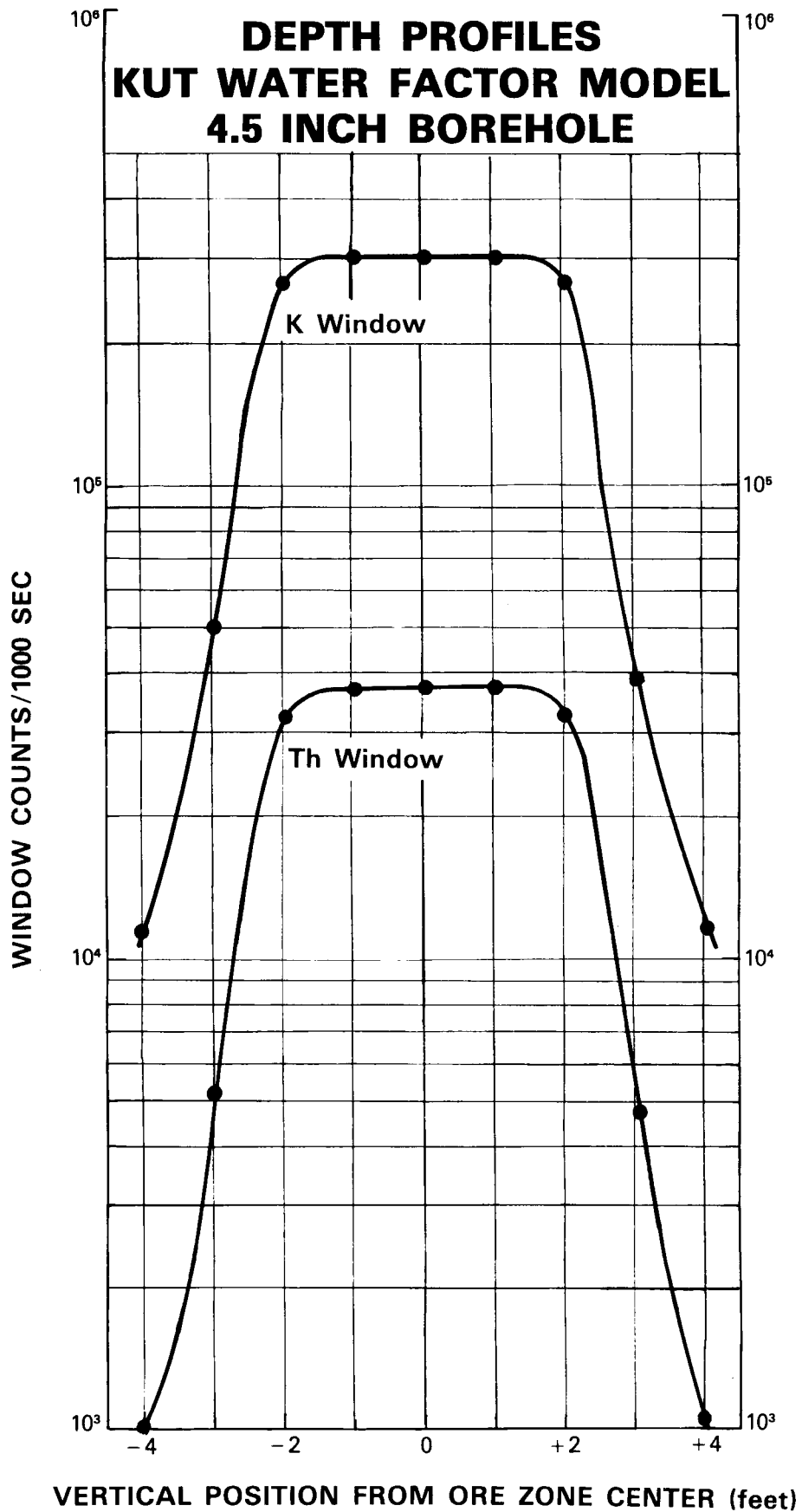
Figure 3-2.   Depth profiles for the 4.5-inch borehole
of the KUT water factor model.
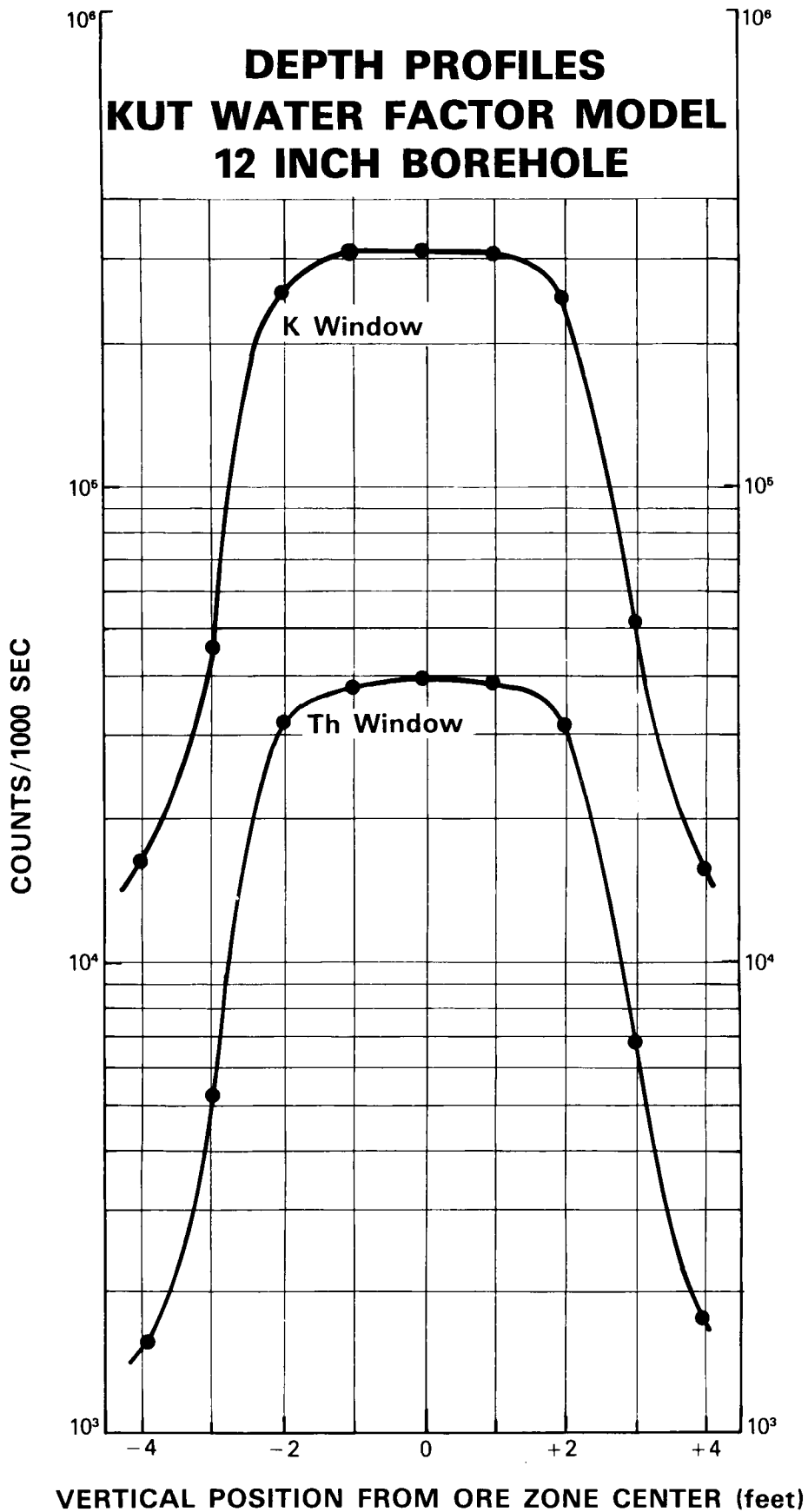
Figure 3-3. Depth profiles for the 12-inch borehole
of the KUT water factor model.

41

Table 3-1. KUT Concentrations for Borehole Assay
of Dry Water Factor Model

Borehole Diameter (inches)	Concentration		
	% K	ppm U	ppm Th
3.0	5.4 ± 0.2	368 ± 1	276 ± 2
4.5	5.2 ± 0.2	371 ± 1	276 ± 2
7.0	5.2 ± 0.2	368 ± 1	275 ± 2
9.0	5.9 ± 0.2	371 ± 1	274 ± 2
12.0	5.0 ± 0.2	369 ± 1	273 ± 2

Note: ± values represent one standard deviation uncertainties
due to water factor data counting statistics. They do not
include uncertainties in the calibration matrix.

profiles. At the 4.5-inch hole size (Figure 3-2) uniformity over the 2-foot
interval about the mixed zone center is excellent for both potassium and
thorium window response. The very slight rounding of the 4.5-inch profile is
quantified in Figure 3-4 as a less than 1 percent effect for both potassium
and thorium windows. Figure 3-3 indicates a significant rounding of the
12.0-inch profile, especially for the thorium window. Uniformity still
appears excellent, although one must remember that the detector used for these
studies was 9 inches in length. Figure 3-4 shows that the rounding of the
12.0-inch profile is approximately a 4 percent effect for the thorium window
and 3 percent for the potassium window for the 2-foot interval.

Probe Response as a Function of Time After Borehole Water Removal

Since water factor correction measurements require wet and dry data for each
borehole size, it was felt necessary to search for any time dependence of the
probe signal after water removal. Such a dependence might be possible in the
short term due to gradual drainage of water from the concrete surrounding the
dry borehole or in the long term due to the change in relative radon emanation
from the concrete.

Probe 253L was placed in the 4.5-inch borehole at the mixed zone center of the
KUT water factor model. The borehole had been previously filled with water
and remained filled for approximately 24 hours prior to the beginning of these
measurements. The borehole was rapidly drained, and consecutive 1,000-second
uranium window counts were begun and continued for about 6 hours. Results are
plotted in Figure 3-5. A very slight time dependence appears here with an
initial drop in count rate of about 1 percent during the first 2 hours after
draining and then a gradual rise of about 1 percent during the next 4 hours.
It is quite possible that these variations are due solely to spectrometer
instabilities. Subsequent measurements showed no dependence of the uranium
window count rates on time after water was added to or removed from the
4.5-inch hole in the D model which is constructed of concrete with
approximately 600 ppm U.
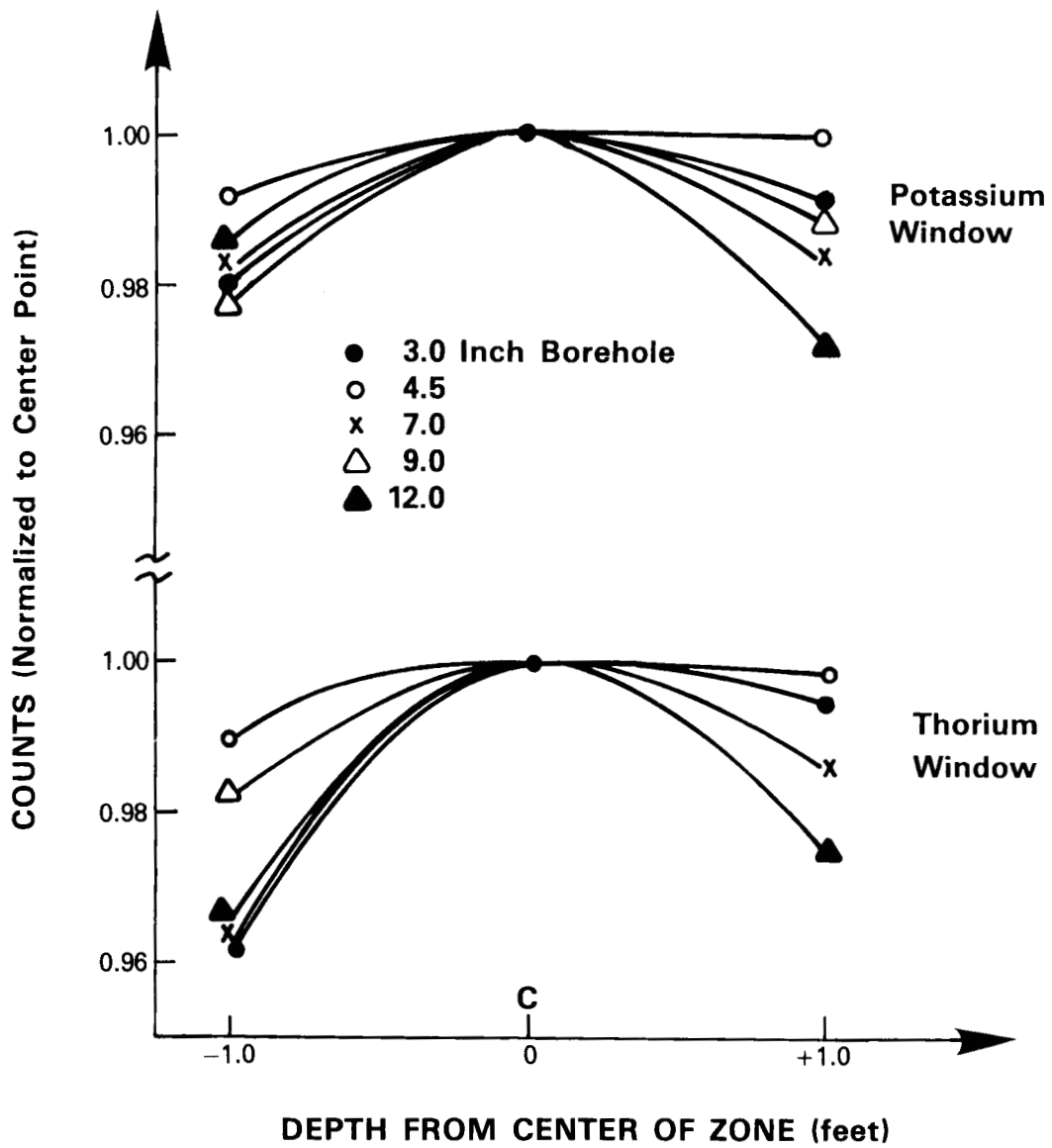
Figure 3-4.   Central zone depth profiles for the KUT
water factor model.
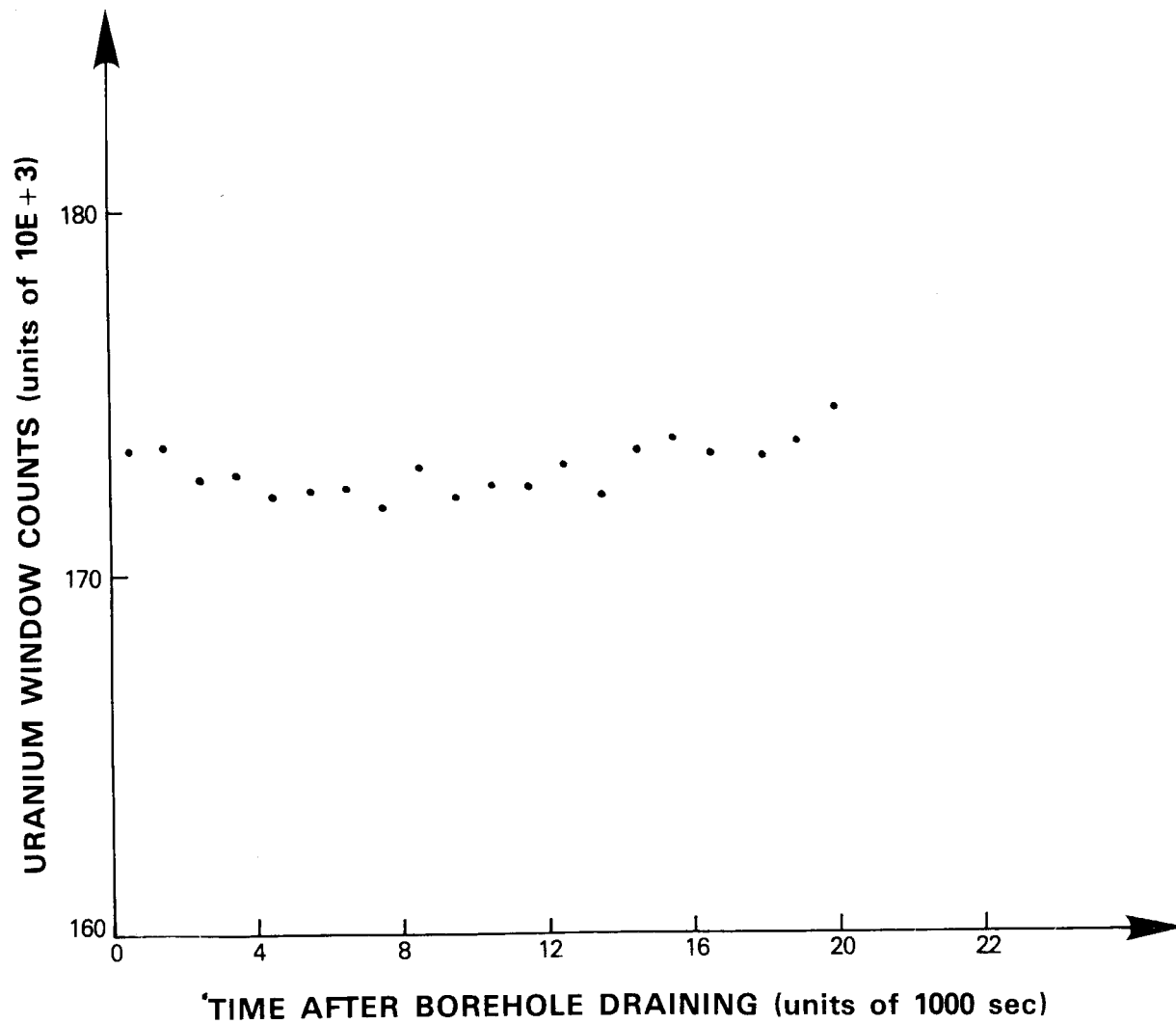
Figure 3-5. Probe response as a function of time after borehole water removal.

Probe Calibration from the K, U, and Th Models

Calibration Matrices

The 1.5-inch x 9-inch NaI(Tℓ) detector of probe 253L has been calibrated
several times over the period from July to September 1978. These calibrations
are for both a wet and dry 4.5-inch-diameter borehole. The calibration of
August 22, 1978 was used in the analysis of the water factor model
measurements. Matrix elements for the A and A^{-1} matrices are given in Table
3-2. The values contained in Table 3-2 agree, within stated uncertainties,
with the calibration performed earlier for the same probe.

Comparison of Stripping Ratios

It is important, in correcting borehole KUT measurements for the presence of
borehole water, to determine whether, and by how much, the window stripping
ratios change with borehole water content. The elements of the A matrix
contained in Table 3-2 permit the calculation of the principal stripping
ratios. Table 3-3 contains the calculated stripping ratios α, β, γ, and A for
the wet and dry borehole and the ratio of wet/dry values. The observed trends
are consistent with the increase in Compton scattering attenuation experienced
by the formation gamma rays as they traverse the borehole water. The most
important stripping ratios in the calibration process are α, β, and γ. As one
would expect, $\beta(Th \rightarrow K)$ changes by the largest fraction (2 percent) for
a dry versus a wet 4.5-inch borehole with a sidewalled 2-inch-diameter probe.
The effect is bound to be larger for larger hole diameters, but the sidewalled
geometry is complicated, and it is not easy to predict how α, β, and γ will
continue to increase with larger, water-filled boreholes. The effect cannot
yet be measured for other hole sizes because the water factor model contains a
mixture of K, U, and Th. There are plans to measure A and γ using the "old"
water factor model which contains only uranium. A separate thorium water
factor model would be required to obtain α and β as a function of water-filled
hole size.

There is some evidence from recent measurements by Princeton Gamma-Tech (PGT)
in the Grand Junction calibration models that at least the $\gamma(U \rightarrow K)$
stripping ratio does not change much as one increases the water-filled hole
size from 4.5 inches to 12 inches. The measurements were performed with a high
resolution intrinsic germanium gamma-ray probe. Figure 3-6 (4 sheets) is an
example of the 4096 channel spectra obtained with the PGT system. The
spectrum was acquired by counting for 300 seconds with the probe sidewalled in
the 4.5-inch, water-filled borehole of the water factor model. The meaning of γ
is slightly different for this probe since the "U window" now is replaced by a
cleanly resolved and background subtracted 1765 keV peak intensity. A
preliminary analysis of the PGT results was performed by ratioing the number
of counts within the "K window" (less the potassium peak intensity) to the
1765 keV ^{214}Bi intensity. This ratio was insensitive to water-filled
borehole diameter to within 3 percent. Since the pulse height distributions
for a given formation source are quite different for sodium iodide and
intrinsic germanium detectors, one can only consider the preceding as indirect
evidence that the stripping ratios will not depend strongly on water-filled
borehole size.

Table 3-2. Calibration Matrices for Probe 253L for Both Wet and Dry Boreholes
of the K, U, and Th Models (August 1978)

Dry 4.5-inch Borehole

$$
A = \begin{pmatrix}
3.4 & \pm 0.2 & 0.67 & \pm 0.04 & 0.17 & \pm 0.01 \\
-0.13 & \pm 0.03 & 0.66 & \pm 0.04 & 0.39 & \pm 0.03 \\
-0.036 & \pm 0.004 & 0.018 & \pm 0.001 & 0.128 & \pm 0.008
\end{pmatrix}
$$

$$
A^{-1} = \begin{pmatrix}
0.29 & \pm 0.01 & -0.31 & \pm 0.01 & 0.54 & \pm 0.02 \\
0.01 & \pm 0.01 & 1.65 & \pm 0.06 & -5.0 & \pm 0.2 \\
0.08 & \pm 0.03 & -0.32 & \pm 0.03 & 8.7 & \pm 0.3
\end{pmatrix}
$$

Wet 4.5-inch Borehole

$$
A = \begin{pmatrix}
2.8 & \pm 0.2 & 0.56 & \pm 0.04 & 0.15 & \pm 0.01 \\
-0.18 & \pm 0.02 & 0.54 & \pm 0.03 & 0.34 & \pm 0.02 \\
-0.051 & \pm 0.003 & 0.014 & \pm 0.001 & 0.110 & \pm 0.007
\end{pmatrix}
$$

$$
A^{-1} = \begin{pmatrix}
0.35 & \pm 0.01 & -0.38 & \pm 0.01 & 0.67 & \pm 0.02 \\
0.01 & \pm 0.02 & 1.99 & \pm 0.07 & -6.1 & \pm 0.2 \\
0.16 & \pm 0.03 & -0.43 & \pm 0.04 & 10.2 & \pm 0.3
\end{pmatrix}
$$

Table 3-3. Stripping Ratios Computed from the August 1978 Calibration
Results of Table 3-2

Stripping Ratio Designation	Dry 4.5-inch Borehole	Wet 4.5-inch Borehole	Wet/Dry Ratio
α (Th$\rightarrow$U)	3.03	3.08	1.01
β (Th$\rightarrow$K)	1.37	1.40	1.02
γ (U$\rightarrow$K)	1.02	1.03	1.01
A (U$\rightarrow$Th)	0.027	0.026	0.95

Stripping ratios defined from the A matrix elements are:

$$\alpha \equiv A_{23}/A_{33}$$

$$\beta \equiv A_{13}/A_{33}$$

$$\gamma \equiv A_{12}/A_{22}$$

$$A \equiv A_{32}/A_{22}.$$
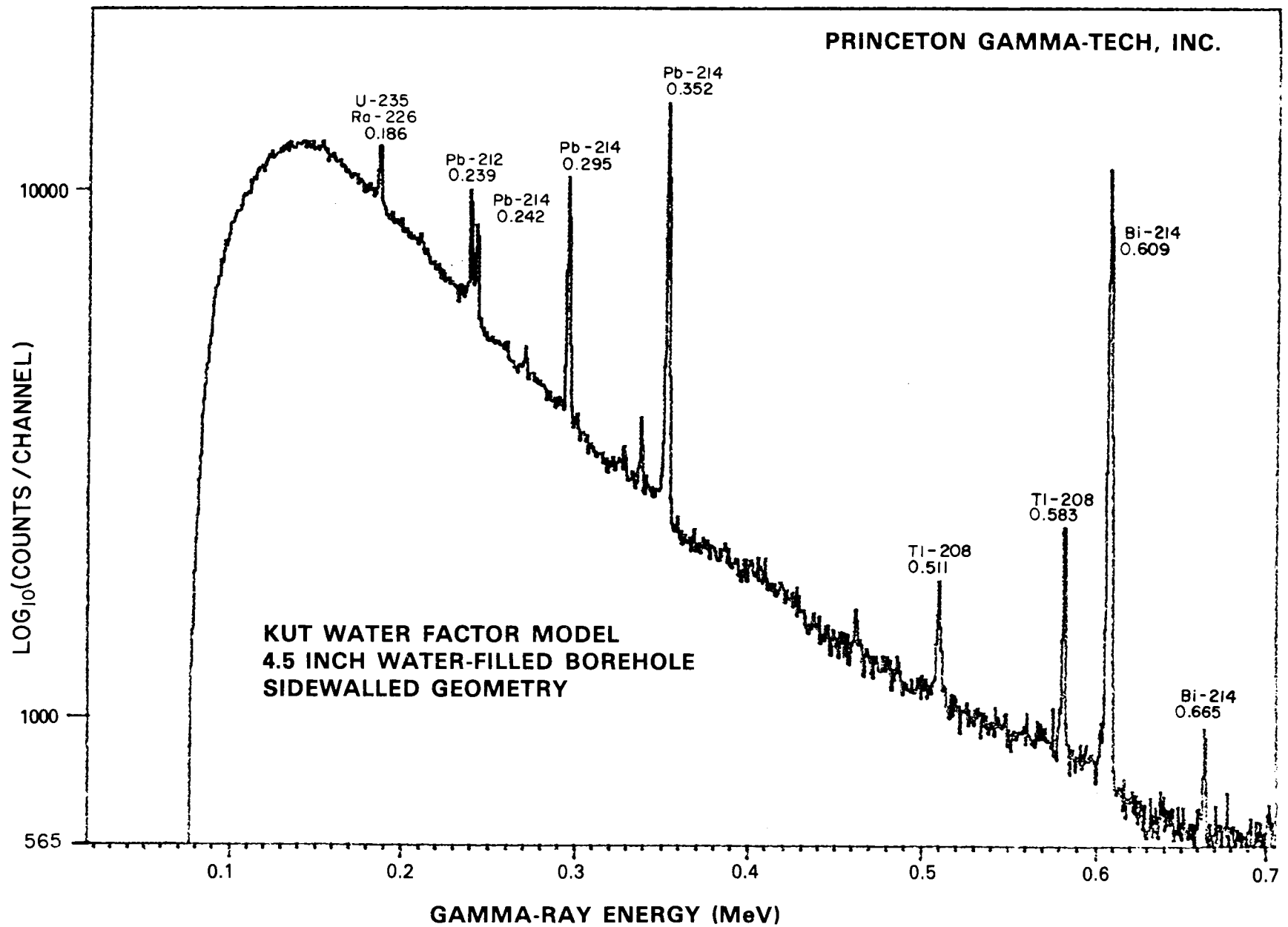
Figure 3-6. High resolution germanium spectrum for the KUT water factor model.
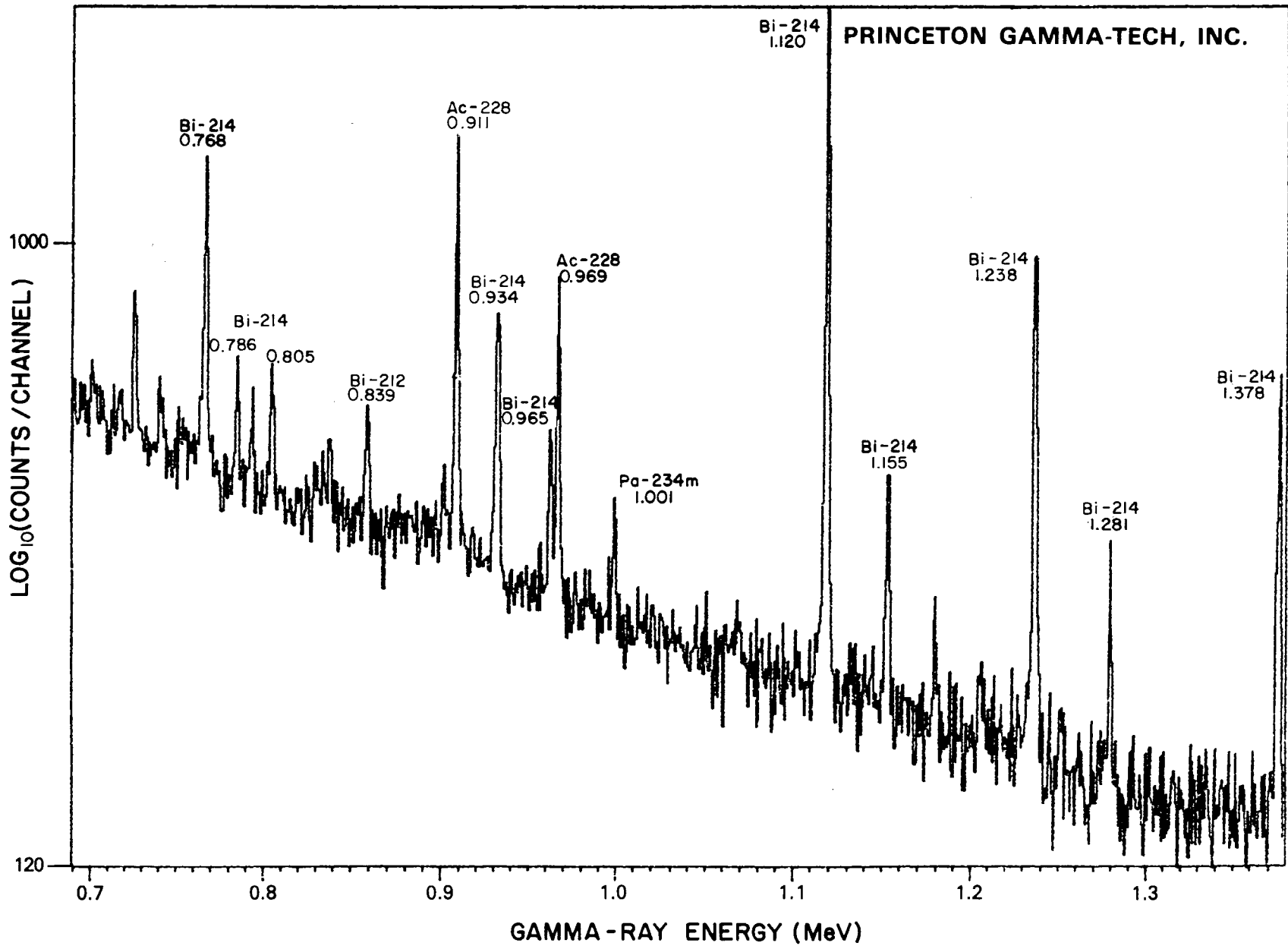
Figure 3-6. Continued
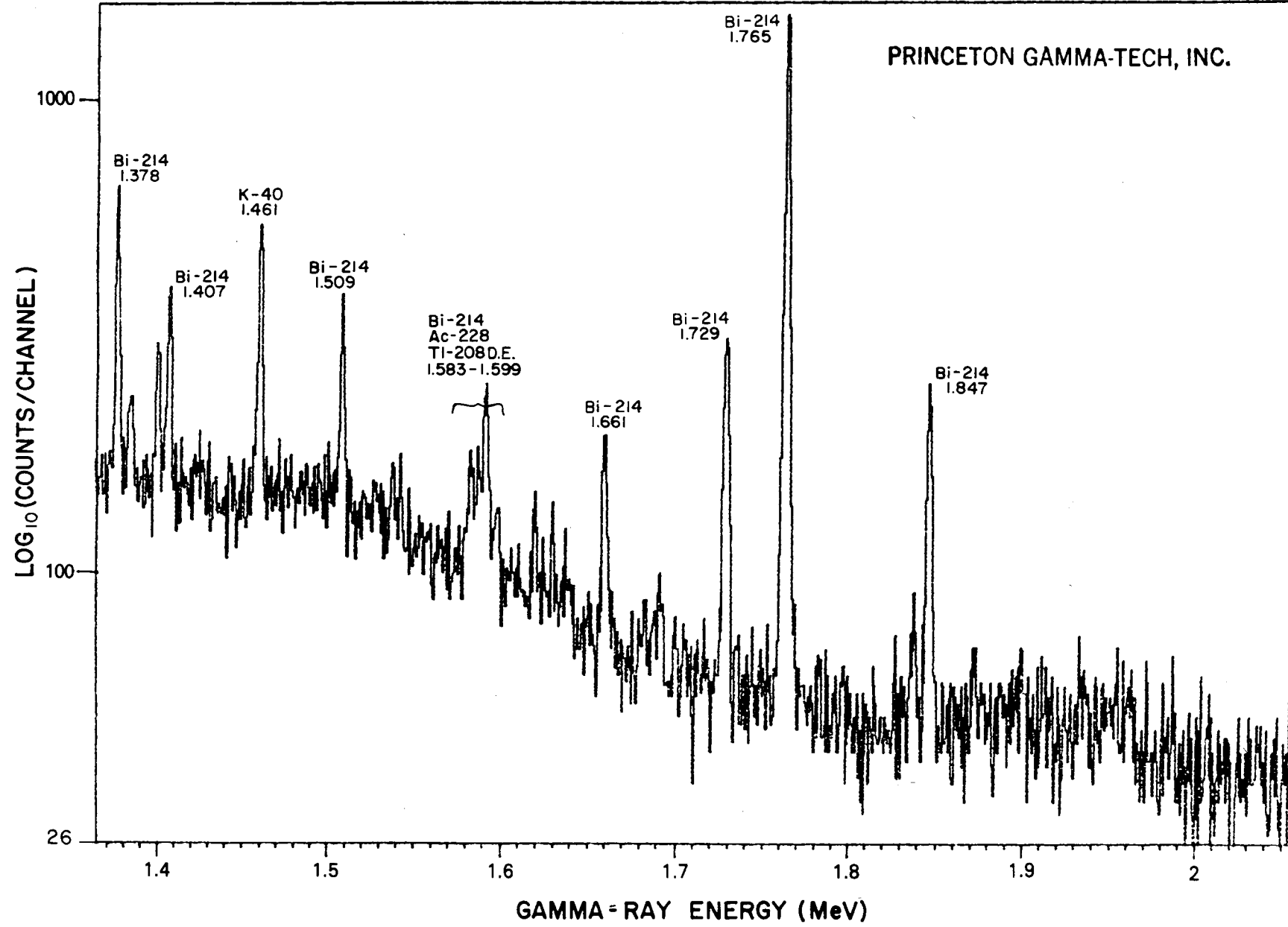
Figure 3-6. Continued
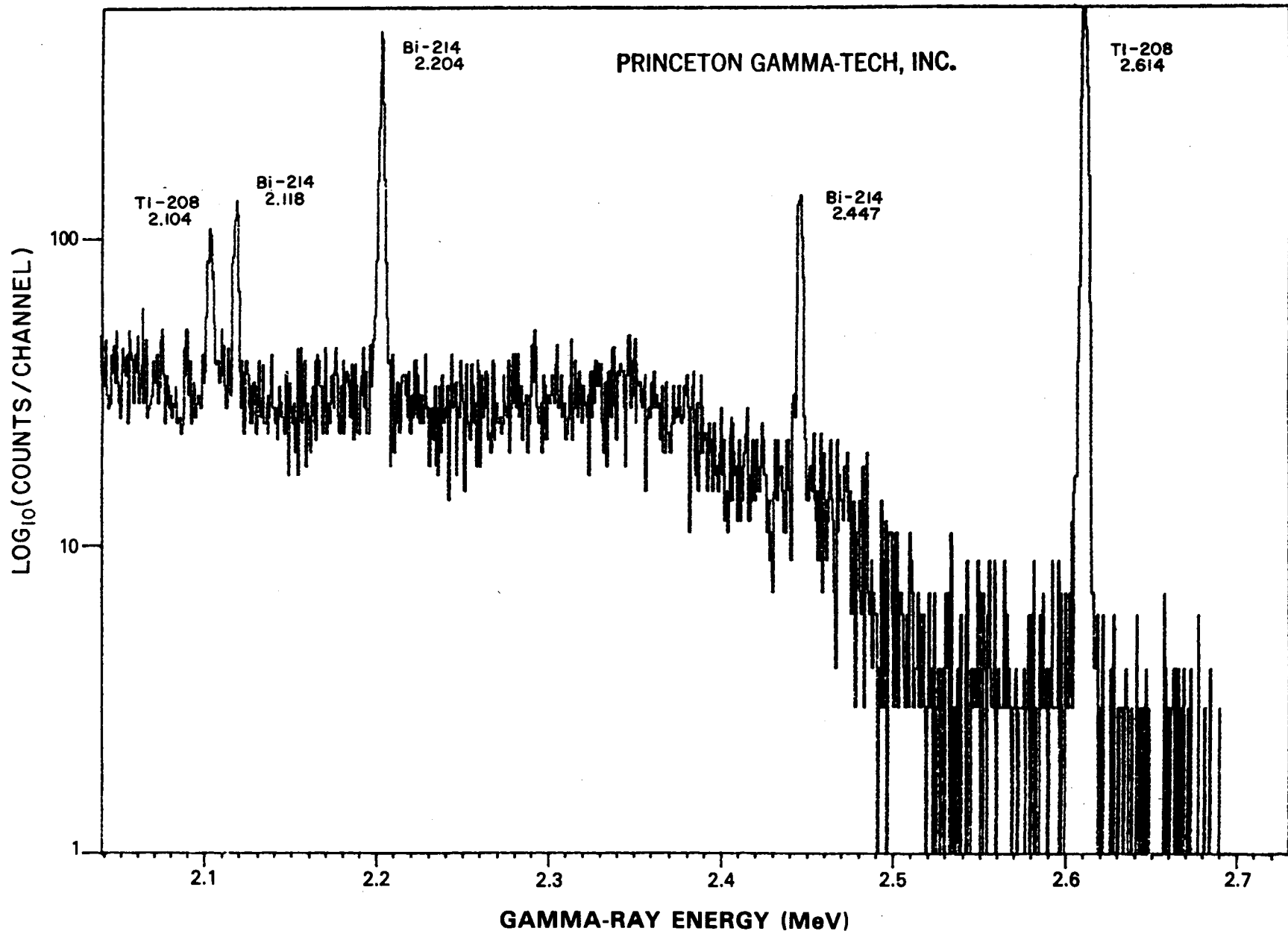
Figure 3-6. Continued

High resolution gamma-ray transport calculations have been performed for the borehole geometry at the Los Alamos Scientific Laboratory. (See Technical Note 9 for a discussion of these calculations.) Results for a centralized probe within a water-filled borehole indicated that the "K window" to 1765 keV gamma-ray flux ratio incident on the detector surface increases by about 7 percent when the 4.5-inch borehole is filled with water. As the water-filled borehole diameter increases to 9 inches, the ratio increases by another 6 percent. These calculations do not include the effect of detector response and hence overestimate the changes in stripping ratio with water-filled hole size.

In the absence of direct measurements of α, β, and γ with varying hole size and considering the indirect evidence from the work of PGT and LASL, it will be assumed for now that the stripping ratios for water-filled boreholes do not change from those for the nominal 4.5-inch case, as given in Table 3-3.

KUT Water Factor For Unstripped Results

Probe 253L with its 1.5-inch by 9-inch NaI(Tℓ) detector was sidewalled at the center of the mixed zone for each hole size of the new KUT water factor model. Spectra for counting periods of 1,000 seconds were acquired for both dry and water-filled boreholes. The K, U, and Th window counts were simply ratioed, dry/wet, for each hole size and the results plotted in Figure 3-7. The results for the three unstripped energy windows can be described by the single solid curve shown in Figure 3-7. The fact that there is little or no difference between the three windows K, U, and Th is a reflection of the strong downscatter contribution to K from U and Th, and indicates that apparently there is little difference in the effect borehole water has on the thorium and uranium window intensities.

KUT Water Factors For Stripped Results

The curve of unstripped dry/wet window intensity ratios can be used to correct KUT data for borehole water attenution only when K, U, and Th are in the relative proportions contained in the water factor model. Since this will rarely be the case for field data, the window intensities must first be stripped before forming the dry/wet ratios for the water factor corrections. Stripping is performed using the dry 4.5-inch borehole calibration matrix A contained in Table 3-2.

A serious difficulty was encountered when the calibration matrix was applied to the KUT water factor data. Stripping corrections to the potassium window count-rates were so large that their associated uncertainties produced stripped potassium results with errors greater than 80 percent. Uranium and thorium water factor results were satisfactory. It was necessary to perform separate measurements in the upper barren zone of the water factor model, where U and Th concentrations were low, to obtain satisfactory potassium data. Dry/wet stripped K, U, and Th window ratios are tabulated in Table 3-4 and plotted in Figure 3-8.

Surprisingly, uranium and thorium seem to exhibit the same water factor correction, and a single solid curve is shown to represent these data. The correction amounts to about 15 perent at 4.5 inches and 48 percent at 12.0 inches. (N.B. Subsequent determinations of water factors have used the KUT water model for only the thorium water factors and have used the D model for

51

Table 3-4.   Water Factor Correction Ratios

for Sidewalled Probe

Borehole Diameter (inches)	Dry/Wet Stripped Window Intensity Ratios		
	*Potassium	Uranium	Thorium
3.0	1.13	1.03	1.05
4.5	1.23	1.15	1.15
7.0	1.39	1.27	1.31
9.0	1.44	1.42	1.37
12.0	1.50	1.48	1.46

Table 3-5.   Water Factor Correction Ratios

for Centralized Probe

Borehole Diameter (inches)	Dry/Wet Stripped Window Intensity Ratios		
	*Potassium	Uranium	Thorium
3.0	1.13	1.09	1.07
4.5	1.26	1.21	1.23
7.0	1.58	1.45	1.47
9.0	1.80	1.71	1.63
12.0	2.38	2.05	2.07

*Potassium results are based on measurements performed in the upper barren zone of the new KUT water factor model. Potassium results from the mixed ore zone were unsatisfactory because of uncertainties in the large stripping corrections required.
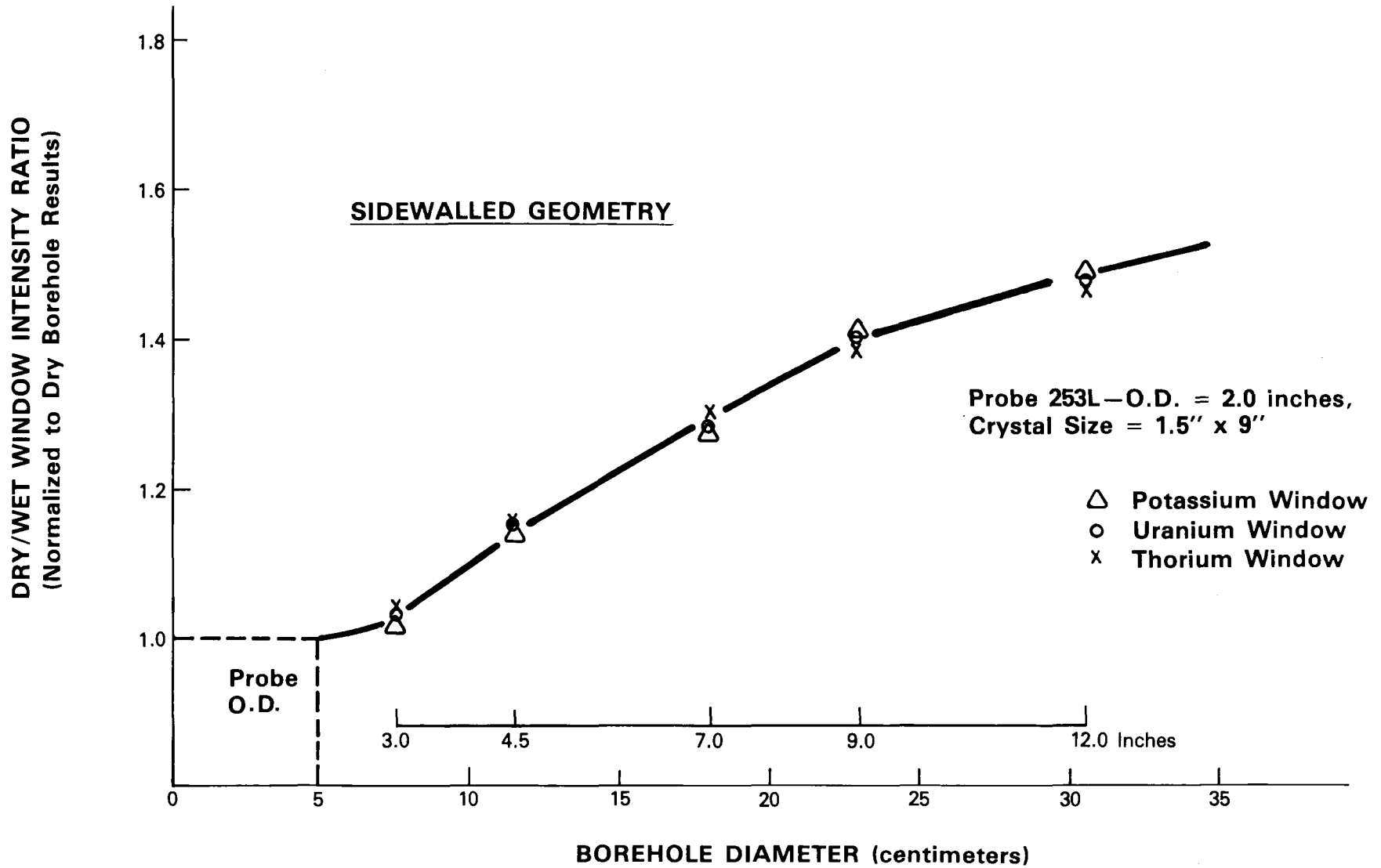
Figure 3-7. KUT water factor data of August 1978 but without spectrum stripping.
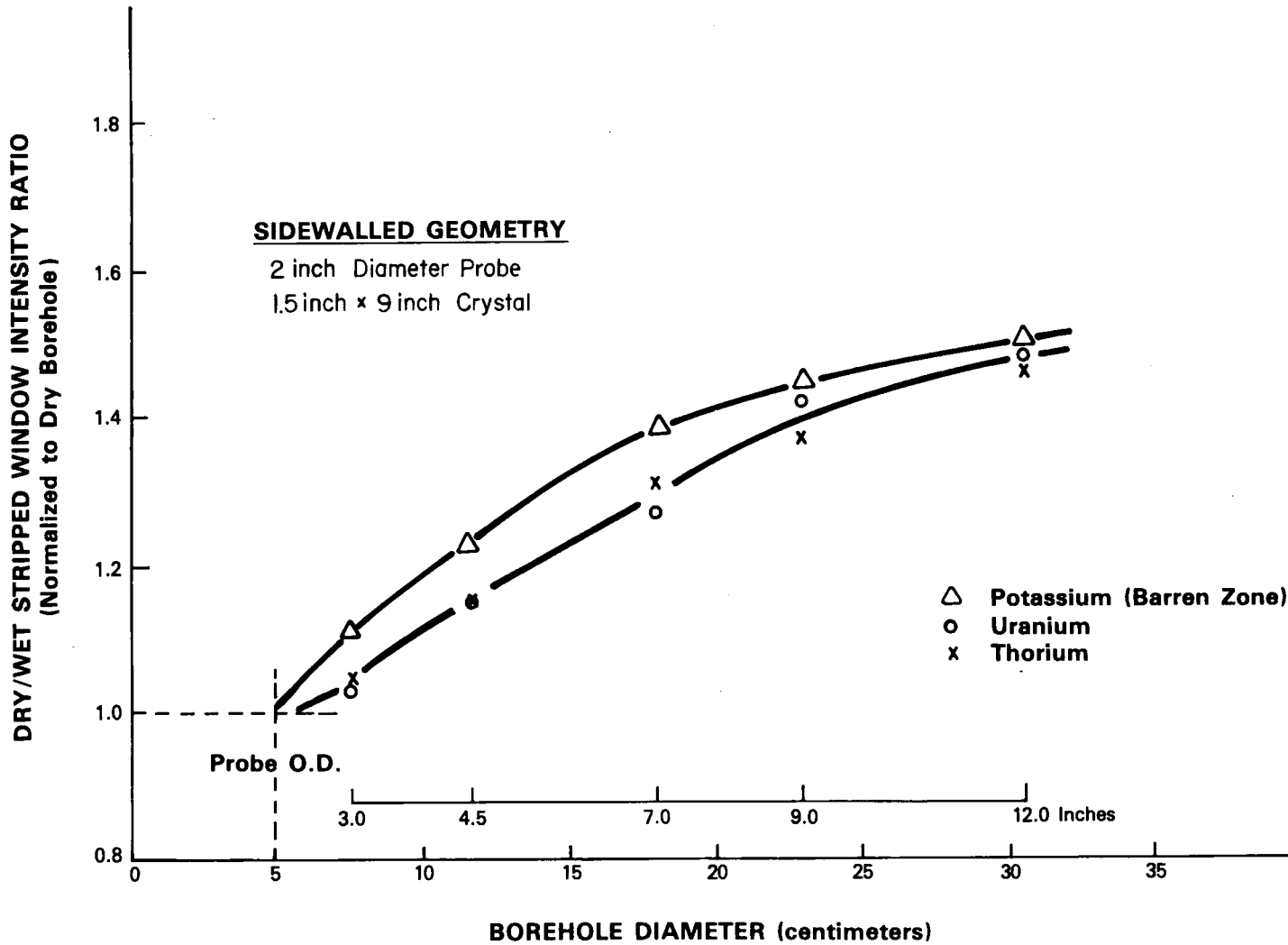
Figure 3-8. KUT water factor corrections after spectrum stripping.

the uranium water factors. This technique leads to correction counts for uranium and thorium which are distinct from each other). The water factor correction for potassium is much greater, as one would expect, ranging from 25 percent at the nominal 4.5-inch hole size to 63 percent at 12.0 inches. These correction curves represent the adjustments required to the sensitivity (diagonal) elements of the calibration matrix. Field data must first be "stripped" before applying these sensitivity corrections.

Comparison of BFEC NaI Results With Princeton Gamma-Tech IG Probe Results

The stripped water factor results presented in Figure 3-8 for BFEC probe 253L were normalized to the water-filled 3.0-inch borehole size in order to compare the NaI(Tℓ) results with the high resolution intrinsic germanium (IG) probe results of PGT. This was necessary because the PGT dry borehole data is not yet available. The renormalized NaI(Tℓ) data is plotted along with the PGT IG results in Figure 3-9. The PGT results are plotted as solid curves, one for the 1120 keV ^{214}Bi gamma ray and another for the 2614 keV ^{208}Tℓ gamma ray. Both the BFEC and PGT probes are 2 inches in diameter. The BFEC results represent correction factors for the potassium (1325-1575 keV), uranium (1650-2390 keV), and thorium (2475-2765 keV) energy windows and hence should fall between the PGT curves. This is what the comparison in Figure 9 shows, although the PGT thorium curve is considerably below the BFEC thorium result.

Comparison of Results for Sidewalled and Concentric Geometries

Measurements were also performed in the KUT water factor model for centralized probe geometry. Correction curves are presented for stripped K, U, and Th windows in Figures 3-10 and 3-11. Numerical results appear in Table 3-5. The figures also include for comparison the previous sidewalled geometry results and LASL gamma-ray transport calculations for the concentric geometry. The observed curve shapes are quite different, as one would expect from geometric considerations. For the concentric case, as borehole diameter increases, the formation signal at the probe continues to decrease due to increasing bore-hole water attenuation. The correction factor then must diverge as water-filled borehole diameter increases without limit. For the sidewalled case, however, as the borehole size increases, the geometry begins to appear to the probe more and more as a plane interface between the formation and the water. Thus, in the limit that water-filled borehole diameter becomes very large, the probe signal will asymptotically approach a constant value. The LASL calculations generally underestimate the observed concentric water factor corrections by about 5 percent except for uranium, where agreement is excellent.

Note from Figures 3-10 and 3-11 that at the nominal borehole diameter of 4.5 inches, the potassium water factor varies by only 3 percent from sidewalled to centralized probe while for uranium and thorium the variation is about 7 percent.

RECOMMENDED WATER FACTOR CORRECTION TECHNIQUE

Principle of the Technique

The difficulties with previous attempts at KUT water factor corrections are that unstripped K, U, and Th window intensities are used in forming the
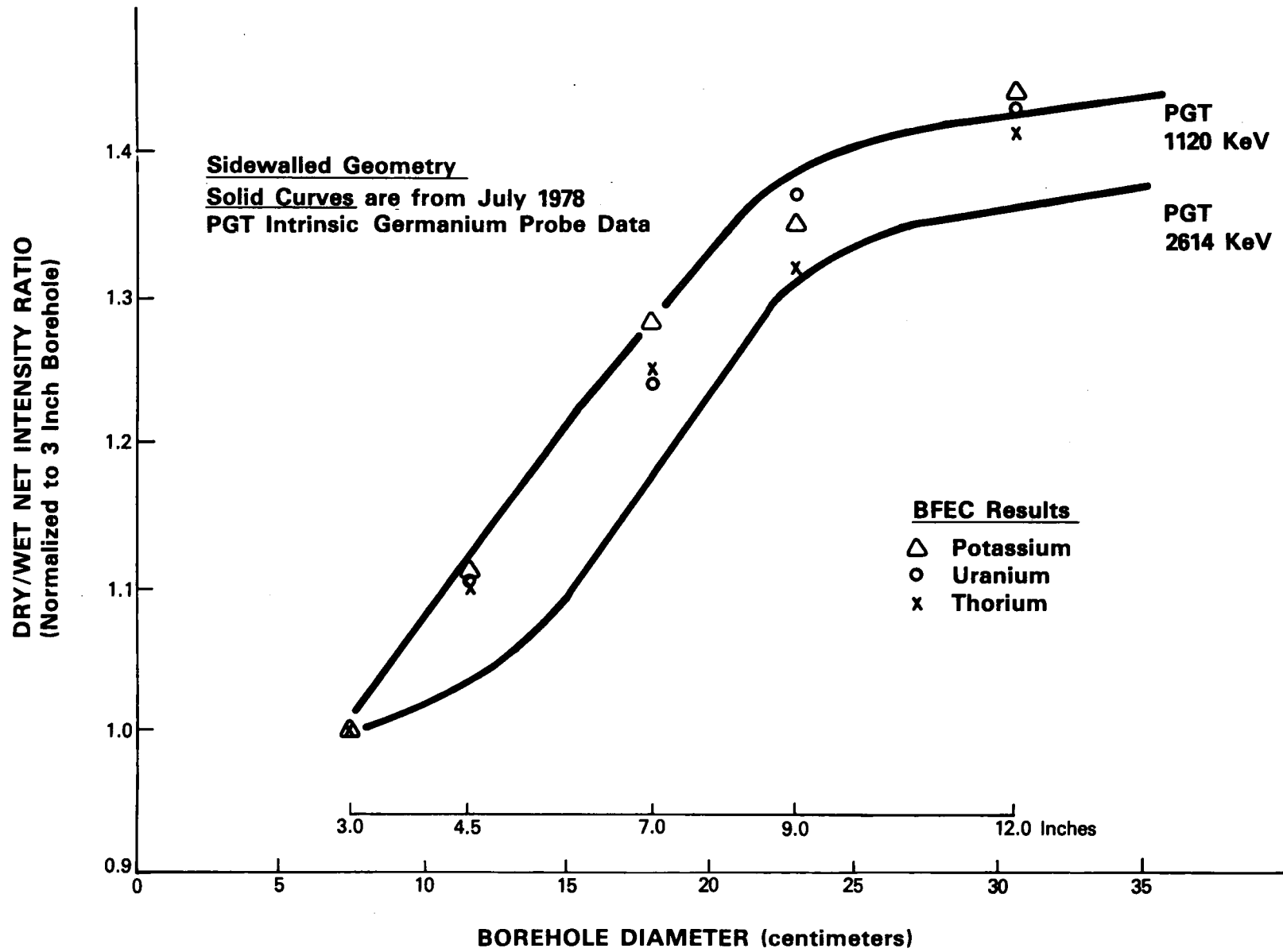
Figure 3-9.   Comparison of BFEC and PGT water factor corrections.
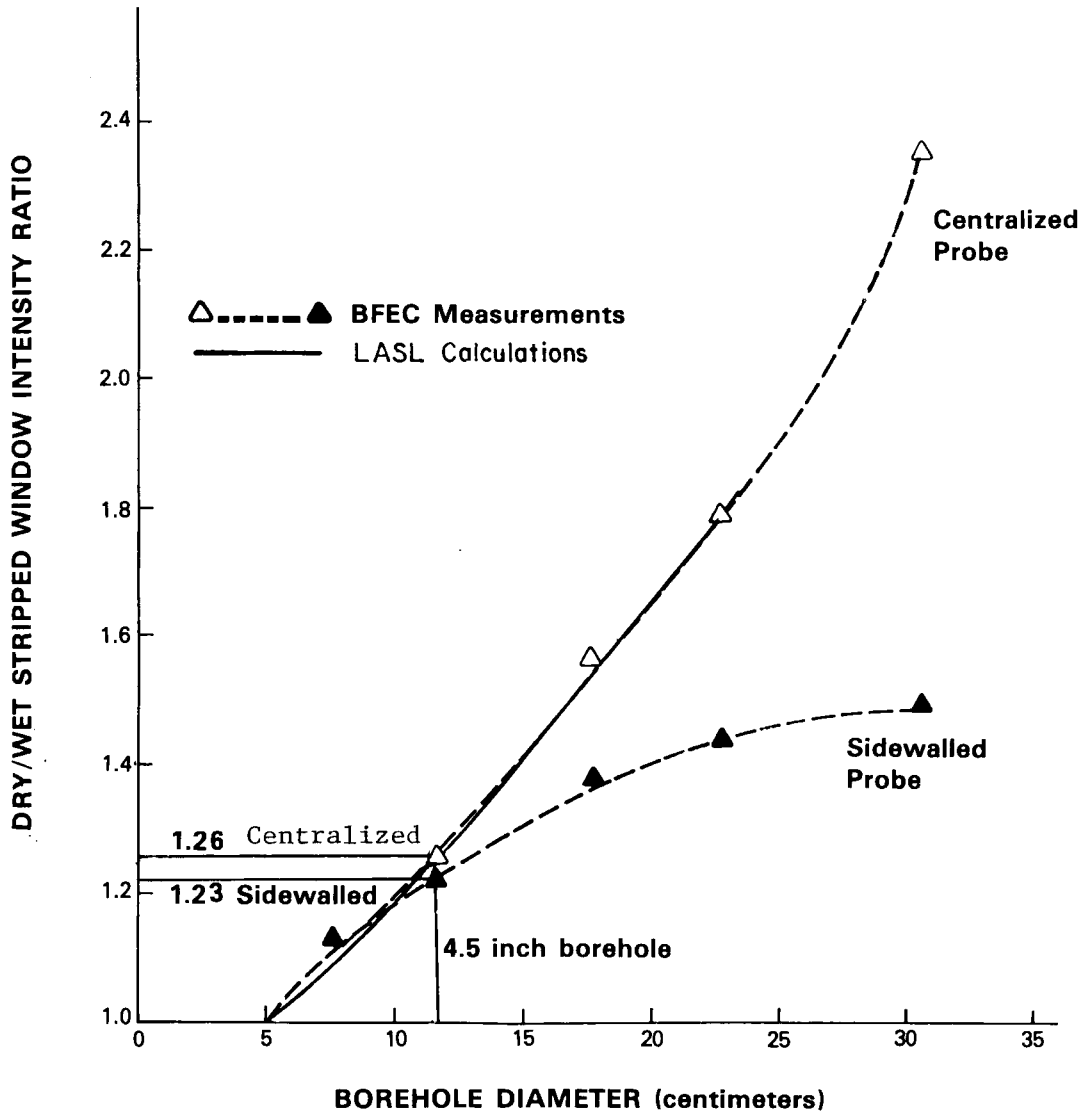
Figure 3-10. Potassium water factor correction for
sidewalled and centralized 2-inch
diameter probe.
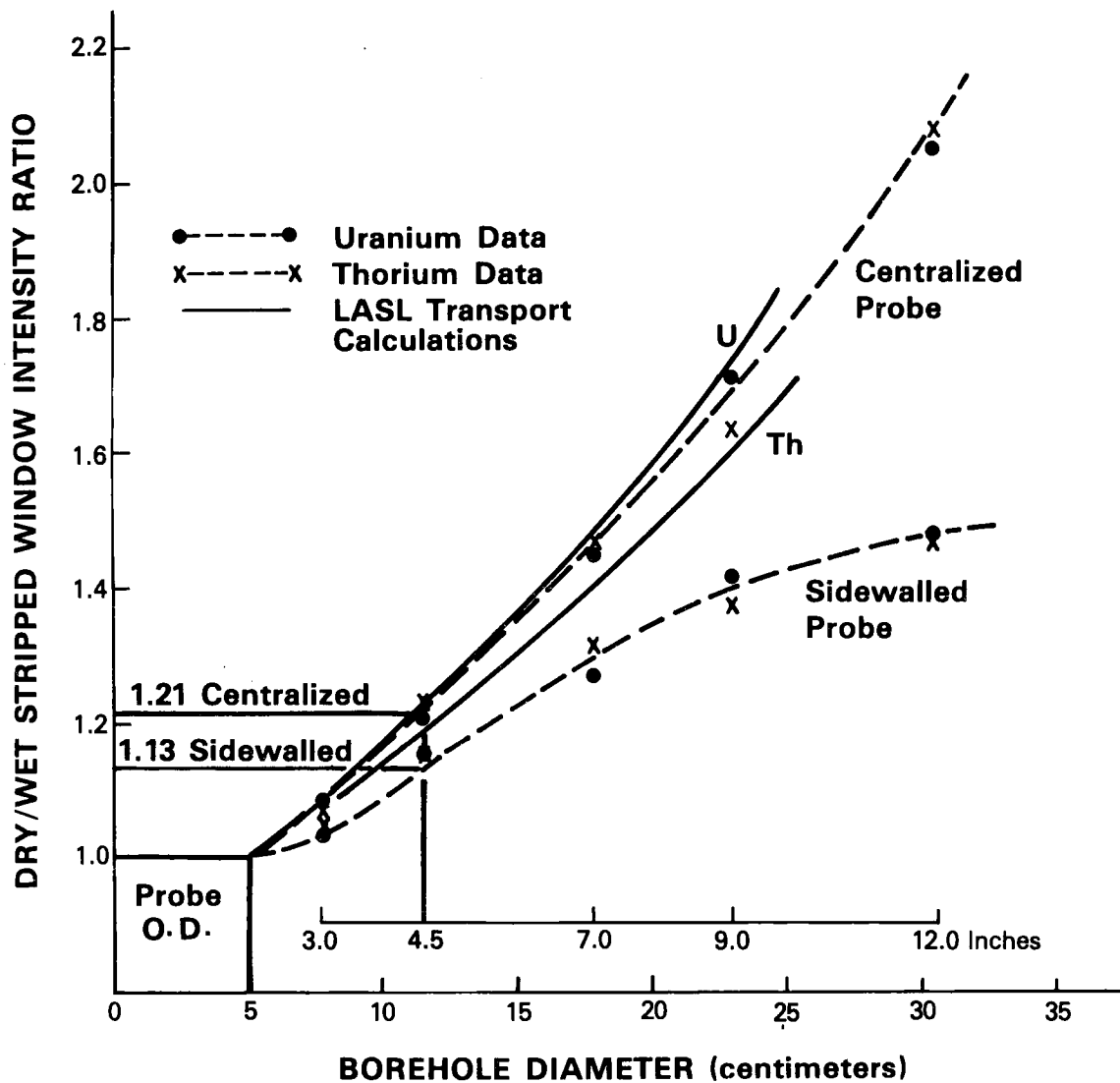
Figure 3-11. Uranium and thorium water factor correction for sidewalled and centralized 2-inch diameter probe.

dry/wet correction ratios. The correction must be based on stripped K, U, and Th window count rates from the new KUT water factor models. Such corrections can then be applied to properly stripped field data.

Since the new water factor model contains a mix of K, U, and Th (the design grades were 4 percent, 350 ppm, and 250 ppm respectively, and our borehole assay gives 5.5 percent, 370 ppm, and 275 ppm respectively), one cannot with this model measure how the window stripping ratios may vary with water-filled borehole size. One must assume that the stripping ratios are invariant with changing hole size and that the ratios obtained from logging the 4.5-inch borehole of the K, U, and Th models may be used. The results from the KUT water factor model previously presented, tend to support this assumption.

Implementation with Field Data

Dry Borehole

Present measurements within the dry borehole of the water factor model show that there is no dependence of K and U window sensitivity on borehole size (see Figure 3-1). A slight decrease in sensitivity amounting to about 1 percent from 3 to 12 inches was observed for the thorium window. It is recommended that no borehole size correction be made to dry borehole data.

Water-filled Borehole

Correction curves for stripped K, U, and Th window sensitivities are presented in Figure 3-8 for water-filled holes. Field data should be stripped using calibration results from the dry 4.5-inch boreholes of K, U, and Th models. The stripped field data will then be multiplied by the appropriate K, U, and Th water factors for the average hole size measured over each logging interval.

Future Development

There is a need for further study of the dependence of window-stripping ratios on water-filled borehole size. Future measurements and additional theoretical calculations by Los Alamos may show that at very large hole sizes a completely new calibration matrix is required. For the range of hole sizes usually encountered in the field, a single set of calibration matrix elements, as recommended here, with a set of corrections to the diagonal sensitivity elements, should prove adequate.

Technical Note 4

CASING CORRECTION FACTORS

INTRODUCTION

When boreholes are drilled in soft material, the holes are often cased to
prevent them from collapsing. Radiation data collected in boreholes subse-
quent to the addition of casing is affected by the presence of casing. The
casing absorbs some of the gamma rays and scatters others to lower energies.
It is, therefore, necessary to apply casing correction factors to data from
cased holes in order to calculate correct concentrations of radioelements in
formations. These correction factors are functions of the casing material and
its thickness. Correction factors for steel casings with thicknesses from
1/16 inch to 1/2 inch are presented below.

DATA COLLECTION

The KUT calibration models at Grand Junction were used in collecting data on
casing effects. A 2-inch diameter probe containing a 1.5-inch x 9-inch NaI
crystal was positioned with the detector in the center of each ore zone, and
various casings were inserted between the probe and the models. These casings
were steel and had the following dimensions:

> Length: 4.5 feet
> Inside Diameter: 3 inches
> Wall Thickness: 1/16-inch, 1/8-inch, 3/16-inch,
> 1/4-inch, 3/8-inch, 1/2-inch.

The counting times for data collection were increased as the casing thickness
increased in order to maintain good counting statistics. Several runs with no
casing present were interspersed with the casing runs to check the stability
of the data collection system. The counts in the potassium (K), uranium (U),
and thorium (Th) energy windows were recorded from a multichannel analyzer.
The count rates obtained for the various casing thicknesses are given in
Tables 4-1, 4-2, and 4-3 for the K, U, and Th models, respectively. The
uncertainties given in the tables are the one standard deviation limits.

ANALYSIS

Variation of Stripping Ratios with Casing Thickness

The data collected in the calibration models were analyzed to determine the
variation in stripping ratios and window sensitivities with casing thickness.
The principal stripping ratios (α, β, and γ) are tabulated in Table 4-4 and
plotted in Figure 4-1. All three ratios show a systematic rise with
increasing casing thickness. The trends can be explained in terms of the
energy differences between the K, U, and Th windows. $\gamma(U \to K)$ shows the
smallest sensitivity to casing thickness because the two windows are adjacent
and the energy difference is not large. On the other hand, $\beta(Th \to K)$ shows the
greatest sensitivity because the energy difference between the thorium and
potassium windows is over 1 MeV.

Table 4-1. Counts Per Second Obtained With Steel Casings in the
Potassium (K) Model

Casing Thickness (inches)	K Energy Window	U Energy Window	Th Energy Window
0	26.5 + 0.2	2.92 + 0.08	0.40 + 0.03
1/16	24.7 + .02	2.75 + 0.06	0.31 + 0.02
1/8	23.2 + 0.2	2.66 + 0.06	0.36 + 0.02
3/16	21.4 + 0.2	2.50 + 0.05	0.28 + 0.02
1/4	20.1 + 0.1	2.40 + 0.05	0.33 + 0.02
3/8	17.3 + 0.1	2.16 + 0.04	0.25 + 0.01
1/2	15.1 + 0.1	1.90 + 0.04	0.23 + 0.01

Table 4-2. Counts Per Second Obtained With Steel Casing in the
Uranium (U) Model

Casing Thickness (inches)	K Energy Window	U Energy Window	Th Energy Window
0	318.8 + 0.8	304.5 + 0.8	9.6 + 0.1
1/16	294.9 + 0.8	278.6 + 0.7	8.4 + 0.1
1/8	270.8 + 0.7	255.3 + 0.7	7.6 + 0.1
3/16	249.7 + 0.6	234.6 + 0.6	6.9 + 0.1
1/4	235.2 + 0.6	220.2 + 0.6	6.7 + 0.1
3/8	204.0 + 0.5	190.9 + 0.5	5.4 + 0.1
1/2	175.4 + 0.4	164.0 + 0.4	4.8 + 0.1

Table 4-3. Counts Per Second Obtained With Steel Casing in the
Thorium (Th) Model

Casing Thickness (inches)	K Energy Window	U Energy Window	Th Energy Window
0	108.0 + 0.2	199.7 + 0.2	61.2 + 0.1
1/16	105.1 + 0.5	193.8 + 0.6	59.3 + 0.3
1/8	96.8 + 0.4	176.5 + 0.6	53.9 + 0.3
3/16	91.0 + 0.4	165.3 + 0.5	49.7 + 0.3
1/4	87.3 + 0.4	158.8 + 0.5	47.8 + 0.3
3/8	78.4 + 0.3	140.9 + 0.4	41.4 + 0.2
1/2	70.1 + 0.3	126.9 + 0.4	36.5 + 0.2

Table 4-4. Stripping Ratios Obtained with Various Thicknesses of Steel Casing

Casing Thickness (inches)	α	β	γ
0	3.00 + 0.01	1.38 + 0.004	1.04 + 0.004
1/16	3.02 + 0.02	1.40 + 0.01	1.05 + 0.004
1/8	3.02 + 0.02	1.42 + 0.01	1.05 + 0.004
3/16	3.08 + 0.02	1.46 + 0.01	1.06 + 0.004
1/4	3.08 + 0.02	1.46 + 0.01	1.06 + 0.004
3/8	3.16 + 0.02	1.52 + 0.01	1.06 + 0.004
1/2	3.24 + 0.02	1.56 + 0.01	1.06 + 0.004

NOTES:

1. Uncertainties are one standard deviation.

2. Uncertainties in the concentrations of the pits are not included in the
    quoted standard deviations because they tend to obscure the variation of
    the stripping ratios.

3. Stripping ratios are for probe 253L.

63
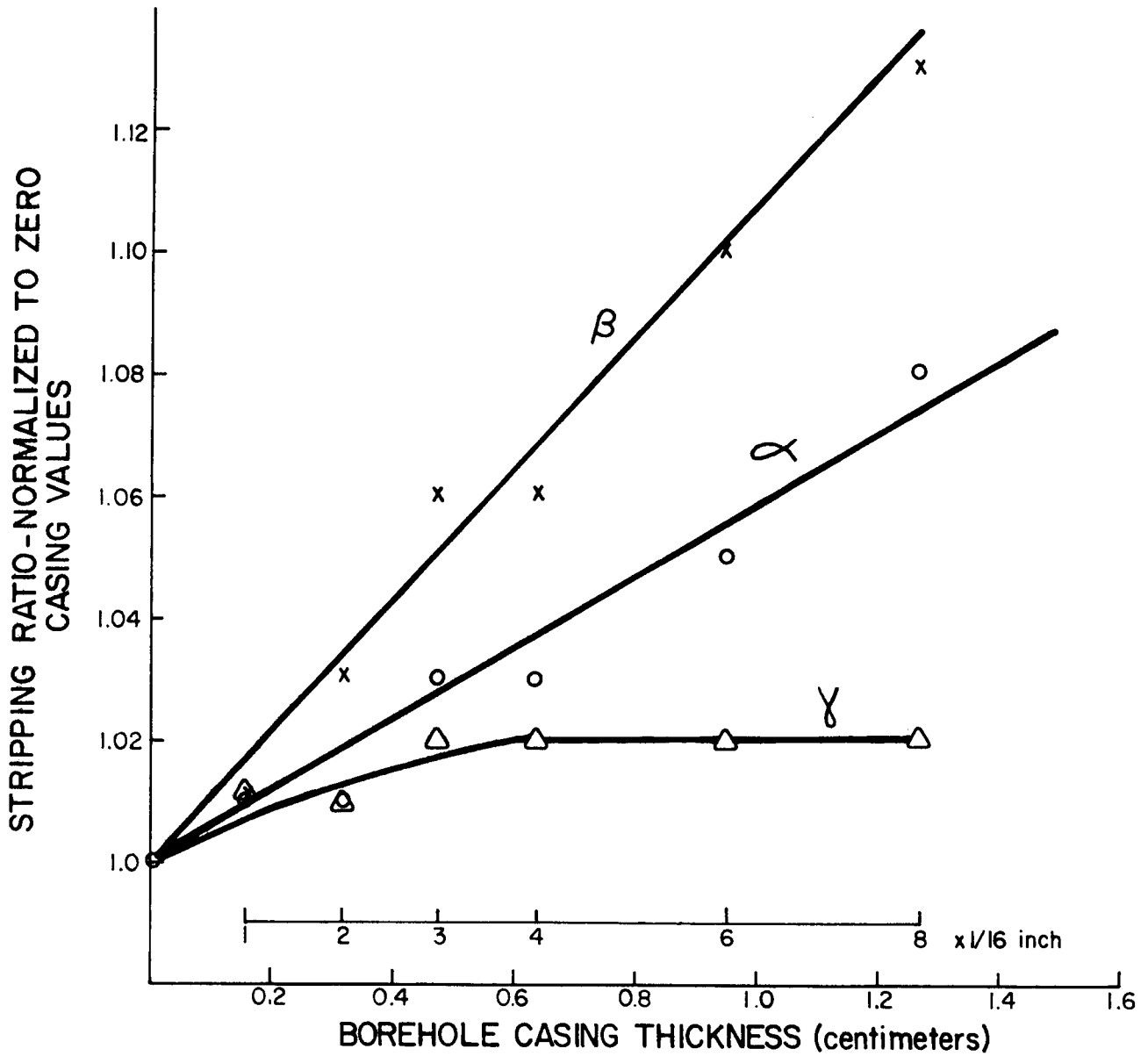
Figure 4-1. Variation of principal stripping ratios with iron casing thickness.

Experimental results in Figure 4-1 show that the γ ratio approaches a constant beyond 3/16-inch casing thickness. γ rises by only 2 percent and can be considered invariant with casing thickness. α and β rise by about 7 and 12 percent, respectively, from zero to 1/2-inch casing thickness.

Variation of Stripped Window Sensitivities with Casing Thickness

Stripped K, U, and Th window intensities, normalized to the zero casing thickness values, are tabulated in Table 4-5 and plotted in Figure 4-2. These values represent the gamma-ray transmissions of these energy windows for the casing thicknesses considered. The plots are in semilogarithmic form, and straight lines were fitted to the thorium and potassium plus uranium results. (Potassium and uranium are combined because they are done in energy and the experimental data for them overlapped.) The straight line fits yield slopes of 1.23 in^{-1} and 1.05 in^{-1}, for the thorium, and for the potassium plus uranium windows, respectively. The sensitivity for the thorium window takes its "half-value" for a steel casing 0.66 inches thick. The corresponding thickness for potassium and uranium is 0.56 inches.

Table 4-5. Stripped Window Intensity Transmission Factors for Steel Borehole Casing

Casing Thickness (inches)	K Energy Window	U Energy Window	Th Energy Window
0	1.000	1.000	1.000
1/16	.926	.914	.967
1/8	.869	.838	.875
3/16	.799	.769	.808
1/4	.743	.722	.775
3/8	.628	.625	.675
1/2	.546	.537	.592

CASING CORRECTION PROCEDURE

It is recommended that corrections be made for the presence of steel casing on both stripping ratios and on sensitivities. This is accomplished by intially performing separate probe calibrations for each casing thickness. The data from the calibrations can be used to determine how the individual elements of the A^{-1} calibration matrix vary with casing thickness. In this way correction factors are obtained for the stripping ratios and sensitivities:

$$\text{Correction factor for } A_{ij}^{-1} (t) = \frac{A_{ij}^{-1} \text{ (casing of thickness } t)}{A_{ij}^{-1} \text{ (no casing)}}$$

The correction factors thus obtained are used to modify (by multiplication) the matrix elements from subsequent calibrations of the probe obtained without casing.
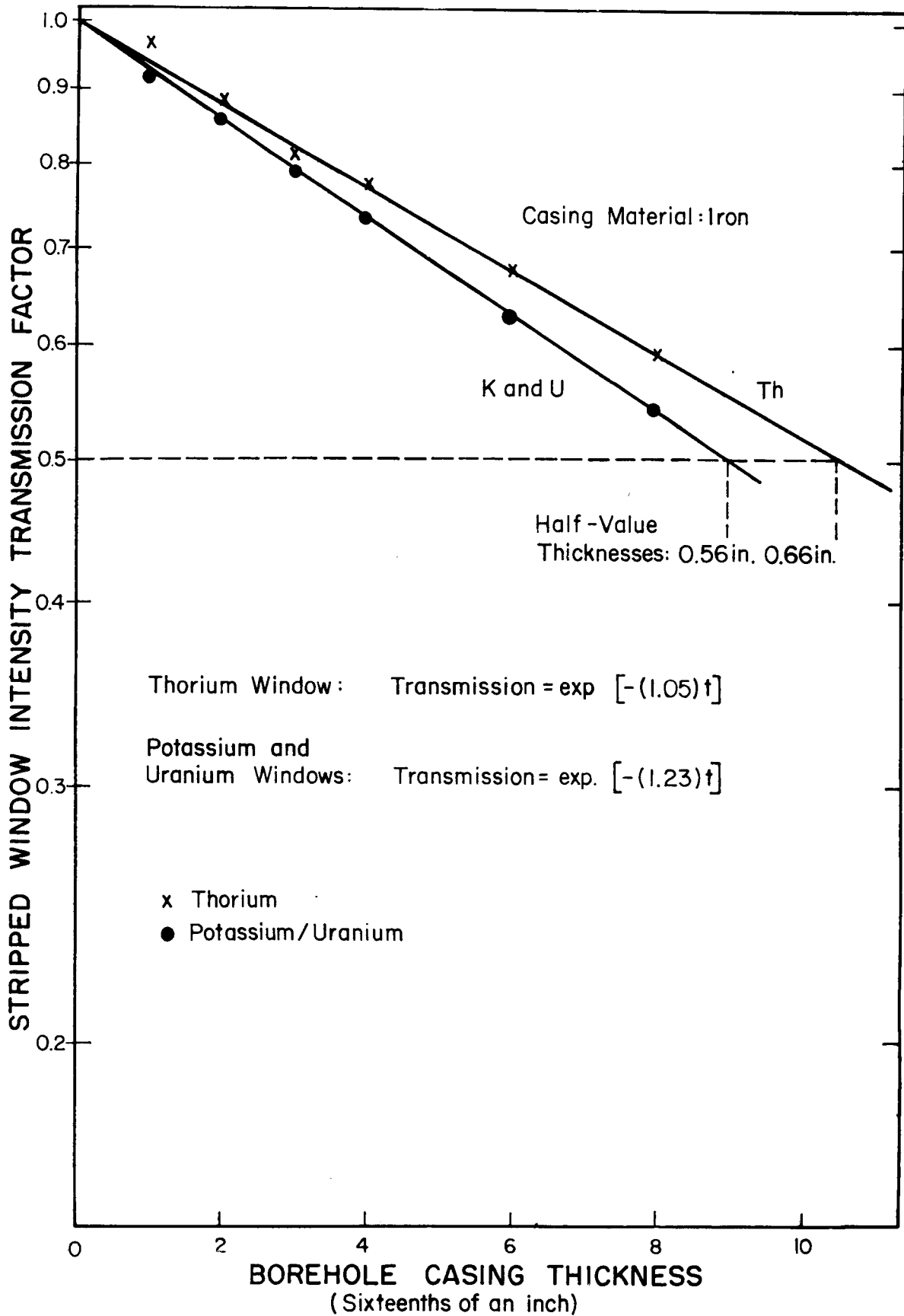
Figure 4-2.   Stripped window intensity transmission for iron
casings.

The effective attenuation coefficients determined in this work are about 40 percent above the values quoted in the literature for steel and for "good" geometry attenuation; that is, for a plane parallel beam of gamma rays incident normally to the thickness t of material. This is because the average angle of incidence for a formation gamma ray, measured from a normal to the casing surface, is something greater than zero. Hence the effective casing thickness is greater by an amount $t/\cos\bar\theta$. The exponential expression for the gamma-ray transmission can then be written:

$$\text{Transmission} = \exp[-\mu t /\cos\bar\theta],$$

where μ is the "good" geometry linear attenuation coefficient for the casing material. A simple model, based on this expression, and the average angle of incidence concept, will permit the calculation of casing correction factors for all materials. These preliminary results indicate the average angle of incidence is about 45 degrees, independent of the energy window. Measurements with additional casing materials are required to determine the usefulness of this model.

SIGNAL DECONVOLUTION

INTRODUCTION

Present KUT log analysis procedures practiced at BFEC do not include a deconvolution of the data. That is, there is no attempt to remove the effects of finite detector length and formation signal penetration from the depth profiles observed with the logging probes. Total or gross gamma-ray logs are routinely deconvolved using the technique developed by James H. Scott and contained in the computer program GAMLOG (Scott, 1962).

This technical note presents results of measurements using a 1.5-inch x 9-inch NaI(Tℓ) detector that are required as input to the GAMLOG program so that it can be used to deconvolve spectral (KUT) gamma-ray data. GAMLOG is then applied to a typical KUT log to illustrate the deconvolved output (K, U, and Th concentrations) versus depth.

ORE ZONE/BARREN ZONE INTERFACE MEASUREMENTS

K Model

The depth profile was measured from a position of about 30 cm above the ore zone center, through the ore zone/barren zone interface, and into the barren zone a distance of about 50 cm. Depth increments of 5.08 cm (2 inches) were used far from the interface while 2.54 cm (1-inch) increments were used across the interface. Counting times varied from 200 to 600 seconds for each depth point. These data were converted to K, U, and Th concentrations using a calibration matrix determined from previous measurements. Numerical values of apparent potassium grade appear in Table 5-1 and are plotted in Figure 5-1. A smooth curve was fit to these data points, shown as the solid line. The differential tool response was then obtained from the smooth curve by forming the ratio Δ (grade)$/\Delta z$, where Δz is a depth increment in centimeters. The differential curve is plotted as "x" in Figure 5-1. A smooth curve was fit to these computed values as well. It takes its maximum value at 74.5 cm, in excellent agreement with the position of the physical interface between ore and barren zones. One expects the maximum at the interface because when one differentiates a step function the result is a delta function. That is, the differential probe response should be that observed for a very thin ore zone located at the interface.

The differential, or thin bed, response exhibits a full width at half-maximum (FWHM) of 24.7 cm, and a full width at tenth-maximum (FWTM) of 47.0 cm.

U Model

Similar profile measurements were performed in the uranium model. Apparent concentrations were computed and equivalent uranium values appear in Table 5-1. Figure 5-2 is a plot of these results. The same procedure used with the K model profile was employed to derive the differential probe response for the uranium model.

Table 5-1. Ore Zone/Upper Barren Zone Depth Profile For Potassium,
Uranium and Thorium Models

Vertical Position Above Ore Zone Center (centimeters)	Apparent Grade			Differential Grade		
	%K	ppm U	ppm Th	$\frac{K(\%)}{cm}$	$\frac{U(ppm)}{cm}$	$\frac{Th(ppm)}{cm}$
30	6.82	506.0	522	0.001		1.1
32			527			
35	7.20	506	513			
40	6.78	496	512		0.8	
45	6.74	495	505	0.006		0.6
50	6.86	492	510		2.3	
52.5						1.6
55	6.63	475	502	0.02		
57.5		453			5.6	3.9
60	6.63	443	464			
62	6.51	424	471	0.078	9.0	7.3
64	6.19	406	453			
66	6.09	380	439		13.5	
68	5.73	351	412	0.138		12.2
70	5.42	330	390		14.9	
72	4.19	290	354	0.170		16.4
74	4.78	257	328		16.0	
75			292			
76	4.44	226	283			17.2
77				0.166		
78	4.12	191	248		16.3	
80	3.91	159	211			
82	3.62	132.0	184	0.140	13.4	15.3
84	3.29	106	151			
85		93.4				
86	3.00	84.2	127		10.0	
88	2.82	65.5	103	0.09		10.5
90	2.68	52.6	85.0		5.8	
92	2.54	42.3	68.4	0.046		6.6
94	2.50	34.3	51.0		3.6	
96		28.2				
98		23.7		0.028	2.2	4.2
100	2.32	18.6	30.3			
102		15.9				
104		13.5			1.4	1.7
105	2.22		23.4	0.008		
106		12.0				
110	2.20					
115	2.27			-0.002		
120	2.32					
125	2.21			-0.001		
129	2.23					

DEPTH PROFILE AND DIFFERENTIAL RESPONSE

POTASSIUM MODEL
Probe 253L
1.5-inch x 9-inch crystal

FWHM = 24.7 cm

POTASSIUM CONCENTRATION (Percent)

Δ(Concentration)/Δz in Percent/Centimeter

VERTICAL POSITION ABOVE ORE-ZONE CENTER
(centimeters)
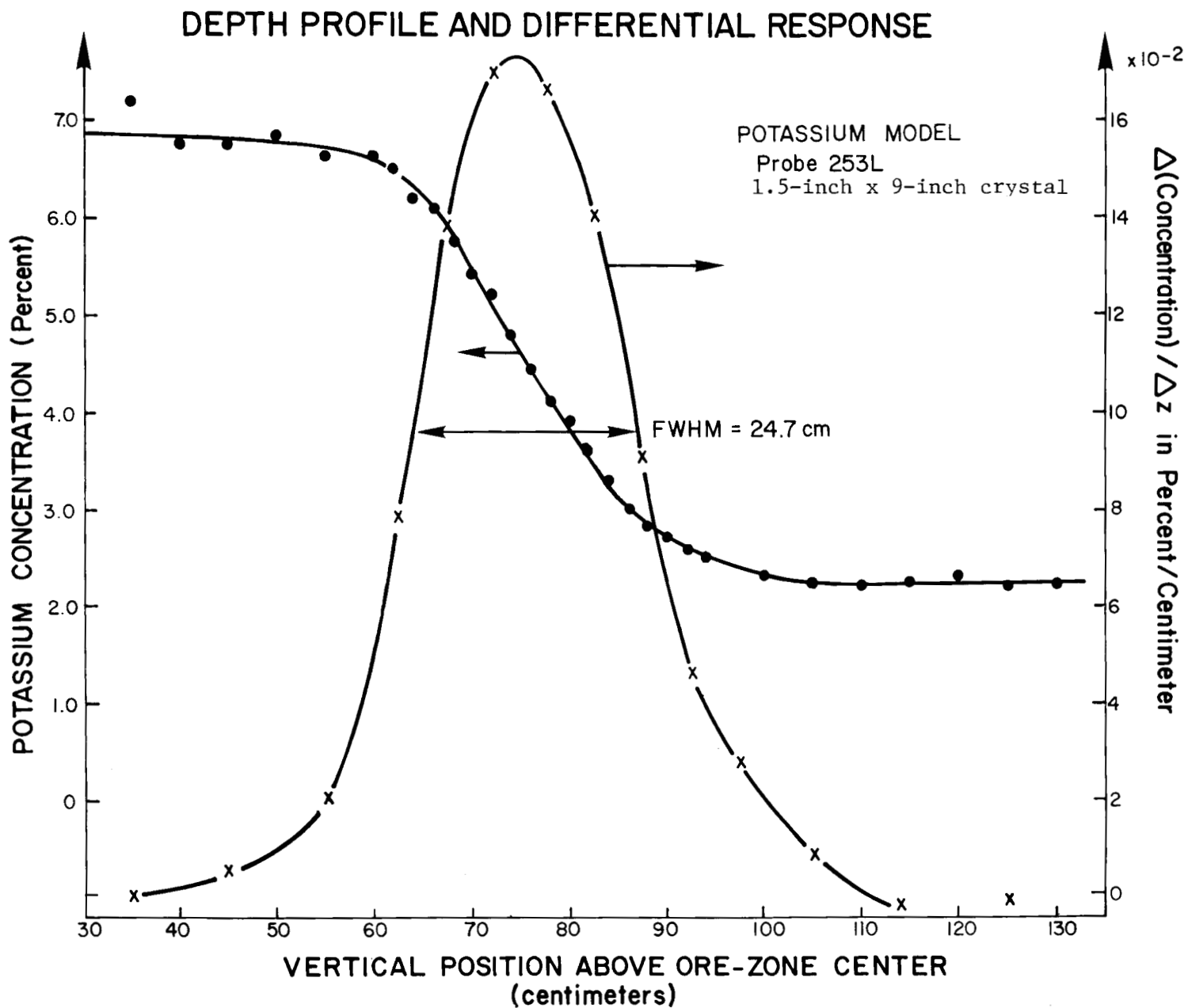
Figure 5-1. Potassium model depth profile and differential response
for 1.5-inch x 9-inch detector.
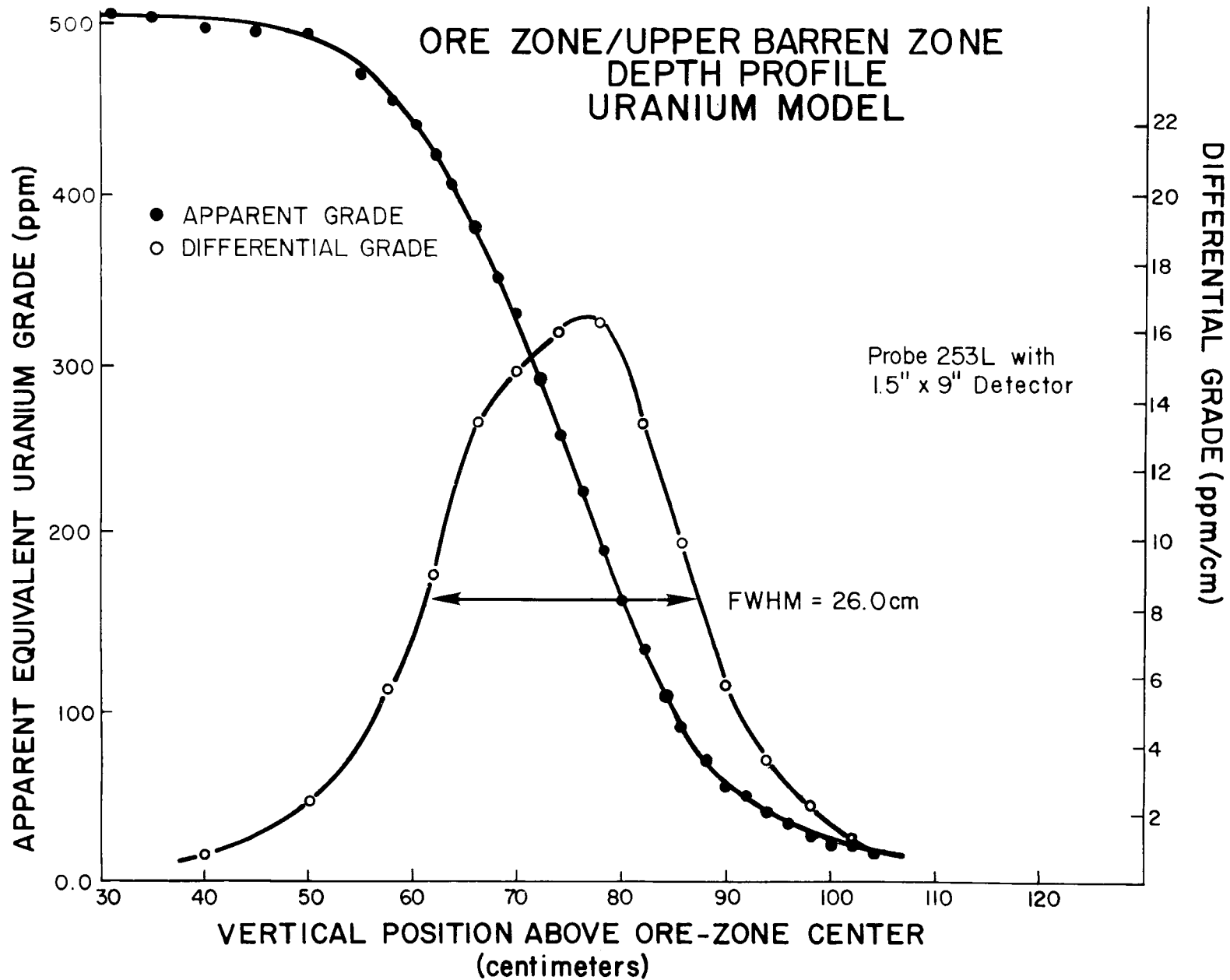
Figure 5-2.   Uranium model depth ~rofile and differential response for
              1.5-inch x 9-inch   ctor.

The differential response is clearly not symmetrical about its maximum value, as expected for a perfect step function ore-barren interface. Apparently there are inhomogeneities or imperfections in the interface between the ore zone and upper barren-zone of the uranium model. The FWHM of the differential curve is 26.0 cm and FWTM is 53.5 cm. However, these differential results cannot be considered the thin uranium bed response function for this probe.

Th Model

Profile measurements were also performed in the thorium model. Appparent thorium concentrations were computed from the previously determined calibration matrix. Numerical values are given in Table 5-1 and are plotted in Figure 5-3. The same procedure described for the potassium profiles was followed to obtain the differential response through the interface region. Differential results also appear in Table 5-1 and are plotted in Figure 5-3. The differential response curve is quite symmetrical about the maximum value with a FWHM of 25.7 cm and a FWTM of 50.0 cm.

Comparison of Differential Response Functions

The differential curves of Figures 5-1 through 5-3 were normalized to unity at the maximum, and their centroids shifted slightly so as to be roughly coincident on a single plot, Figure 5-4. Dashed and solid lines were fit to the potassium and thorium results, respectively, to emphasize the wider thin bed functions obtained for thorium. Uranium results are not accurate because of problems with the interface region of the uranium model. The skewed shape of the uranium function is obvious when compared to the potassium and thorium shapes.

THIN URANIUM BED MEASUREMENTS

Presentation of Results

In an effort to obtain thin bed probe response functions that were more accurate than those obtained by differentiating interface profiles, measurements were performed in the horizontal thin bed model. The apparent uranium grade, after application of the calibration matrix, appears in Table 5-2 for a range of positions about the bed center of ± 30 inches in 1, 2, or 3-inch increments. The uranium bed is 2 inches thick and the detector is 9 inches long. The results of Table 5-2 are plotted in Figure 5-5. The FWHM of 26 cm and FWTM of 55 cm agree well with the differential interface response measurements from the U model (see Figure 5-2), even though the curve shape observed was asymmetric. Also presented in Table 5-2 and Figure 5-5 are the observed values of the uranium-to-potassium stripping ratio (sometimes referred to as γ) as a function of position relative to the bed center. γ was computed by forming the ratio: (K window counts – contribution from known percent K) / (U window counts – contribution from known ppm Th). The trend observed in Figure 5-5 is quite interesting. γ takes its minimum value (0.97) at about the thin bed center and rises to about 1.5 for distances of ± 40 cm from the center. Also shown is the value of γ determined from the "thick bed" calibration with the K, U, and Th models ($\gamma = A_{12}/A_{22} = 1.02$). The barren zone uranium content contributes negligibly to the window count rates for axial positions less than ± 40 cm from the thin bed. For greater distances, this contribution is not negligible and the effect is to under-

ORE ZONE/UPPER BARREN ZONE DEPTH PROFILE THORIUM MODEL

Probe 253L with
1.5″ x 9″ Detector

FWHM = 25.7 cm.

APPARENT EQUIVALENT THORIUM GRADE (ppm)

GRADE DIFFERENTIAL (ppm/cm)

VERTICAL POSITION ABOVE ORE ZONE CENTER (centimeters)
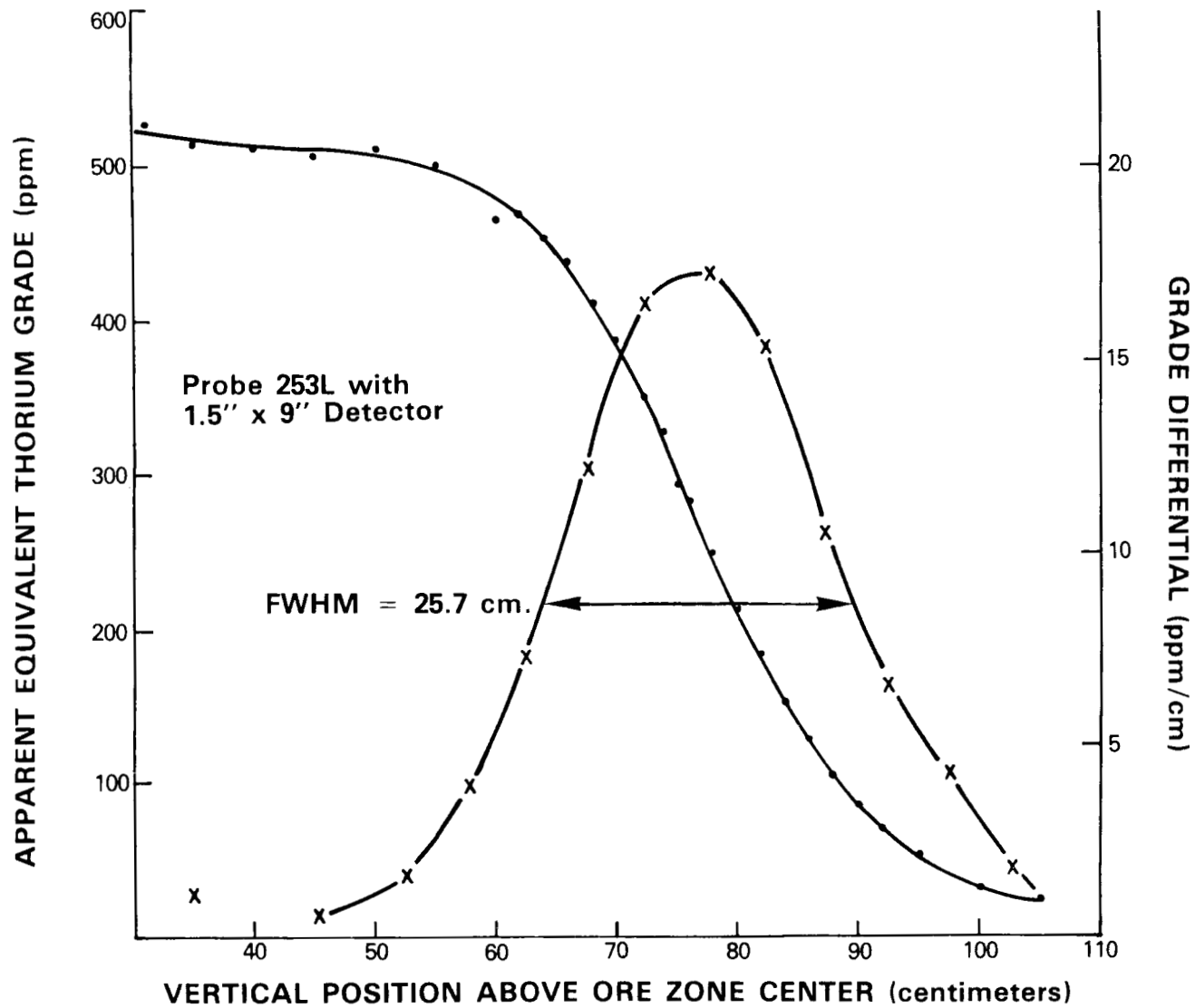
Figure 5-3.   Thorium model depth profile and differential response for
1.5-inch x 9-inch detector.
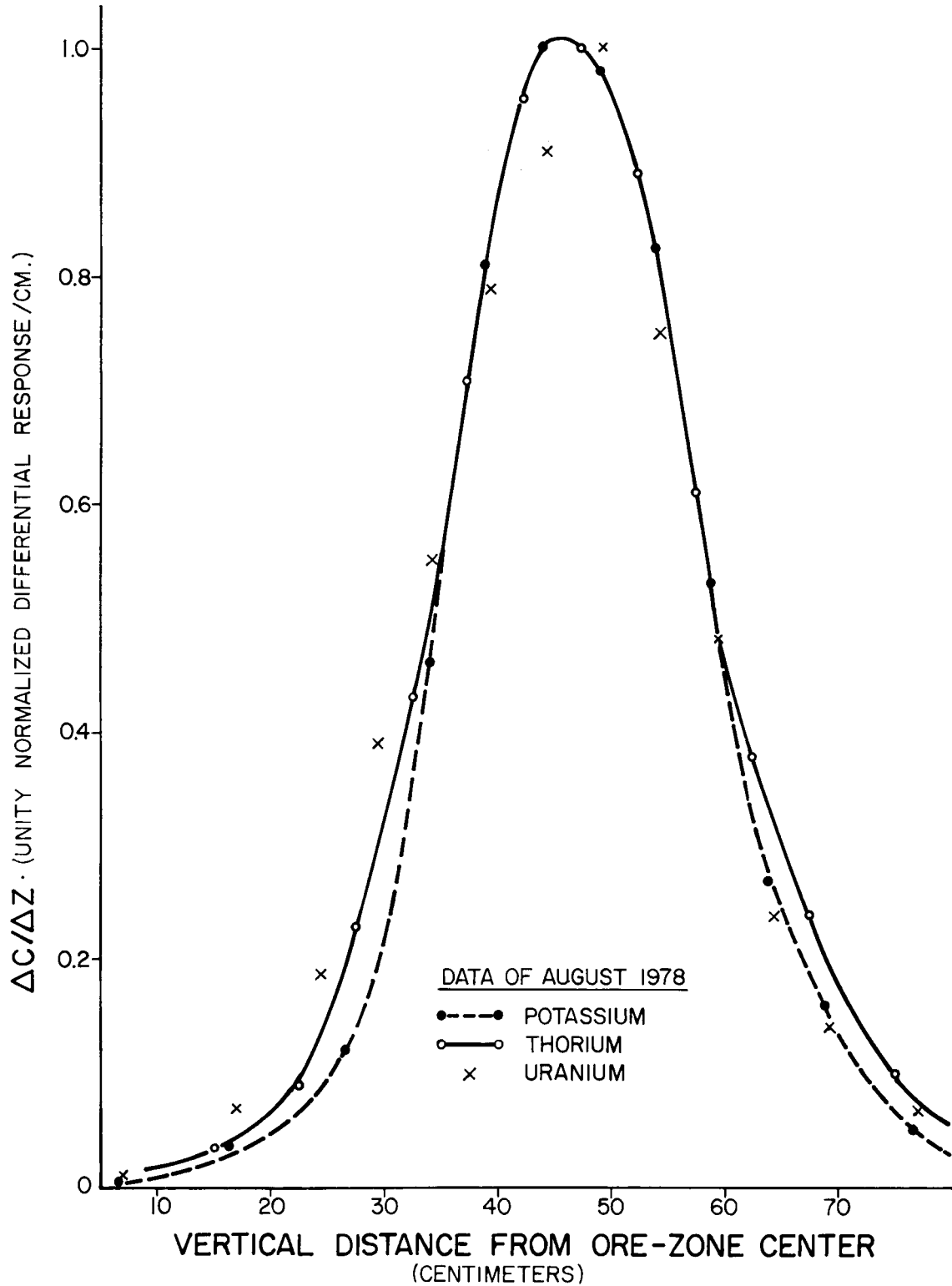
Figure 5-4. Unity normalized differential probe response for the ore
zone/barren zone interface region of the K, U, and Th models.

75

Table 5-2. Spectral Gamma-Ray Probe Response To A Thin Uranium Bed

Borehole Position (inches)	Apparent Equivalent Uranium Grade (ppm U)	Uranium to Potassium Stripping Ratio
(East) 30	2.9	2.10
24	4.2	1.71
21	5.4	1.61
18	7.9	1.39
15	14.4	1.21
12	27.1	1.091
10	45.6	1.068
8	78.0	1.021
7	105.3	
6	142.6	1.016
5	195.7	
4	255.3	0.987
3	307.0	
2	341.1	0.990
(Bed 1	359.9	
Center) 0	365.8	0.990
1	350.1	
2	327.9	1.00
3	283.8	
4	228.6	1.04
5	177.3	
6	135.1	1.07
7	98.1	
8	73.4	1.10
10	42.9	1.12
13	20.1	1.16
16	10.7	1.32
20	5.6	1.53
24	3.7	1.70
(West) 30	2.8	1.79

estimate the γ stripping ratio. The observed trend for γ can be explained by the fact that as one proceeds away from the thin bed, the intervening attenuating medium (water-saturated sand) causes a "build-up" of scattered radiation relative to the transmitted, unattenuated radiation observed in the U window. The value of γ then rises. It eventually should approach a constant value as the spectrum shape stabilizes farther from the thin bed source. γ is lower than the thick bed case at the thin bed center because the scattered component is smaller. It is reassuring that for the range of distances containing over 90 percent of the thin bed signal, γ changes by only 2 percent. This means that the deconvolution process will not require any variations in the stripping ratios. It will only be necessary to consider variations in the sensitivity of each channel (the A_{11}, A_{22}, and A_{33} elements of the calibration matrix) by use of appropriate K, U, and Th weighting factors.
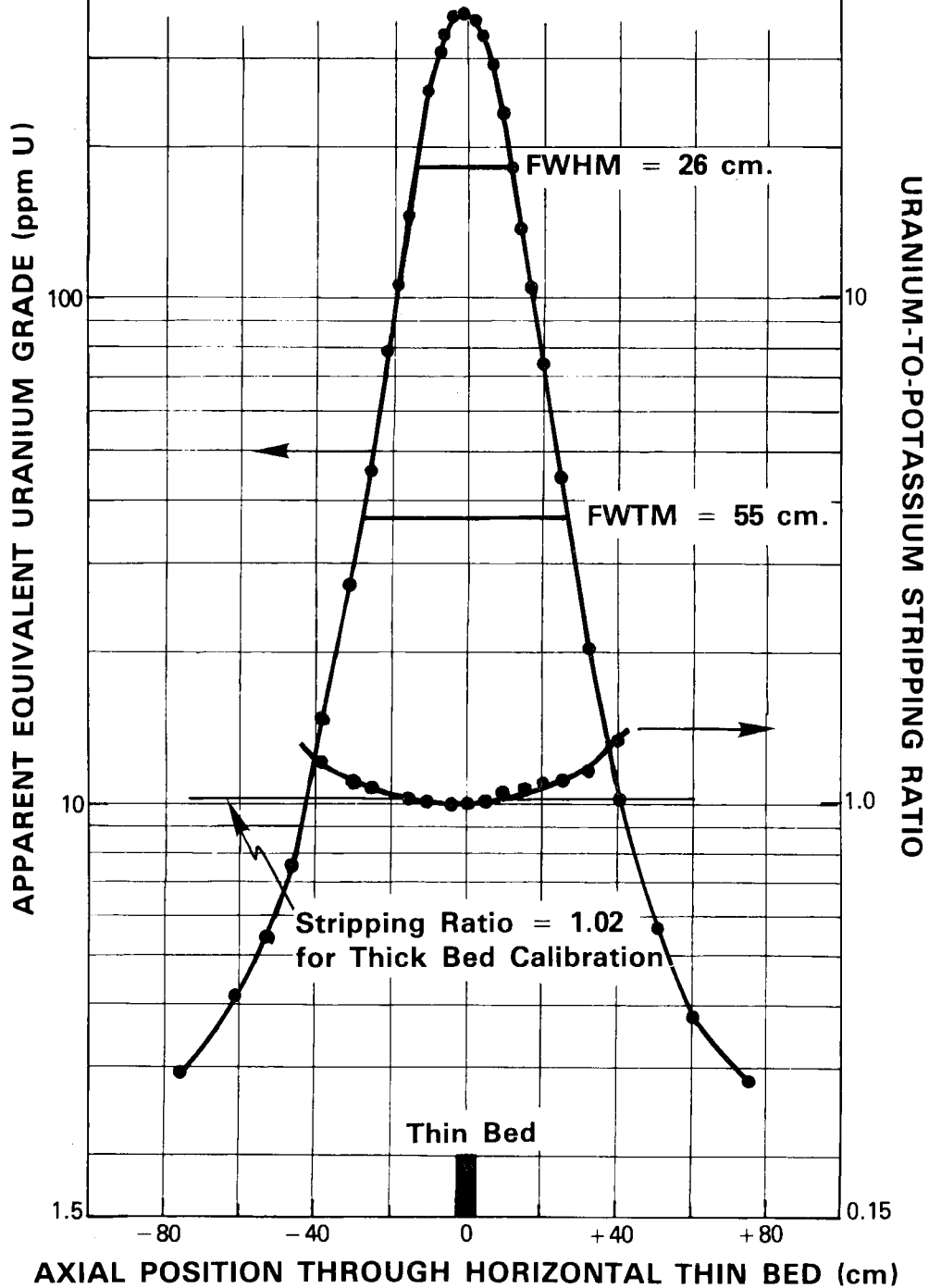
Figure 5-5.   Response of a 1.5-inch x 9-inch detector to a thin uranium
bed perpendicular to the borehole.

Derivation of Weighting Factors

0.5-Foot Anomaly

The thin uranium bed response of Figure 5-5 was corrected for the contributions from the 3.5 ppm barren zone uranium concentration and then used to simulate the probe response for a 0.5-foot thick uranium anomaly. Weighting factors derived from this simulated function are required as input to the GAMLOG deconvolution program. Numerical results are presented in Table 5-3 and plotted in Figure 5-6. Note that the FWHM has increased to 27.5 cm from the 26.0 cm value for the 2-inch thick thin bed. The increase is not large because the crystal is 23 cm (9 inches) in length. The values from this curve for positions at +0.5, +1.0, and +1.5 feet from the anomaly center are the 0.5-foot anomaly weighting coefficients required for the uranium window for the GAMLOG computer program. These values are shown on Figure 5-6 and tabulated in Table 5-4. Also tabulated, for comparison, are weighting coefficients determined several years ago by J. H. Scott (Scott, 1962) for a small sodium iodide crystal and for the "total gamma" signal. The +1.0 and +1.5-foot values for K and Th are not yet available due to insufficient data from the K and Th model profile measurements. These profiles will have to be repeated so that they include greater distances from the ore zone/barren zone interface. Note that there is a systematic increase in the +0.5-foot weighting coefficients from K to Th signals. This is expected since the gamma-ray energy is increasing, yielding a greater depth of penetration for the thorium signal.

1.0-Foot Anomaly

The 0.5-foot and 1.0-foot simulated anomalies are derived from the thin bed response by performing a sliding average over the thin bed data using the appropriate depth interval. Values for the 1.0-foot simulated anomaly also appear in Table 5-3. Figure 5-7 shows a plot of the 1.0-foot anomaly. The FWHM of 36.0 cm is substantially greater than the thin bed FWHM of 26.0 cm. Now the anomaly is significantly thicker than the detector length and a larger change in the width of the simulated response should be observed. Values of the weighting coefficients for the 1.0-foot anomaly are obtained from the curve in Figure 5-7 at +1 feet and +2 feet. The values are shown in the figure and are tabulated in Table 5-4.

GAMLOG DECONVOLUTION RESULTS FOR KUT WEIGHTING FACTORS

The weighting coefficients determined for the uranium channel in spectral gamma-ray (KUT) probes have been inserted into the computer program GAMLOG (Scott, 1962). This program was originally written to deconvolve gross count gamma-ray logging data, but it has been modified recently to process uranium-channel KUT data also. GAMLOG is now part of an extensive log analysis system placed in operation at the Oak Ridge DEC-10 computer facility by R. Price and K. Hayer.

The new weighting coefficients have been tried with a test set of field data. The results are shown in Table 5-5 along with natural (gross count) gamma data from the same hole. In the table, column 1 contains the depth information, column 2 the counts per second from the natural gamma-ray probe, and columns 3 through 5 the stripped count-rates from the spectral gamma-ray probe. The

Table 5-3. Simulated Probe Response for 0.5 and 1.0-Foot-Thick
Uranium Anomalies

Distance from Anomaly Center (inches)	Simulated Probe Response Normalized to Unity at Maximum	
	0.5-foot	1.0-foot
-27	0	0.003
-22		0.006
-21	0.007	
-20		0.012
-18	0.017	0.022
-16		0.037
-15	0.030	
-14	0.040	0.066
-13	0.052	
-12	0.069	0.117
-11	0.191	
-10	0.121	0.215
- 9	0.162	0.290
- 8	0.218	0.359
- 7	0.298	0.476
- 6	0.401	0.578
- 5	0.523	0.682
- 4	0.654	0.777
- 3	0.779	0.864
- 2	0.888	0.932
- 1	0.965	0.978
0	1.000	1.000
+ 1	0.988	0.997
+ 2	0.934	0.968
+ 3	0.843	0.912
+ 4	0.730	0.838
+ 5	0.606	0.747
+ 6	0.481	0.646
+ 7	0.369	0.544
+ 8	0.277	0.443
+ 9	0.206	0.349
+10	0.152	0.267
+11	0.114	0.201
+12	0.086	0.150
+13	0.064	0.110
+14	0.049	0.083
+15	0.036	
+16	0.027	0.046
+17	0.021	
+18		0.025
+19	0.009	
+20		0.015
+22		0.007
+23	0.002	
+24		0.003
+27	0	

Figure 5-6. Simulated probe response for a 0.5-foot uranium anomaly and a 1.5-inch x 9-inch detector.

Figure 5-7. Simulated probe response for a 1.0-foot uranium anomaly and a 1.5-inch x 9-inch detector.

Table 5-4. KUT Weighting Factors For Use In The Gamlog
Deconvolution Program

Distance from Anomaly Center (feet)	0.5-Foot Anomaly Weighting Factors			
	K	U	Th	Total Gamma*
0.0	1.000	1.000	1.000	1.00
+0.5	0.395	0.430	0.441	0.40
+1.0	---	0.078	---	0.08
+1.5	---	0.014	---	0.02
Distance from Anomaly Center (feet)	1.0-Foot Anomaly Weighting Factors			
	K	U	Th	Total Gamma*
0.0	1.000	1.000	1.000	1.00
+1.0	---	0.132	---	0.14
+2.0	---	0.005	---	0.007

*These weighting factors are for a small total gamma crystal as reported by Scott in his GAMLOG report.

grades (percent eU_3O_8) calculated by GAMLOG are given in column 6 for the natural gamma data and in column 7 for the uranium-channel data of the spectral data. A strict comparison between these grades should not be attempted at this time because the information in Table 5-5 is preliminary. In column 8 of the table, the ratio is given of the grades spectral gamma to natural gamma. The ratio is expressed as a percentage. Finally, a histogram of the natural gamma grades is presented along the right edge of the table.

Additional work is planned to test the weighting coefficients and use them in GAMLOG-type analyses which deconvolve spectral signals according to their origin along the borehole axis.

Table 5-5. Gamlog Results for Spectral Gamma-Ray and Natural Gamma-Ray Data

GAMLOG VS. K-U-T ANALYSIS FOR PROJECT NUMBER ( ) V1.0 27-SEP-78

HOLE: NORTH: ELEVATION: HOLE:
          EAST: H2O DEPTH:

REMARKS:

(NO WARRANTY OR REPRESENTATION IS MADE WITH RESPECT TO THE ACCURACY OR COMPLETENESS OF THE INFORMATION CONTAINED HEREIN.)

******** GAMLOG ANALYSIS PARAMETERS ******** ********************** K-U-T ANALYSIS PARAMETERS**************************

LOGGED-	K-FACTOR-	LOGGED-	A INVERSE MATRIX	BACKGROUND-
UNIT NO.-	DEAD TIME-	UNIT NO.-		WATER FACTOR-
PROBE NO.-	WATER FACTOR-	PROBE NO.-		FORMATION FACTOR-

GAMLOG AND K-U-T INTERPRETED VALUES ARE NON-CORRECTED FOR DIS-EQUILIBRIUM. CUTOFF GRADE FOR GAMLOG PRINTING IS .0000

DEPTH (FT.)	NAT. GAM. (CPS)	STRIPPED K-U-T K (CPS)	STRIPPED K-U-T U (CPS)	STRIPPED K-U-T TH (CPS)	GAMLOG GRADE (%eU3O8) NATURAL GAMMA	GAMLOG GRADE (%eU3O8) SPECTRAL GAMMA	SPECTRAL GAMMA / NATURAL GAMMA	NATURAL GAMMA HISTOGRAM
FEET SKIPPED = 480.0								
480.0	508.0	4.2	7.8	0.5	.0069	.0047	68.2	*******
481.0	419.0	3.8	11.0	0.1	.0056	.0076	134.9	******
482.0	294.0	2.6	5.2	0.7	.0038	.0031	81.3	****
483.0	220.0	5.3	2.4	1.0	.0028	.0012	42.2	***
484.0	218.0	4.4	4.8	0.5	.0025	.0031	121.1	***
485.0	452.0	3.6	6.1	0.7	.0066	.0039	59.0	*******
486.0	297.0	3.4	8.3	-0.0	.0038	.0058	152.1	****
487.0	248.0	5.2	3.6	0.4	.0032	.0019	60.2	***
488.0	272.0	4.9	3.9	0.2	.0036	.0025	68.8	****
489.0	308.0	6.9	2.9	0.7	.0041	.0017	40.6	****
490.0	332.0	6.5	4.8	0.4	.0041	.0029	71.8	****
491.0	584.0	4.5	7.4	0.2	.0081	.0046	56.5	********
492.0	612.0	3.6	12.1	0.4	.0079	.0082	104.0	********
493.0	802.0	5.5	10.1	0.1	.0103	.0058	56.2	**********
494.0	1206.0	6.6	14.5	1.2	.0161	.0085	52.5	***************
495.0	1627.0	2.6	29.2	0.1	.0231	.0198	85.6	***********************
496.0	1109.0	1.1	27.8	0.3	.0134	.0178	132.3	**************
497.0	1435.0	6.3	25.3	0.2	.0178	.0150	84.4	******************
498.0	2541.0	1.1	31.7	0.4	.0337	.0178	52.9	**
499.0	3857.0	0.8	68.6	0.5	.0552	.0465	84.4	**
500.0	2839.0	7.3	67.6	0.5	.0373	.0442	118.7	**
501.0	2344.0	-0.6	54.6	-0.3	.0324	.0357	110.0	**
502.0	1043.0	6.2	27.7	0.2	.0125	.0161	128.2	**************
503.0	620.0	0.8	19.8	0.4	.0076	.0124	163.1	********
504.0	556.0	4.9	11.0	0.2	.0075	.0064	85.2	*******
505.0	430.0	4.6	9.7	0.2	.0055	.0060	108.7	******
506.0	423.0	1.8	8.5	0.2	.0056	.0053	94.5	******
507.0	414.0	1.3	8.5	0.2	.0055	.0056	101.9	*****
508.0	440.0	4.8	5.8	0.9	.0059	.0034	57.0	******
509.0	426.0	4.8	8.0	0.3	.0055	.0052	93.1	******
510.0	492.0	1.7	8.7	0.5	.0065	.0056	86.0	*******
511.0	589.0	3.7	8.1	0.9	.0082	.0049	59.5	********
512.0	452.0	0.3	12.2	-0.0	.0059	.0085	143.2	******

Technical Note 6

RESULTS OF DYNAMIC LOGGING OF THE CALIBRATION MODELS

INTRODUCTION

The spectral gamma-ray calibration models at Grand Junction have been logged dynamically with a 2-inch x 10-inch NaI(Tℓ) detector using various speeds and counting periods. The logging speeds ranged from 1 ft/minute to 10 ft/minute, and the counting periods ranged from 1 second to 10 seconds. The data have been analyzed to calculate the concentrations of the models for comparison to the known concentrations. In addition, statistical uncertainties have been calculated to determine the effect of the counting period on the uncertainties. These results are applicable to field data which is presently collected at 5 ft/minute and 10-second periods.

CALIBRATION MODELS

The KUT calibration models at Grand Junction are pits constructed of concrete mixed with radioactive ores. There are three models, each having an enhanced concentration of potassium, uranium, or thorium. In each model, there is a central ore zone with barren zones (plain concrete) above and below the central ore zone. The concentrations in the ore zones and barren zones are given in Table 6-1. The models are cylindrical each having a diameter of 4 feet with a 4.5-inch hole along the axis for probe insertion.

DYNAMIC LOGGING DATA

The calibration models were logged from bottom to top at various probe speeds. The shallowness of the models as compared to actual field holes limits the quantity of data because the probe passes quickly through the ore zones. However, some data from the ore zones have been obtained. These data are given in Tables 6-2, 6-3, and 6-4 for the potassium (K) model, uranium (U) model, and thorium (Th) model, respectively.

CALCULATED CONCENTRATIONS

The data in Tables 6-2 through 6-4 have been used to calculate concentrations of potassium, uranium, and thorium in models. The equation used for the data reduction is the matrix equation:

$$C = A^{-1} R \qquad (1)$$

where C = calculated concentration matrix (3x1)

A^{-1} = calibration matrix (3x3)

R = count rate matrix (3x1) from data in Tables 2-4

The calibration matrix A^{-1} was determined by using static data taken in the models 3 days prior to the dynamic tests. These static calibration data are given in Table 6-5. The concentrations calculated using equation (1) with the dynamic data are given in Tables 6-6, 6-7, and 6-8 for the potassium (K)

85

Table 6-1. Concentrations of Calibration Models

Model	Zone	Zone Thickness(feet)	Percent K	ppm U	ppm Th
K	upper barren	3	2.00 ± 0.07	2.6 ± 0.3	7.4 ± 0.8
	ore	5	6.76 ± 0.18	2.7 ± 0.3	2.4 ± 0.6
	lower barren	3	1.89 ± 0.05	2.7 ± 0.3	7.4 ± 1.3
U	upper barren	3	2.01 ± 0.05	2.6 ± 0.2	8.0 ± 0.4
	ore	5	0.84 ± 0.24	498.3 ± 12.1	5.6 ± 1.3
	lower barren	3	2.16 ± 0.09	3.4 ± 0.6	8.7 ± 0.5
Th	upper barren	3	1.98 ± 0.04	2.4 ± 0.2	8.0 ± 0.7
	ore	5	1.44 ± 0.08	28.3 ± 1.0	505.5 ± 12.1
	lower barren	3	not available	not available	not available

Note: 1) Statistical uncertainties are one standard deviation.

2) No samples were collected for analysis from the Th, lower barren zone.

Table 6-2. Data Obtained from Dynamic Logging of the Potassium (K) Model

Logging Speed (ft/minute)	Counting Period (seconds)	K-Window (Counts)	U-Window (Counts)	Th-Window (Counts)
1	5	201 210 195	29 34 31	3 6 2
5	2	70 88 87	4 8 11	1 0 0
5	5	224 212 211	31 22 27	0 4 3
5	10	432 412 434	47 50 50	6 9 4
10	2	102 94 88	6 17 6	2 2 1
10	5	210 212 230	23 23 17	2 5 5
15	1	47 39 47	1 6 7	1 0 1
15	2	89 83 83	10 9 11	1 1 0

Table 6-3. Data Obtained from Dynamic Logging of the Uranium (U) Model

Logging Speed (ft/minute)	Counting Period (seconds)	K-Window (Counts)	U-Window (Counts)	Th-Window (Counts)
1	5	2413 2427 2406	2224 2187 2266	54 59 52
5	2	986 929 943	921 863 921	18 29 14
5	5	2381 2445 2378	2164 2244 2233	54 49 54
5	10	5017 4746 4848	4342 4380 4358	97 88 100
10	2	995 971 1003	881 873 854	24 15 19
10	5	2361 2329 2446	2109 2202 2116	66 56 55
15	1	471 482 494	414 444 489	7 9 5
15	2	903 903 920	861 857 845	23 17 24

Table 6-4. Data Obtained from Dynamic Logging of the Thorium (Th) Model

Logging Speed (ft/minute)	Counting Period (seconds)	K-Window (Counts)	U-Window (Counts)	Th-Window (Counts)
1	5	804 821 914	1660 1761 1685	420 453 517
5	2	330 328 324	657 671 676	183 159 198
5	5	869 879 889	1771 1690 1690	425 413 427
5	10	1716 1777 1754	3325 3358 3380	900 870 868
10	2	359 338 371	679 714 656	174 184 183
10	5	917 895 885	1668 1724 1741	462 452 450
15	1	160 161 158	320 325 345	84 96 95
15	2	276 356 347	680 716 702	185 196 190

Table 6-5. Static Calibration Data from the Models

Model	K-Window Counts	U-Window Counts	Th-Window Counts	Counting Time (Seconds)
Lead Cylinder (background)	2,338	2,172	415	900
K	72,979	7,727	921	1,500
U	430,843	415,225	9,261	900
Th	159,374	308,032	81,652	900

Note: Data collected with probe 241-L.

Table 6-6. Concentrations Calculated from Dynamic Logging Data for the
Potassium (K) Model

Logging Speed (ft/minute)	Counting Period (seconds)	Percent K	ppm U	ppm Th
1	5	5.33 $\pm$ 0.52 5.65 $\pm$ 0.55 5.01 $\pm$ 0.52	3.5 $\pm$ 1.9 2.2 $\pm$ 2.5 4.8 $\pm$ 1.8	1.9 $\pm$ 2.2 5.4 $\pm$ 3.1 0.5 $\pm$ 1.8
5	2	5.12 $\pm$ 0.71 6.02 $\pm$ 0.79 5.69 $\pm$ 0.80	-0.6 $\pm$ 2.4 3.9 $\pm$ 1.7 5.6 $\pm$ 2.0	1.6 $\pm$ 3.1 -1.4 $\pm$ 0.7 -1.6 $\pm$ 0.7
5	5	5.77 $\pm$ 0.54 5.98 $\pm$ 0.54 5.71 $\pm$ 0.54	6.4 $\pm$ 1.4 1.0 $\pm$ 2.0 3.0 $\pm$ 1.9	-1.7 $\pm$ 0.6 3.4 $\pm$ 2.5 2.0 $\pm$ 2.2
5	10	5.98 $\pm$ 0.41 5.72 $\pm$ 0.40 5.89 $\pm$ 0.41	2.2 $\pm$ 1.3 1.3 $\pm$ 1.5 3.4 $\pm$ 1.2	2.2 $\pm$ 1.6 3.9 $\pm$ 1.9 0.9 $\pm$ 1.4
10	2	7.62 $\pm$ 0.88 6.08 $\pm$ 0.89 6.36 $\pm$ 0.80	-1.4 $\pm$ 3.3 5.0 $\pm$ 3.8 0.6 $\pm$ 2.5	5.2 $\pm$ 4.4 4.2 $\pm$ 4.4 1.9 $\pm$ 3.1
10	5	5.74 $\pm$ 0.53 6.01 $\pm$ 0.54 6.77 $\pm$ 0.56	2.9 $\pm$ 1.6 0.5 $\pm$ 2.2 -0.9 $\pm$ 2.1	0.9 $\pm$ 1.8 4.6 $\pm$ 2.8 4.9 $\pm$ 2.8
15	1	7.33 $\pm$ 1.15 4.91 $\pm$ 1.07 6.33 $\pm$ 1.22	-3.7 $\pm$ 4.3 6.2 $\pm$ 2.9 3.3 $\pm$ 5.2	5.4 $\pm$ 6.2 -1.9 $\pm$ 0.7 4.4 $\pm$ 6.2
15	2	6.10 $\pm$ 0.82 5.72 $\pm$ 0.79 5.38 $\pm$ 0.78	3.0 $\pm$ 2.8 2.4 $\pm$ 2.7 5.6 $\pm$ 2.0	1.6 $\pm$ 3.1 1.5 $\pm$ 3.1 -1.7 $\pm$ 0.7

Note: Statistical uncertainties are one standard deviation.

Table 6-7. Concentrations Calculated from Dynamic Logging Data for the Uranium (U) Model

Logging Speed (ft/minute)	Counting Period (seconds)	Percent K	ppm U	ppm Th
1	5	4.38 + 4.03	476.8 + 21.2	11.6 + 13.4
		6.40 + 4.01	464.1 + 21.0	19.0 + 13.7
		2.63 + 4.05	488.3 + 21.4	7.7 + 13.3
5	2	2.76 + 4.97	502.6 + 26.5	-1.5 + 16.6
		5.06 + 4.78	446.0 + 26.3	35.7 + 19.3
		-1.27 + 4.88	510.8 + 26.1	-14.7 + 15.3
5	5	5.39 + 3.96	462.8 + 20.7	13.2 + 13.2
		4.37 + 4.06	485.6 + 21.2	5.1 + 13.2
		2.99 + 4.01	478.9 + 21.2	11.0 + 13.4
5	10	8.75 + 3.72	469.0 + 18.8	7.3 + 11.6
		3.59 + 3.64	477.0 + 18.8	0.1 + 11.2
		5.95 + 3.67	469.6 + 18.8	8.2 + 11.5
10	2	7.83 + 4.92	466.9 + 26.2	20.2 + 18.3
		5.09 + 4.84	480.6 + 25.3	-7.2 + 15.5
		9.85 + 4.87	461.4 + 25.3	7.3 + 16.7
10	5	7.43 + 3.91	440.0 + 20.5	29.6 + 13.9
		2.64 + 3.95	470.0 + 21.0	14.0 + 13.4
		9.08 + 3.97	450.7 + 20.4	16.6 + 13.3
15	1	6.41 + 5.82	456.3 + 30.6	-7.2 + 19.0
		3.81 + 6.02	483.3 + 32.4	0.6 + 21.1
		-3.22 + 6.22	552.4 + 33.2	-30.7 + 17.5
15	2	2.17 + 4.71	457.1 + 25.7	16.9 + 17.6
		1.48 + 4.69	467.1 + 25.1	-1.2 + 15.9
		5.00 + 4.72	445.7 + 25.5	21.6 + 17.9

Note: Statistical uncertainties are one standard deviation.

Table 6-8. Concentrations Calculated from Dynamic Logging Data for the Thorium (Th) Model

Logging Speed (ft/minute)	Counting Period (seconds)	Percent K	ppm U	ppm Th
1	5	-1.69 + 3.02	43.8 + 25.6	465.3 + 29.9
		-2.27 + 3.16	40.4 + 26.9	502.6 + 31.3
		7.56 + 3.23	-29.8 + 28.2	584.3 + 34.0
5	2	0.62 + 4.11	19.5 + 36.3	510.5 + 45.0
		-3.32 + 3.98	66.4 + 34.2	437.2 + 41.6
		2.65 + 4.18	-10.7 + 37.5	556.3 + 47.0
5	5	-3.03 + 3.15	65.7 + 26.3	468.3 + 30.1
		-0.84 + 3.07	56.6 + 25.6	456.3 + 29.6
		0.43 + 3.09	45.1 + 26.0	473.6 + 30.2
5	10	1.97 + 2.67	19.8 + 22.4	502.4 + 25.1
		1.33 + 2.68	36.0 + 22.1	483.7 + 24.6
		0.54 + 2.68	39.4 + 22.2	482.1 + 24.5
10	2	1.00 + 4.11	40.3 + 35.6	483.2 + 43.8
		-1.84 + 4.21	40.3 + 36.8	510.6 + 45.2
		5.40 + 4.12	8.4 + 36.0	512.9 + 45.0
10	5	4.44 + 3.14	11.3 + 26.8	517.4 + 31.7
		1.20 + 3.16	32.6 + 26.8	503.2 + 31.3
		0.19 + 3.16	38.2 + 26.8	500.1 + 31.2
15	1	0.19 + 5.20	29.8 + 46.1	467.2 + 58.5
		3.63 + 5.38	-13.6 + 48.8	540.0 + 62.8
		-0.52 + 5.44	13.9 + 49.0	530.5 + 62.5
15	2	-3.65 + 4.07	18.3 + 36.5	515.1 + 45.3
		1.46 + 4.29	16.9 + 37.8	547.6 + 46.8
		0.89 + 4.22	21.0 + 37.1	530.1 + 46.0

Note: Statistical uncertainties are one standard deviation.

model, uranium (U) model, and thorium (Th) model, respectively. The statistical uncertainties in the tables are one standard deviation; they represent the total uncertainty due to both the counting statistics in the dynamic data and the uncertainty in the probe calibration, A^{-1}.

The uncertainties in the calculated concentrations in Tables 6-6 through 6-8 decrease as the counting period increases for fixed logging speeds. For example, at a logging speed of 5 ft/minute the average uncertainty in the calculated potassium concentration in the potassium model decreases from 0.77 to 0.54 to 0.41 percent as the counting period increases from 2 seconds to 5 seconds to 10 seconds. This behavior is typical for all the models and logging speeds. If there were no uncertainty in the probe calibration A^{-1}, the concentration uncertainties would vary as the square root of the counting period. Thus, when the counting time is doubled, the statistical uncertainty will improve by a factor of $1/\sqrt{2}$. The inclusion of the uncertainty in the calibration tends to obscure the theoretical square root dependence in the tables.

The uncertainties in Tables 6-6 through 6-8 do not vary significantly with logging speed when the counting period is held constant. For example, the uranium concentrations calculated for the uranium model have average uncertainties of 21.2 ppm, 21.0 ppm, and 20.6 ppm for the logging speeds 1 ft/minute, 5 ft/minute, and 10 ft/minute when the counting period is 5 seconds. Logging speed does not directly affect the statistical uncertainty of the calculated concentrations, but it does affect the distance over which the signal is averaged. When the probe moves more rapidly, the spatial resolution of the signal along the borehole axis decreases for fixed counting periods. At a logging speed of 1 ft/minute, the probe moves approximately 0.1-foot in 5 seconds, whereas at a speed of 10 ft/minute it moves approximately 1 foot in 5 seconds.

The selection of a logging speed is necessarily a compromise between the desire to log rapidly and the need for acceptable spatial resolution. The counting period is also a factor for consideration because it determines the uncertainty in the concentrations calculated from the logging data. This reduces the desirability of counting for short periods to regain good spatial resolution at high speeds. The proper procedures for selecting a logging speed are as follows: (1) determine what statistical uncertainties in the calculated concentrations are acceptable, (2) determine the spatial resolution desired along the borehole, and (3) select the fastest logging speed that will provide the required uncertainties and resolution. If the resulting logging speed is too slow for economic operation, it may be necessary to log only zones of interest identified by gross gamma-ray logs as having sufficient merit for KUT investigation.

For ease in comparison, concentrations from Tables 6-6 through 6-8 have been averaged to get single concentrations of K, U, Th at selected logging speeds and counting periods. The resulting concentrations are given in Table 6-9 along with the "known" concentrations of the models' ore zones. The calculated concentrations are generally slightly lower than the known concentrations, but both values are consistent in all cases to within the statistical uncertainty of 2 standard deviations (95 percent confidence intervals). The same dynamic data have been analyzed using calibration of the probe performed one month earlier. The resulting concentrations are shown in

Table 6-9. Calculated Concentrations with Comparison to Known Concentrations Using Probe Calibration on 4/11/78

Model	Logging Speed (ft/minutes)	Counting Period (seconds)	Percent K	ppm U	ppm Th
K	5	10	5.87 $\pm$ 0.40	2.3 $\pm$ 1.3	2.3 $\pm$ 1.6
K	5	5	5.82 $\pm$ 0.54	3.5 $\pm$ 1.7	1.2 $\pm$ 1.8
K	1	5	5.33 $\pm$ 0.53	3.5 $\pm$ 2.1	2.6 $\pm$ 2.4
K	Known Concentration		6.76 $\pm$ 0.18	2.7 $\pm$ 0.3	2.4 $\pm$ 0.6
U	5	10	4.43 $\pm$ 3.68	471.9 $\pm$ 18.8	5.2 $\pm$ 11.4
U	5	5	4.25 $\pm$ 4.01	475.8 $\pm$ 21.0	9.8 $\pm$ 13.3
U	1	5	4.47 $\pm$ 4.03	476.4 $\pm$ 21.2	12.8 $\pm$ 13.5
U	Known Concentration		0.84 $\pm$ 0.24	498.3 $\pm$ 12.2	5.6 $\pm$ 1.3
Th	5	10	1.28 $\pm$ 2.68	31.6 $\pm$ 22.2	489.4 $\pm$ 24.7
Th	5	5	-1.15 $\pm$ 3.10	55.8 $\pm$ 26.0	466.1 $\pm$ 30.0
Th	1	5	1.20 $\pm$ 3.14	18.1 $\pm$ 26.9	517.4 $\pm$ 31.7
Th	Known Concentration		1.44 $\pm$ 0.08	28.3 $\pm$ 1.0	505.5 $\pm$ 12.1

Note: Concentrations in this table are selected averages from tables 6-6 through 6-8. The known concentrations are the ore zone values from Table 6-1.

Table 6-10, and and they are very similar to the concentrations in Table 6-9. The concentrations calculated from the two calibrations agree within the statistical uncertainties. This agreement suggests that probe calibration parameters do not vary rapidly and that monthly calibrations should be adequate for operational logging.

The uncertainites in the calculated potassium concentrations in the U and Th models are large; they have the same magnitude as the concentrations themselves. The resulting percent uncertainties (uncertainty $\div$ concentration X 100 percent) are typically 100 percent to 300 percent for the potassium concentrations. These large uncertainties are due to the stripping of the uranium and thorium counts from the potassium. The large uncertainties are not caused by improper calibration or stripping; rather, they are inevitable whenever there is a high concentration of uranium or thorium. Stripping removes the Compton-scattered uranium and thorium gamma rays from the potassium energy window. The net potassium counts are:

$$\text{Potassium counts} = \text{Total in potassium window} - U - Th,$$

where

$$U = \text{Compton scattered and low energy U counts}$$

$$Th = \text{Compton scattered and low energy Th counts.}$$

From nuclear statistics, the resulting uncertainty in the potassium is

$$\text{Potassium uncertainty} = \sqrt{\text{Total} + U + Th}$$

The "+" signs under the square root are the reasons for the large uncertainty in calculated potassium when mineralized zones of U and Th are encountered. The large uncertainties in potassium make it easy to get "negative" potassium concentrations from logging data. The concentrations are not actually negative, but the statistical fluctuations cause them to appear so (e.g., -2 percent potassium with an uncertainty of ± 4 percent potassium).

The uncertainties in concentrations calculated from logging data are due to both calibration uncertainties and logging uncertainties related to counting period. It is possible to separate these uncertainties to determine their independent contributions. This has been done for a single data point in each of the three models using dynamic data taken at 5 ft/minute and 10-second counting periods. The results are given in Table 6-11. For the K model, most of the uncertainty in this example comes from the counting of the 10-second logging intervals. In the U and Th models the calibration contributes the majority of the uncertainty. (In the calibration, most of the uncertainty is due to the uncertainties in the "known" concentrations of the models.) The 10-second counting period thus appears to be good for the probe used to collect the data in Table 6-11.

Table 6-10. Calculated Concentrations with Comparison to Known Concentrations
Using Probe Calibration on 3/9/78

Model	Logging Speed (ft/minutes)	Counting Period (seconds)	Percent K	ppm U	ppm Th
K	5	10	5.90 + 0.41	1.6 + 1.3	2.3 + 1.6
K	5	5	5.85 + 0.54	3.4 + 1.7	1.2 + 1.8
K	1	5	5.35 + 0.54	3.4 + 2.0	2.4 + 2.4
K	Known Concentration		6.76 + 0.18	2.7 + 0.3	2.4 + 0.6
U	5	10	4.14 + 3.76	473.3 + 19.0	5.6 + 11.6
U	5	5	3.93 + 4.10	477.2 + 21.1	9.6 + 13.4
U	1	5	4.15 + 4.12	477.8 + 21.3	12.6 + 13.6
U	Known Concentration		0.84 + 0.24	498.3 + 12.1	5.6 + 1.3
Th	5	10	1.10 + 2.74	35.5 + 22.2	480.6 + 24.8
Th	5	5	-1.37 + 3.17	59.3 + 25.7	455.5 + 30.0
Th	1	5	1.02 + 3.20	22.0 + 26.9	508.1 + 31.7
Th	Known Concentration		1.44 + 0.08	28.3 + 1.0	505.5 + 12.1

Note: Concentrations in this table are selected averages from tables 6-6 through 6-8.
The known concentrations are the ore zone values from Table 6-1.

97

Table 6-11. Concentration Uncertainties Separated According to Their Origin

Model	Origin of Uncertainty	Percent K	ppm U	ppm Th
K	Calibration & Logging	6.01 ± 0.41	2.1 ± 1.3	2.1 ± 1.6
K	Calibration only	6.01 ± 0.20	2.1 ± 0.3	2.1 ± 0.6
K	Logging only	6.01 ± 0.36	2.1 ± 1.3	2.1 ± 1.5
K	None	6.01 ± 0.00	2.1 ± 0.0	2.1 ± 0.0
U	Calibration & Logging	8.50 ± 3.81	470.5 ± 18.9	8.2 ± 11.8
U	Calibration only	8.50 ± 3.45	470.5 ± 16.8	8.2 ± 10.0
U	Logging only	8.50 ± 1.62	470.5 ± 8.7	8.2 ± 6.2
U	None	8.50 ± 0.00	470.5 ± 0.0	8.2 ± 0.0
Th	Calibration & Logging	0.34 ± 2.74	43.0 ± 22.2	473.2 ± 24.6
Th	Calibration only	0.34 ± 2.24	43.0 ± 17.4	473.2 ± 16.7
Th	Logging only	0.34 ± 1.57	43.0 ± 13.7	473.2 ± 18.0
Th	None	0.34 ± 0.00	43.0 ± 0.0	473.2 ± 0.0

Notes: 1. Only one data point used from each model.

2. Data taken at 5 ft/minute and 10-second counting period.

3. Probe used: 241-L (2-inch x 10-inch NaI crystal).

4. Uncertainties are one standard deviation.

SUMMARY

The spectral gamma-ray calibration models at Grand Junction have been logged dynamically to assess the importance of counting time on predicted concentrations of potassium, uranium, and thorium and their uncertainties. Logging speed has no significant effect on the predicted concentrations; although, it does affect the spatial interval over which signals are averaged along the borehole axis. Counting-time affects the statistical uncertainties in the data and in the calculated concentrations. Long counting-times provide superior statistical results, but they lengthen the spatial interval over which the signals are averaged. For the probe used to collect the dynamic data in this study (probe 241-L with a 2-inch x 10-inch NaI crystal), a logging speed of 5 ft/minute and a counting time of 10 seconds provided acceptable data.

ENERGY STABILIZATION METHODS

INTRODUCTION

For spectral gamma-ray probes, it is necessary to have a stable reference
signal from the detector to insure proper energy discrimination of the gamma
rays. In the probes built and operated by Bendix Field Engineering
Corporation (BFEC) for the U.S. Department of Energy (DOE), a ^{54}Mn
radioactive source is attached to the detector to provide this reference
signal, and an analog gain control amplifier is used to keep the ^{54}Mn pulses
at a constant value. A block diagram of the electronic system, including the
gain stabilization, is shown in Figure 7-1.
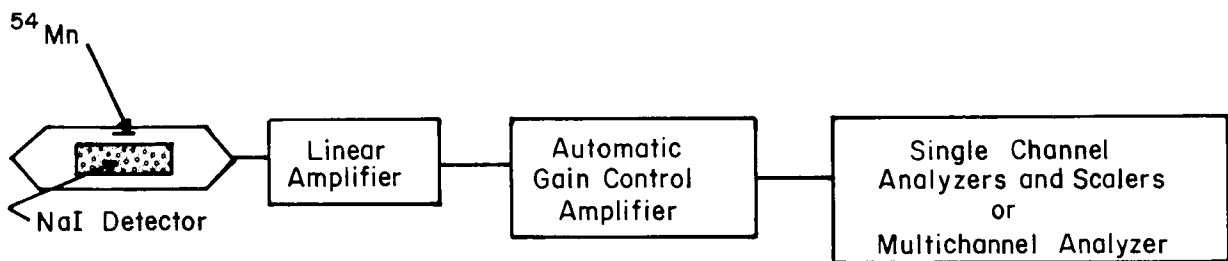
Figure 7-1. Electronic system used by Bendix/DOE to collect spectral
gamma-ray data in the field.

The use of ^{54}Mn to provide the reference signal creates some problems,
however, because the gamma rays from ^{54}Mn interfere with the natural
gamma-ray spectrum in the borehole. Alternate methods of providing reference
signals which do not use gamma rays have been investigated. Specifically,
alpha-particle sources and light-emitting diodes have been tested for use in
borehole probes. Attention has been focused in these tests on the temperature
dependence of the reference signals because this is the main cause of
instability when operating in borehole environments.

THEORETICAL CONSIDERATIONS

Gamma-Ray Reference

Gamma-ray sources provide the simplest means of obtaining a reference pulse of
constant energy. Compton scattering of the gamma rays makes it essential to
select a stabilization source with gamma rays of lower energy than those in
the natural spectrum. For spectral gamma-ray logging, the 1460 keV gamma ray
from ^{40}K is the lowest energy gamma ray which is typically used in the
natural spectrum. There are other, lower energy gamma rays in both the
uranium and thorium decay series (e.g., 609 keV and 1120 keV from ^{214}Bi),
but they are not generally used. The gamma ray from the stabilization source
must have an energy low enough ($\simeq$1200 keV) to avoid interference with the

potassium gamma ray. The radioactive source used for stabilization must also have a half-life sufficiently long to make its use practical in probes. The following gamma-ray sources are suitable for use:

^{241}Am (half life = 458 years; gamma-ray energy = 60 keV)

^{133}Ba (half life = 7.2 years; energy = 302 keV and 356 keV)

^{54}Mn (half life = 303 days; energy = 835 keV).

The necessity for having the stabilization gamma ray lower in energy than the natural gamma rays presents two problems: (1) slight drifts in energy stabilization based on the low energy reference are magnified at the higher energies, and (2) the presence of the stabilization source prevents counting of low energy gamma rays from the formation (e.g., it is not possible to collect simultaneously both spectral data and total count data with a low threshold). Stabilization using a gamma-ray source with high energy is not practical because of Compton scattering into the lower energies of interest.

Alpha-Particle Reference

Alpha particle emitting sources, such as ^{241}Am, do not create problems with Compton scattering. Alpha particle stabilization is achieved by implanting into the main detectors small chips of scintillators which have been impregnated with ^{241}Am. Placement of the reference peak in the energy spectrum depends on the fabrication process, and it cannot be readily reproduced. For NaI(Tℓ) chips with ^{241}Am, the reference pulse can have a gamma-ray equivalent energy up to approximately 6 MeV. This is adequate for borehole spectrometry; a reference pulse of 3 to 4 MeV is most desirable. The disadvantage of using alpha particle sources is that the light output from alpha particle interactions in scintillators varies with temperature in a manner different from the light output from gamma-ray interactions. As the temperature changes, the apparent energies of gamma rays will shift with respect to the alpha reference. The shift can be corrected if a computer is used in the data collection system and the temperature is monitored. Usually, however, the equipment required for making these corrections is not available. If the amount of relative shift between alpha- and gamma-ray interactions is small enough, the error introduced by ignoring the shift can be negligible compared to other uncertainties. By using different scintillators for the alpha interactions in the impregnated chip and for the gamma-ray interactions in the main detector, offsetting temperature dependencies can sometimes be obtained to reduce the relative movement of the peaks. In particular, CsI(Tℓ) chips impregnated with ^{241}Am provide much better tracking than do NaI(Tℓ) chips when used with NaI(Tℓ) as the main, gamma-ray detector.

Light-Emitting Diode Reference

A light-emitting diode (LED) can be used to provide a reference pulse for energy stabilization. The LED produces a light pulse into the detector which simulates the flash of light from a gamma-ray interaction. The light output from the LED can be adjusted to position the resulting peak higher in the energy spectrum than all the natural gamma rays of interest, and the LED does not produce Compton scattering to interfere with the lower energy gamma rays. The light output from the LED depends on temperature, and a temperature-

sensitive electronic network is required to match the LED's light output to
that of gamma rays. For the Bendix probe with a LED, the temperature
compensation is achieved by a network of temperature-sensitive resistors. The
resistance required for proper light output from the LED has been determined
experimentally, and a network of resistors has been assembled to approximate
the desired behavior. An alternate technique for temperature compensation is
to automatically switch fixed-value resistors in and out of the circuit
depending upon the temperature. This technique has not been used in Bendix
Field Engineering borehole probes; however, some commercial surface
spectrometers use this method.

TEST RESULTS

Small crystals of NaI(Tℓ) and CsI(Tℓ) impregnated with [241]Am were obtained
for the stabilization tests. They were mounted in a light pipe facing the
photocathode of a single photomultiplier tube (PMT), and the light pipe was
placed between the PMT and a 2-inch x 5-inch NaI(Tℓ) crystal which contained a
light emitting diode (LED). This arrangement allowed simultaneous temperature
tests of alpha stabilization in CsI(Tℓ) and NaI(Tℓ) and also LED stabiliza-
tion. A diagram of the detector assembly is shown in Figure 7-2. The
assembly was mounted in a spectral gamma-ray borehole probe which was placed
in a temperature chamber for the tests. The supporting electronic equipment
was kept at room temperature and connected to the probe by approximately 6,000
feet of 4HO logging cable to simulate field use.
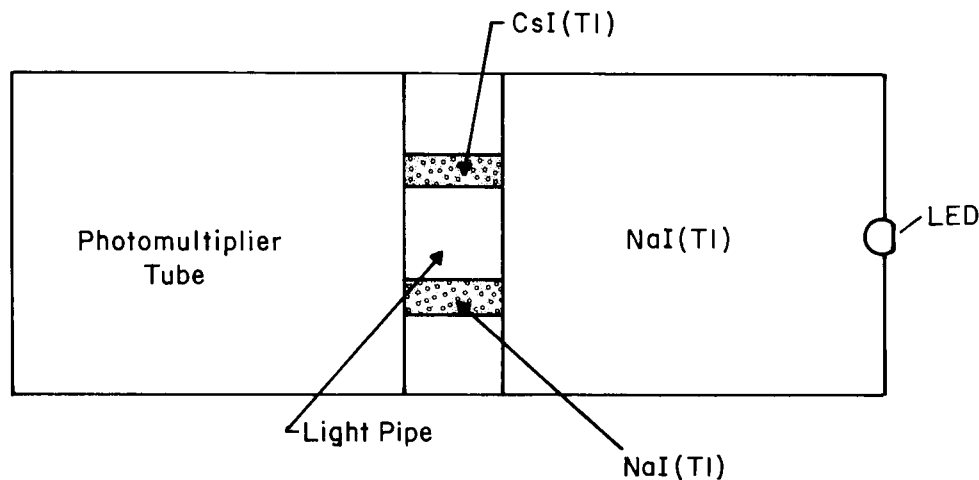
Figure 7-2. Detector assembly for simultaneous stabilization tests
             of alpha sources in CsI(Tℓ) and NaI(Tℓ) and of light
             emitting diode (LED).

Data were collected in both the stabilized and unstabilized modes by using the
equipment shown in Figure 7-3. The pulse shaping time constants for both
linear amplifiers were 1 μs, and the window of the automatic gain stabilizer
was set to a width of 0.2 volts on the 662 keV gamma ray from [137]Cs.
[137]Cs and [60]Co (1173 keV, 1332 keV and sum 2505 keV) were used to provide
gamma rays for comparison to the alpha peaks and the LED. A spectrum showing

all the alpha, gamma-ray, and LED peaks is given in Figure 7-4. The position of the alpha peaks near the gamma-ray peaks provides good comparison for their relative movement with temperature variation. The LED peak at the upper end of the energy spectrum is somewhat removed from the other peaks, but it is in a position desirable for spectral gamma-ray logging (i.e., its energy is greater than that of the natural gamma rays).
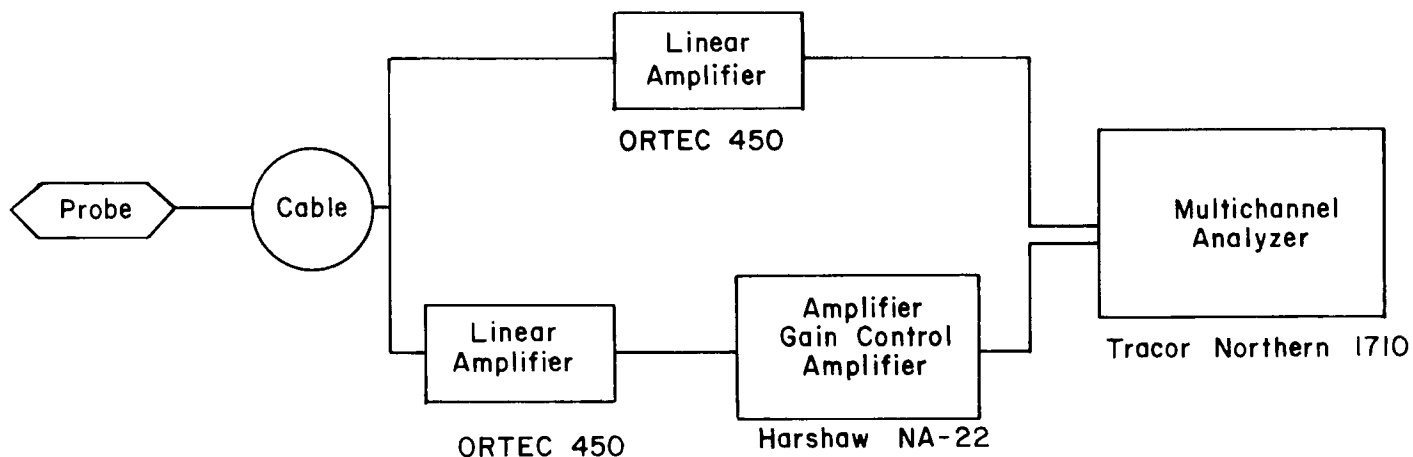
Figure 7-3. Electronics used for temperature tests in both stabilized and unstabilized modes of operation.

The data collected in the simultaneous temperature tests of CsI(Tℓ), NaI(Tℓ), and LED are given in Table 7-1 for the stabilized mode of operation and in Table 7-2 for the unstabilized mode. Approximately 3 hours were allowed for each temperature change before the data were recorded. From Table 7-1, it can be seen that none of the gamma-ray peaks moved significantly when the system was stabilized on the 662 keV peak from [137]Cs. Furthermore, the alpha peak from CsI(Tℓ) moved much less than did the alpha peak from NaI(Tℓ). The LED peak position decreased as the temperature increased. This was due to incomplete temperature compensation in the electronic driving network of the LED. Significant modifications were made to the electronic circuit after the compensation had been determined, and a futher revision for temperature compensation is needed for a critical evaluation of the LED. The present results for the LED should not be taken as a limit on the accuracy of this technique for stabilization.

The gamma-ray data in Table 7-2 have been used to determine a separate energy calibration to convert from channel number to energy at each temperature. From these calibrations, the equivalent gamma-ray energies of the alpha and LED peaks have been calculated, and they are listed in Table 7-3. The percent change in the peak locations with temperature are plotted in Figure 7-5 for the two alpha peaks and the LED. Over the temperature range of 30° to 118°F, the alpha peak in CsI(Tℓ) moved 1.3 percent, the alpha peak in NaI(Tℓ) moved 12.0 percent, and the LED peak moved 3.5 percent. With proper temperature compensation, it is expected that the LED movement can be reduced to less than 2 percent. The relatively large movement of the alpha peak in NaI(Tℓ) shows that [241]Am implanted in NaI(Tℓ) is not suitable for stabilization reference
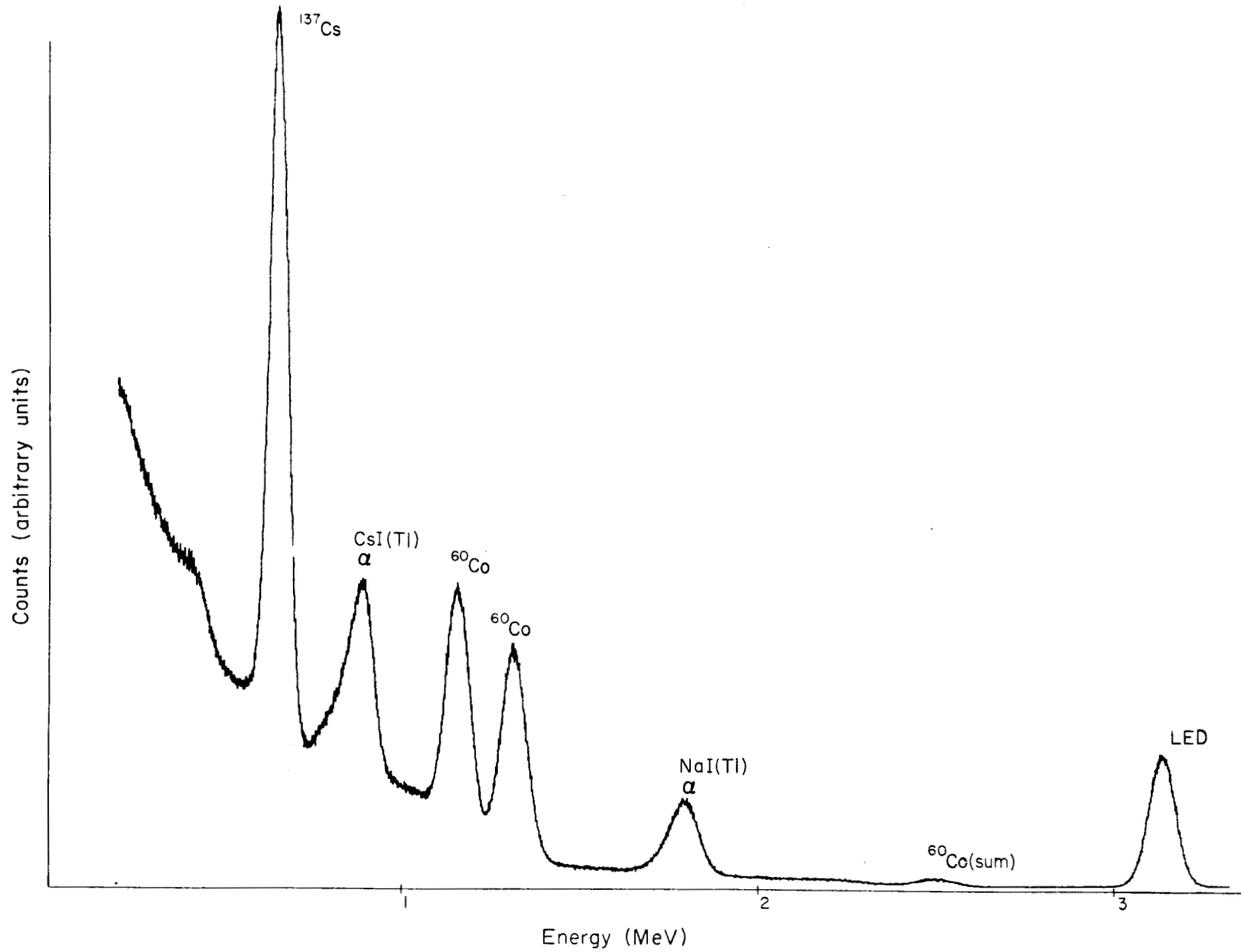
Figure 7-4. Spectrum showing peaks from gamma rays of ^{137}Cs and ^{60}Co, alphas in CsI(Tℓ) and NaI(Tℓ), and light emitting diode (LED).

Table 7-1. Temperature dependence of alpha peaks in CsI(Tℓ) and in NaI(Tℓ), gamma rays, and light emitting diode (LED) for a system stabilized on the 662 keV gamma ray from ^{137}Cs

Peak Location (Channel Number)

Temp (°F)	662 keV Gamma Ray	CsI(Tℓ) Alpha	1173 keV Gamma Ray	1332 keV Gamma Ray	NaI(Tℓ) Alpha	2505 keV Gamma Ray	LED
30	909	1209	1560	1796	2470	3253	4080
53	909	1214	1560	1769	2347	3249	4026
75	909	1219	1561	1770	2300	3252	4005
97	910	1225	1564	1769	2247	3258	3990
118	909	1223	1565	1769	2202	3250	3950

Table 7-2. Temperature dependence of alpha peaks in CsI(Tℓ) and NaI(Tℓ), gamma rays, and light emitting diode (LED) for an unstabilized system

Peak Location (Channel Number)

Temp (°F)	662 keV Gamma Ray	CsI(Tℓ) Alpha	1173 keV Gamma Ray	1332 keV Gamma Ray	NaI(Tℓ) Alpha	2505 keV Gamma Ray	LED
30	888	1197	1549	1754	2485	3302	4195
53	887	1195	1548	1756	2385	3306	4138
75	868	1176	1513	1714	2257	3228	4020
97	814	1109	1418	1607	2065	3024	3752
118	732	993	1274	1443	1819	2719	3337

106
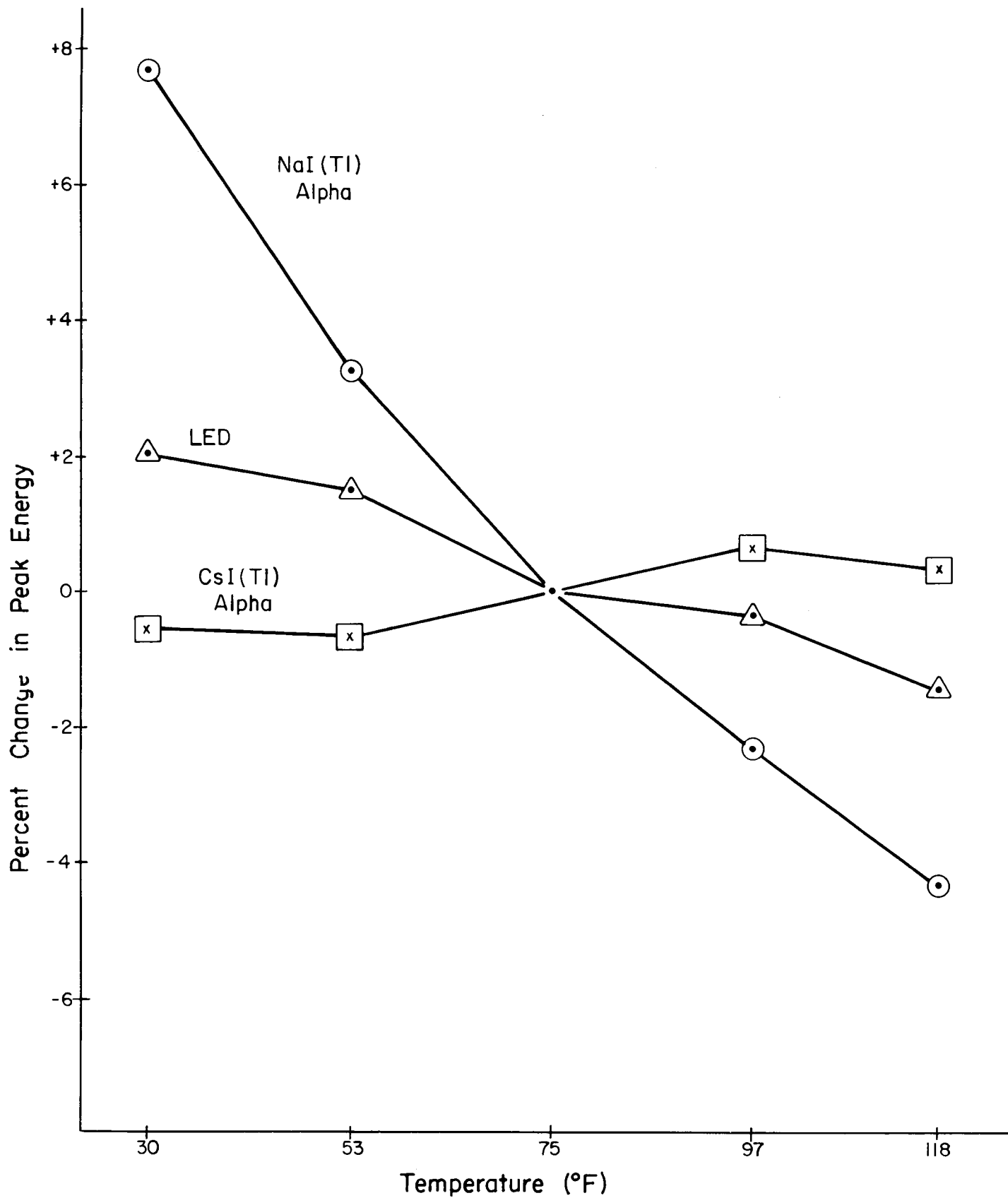
Figure 7-5. Percent change in peak energy versus temperature. Changes are relative to 75°F values.

107

Table 7-3. Temperature dependence of the equivalent gamma-ray energies of the alpha peaks from [241]Am in CsI(Tℓ) and in NaI(Tℓ) and of the LED peak. The energies were determined from data in Table 7-2.

Equivalent Gamma-ray Energy (keV)

Temperature ($°F$)	CsI(Tℓ) Alpha	NaI(Tℓ) Alpha	LED
30	902	1884	3188
53	901	1807	3140
75	907	1750	3125
97	913	1709	3114
118	910	1674	3080

unless the temperature is monitored and a correction is made during data collection for the drift of the reference peak. The alpha peak from [241]Am in CsI(Tℓ) provides a reference peak stable enough for use in spectral gamma-ray logging, but it is not known if an alpha peak can be obtained in CsI(Tℓ) above an equivalent gamma-ray energy of 3 MeV. The light output from CsI(Tℓ) is less than from NaI(Tℓ), and it may be impossible to produce sufficient light for the needed high-energy reference peak.

CONCLUSION

Three methods of obtaining a reference signal for energy stabilization have been investigated: gamma ray, alpha particle, and light-emitting diode. Stabilization on the 835 keV gamma ray from [54]Mn is currently used by BFEC because of its simplicity, but there are significant problems with this method caused by interference of the stabilizing gamma ray with the natural gamma rays from the formation being logged.

Alpha particle sources and light-emitting diodes provide potential energy reference signals which do not interfere with the natural spectrum. The [241]Am alpha source implanted in NaI(Tℓ) was found to be too temperature dependent for practical logging use because its peak shifted by 12 percent from that of gamma-ray interactions over the temperature range of 30° to 118°F. [241]Am in CsI(Tℓ), however, provided a variation of only 1.3 percent when compared to gamma-ray light output over the same temperature range. The sample of CsI(Tℓ) with [241]Am used for these tests, had its alpha peak at an apparent gamma-ray energy of less than 1 MeV, and it is not known if a peak above 3 MeV can be obtained. If this is not possible, then [241]Am in CsI(Tℓ) cannot be used for a stabilization reference in borehole logging. CsI(Na) with [241]Am may provide higher light output than CsI(Tℓ), but a sample of this crystal has not yet been obtained for evaluation.

The light from a light-emitting diode was found to vary by 3.5 percent over the temperature range of 30° to 118°F. With proper temperature compensation in the LED's electronic driving network, it is expected that this variation can be reduced to less than 2 percent. At this value the LED will provide an acceptable stabilization reference for spectral gamma-ray borehole logging.

Technical Note 8

LOG DECONVOLUTION WITH THE INVERSE DIGITAL FILTER

INTRODUCTION

Previous efforts at KUT log deconvolution have utilized the iterative procedure contained in the program GAMLOG. These efforts are described in Technical Note 5. Recently, a new approach to gamma-ray log deconvolution has been described by J. G. Conaway (Conaway and Killeen, 1978). Conaway's technique employs the inverse digital filter method to obtain uranium grade versus depth from the gamma-ray log response.

Extensive measurements were performed with the Grand Junction models to determine the sensitivity of the inverse filter parameter to detector size and to borehole conditions. Results of these measurements are presented and discussed.

Grand Junction model N5 was then logged with a KUT probe. This model consists of several layers with differing grades and thickness. The inverse filter technique was used to deconvolve these data. The results are quite satisfactory and indicate that deconvolution in "real time" will now be possible with mini-computer based field logging systems.

INVERSE FILTER DECONVOLUTION TECHNIQUE

This approach to log deconvolution is based on the theory of digital time series analysis. Given an appropriate function to describe the logging probe response to a thin uranium zone, this theory predicts an inverse, discretized function or filter that, when applied to the digital gamma-ray log, yields uranium distribution with depth.

The work published by Conaway uses a two-sided exponential function to describe the probe response to a thin zone. This function was apparently first used by Czubek, (Czubek, 1961), and can be written

$$I(z) = \frac{\alpha}{2} \exp\left(-\alpha|z|\right),\tag{1}$$

where $I(z)$ is the unity normalized probe response at position z along the borehole axis from the thin zone, and α is a parameter dependent on gamma-ray energy, borehole conditions, formation composition, and formation density. $I(z)$ is called "the Geologic Impulse Function" by Conaway. The function is

realistic only for point detectors or for detectors whose length is much less than $1/\alpha$. When the effect of the detector length is included, the function becomes more complicated (George, 1979a):

$$
I(z) = \begin{cases} \frac{1}{L} \sinh\left(\frac{\alpha L}{2}\right) \exp\left(-\alpha|z|\right) & |z| \geq L/2 \\[2em] \frac{1}{L}\left[1 - \cosh(\alpha z)\,\exp\left(-\alpha L/2\right)\right] & |z| < L/2 \end{cases} \tag{2}
$$

where L is the detector length. If one assumes zero detector length and uses equation (1), it can be shown that the discretized inverse filter operator is given by the triad:

$$
\left(\frac{-1}{(\alpha \Delta z)^2}\, ,\; 1 + \frac{2}{(\alpha \Delta z)^2}\, ,\; \frac{-1}{(\alpha \Delta z)^2} \right) \tag{3}
$$

where Δz is the depth interval utilized for the digital gamma-ray log. Since this filter does not account for finite detector length, the sampling interval Δz must be no smaller than L, the detector length.

The successful deconvolution of gamma-ray logging data with this inverse filter technique depends on the correct choice for the parameter α. In addition, the data must ideally be free of noise. The introduction of noise (e.g., uncertainties from counting statistics) degrades the performance of the deconvolution filter.

The parameter α in the geologic impulse function is best determined by direct experimental measurement. The most precise data are obtained if probe response is measured through a thin zone of the radioactive species of interest (potassium, equilibrium uranium, or thorium). A "thin zone" is one whose thickness is less than about half the detector length. The 2-inch zones of the Grand Junction models are adequate for most detectors in use for spectral gamma-ray logging. If thin zones are not available, the parameter α may be determined by measuring the probe response across a plane interface between a homogeneous ore zone and a perfectly barren zone. Both zones must have the same bulk density and be at least 2 feet thick to approximate semi-infinite media.

Calculations have been performed by Czubek that predict the values of α for various values of the gamma-ray linear attenuation coefficient and borehole diameter (Czubek, 1973). These calculations apply only to unscattered, unattenuated gamma rays from a cylindrical source. They assume a point detector in a dry borehole.

In the sections that follow, both the thick zone interface and thin bed experimental approaches are utilized and results are compared to Czubek's calculations.

MEASUREMENTS OF FILTER PARAMETER α

Ore Zone/Barren Zone Results

K Model

The GJO potassium model depth profile was measured for 1.5-inch x 3.0-inch and 1.5-inch x 9.0-inch crystals. Tables 8-1 and 8-2 contain numerical values of apparent potassium grade, and results are plotted in semilogarithmic form in Figures 8-1 and 8-2. The results presented in Table 8-2 are from earlier work (Table 5-1 in Technical Note 5). Both detectors were first calibrated at the centers of the K, U, and Th models to determine the thick zone calibration matrix. The matrix was then applied to data taken as the probe moved through the interface giving apparent grade versus depth.

Table 8-1. Ore Zone/Upper Barren Zone Depth Profile Potassium Model
Probe 253L 1.5-inch x 3.0-inch Crystal

Depth (cm)	Apparent Grade (percent K)	Depth (cm)	Apparent Grade (percent K)	Depth (cm)	Apparent Grade (percent K)
16	2.06	80	2.76	104	6.23
24	1.86	82	3.01	108	6.38
32	2.05	84	3.16	112	6.38
40	2.04	86	3.50	116	6.52
48	2.13	88	3.87	120	6.71
56	2.11	90	4.19	124	6.47
60	2.10	92	4.60	128	6.70
64	2.14	94	5.06	136	6.88
68	2.37	96	5.45	144	6.67
72	2.47	98	5.59	152	6.73
76	2.48	100	5.97	160	6.61
78	2.64	102	6.12	168	6.65

Table 8-2. Ore Zone/Upper Barren Zone Depth Profile Potassium Model
Probe 253L 1.5-inch x 9.0-inch Crystal

Depth (cm)	Apparent Grade (percent K)	Depth (cm)	Apparent Grade (percent K)	Depth (cm)	Apparent Grade (percent K)
39	2.23	82	3.00	104	6.19
43	2.21	84	3.29	106	6.51
48	2.32	86	3.62	108	6.63
53	2.27	88	3.91	113	6.63
58	2.20	90	4.12	118	6.86
63	2.22	92	4.44	123	6.74
68	2.32	94	4.78	128	6.78
74	2.50	96	5.19	133	7.20
76	2.54	98	5.42	138	6.82
78	2.68	100	5.73		
80	2.82	102	6.09		
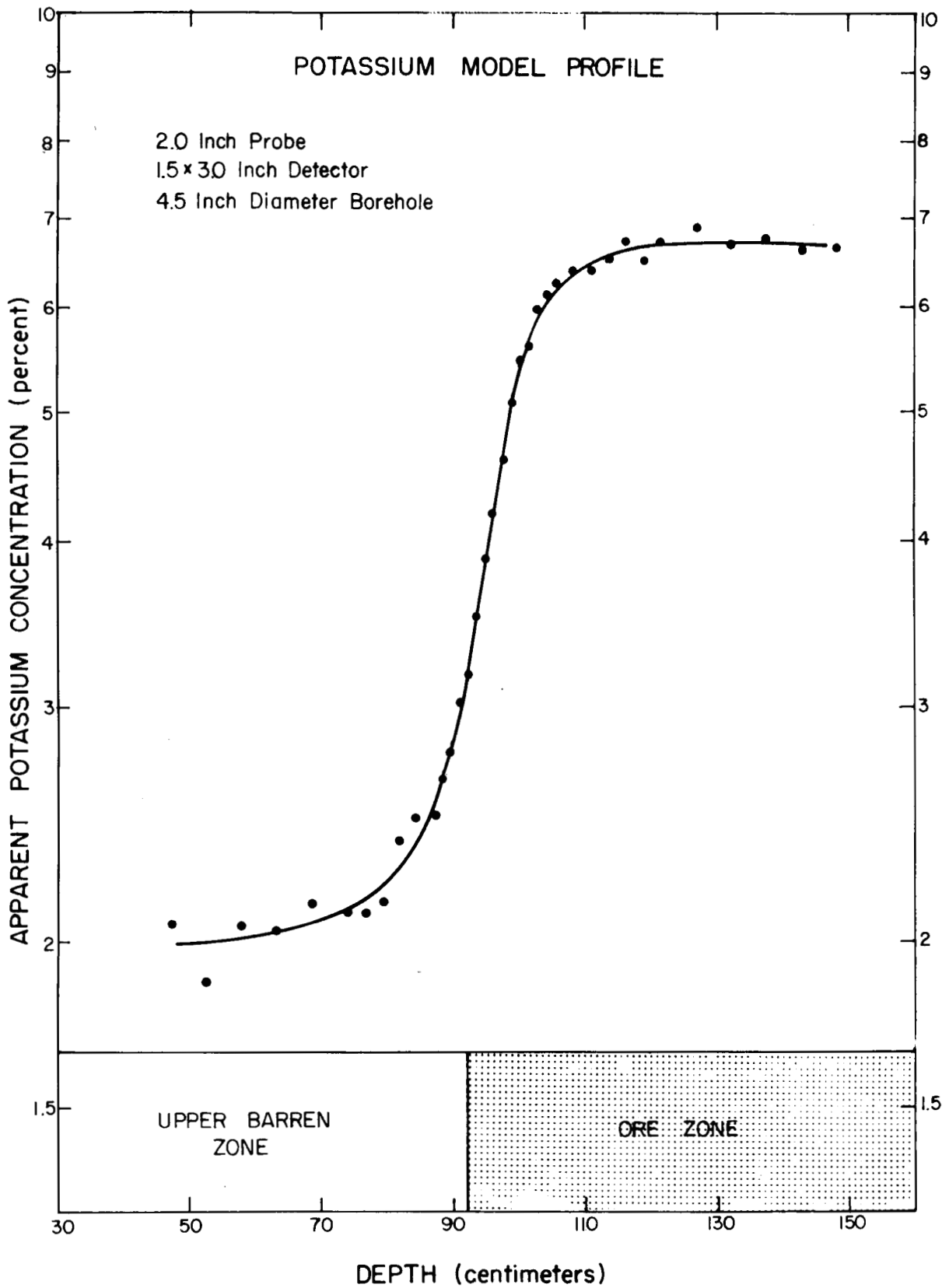
Figure 8-1. Potassium model profile for a 1.5-inch x 3-inch detector.

112
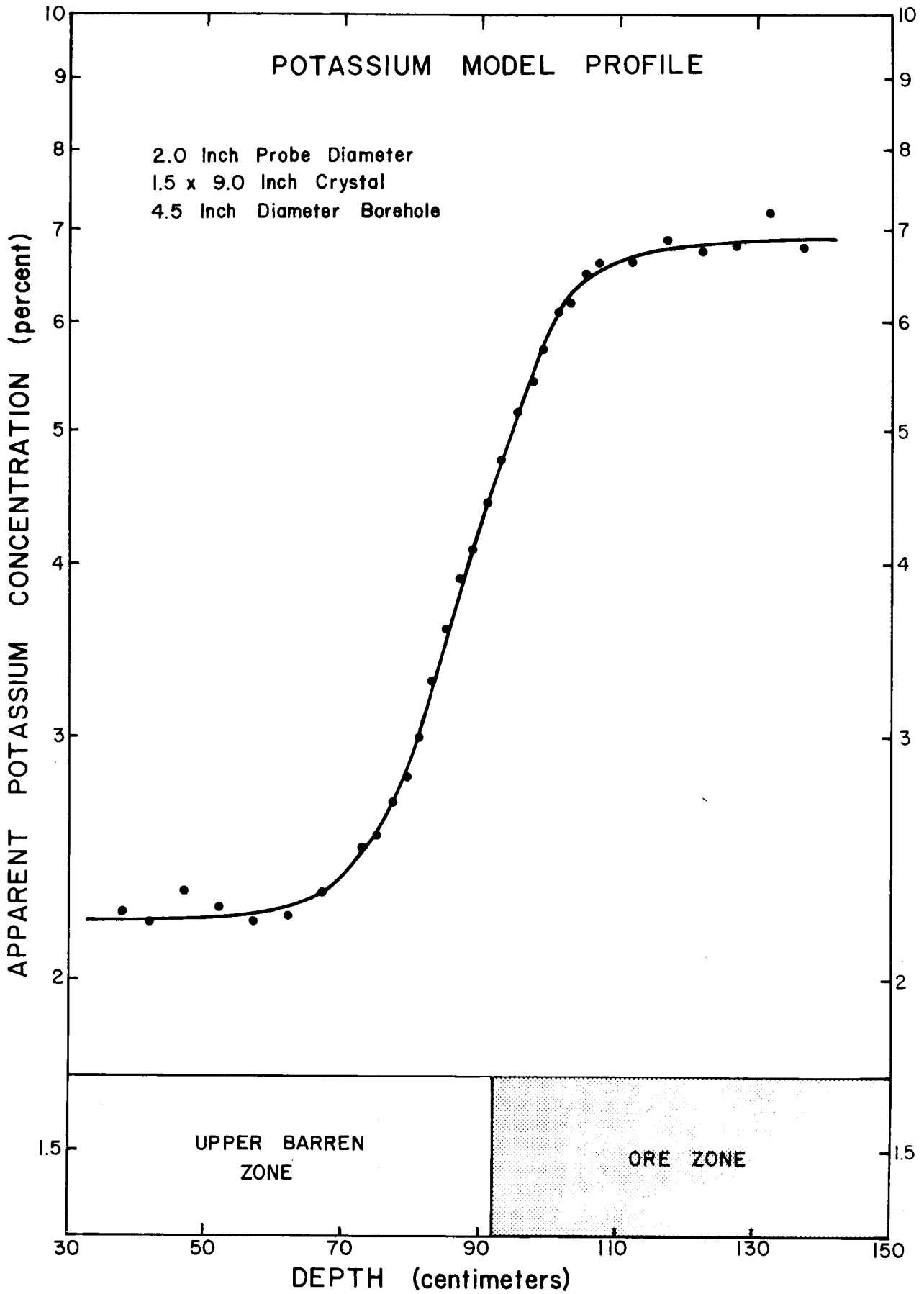
Figure 8-2.   Potassium model profile for a 1.5-inch x 9-inch detector.

113

These data were then fit with smooth curves and differential grades were computed. Table 8-3 contains differential potassium grades for the 1.5-inch x 3.0-inch and 1.5-inch x 9.0-inch crystals. Semilogarithmic plots appear in Figures 8-3 and 8-4. These curves represent the geologic impulse functions for a potassium source in a concrete medium with a dry 4.5-inch diameter borehole and for the 3.0-inch and 9.0-inch detector lengths.

Table 8-3. Ore Zone/Upper Barren Zone Depth Profile for Potassium Model

1.5-inch x 3.0-inch Crystal		1.5-inch x 9-inch Crystal	
Depth (cm)	Differential Grade (percent/cm)	Depth (cm)	Differential Grade (percent/cm)
47	0.003	45	0.002
53	0.005	50	0.003
59	0.011	55	0.004
65	0.018	60	0.008
71	0.032	65	0.013
74	0.045	70	0.024
77	0.058	74	0.042
80	0.078	78	0.075
83	0.118	82	0.123
86	0.158	86	0.148
89	0.178	88	0.150
92	0.205	90	0.155
95	0.183	92	0.155
98	0.130	94	0.160
101	0.085	96	0.170
104	0.050	98	0.162
107	0.032	100	0.140
110	0.025	105	0.081
116	0.015	110	0.033
122	0.009	115	0.015
		120	0.008
		125	0.007
		130	0.007

The shorter detector exhibits an impulse function that is narrower by 9 centimeters at FWHM and by only 2 centimeters at FWTM. The maximum apparent differential grades occur at the known interface between the two zones (92 centimeters in depth). The observed maximum is higher for the short detector, as expected.

The inverse filter parameter α can be obtained from the differential curves in Figures 8-3 and 8-4. Equation (2) shows that the predicted geologic impulse function for a detector of length L falls off exponentially with slope α for $|z| \geq L/2$. The derivation of equation (2) by D. George was apparently stimulated by discussions with John Conaway in which Conaway suggested α could be obtained from a semilogarithmic plot of the geologic impulse response, independent of detector length and zone thickness (Conaway, 1979a). This approach

114
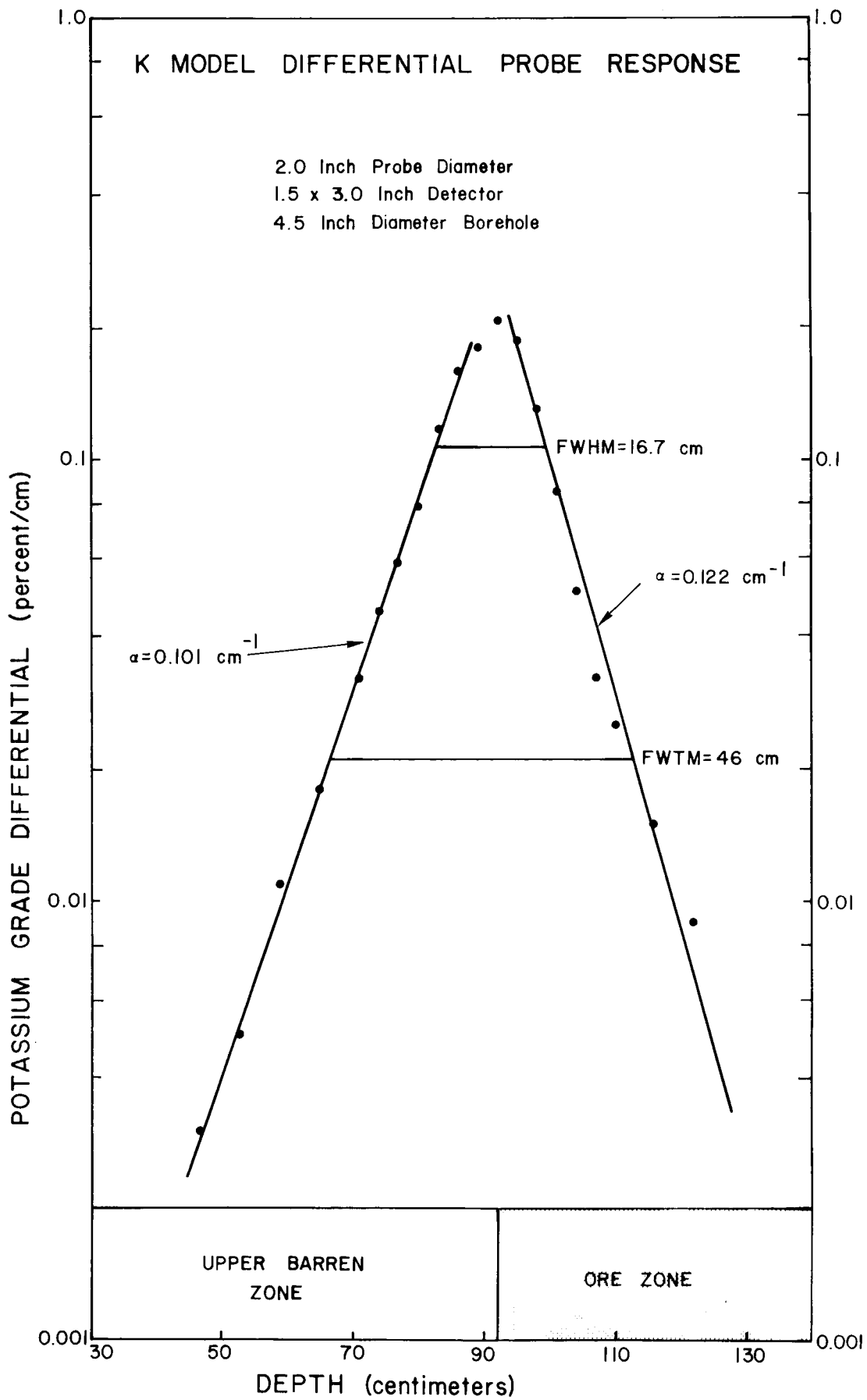
Figure 8-3. Potassium model differential response for a
1.5-inch x 3-inch detector.

115
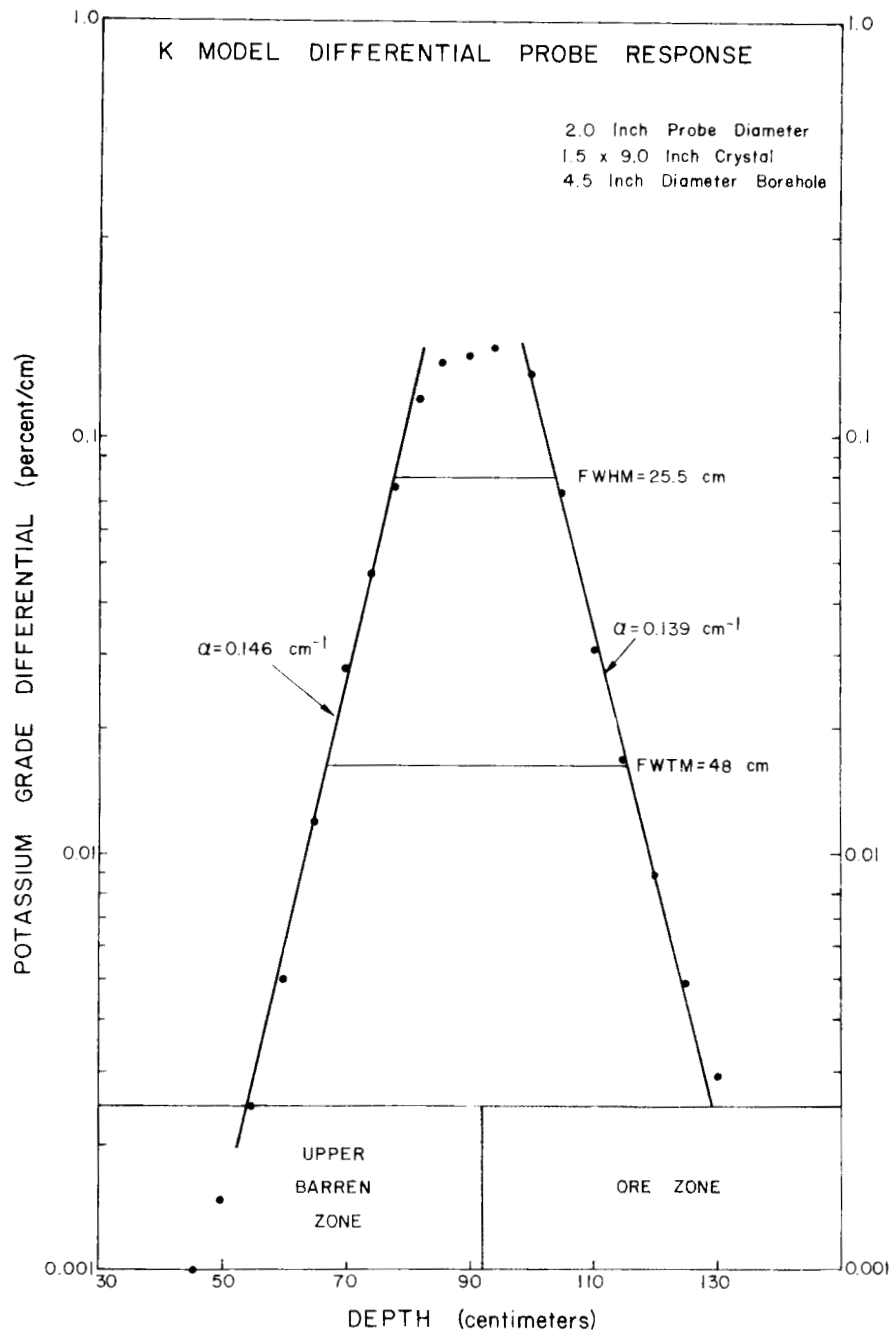
Figure 8-4. Potassium model differential response
for a 1.5-inch x 9-inch detector.

116

follows from the derivation of equation (2). Since the functions are plotted in semilogarithmic form in Figures 8-3 and 8-4, they should fall linearly for values of depth above and below the interface at 92 cm by more than L/2. For the 9-inch-long (22.86 cm) detector the function is in fact nearly linear for depths less than 92 - (22.86/2) = 80.57 cm and greater than 92 + (22.86/2) = 103.43 cm (see Figure 8-4). The slope computed from straight line fits in these regions gives the value of α directly. This procedure was used to determine α for both detector lengths. Values are given on Figures 8-3 and 8-4 and in Table 8-4 as "Measured α ."

The geologic impulse response function represented by equation (2) assumes that α is independent of detector length. The theoretical calculations of Czubek were applied to obtain α values for the 1.46 MeV potassium gamma ray in the concrete medium of both the upper barren zone and the ore zone. The results are given in Table 8-4 as "Calculated α." α is predicted as larger in the barren zone because of its higher bulk density.

Table 8-4. α Parameter for Potassium Model

Detector Size	Measured α (cm^{-1})		Calculated α (cm^{-1})	
(inches)	Upper Barren Zone	Ore Zone	Upper Barren Zone	Ore Zone
1.5 x 3.0	0.101	0.122	0.113	0.102
1.5 x 9.0	0.146	0.139		

The calculated values are in fair agreement with the measured α for the 1.5-inch x 3-inch detector. However, the 1.5-inch x 9-inch detector yields a higher measured value than calculated value of α . Apparently, α depends on detector length. Perhaps this dependence is caused by detector self-shielding effects. As the detector length becomes greater than its diameter, gamma rays incident on the detector along its length are self-shielded, yielding lower count rates per unit detector length. This effect is more pronounced when a large fraction of incident gamma rays are directed along the length of the detector. Since this fraction increases with increasing distances from a thin source layer, the result is an apparent increase in the slope of the impulse function α.

U Model

The uranium model depth profile was measured for the 1.5-inch x 3-inch crystal. Table 8-5 contains numerical values of apparent equivalent uranium grade, and results are plotted in Figure 8-5. Following the same procedure as with the K model results, the differential uranium grade profile was computed and is plotted on Figure 8-5 as "X." Numerical values for the differential grade appear in Table 8-6. This uranium impulse function was plotted together

117

with the profile data ("dots") to show the near coincidence in slope between
the linear portion of the semilogarithmic profile plot and the slope for each
side of the differential plot. This is true whenever one of the two regions
forming the interface is truly barren. This was not the case for the K model
but is nearly true for the U and Th models. The average α from the
differential grade function is 0.112 cm^{-1} and is slightly higher than the
value of 0.109 cm^{-1} from the grade profile. However, the slope is more
easily obtained from the interface profile.

Table 8-5. Ore Zone/Upper Barren Zone Depth Profile Uranium Model
Probe 253L 1.5-inch x 3.0-inch Crystal

Depth (cm)	Apparent Grade (ppm U)	Depth (cm)	Apparent Grade (ppm U)	Depth (cm)	Apparent Grade (ppm U)
16	2.8	80	67.7	112	476
22	2.3	82	84.3	114	485
28	3.1	84	108	116	487
34	4.1	86	130	120	488
40	3.8	88	170	124	502
46	4.5	90	206	128	501
52	6.8	92	257	132	489
56	—	94	302	136	499
60	12.0	96	340	140	493
64	14.6	98	372	144	503
68	21.5	100	396	148	502
70	24.8	102	417	152	501
72	30.2	104	436	158	506
74	38.4	106	444	164	502
76	46.1	108	468	170	500
78	55.3	110	468	176	510

Table 8-6. Ore Zone/Upper Barren Zone Depth Profile Uranium Model
1.5-inch x 3.0-inch Crystal

Depth (cm)	Differential Grade (ppm/cm)	Depth (cm)	Differential Grade (ppm/cm)
25	0.05	82.5	9.8
30	0.064	85	13.0
35	0.076	87.5	17.2
40	0.104	90	22.6
45	0.154	92.5	23.4
50	0.28	95	19.8
55	0.52	97.5	15.2
60	0.86	100	12.0
65	1.42	102.5	9.8
70	2.30	105	7.6
72.5	3.0	107.5	5.6
75	3.9	110	3.6
77.5	5.5	115	1.6
80	7.5	120	1.2
		125	0.7
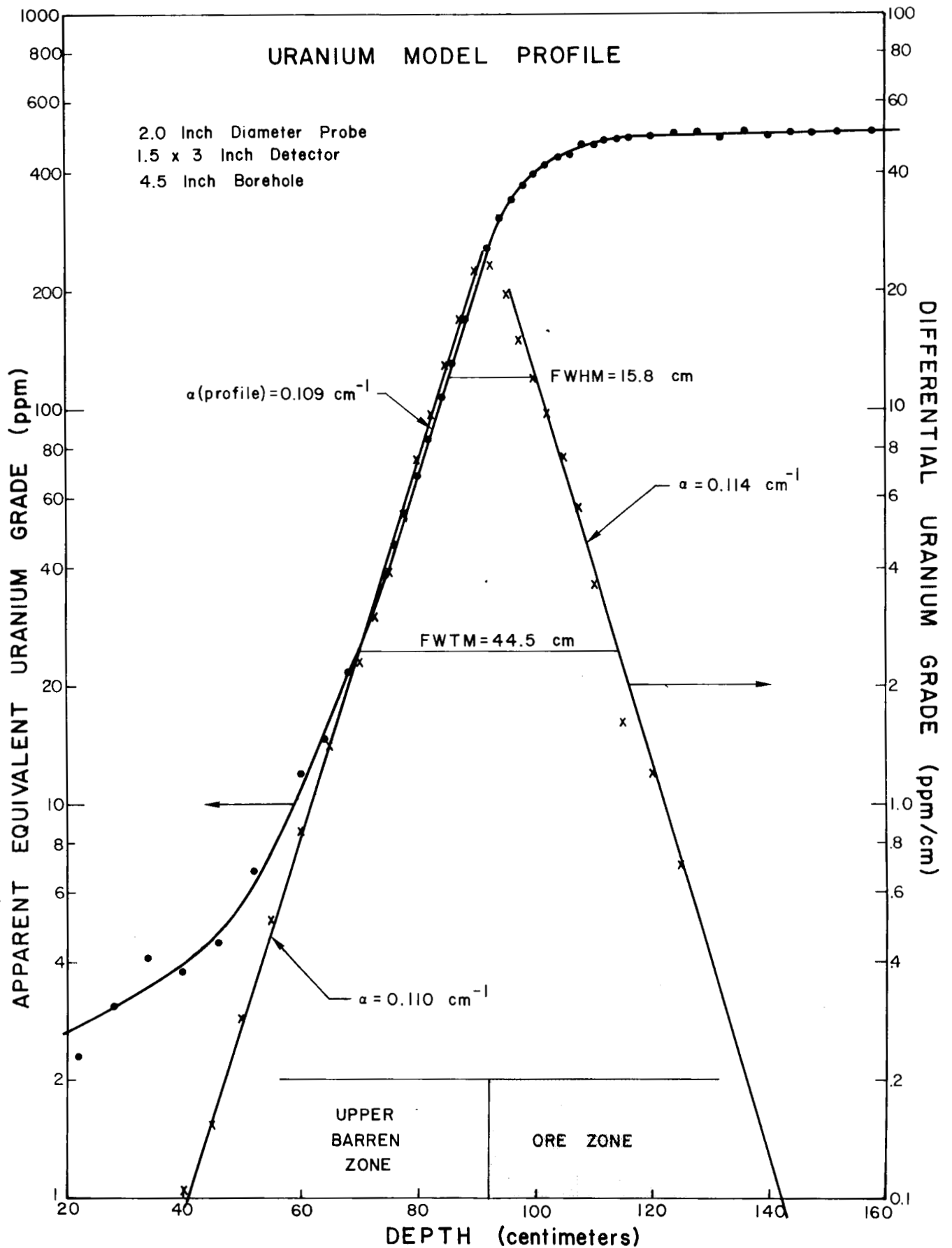
Figure 8-5.   Uranium model profile for a 1.5-inch x 3-inch detector.

The previously measured uranium profile for the 1.5-inch x 9-inch detector (see Technical Note 5) has been replotted in semilogarithmic fashion in Figure 8-6. Table 8-7 contains the uranium model depth profile results from Technical Note 5. The value of α obtained from the profile in Figure 8-6 for the 1.5-inch x 9-inch detectors is 0.112 cm^{-1}. Table 8-8 contains numerical values for the differential grade function obtained from Figure 8-6. The differential response is plotted in Figure 8-7. The average α value is 0.123 cm^{-1}. Again, the value of α from the differential grade function is higher than that obtained from the interface profile. The profile values of α are low because the "barren zone" is not truly barren of uranium. The differential grade function yields more reliable α values.

Table 8-7. Ore Zone/Upper Barren Zone Depth Profile Uranium Model
1.5-inch x 9.0-inch Crystal

Depth (cm)	Apparent Grade (ppm)	Depth (cm)	Apparent Grade (ppm)
62	12.0	92	226
64	13.5	94	257
66	15.9	96	290
68	18.6	98	330
70	23.7	100	351
72	28.2	102	380
74	34.3	104	406
76	42.3	106	424
78	52.6	108	443
80	65.5	110.5	453
82	84.2	113	475
83	93.4	118	492
84	106	123	495
86	132	128	496
88	159	133	506
90	191	138	506

Table 8-8. Ore Zone/Upper Barren Zone Depth Profile Uranium Model
1.5-inch x 9.0-inch Crystal

Depth (cm)	Differential Grade (ppm/cm)	Depth (cm)	Differential Grade (ppm/cm)
64	0.9	96	17.5
68	1.7	100	13.3
72	2.9	104	11.2
76	4.8	108	8.3
80	7.4	112	5.0
84	12.4	116	3.0
88	14.5	120	2.0
92	17	130	0.7

Figure 8-6. Uranium model profile for a 1.5-inch x 9-inch detector.

121
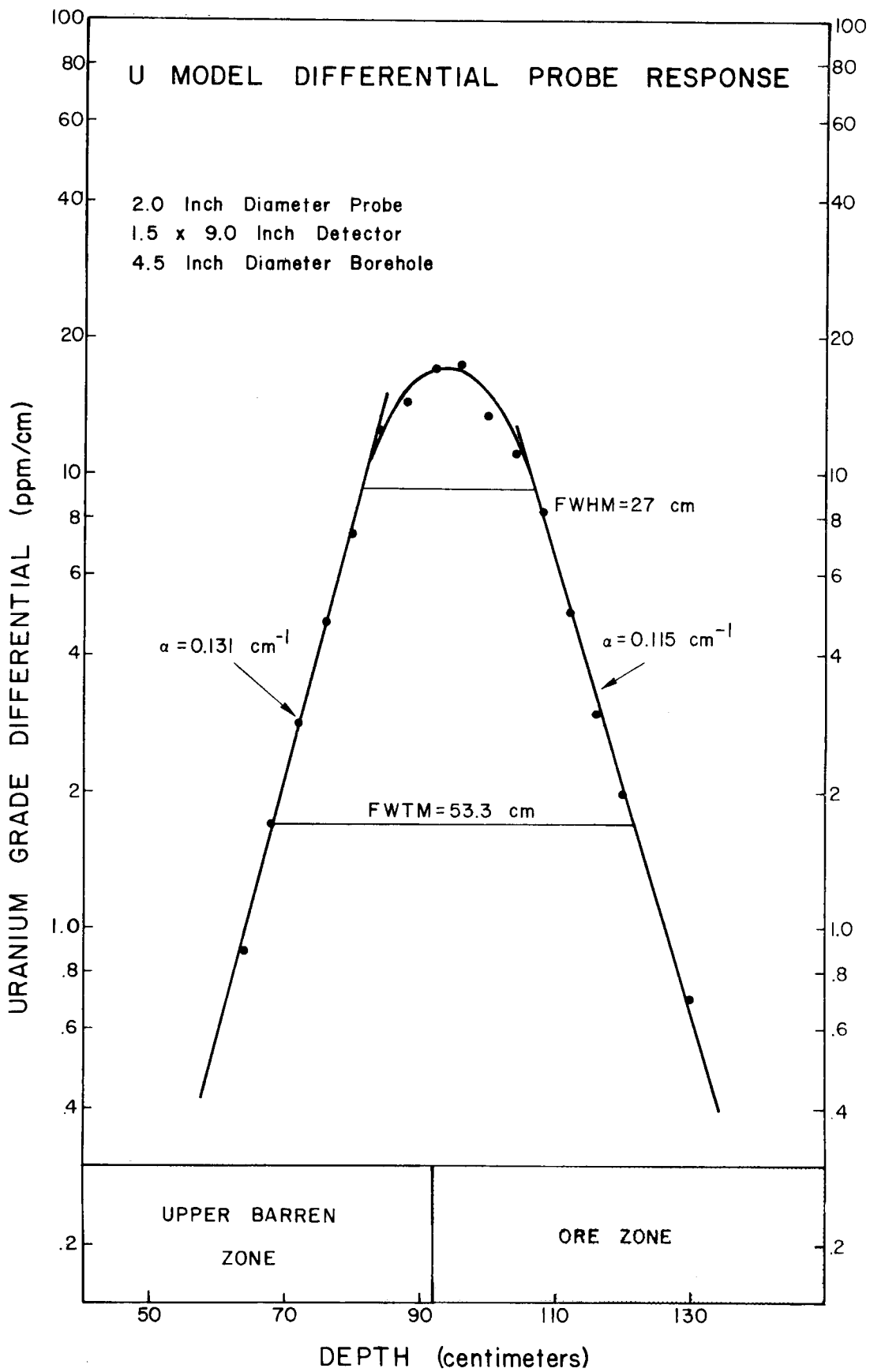
Figure 8-7. Uranium model differential response for a 1.5-inch x 9-inch detector.

A summary of α values for the U model is given in Table 8-9. As with the K model results of Table 8-4, α is larger for the larger detector. α for the 3-inch long detector is essentially the same for K and for U. For the 9-inch detector, α is smaller for U than for K. Perhaps the self-shielding effect is larger for the lower energy potassium gamma ray than for uranium, causing a larger slope α for the K model differential response function.

Table 8-9. α Parameter for Uranium Model

Detector Size (inches)	Measured α (cm^{-1})		Calculated α (cm^{-1})	
	Upper Barren Zone	Ore Zone	Upper Barren Zone	Ore Zone
1.5 x 3.0	0.110	0.114	0.108	0.116
1.5 x 9.0	0.131	0.115		

Th Model

The thorium model profile was measured for the 1.5-inch x 3-inch detector. Table 8-10 contains numerical values of apparent thorium grade. Figure 8-8 contains a semilogarithmic plot of both the apparent and dif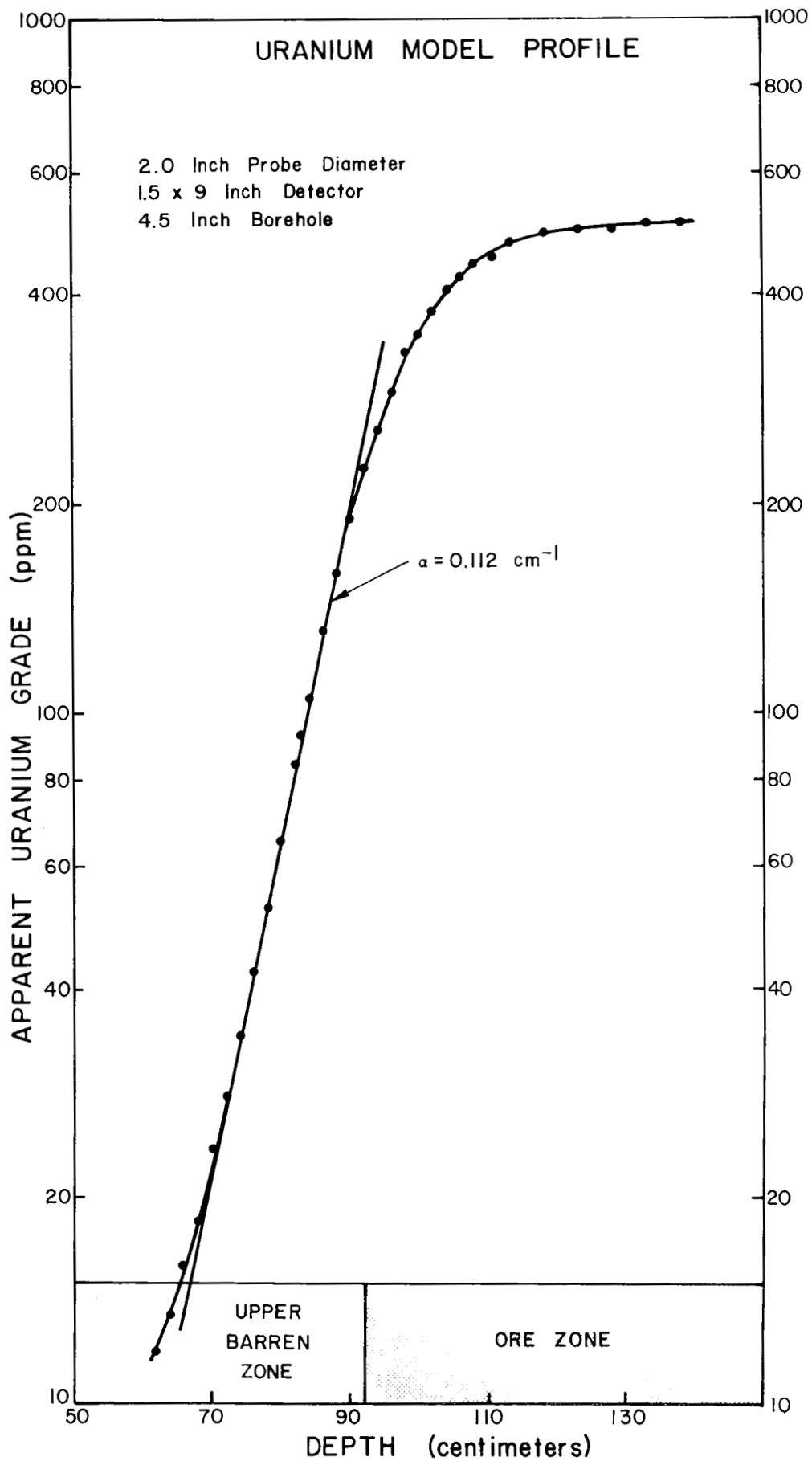ferential thorium grade. The previously measured thorium profile for the 1.5-inch x 9-inch detector (see Technical Note 5) is reported in Table 8-11 and has been replotted in semilogarithmic form in Figure 8-9. Figure 8-10 contains the differential grade function derived from the smooth curve fit in Figure 8-9. Computed differential grades are contained in Table 8-12. Results were analyzed for the parameter α and are summarized in Table 8-13. A comparison of Tables 8-4, 8-9, and 8-13 shows that for the 1.5-inch x 3-inch crystal α is essentially the same for K, U, and Th. For the longer 1.5-inch x 9-inch detector, α values are larger. There is no observable correlation in trends between measured and calculated α values.

THIN URANIUM BED RESULTS

Interface profile measurements of the type presented in the last section are difficult to perform because they are time-consuming, especially for smaller detectors. Furthermore, the calculation required to determine the differential shape introduces considerable noise to the result.

Better results are obtained when thin beds of the radioactive material are available. The 2-inch thick horizontal uranium bed of the Grand Junction models was used to measure the geologic impulse function for a variety of detector sizes and borehole conditions. Thin beds of potassium or thorium are not available so the differential profile responses in the K and Th models represent the only measure of potassium and thorium geologic impulse functions.

Table 8-10. Ore Zone/Upper Barren Zone Depth Profile Thorium Model
Probe 253L 1.5-inch x 3.0-inch Crystal

Depth (cm)	Apparent Grade (ppm Th)	Depth (cm)	Apparent Grade (ppm Th)	Depth (cm)	Apparent Grade (ppm Th)
20	8.2	82	115	112	469
26	8.8	84	133	114	492
32	8.1	86	177	116	484
38	10.0	88	208	118	481
44	9.8	90	257	120	477
50	13.1	92	305	122	487
56	15.6	94	338	126	488
62	21.3	96	365	130	496
66	26.4	98	398	134	497
70	35.9	100	424	138	495
72	43.3	102	433	144	487
74	51.7	104	447	150	492
76	61.1	106	462	156	499
78	82.0	108	475	162	509
80	92.3	110	473	168	511

Table 8-11. Ore Zone/Upper Barren Zone Depth Profile Thorium Model
1.5-inch x 9.0-inch Crystal

Depth (cm)	Apparent Grade (ppm)	Depth (cm)	Apparent Grade (ppm)
63	23.4	96	354
68	30.3	98	390
74	51.0	100	412
76	68.4	102	439
78	85.0	104	453
80	103	106	471
82	127	108	464
84	151	113	502
86	184	118	510
88	211	123	505
90	248	128	512
92	283	133	513
93	292	136	527
94	328	138	522
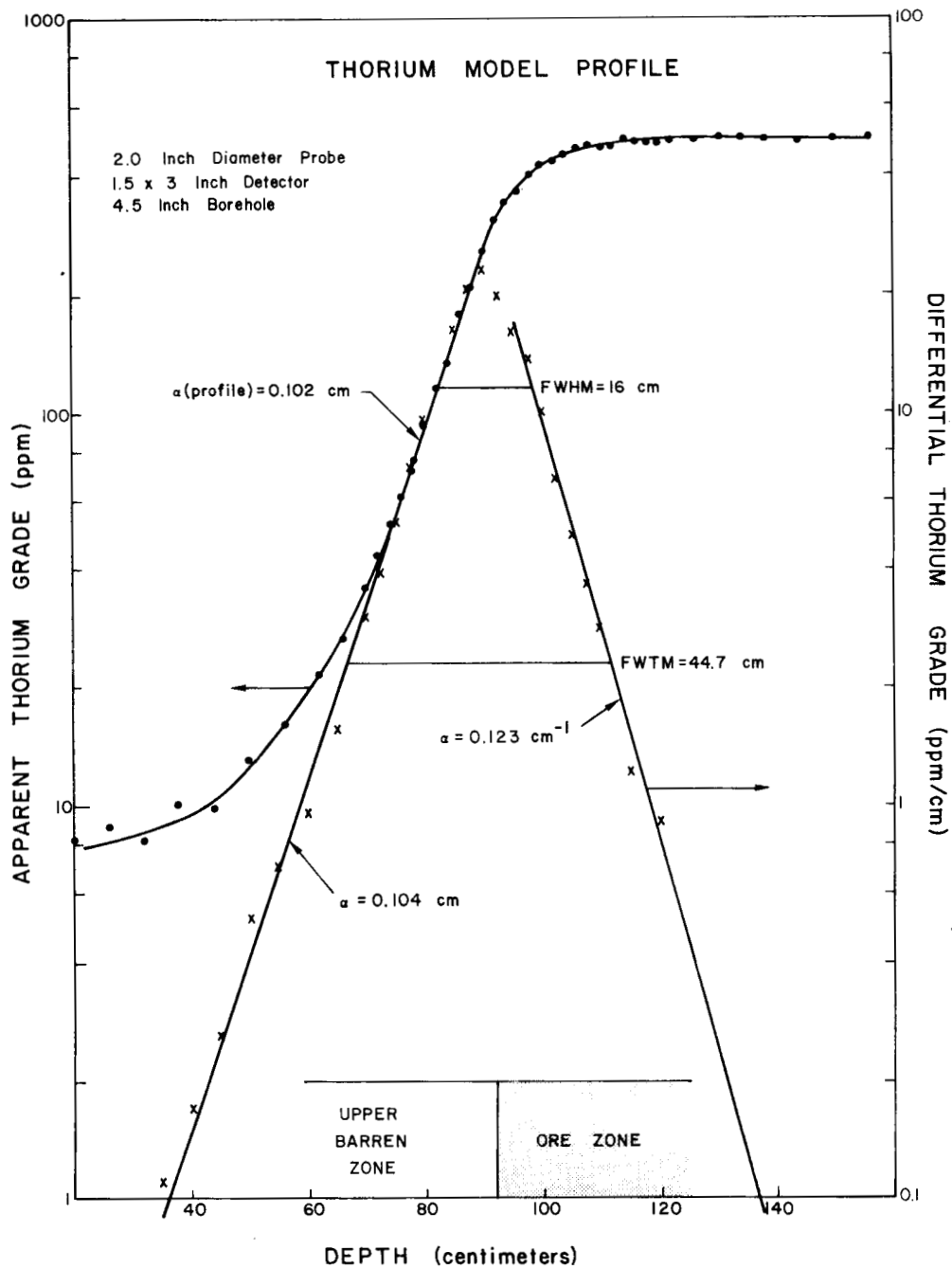
Figure 8-8. Thorium model profile and differential response for a 1.5-inch x 3-inch detector.
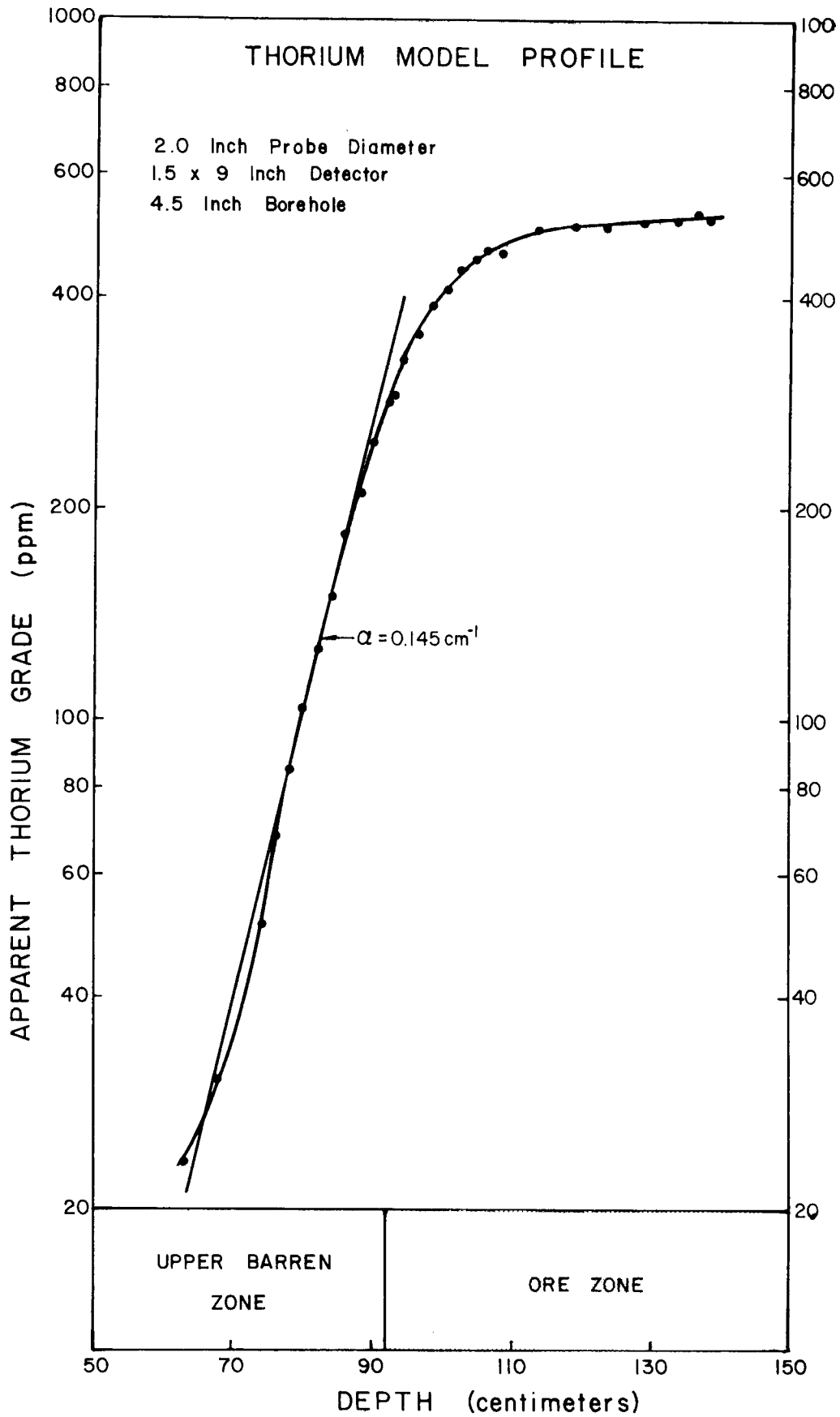
Figure 8-9. Thorium model profile for a 1.5-inch x 9-inch detector.

126
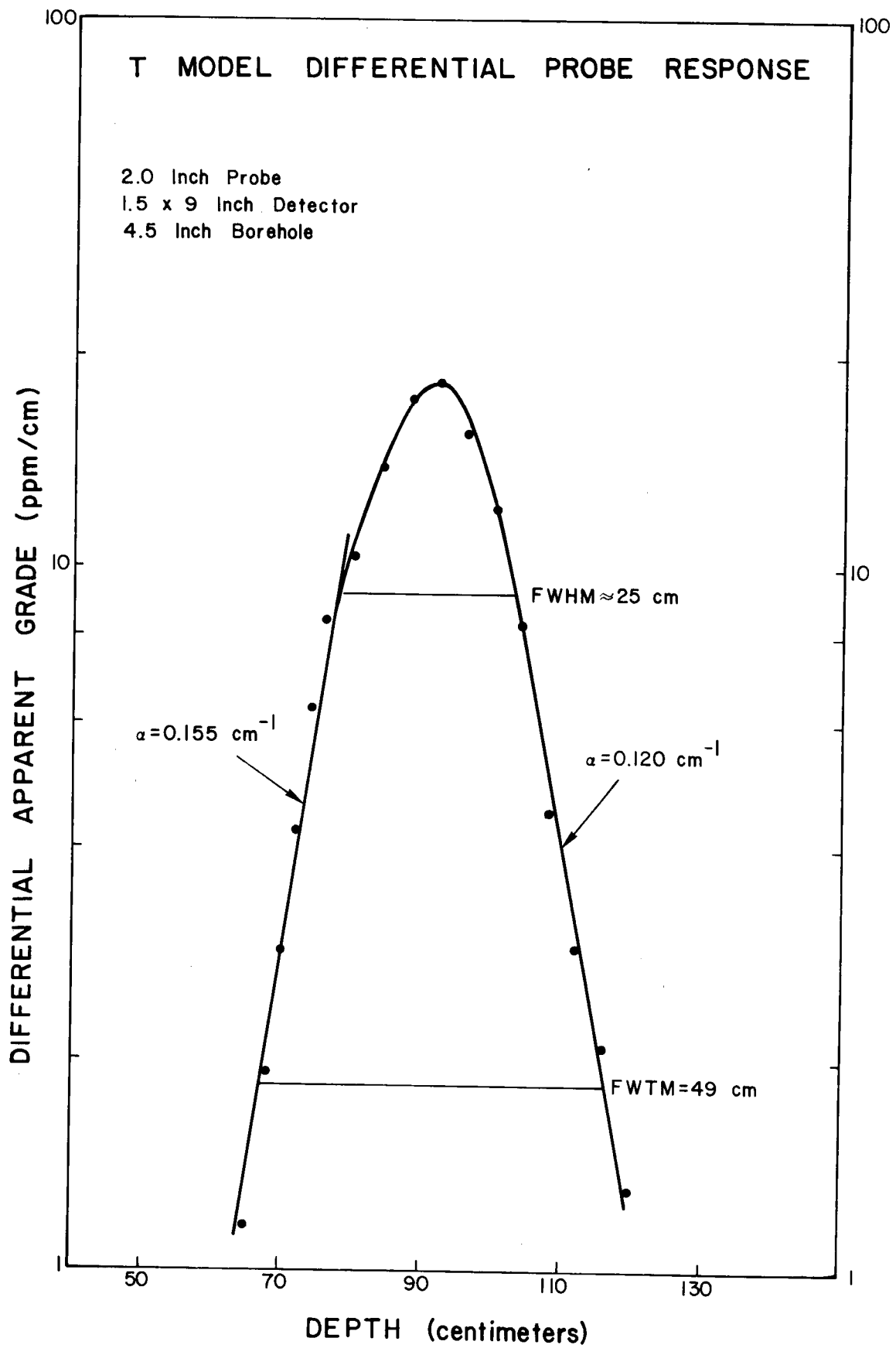
Figure 8-10. Thorium model differential response for a
1.5-inch x 9-inch detector.

Table 8-12. Ore Zone/Upper Barren Zone Depth Profile Thorium Model

1.5-inch x 3.0-inch Crystal		1.5-inch x 9.0-inch Crystal	
Depth (cm)	Differential Grade (ppm/cm)	Depth (cm)	Differential Grade (ppm/cm)
25	0.06	65	1.16
30	0.09	68	1.93
35	0.11	70	2.88
40	0.17	72	4.25
45	0.26	74	6.35
50	0.52	76	8.47
55	0.70	80	10.4
60	0.96	84	14.0
65	1.6	88	17.3
70	3.0	92	18.3
72.5	3.9	96	15.7
75	5.2	100	12.2
77.5	7.2	104	8.3
80	9.6	108	4.5
82.5	12.5	112	2.9
85	16.2	116	2.1
87.5	20.6	120	1.3
90	23.0	130	0.9
92.5	19.6		
95	16.0		
97.5	13.4		
100	10.0		
102.5	6.8		
105	4.8		
107.5	3.6		
110	2.8		
115	1.2		
120	0.9		

Table 8-13. α Parameter for Thorium Model

Detector Size (inches)	Measured α (cm^{-1})		Calculated α (cm^{-1})	
	Upper Barren Zone	Ore Zone	Upper Barren Zone	Ore Zone
1.5 x 3	0.104	0.123	0.096	0.089
1.5 x 9	0.155	0.120		

1.5-inch x 9-inch Detector

The first attempt to perform a KUT measurement in the thin uranium bed occurred in 1978. The 1.5-inch x 9-inch detector was used for these measurements and results were presented in Table 5-2 and Figure 5-5 of Technical Note 5. Since then, it was realized that the barren zone uranium content of 3.5 ppm should be subtracted from the results. When this correction is made, the probe response of Figure 8-11 results. Corrected numerical results are given in Table 8-14. Comparing Figure 8-11 to Figure 5-5 of Technical Note 5, the most obvious effect is that now the curve is more nearly exponential for larger distances on either side of the thin bed. Also, the full width at half maximum (FWHM) has dropped by 1 cm to 25 cm and the full width at tenth maximum (FWTM) has dropped by 2 cm to 53 cm. The α parameters obtained from the linear portions of the curve are given on Figure 8-11. The average value of 0.116 cm^{-1} is slightly lower than the average value of 0.123 cm^{-1} from the uranium model differential profile results of Table 8-9. This difference is probably due to the slightly lower bulk density of the thin bed barren zone.

1.5-inch x 3-inch Detector

Thin bed measurements for this detector were performed with and without a 7 inch long by 0.25-inch thick lead filter surrounding the detector. The lead filter was required for later measurements in the high grade uranium zones of model N5. Separate calibrations were performed for each configuration to obtain apparent grades. Results are given in Table 8-15 and plotted in Figures 8-12 and 8-13. There is very little difference in geologic impulse function with and without the filter although the filtered response is slightly wider at one-tenth maximum (55.6 cm versus 54 cm).

Table 8-14. KUT Probe Response to a Thin Uranium Bed Perpendicular to the Borehole 2.0-inch Probe Diameter 1.5-inch x 9-inch Crystal 2-inch Bed Thickness 4.5-inch Diameter Dry Borehole

Borehole Position (cm)	Apparent Grade* (ppm U)	Borehole Position (cm)	Apparent Grade* (ppm U)
(east) 76.2	-0.6	2.5	346.6
61.0	0.7	5.1	324.4
53.3	1.9	7.6	280.3
45.7	4.4	10.2	225.1
38.1	10.9	12.7	173.8
30.5	23.6	15.2	131.6
25.4	42.1	17.8	94.6
20.3	74.5	20.3	69.9
17.8	101.8	25.4	39.4
15.2	139.1	33.0	16.6
12.7	192.2	40.6	7.2
10.2	251.8	50.8	2.1
7.6	303.5	61.0	0.2
5.1	337.6	(west) 76.2	-0.7
2.5	356.4		
(thin bed) 0	362.3		

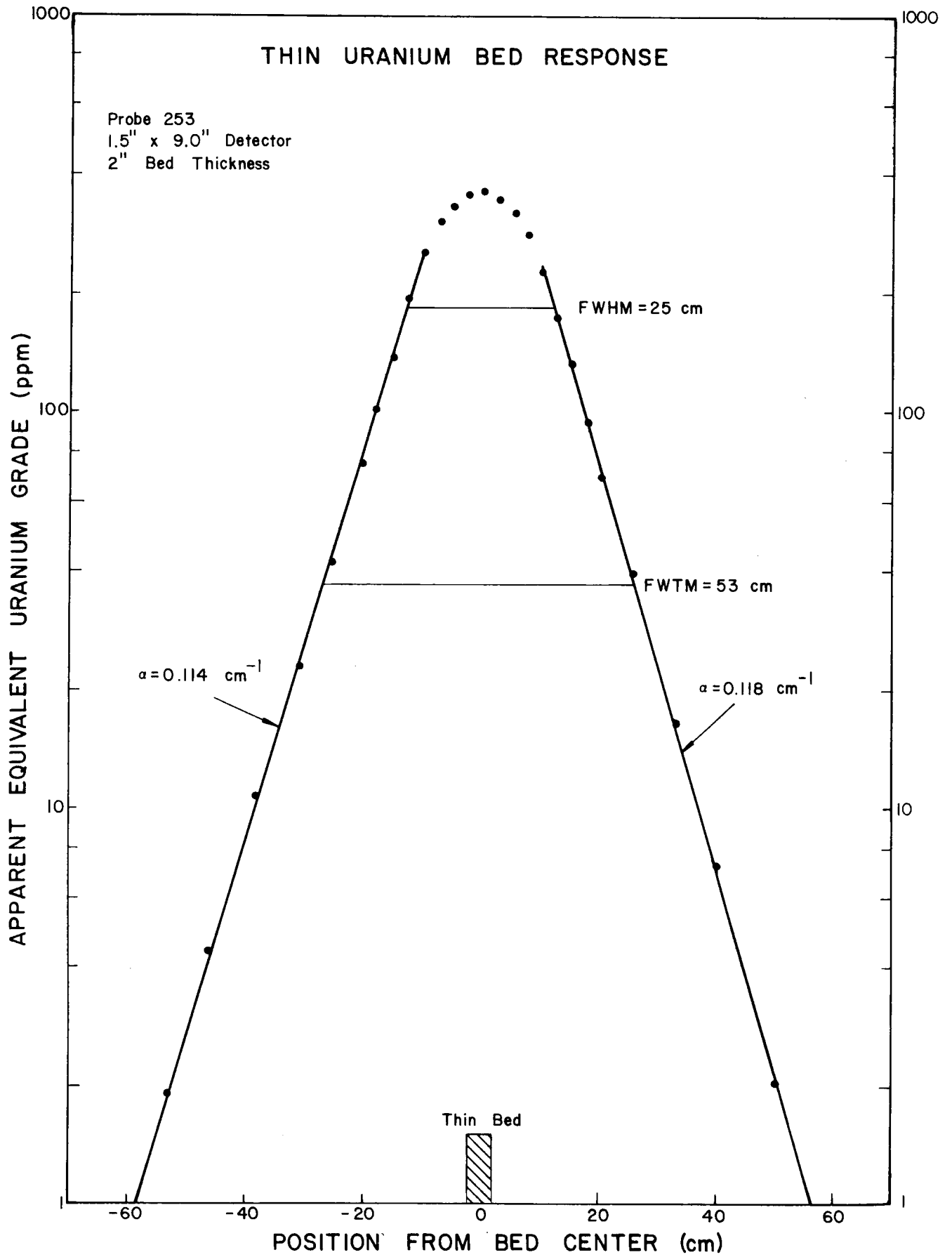*Barren zone uranium content of 3.5 ppm U has been subtracted from these data.

Figure 8-11. Thin uranium bed response for a 1.5-inch x 9-inch detector.

Table 8-15. KUT Probe Response to a Thin Uranium Bed Perpendicular to the Borehole 2.0-inch Probe Diameter 1.5-inch x 3-inch Crystal 2-inch Bed Thickness 4.5-inch Diameter Dry Borehole

Borehole Position (cm)	Apparent Grade* (ppm U)		Borehole Position (cm)	Apparent Grade* (ppm U)	
	Unfiltered	1/4-inch Lead		Unfiltered	1/4-inch Lead
(east) 90	3.2		0 (thin bed)	516.4	515.0
80	2.0		2	484.8	485.0
70	3.6		4	434.3	440.7
60	6.6		6	376.5	368.5
50	9.4	12.4	8	319.9	313.1
40	16.0	23.5	10	257.8	254.2
35	29.3	32.5	12	211.4	206.0
30	41.0	48.7	14	171.7	163.6
25	68.0	72.6	19	107.2	101.2
20	109.5	-	24	66.2	63.5
18	130.9	141.6	29	42.1	44.1
16	162.9	164.7	34	28.6	30.4
14	198.3	198.3	39	18.6	30.8
12	238.5	239.6	49	9.4	11.7
10	290.6	300.6	59	3.7	7.2
8	347.2	356.8	69	3.3	3.7
6	405.4	416.4	79	3.9	4.5
4	488.5	464.9	89 (west)	3.5	4.8
2	506.2	499.2			

*Barren zone uranium content of 3.5 ppm U has been subtracted from these data.

Values for the parameter α have been computed from the plots of Figure 8-12 and 8-13. The average α value is 0.095 cm^{-1}. This is significantly smaller than the 0.116 cm^{-1} value obtained for the 9-inch long detector.

2-inch x 5-inch Detector

Thin bed measurements for this detector were performed with and without a water-filled borehole. Results are given in Table 8-16 and are plotted in Figures 8-14 and 8-15 for dry and water-filled boreholes, respectively.

For the dry borehole case, the average α value is 0.112 cm^{-1}. For the water-filled borehole, the average value of the α parameter is 0.118 cm^{-1}. This represents a "sharpening" of several percent in the impulse function when the borehole is water-filled. The apparent grade measured with the water-filled borehole is systematically lower because the probe was calibrated for a dry borehole.

THIN URANIUM BED RESPONSE

Probe 253
1.5" x 3.0" Detector
2" Bed Thickness

FWHM = 21 cm

$\alpha = 0.095$ cm^{-1}

$\alpha = 0.099$ cm^{-1}

FWTM = 54 cm

Thin
Bed

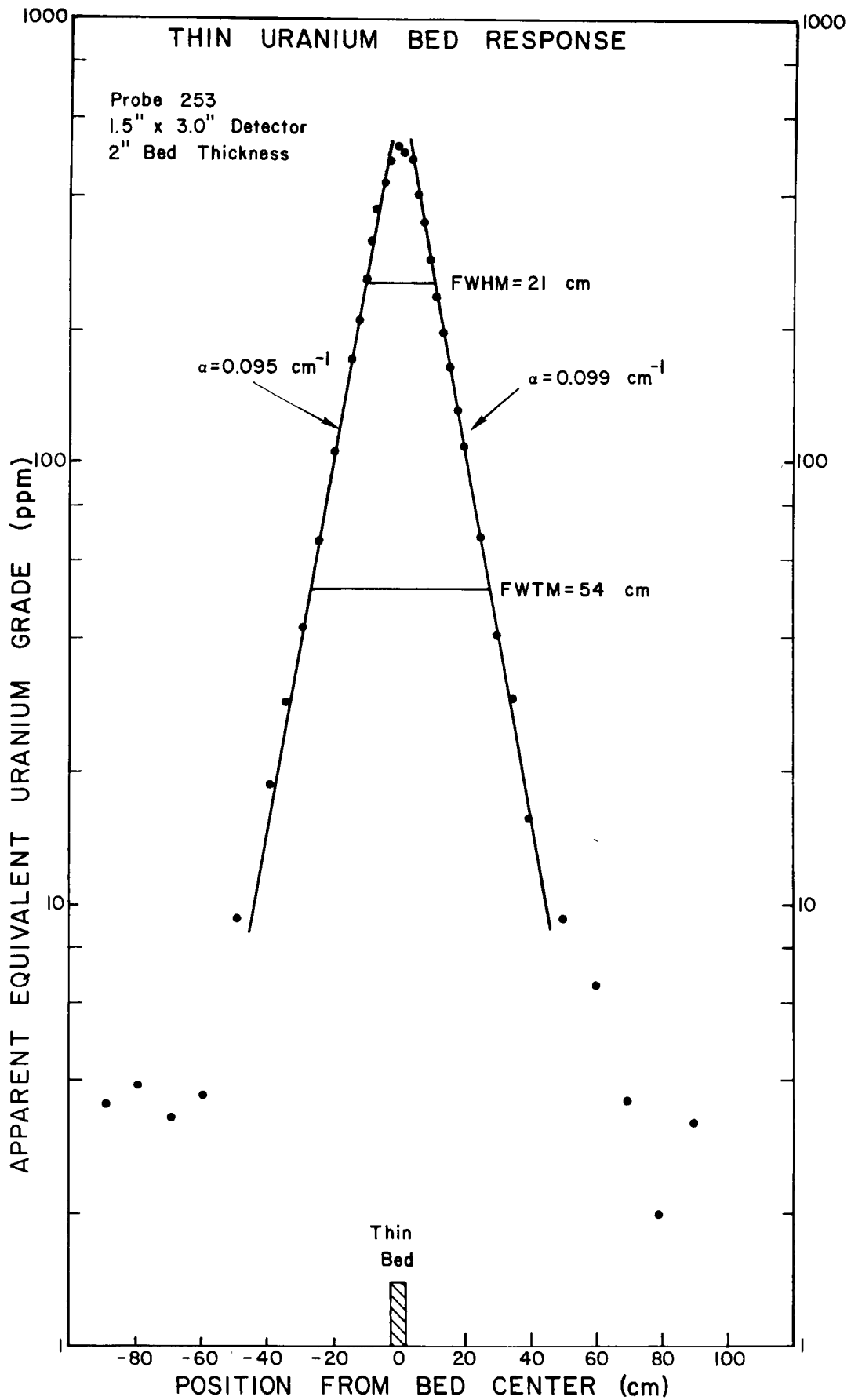APPARENT EQUIVALENT URANIUM GRADE (ppm)

POSITION FROM BED CENTER (cm)

Figure 8-12.   Thin uranium bed response for a
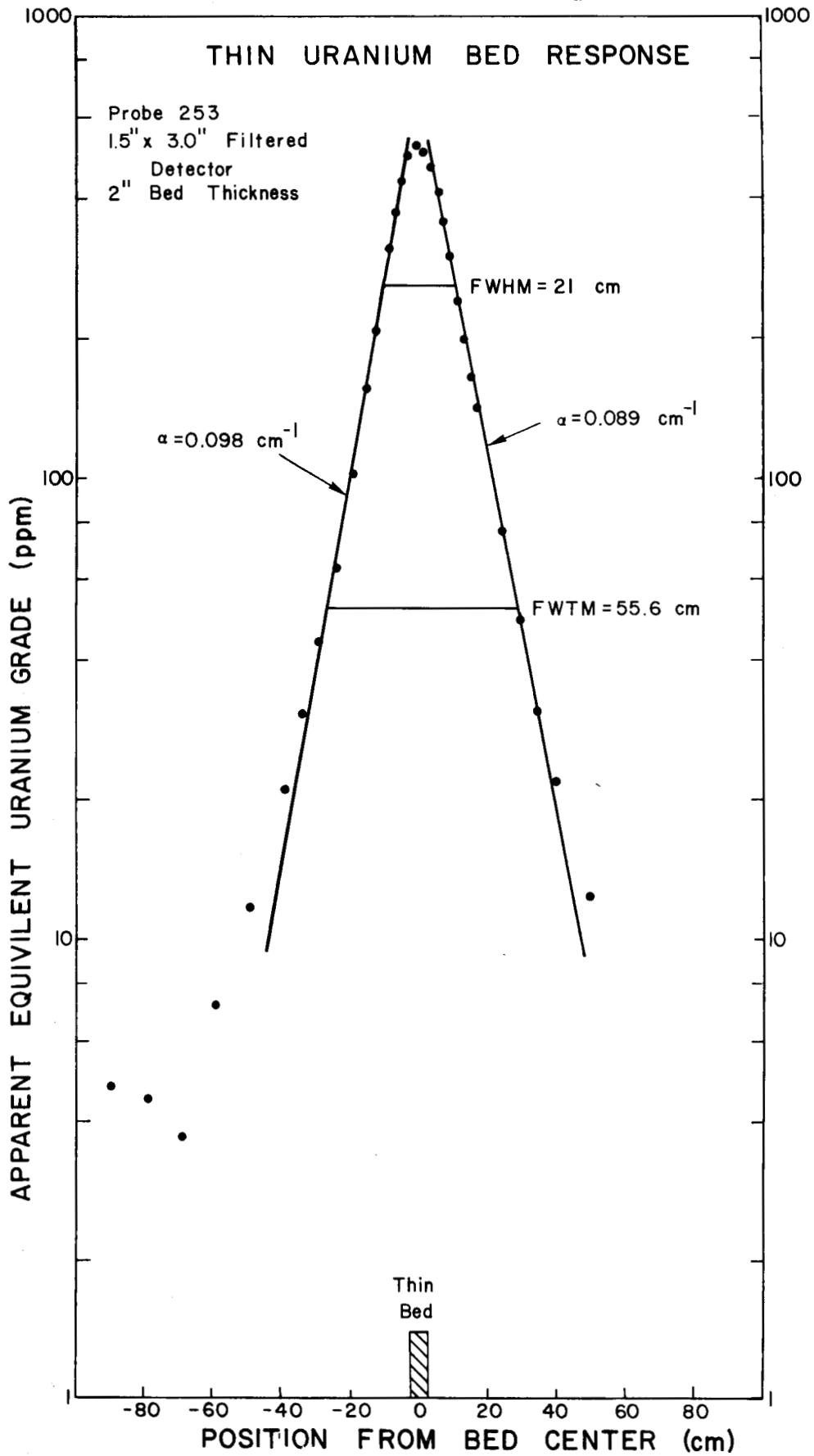1.5-inch x 3-inch detector.

132

Figure 8-13.   Thin uranium bed response for a
1.5-inch x 3-inch filtered
detector.

Table 8-16. KUT Probe Response to a Thin Uranium Bed Perpendicular
to the Borehole 2.675-inch Probe Diameter 2-inch x 5-inch Crystal
2-inch Bed Thickness 4.5-inch Diameter Borehole

Borehole Position (cm)	Apparent Grade* (ppm U)		Borehole Position (cm)	Apparent Grade* (ppm U)	
	Dry Borehole	Water Filled Borehole		Dry Borehole	Water Filled Borehole
122 (east)	3.1	3.0	2.5	427.0	397.5
107	2.5	2.7	5.1	351.0	325.0
91.4	2.8	3.0	7.6	264.1	249.9
76.2	3.3	2.9	10.2	194.0	175.2
61.0	4.5	3.5	12.7	140.1	130.6
50.8	6.2	5.1	15.2	105.3	94.5
40.6	12.2	9.6	17.8	79.6	69.7
30.5	28.4	23.2	20.3	58.4	51.2
25.4	47.2	38.9	25.4	34.5	29.6
20.3	80.9	68.3	30.5	21.0	17.9
17.8	108.4	91.6	40.6	9.7	7.7
15.2	144.7	124.7	50.8	6.2	4.5
12.7	197.6	167.1	61.0	4.2	3.1
10.2	264.9	231.8	76.2	3.7	3.2
7.6	345.0	308.1	91.4	3.9	3.3
5.1	431.3	378.6	107	6.1	4.5
2.5	469.4	429.3	122 (west)	12.7	10.1
0 (thin bed)	468.0	431.2			

*Barren zone uranium content of 3.5 ppm U has been subtracted from these data

If the area under each curve is measured for the distance range of ±40
centimeters, the ratio of dry/water-filled areas is 1.14. This compares
favorably with the water factor correction of 1.17 obtained for this probe and
borehole diameter from the thick bed measurements presented in Technical Note
3. The agreement of these results indicates that the thick bed water factor
corrections measured in the KUT water factor model can be applied to thin bed
results as well.

1-inch x 2-inch Detector

The thin bed response function for this detector and for a dry borehole is
tabulated in Table 8-17 and plotted in Figure 8-16. The average value of α
obtained from this plot is 0.108 cm^{-1}. This result is in excellent
agreement with the value 0.104 cm^{-1} computed from the theoretical results of
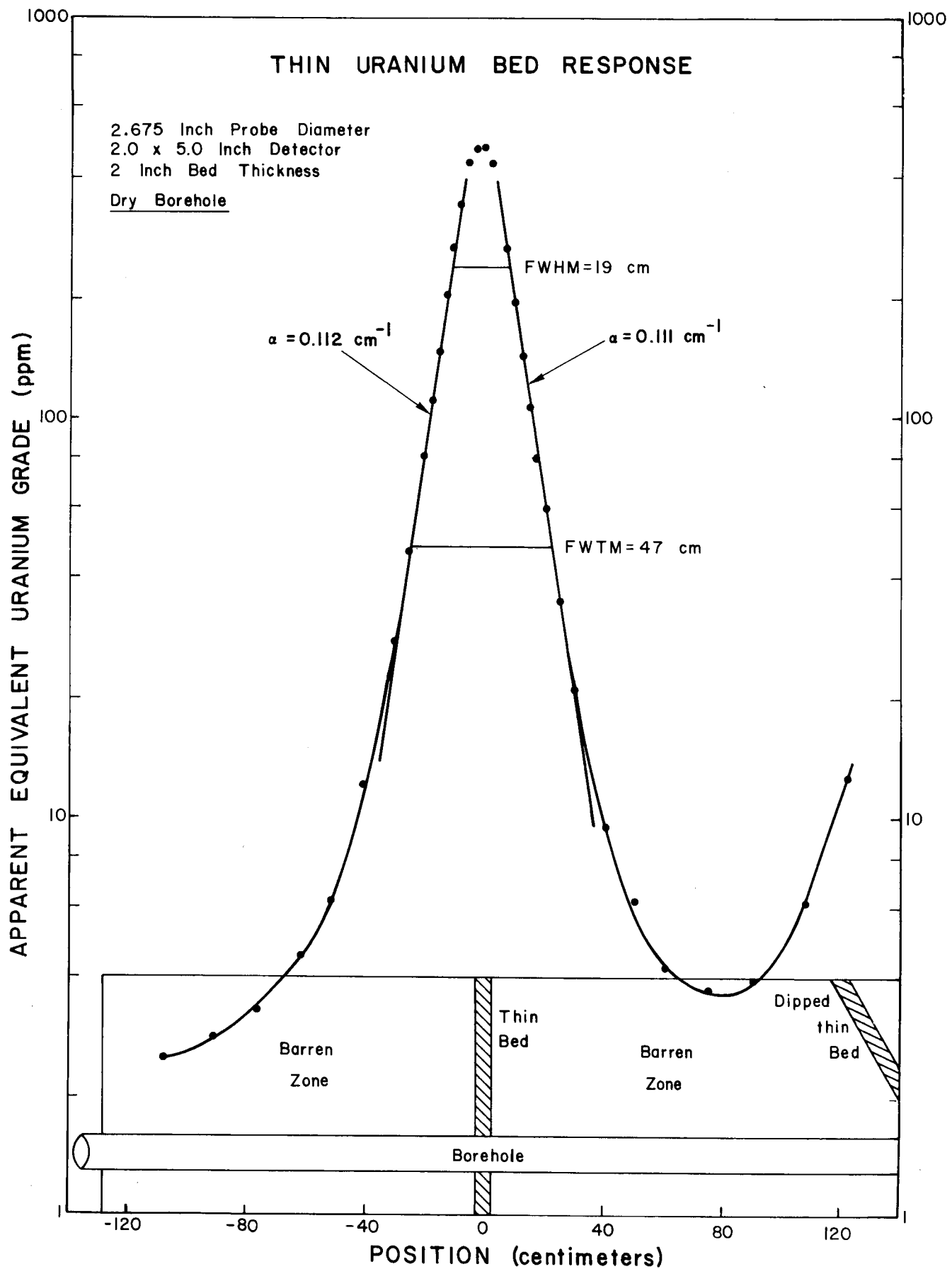Czubek.

Figure 8-14. Thin uranium bed response for a 2-inch x 5-inch detector and dry borehole.
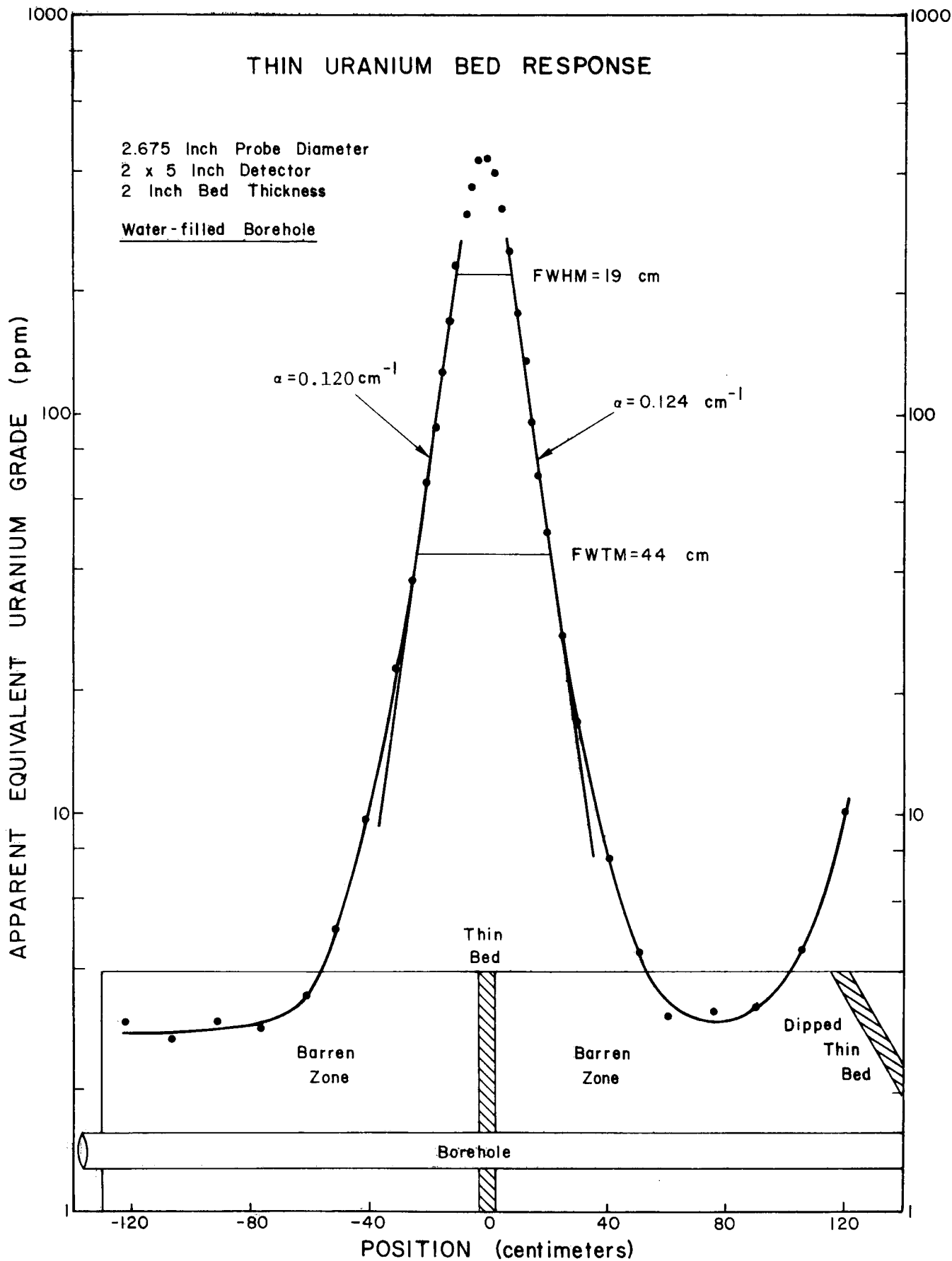
Figure 8-15. Thin uranium bed response for a 2-inch x 5-inch detector and a water-filled borehole.

Table 8-17. KUT Probe Response to a Thin Uranium Bed Perpendicular
to the Borehole 2.0-inch Probe Diameter 1-inch x 2-inch Crystal
2-inch Bed Thickness 4.5-inch Diameter Dry Borehole

Borehole Position (cm)	Apparent Grade* (ppm U)	Borehole Position (cm)	Apparent Grade* (ppm U)
91.4 (east)	4.8	2.5	460.5
76.2	5.1	5.1	370.3
61.0	6.8	7.6	282.1
50.8	8.2	10.2	212.3
40.6	13.9	12.7	165.4
30.5	28.8	15.2	128.2
25.4	48.5	17.8	94.1
20.3	71.3	20.3	75.1
17.8	94.4	25.4	43
15.2	126.1	30.5	29.8
12.7	164.1	40.6	15.9
10.2	222.1	50.8	10.5
7.6	301.8	61.0	8.3
5.1	397.8	76.2	6.0
2.5	486.1	91.4 (west)	6.3
0 (thin bed)	526		

*Barren zone uranium content of 3.5 ppm U has been subtracted from these
results.

INTERPRETATION AND SUMMARY OF MEASUREMENTS

Measured and calculated values of the geologic impulse parameter α for the
various detector sizes and borehole conditions are summarized in Table 8-18.
This table also contains the value of full width at half-maximum (FWHM) and at
tenth-maximum (FWTM) for all measured impulse functions. Measured α values
were in all cases determined from linear portions of a semilogarithmic plot on
either side of the geologic impulse function. For the differential profile
type measurement, this linear portion occurred either in the ore zone or in
the upper barren zone. For the thin bed type of measurement, it occurs either
east or west of the thin bed location. For a given gamma-ray signal, the
differences in computed α values for these different regions are caused by the
difference in bulk density reported for the concrete and ore mixture. For
example, the reported bulk density in the upper barren zone of the K model is
2.23 gm/cc while in the ore zone the density is 1.86 gm/cc. This means the
1.46 MeV potassium gamma ray is more heavily attenuated in the upper barren
zone, and hence the predicted α is larger (see Table 8-18). If all bulk
densities and compositions were identical, then calculated α values would be
identical for a given signal window and would systematically decrease from
potassium to thorium energies. This trend is not observed in Table 8-18
because of variations in bulk density. Further, measured α values do not
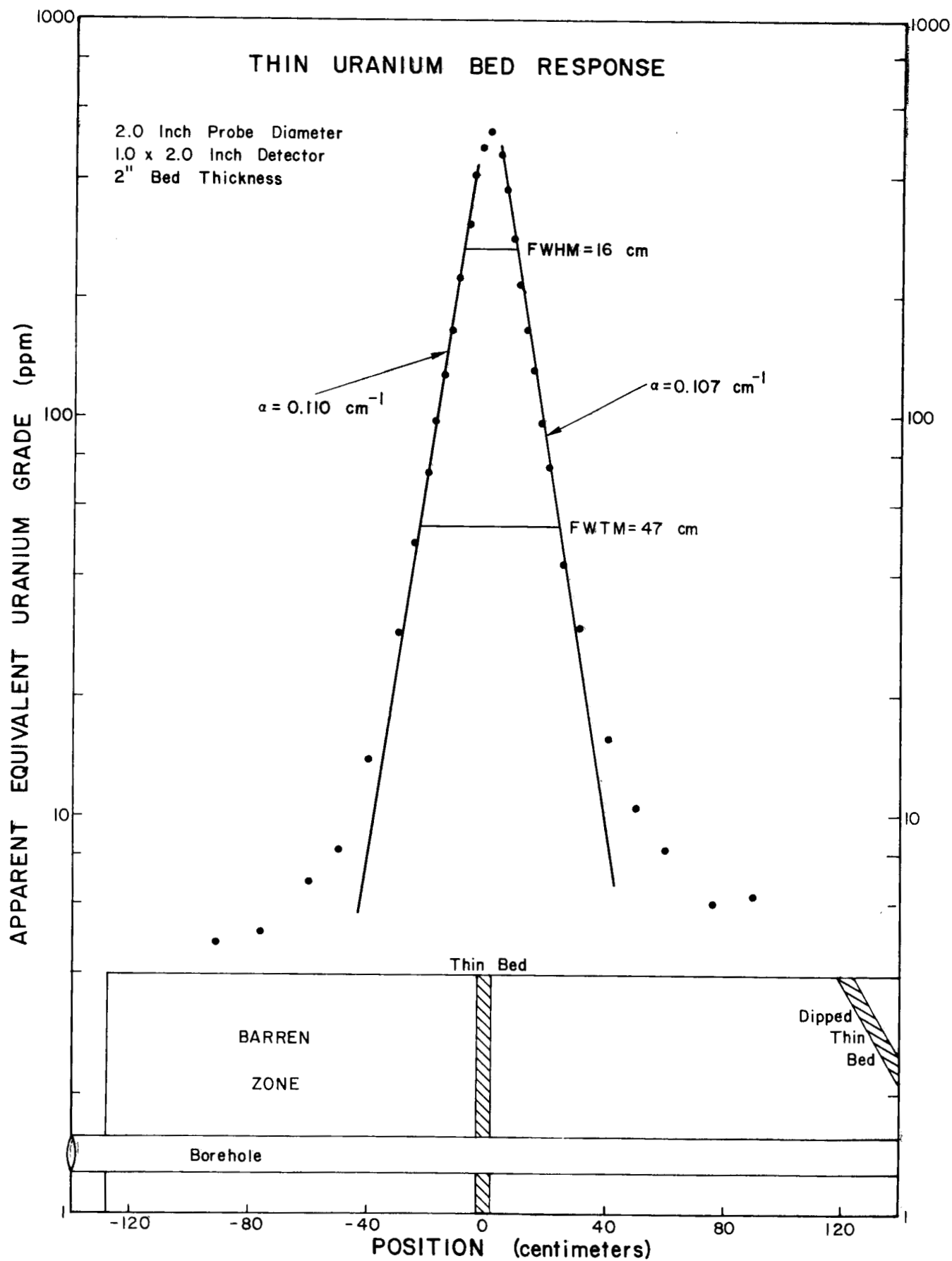
Figure 8-16.   Thin uranium bed response for a 1-inch x 2-inch detector.

Table 8-18. Geologic Impulse Parameter α

Gamma-Ray Signal Window (keV)	Measurement Type	Detector Size (Inches)	4.5-Inch Borehole Condition	FWHM (cm)	FWTM (cm)	Parameter α (cm^{-1})			
						Measured		Calculated	
						Ore Zone	Barren	Ore Zone	Barren
Potassium (1320-1575)	K Model Differential Profile	1.5 x 3	Dry	16.7	46	0.122	0.101	0.102	0.113
		1.5 x 9	Dry	25.5	49	0.139	0.146		
Uranium (1650-2390)	U Model Differential Profile	1.5 x 3	Dry	15.8	44.5	0.114	0.110	0.116	0.108
		1.5 x 9	Dry	26.9	53.3	0.115	0.131		
						West	East		
	Thin Horizontal U Bed	1 x 2	Dry	16	47	0.107	0.110	0.104	
		2 x 5	Dry	19	47	0.112	0.111		
		2 x 5	Water-Filled	19	44	0.120	0.124		
		1.5 x 3	Dry	21	54	0.095	0.099		
		1.5 x 3 (Filtered)	Dry	21	56	0.098	0.089		
		1.5 x 9	Dry	25	53	0.118	0.114		
						Ore Zone	Barren	Ore Zone	Barren
Thorium (2475-2765)	Th Model Differential Profile	1.5 x 3	Dry	16	44.7	0.123	0.104	0.089	0.096
		1.5 x 9	Dry	25	49	0.120	0.155		

follow the variations predicted by the calculations. For example, the measured α values for the thorium signal are comparable to those observed for the potassium signal; measured α values are often lower in the higher density zones, in disagreement with prediction.

Certain trends in the value of α are apparent. There is a systematic increase in α with increasing detector length for the 1.5-inch diameter detector. This effect is observed for all the signal windows and for all measurement types. The detector shape and resulting variations in angular sensitivity seem to play a more important role in determining the α parameter than do the transport properties of the gamma rays themselves. The longer detectors exhibit reduced sensitivity for gamma rays directed along the axis, and since the incident flux of gamma rays is directed more nearly along the axis for large distances from the thin bed and for the upper barren zones of the K, U, and Th models, the detector response will drop more rapidly than the gamma-ray flux itself, resulting in values of the parameter α higher than predicted by the calculations of Czubek.

There is an apparent discrepancy in the measured values of α for the 1.5-inch x 3-inch detector. The thin bed results are about 13 percent lower than the U model differential profile results. Part of this difference (about 7 percent) can be explained by the lower barren zone bulk density of the thin bed model. The remaining discrepancy may be caused by the "finite thickness" of the thin bed (2 inches thick). This conclusion is reinforced by the fact that for the long 1.5-inch x 9-inch detector, where the 2-inch bed thickness should appear truly thin, the difference between thin bed and U model profile α values is very close to the 7 percent predicted by the bulk density difference of the models.

STATIC KUT LOG OF MODEL N-5

Presentation of Results

Using the Mt. Sopris Model 3000 portable logger and a BFEC spectral gamma-ray probe, a static KUT log was acquired for Grand Junction Model N5 with no water in the borehole. The depth encoder for this unit is calibrated in feet so measurement intervals of 0.1 feet were chosen. KUT window counts were acquired at each depth for times varying from 100 seconds in the barren zone to as short as 10 seconds in the highest grade zone. A 0.25-inch thick lead filter covered the 1.5-inch x 3-inch detector to ensure acceptable count rates in the high grade zone. The probe was calibrated with the lead filter in place using the K, U, and Th models, and apparent uranium grades were computed for each depth within N5. The resulting grade profile for N5 is contained in Table 8-19. The grade is labelled "apparent" because the static log is not deconvolved to remove the effect of the geologic impulse response. The apparent uranium grade versus depth is plotted as dots in Figure 8-17. In this figure, depth is measured from the detector center to the top of model N5. The semilogarithmic scale covers a range of 5 decades, from 1 to 100,000 ppm equivalent uranium.

140

Table 8-19. Apparent Equivalent Uranium Grade Model N-5
1.5-inch x 3-inch Filtered Detector

Depth (feet)	eU (ppm)	Depth (feet)	eU (ppm)	Depth (feet)	eU (ppm)
5.3	16.3	8.2	7803.9	11.1	4314.8
5.4	16.4	8.3	9185.5	11.2	2749.7
5.5	16.4	8.4	9827.7	11.3	2417.3
5.6	19.7	8.5	9884.5	11.4	2170.5
5.7	20.8	8.6	8643.4	11.5	2033.4
5.8	22.7	8.7	6958.3	11.6	2002.9
5.9	25.7	8.8	5144.9	11.7	1905.7
6.0	32.8	8.9	3799.6	11.8	1765.5
6.1	37.6	9.0	2944.5	11.9	1615.6
6.2	45.1	9.1	2517.2	12.0	1459.2
6.3	53.5	9.2	2454.9	12.1	1117.1
6.4	65.8	9.3	2535.6	12.2	825.1
6.5	75.9	9.4	2831.5	12.3	609.0
6.6	95.7	9.5	3219.5	12.4	435.5
6.7	116.3	9.6	3700.8	12.5	326.8
6.8	146.7	9.7	4568.0	12.6	233.3
6.9	177.9	9.8	5387.6	12.7	175.3
7.0	218.7	9.9	6480.9	12.8	138.8
7.1	280.8	10.0	7295.5	12.9	101.6
7.2	357.4	10.1	7677.4	13.0	79.5
7.3	478.5	10.2	8887.5	13.1	63.2
7.4	610.1	10.3	9087.5	13.2	51.9
7.5	785.0	10.4	7965.2	13.3	41.9
7.6	1048.3	10.5	8000.3	13.4	37.1
7.7	1392.0	10.6	7777.7	13.5	29.4
7.8	1942.9	10.7	7425.5	13.6	27.9
7.9	2828.4	10.8	7083.5	13.7	22.8
8.0	4059.5	10.9	6384.6	13.8	20.4
8.1	5802.9	11.0	5151.9	13.9	19.0

Deconvolution with the Inverse Digital Filter

The numerical values for the inverse filter operator can be computed from
Equation (3) when the parameter α is known and when the discrete depth
interval Δz is given. Since Δz was measured in units of feet, the filter
parameter α must have units of $feet^{-1}$. α values for the 1.5-inch x 3-inch
detector were determined from differential U model measurements and from thin
bed responses with and without the lead filter. These values were given in
cm^{-1} in Table 8-18. In the absence of bulk density data for model N5, the
best estimate that one can make for the parameter α is to assume the same
density as the U model and to employ the average α obtained from the U model
differential profile. This value of 0.112 cm^{-1} is modified by a factor to
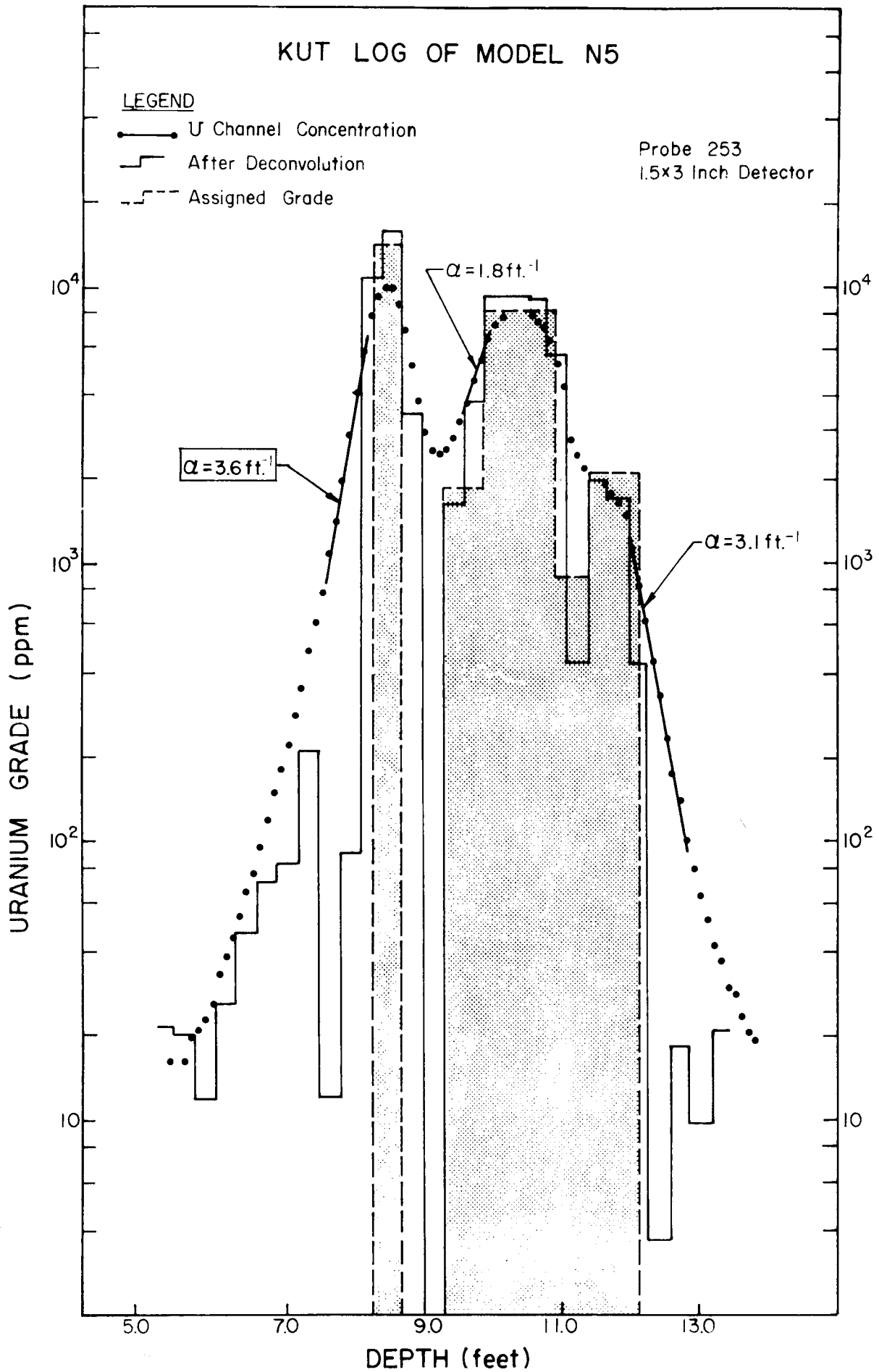account for the slight widening of the thin bed function when the lead filter
is added:

Figure 8-17. Presentation of a KUT log for model N-5 before and after spatial deconvolution with the inverse digital filter.

$$\text{Filter factor} = \frac{\text{Average thin bed } \alpha \text{ with filter}}{\text{Average thin bed } \alpha \text{ without filter}}$$

$$= \frac{0.089 + 0.098}{0.095 + 0.099} = 0.96$$

$$\alpha \text{ Estimate for N5} = (\text{Filter Factor}) \cdot (\alpha \text{ from U model})$$

$$= (0.96)(0.112)$$

$$= 0.108 \text{ cm}^{-1}$$

Or, in units of feet^{-1},

$$\alpha \text{ Estimate for N5} = 3.29 \text{ feet}^{-1}.$$

The inverse digital filter operator (equation 3) was computed for this α value and for a 0.1-foot depth interval Δz. When this filter was applied to the N5 static log, oscillatory results were obtained. α was varied in an effort to remove the oscillations but little improvement was observed. With α fixed at 3.3 feet^{-1}, the depth interval was increased to 0.3-foot, slightly larger than the 3-inch detector length. A dramatic improvement was observed although the deconvolved results tend to be negative when the apparent grade rises rapidly from near zero to very large values. The inverse filter operator from equation (3) is valid only for a point detector. In practice, this apparently limits its application to depth (or sampling) intervals which are at least as large as the detector length.

With the depth interval fixed at 0.3-foot, the parameter α was varied to values higher than estimated from the U model differential profile results. Table 8-20 contains deconvolved grade versus depth for α = 3.4, 3.6, and 3.8 feet^{-1}. The value of 3.6 feet^{-1} gives the best agreement with assigned grades and shows the best definition of the thin barren zone at 9 feet without giving strongly negative results. Figure 8-17 contains a semilogarithmic plot of the deconvolved result with the filter parameter α fixed at 3.6 feet^{-1}. For comparison, the shaded region shows the assigned grades of the several thin zones. The action of the filter is quite dramatic and shows an unidentified low grade uranium zone beginning with 12 ppm at 5.8 feet and increasing to 210 ppm at 7.13 feet.

Uncertainty exists in the official (Mathews, et al., 1978) assigned thickness for the bottom two ore zones and in the order of appearance of the barren zone at 9.0 feet and the ore zone immediately above. There is evidence from data collected by the Geologic Survey of Canada (Conaway, 1979b) and by BFEC (George, 1979b) to support the assignment shown in Figure 8-17. This assignment represents an interchange of thickness for the bottom two zones and an exchange of order for the barren zone and ore zone above the barren zone. Measurements are in progress to resolve this uncertainty. The grade assignments of Figure 8-17 are the author's best estimate as of June 1979.

Table 8-20. Equivalent Uranium Grade for Model N-5 After Deconvolution
with Inverse Filter

$$\left(-\ \frac{1}{(\alpha \Delta z)^2}\ ,\quad 1 + \frac{1}{(\alpha \Delta z)^2}\ ,\quad -\ \frac{1}{(\alpha \Delta z)^2} \right)$$

α = 3.4, 3.6, 3.8 feet $^{-1}$

Δz = 0.3 feet

Depth (feet)	Equivalent Uranium (ppm)		
	α = 3.4 ft^{-1}	α = 3.6 ft^{-1}	α = 3.8 ft^{-1}
6.1	25	26	27
6.4	44	47	49
6.7	66	72	76
7.0	67	84	98
7.3	180	213	240
7.6	-115	12	117
7.9	-244	92	370
8.2	10,583	10,290	10,031
8.5	16,436	15,736	15,132
8.8	3,113	3,338	3,520
9.1	-312	-2.4	253
9.4	1,463	1,615	1,737
9.7	3,614	3,722	3,805
10.0	9,271	9,064	8,879
10.3	9,124	9,007	8,896
10.6	9,089	8,916	8,760
10.9	5,593	5,550	5,507
11.2	186	430	632
11.5	1,976	1,981	1,982
11.8	2,002	1,678	1,926
12.1	544	430	600
12.4	28	3.7	88
12.7	31	18.2	52
13.0	16	9.7	25
13.3	26	20.5	28

The shape of the static log between 7.5 and 8 feet provides support for the choice of 3.6 feet^{-1} for α . Since this region is near the interface between a high grade ore zone and a nearly barren zone, the semilogarithmic plot should contain a linear portion whose slope is the parameter α . The computed slope is very close to 3.6 feet^{-1}, in agreement with the value obtained by varying α until the best agreement with assigned grade was obtained. Since probe and borehole conditions are the same as for the U model profile measurements, the 10 percent difference in α must be due to a bulk density or composition difference between models U and N5. Also shown on Figure 8-17 are α values computed from other portions of the static log where the semilogarithmic plot is linear. The value of 1.8 feet^{-1} obtained between 9.5 and 10 feet is clearly too low. This value was included to illustrate the fact that only near the interface between two zones of highly different grade can one hope to obtain a linear slope that is close to the correct value of α . Ideally, one of the two zones should be completely barren of uranium. Any other situation will give α estimates that are too small. The value of α obtained from the linear region between 12 and 13 feet is 3.1 feet^{-1}. Apparently, the grade differential between ore and barren zones at 12.1 feet is not sufficiently large to approach the ideal, and hence the α value is about 15 percent low.

SUMMARY

Extensive measurements of the thin bed or "geologic impulse" response have been performed for KUT borehole probes. The geologic impulse response for the potassium and thorium gamma rays were determined by differentiating K model and Th model depth profiles. The geologic impulse response for the uranium signal was determined both from U model differential profiles and from thin uranium bed measurements. A wide range of sodium iodide detector sizes was considered. The effect of a water-filled borehole was studied for the 2-inch x 5-inch detector size.

Geologic impulse responses were analyzed for the inverse digital filter parameter α . The filter parameter α appears to be more sensitive to detector size than to formation bulk density or to energy differences for the K, U, and Th gamma rays.

A static KUT log of model N5 was made with the 1.5-inch x 3-inch detector, and results were successfully deconvolved with the inverse digital filter technique. The value of parameter α required for the most satisfactory deconvolution was 3.6 feet^{-1} (0.12 cm^{-1}), 9 percent higher than the 3.3 feet-1 value from the thin bed studies.

The filter parameter for model N5 was determined directly from the semilogarighmic plot of the static log and was 3.6 feet^{-1}, exactly equal to the value obtained by trial and error variation of α. This result confirms the feasibility of determining α dynamically in the field as proposed by J. Conaway (Conaway, 1979a), by observing the slope of the logarithmic stripped count-rate versus depth curve. A major difficulty with this technique, though, is that one must make this observation near the interface between zones differing in grade by more than two orders of magnitude.

Technical Note 9

INTERPRETATION OF HIGH RESOLUTION GAMMA-RAY
TRANSPORT CALCULATIONS

INTRODUCTION

In 1976 the Grand Junction Office (GJO) of the Department of Energy (DOE)
began funding a project at the Los Alamos Scientific Laboratory (LASL) to
perform high resolution gamma-ray transport calculations for the borehole
environment. The project is continuing and is designed to assist in the
understanding and interpretation of spectral gamma-ray logging data.

This technical note discusses the results of this project as of February,
1979, and how these results impact the interpretation of KUT logging data.

INFINITE MEDIUM RESULTS

Discussion of Potassium, Equilibrium Uranium, and Thorium Spectra

Gamma-ray flux spectra were computed within infinite media of sandstone and
shale and for a variety of water saturated porosities using the gamma rays
from the naturally radioactive isotopes of potassium, equilibrium uranium, and
thorium. Figure 9-1 contains the source spectra for these three elements.
The LASL discrete ordinates transport code ONETRAN (Hill, 1975) was upgraded to
perform gamma-ray spectral calculations with 10 keV energy resolution.
Infinite medium potassium, equilibrium uranium, and thorium spectra are
presented in Figure 9-2. The medium is an idealized sandstone with zero
porosity. Similar calculations also exist for shale and for differing
porosities and water saturations. These plots illustrate the excellent energy
resolution of the calculations and that the continuum portion of each spectrum
becomes increasingly important at the lower energies. The spectra are those
which one would observe if a "perfect" gamma-ray detector was placed at any
location within an infinite medium containing uniformly distributed potassium,
equilibrium uranium, or thorium sources. There is no perfect detector, and
when, for example, a germanium or sodium iodide detector observes these
spectra, it will respond by enhancing the lower energy regions of the spectra
and by introducting additional continuum components and resolution smearing of
the spectra. LASL has developed the fast-running, Monte Carlo computer code
GAMRES (Evans, et al., 1977) to compute the effects of detector response. The
code is presently being adapted for enfolding borehole gamma-ray detector
responses with the computed spectra. The spectra of Figure 9-2 should
accurately represent the actual gamma-ray flux for energies above about 150 keV.
For lower energies, the uranium and thorium fluxes are probably somewhat low
because the effect of x-ray fluorescence from the K-shells of uranium and
thorium following photoelectric absorption have not been included in the
transport calculations.

Formation Density and Composition Effects

The three basic mechanisms for gamma ray interactions in any material are with
atomic electrons. The three mechanisms are described in Table 9-1. The
table gives the exact energy dependence for the Compton scattering process.
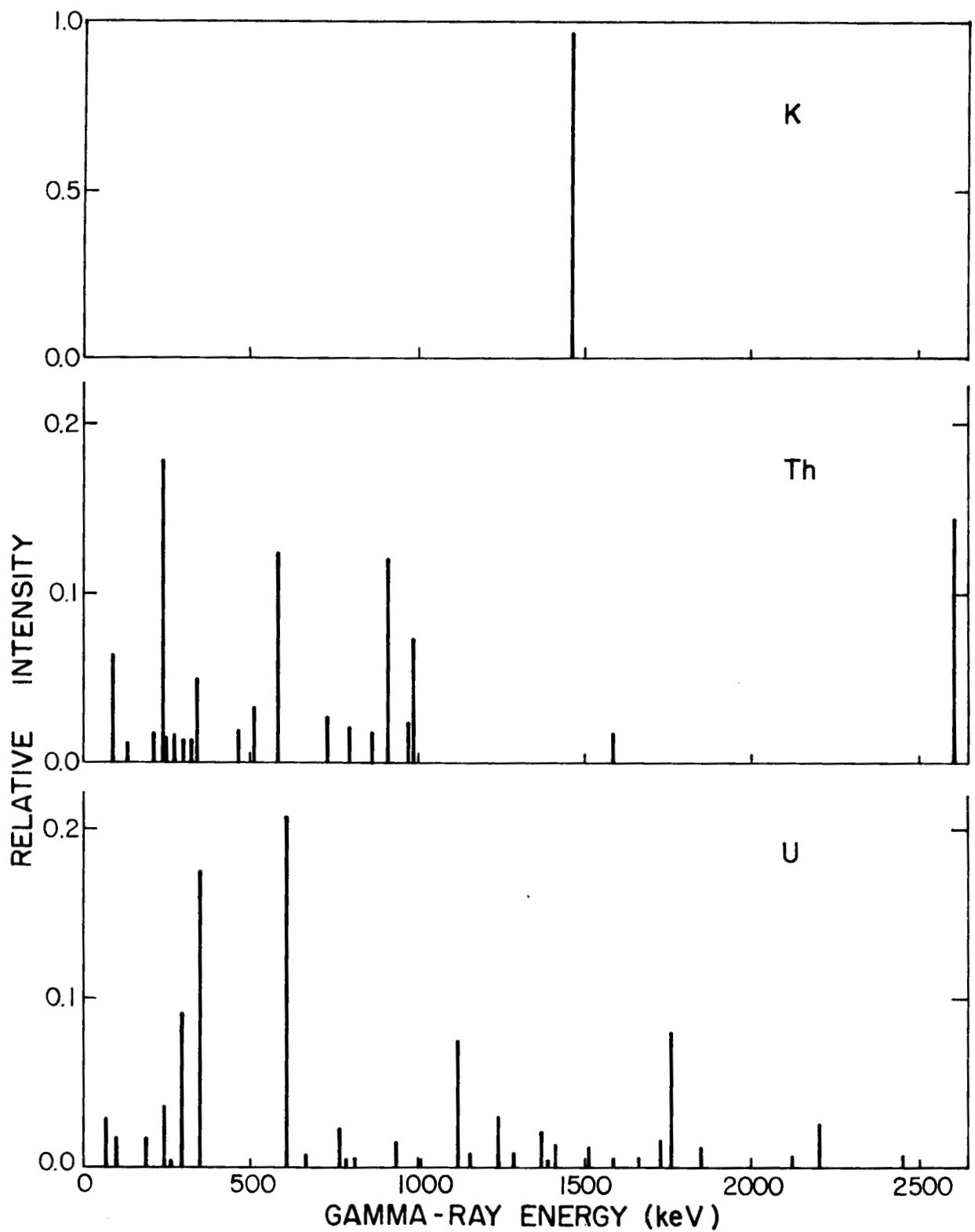
147

Figure 9-1. Gamma-ray source energies and relative intensities for borehole transport calculations.
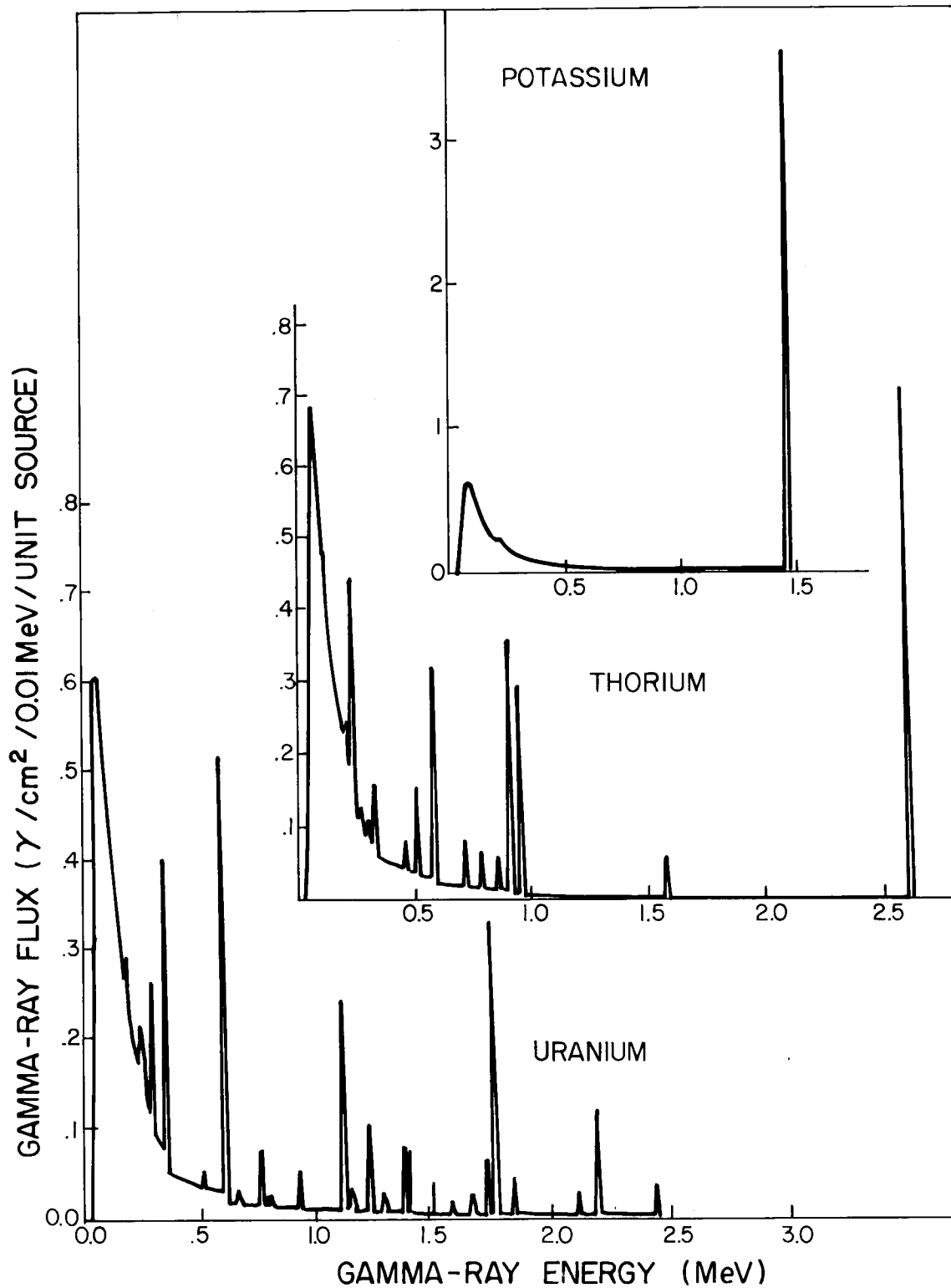
Figure 9-2. Calculated spectra for potassium, equivalent uranium and thorium sources uniformly distributed in an infinite sandstone medium.

Table 9-1. Gamma-Ray Interaction Mechanisms (Per Atom)*

Interaction Type	Atomic Number Z Dependence	Gamma-ray Energy E Dependence	Energy at which one-half of Interactions are by this Type (Z=13)
Photoelectric Effect	Z^n n=4 at 0.1 MeV n=4.6 at 3 MeV	E^3	0.046 MeV
Compton Effect	Z	$\frac{1+E}{E^3}\left[\frac{2E(1+E)}{1+2E} - \ln(1+2E)\right]$ $+ \frac{1}{2E}\ln(1+2E) - \frac{1+3E}{(1+2E)^2}$	Dominates range $0.1 \leq E < 10$ MeV
Pair Production	Z^2	Threshold at 1.02 MeV and weakly increasing with E	15 MeV

*Analytical expressions are taken from (Evans, 1955)

This energy dependence is complicated in form but does not yield a strong variation over the energy range 0.1 to 10 MeV where Compton scattering tends to dominate the gamma-ray attenuation process. This range of dominance for the Compton effect is valid for atomic number Z=13 (aluminum), and this is typical of the average Z for geologic formations. Table 9-1 also contain the approximate Z and E dependence of the photoelectric and pair production mechanisms. For higher values of Z the energy at which the photoelectric effect produces one-half of the total interactions increases as shown in Table 9-2.

Table 9-2. Energy at Which Photoelectric Effect
Provides One-Half the Total Absorption Coefficient (Shaeffer, 1973)

Element	Z	E (MeV)
A	13	0.046
Ca	20	0.079
Fe	26	0.11
Pb	82	0.50
U	92	0.62

For typical geologic formations, Z ranges from 12 to 18. One can assume then that the single interaction mechanism of importance over the range from about 0.1 MeV to 10 MeV is Compton scattering. When high grade uranium zones or zones of other high Z materials are encountered, the lower limit of this "Compton range" must be increased.

Table 9-1 shows that the Compton interaction probability, or cross section, per atom varies directly with Z. This is because the cross section per electron σ_{ce} (cm^2/electron) is a constant and there are Z electrons per atom. For a mixture of n elements with atomic number Z_i for each species, the average Compton cross-section per centimeter is:

$$\mu_{ce}(cm^{-1}) = \sigma_{ce}(\frac{cm^2}{electron}) \sum_{i=1}^{n} N_i(\frac{atoms}{cm^3}) \ Z_i(\frac{electrons}{atom}) , \quad (1)$$

where N_i is the atomic number density for each species and the summation is over all n elements of the formation. The atomic density can be written as:

$$N_i = \frac{N_o(\frac{atoms}{GAW}) \ \rho_i(\frac{grams}{cm^3})}{A_i(\frac{grams}{GAW})} , \quad (2)$$

151

where N_0 is Avogadro's number, ρ_i is the partial density of element i, and A_i is its atomic weight. Substituting equation (2) into equation (1):

$$\mu_c (\text{cm}^{-1}) = \sigma_{ce} \, N_0 \sum_{i=1}^{n} \frac{\rho_i Z_i}{A_i} \qquad (3)$$

If one defines a partial density weighted average Z/A for the formation as follows:

$$\left(\frac{\overline{Z}}{A}\right) \equiv \frac{1}{\rho_B} \sum_{i=1}^{N} \frac{\rho_i Z_i}{A_i} \qquad (4)$$

where ρ_B is the formation bulk density and is the sum of all partial densities, then equation (3) may be rewritten:

$$\mu_c (\text{cm}^{-1}) = \sigma_{ce} N_0 \, \rho_B \left(\frac{\overline{Z}}{A}\right) \qquad (5)$$

The Compton cross section per centimeter μ_c is called the Compton linear attenuation coefficient. Similar expressions can be written for the photoelectric and pair production mechanisms, but σ_{pe} and σ_{pp} will be functions of each Z_i.

Since the Compton scattering mechanism dominates the gamma-ray interaction process for typical formations from energies of 0.1 MeV to 10 MeV, equation (5) suggests that the gamma-ray fluxes computed by LASL should scale inversely with formation bulk density ρ_B and with partial density weighted average Z/A.

LASL has verified that infinite media gamma-ray flux spectra scale exactly with the inverse of formation bulk density when composition remains unchanged. LASL has also compared gamma-ray flux ratios for the composition change resulting when water-saturated porosity is introduced to a sandstone formation. Figure 9-3 contains a plot of gamma-ray flux ratio as a function of energy for sandstone with water-saturated porosities of 0.1 and 0.3. The ratio is constant from the highest energy of interest to natural gamma-ray logging at 2.6 MeV down to an energy of about 0.1 MeV. Below this energy, the composition dependent change in the photoelectric cross-section, which increases strongly with decreasing energy (see Table 9-1), causes the flux ratio to drop rapidly because of the higher average Z of the lower porosity water-saturated formation. The constant nature of the flux ratio to 2.6 MeV indicates that pair production is unimportant to this problem, as already stated in Table 9-1. From Figure 9-3 the constant value of the flux ratio predicted by the LASL transport calculations is 0.875. This result is predicted quite accurately by inverse scaling with bulk density and average Z/A.
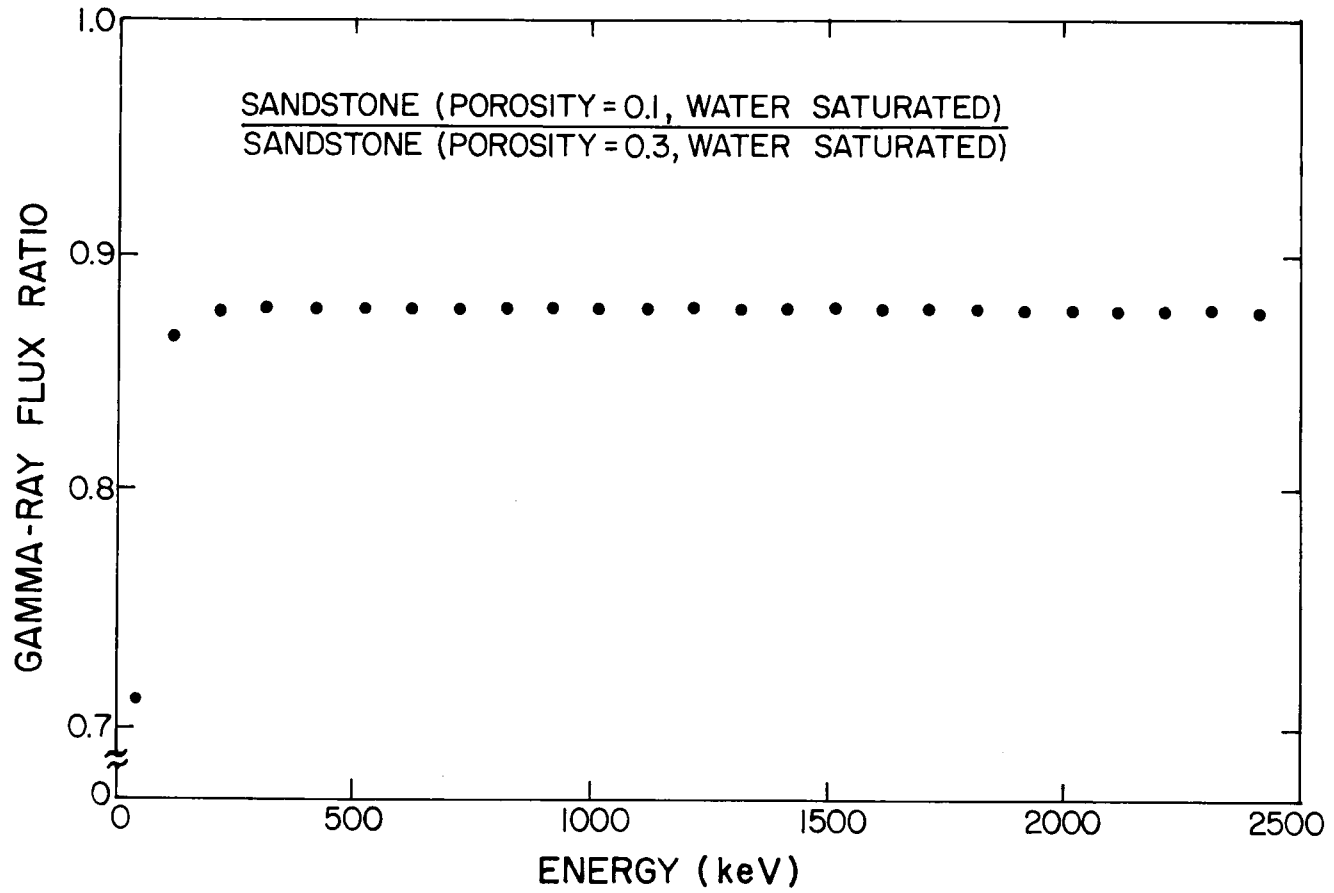
Figure 9-3. Gamma-ray flux ratio versus energy for sandstone media with water saturated porosities of 0.1 and 0.3.

The scaling factor for bulk density is computed as follows:

$$\text{Inverse bulk density ratio} = \frac{(0.7)(\text{Sandstone Matrix Density}) + (0.3)(1.0\,\text{g/cm}^3)}{(0.9)(\text{Sandstone Matrix Density}) + (0.1)(1.0\,\text{g/cm}^3)} \tag{6}$$

LASL used a sandstone matrix density of 2.6263 g/cm^3 so that the inverse ratio becomes:

$$\text{Inverse bulk density ratio} = \frac{(0.7)(2.6263) + (0.3)(1.0)}{(0.9)(2.6263) + (0.1)(1.0)} + \frac{2.1384}{2.4637} = 0.8680. \tag{7}$$

The scaling factor for average Z/A is computed as follows:

$$\text{Inverse } \left(\frac{\overline{Z}}{A}\right) \text{ ratio} = \left[\frac{(\overline{Z/A})_{\Delta\Delta}\,(0.7)(2.6263) + (\overline{Z/A})_{H_2O}\,(0.3)}{(\overline{Z/A})_{\Delta\Delta}\,(0.9)(2.6263) + (\overline{Z/A})_{H_2O}\,(0.1)} \right] \times \left[\frac{2.4637}{2.1384} \right]. \tag{8}$$

The partial density weighted average values of Z/A for sandstone and water are:

$$\left(\frac{\overline{Z}}{A}\right)_{\Delta\Delta} = 0.499$$

$$ \tag{9}$$

$$\left(\frac{\overline{Z}}{A}\right)_{H_2O} = 0.551$$

so that,

$$\text{Inverse } \left(\frac{\overline{Z}}{A}\right) \text{ Ratio} = \frac{(0.499)(1.8384) + (0.551)(0.3)}{(0.499)(2.3637) + (0.551)(0.1)} \times \frac{2.4637}{2.1384}$$

$$ \tag{10}$$

$$\text{Inverse } \left(\frac{\overline{Z}}{A}\right) \text{ Ratio} = \frac{1.0827}{1.2346} \cdot \frac{2.4637}{2.1384} = 1.0104.$$

The product of the $(\overline{Z/A})$ and bulk density inverse scaling factors from equations (7) and (10) predicts the gamma-ray flux ratio based on the change in the Compton linear attenuation coefficient:

$$\text{Flux Ratio} = (0.868)(1.0104) = 0.877. \tag{11}$$

154

The result of equation (11) is in excellent agreement with the result of 0.875 from Figure 9-3, as predicted from the LASL transport calculations.

When Compton scattering dominates the gamma-ray attenuation process, the effect of formation bulk density and composition changes on the gamma-ray flux can be accurately computed by this simple scaling technique. The development of equations (6) through (11) shows that the effect of changing formation moisture content on gamma-ray flux is principally through the change in bulk density. The change in formation $(\overline{Z/A})$ due to an increase from 10 percent to 30 percent by volume in moisture content leads to a small 1-percent change in gamma-ray flux while the resulting bulk density change leads to a 13-percent change in gamma-ray flux.

The effect of a large concentration of high Z elements, such as uranium (Z=92), has been considered explicity by LASL. Energy dependent flux ratios have been computed for uranium concentrations of 0.06, 0.2, 0.6, 2.0 and 6.0 percent uranium, by weight. The results are shown in Figures 9-4 and 9-5. The flux ratios are formed by computing the flux spectrum at the stated uranium grade and dividing by the result for the same gamma-ray source strength (Figure 9-1) but for a transport formation free of the element uranium. Formation bulk density was held constant throughout. For uranium grades less than or equal to 0.6 percent, the flux ratio is near unity from 1.0 to 2.6 MeV and begins to drop at lower energies, to about 0.98 at 0.5 MeV and to 0.95 at 0.3 MeV. This so-called "Z-effect" then amounts to a 5 percent reduction in gamma-ray flux at 0.3 MeV for a 0.6 percent uranium concentration. For uranium grades below 0.6 percent and for energies greater than 0.5 MeV, the uranium "Z effect" may be neglected. For uranium grades above 0.6 percent the Z effect is increasingly important at low energies. For the 6-percent case, the flux ratio at 0.3 MeV has decreased to about 0.7, a 30 percent drop in the gamma-ray flux. From 0.3 MeV to about 1.5 MeV, the flux ratio rises to a value of 0.975 and remains constant at higher energies (see Figure 9-4). This means that the photoelectric effect is important to energies of about 1.5 MeV when the uranium concentration is in the percent range. The constant flux ratio of 0.975 at energies above 1.5 MeV is explained by the inverse $(\overline{Z/A})$ scaling of the Compton cross section that results from the composition change.

Conclusions

The infinite medium gamma-ray transport results performed by Los Alamos have led to some important conclusions concerning formation corrections to spectral gamma-ray logs.

1. For virtually all formations of interest ($13 \leq Z < 20$) the Compton scattering process is the only significant gamma-ray attenuation mechanism for energies between 0.1 and 10 MeV.

2. The gamma-ray flux at any energy within this range will scale inversely with the formation bulk density ρ_B and with the formation $(\overline{Z/A})$.
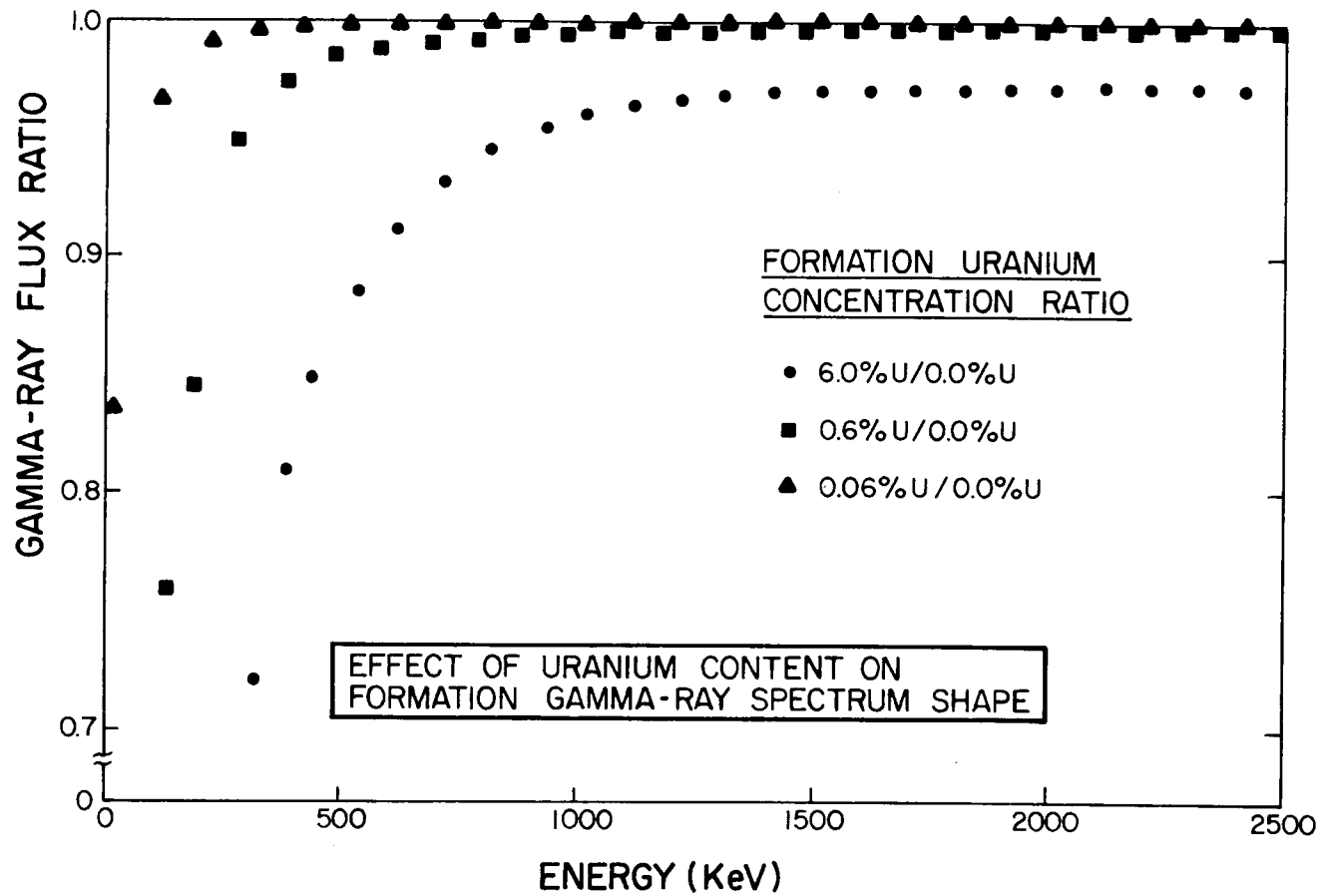
Figure 9-4. Gamma-ray flux ratio versus energy for sandstone media
containing differing uranium concentrations with the
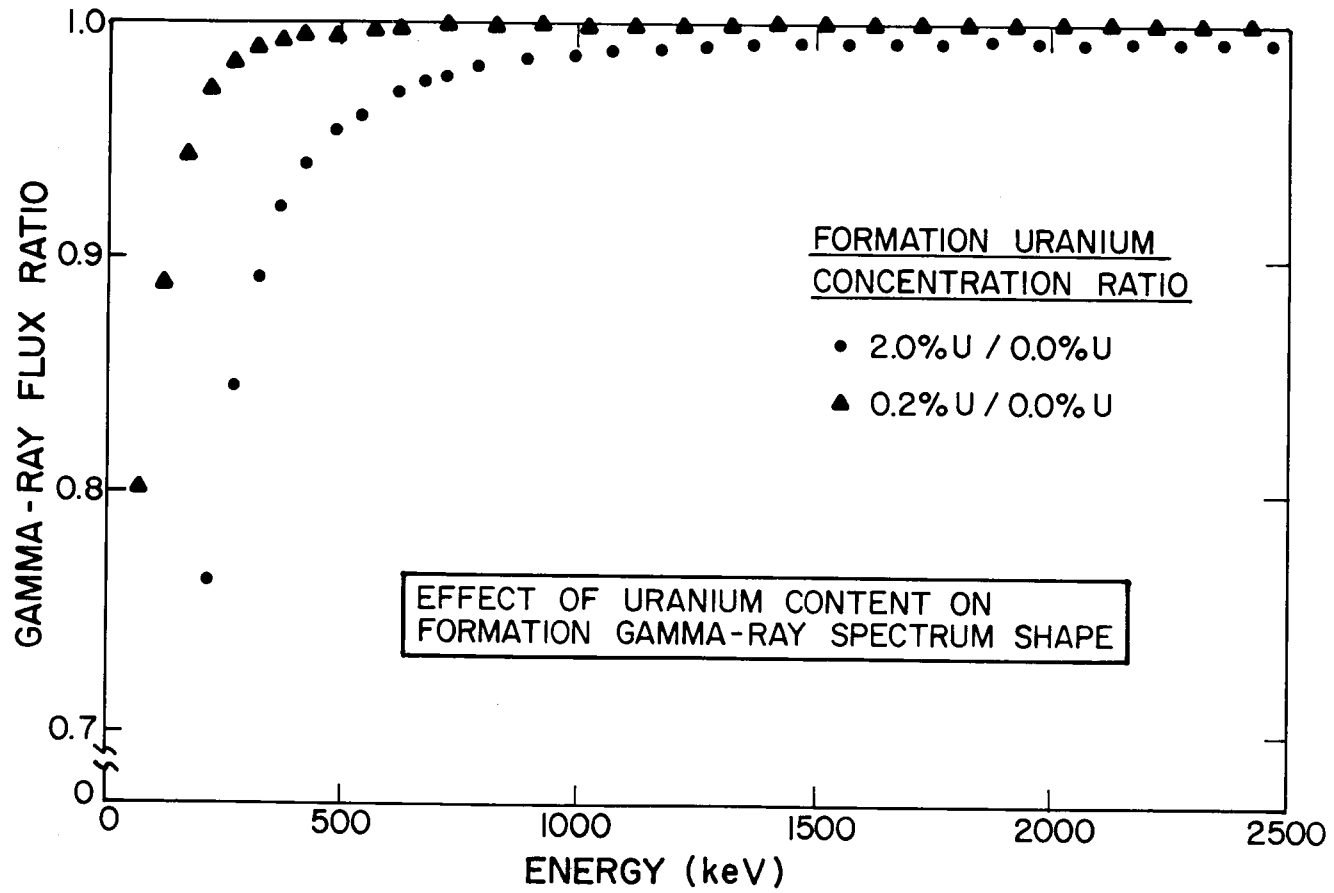gamma-ray source strength held constant.

Figure 9-5. Gamma-ray flux ratio versus energy for sandstone media
containing differing uranium concentrations.

3. The formation (Z/A) varies little from the nominal value of 0.500.
    Usually the largest changes in (Z/A) are caused by variations in
    formation moisture content. But even the largest practical
    variations in moisture content yield less than a 2-percent change in
    (Z/A) for the formation.

4. For the energy range of interest in spectral gamma-ray logging, the
    effect of formation changes on gamma-ray flux is well described by a
    simple inverse bulk density scaling. This is true, within a percent
    or two, even when the formation change is caused by a large variation
    in moisture content.

5. Given a certain gamma-ray source per unit volume from potassium,
    equilibrium uranium, or thorium, the percent concentration by weight
    scales inversely with any increase in bulk density due to additions
    of other constituents, such as moisture. Since the gamma-ray flux
    also scales nearly exactly with the inverse of bulk density, the
    gamma-ray flux characteristic of a given element will always be
    proportional to the concentration by weight, for the element,
    regardless of bulk density. The formation bulk density is required
    only when converting the elemental concentration (in percent or ppm)
    obtained from the borehole log to quantity of the element (in
    kilograms/m^3).

6. Spectral gamma-ray field logs can be calibrated for concentration in
    percent or ppm by weight without knowledge of the formation moisture
    content, if the same moisture content is assumed to exist in both the
    calibration model and the field formations. If in-situ concentra-
    tions were specified for the calibration model, the error introduced
    by making this assumption is related to (Z/A), and it generally
    amounts to only about 1 percent.

7. Concentrations of elements with large atomic numbers (including
    uranium) do not affect gamma-ray transport for the energy range from
    0.5 MeV to 2.6 MeV provided their concentrations are less than 0.6
    percent. For higher concentrations, the gamma-ray flux at the lower
    energies become increasingly attentuated, and at 6-percent uranium
    concentrations the flux is attenuated by approximately 30 percent at
    0.3 MeV. However, for the energy range from 1 to 2.6 MeV, which is
    of particular interest to spectral gamma-ray logging, the flux at
    6-percent uranium is attenuated by only 3-percent.

BOREHOLE GEOMETRY RESULTS

Borehole Diameter Effects

LASL transport calculations have also been completed for a borehole introduced
to the infinite homogeneous medium. Angular and energy dependent gamma-ray
fluxes were calculated at two radial positions within the borehole, corre-
sponding to the surface of detectors with diameters of 3.81 cm and 5.08 cm
placed concentric with the borehole axis. A 3.334 cm (1.313-inch) radius by
0.732 cm (0.29-inch) thickness of iron was introduced to simulate the probe
shell and detector housing materials. Results are virtually independent of

radial position within the probe shell region. Figures 9-6 through 9-11 show computed spectra for equilibrium uranium, and thorium spectra for the region within the probe housing. The borehole was 11.42 cm (4.5-inch) in diameter. Both dry and water-filled conditions were considered. Recall that the energy resolution for these calculations is 10 keV. Consider the dry borehole potassium spectrum of Figure 9-6 . It appears that the discrete, uncollided source gamma-ray line at 1.46 MeV dominates this spectrum. But one must remember that all of this intensity is confined to a 10 keV wide energy bin. If one sums the intensity of the continuum portion from 0 to 1.455 MeV, the result is larger than the uncollided line intensity by a factor of about 3. The continuum components of these spectra are very important to the interpretation of gamma-ray logging data. This is especially true when the window method of spectrum analysis is employed with probes that use sodium iodide detectors.

The effect of borehole water on the gamma-ray spectra may be observed by comparing Figure 9-6 with 9-7, Figure 9-8 with 9-9, and Figure 9-10 with 9-11. For example, the water attenuation factor for the uncollided potassium gamma-ray at 1.46 MeV is 0.844 while for the lowest energies of the continuum portion of the spectrum, the attenuation factor is 0.934. The continuum component is much less affected by borehole water because of multiple scattering "build-up" effects.

The potassium window used for sodium iodide detector data analysis has an energy range of 1.325 MeV to 1.575 MeV. If the continuum component within this window is summed for the dry and water-filled conditions, the resulting attentuation factor is 0.947. The total K window response is the sum of the continuum and the discrete 1.46 MeV line components. The ratio of total K window responses for the water-filled and dry borehole gives the resulting water attenuation factor of 0.855 for the 11.73 cm diameter borehole. The reciprocal of this ratio is the correction factor required to compensate the K window response for borehole water attenuation. This type of analysis was performed for borehole diameters of 3.0, 4.5, 6.25, 8.0, and 10.0 inches. Flux intensities are tabulated in Table 9-3 for the K, U, and Th window responses, as well as for the corresponding discrete lines at 1.46, 1.76, and 2.61 MeV, respectively. Corresponding correction factors are given in Table 9-4. The energy range for the uranium window is 1.650 MeV to 2.390 MeV, and for the thorium window the range is 2.475 MeV to 2.765 MeV. The relatively wide uranium window gives a response that is more sensitive to the continuum component than either the K or the Th windows. Table 9-3 shows that more than half the U window response is from gamma rays other than the discrete signature at 1.76 MeV. The results of Table 9-3 also show that borehole diameter has no effect on gamma-ray flux when the borehole is dry.

The calculated correction factors contained in Table 9-4 are compared to BFEC measurements in Figures 9-12, 9-13, and 9-14. Measured results are taken from Table 3-5 of Technical Note 3. The LASL results have been plotted at an adjusted borehole diameter to account for the 0.625-inch smaller probe diameter used for the measurements. These results are for a centralized probe geometry. The computed window correction factors are consistently lower than the measured results. The comparison is imperfect, though, because the LASL calculations do not yet account for detector response. Detector response has the effect of emphasizing the lower energy component of the window intensity relative to the higher energy component. The result is a larger measured correction factor than one would compute solely on the basis of energy fluxes incident on the detector.
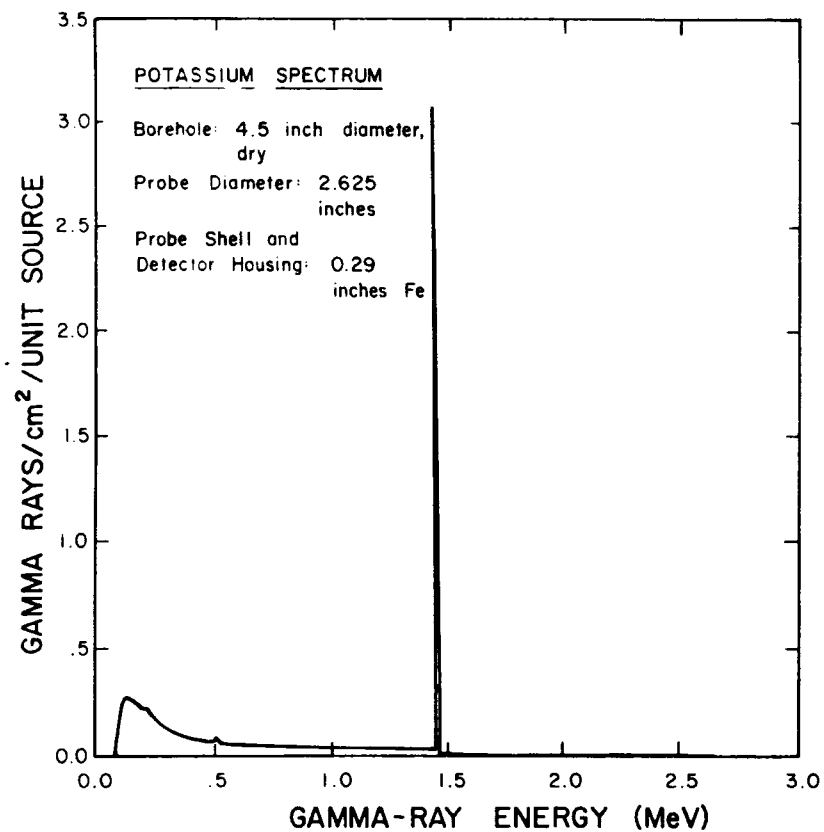
Figure 9-6. Calculated energy-dependent gamma-ray flux within a dry borehole surrounded by sandstone containing a potassium source.
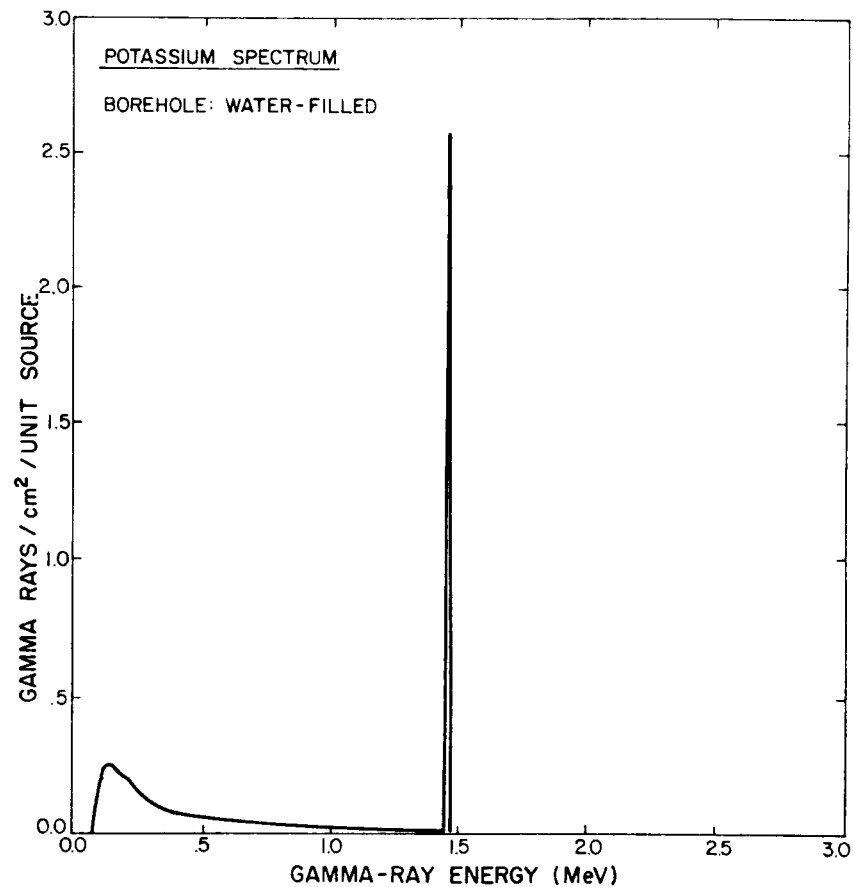
Figure 9-7. Calculated energy-dependent gamma-ray flux within a water-filled, 4.5-inch borehole surrounded by sandstone containing a potassium source.

EQUILIBRIUM URANIUM SPECTRUM

Borehole: 4.5 inch diameter, dry
Probe Diameter: 2.625 inches
Probe Shell and
Detector Housing: 0.29 inches
Fe

GAMMA RAYS/cm^2/UNIT SOURCE

GAMMA-RAY ENERGY (MeV)

EQUILIBRIUM URANIUM SPECTRUM
BOREHOLE: WATER-FILLED

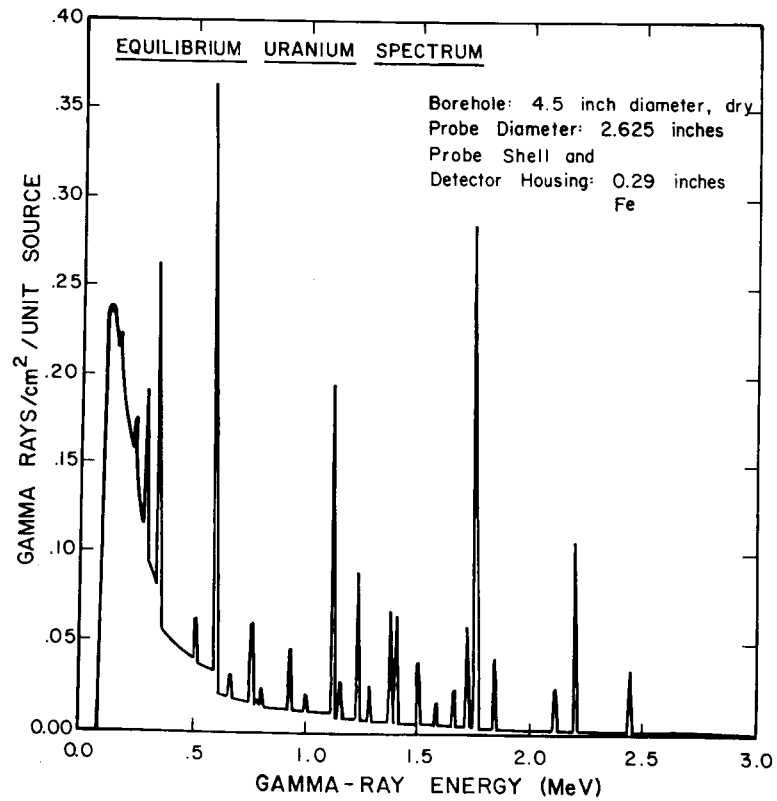GAMMA RAYS/cm^2/UNIT SOURCE

GAMMA-RAY ENERGY (MeV)

Figure 9-8. Calculated energy dependent gamma-ray
flux within a dry borehole surrounded
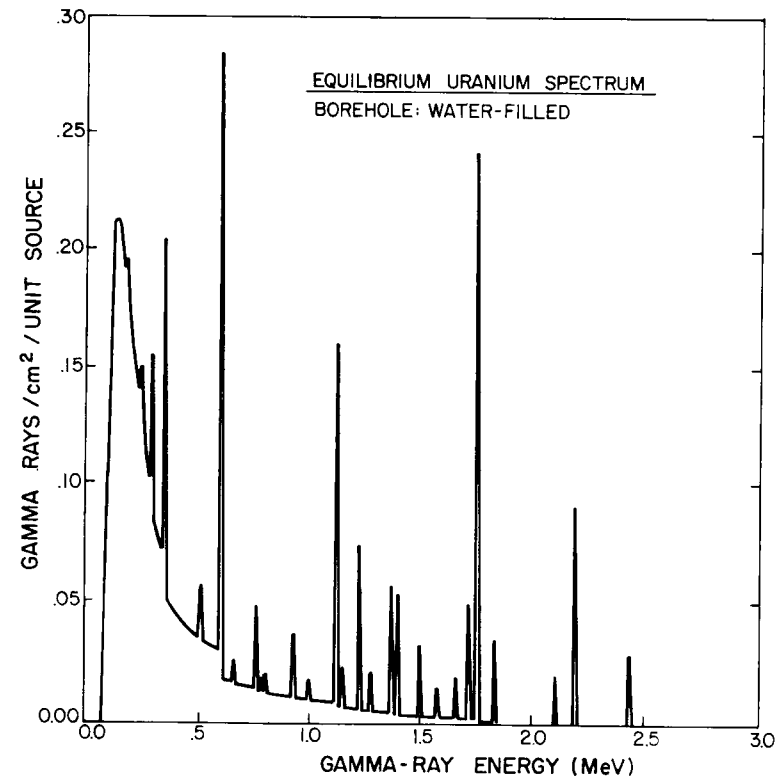by sandstone containing a uranium
source.

Figure 9-9. Calculated energy dependent gamma-ray
flux within a water-filled, 4.5-inch
borehole surrounded by sandstone
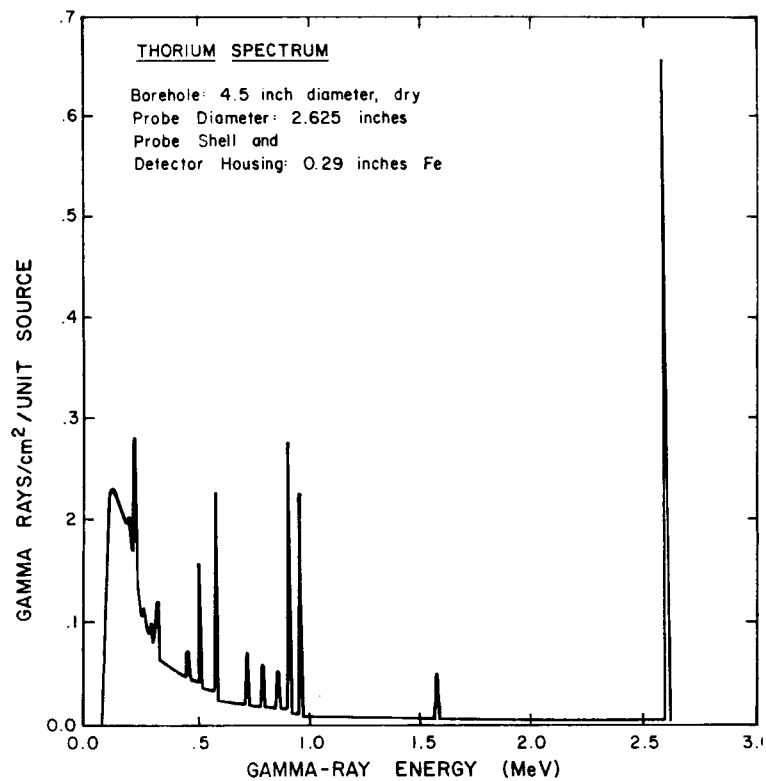containing a uranium source.

Figure 9-10. Calculated energy dependent gamma-ray
flux within a dry, 4.5-inch borehole
surrounded by a sandstone containing
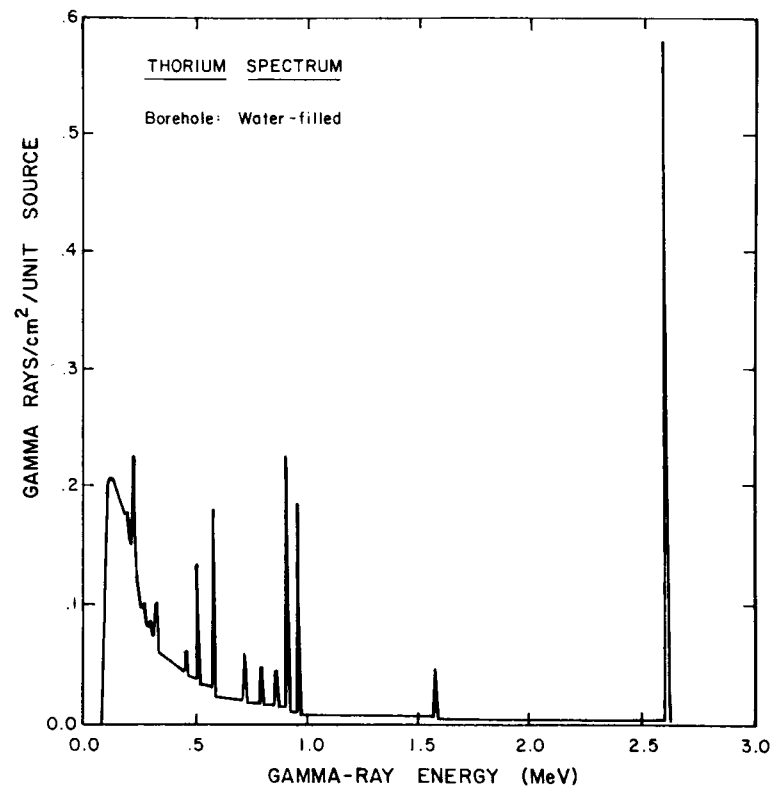a thorium source.

Figure 9-11. Calculated energy dependent gamma-ray
flux within a water-filled, 4.5-inch
borehole surrounded by a sandstone
containing a thorium source.

Table 9-3. Calculated Borehole Gamma-Ray Flux Intensities

Borehole Condition			Discrete Gamma-Ray Line Intensity (γ/cm^2/unit source)			Window Integral Intensity (γ/cm^2/unit source)		
Diameter (inches)	Wet/Dry	Casing	K (1.46 MeV)	U (1.76 MeV)	Th (2.61 MeV)	K (1.320–1.575 MeV)	U (1.650–2.390 Mev)	Th (2.475–2.765 MeV)
3.0 4.5 6.25 8.0 10.0	Dry	None	3.066	0.2832	0.6518	3.445	0.5923	0.6831
3.0	Wet	None	2.959	0.2742	0.6348	3.335	0.5780	0.6660
4.5	Wet	None	2.587	0.2426	0.5743	2.946	0.5172	0.6047
6.25	Wet	None	2.219	0.2110	0.5123	2.557	0.4597	0.5414
8.0	Wet	None	1.906	0.1839	0.4576	2.222	0.4049	0.4857
10.0	Wet	None	1.603	0.1572	0.4027	1.894	0.3521	0.4293
4.5	Dry	0.125 Inch Steel	2.641	0.2469	0.5799	3.002	0.5253	0.6102

Table 9-4. Calculated Borehole Gamma-Ray Flux Correction Factors

|								
				Dry/Wet Intensity Ratio				
Borehole Condition	Discrete Gamma-Ray Lines			Window Integrals		
Diameter (inches)	Wet/Dry	Casing	K (1.46 MeV)	U (1.76 MeV)	Th (2.61 MeV)	K (1.325-1.575 MeV)	U (1.650-2.390 MeV)	Th (2.475-2.765 MeV)
3.0	Wet	None	1.036	1.033	1.027	1.033	1.025	1.026
4.5	Wet	None	1.185	1.167	1.135	1.169	1.145	1.130
6.25	Wet	None	1.382	1.342	1.272	1.347	1.288	1.262
8.0	Wet	None	1.609	1.540	1.424	1.550	1.463	1.406
10.0	Wet	None	1.913	1.802	1.619	1.819	1.682	1.591
4.5	Dry	0.125 Inch Steel	1.161	1.147	1.124	1.148	1.128	1.120
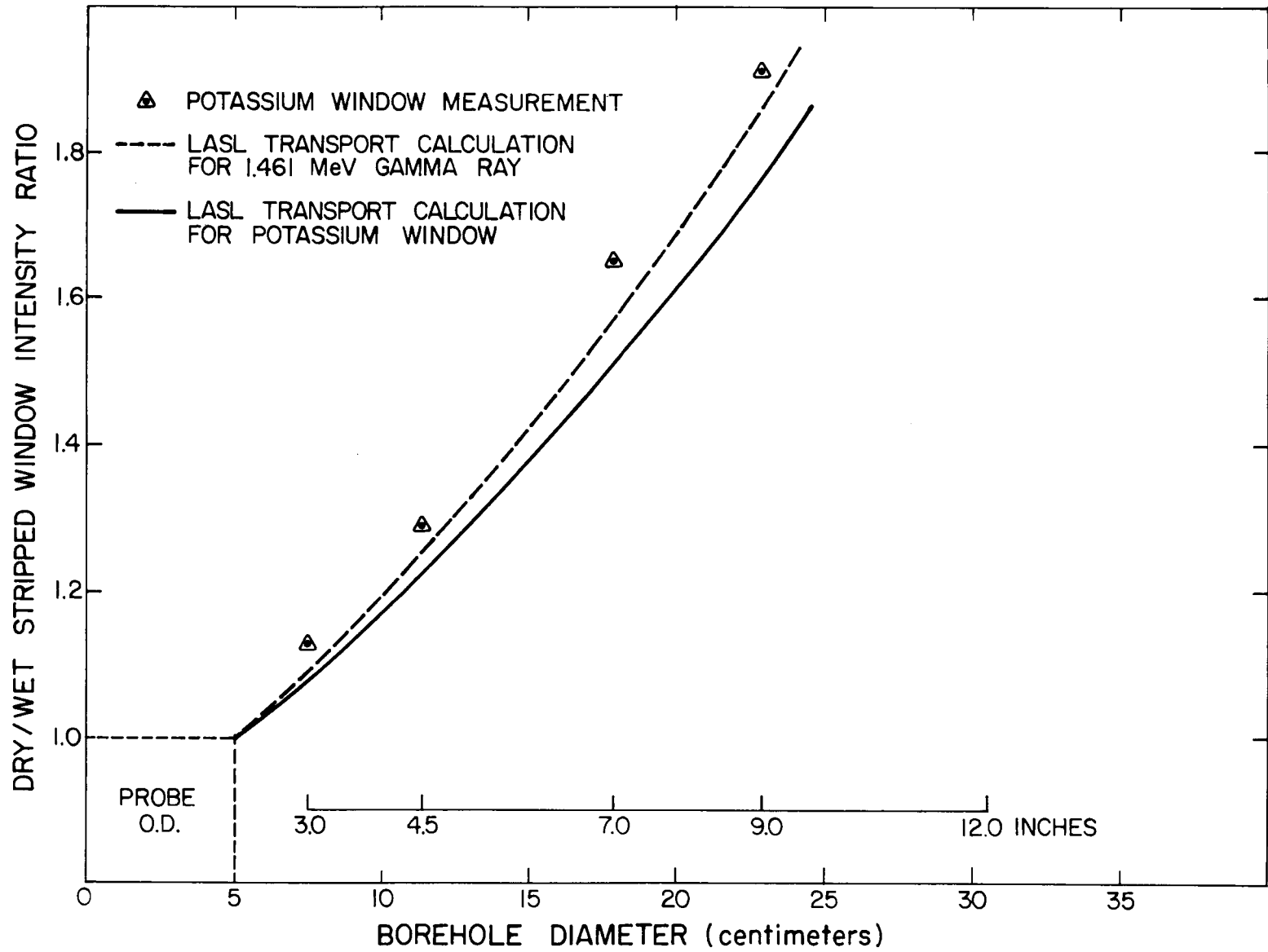
Figure 9-12. Comparison of measured and calculated borehole water correction
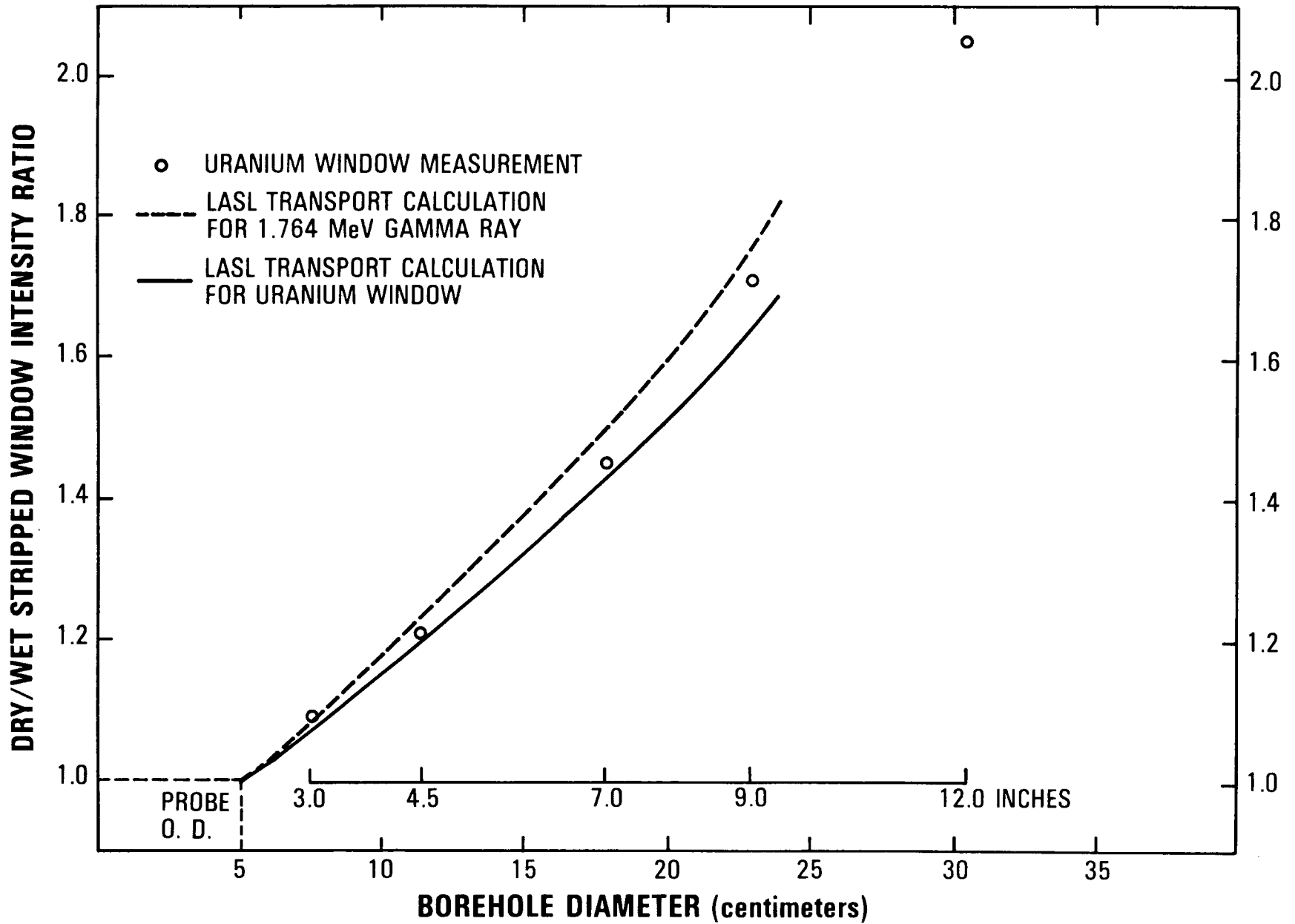for potassium.

Figure 9-13. Comparison of measured and calculated borehole water correction for uranium.
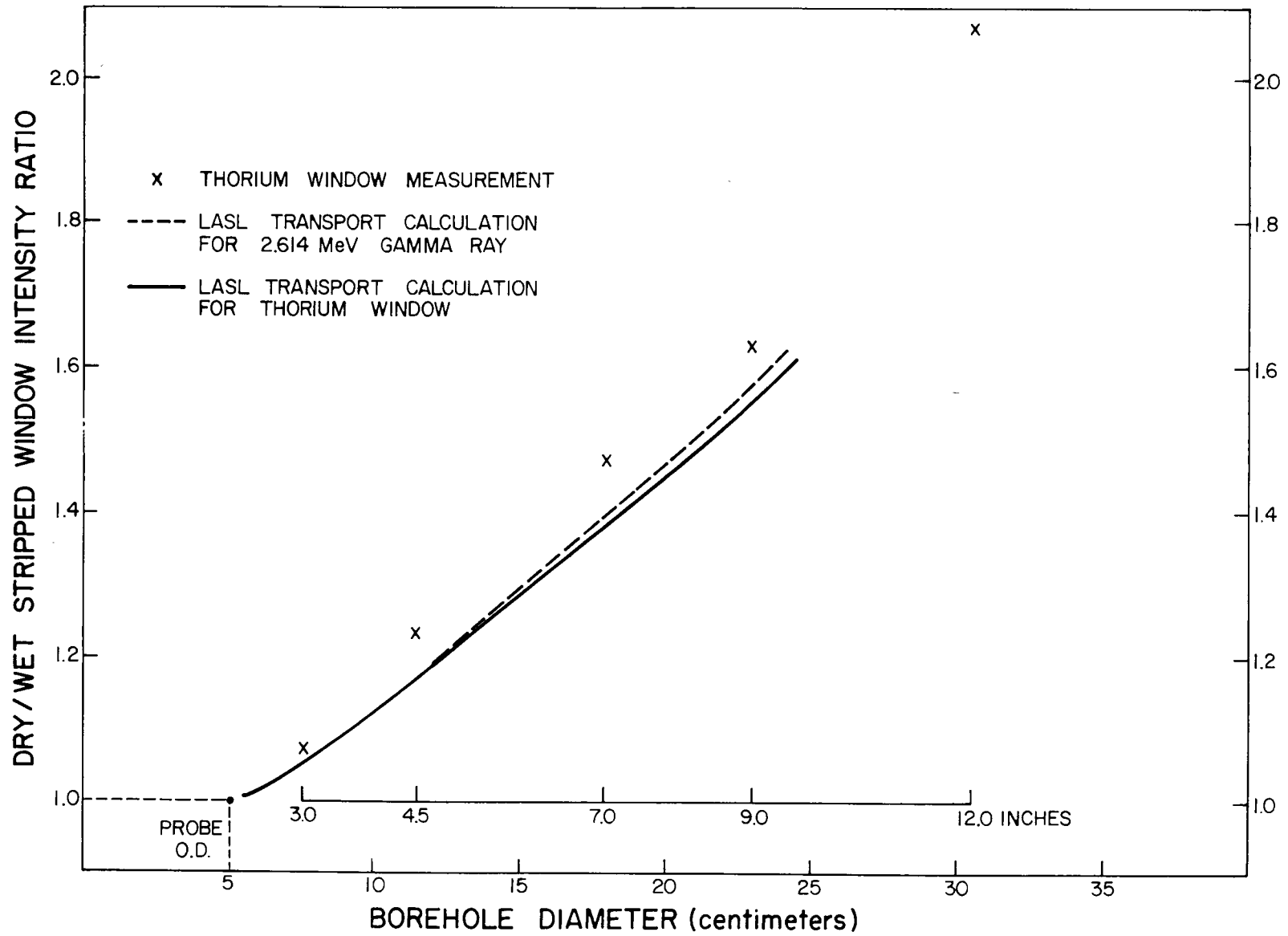
Figure 9-14. Comparison of measured and calculated borehole water correction for thorium.

The magnitude of this effect depends on the window width and on the distribution of gamma-ray energies within the window. It remains to be seen if the inclusions of detector response will bring the LASL calculations into agreement with the measurements.

Borehole Casing Effects

LASL has performed transport calculations of dry borehole spectra for a single iron casing thickness and for two thicknesses of PVC casing. The results for iron appear in Tables 9-3 and 9-4. The iron casing correction factors are compared to BFEC measurements in Table 9-5. The BFEC results are from Figure 4-2 of Technical Note 4. The LASL calculations are systematically below the BFEC measured casing corrections. This is the same trend observed when comparing calculated and measured water factor corrections and can be attributed to the effect of detector response.

Table 9-5. Comparison of Calculated and Measured
Casing Correction Factors

Energy Window	LASL Calculation	BFEC Measurement
K	1.148	1.17
U	1.128	1.17
Th	1.120	1.14

SUMMARY

Gamma-ray transport calculations completed by the Los Alamos Scientific Laboratory predict the effects of formation matrix and moisture conditions and of borehole fluid and casing conditions on the calibration of spectral gamma-ray logging probes.

Comparisons to BFEC measured borehole water and casing corrections show that the calculations underestimate the required corrections. The differences are attributed to the fact that detector response has not yet been included in the calculations. It is expected that future calculations, which will include detector response and sidewalled probe geometries, will provide more accurate estimates of borehole correction factors.

COMPARISON OF SODIUM IODIDE, CESIUM IODIDE, AND BISMUTH
GERMANATE SCINTILLATORS FOR BOREHOLE GAMMA-RAY LOGGING

ABSTRACT

Three types of scintillation detectors have been tested for application to
gamma-ray borehole logging. $NaI(T\ell)$, $CsI(Na)$, and $Bi_4Ge_3O_{12}$ detectors
were installed in borehole probes and used to collect gamma-ray data at the
U.S. Department of Energy's calibration facility at Grand Junction, Colorado.
Spectral data were collected with all three detectors to determine their
ability to assay ^{40}K, ^{214}Bi (a decay product of uranium) and $^{208}T\ell$ (a
decay product of thorium). Gross count data were also obtained with small
$NaI(T\ell)$ and $Bi_4Ge_3O_{12}$ detectors.

Both $CsI(Na)$ and $Bi_4Ge_3O_{12}$ offer enhanced gamma-ray counting efficiency
over that provided by $NaI(T\ell)$ which is the most common scintillator used in
uranium exploration. Tests in the calibration boreholes showed that $CsI(Na)$
averaged 45 percent higher spectral counting efficiency than did the same size
$Na(T\ell)$ detector. $Bi_4Ge_3O_{12}$ gave an average spectral counting efficiency
310 percent higher than did the same size $NaI(T\ell)$ detector. The greater
efficiency is accompanied by poorer energy resolution than is obtained from
$NaI(T\ell)$. However, the poorer energy resolution did not adversely affect the
stripping ratios calculated for $CsI(Na)$ and $Bi_4Ge_3O_{12}$. On the contrary,
the stripping ratios to remove downward scattering were lower for these
detectors than they were for $NaI(T\ell)$.

Finally, for gross count applications, $Bi_4Ge_3O_{12}$ produced a count rate
50 percent greater than did the same size $NaI(T\ell)$ detector in an unfiltered
gamma-ray probe. When a graded filter was placed around the detectors to
reduce the number of low energy gamma rays detected, the count rate obtained
from $Bi_4Ge_3O_{12}$ was 90 percent greater than from $NaI(T\ell)$.

INTRODUCTION

At the present time, Bendix uses only $NaI(T\ell)$ scintillation detectors in its
gamma-ray logging probes for the U.S. Department of Energy. Different types
of scintillators are commercially available, but they have not been widely
used in the logging industry. Two of these scintillators, $CsI(Na)$ and
$Bi_4Ge_3O_{12}$, have been obtained for evaluation as gamma-ray detectors in
logging probes.

The two new scintillators offer the ability to detect more gamma rays per
second for equal size detectors due to the higher density and higher average
atomic number of these scintillators compared to $NaI(T\ell)$. They have the
disadvantages, however, of poorer energy resolution and greater purchase
price. Comparison tests have been performed using the Grand Junction
calibration models to quantify the performance differences of the
scintillators for the specific application of logging.

CHARACTERISTICS

NaI(Tℓ) has been the most common scintillation material used in borehole gamma-ray logging. Its wide usage can be attributed to its generally acceptable performance characteristics, its availability from two major United States manufacturers (Harshaw Chemical Company and Bicron Corporation), and its moderate price. The harsh environment of a logging probe, however, causes NaI(Tℓ) detectors to be susceptible to failure. Rapid temperature changes can cause the detectors to crack from thermal stress, and mechanical shock can also fracture the detectors. When a cold detector is warmed, the protective metal can surrounding the detector may expand faster than the detector itself. If this occurs, the reflective oxide packing between the metal and the detector can shift and degrade the energy resolution of the detector. Finally, NaI(Tℓ) is hygroscopic and can be ruined if the moisture seal is broken.

CsI(Na) is less susceptible to breakage than is NaI(Tℓ), but it is hygroscopic. Its energy resolution, however, is slightly poorer than that of NaI(Tℓ), but its density is greater with the result that it can stop gamma rays more efficiently. CsI(Na) costs approximately 20 percent more than does NaI(Tℓ), and it is manufactured by only one United States company (Harshaw).

$Bi_4Ge_3O_{12}$ (bismuth germanate, abbreviated BGO) is a relatively new scintillator made by Harshaw. Its main advantage over NaI(Tℓ) and CsI(Na) is its high density and high average atomic number. Thus, per unit volume it has a significantly enhanced gamma-ray stopping power, especially for the high energy gamma rays (Evans, 1979) between 1 MeV and 3 MeV used as signatures for potassium, uranium, and thorium. BGO costs approximately six times as much as NaI(Tℓ), but the enhanced efficiency (although with poorer energy resolution) makes it especially attractive for slim probes. Some of the characteristics of NaI(Tℓ), CsI(Na), and BGO are given in Table 10-1.

Table 10-1. Scintillator Characteristics

	NaI(Tℓ)	CsI(Na)	$Bi_4Ge_3O_{12}$
Density (g/cm^3)	3.67	4.51	7.13
Wave Length of Maximum Emission (nm)	413	420	480
Decay Constant (ns)	230	650	300*
Nominal Energy Resolution at 662 keV (percent)	8	11	20
Nominal Pulse Height (light output) relative to NaI(Tℓ) (percent)	100	65-83	8*
Hygroscopic	Yes	Yes	No

*Varies with temperature

SPECTRAL TESTS

Sodium Iodide and Cesium Iodide

CsI(Na) and NaI(Tℓ) were tested using detectors 2 inches in diameter and 5 inches in length. They were installed separately in a Bendix spectral gamma-ray KUT logging probe (George, et al., 1979) using the same 2-inch photomultiplier tube (RCA-4523) for each crystal. A ^{54}Mn radioactive source which emits an 835 keV gamma ray was placed on the side of the detector to obtain a reference pulse for energy stabilization (Stromswold and Kosanke, 1979). Upon switching from the NaI(Tℓ) detector to the CsI(Na) detector, the high voltage in the probe had to be increased from 928 volts to 1070 volts to maintain the pulse height from manganese at a constant value. This adjustment was necessary due to the lower light output of CsI(Na).

A block diagram of the equipment used to collect the comparison data is given in Figure 10-1. The probe was connected to the uphole electronics by 3,000 feet of 4HO logging cable. The pulse shape uphole was adjusted using a pole zero control at the input to the linear amplifier. A shape was selected which provided rapid return of the pulse to the baseline with minimal undershoot. The pulse shaping time constant of the linear amplifier was 1 μs. The Tracor-Northern NS-454 gain stabilizer held the reference peak from manganese in a fixed channel in the multichannel analyzer, and the lower level discriminator on the analog to digital converter was used to cut off pulses from gamma rays below the manganese reference level.

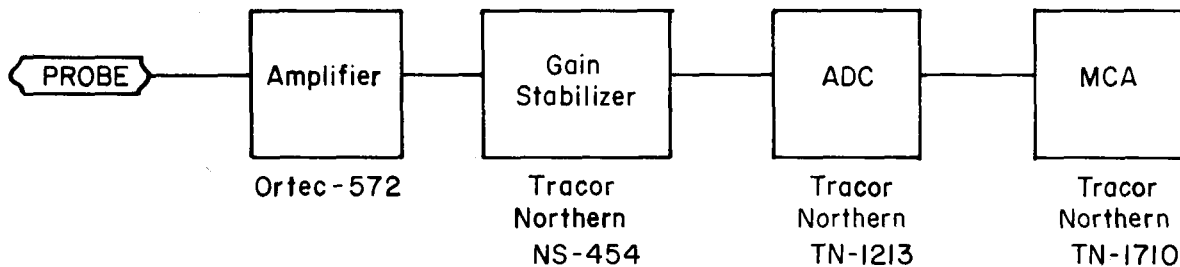| PROBE	—	Amplifier	—	Gain Stabilizer	—	ADC	—	MCA
		Ortec-572		Tracor Northern NS-454		Tracor Northern TN-1213		Tracor Northern TN-1710

Figure 10-1. Equipment used in spectral comparison tests.

A calibration was performed for each detector by collecting data in the Grand Junction K, U, and Th models. Counting times ranged from 3,000 seconds to 7,500 seconds depending upon the model used. The unstripped count rates obtained for the two scintillators are given in Table 10-2. Two sets of count rates are listed for CsI(Na); the first set was obtained using the standard energy windows for Bendix KUT systems, and the second set was obtained using windows which had been widened to better correspond to the broader peaks produced by CsI(Na). The energy limits for the two sets of windows are also given in Table 10-2.

Table 10-2. Comparison of Count Rates for 2-inch x 5-inch
NaI(Tℓ) and CsI(Na) Detectors.

Model	Energy Window	NaI(Tℓ)[a]	CsI(Na)[a]	CsI(Na)[b]
Lead	K	5.59	9.75	9.93
Lead	U	2.45	4.49	5.04
Lead	Th	0.29	0.27	0.35
K	K	29.04	42.76	42.69
K	U	4.28	7.09	7.75
K	Th	0.36	0.47	0.53
U	K	244.01	317.56	320.31
U	U	251.50	342.47	353.98
U	Th	7.70	8.74	12.25
Th	K	89.65	116.60	124.04
Th	U	163.50	201.12	205.48
Th	Th	60.76	80.23	88.71

[a]NaI windows: K(1320-1575 keV), U(1650-2390 keV), Th(2475-2765 keV).
[b]CsI windows: K(1334-1604 keV), U(1631-2368 keV), Th(2440-2862 keV).

The more valid comparison between count rates from NaI(Tℓ) and CsI(Na) is obtained when the standard windows are used for the NaI data and the wide windows are used for the CsI data. Notice, however, that in Table 10-2 there is no great difference between the count rates for the two different window sets for CsI(Na). As shown in Table 10-2, the CsI(Na) detector produced significantly more counts per second than did the NaI(Tℓ) detector. For example, the count rate in the potassium window in the potassium model was 29.04 counts per second from NaI(Tℓ) and 42.69 counts per second from CsI(Na). This corresponds to a 47 percent increase in count rate for CsI(Na) over that of NaI(Tℓ). For the uranium window in the uranium model and for the thorium window in the thorium model the increases in count rates were 41 percent and 46 percent, respectively. The average increase in count rate for CsI(Na) was 45 percent for the three photopeaks.

The data from the calibrations of the two detectors were processed through the computer program PADCAL to obtain the calibration matrices used by Bendix in reducing KUT data (Stromswold and Kosanke, 1978). The matrix elements obtained from this program are given in Table 10-3 and the conventional stripping ratios are given in Table 10-4. The three primary stripping ratios (alpha, beta, and gamma) are lower for CsI(Na) than for NaI(Tℓ). This is somewhat surprising because more interference between peaks in the spectrum might be expected from the poorer energy resolution of CsI(Na). Apparently CsI(Na) has a higher percentage of the gamma rays in the photopeaks versus the Compton continuum than does NaI(Tℓ). The lower stripping ratios for CsI(Na) are highly desirable for borehole logging because they result in smaller corrections to the raw data to obtain concentrations of radioelements. The only stripping ratio which increased for CsI(Na) is the upward ratio A (uranium to thorium), and this stripping ratio is small in comparison to the three primary ones. The remaining two upward stripping ratios B (potassium to thorium) and G (potassium to uranium) are seen to be small and negative in Table 10-4. The uncertainty in these elements is large, and these stripping ratios should be considered to be zero.

Spectra collected in the uranium, (498 parts per million) and thorium (505 parts per million) models are shown in Figures 10-2 and 10-3. These spectra were collected without a manganese stabilization source in the probe; instead, the spectra were stabilized on natural peaks from the formation. In each figure the counts from the CsI(Na) detector are seen to be greater than those from the NaI(Tℓ) detector. Also the peaks in the CsI(Na) spectra are clearly broader than the corresponding peaks in the NaI(Tℓ) spectra.

Sodium Iodide and Bismuth Germanate

NaI(Tℓ) and BGO were compared using detectors 1.5 inches in diameter and 3 inches in length. It would have been desirable to have NaI, CsI, and BGO detectors which were all the same size for these tests, but they were not available. Consequently, the comparisons were made separately using two NaI(Tℓ) detectors—one the size of the CsI detector and one the size of the BGO detector. The detectors were attached to a 2-inch diameter photomultiplier tube and operated in the same borehole probe used in the NaI-CsI comparison. The low light output of BGO made it necessary to raise the high voltage to 1200 volts to obtain pulse heights equivalent to those from NaI. A pulse shaping time constant of 1 us was used on the spectroscopy amplifer. The equipment used in the NaI-BGO comparison tests was the same as that used for the NaI-CsI comparison and is shown in Figure 10-1.

Table 10-3. Comparison of Calibration Matrix
Elements for 2-inch x 5-inch NaI(Tℓ) and CsI(Na) Detectors.

Matrix Elements	NaI(Tℓ)[a]	CsI(Na)[a]	CsI(Na)[b]
A_{11}^{-1}	0.311	0.219	0.222
A_{12}^{-1}	-0.306	-0.203	-0.201
A_{13}^{-1}	0.408	0.224	0.187
A_{21}^{-1}	-0.041	-0.022	-0.029
A_{22}^{-1}	2.198	1.592	1.563
A_{23}^{-1}	-5.330	-3.508	-3.187
A_{31}^{-1}	0.103	0.049	0.059
A_{32}^{-1}	-0.348	-0.197	-0.249
A_{33}^{-1}	9.144	6.741	6.208

[a]NaI windows: K(1320-1575 keV), U(1650-2390 keV), Th(2475-2765 keV).
[b]CsI windows: K(1334-1604 keV), U(1631-2368 keV), Th(2440-2862 keV).

Table 10-4. Comparison of Stripping Ratios for
2-inch x 5-inch NaI(Tℓ) and CsI(Na) Detectors.

Stripping Ratio	NaI(Tℓ)[a]	CsI(Na)[a]	CsI(Na)[b]
Alpha(Th→U)	2.445	2.231	2.059
Beta(Th→K)	1.098	1.044	1.028
Gamma(U→K)	0.950	0.902	0.881
A(U→Th)	0.027	0.023	0.032
B(K→Th)	-0.012	-0.007	-0.010
G(K→U)	-0.010	-0.002	-0.001

[a]NaI windows: K(1320-1575 keV), U(1650-2390 keV), Th(2475-2765 keV).
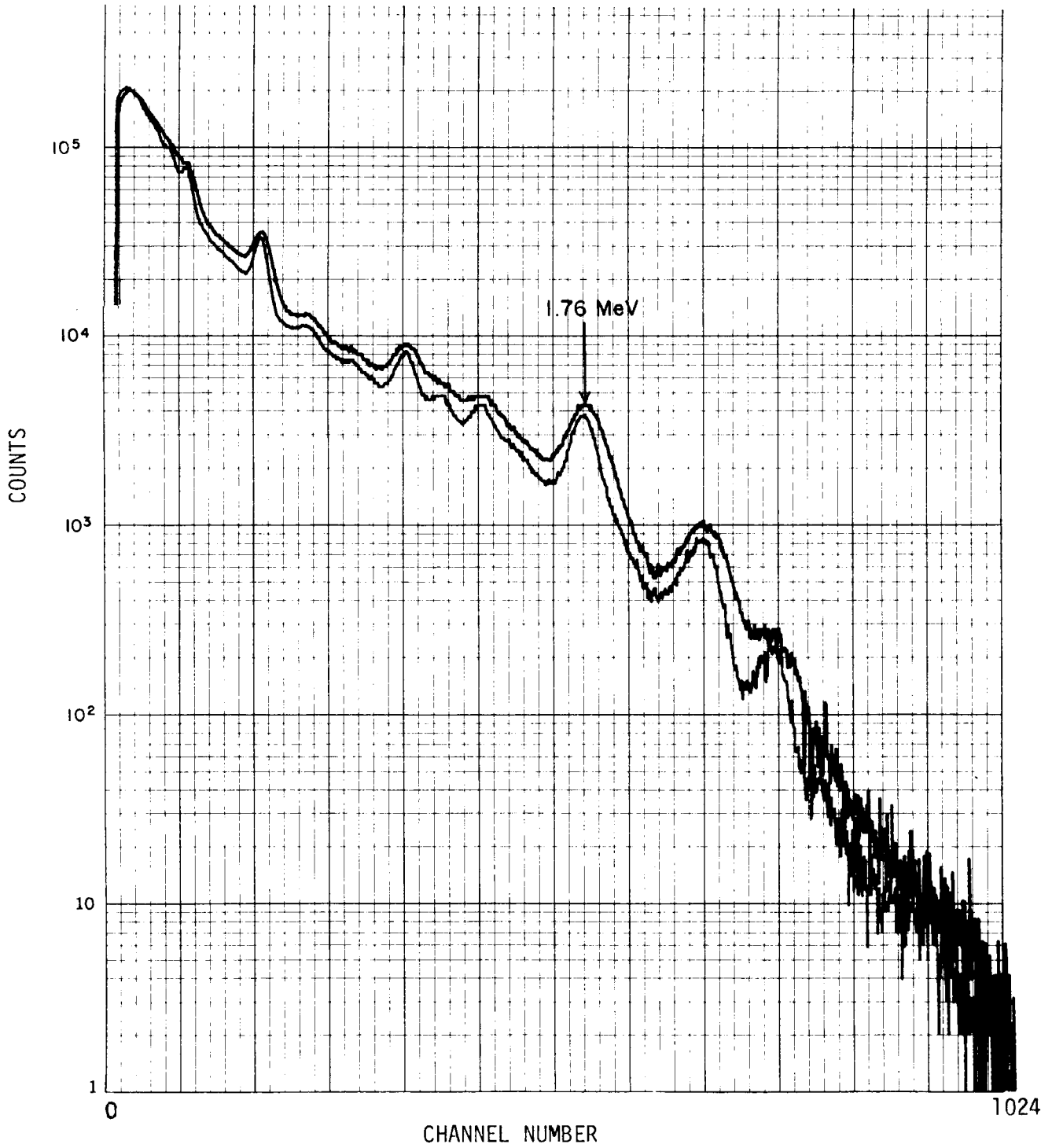[b]CsI windows: K(1334-1604 keV), U(1631-2368 keV), Th(2440-2862 keV).

Figure 10-2. Comparison spectra from U model obtained using a 2-inch x 5-inch CsI(Na) detector (upper trace) and a 2-inch x 5-inch NaI(Tℓ) detector (lower trace), counting time = 1000 sec.
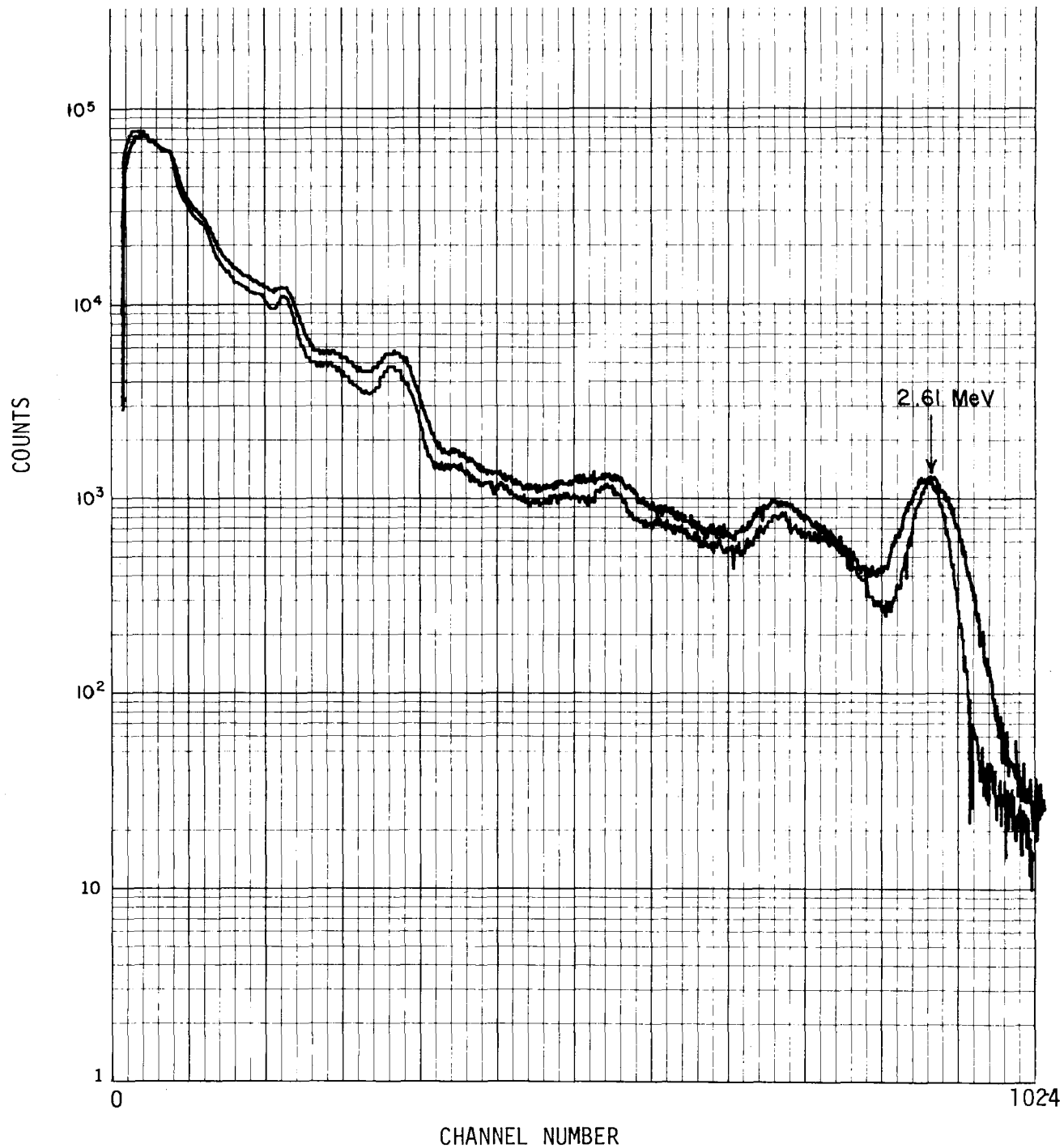
Figure 10-3. Comparison spectra from Th model obtained using a 2-inch x
5-inch CsI(Na) detector (upper trace) and a 2-inch x
5-inch NaI(Tℓ) detector (lower trace), counting time = 1000
sec.

175

Calibration data were collected in the Grand Junction models. The unstripped count rates obtained for the 1.5-inch x 3-inch NaI(Tℓ) and BGO detectors are given in Table 10-5. Two sets of count rates are given for BGO; the first set corresponds to the standard energy windows used for NaI, and the second set corresponds to wider windows which are more suitable for the broad peaks from BGO. The wide windows were selected visually to cover the peaks in the spectra obtained in the KUT calibration models. The separation between the potassium peak and the uranium peak was insufficient to allow the desired windows to cover both the potassium and uranium peaks completely. Consequently, the upper end of the potassium window was truncated with the loss of approximately 10 percent of the total potassium counts available in a full width window. In comparing the count rates between the NaI and BGO detectors, the results for the wider windows should be used for BGO.

From Table 10-5 it can be seen that the count rate in the potassium window in the potassium model was 7.61 counts per second for the NaI detector and 33.03 counts per second for the BGO detector. This corresponds to a 330 percent increase in the BGO count rate over that of NaI. For the uranium window in the uranium model and for the thorium window in the thorium model, the count rates from BGO were higher by 230 percent and 360 percent, respectively. The average increase in count rate for the potassium, uranium, and thorium photopeaks was 310 percent.

The calibration data for the two detectors were processed through the program PADCAL to obtain calibration matrices and stripping ratios. The resulting matrix elements are given in Table 10-6, and the stripping ratios are given in Table 10-7. As shown in Table 10-7 the three primary stripping ratios are smaller for BGO than they are for the same size NaI detector. The largest difference is seen for alpha (thorium to uranium) which is 3.230 for NaI and only 1.264 for BGO. The smaller stripping ratio for BGO is due to its increased efficiency in stopping high energy gamma rays rather than just scattering them. The upward stripping ratios A (uranium to thorium) and G (potassium to uranium) are larger for BGO than for NaI because of the greater overlap of the peaks from BGO. However, for both BGO and NaI the upward stripping ratios are small in comparison to the downward ratios. The decrease in the primary stripping ratios and the increase in counting efficiency of BGO make this scintillator very attractive for use in spectral gamma-ray logging.

Table 10-5. Comparison of Count Rates for 1.5-inch x 3-inch NaI(Tℓ) and BGO Detectors.

Model	Energy Window	NaI(Tℓ)[a]	.BGO[a]	BGO[b]
Lead	K	1.01	5.30	7.05
Lead	U	0.49	1.64	2.18
Lead	Th	0.08	0.21	0.28
K	K	7.61	28.52	33.03
K	U	0.93	3.29	4.22
K	Th	0.11	0.38	0.49
U	K	76.99	181.53	241.57
U	U	73.69	227.73	245.01
U	Th	1.74	7.20	12.47
Th	K	28.50	65.00	86.20
Th	U	56.93	102.35	110.78
Th	Th	16.37	65.71	75.87

[a]NaI windows: K(1320-1575 keV), U(1650-2390 keV), Th(2475-2765 keV)
[b]BGO windows: K(1276-1614 keV), U(1616-2395 keV), Th(2397-2855 keV)

Table 10-6. Comparison of Calibration Matrix
Elements for 1.5-inch x 3-inch NaI(Tℓ) and
BGO Detectors.

Matrix Elements	NaI(Tℓ)[a]	BGO[a]	BGO[b]
A_{11}^{-1}	1.096	0.307	0.281
A_{12}^{-1}	-1.178	-0.239	-0.274
A_{13}^{-1}	2.323	0.110	0.118
A_{21}^{-1}	-0.005	-0.026	-0.050
A_{22}^{-1}	7.349	2.320	2.240
A_{23}^{-1}	-23.729	-3.112	-2.792
A_{31}^{-1}	0.312	0.062	0.065
A_{32}^{-1}	-1.017	-0.274	-0.401
A_{33}^{-1}	34.044	8.082	7.195

[a]NaI windows: K(1320-1575 keV), U(1650-2390 keV), Th(2475-2765 keV)
[b]BGO windows: K(1276-1614 keV), U(1616-2395 keV), Th(2397-2855 keV)

Table 10-7. Comparison of Stripping Ratios for
1.5-inch x 3-inch NaI(Tℓ) and BGO Detectors.

Stripping Ratio	NaI(Tℓ)[a]	BGO[a]	BGO[b]
Alpha (Th→U)	3.230	1.349	1.264
Beta (Th→K)	1.353	0.693	0.811
Gamma (U→K)	1.032	0.768	0.955
A (U→Th)	0.020	0.028	0.047
B (K→Th)	-0.010	-0.008	-0.008
G (K→U)	-0.032	-0.001	0.011

[a]NaI windows: K(1320-1575 keV), U(1650-2390 keV), Th(2475-2765 keV)
[b]BGO windows: K(1276-1614 keV), U(1616-2395 keV), Th(2397-2855 keV)

Figures 10-4 and 10-5 show spectra collected in the uranium and thorium models
with the two detectors. The manganese stabilization source was removed prior
to collecting the spectra, and stabilization was performed on the gamma rays
from the formation. The figures clearly show the greater counts and broader
peaks in the BGO spectra compared to those in the NaI(Tℓ) spectra.

GROSS COUNT GAMMA TESTS

NaI(Tℓ) and BGO detectors having a diameter of 0.75-inch and a length of 2
inches were used to compare these scintillators for gross count gamma-ray
logging applications. They were installed in a Bendix gross-gamma probe, and
the signals were processed using a Bendix live-time ratemeter/scaler system
(LPI Model 5). The energy threshold was set at 100 mV, and the gain was
adjusted in each case to obtain minimum sensitivity of the count rate to gain
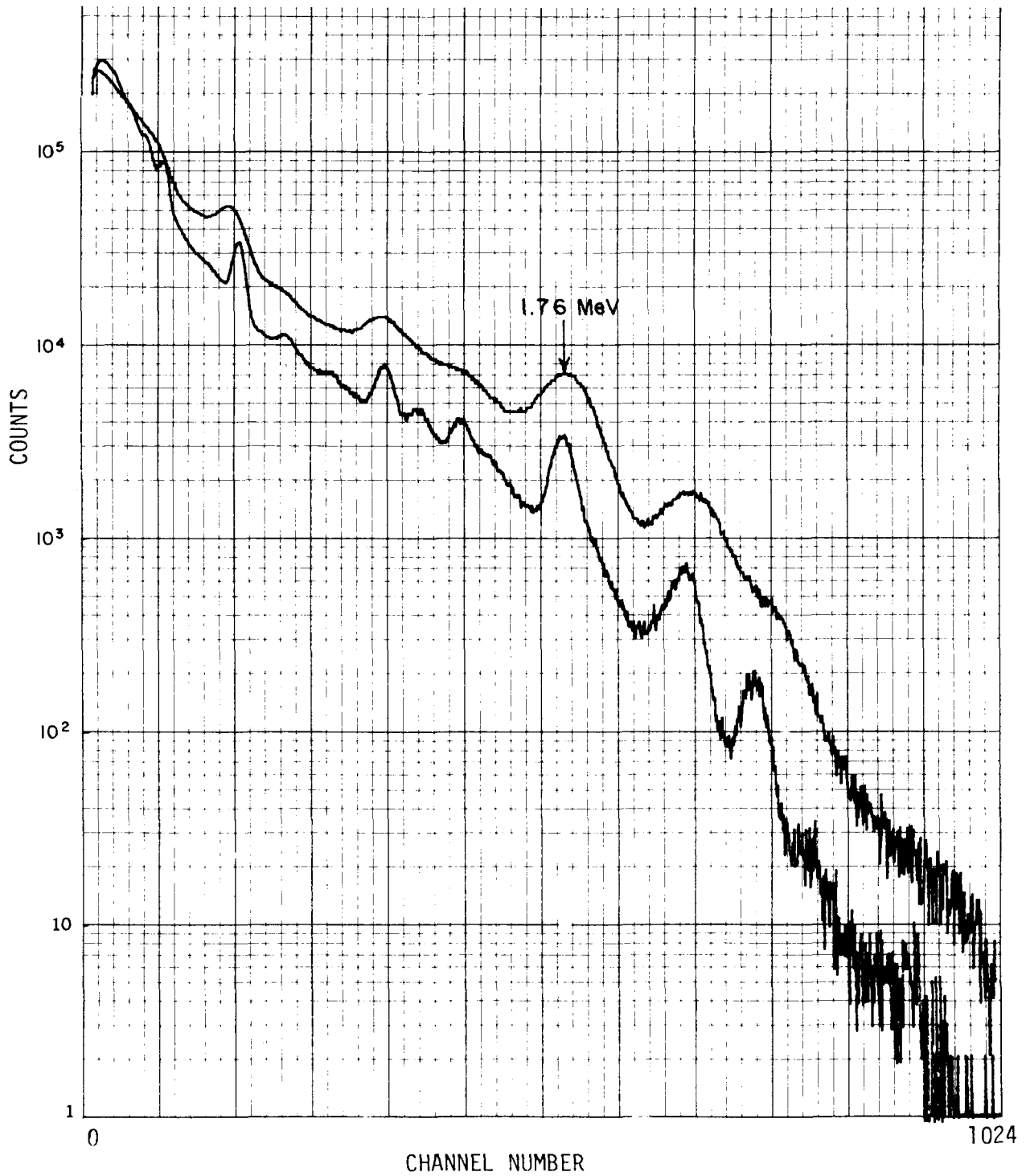changes (i.e., the system was "plateaued").

Figure 10-4. Comparison spectra from U model obtained using a 1.5-inch x
            3-inch BGO detector (upper trace) and a 1.5-inch x
            3-inch NaI(Tℓ) detector (lower trace), counting = 3000
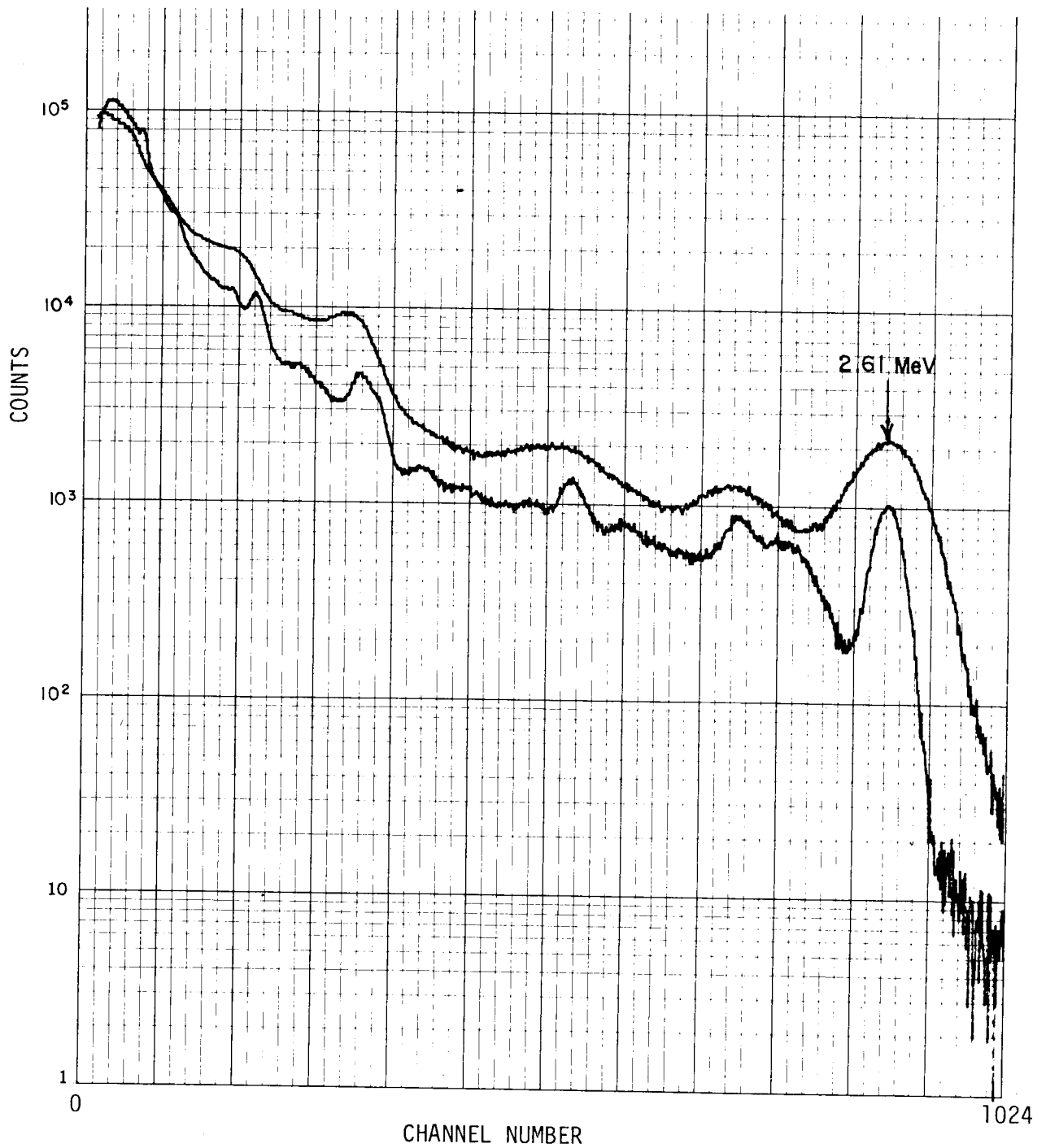   sec.

Figure 10-5. Comparison spectra from Th model obtained using a 1.5-inch x
3-inch BGO detector (upper trace) and a 1.5-inch x
3-inch NaI(Tℓ) detector (lower trace), counting time = 3000
sec.

179

Data were collected with the detectors in the center of the ore zones of the dry calibration models U1, U2, U3, and N3 at Grand Junction. Counting times ranged from 200 to 600 seconds. For both detectors, data were collected both with and without a graded filter around the detector. The filter was 0.25-inch thick and made of lead, cadmium, and copper. The lead reduced the number of low energy gamma rays reaching the detector, and the cadmium and copper stopped x-rays generated in the filter.

Data collected in the calibration models are given in Table 10-8. The count rate for the filtered BGO detector was 90 percent greater than for the filtered NaI(Tℓ) detector. When the detectors were not filtered, the count rate was 50 percent greater than from the BGO detector. The smaller difference between the two unfiltered count rates was due to the lower averge energy of the gamma rays reaching the detectors. For low energy gamma rays the higher density and average atomic number of BGO became less important.

Table 10-8. Gross count gamma-ray data collected in the calibration models with 0.75-inch x 2-inch NaI(Tℓ) and BGO detectors (1000 counts per second).

Model	NaI Filtered	NaI Unfiltered	BGO Filtered	BGO Unfiltered
U1	16.7	66.0	31.6	99.1
U2	8.0	35.6	15.1	53.5
U3	3.1	14.8	5.8	22.2
N3	1.6	8.1	3.1	12.1

For uranium exploration it is desirable to perform gross count gamma-ray logging with a filtered detector in order to avoid problems with the "Z effect". When the detectors are unfiltered, they are sensitive to the low energy gamma rays which can be absorbed through the photoelectric effect. The "Z effect" produces a drop in observed count rate due to enhanced photoelectric absorption of the low energy gamma rays in formations with high atomic number (Z). This can produce a non-linear dependence of count rate on uranium grade. A BGO detector can reduce problems from the "Z effect" by providing improved sensitivity to higher energy gamma rays and by allowing the use of smaller detectors which leave room for graded filters in slim probes.

CONCLUSION

Comparison data have been collected in the Grand Junction calibration models using three different scintillators: sodium iodide, cesium iodide, and bismuth germanate. Sodium iodide had the best energy resolution, but both cesium iodide and bismuth germanate provided better counting efficiencies and smaller stripping ratios.

Enhanced counting efficiency is important for spectral gamma-ray logging because of the low radiation levels encountered in many logging operations. If a more efficient detector is used, then several benefits become available:

1. Faster logging speeds;
2. Better precision in the data;
3. Improved thin bed resolution;
4. Slimmer probe construction.

The decrease in the magnitudes of the primary stripping ratios for cesium iodide and bismuth germanate is advantageous to logging data reduction. Because of the smaller stripping ratios less correction has to be made to the raw data to remove interferences between the energy windows of interest. Errors caused by neglecting variations in stripping ratios due to changing borehole conditions should be less significant for detectors with smaller stripping ratios.

For gross count gamma-ray logging, bismuth germanate has a greater counting efficiency than does sodium iodide, but its main advantage appears to be its enhanced sensitivity to the high energy gamma rays present in boreholes. This may make it possible to replace unfiltered sodium iodide detectors with filtered bismuth germanate detectors, even in slim probes, and thus avoid problems from the "Z effect."

Additional studies need to be done on bismuth germanate to test its reliability under field conditions. Also, its light output must be investigated for borehole logging applications to determine if its rather large variation in light output depending on temperature, approximately -1.5-percent change per degree centigrade (Henry, 1980), will be acceptable with present gain stabilization methods.

REFERENCES

Conaway, J.G. (Geologic Survey of Canada), 1979a, (private communication).

Conaway, J.G. (Geologic Survey of Canada), 1979b, (private communication).

Conaway, J.G., and Killeen, P.G., 1978, Quantitative uranium determination from gamma-ray logs by application of digital time series analysis: Geophysics, v. 43, p. 1204-1221.

Czubek, J.A., 1961, Some problems of the theory and quantitative interpretation of the gamma-ray logs: Acta Geophysica Polonica A, no. 112, p. 121-137.

Czubek, J.A., 1973, New theory, possibilities, and practice in digital interpretation of gamma-ray logs: SPWLA Fourteenth Annual Logging Symposium Transactions, paper W.

Evans, A.E., 1979, Application of bismuth germanate scintillators to detection of high-energy gamma radiation: American Nuclear Society Transactions, v. 33, p. 693-696.

Evans M.L., 1977, NDA technology for uranium resource evaluation: Los Alamos Scientific Laboratory Report LA-6996-PR, p. 2-12.

Evans R.D., 1955, The atomic nucleus: New York, McGraw-Hill Book Company, p. 684, 698-699, 706.

George, D.C. (Bendix Field Engineering Corporation), 1979a, (private communication).

George, D.C. (Bendix Field Engineering Corporation), 1979b, (private communication).

George, D.C., Evans, H.B., Allen, J.W., Key, B.N., Ward, D.L., and Mathews, M.A., 1979, A borehole gamma-ray spectrometer for uranium exploration: Twentieth Annual Logging Symposium Transactions, v. 1, paper X.

Henry, D. (Harshaw Chemical Co.), 1980, (private communication).

Hill, T.R., 1975, ONETRAN: A discrete ordinates finite element code for the solution of the one-dimensional multi-group transport equation: Los Alamos Scientific Laboratory Report LA-5990-MS.

Mathews, Mark A., Koizumi, Carl J., and Evans, Hilton B., 1978, DOE-GJ logging model data synopsis: Bendix Field Engineering Corporation Open-File Report GJBX-76(78), p. 11.

Scott, James H., 1962, The GAMLOG computer program: U.S. Atomic Energy Commission Report RME-143, p. 11.

Shaeffer, N.M., 1973, Reactor shielding for nuclear engineers: U.S. Atomic Energy Commission Report TID-25951, p. 70.

REFERENCES

Stromswold, D.C., and Kosanke, K.L., 1978, Calibration and error analysis
for spectral radiation detectors: IEEE Transactions on Nuclear
Science, v. N5-25, no. 1, p. 782-786.

Stromswold, D.C., and Kosanke, K.L., 1979, Spectral gamma-ray logging I:
Energy stabilization methods: SPWLA Twentieth Annual Logging
Symposium, v. 2, paper DD.

APPENDIX

EQUIPMENT

The equipment used to collect the data in this report evolved over the performance period. The same winch (Mount Sopris NB-3000) and cable (3,000 ft., 4HO) were used all the time, but the uphole electronics changed.

Uphole Electronics

The electronics for the early experiments are shown in Figure A-1. The linear amplifier was an Ortec 450 with shaping constants set at 1 microsecond. The amplified signals were stabilized using a Harshaw NA-22 analog gain stabilizer which held pulses from a ^{54}Mn reference source in the probe fixed in amplitude. The signals were processed by a Canberra Series 30 multichannel analyzer, and 1024 channels were generally used for the spectrum. When the spectra were recorded on tape, a Texas Instrument 733 data terminal with cassettes was used.
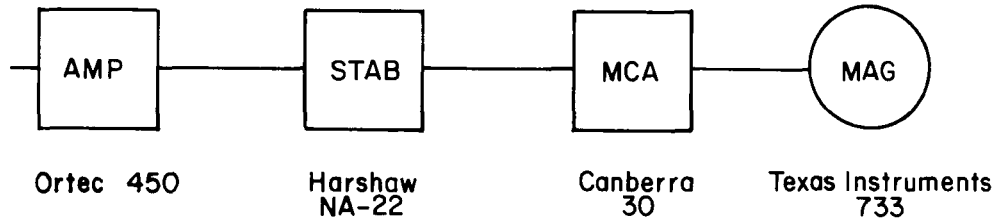
Figure A-1. Uphole electronics used in early experiments.

The equipment used in the experiments changed gradually and in the end existed as shown in Figure A-2. Signals from an Ortec 572 linear amplifier were stabilized in a Tracor Northern NS-454 digital gain stabilizer. The spectra from the calibration models were stabilized using the natural peaks in the spectra so that the ^{54}Mn source could be removed from the probe. The digital stabilizer operated in conjunction with a Tracor Northern TN-1213 analog to digital converter (ADC). The ADC was mounted in a NIM bin and interfaced with a Tracor Northern TN-1710/8K multichannel analyzer through a digital input module (TN-1710-42) in the MCA. Spectra selected for recording were placed on floppy disk using a TN-1117 dual floppy disk system.
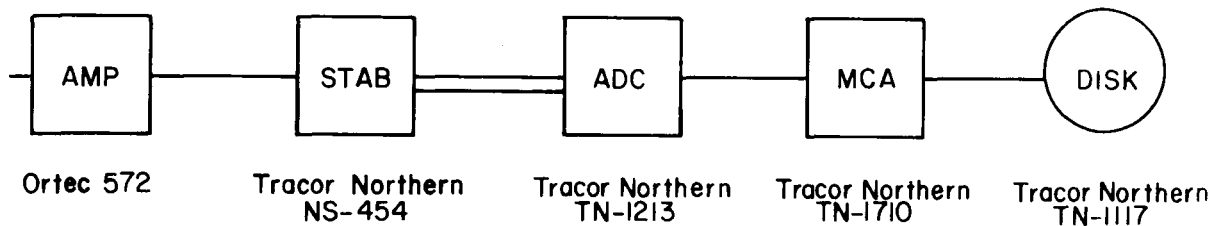

Figure A-2. Uphole electronics final configuration.

185

Probes

The spectral probes used in the experiments were built by Bendix Field
Engineering Corporation at Grand Junction. Probe diameters ranged from 2 to
2.625 inches. The electronics in all the probes were essentially the same and
are shown in Figure A-3. Pulses from the probe were sent analog up the
logging cable. The detectors in the probes were NaI(Tℓ) crystals with
ruggedized construction made by Harshaw and Bicron. RCA photomultiplier
tubes (generally type 4855) were coupled to the crystals. The tubes were
wrapped with magnetic shielding but limited space in the probes restricted
the amount of magnetic shielding used. High voltage for the photomultiplier
tubes was provided by a Velonex Pico-pac power supply in the probe.
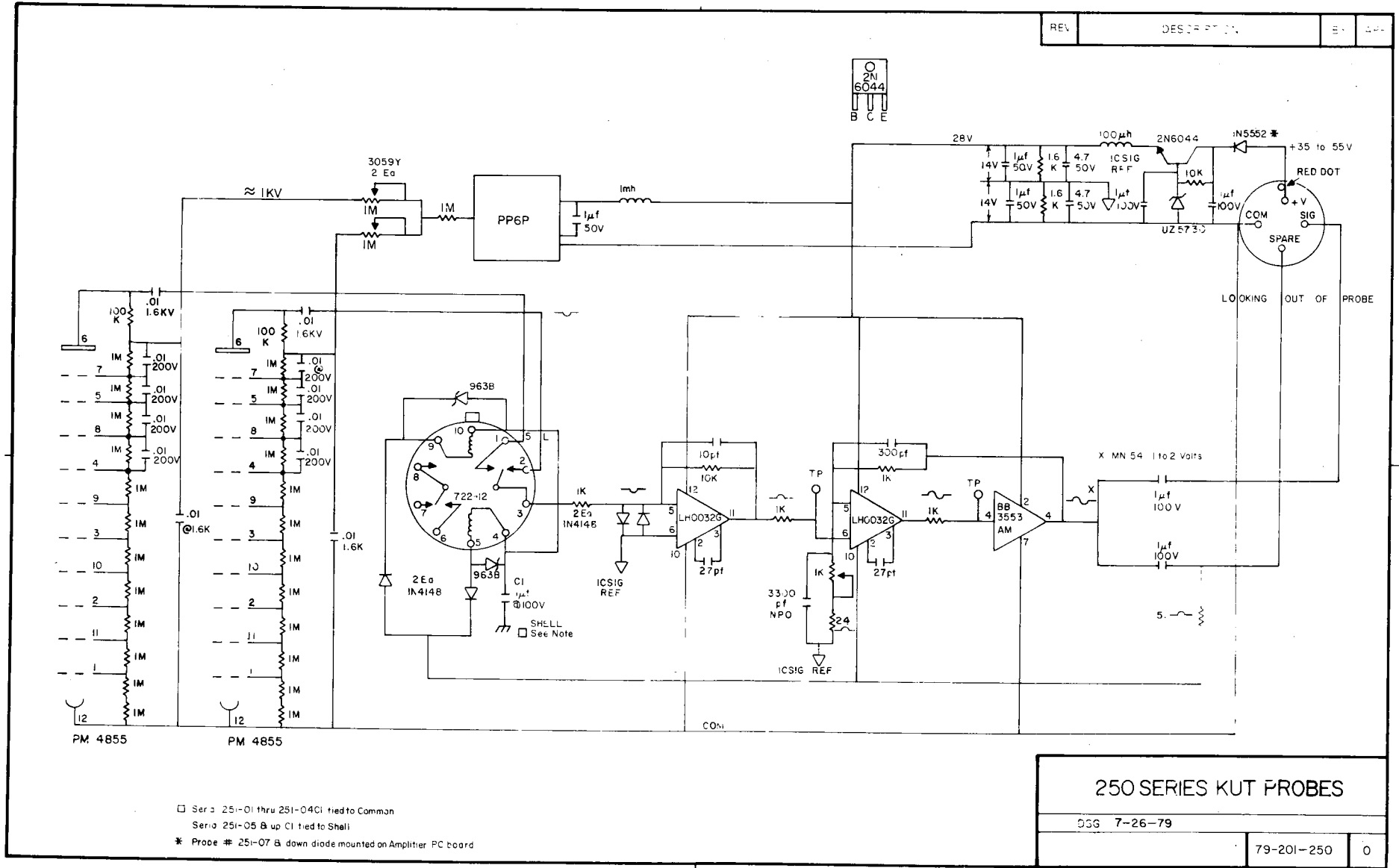
Figure A-3. Schematic drawing of spectral probe electronics.

AIRBORNE AND VEHICLE MOUNTED GEOPHYSICAL DATA ACQUISITION
SYSTEM CONTROLLED BY NOVA MINICOMPUTERS

Q. Bristow

Geological Survey of Canada

AIRBORNE AND VEHICLE MOUNTED GEOPHYSICAL DATA ACQUISITION SYSTEMS CONTROLLED BY NOVA MINICOMPUTERS

Quentin Bristow, Geological Survey of Canada

BACKGROUND

One of the activities of the Geological Survey of Canada (GSC) is a continuing programme of research directed toward the introduction of improved techniques and nationally accepted standards for geophysical and geochemical data collection and presentation. A part of this work is concerned with the measurement of the distribution of the naturally occurring radio-elements potassium, uranium and thorium by means of gamma-ray spectrometry. All three of these elements generate (directly or indirectly) gamma radiation which is sufficiently penetrating to be detected by airborne equipment, and by metal probes containing scintillation detectors lowered down field boreholes which are drilled for exploration purposes. The two research-oriented systems which were developed at the GSC to meet these two particular applications are the subject of this paper.

RADIATION MEASUREMENT - A RECAP

Figure 1 shows that part of the electromagnetic radiation spectrum in which measurements are commonly made. As can be seen it encompasses everything from radio waves with very long wavelengths (several kilometres) used for navigational purposes, to cosmic radiation with wavelengths of the order of 10^{-7} nm (nanometres).
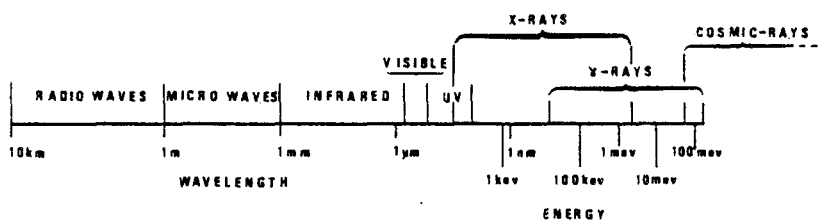

Figure 1: The portion of the electromagnetic radiation spectrum in which measurements are commonly made.

The methods of detection of radio waves, micro-waves, infra-red and visible radiation involve a variety of well known devices such as conventional antennae, dishes, bolometers and photo-cells. In the case of visible radiation the human eye responds differently to different wavelengths to give the sensation of colour. The measurement parameter traditionally used for radiation in these portions of the EM spectrum is wavelength, the shorter the wavelength the greater the energy associated with the radiation. Beyond the UV wavelengths EM radiation has sufficient energy to ionise matter. X-rays, gamma-rays and cosmic radiation are all capable of disrupting individual atoms of the matter they strike by knocking orbiting electrons from them to form ions. The measurement parameter most commonly used for this type of radiation is energy expressed in thousands or millions of electron-volts (keV, meV) rather than wavelength. The gamma radiation from the naturally occurrring radioisotope of potassium (^{40}K) has an energy of 1.46 meV, while that generated from one each of the many radioisotopic · daughter elements of uranium and thorium (^{214}Bi and ^{208}Tl) have energies of 1.76 and 2.62 meV respectively. Since all three frequently occur together in the earth's crust it is desirable to have some means of being able to distinguish between these different radiation energies. In the visible spectrum this would be
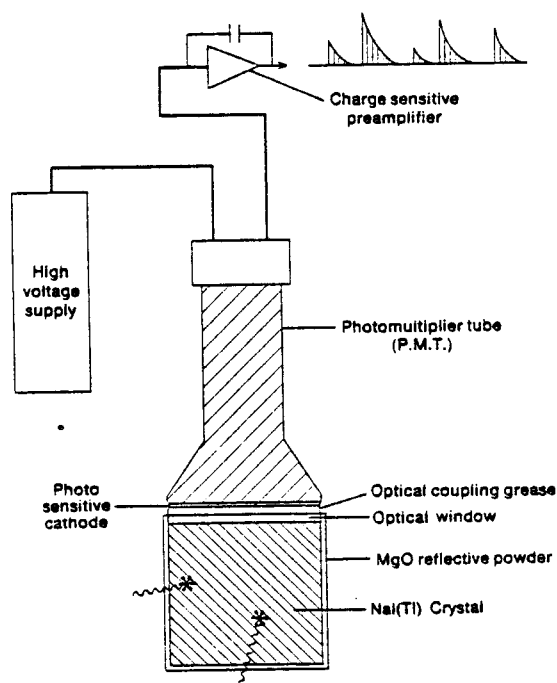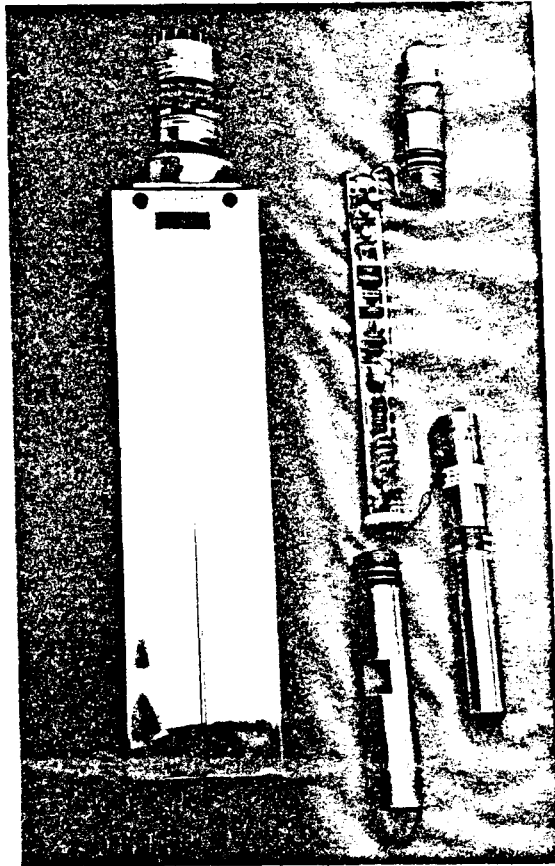

Figure 2:   The scintillation detector is used for sensing and resolving gamma radiation into an energy spectrum. It is analagous to devices which resolve visible light into a spectrum of colours.

equivalent to saying that it would be desirable to have a detection device capable of distinguishing between radiation of different colours. This analogy is accurate and worth bearing in mind for the discussion which follows.

Figure 2 shows the scintillation detector, which is the most commonly used device for detecting and resolving gamma radiation into a spectrum of energies of "colours". When gamma-rays, or sufficiently energetic X-rays, interact with the thallium-doped sodium iodide crystal, tiny scintillations or light flashes occur, the intensities of which are proportional to the energies of the gamma or X-rays which caused them. These are sensed by the photomultiplier tube attached to the crystal which generates corresponding electrical pulses having amplitudes proportional to the original radiation energies.

Figure 3: The large scintillation detector (left) is used in airborne equipment. The top portion houses the photomultiplier tube. The small detector (right) is used to record radiation profiles in boreholes; it is contained in a metal tube (not shown) with electronics. "O" ring seals on nose-weight and connector assembly keep water out.

Figure 3 shows the scintillation detectors which are used in our systems. The one on the left contains a sodium iodide crystal made in the form of a rectangular prism 400 mm (16") long with a 102 mm (4") square cross-section and weighs over 15 kg. Twelve of these are used in the airborne system. The one on the right contains a cylindrical crystal 25 mm in diameter by 76 mm in length and is used for measurements in boreholes (borehole logging).

ACQUISITION OF GAMMA-RAY SPECTRA

The problem of detecting and sorting individual gamma-rays is analagous in some ways to that of trying to count and sort rain drops according to size as they fall during a shower. The time between the events is random and decreases on average the heavier the shower. The measurements of terrestial radiation with which we are concerned can involve average gamma-ray count rates as high as 50,000 c/s, and more in extreme cases where boreholes intersect formations with very high uranium or thorium concentrations. The method of sorting or acquiring a spectrum showing the energies of the individual gamma-rays is to feed the corresponding pules from the photomultiplier tube (PMT) of the scintillation detector to a special analogue-to-digital converter (ADC). This converter is essentially a high speed digital voltmeter which generates in a few microseconds a binary number corresponding to the height of an incoming pulse and hence to the energy of the gamma-ray which was detected. Such converters are commercially available in the popular nuclear instrument module (NIM) package and are used in our systems.

The NOVA Minicomputer is ideally suited for the next step in the process which is to keep track of the number of pulses and their amplitudes as read from the output of the ADC. A feature of the NOVA data channel (direct memory access) interface is a "memory increment" capability. If the digital representation of each gamma-ray energy generated by the ADC is interpreted as a memory location, then the contents of that location will be incremeted by one.
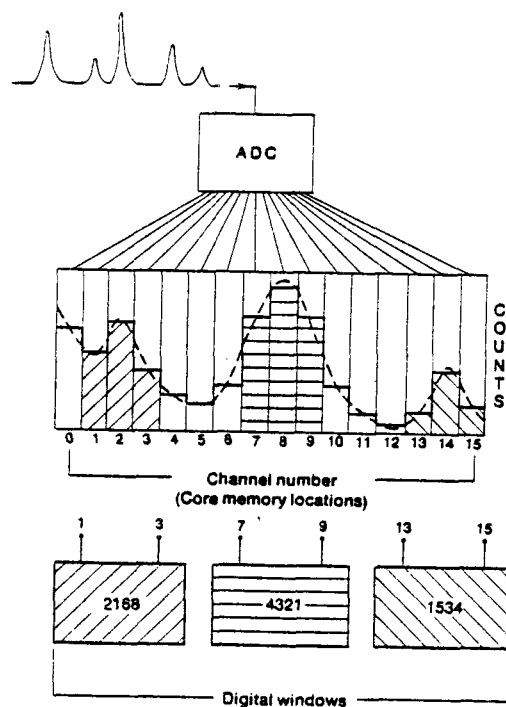
Figure 4: *A pulse-height analogue-to-digital converter (ADC) in conjunction with a memory allows histogram of spectrum to be accumulated, showing the distribution of gamma energies detected by a scintillation detector.*

Figure 4 shows how this process causes a spectrum of the detected gamma-ray energies to be built up in a block of memory, each location representing a channel or energy slot. It also shows that the intensity of one particular "colour" of radiation can be estimated by summing the contents of the channels in a window encompassing the energy range of that particular "colour". This is the basis of gamma-ray spectrometry using scintillation detectors and is exactly analagous to optical spectrometry where a prism or diffraction grating would be used. Figure 5 shows a typical spectrum of the gamma radiation from natural sources which was acquired by the GSC airborne gamma-ray spectrometry system.
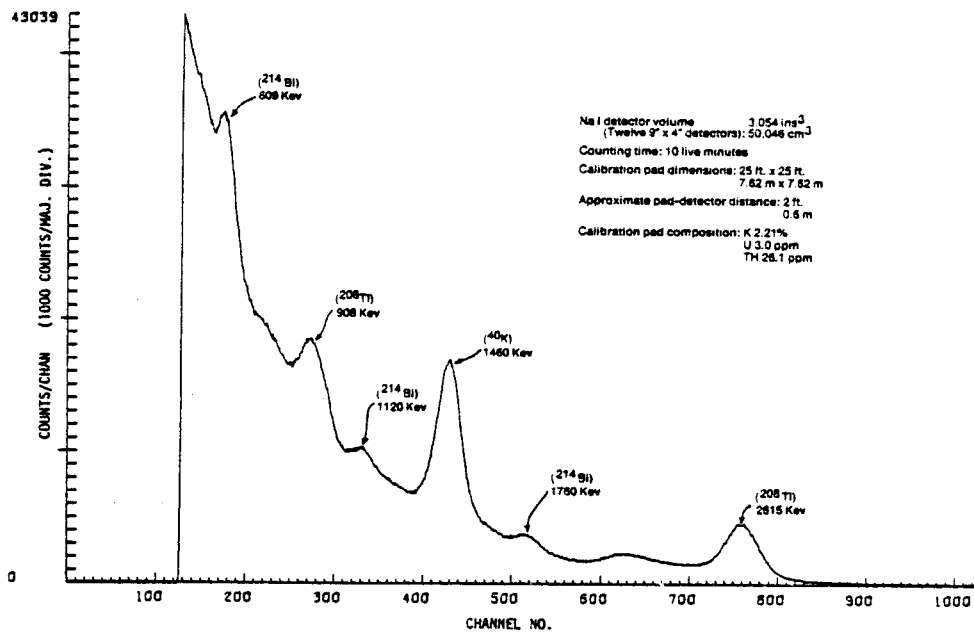
Figure 5: A typical gamma radiation spectrum from natural sources. The peaks identified as ^{40}K, ^{214}Bi and ^{208}Tl indicate the presence of potassium, uranium and thorium respectively.

FUNCTIONAL CONFIGURATION OF THE TWO SYSTEMS

Figures 6 and 7 are block diagrams of the airborne and vehicle mounted systems respectively. A comparison shows that most of the major components are common to both systems. Specifically these are:

- NOVA 1220 minicomputer
- Special CRT display
- Pulse-height A/D converter
- Nine-track mag. tape unit
- Hard copy terminal
- Six-channel strip chart recorder
- Operational software (approximately 80% common to both systems)

The functions of these various components in extracting data relating to the distribution of potassium, uranium and thorium can be understood from the pictorial representation of figure 8. This shows a scintillation detector (in this case being lowered into a borehole) generating pulses caused by the detection of individual gamma-rays which are digitized by the ADC and accumulated by the NOVA to form a series of complete energy spectra. The accumulation time for each spectrum is normally one second. Two blocks of NOVA memory are reserved

for this purpose so that while a new spectrum is accumulating in one, the spectrum just acquired in the other is being processed. One part of this processing is the generation of profiles in real-time on the strip chart recorder of the intensities of certain energy windows (or "colours" to follow the earlier analogy). In particular we need those which correspond to the intensities of the potasssium, uranium and thorium energies since they will be an indirect measure of the concentrations of these elements in the vicintiy of the gamma-ray detector at any time.

The three broken lines running over the spectral peaks in figure 8 would be the intensity profiles in that case for the five second interval shown. The NOVA sums the contents of the channels encompassed by the appropriate peaks in each specrtrum to provide these data at one second intervals or at whatever interval is selected. The numbers are then converted to analogue signals which drive the strip chart recorder pens. The CRT display is used to present the counts in up to ten such energy windows as well as depth or navigational data, all updated once per sampling interval. It also displays spectra in graphical form with selected energy windows intensified. The hard copy terminal (a Texas Instruments KSR 743 "silent 700" unit) is used to enter processing constants and other operational parameters, to select and/or copy any one of the 20 CRT display pages, and to list the spectra contained in memory on a channel by channel basis. The magnetic tape unit records complete spectra as acquired along with window profile data, current operational parameters as entered via the terminal, and depth or navigational data as the case may be.
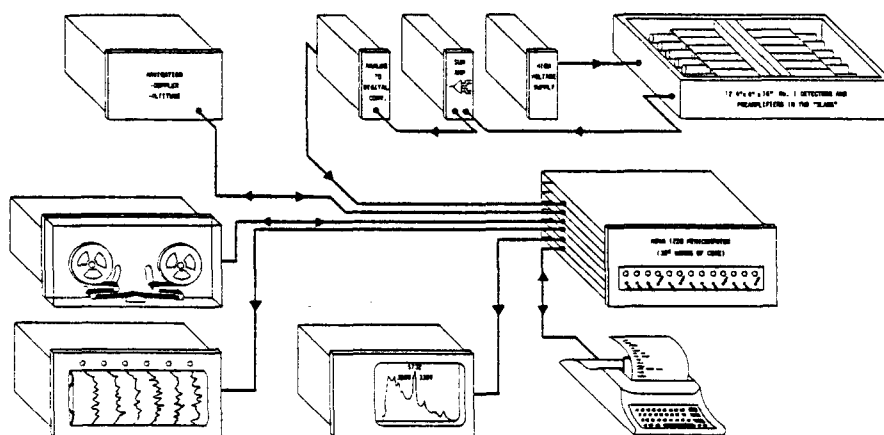

Figure 6: The main components of the Geological Survey of Canada airborne gamma-ray spectrometer. A NOVA minicomputer controls the system.
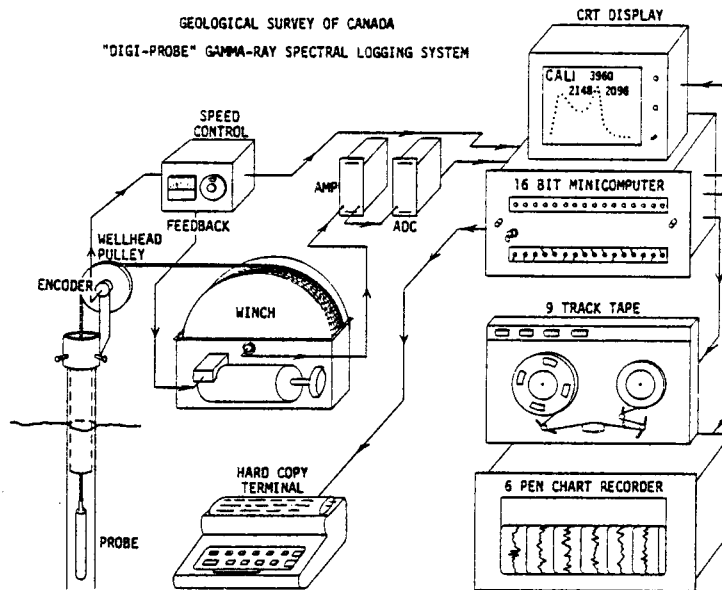
GEOLOGICAL SURVEY OF CANADA
"DIGI-PROBE" GAMMA-RAY SPECTRAL LOGGING SYSTEM

Figure 7: *The vehicle mounted gamma-ray spectrometry system is similar to the airborne system of Fig. 6 and is also controlled by a NOVA minicomputer.*

AIRBORNE GAMMA-RAY SPECTROMETER SYSTEM

Two views of this system are shown in figure 9. The twelve scintillation detectors (one of which is shown at the left of figure 3) are housed in a two-compartment box which is heavily lagged with polyurethane foam and additional hard foam to minimize thermal and mechanical shock to the crystals as they are particularly vulnerable to both of these hazards. This box is 1.6 m long, by 0.5 m high by 1.1 m wide (63" x 20" x 43"). It is bolted to a dual 19" rack cabinet which contains the NOVA, its peripherals and other electronics, this cabinet being 1.1 m wide by 1.2 m high by 0.76 m deep (43" x 46" x 30"). The integral package formed by these two units weighs about 540 kg (1200 lbs) and is mounted on caster wheels for easy transfer between the aircraft in which it is used and a special loading trolley.

Surveys are normally carried out at a terrain clearance of about 120 m (400 ft) along regularly spaced flight lines. The spacing of these lines varies from 0.5 km or so for detailed coverage to several km for broad reconnaissance surveys where very large areas are involved. The navigational and spectral data from the small (8 1/2" reel) tapes are subsequently reformatted off-line with some preprocessing onto standard 2400 ft. tapes using an S130 ECLIPSE based system.

These tapes in turn become the data base from which computer generated contour maps are made of the uranium, potassium and thorium distributions using an APPLICON Corp. Colour plotter.

Figure 10 shows the twin turbo-prop STOL "Skyvan" aircraft, manufactured by Shorts Ltd. of N.-Ireland, which is used for these surveys. It has a tail door for unimpeded access to the fuselage cargo section and flight characteristics which make it eminently suitable for low level survey operations.

VEHICLE MOUNTED SYSTEM FOR BOREHOLE LOGGING

This system is mounted in a four wheel drive three-quarter-ton truck fitted with a camper-back. The NOVA with peripherals and other electronics is mounted in a single 19" rack secured to the camper-back. Power for this system, the electrically driven cable winch and a small air conditioning unit is supplied from an auxilliary generator mounted in the roof section of the camper back over the passenger cab of the truck.
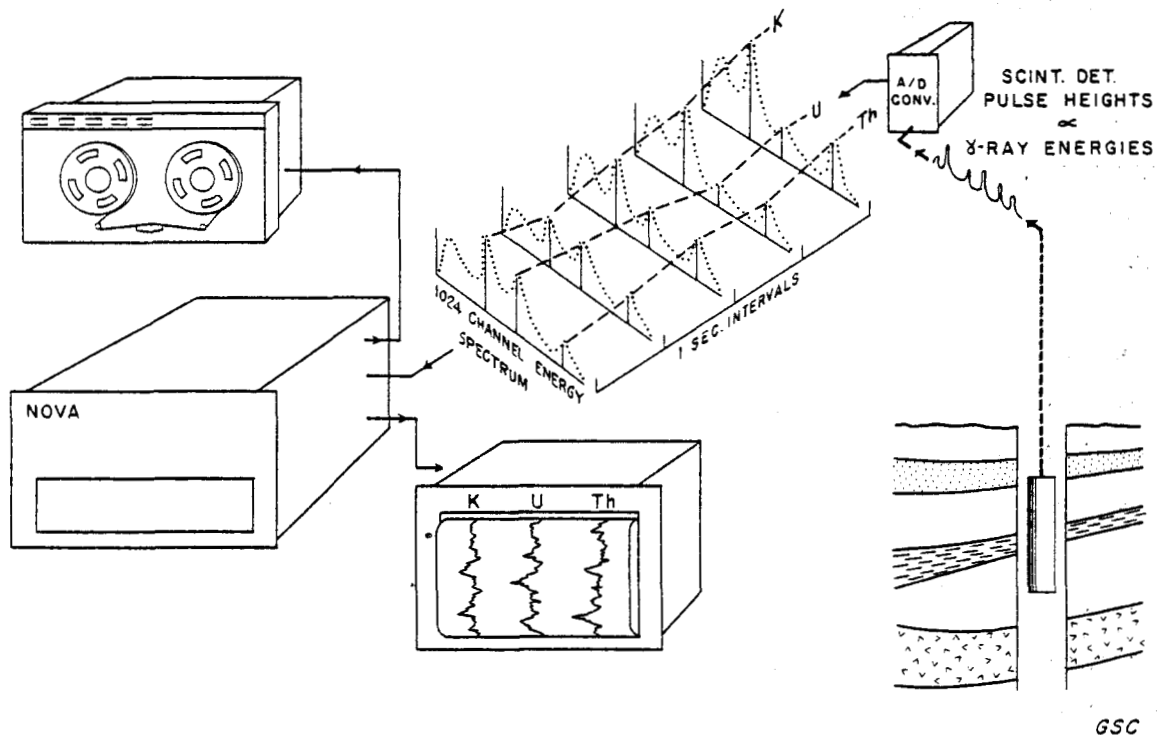

Figure 8:   The intensities of three peaks in each spectrum are processed by the NOVA in real-time to generate profiles marked "K", "U" and "Th" which can be related to the concentrations of potassium, uranium and thorium scanned by the gamma-ray detector.

signal giving direction (up or down). These signals are acquired by the NOVA via an I/O interrupt interface for probe depth and velocity calculations and are also used via separate hardware to maintain the winch speed at a constant level which can be preset. The NOVA interface also has a line to the winch controller which allows automatic stops under software control at predetermined depths entered via the keyboard. Figure 11 shows some of the equipment in the vehicle and a view of a typical set-up for logging a borehole.

NOVA INTERFACES

Full advantage was taken of the interfacing flexibility afforded by the standard NOVA general purpose boards in designing the special interfaces required in these systems. The field environment and the number of physical connections to be made between the NOVA and the devices which it controls made it necessary to add a bracket to the rear of the chassis on which are mounted a variety of multi-pin bayonet and BNC connectors as shown in the photograph of figure 12.
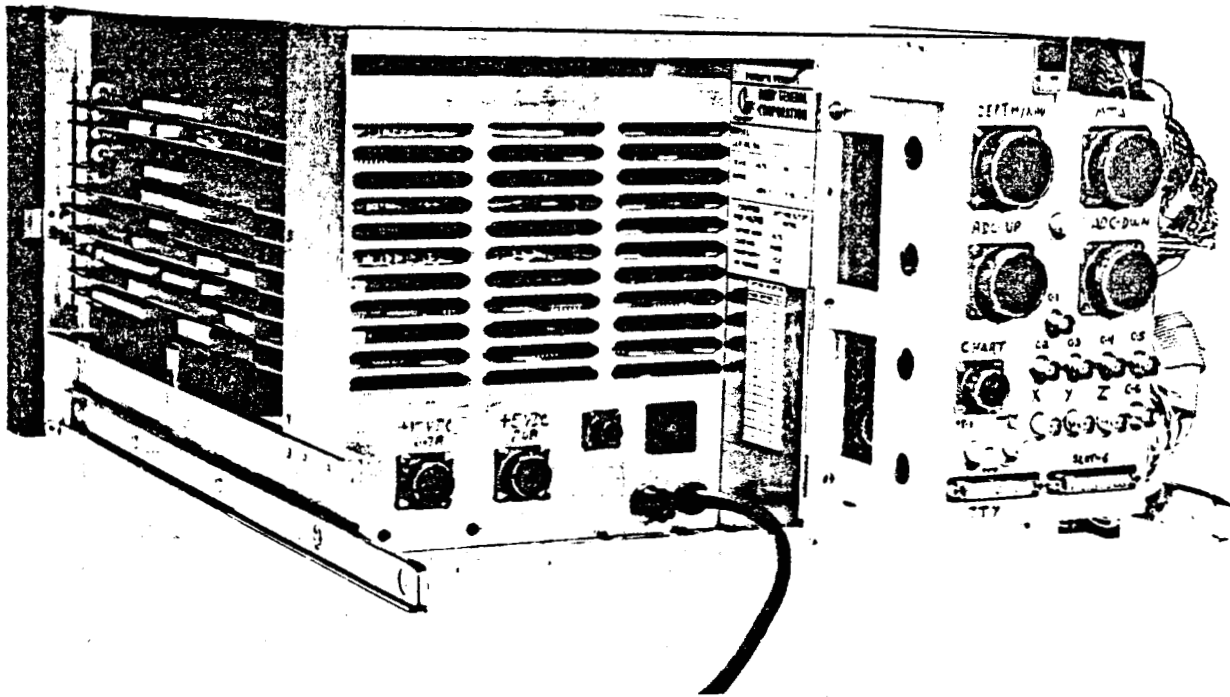

Figure 12: A useful modification to the NOVA allows a variety of peripherals and special devices to be connected with maximum convenience and reliability.

Two industry standard RS232-C connectors are also included for easy connection of devices using this mode of communication. Each connector is wired to the edge board connectors which plug onto the backplane circuit board.

The interface for the pulse-height ADC, a real-time clock (non standard) and the six channel strip chart recorder are all contained on one general purpose board. The block diagram is shown in figure 13. The data channel logic with the jumper-selectable "increment memory" feature already on this board required only three additional ICs and the connection of the ten data input and two "handshake" lines to accomplish the ADC interface.

The general purpose output register is connected to six simple 8 bit D/A converters consisting of CMOS gates and R-2R ladder networks. The six most significant bits of this reigster are reserved for selecting the six D/As (one for each), allowing test patterns to be fed to all chart pens in parallel or different data profiles to be assigned to different ones as required. The NOVA crystal controlled clock on the CPU board (available via the back plane) is divided down for use as a real-time clock. A special requirement here is a tally of the times during which the pulse-height ADC is busy making a conversion ("dead time").
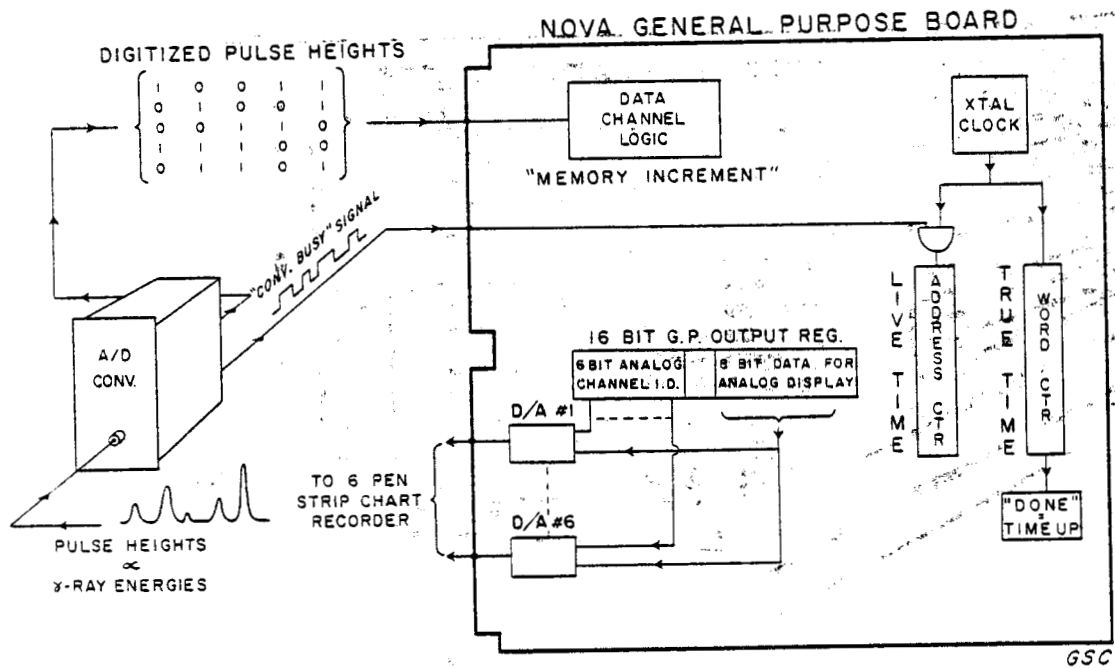

Figure 13: The pulse-height ADC interface, a special real-time clock and six D/A converters for operating the six pen strip chart recorder, are all contained in one NOVA general-purpose board.

This is accomplished by preloading both the WORD and ADDRESS counters already on the general purpose board with the twos complement of the required spectrum accumulation time, and interrupting the clock frequency to one of them whenever the ADC is busy. When the uninterrupted one reaches zero, marking the end of the preset time interval, the other one will contain a residual which is the ADC dead time. The contents of this are brought back into memory by software and used to correct measured gamma-ray countrates.

The requirements for the CRT display were light weight, with a capability for displaying both text and gamma-ray spectra, ie a limited graphics capability. The solution eventually adopted was the use of a simple X-Y monitor CRT, the Tektronix 604A, which has only X and Y deflection and intensity (z) modulation inputs.

The necessary circuitry for character generation (an LSI chip), D/A conversion and line counting etc. was built onto a single NOVA general purpose board. The only external connections required from this board to the monitor are for the X, Y and Z inputs. The NOVA memory itself is used to store the pages of text to be displayed as ASC11 characters, the appropriate blocks of memory being accessed via the data channel logic on the general purpose board. Figure 14 shows
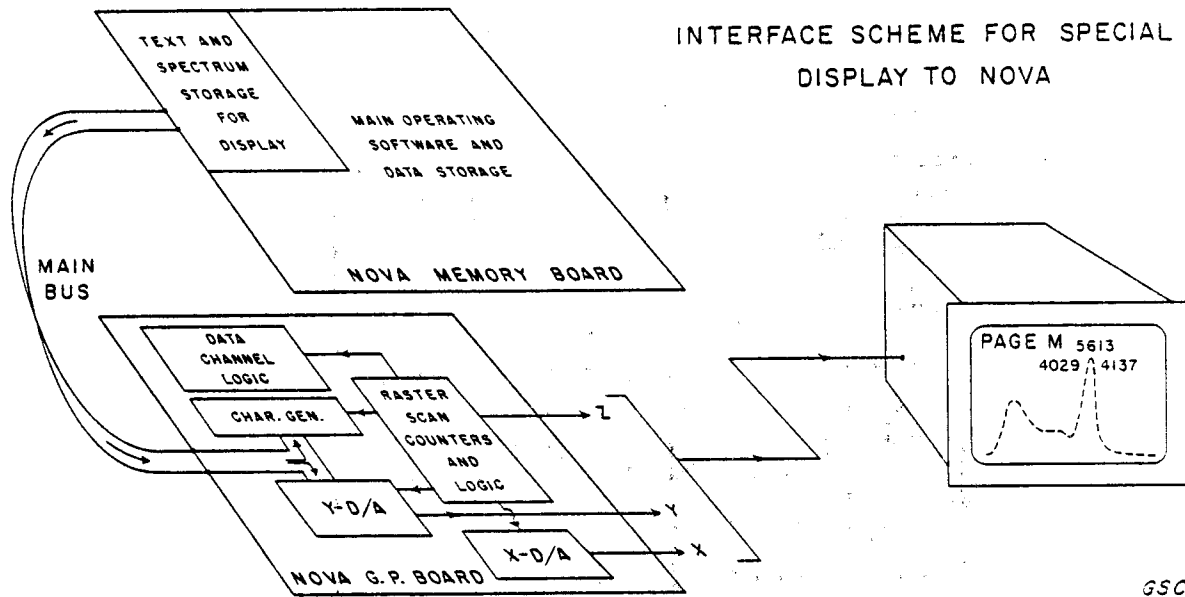

INTERFACE SCHEME FOR SPECIAL
DISPLAY TO NOVA

Figure 14: The CRT display circuitry on a NOVA general purpose board scans the text and gamma-ray spectra stored in the NOVA memory via the data channel to provide visual data on the X-Y monitor CRT unit.

a block diagram of the arrangement. An interrupt is generated at the end of each page scan at which time the software restarts the scan to maintain a continuous refresh rate. This approach has a number of advantages; no external memory is required, no massive high speed data transfers are required from the NOVA to an external memory in order to change a page, and when updates are made to memory locations in a page via the software (e.g. posting new countrate data once per second,) then these automatically appear on that display during the next scan of that page without any special software to implement them. By having the display scan a block of memory where a gamma-ray spectrum is accumulating, a "live" spectrum display is obtained, which greatly facilitates calibration of the system and which would be complicated to implement with a standard commercially available CRT display unit. Figure 15 shows some typical display pages photographed directly from the CRT.
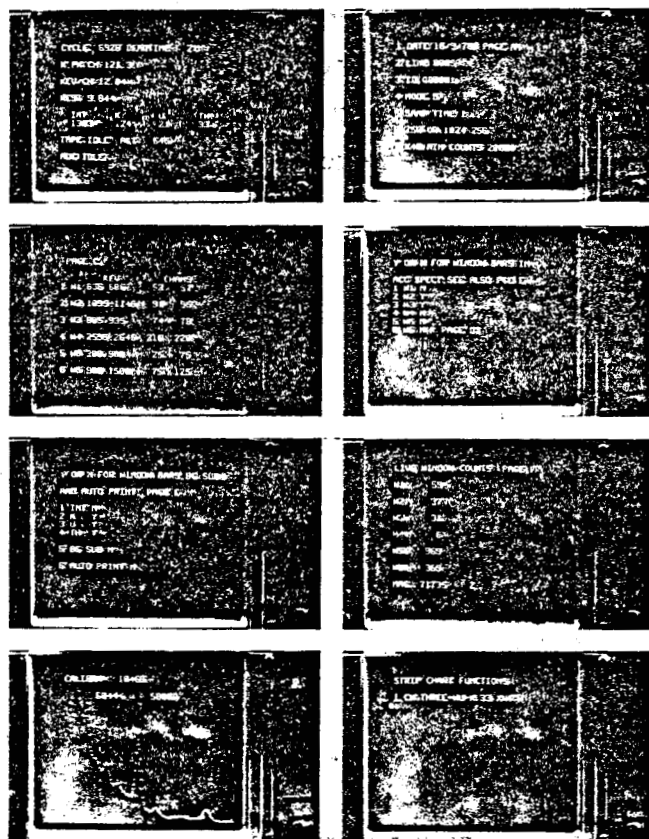

Figure 15: Typical display pages scanned from NOVA memory. Updating numbers in memory automatically updates displayed data.

The interface for the acquisition of depth pulses for the borehole logging system and navigational data for the airborne system are virtually identical. One general purpose NOVA board is used in each case with the interrupt logic being arranged to set the "DONE" flag when new data are received in the general purpose input register.

OPERATIONAL SOFTWARE

The entire software package for the two systems was written in assembly language rather than in FORTRAN or some other higher level language. This was done in order to minimize the execution time involved in processing spectra on line, and because the standard software modules available did not lend themselves readily to handling the locally developed and other speciallized peripherals that are interfaced to the NOVA. Other secondary benefits of this approach are the comparatively small core requirement (approximately 16 K words including 6 K of data storage in this case), and the relative ease with which modifications can be made to suit the needs of the moment. A utility is included which allows octal code to be entered via the keyboard with the address automatically being printed alongside when every second entry is complete. It also incudes commands for dumping portions of memory in the same format and for replacing the contents with zeros. This has been used repeatedly in field situations to patch in blocks of code to meet various temporary requirements. The main functions of the operating software are:

- The continuous acquisition of gamma-ray spectra, with the spectra accumulated during successive time intervals being stored ping-pong fashion in two different blocks of memory.

- Summing of the contents of spectral channels in up to ten energy windows specified by keyboard entry.

- Correction of sums so obtained for "dead time".

- Processing of the profiles generated by successive window count rate data for presentation on the six channel strip chart recorder.

- Acquisition and computation of navigational or depth data.

- Recording of data on magnetic tape.

- Accepting keyboard entries for changes in operational parameters.

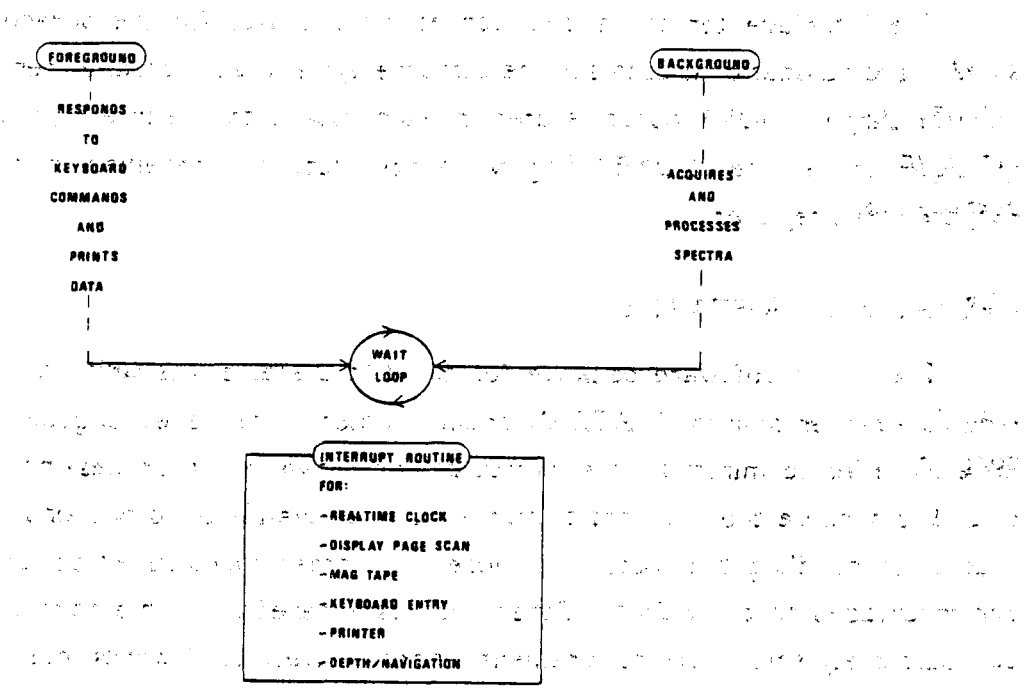- Listing displayed data on the hard copy terminal.

Figure 16: Software operating system operates in a background/foreground mode
to allow keyboard access while data is being acquired.

The software operates in a background/foreground mode as shown in Figure 16 when the spectrometer is acquiring data. Under these conditions the foreground portion, accessible via the terminal keyboard, allows parameters to be changed and display pages to be called or copied while the cycle of data acquisition and computation proceeds in the background. This cycle has absolute priority over the foreground; for example if a keyboard or printer interrupt occurs during the computation cycle it is recognized by the interrupt service routine but service is delayed until computation is complete for the current cycle. Servicing of other interrupts which require insignificant execution times such as restarting a display page scan or pulling in navigational data from a register is done in the interrupt routine as they occur, with immediate return to the computation in progress. One accumulation time interval (normally one second) is available for the necessary computation to be carried out on the spectrum most recently acquired, with what is left being used for any foreground tasks still pending. During this interval the next spectrum is accumulating in a second memory block via the data channel. Once the real-time clock signals the end of the interval, computation must immeditely begin again on the new spectrum.

In the case of the bore-hole logging system, a fairly sophisticated digital inverse filter combined with a smoothing filter is applied to one of the window countrate profiles. The calculation of each point involves storage of up to 30 consecutive raw data values. Both systems have keyboard programmable profile functions which allow scaling of window data to fit the full scale chart pen ranges (256 each) imposed by the 8 bit D/A converters. These programmable functions also allow ratios, sums, differences, etc. of various window profiles to be plotted on any channel.

Both systems also have provision for tracking the position of a spectral peak. If the gains of the scintillation detectors stay constant, then a peak with given energy will always be found in the same spectral channel. However, the gains do vary causing the horizontal (energy) scale of the spectrum to compresss or expand by a small amount. The software periodically calculates the channel number of the centroid of the area under one particular peak and corrects all the limits of the currently specified energy windows to allow for this variation.

Figure 17 shows how the mode switching between background and foreground is accomplished. Whenever the current background computation cycle is finished and the current foreground task is awaiting a hardware interrupt, the program enters a wait loop. It remains there until either the foreground software flag or the background software flag is set in the interrupt routine as a result of an interrupt being received. Separate entry and exit routes allow current status information to be stored and recovered for the mode it has left or to which it is about to return. Once a flag has been set as a result of a hardware interrupt, it will remain set until the program re-enters the wait loop via the corresponding route and resets it. The RUBOUT key is recognized in the TTY interrupt routine as a special character. Whenever it is received the current foreground task is terminated and the foreground program is set to await new keyboard commands.

The software system thus appears to operate as two independent and concurrent programs, with much of the sophistication of more elaborate high level language systems, but with the economy of core space and execution time typical of an assembly language compilation.